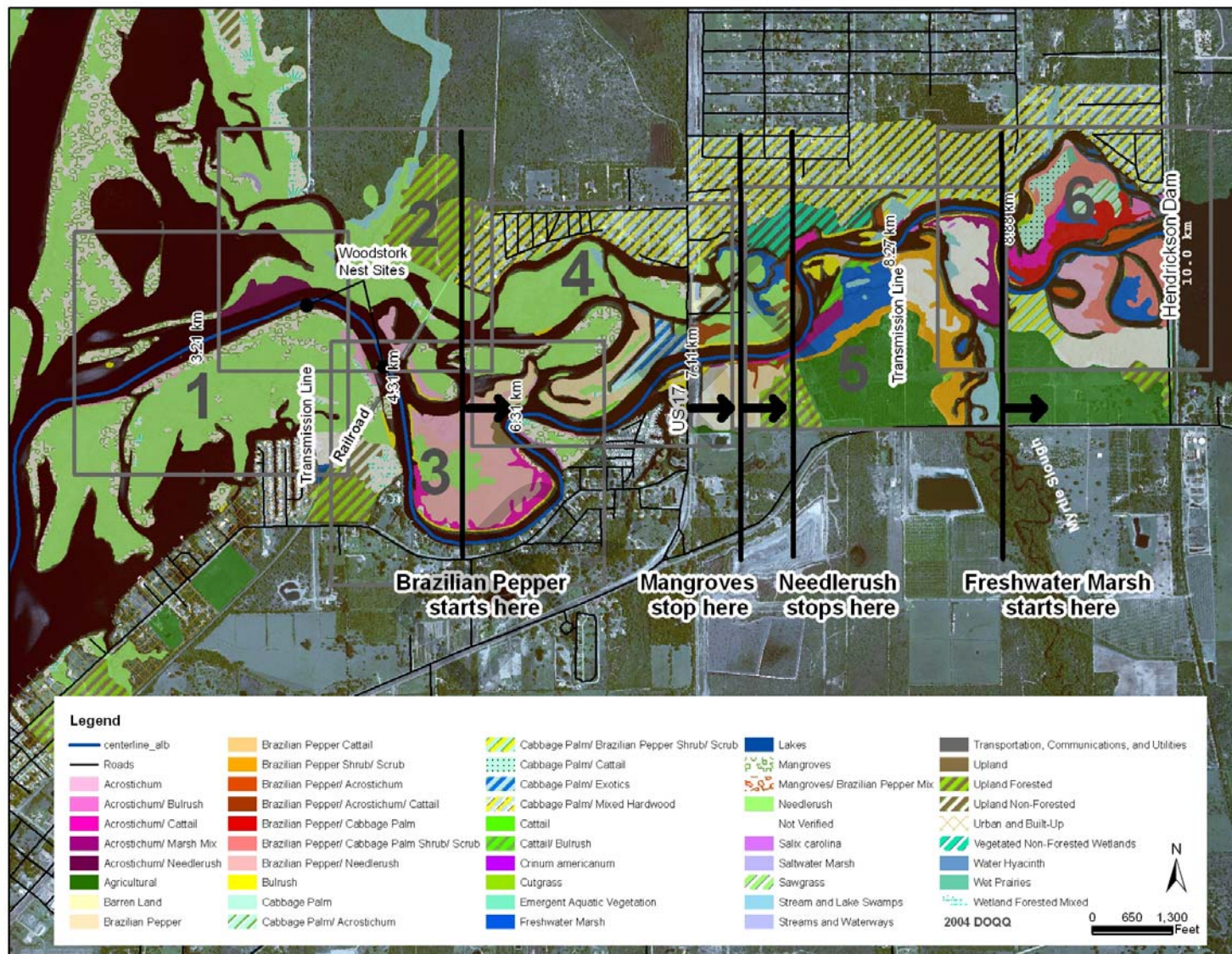
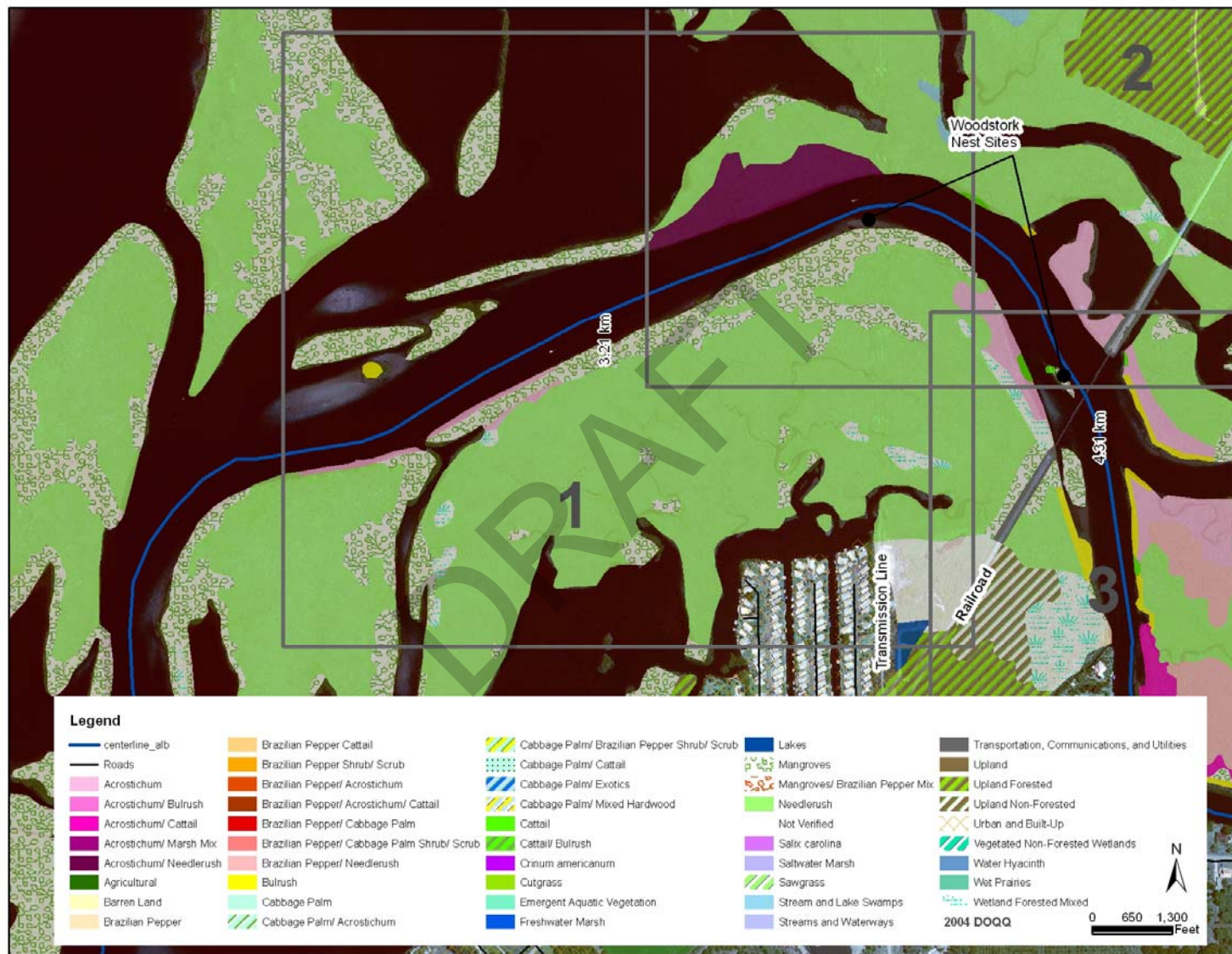
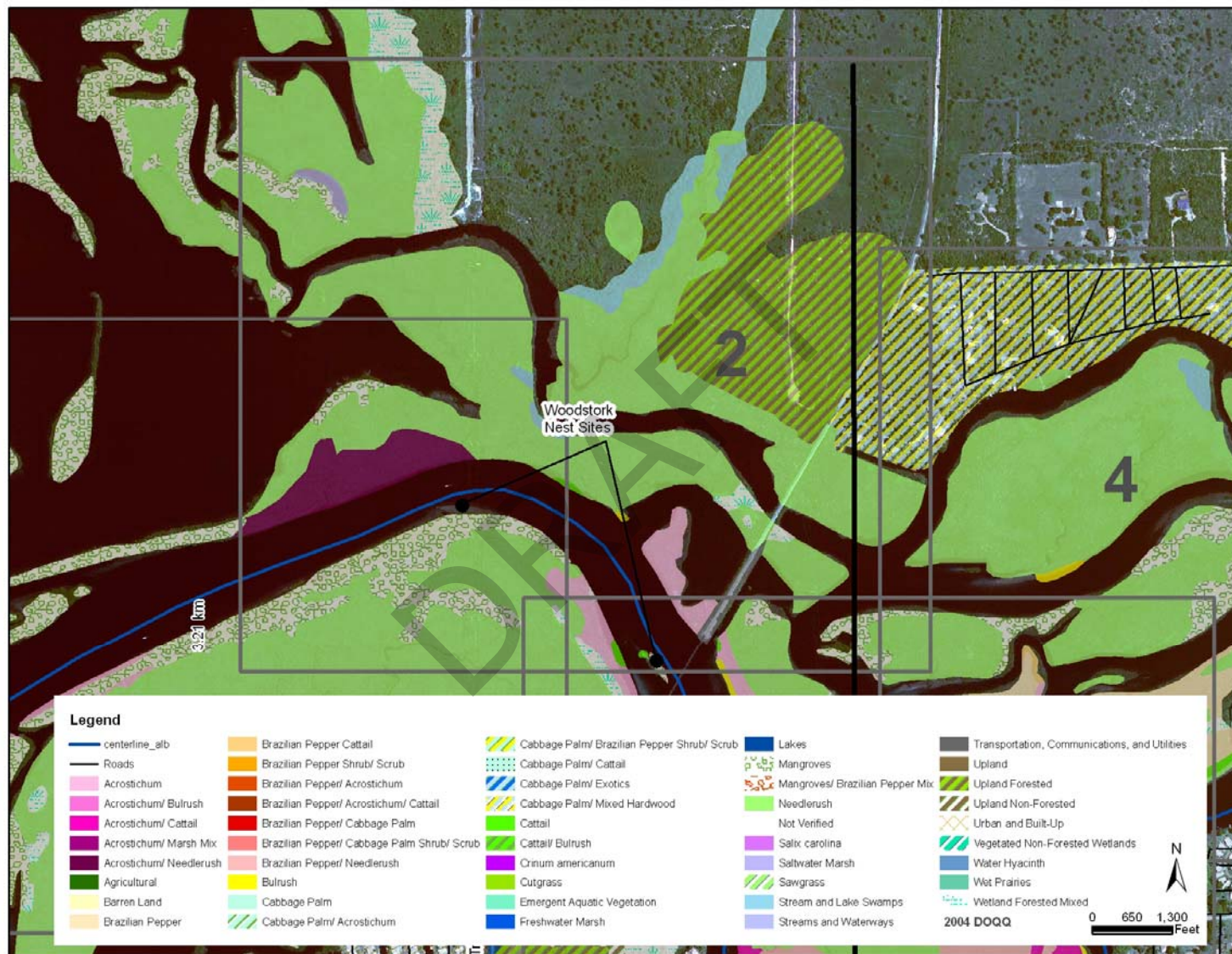


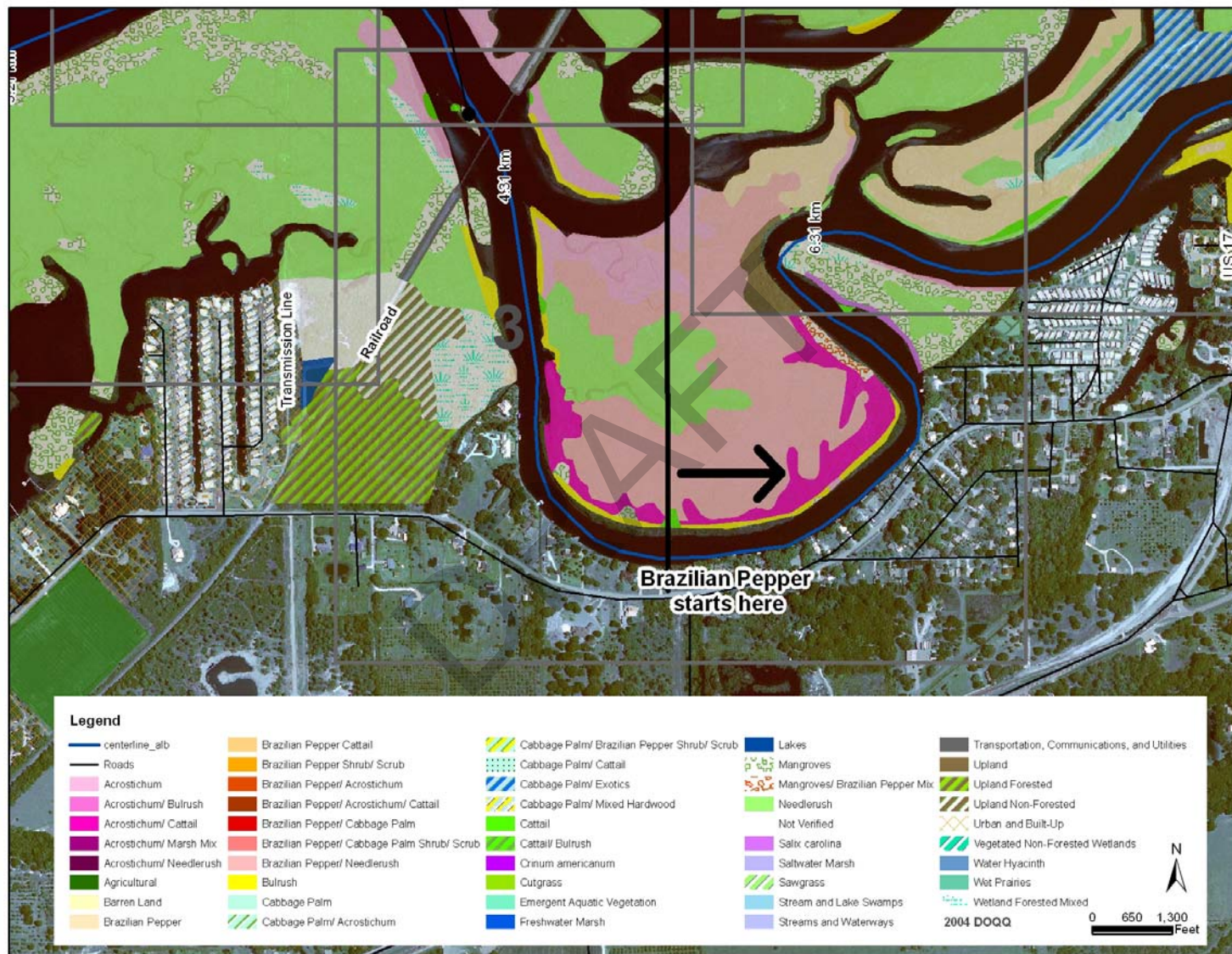
Appendix 2-1

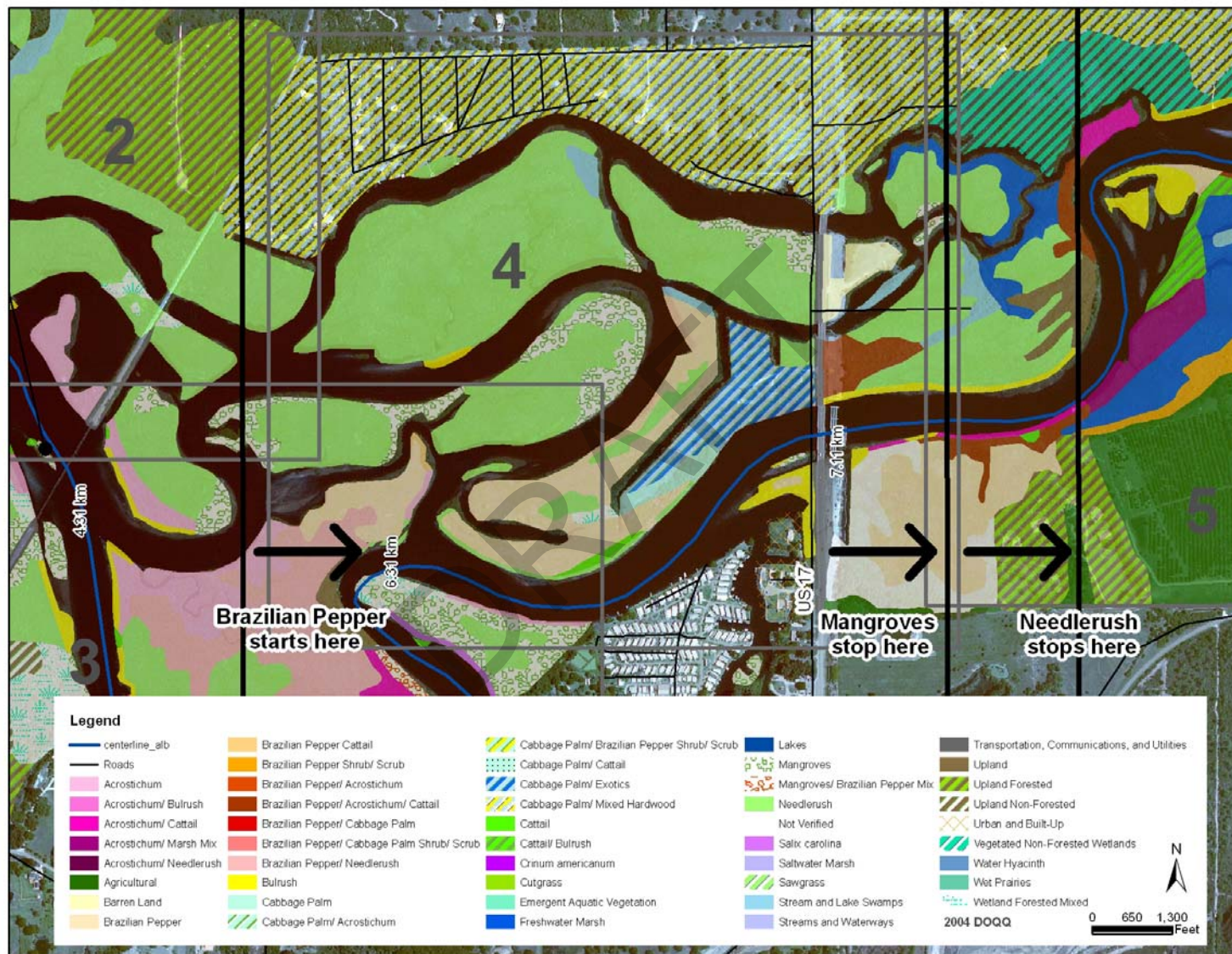
Shell Creek Vegetation Maps (PBS&J, 2006)

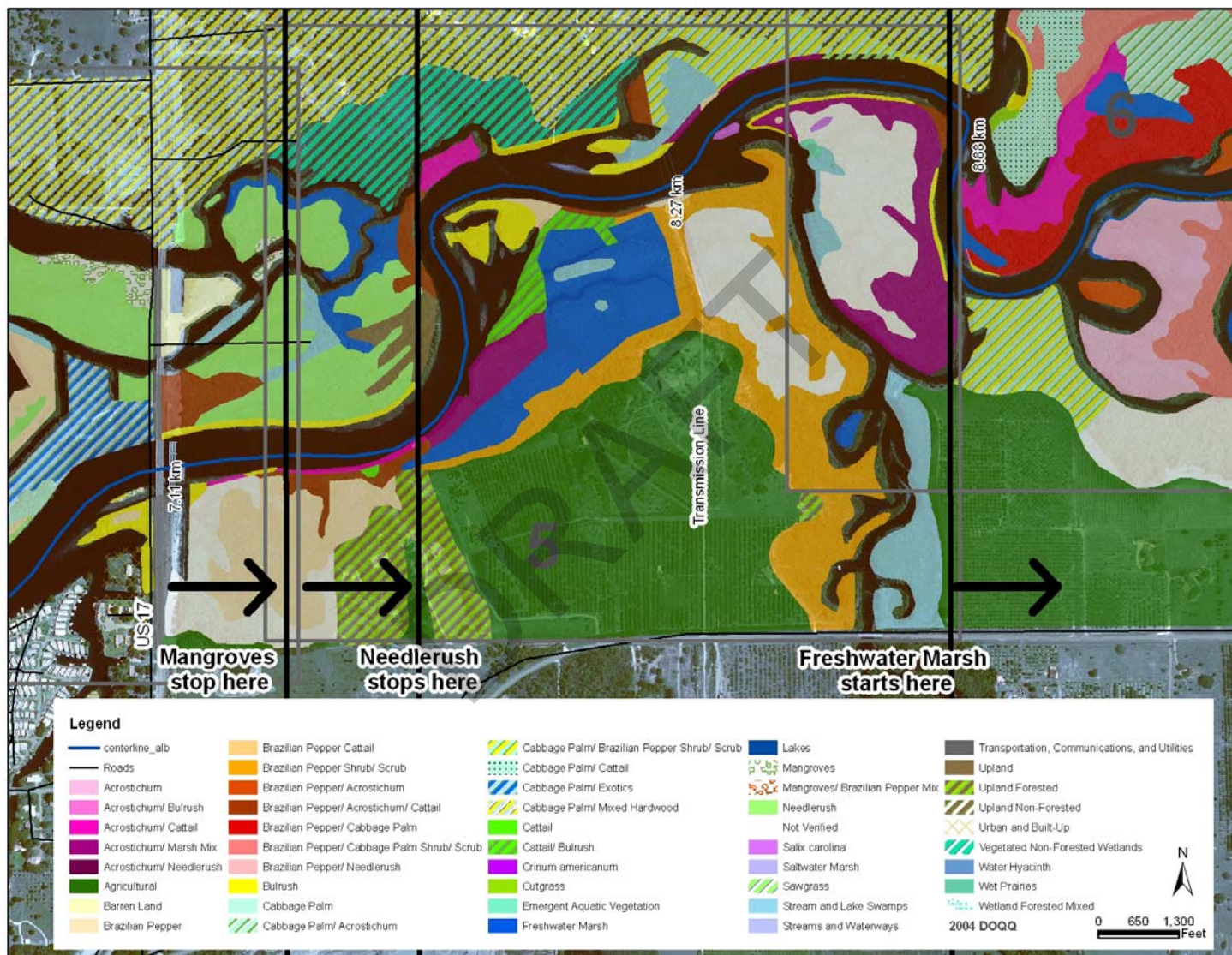








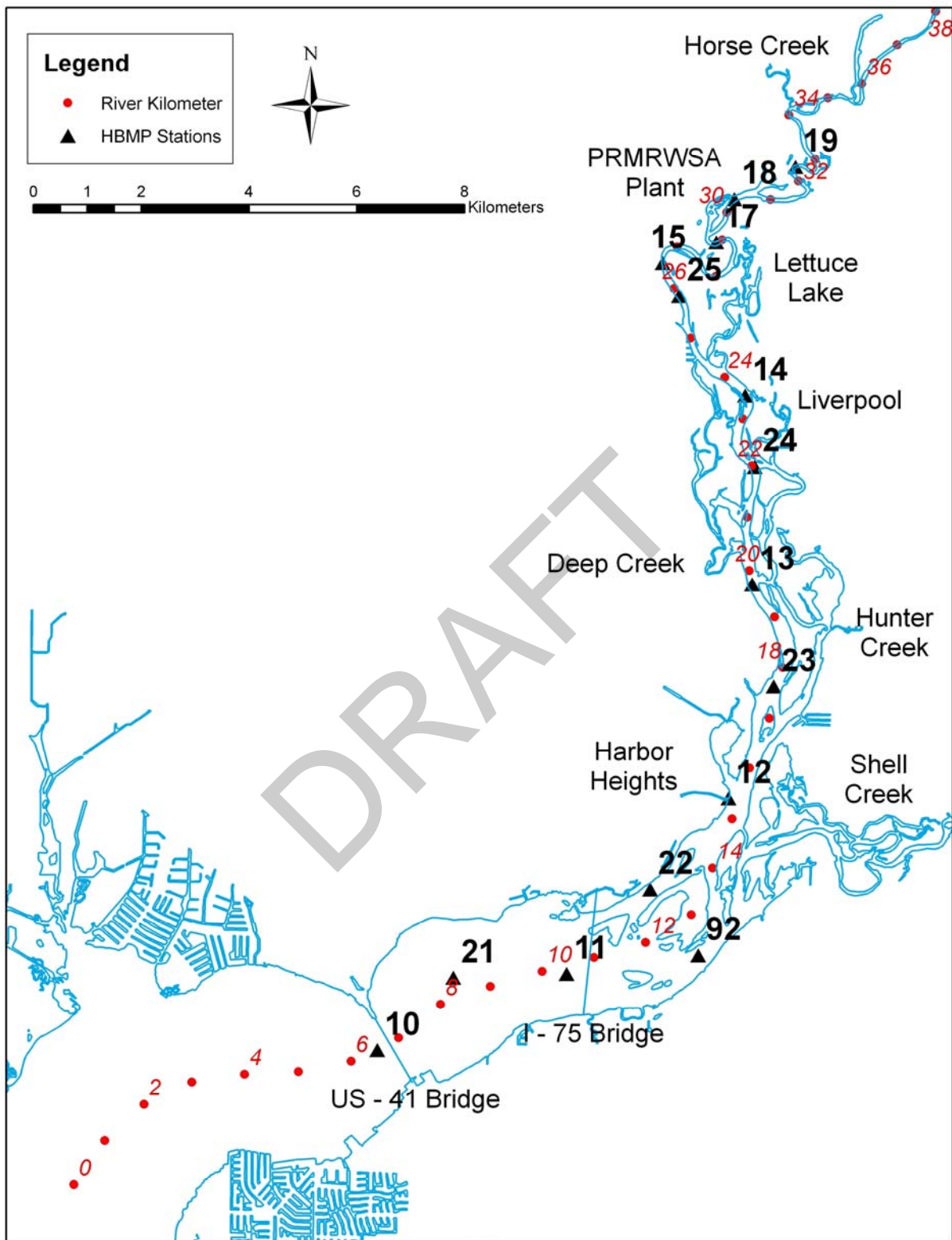


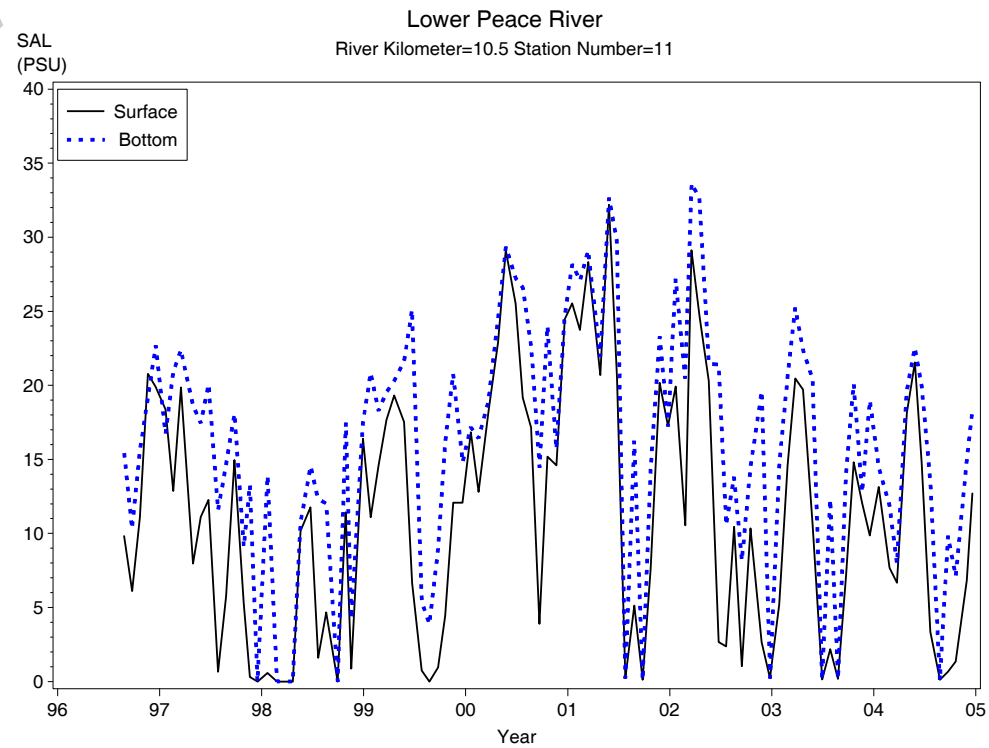
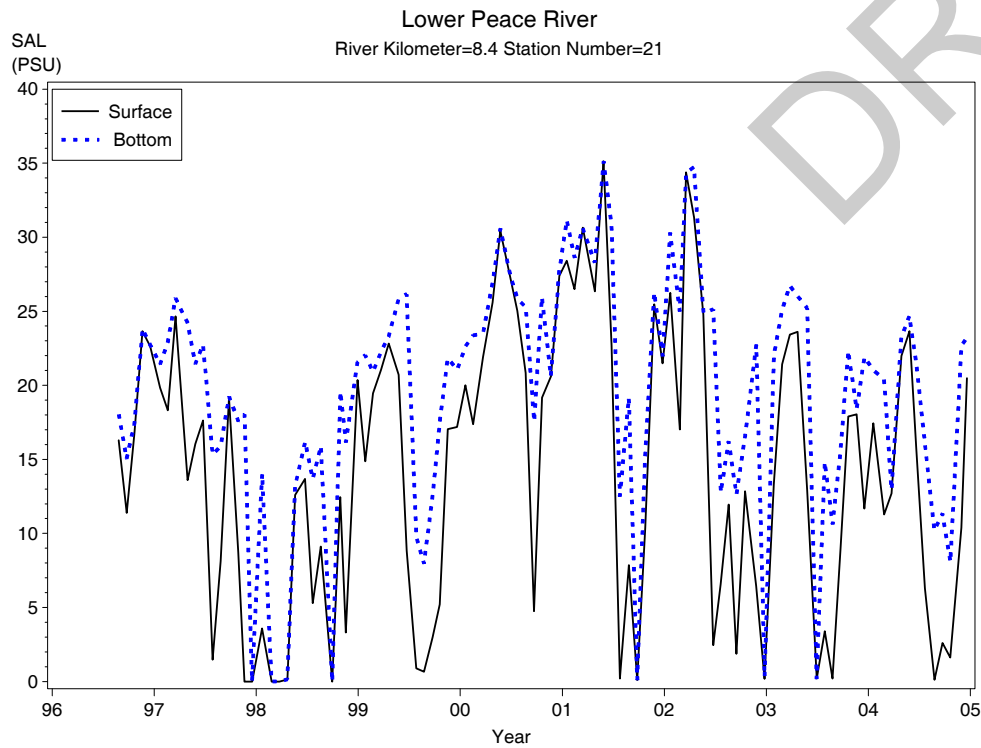
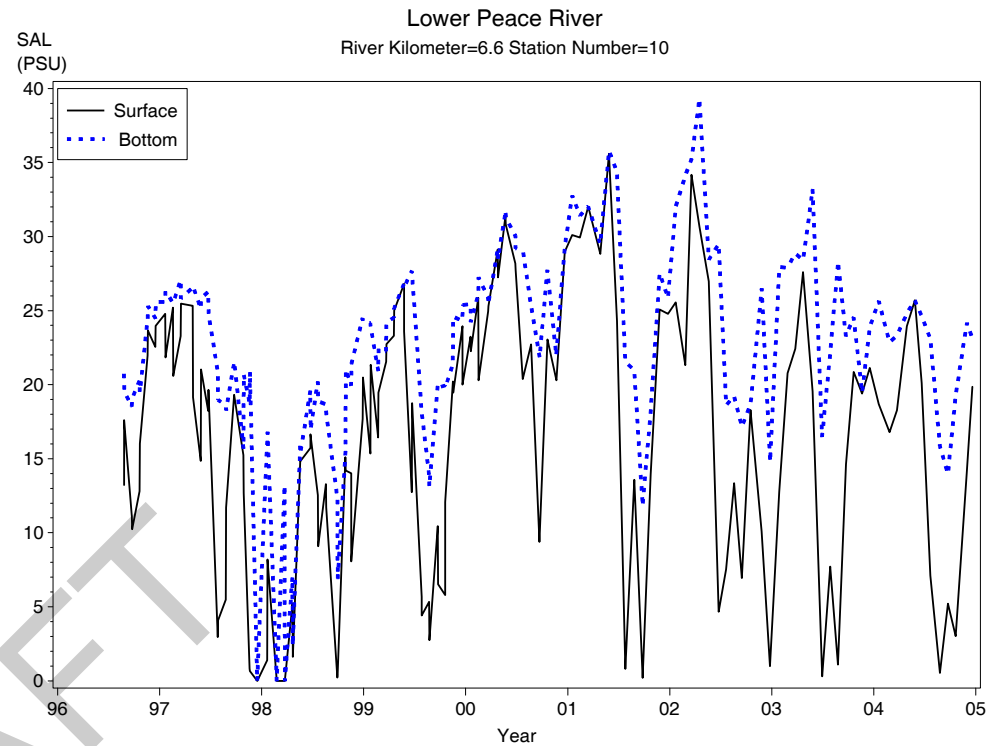
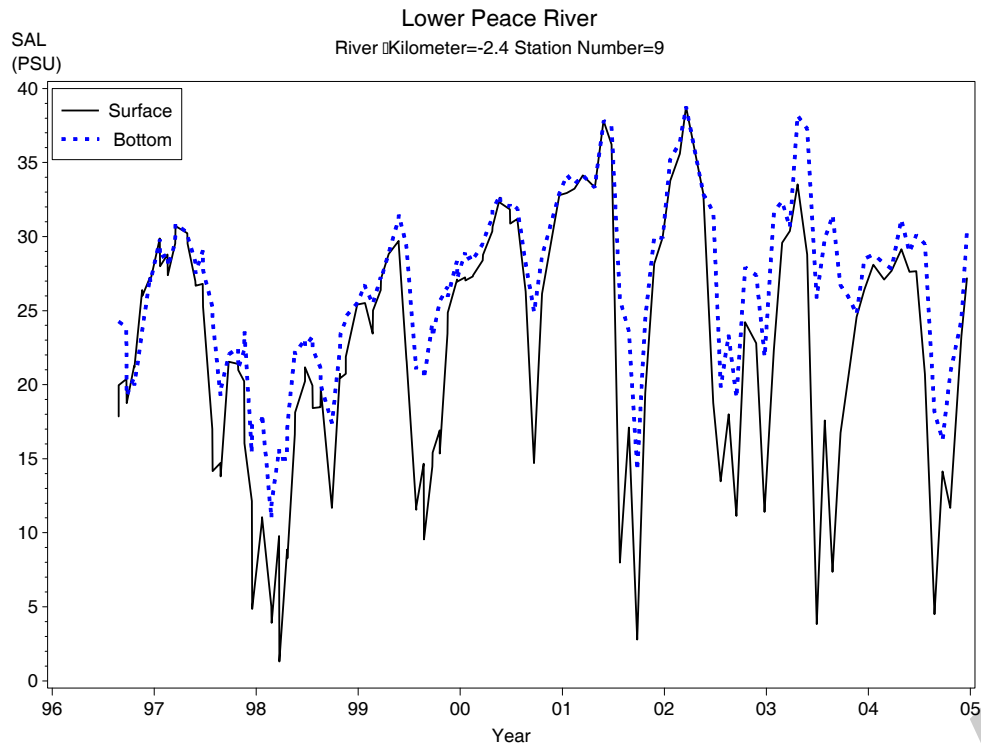


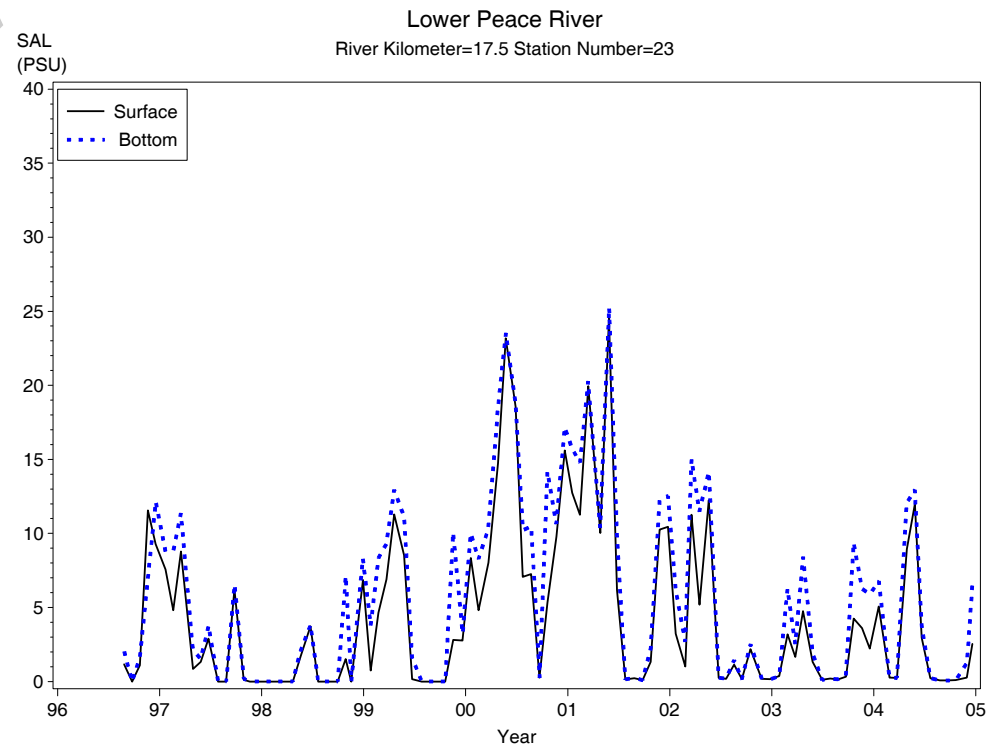
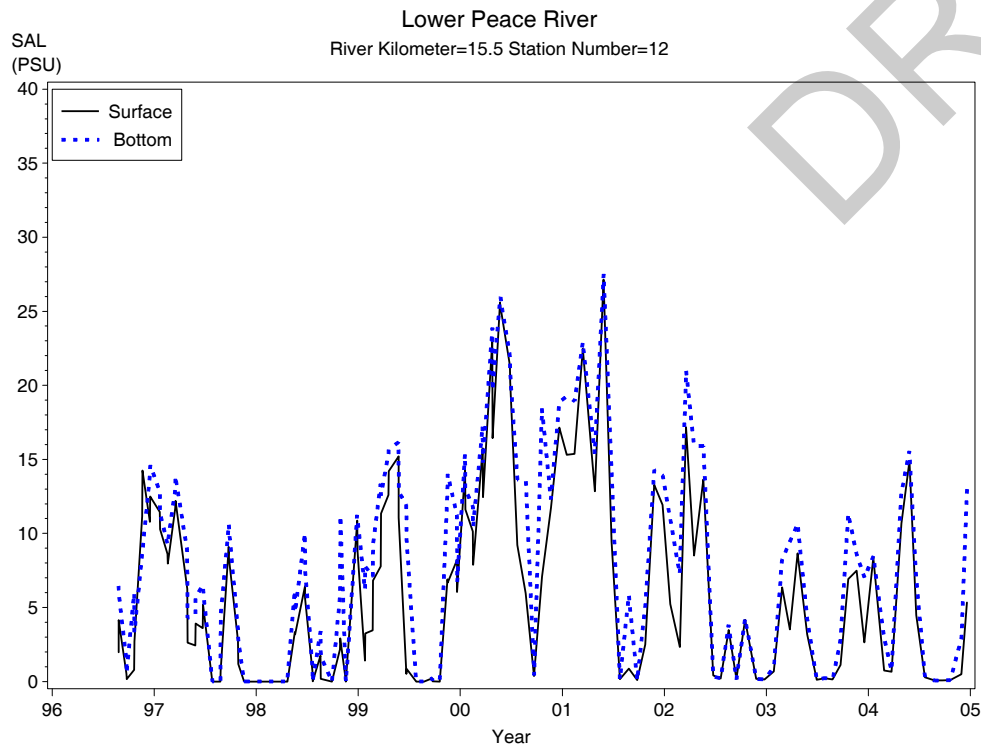
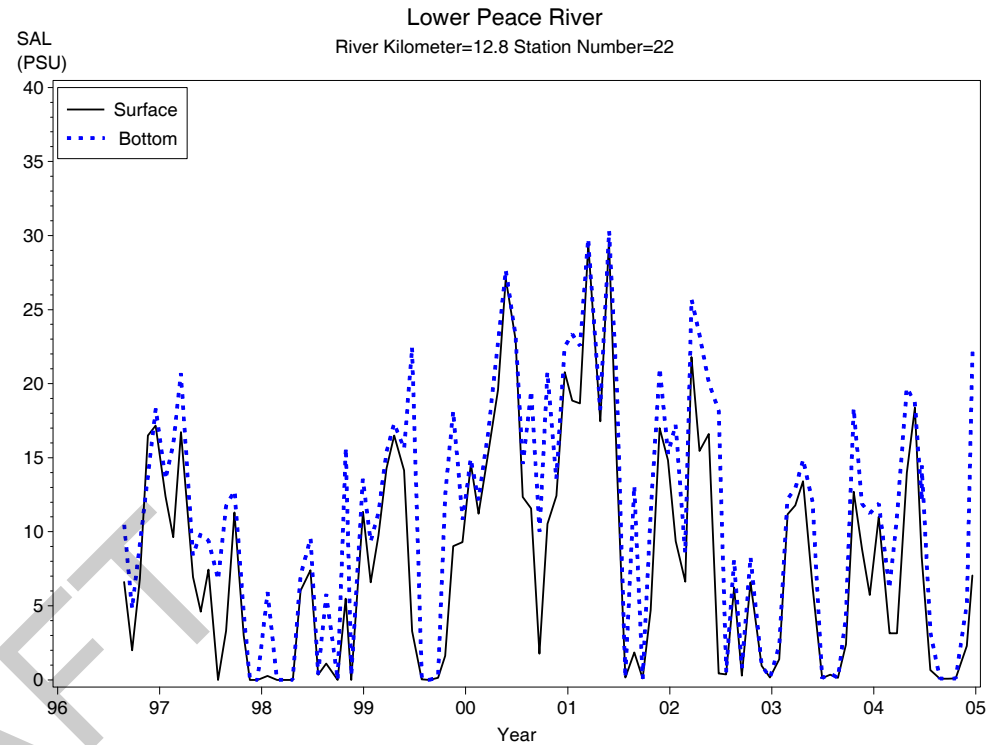
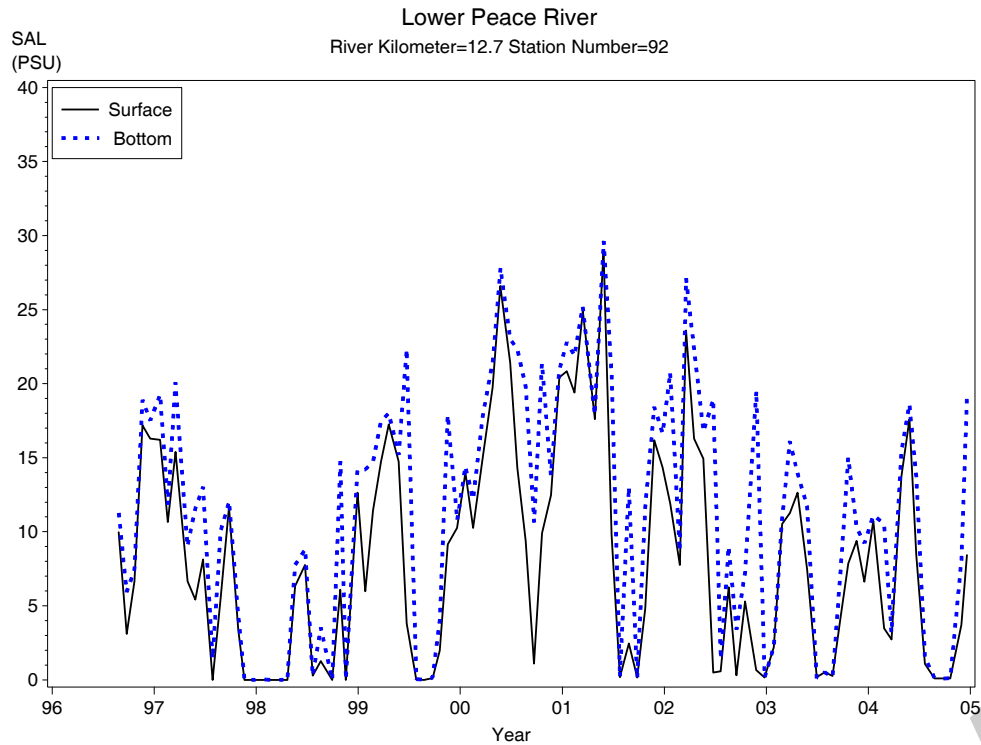


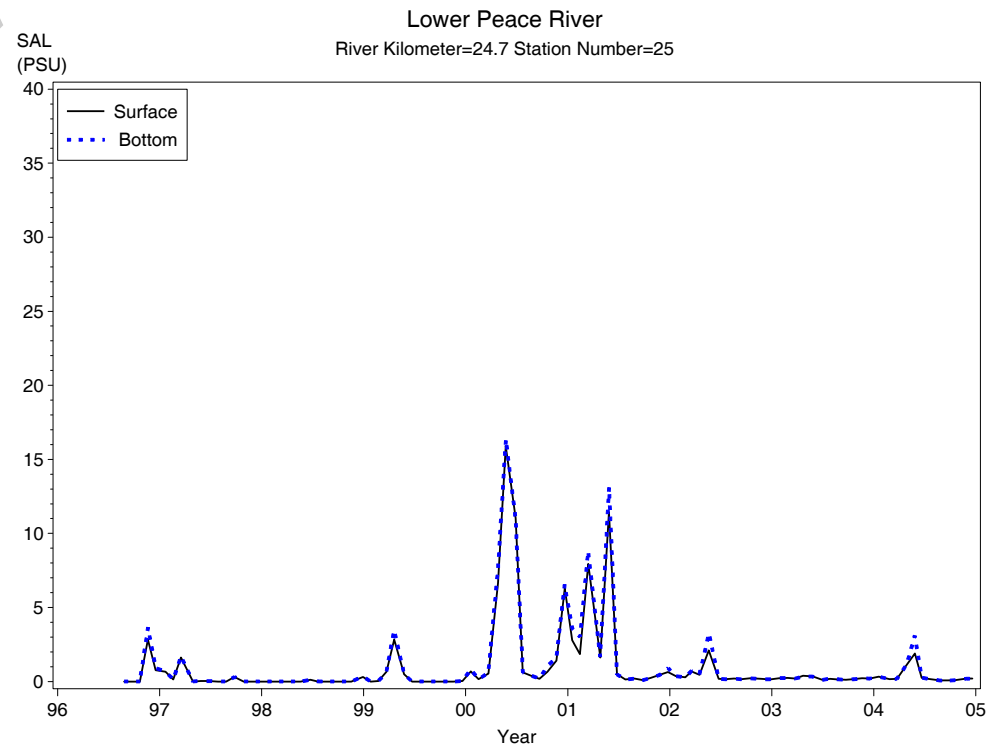
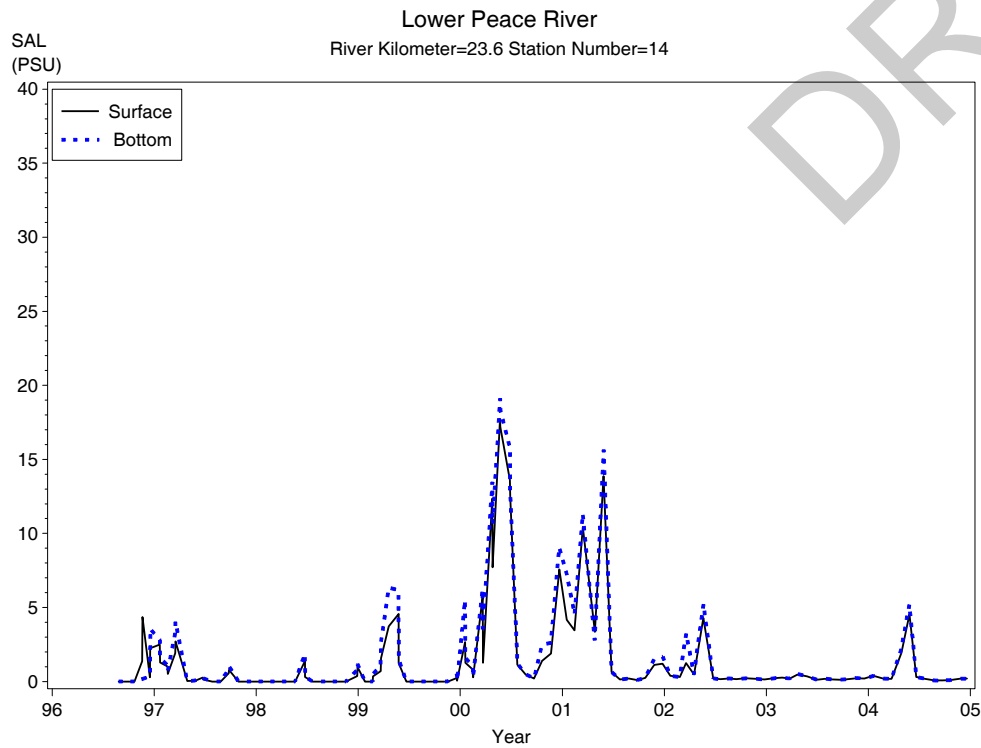
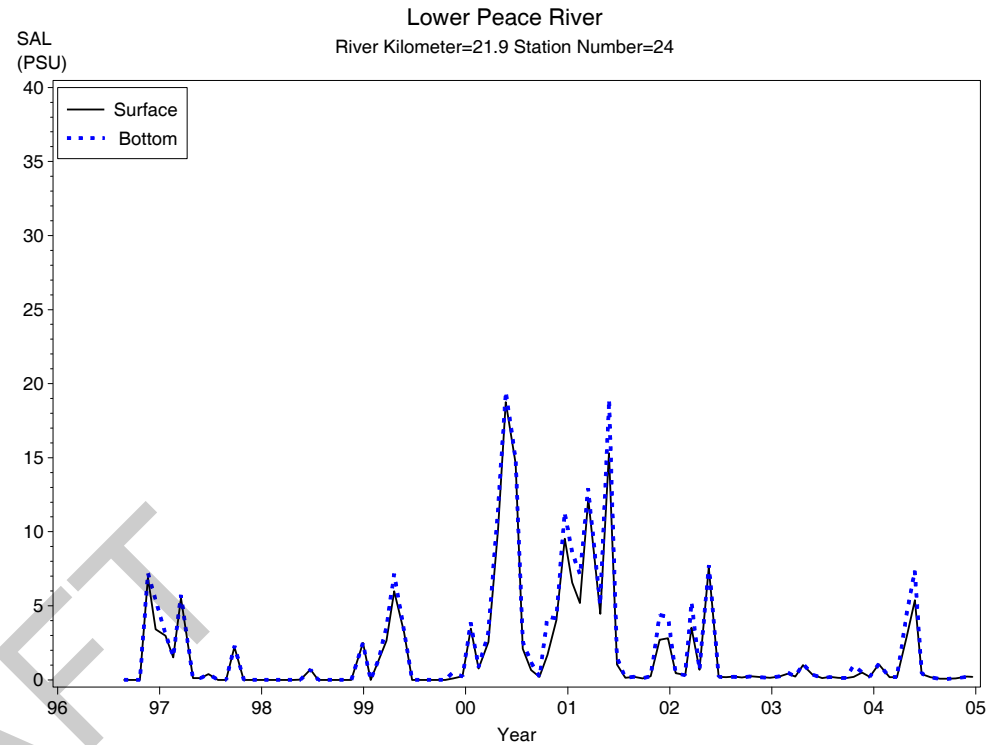
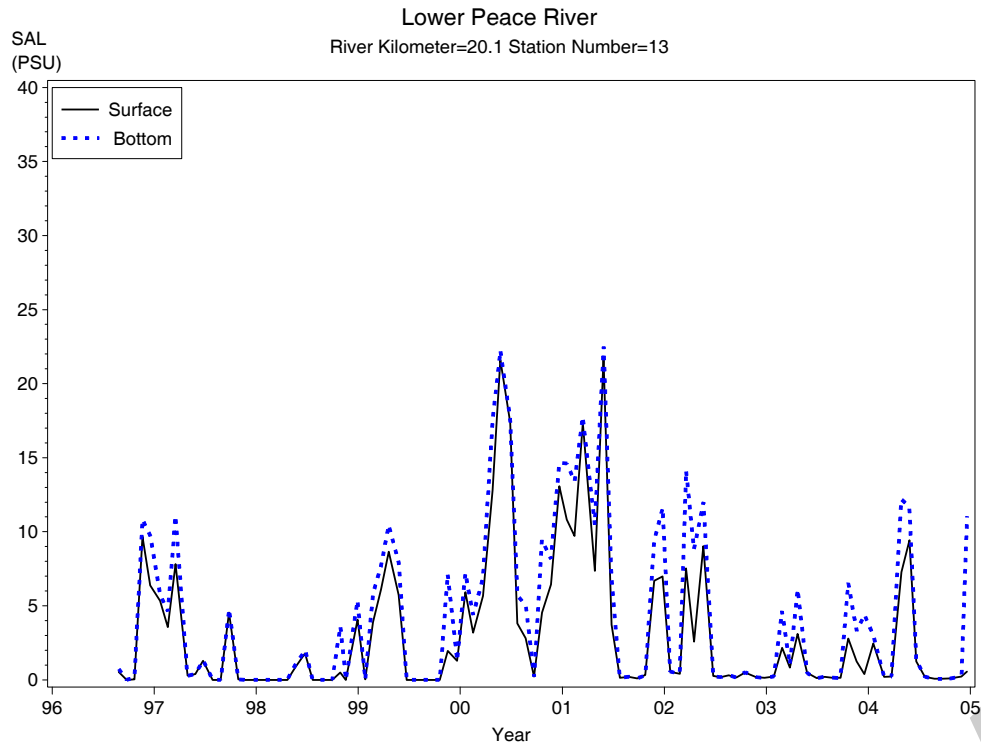
Appendix 3-1

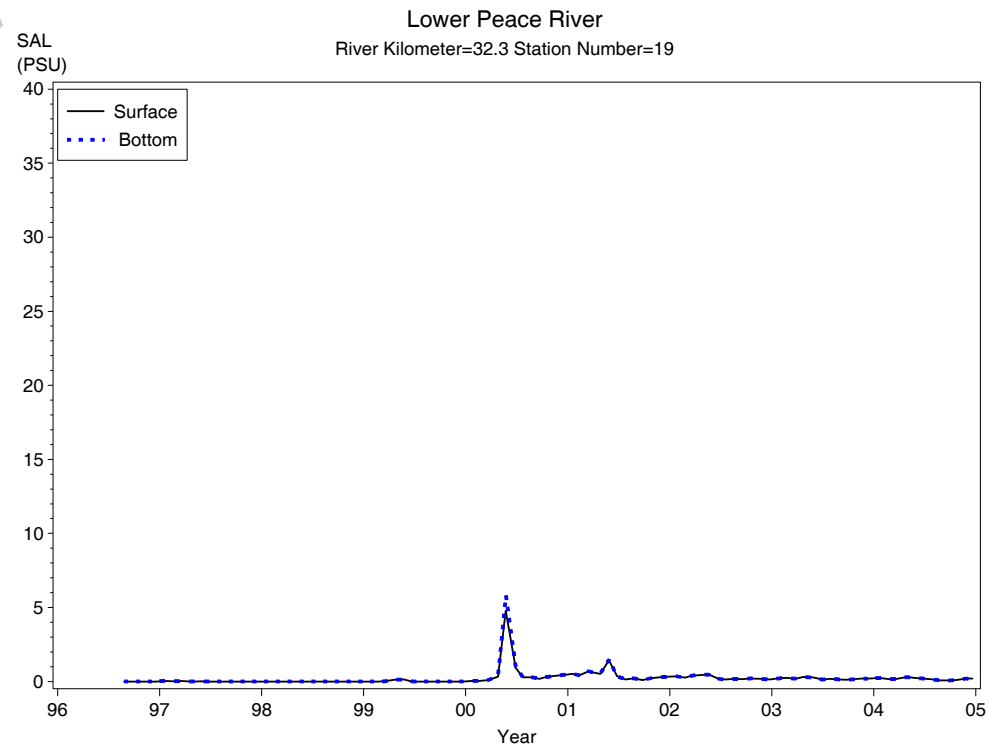
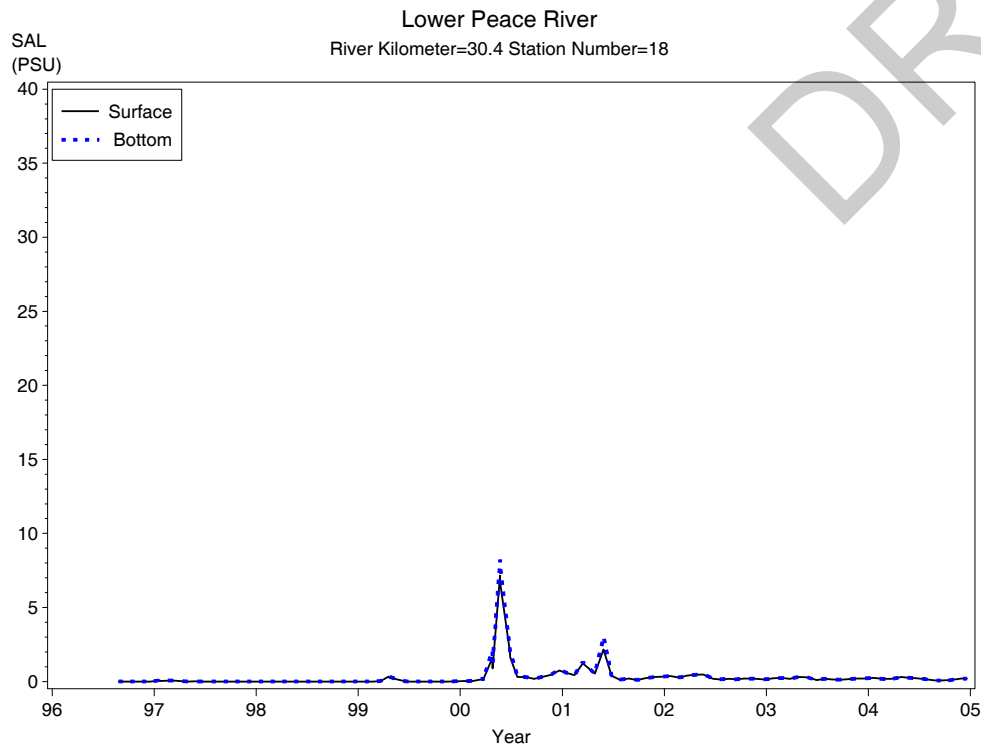
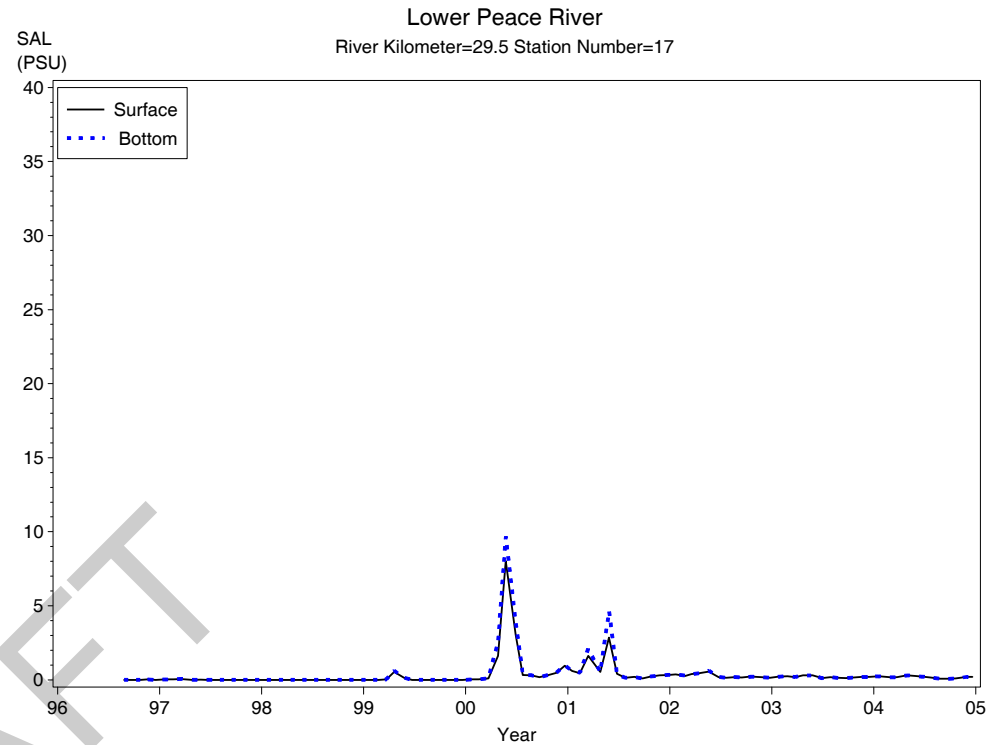
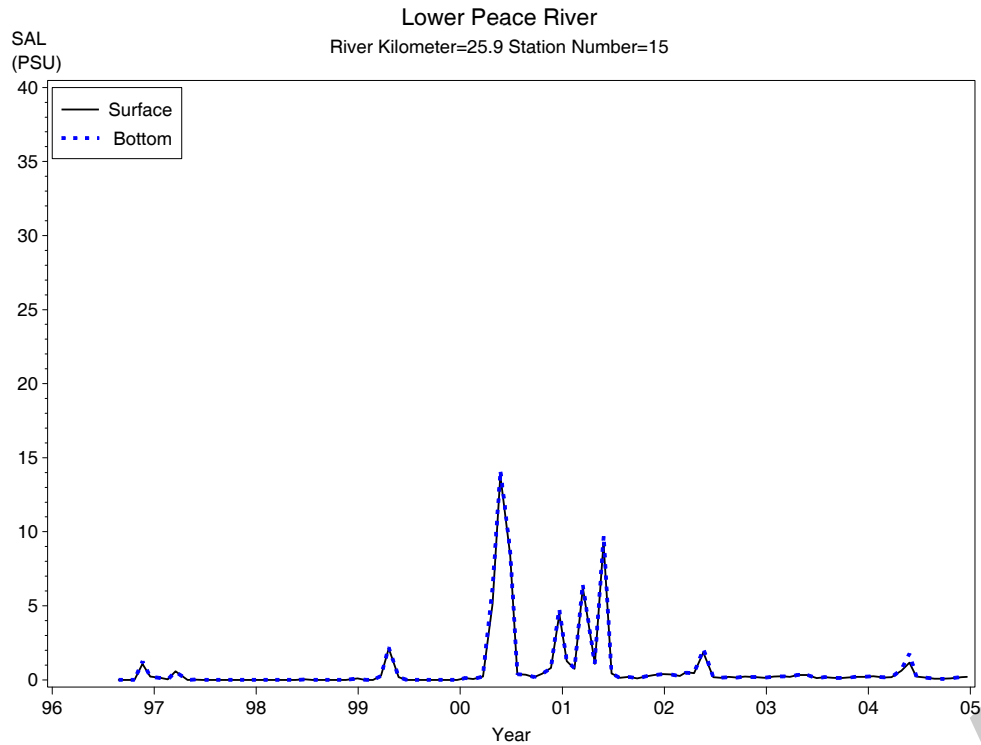
Annual Variation in Lower Peace River Water Quality Constituents

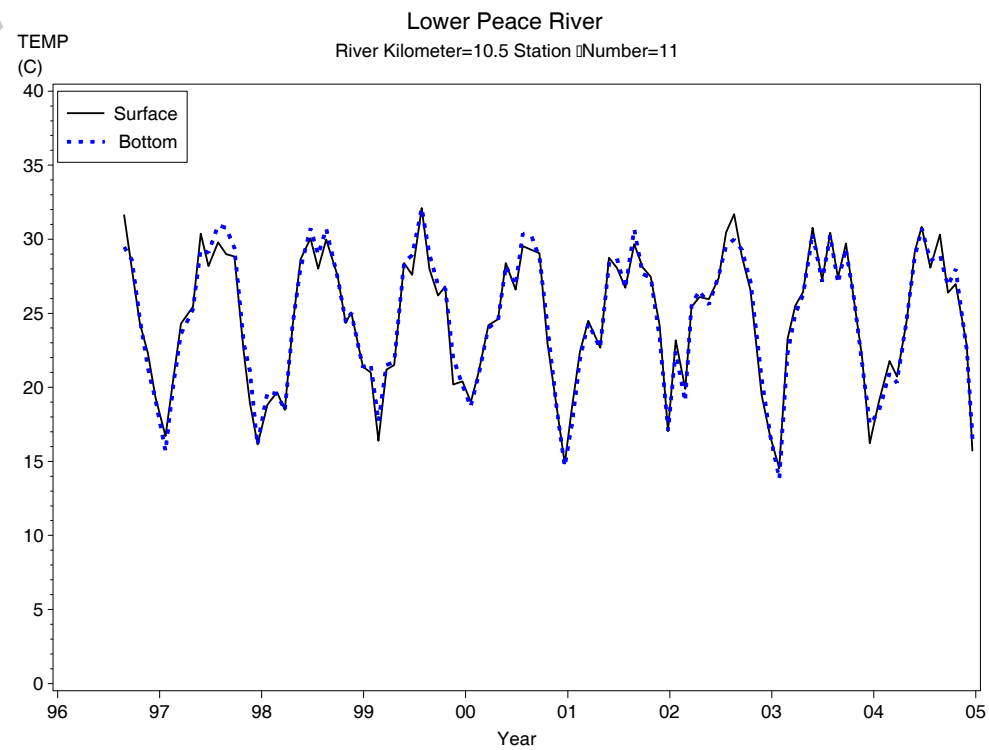
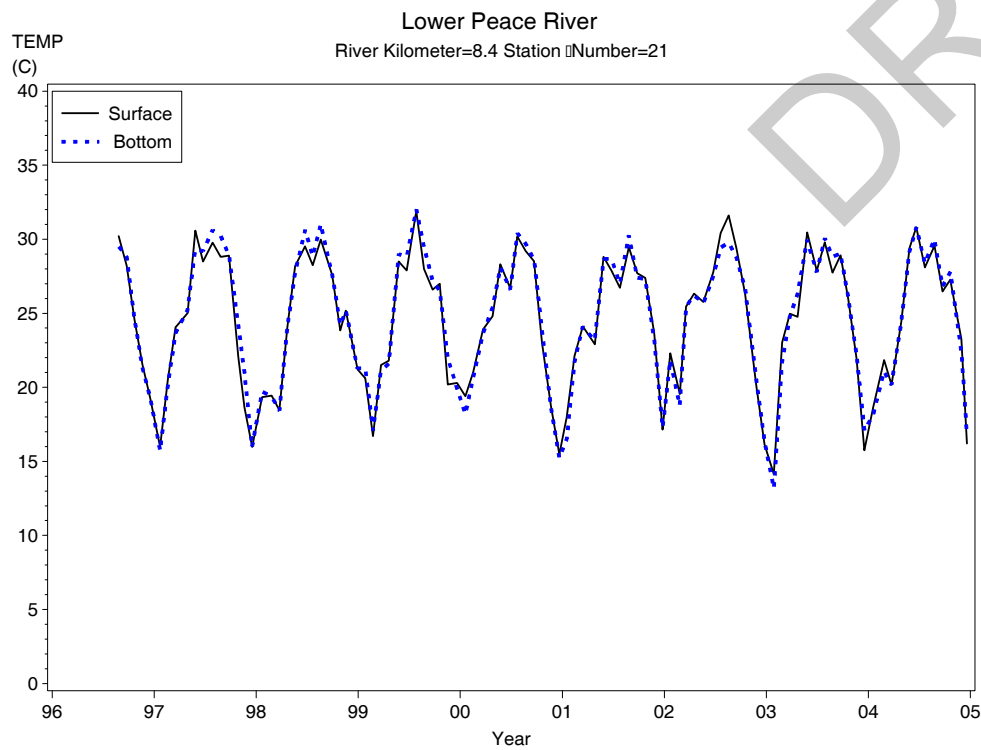
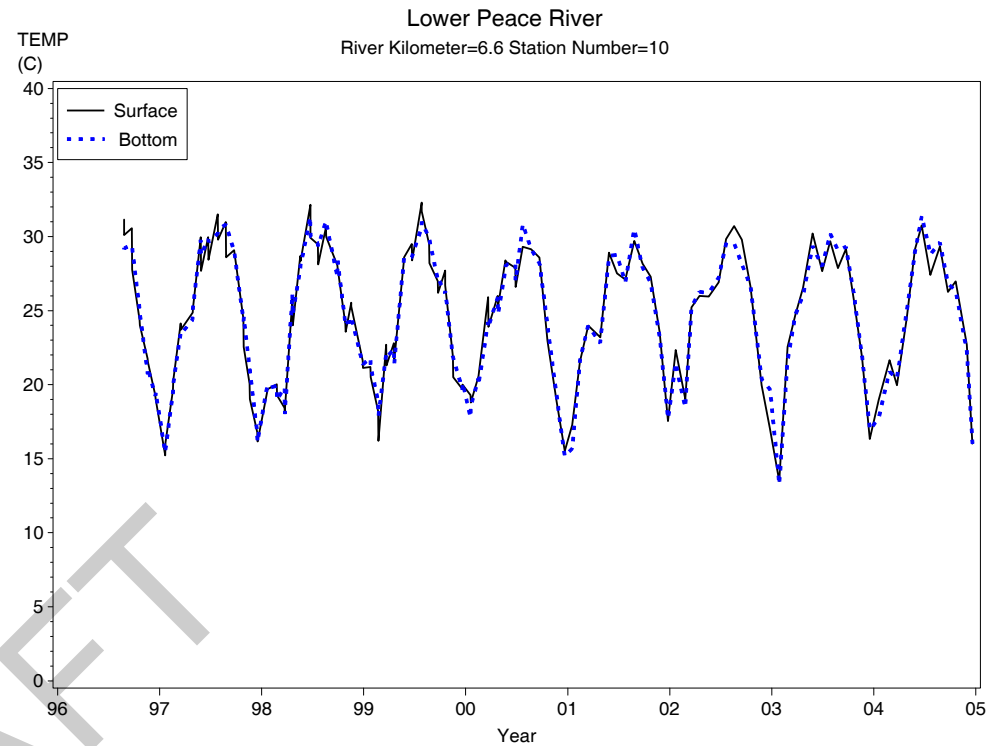
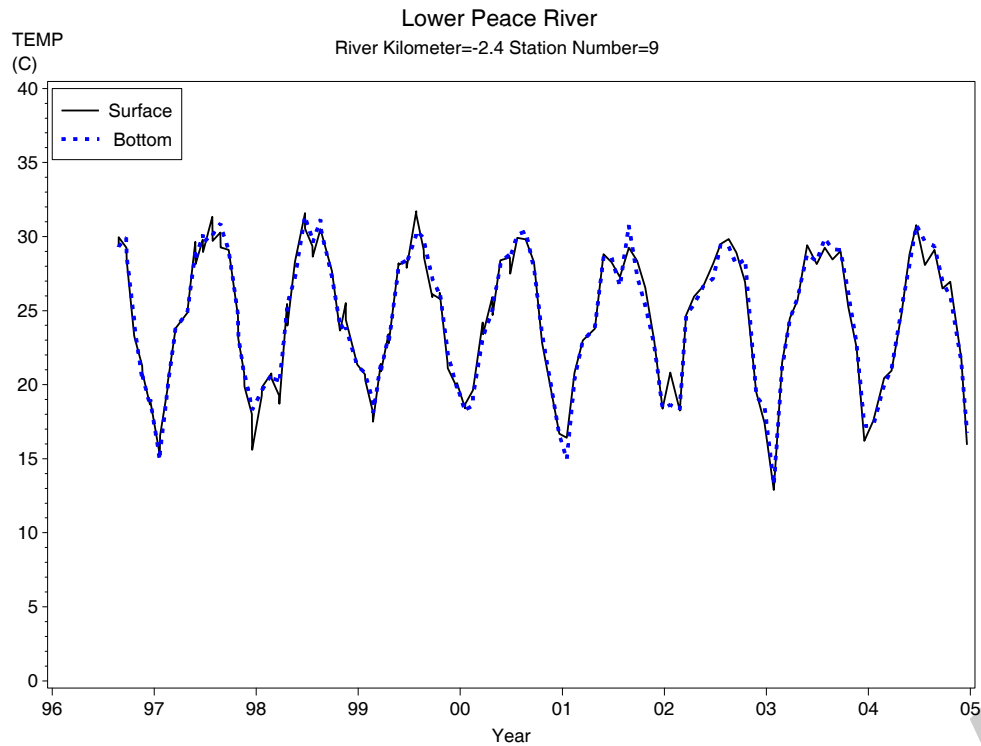


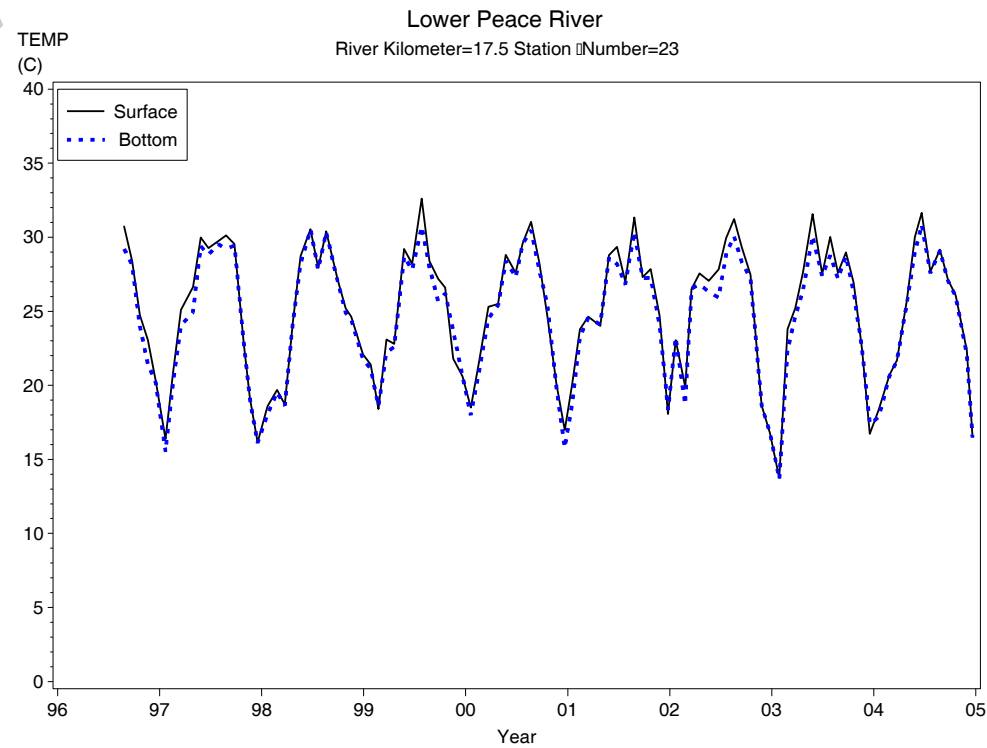
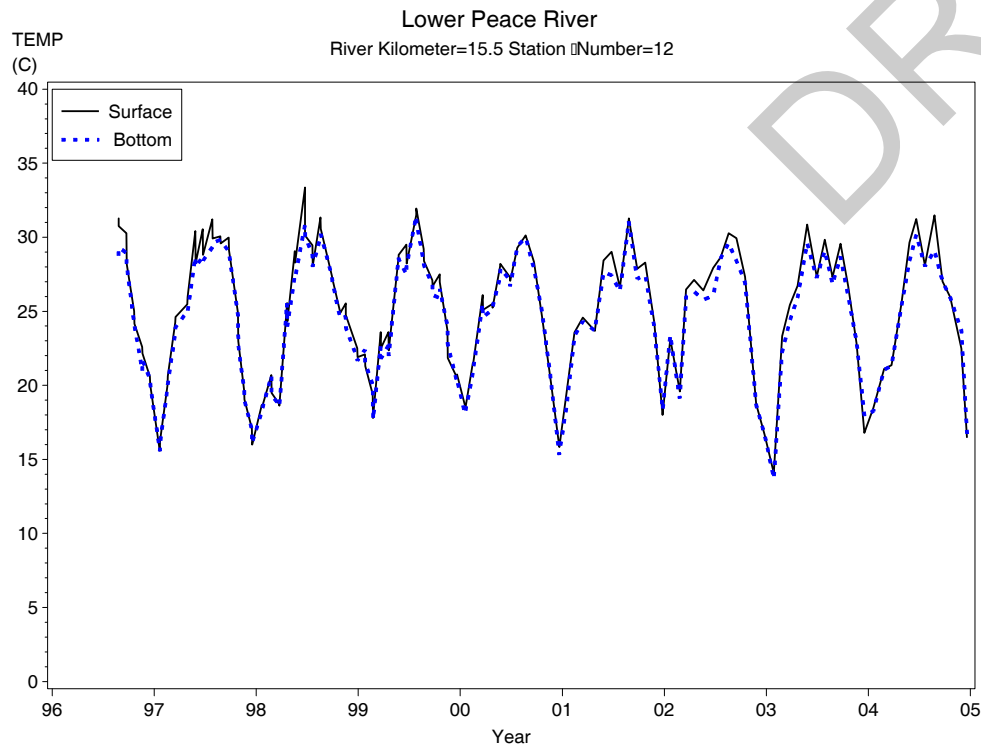
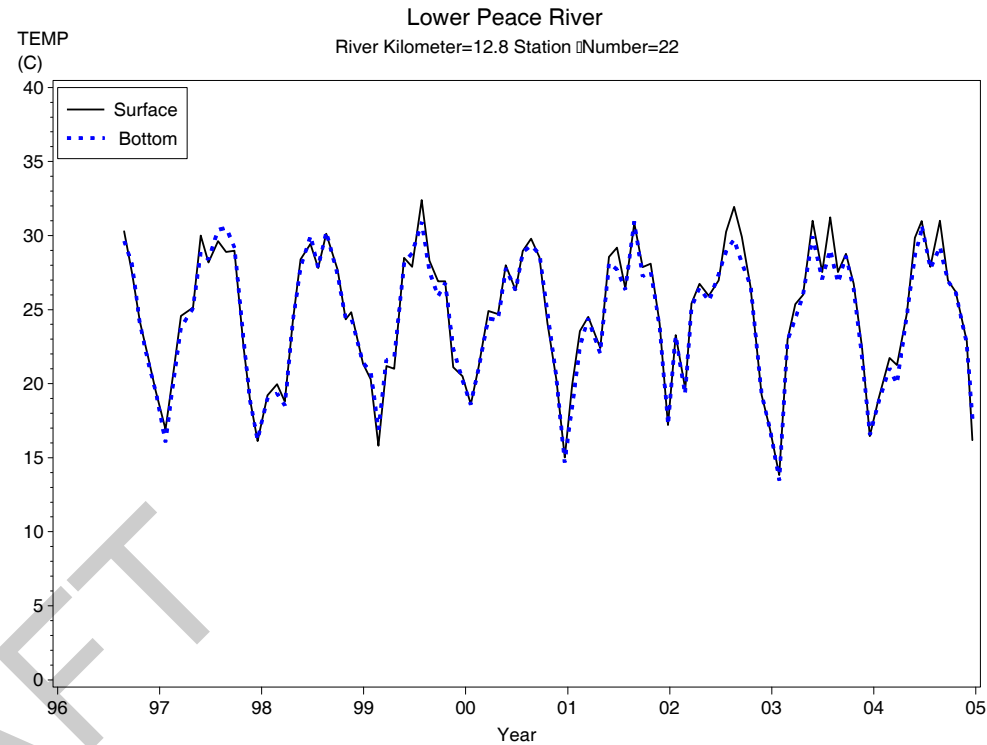
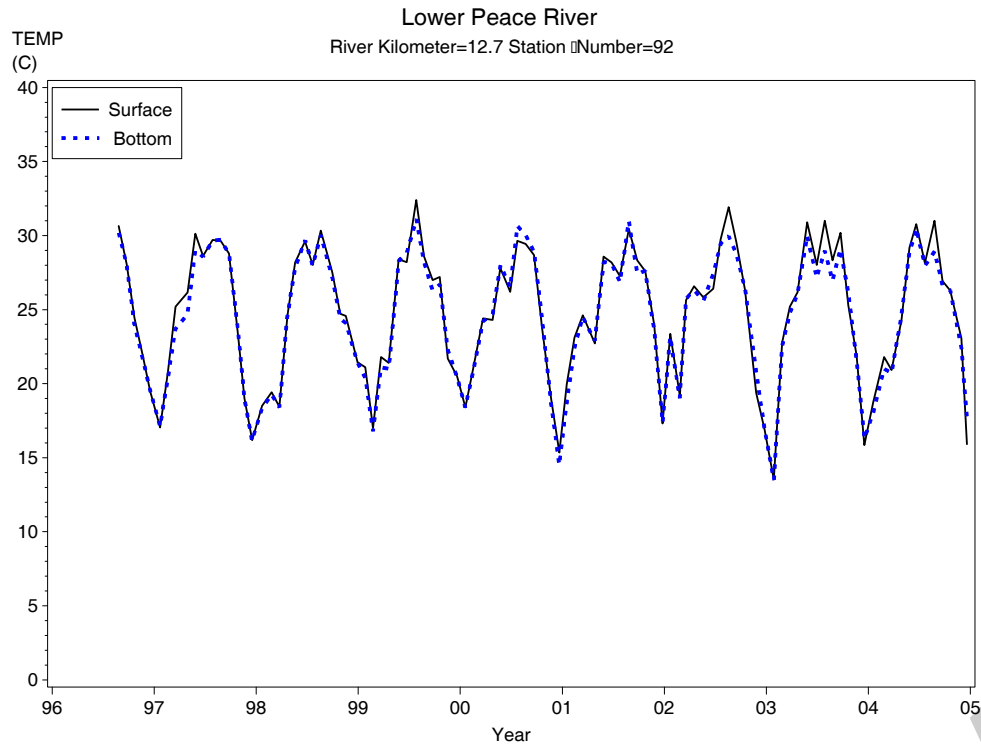


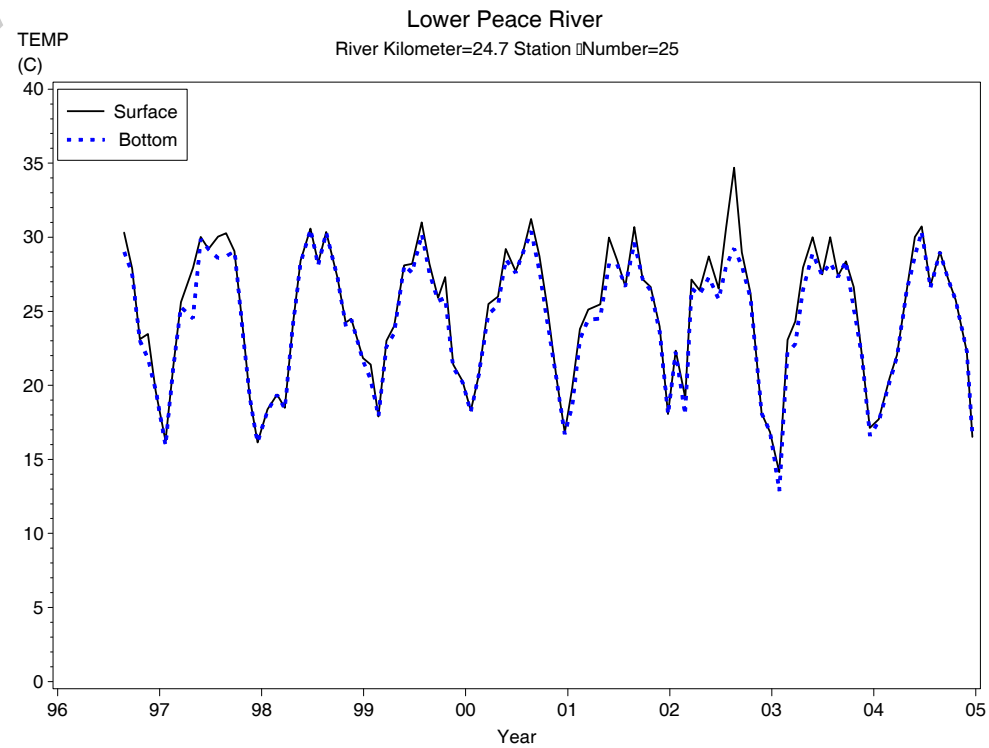
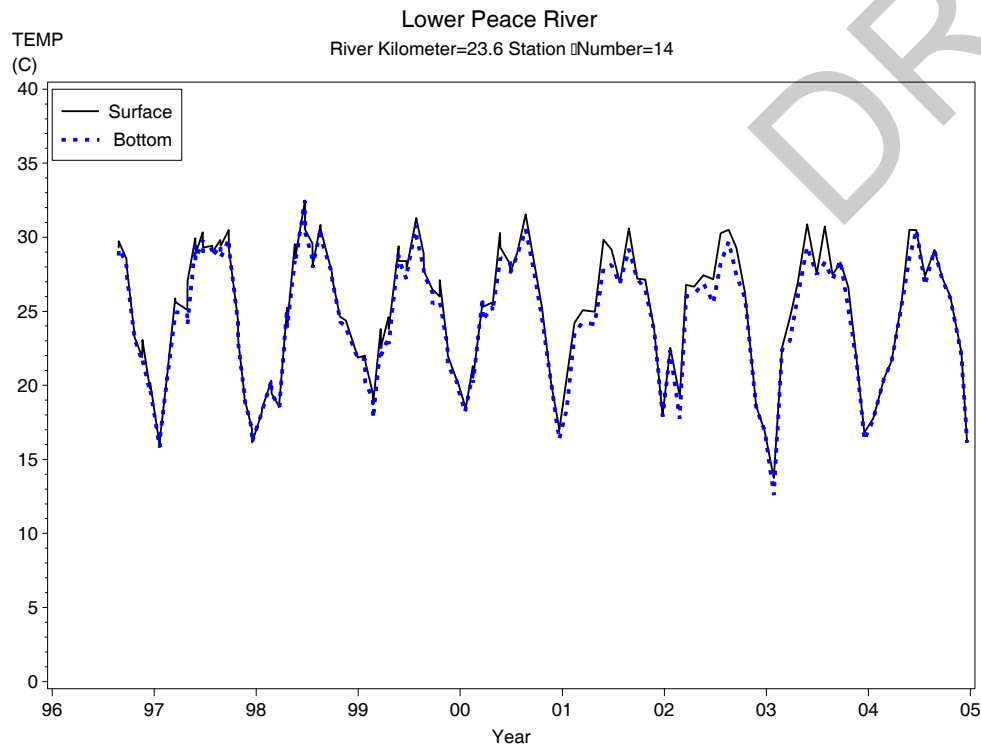
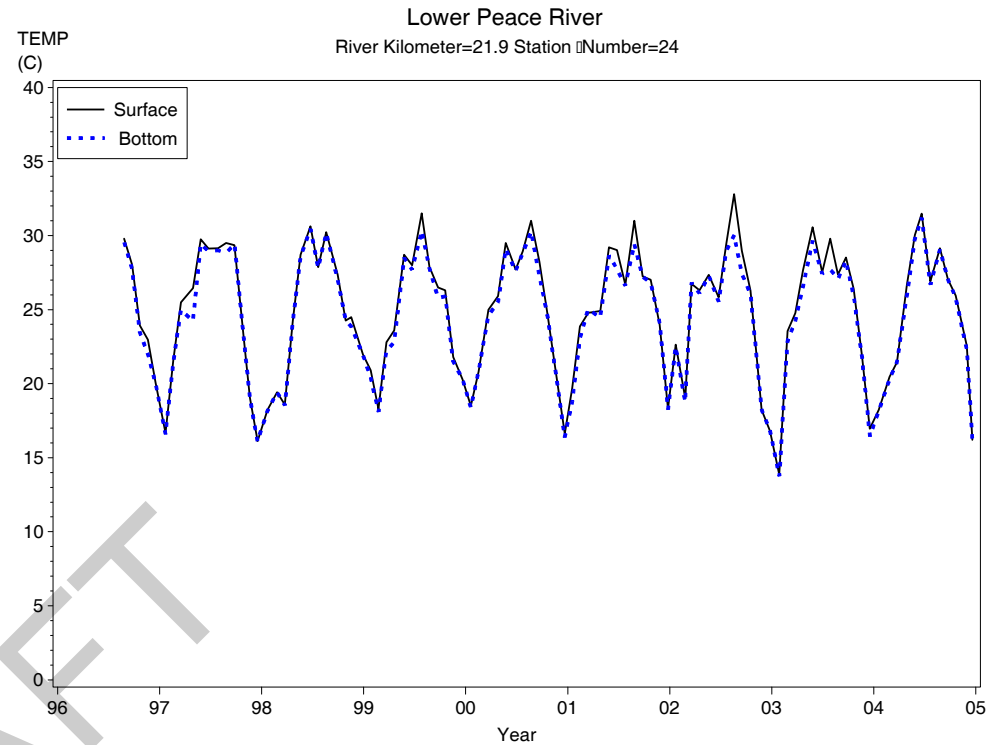
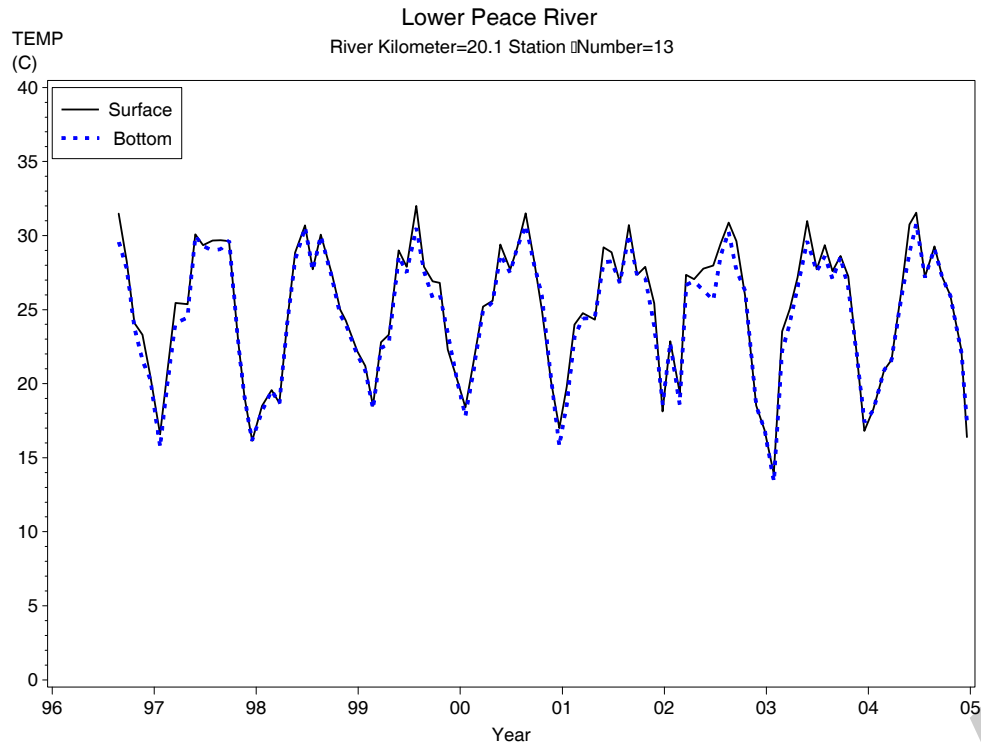


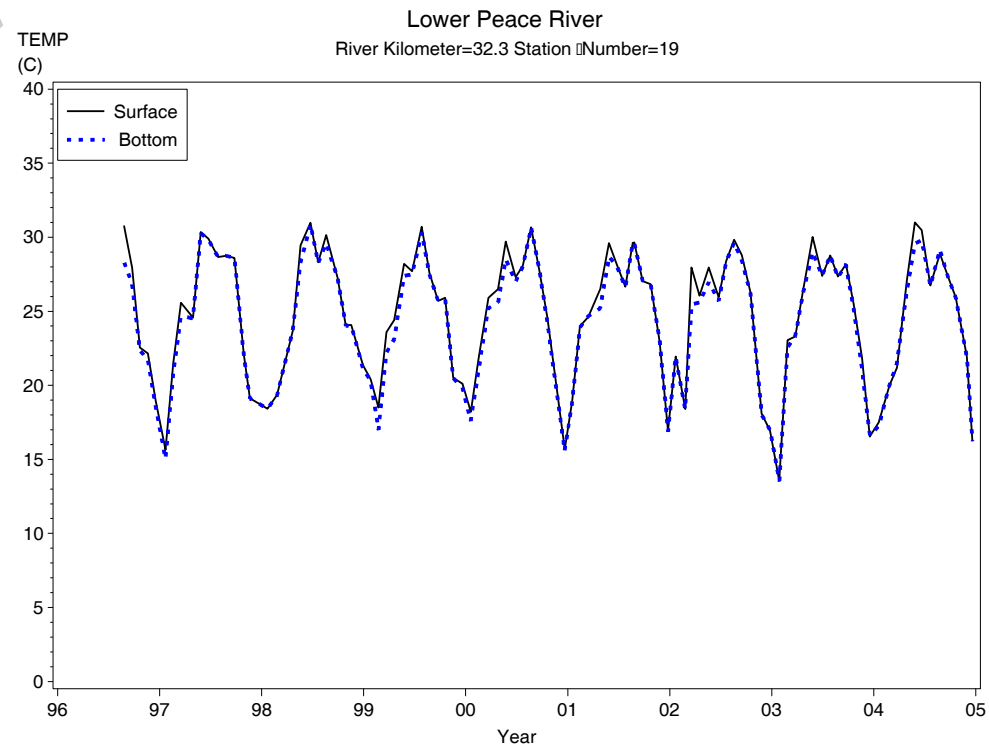
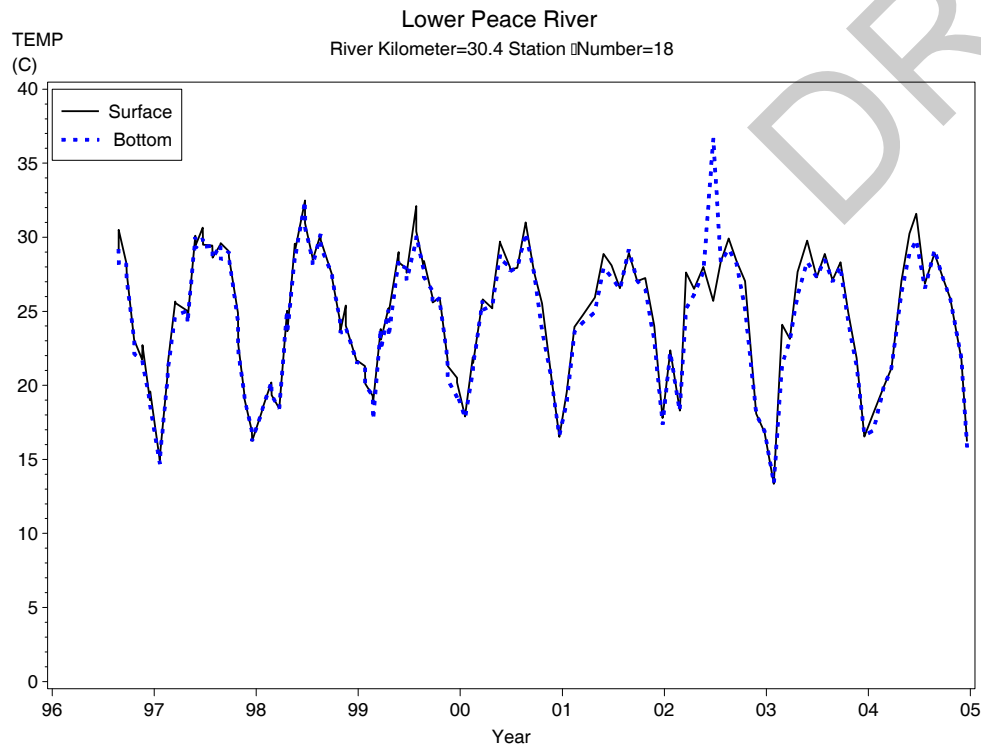
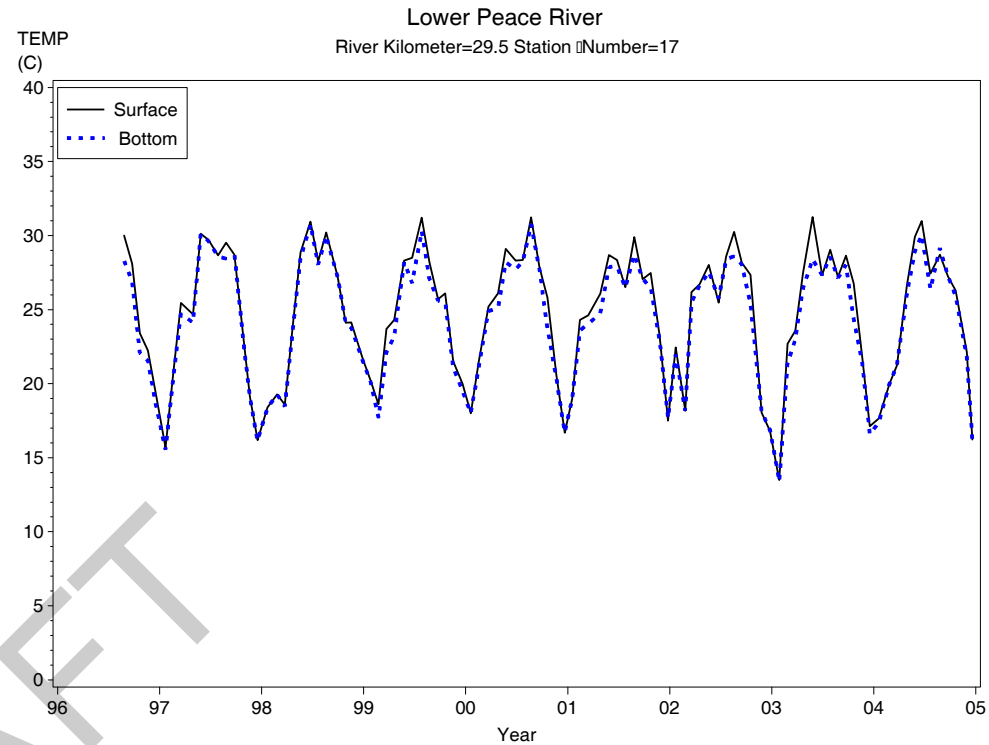
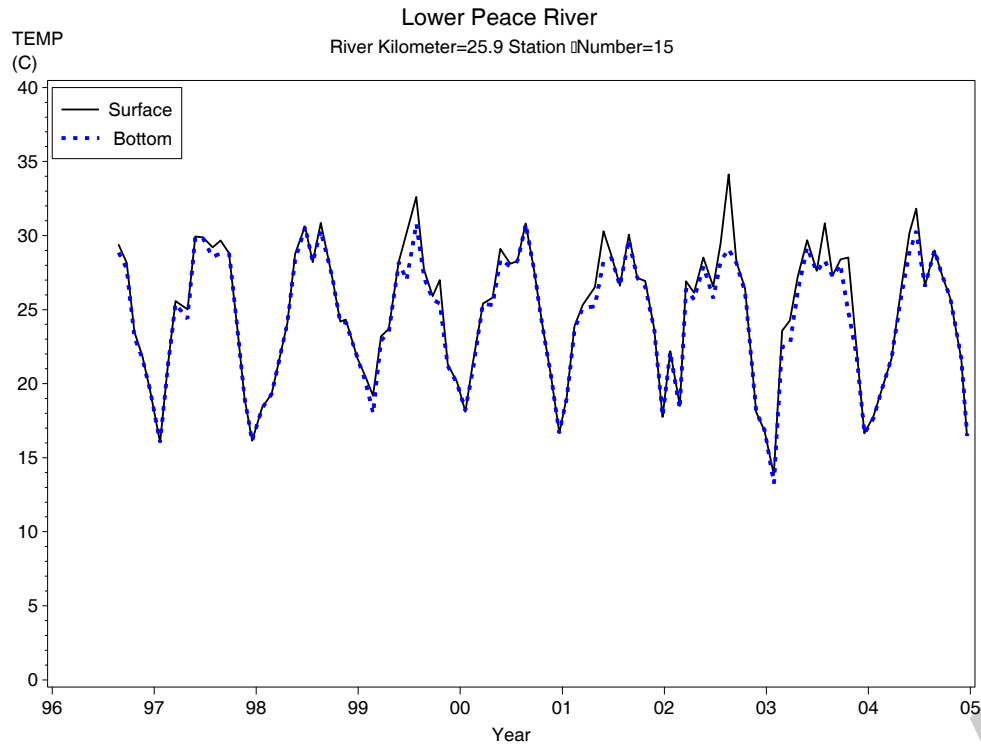


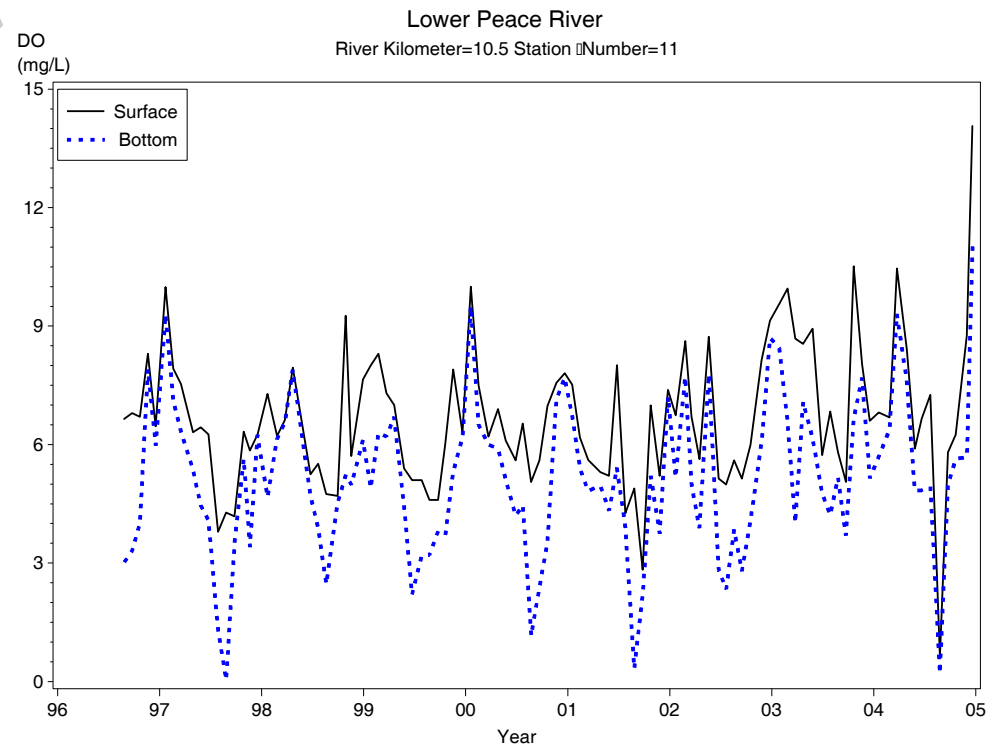
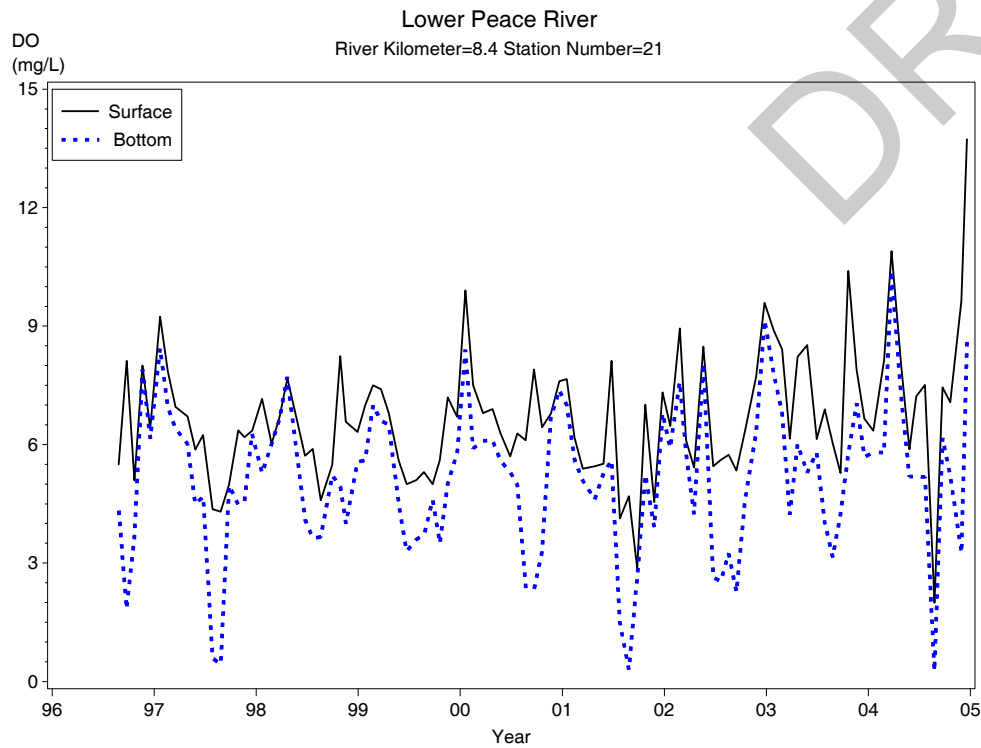
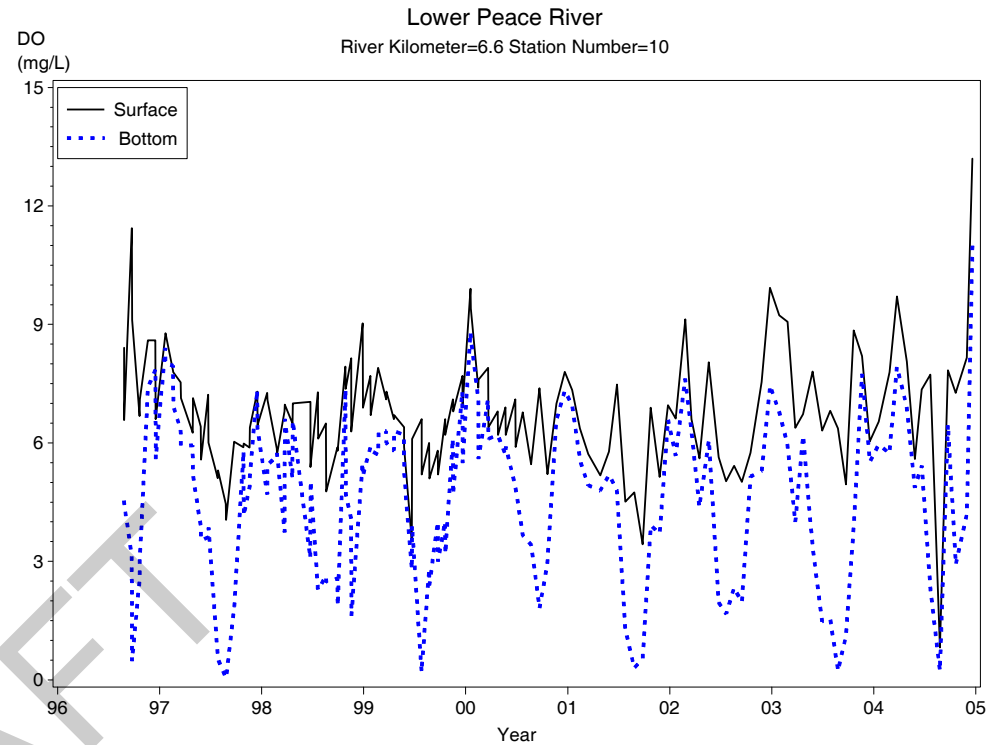
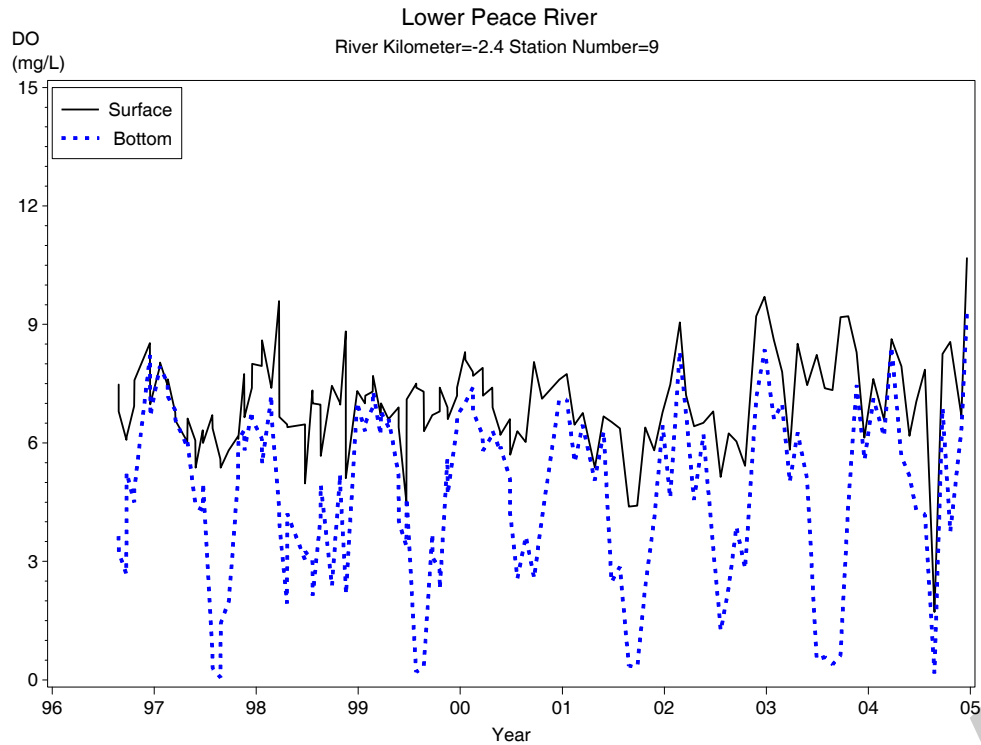


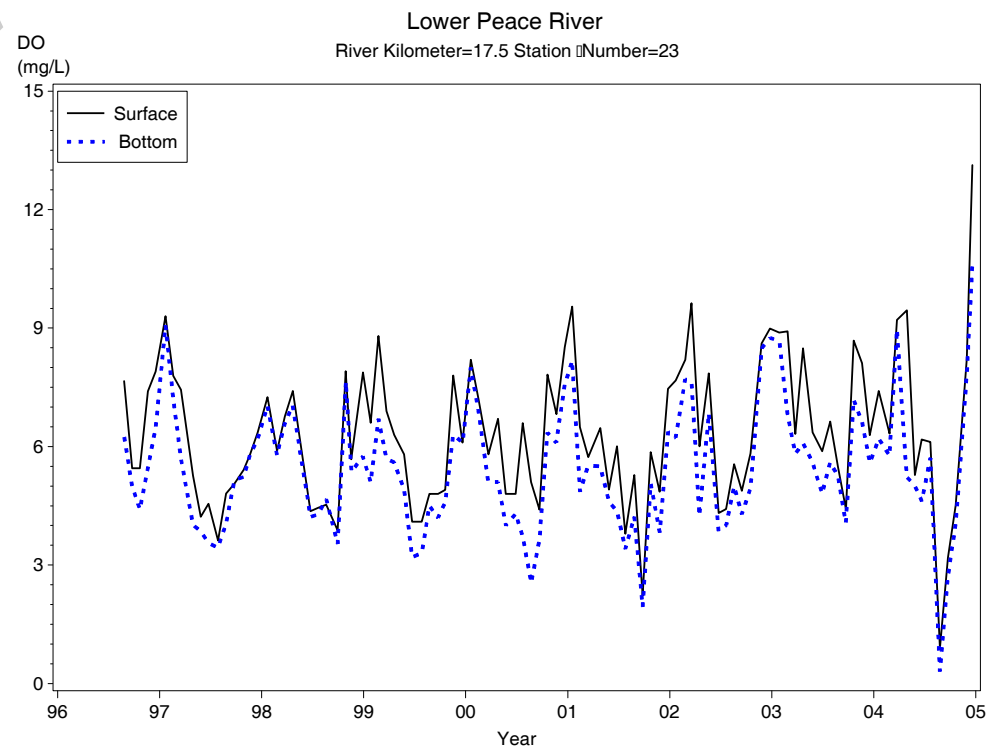
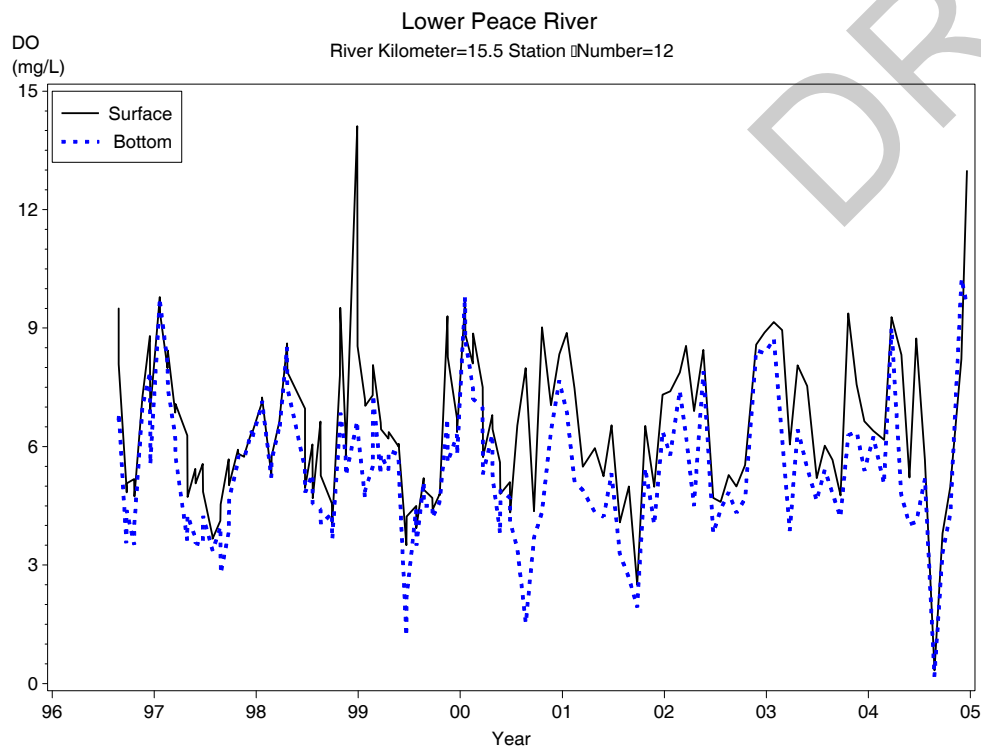
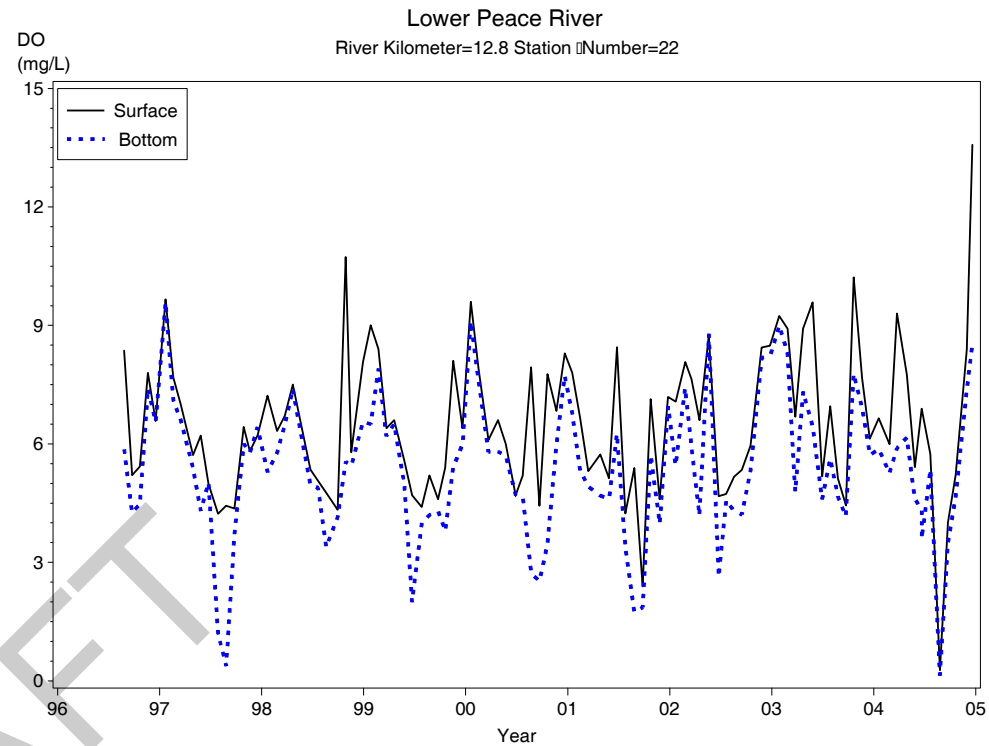
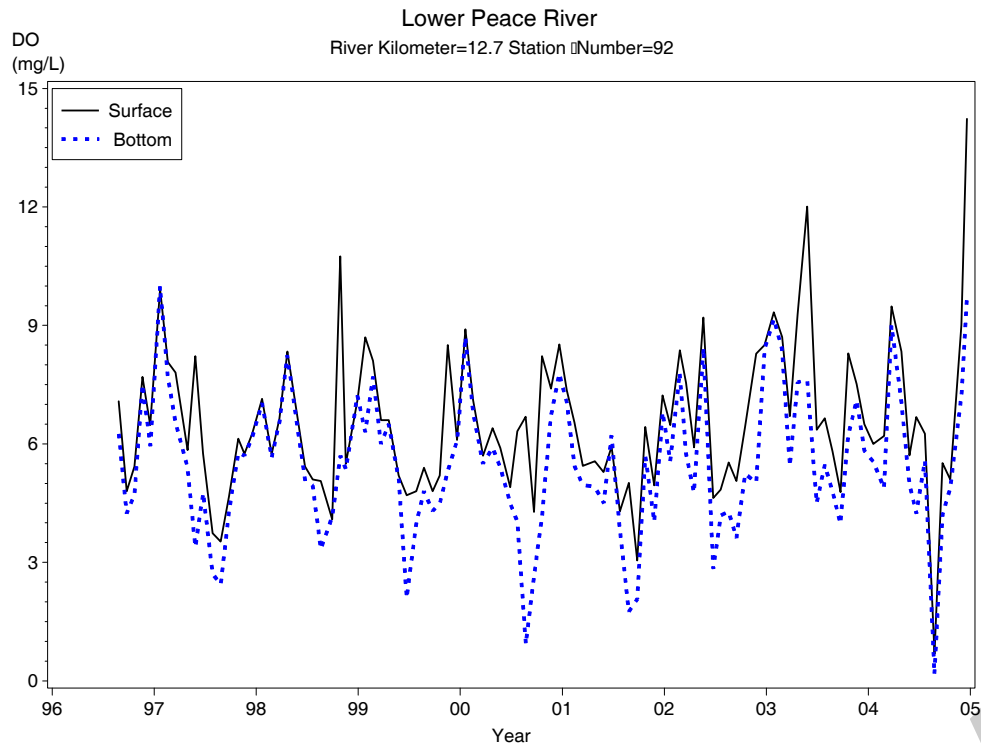


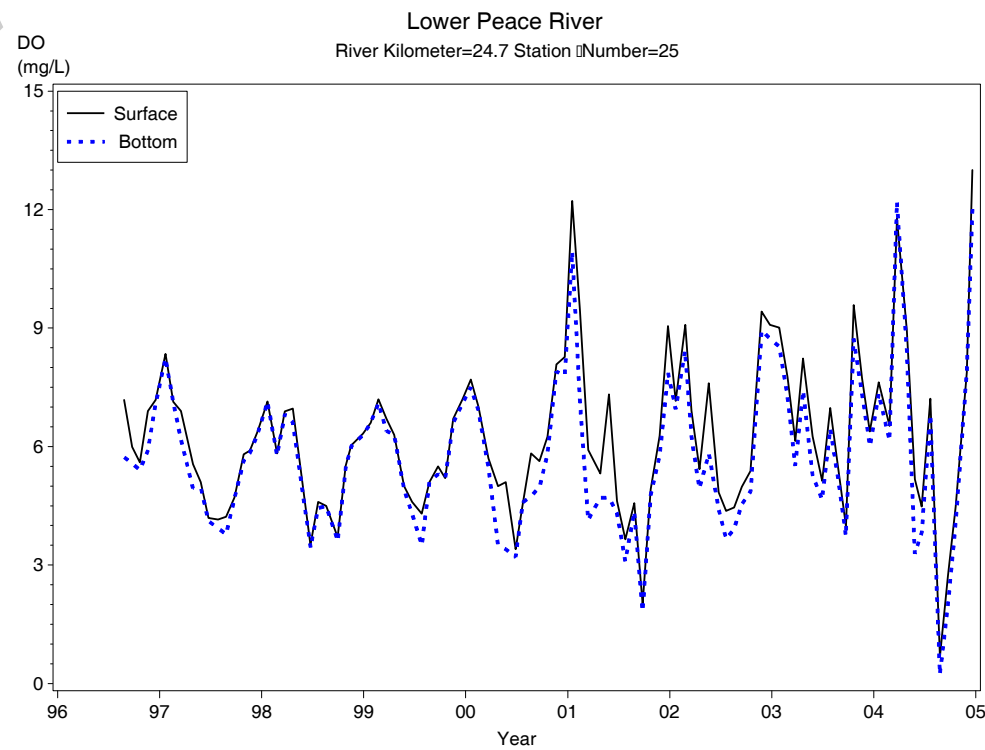
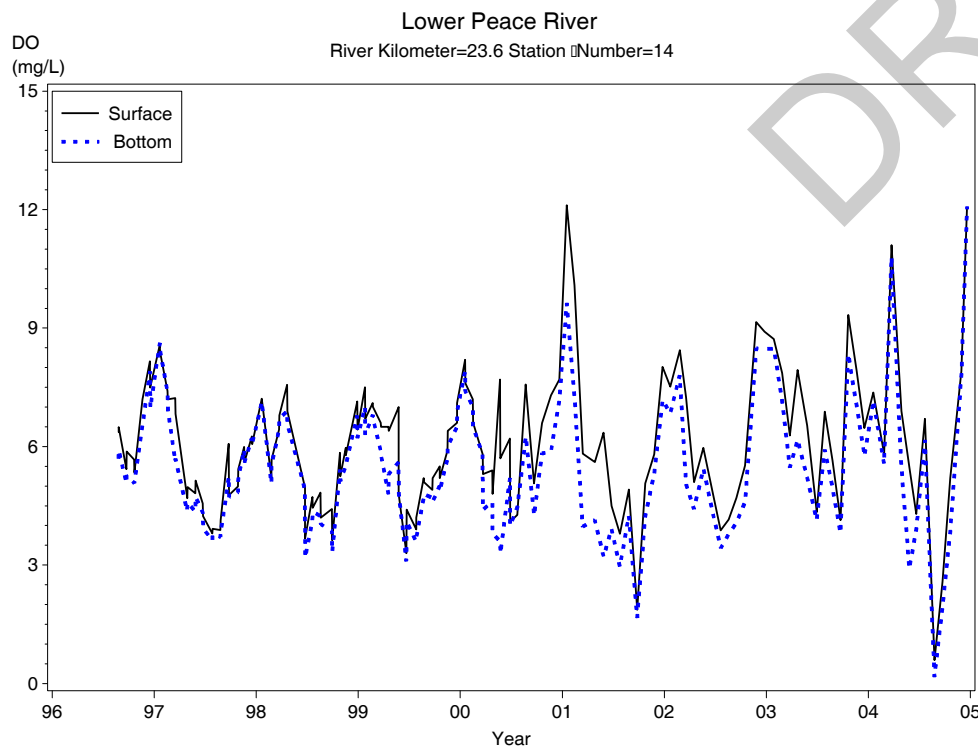
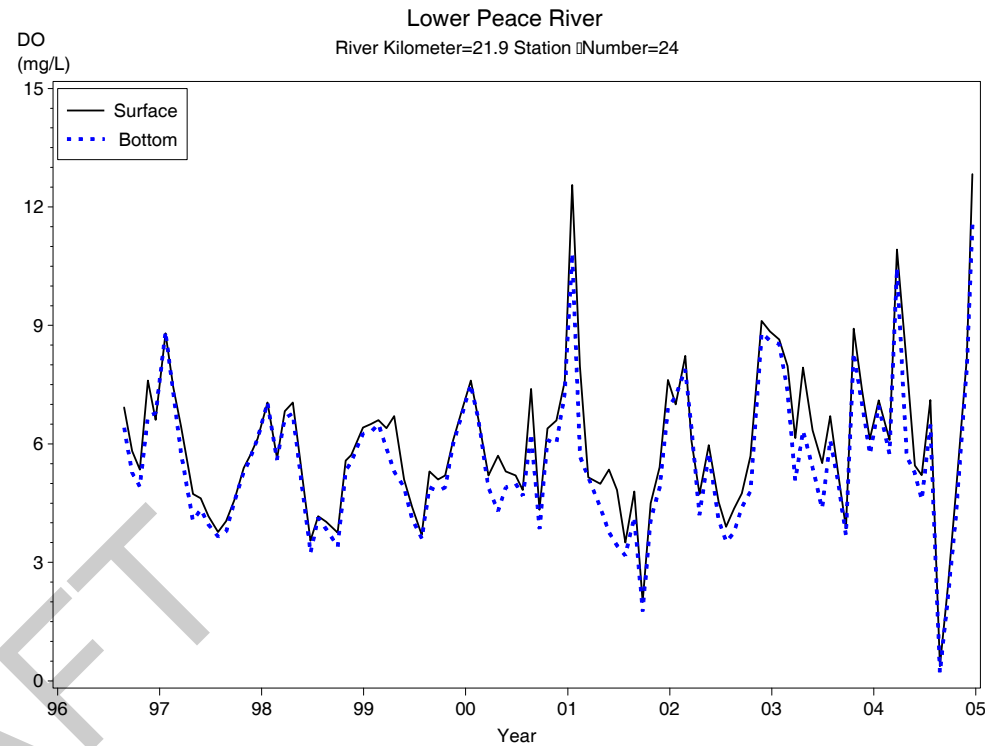
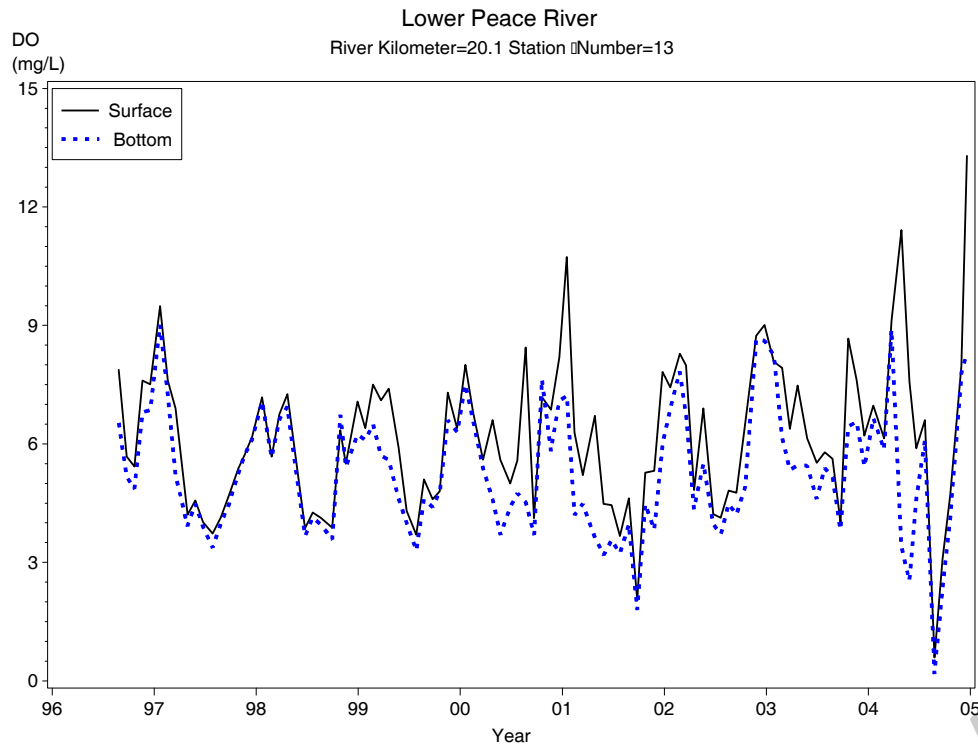


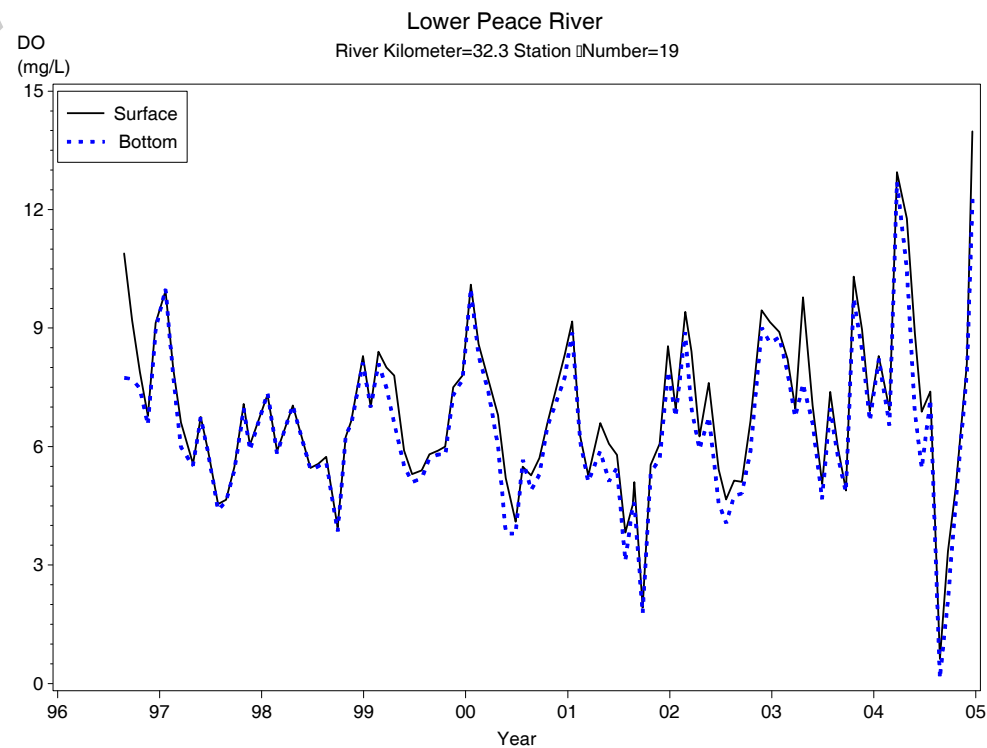
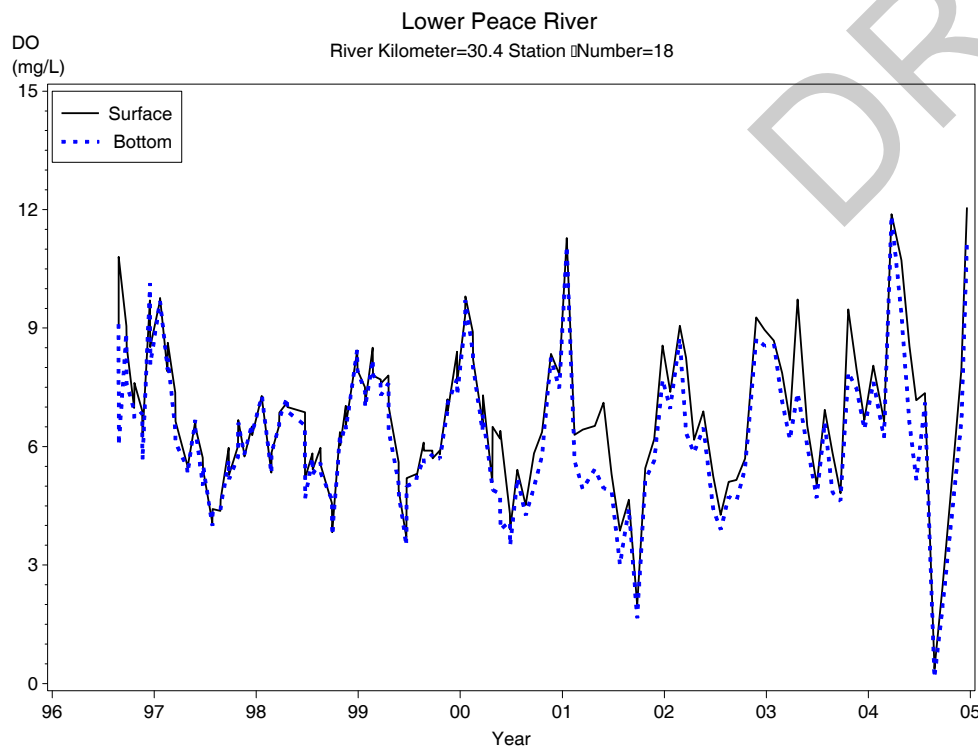
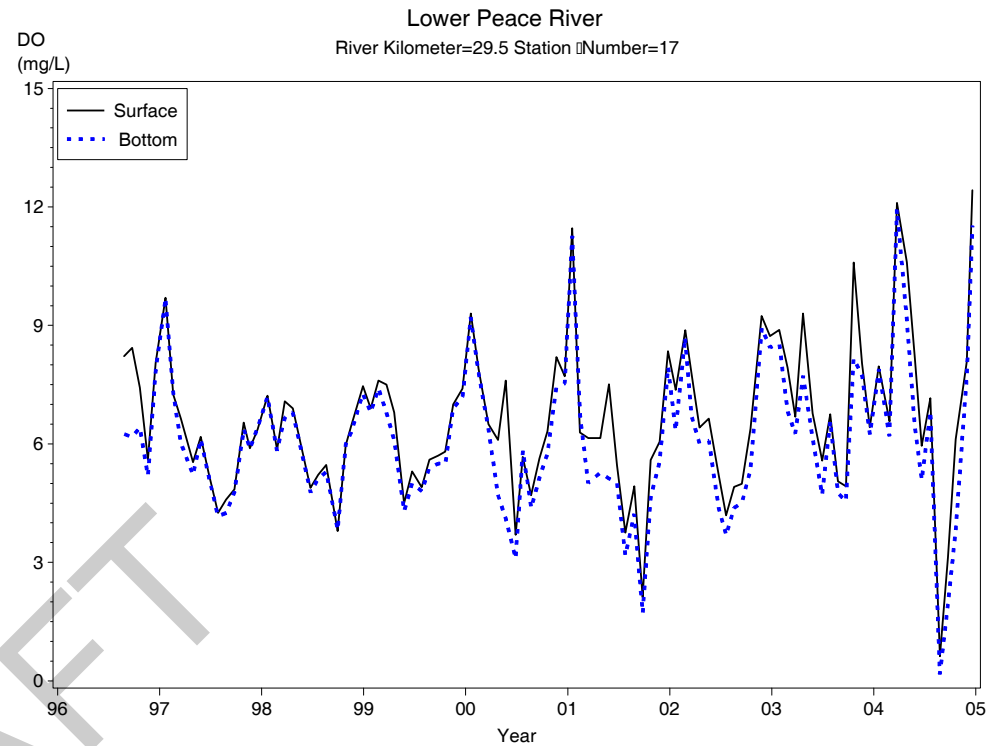
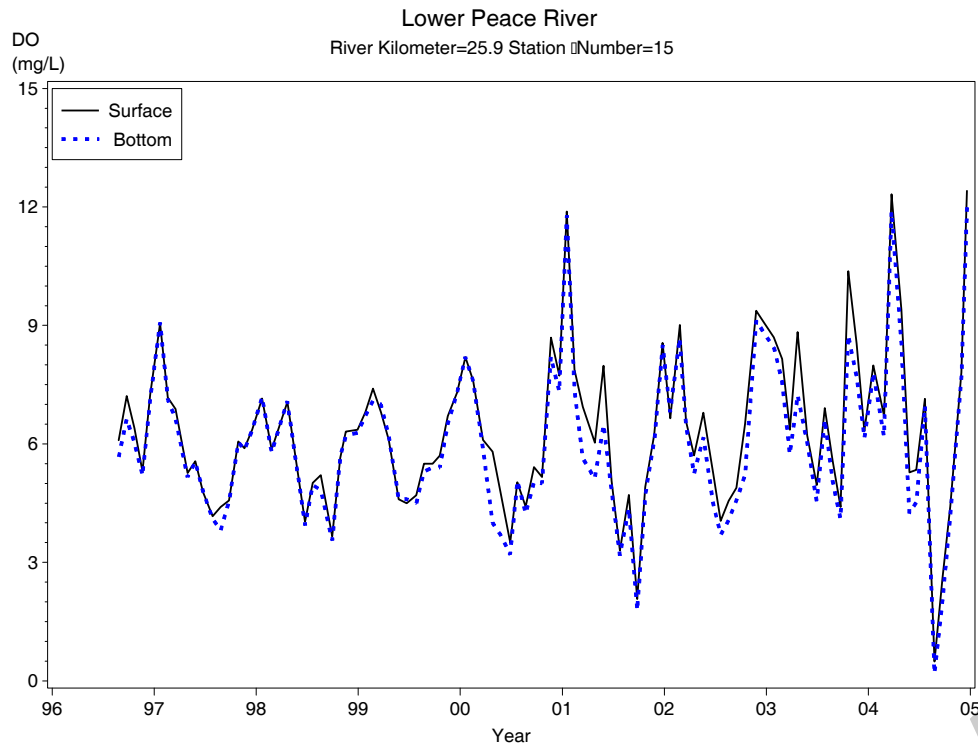


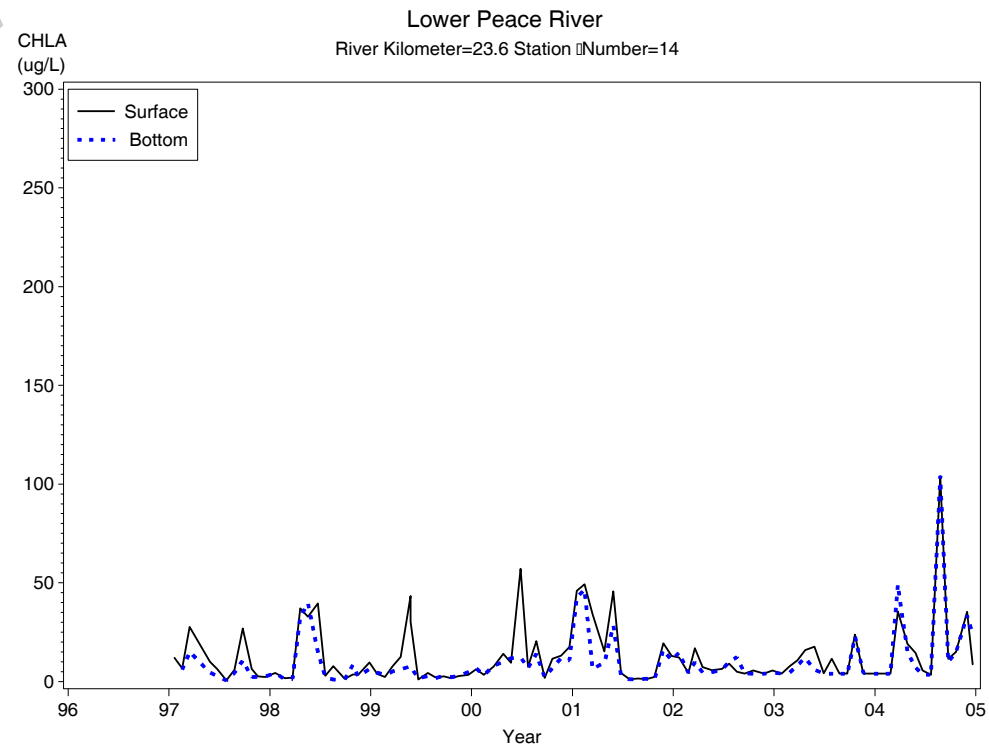
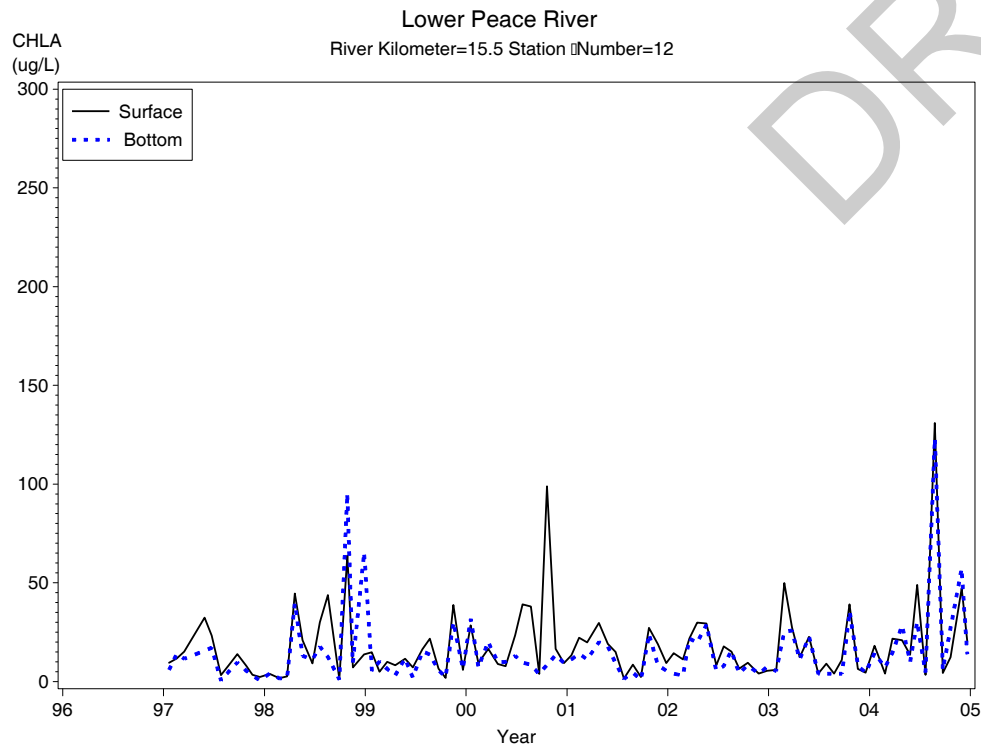
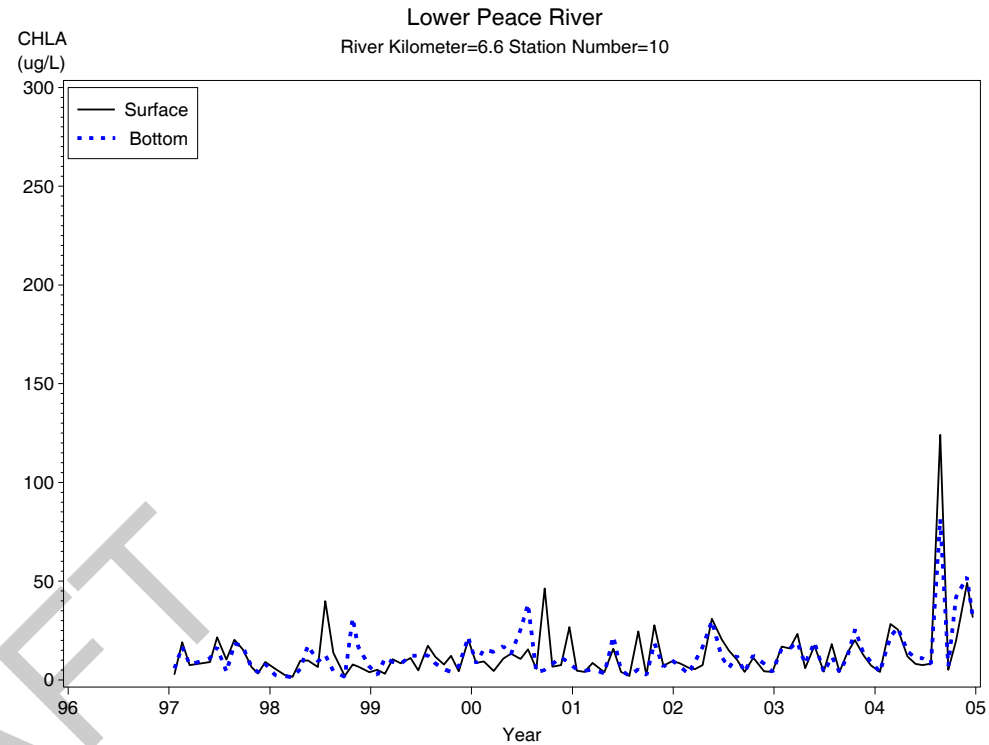
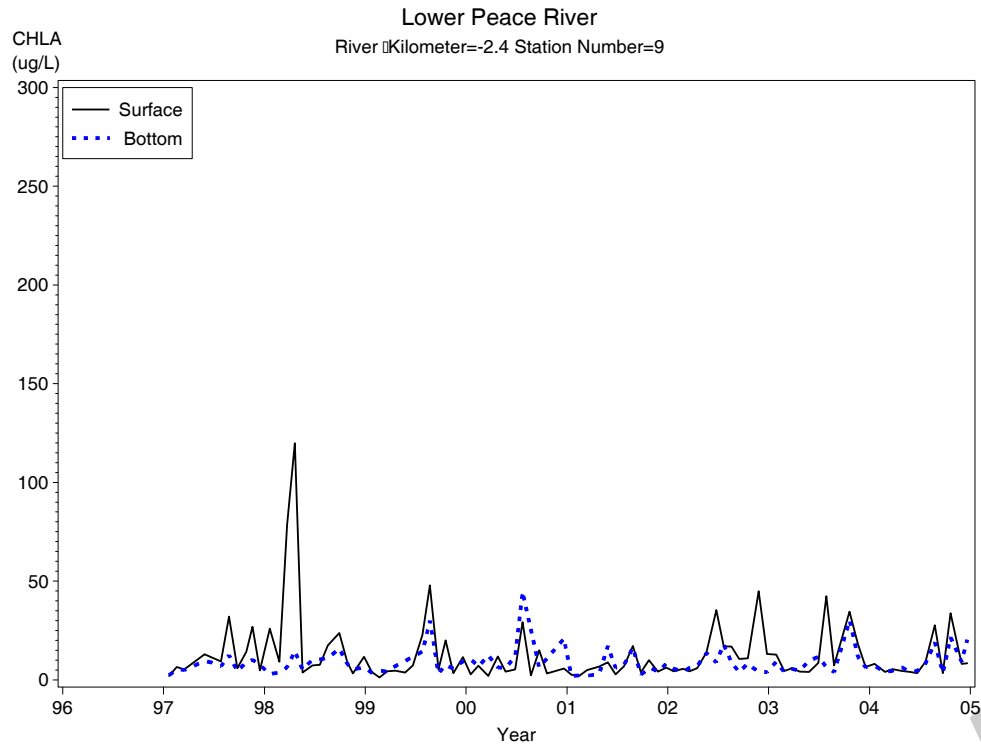


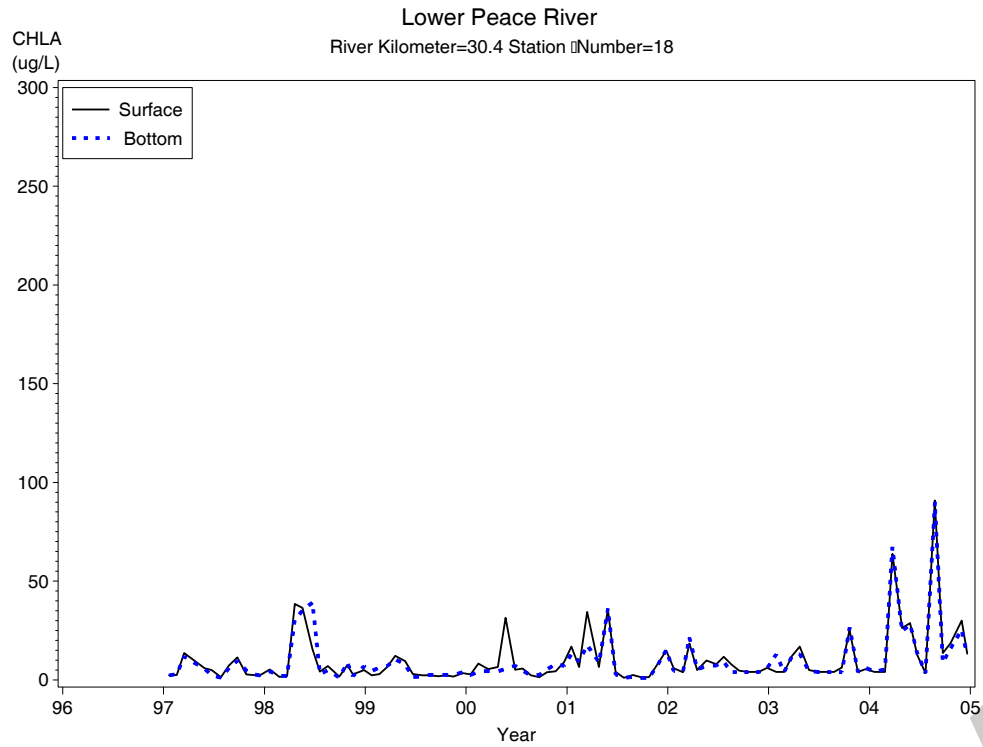


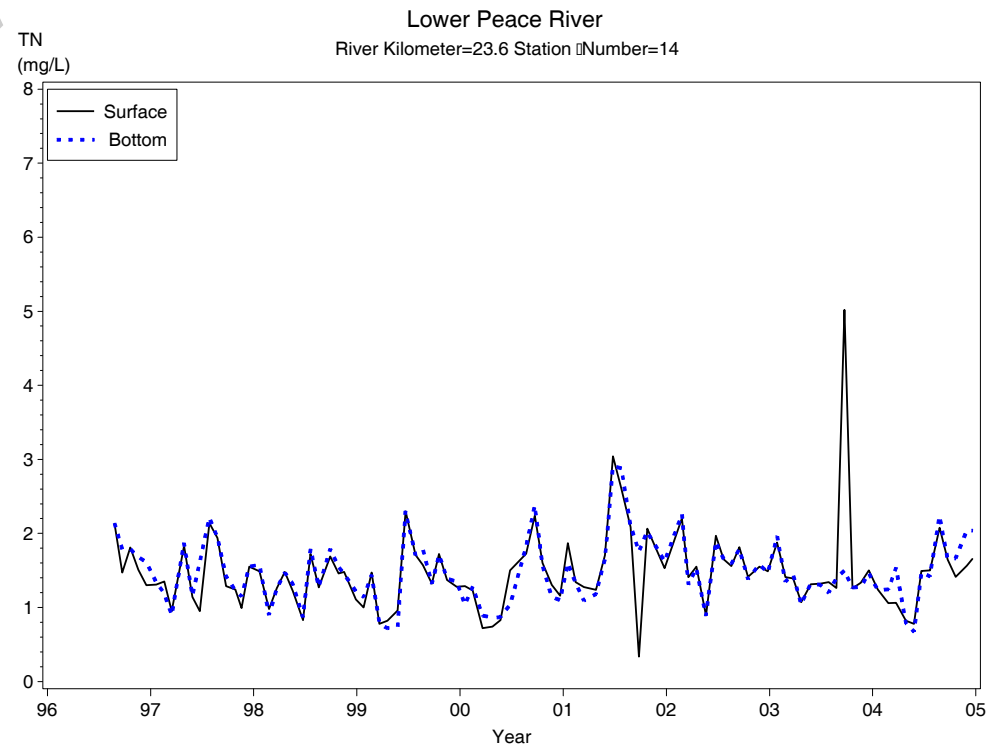
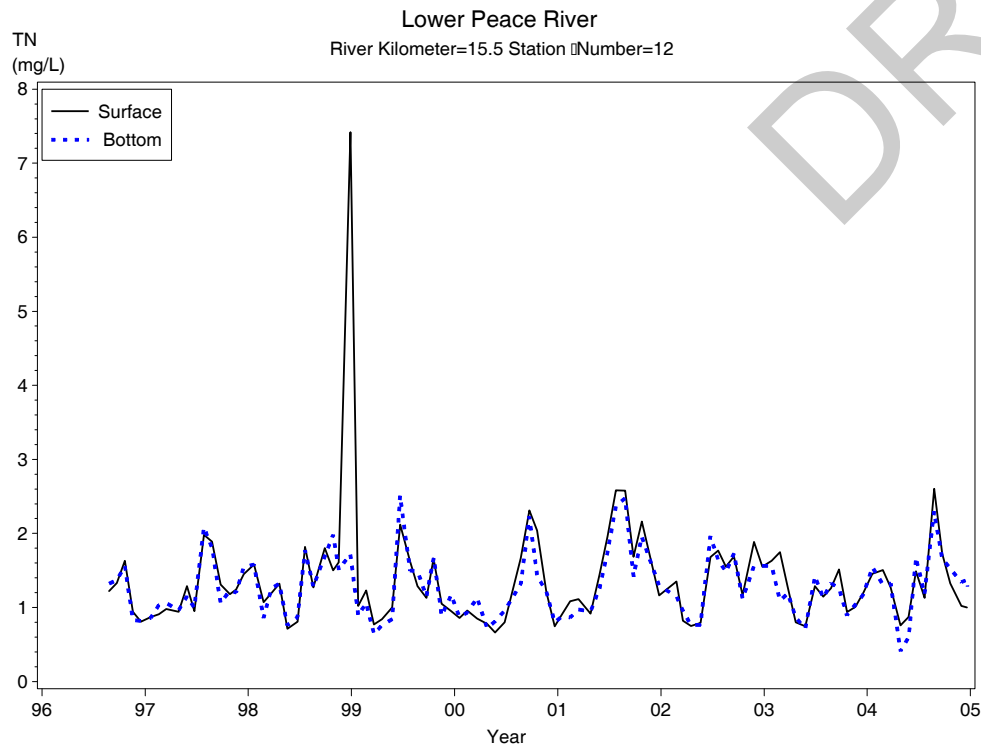
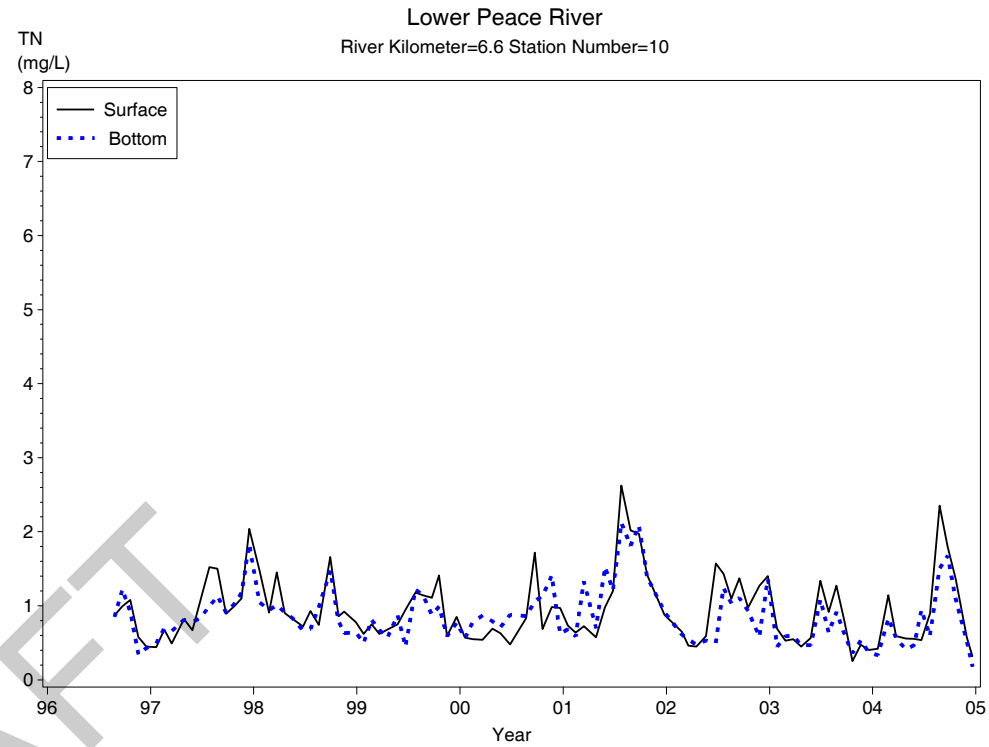
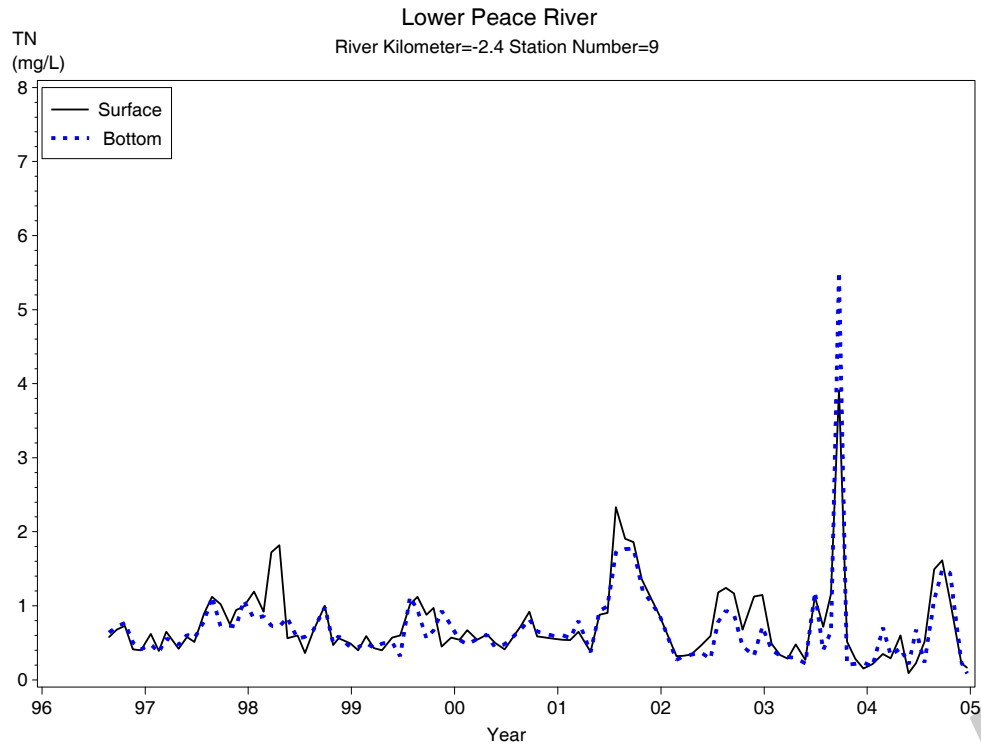


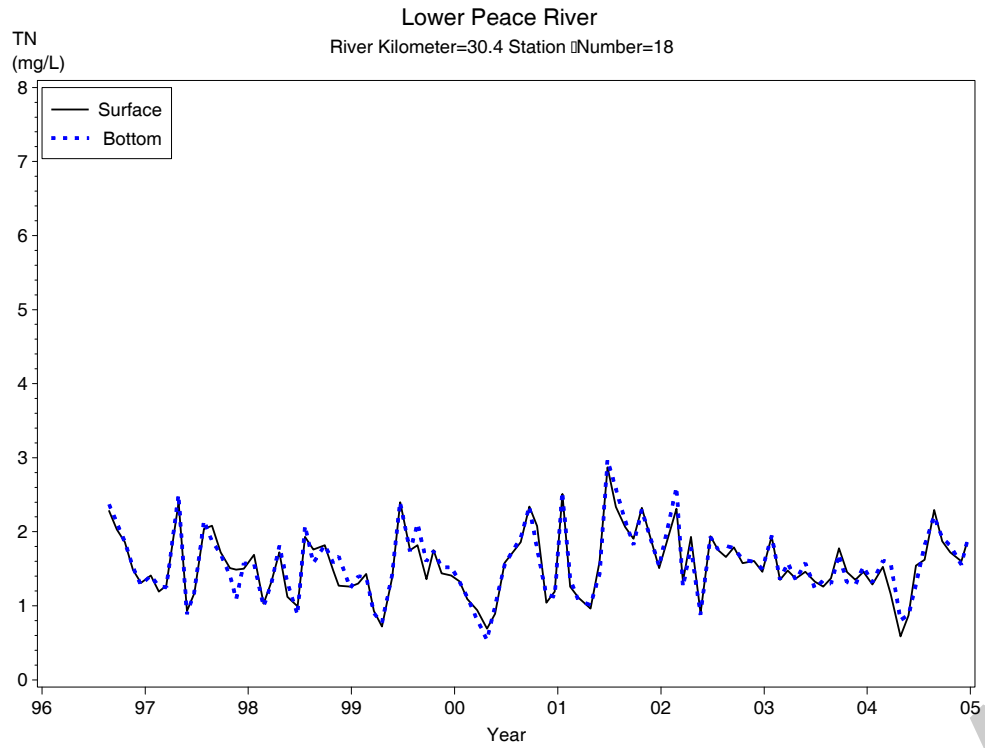


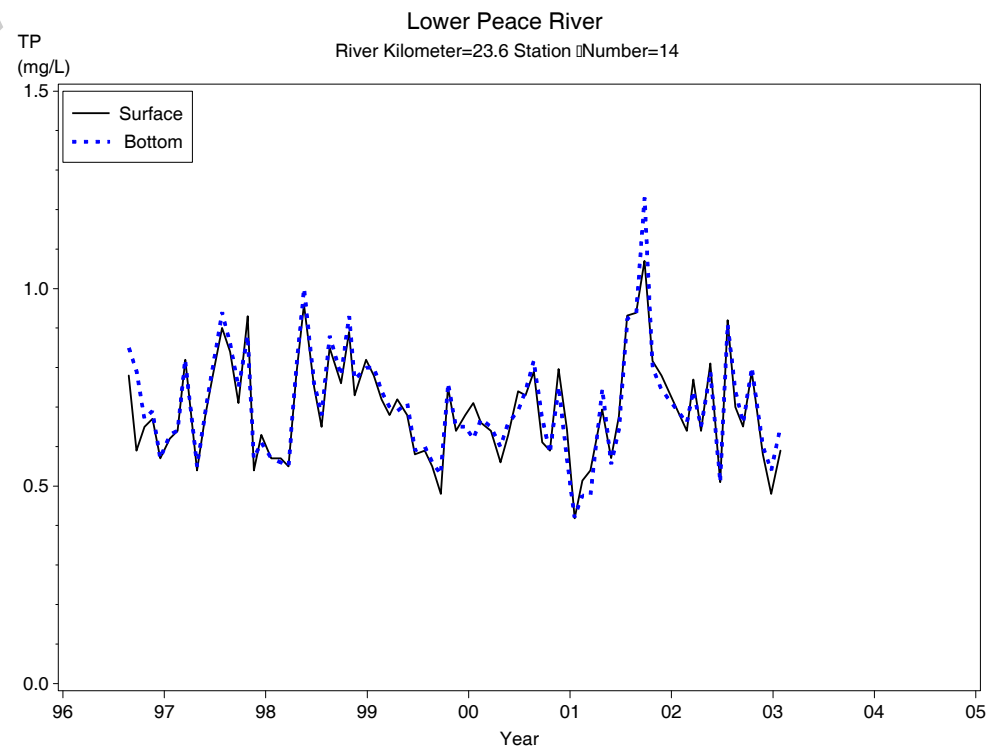
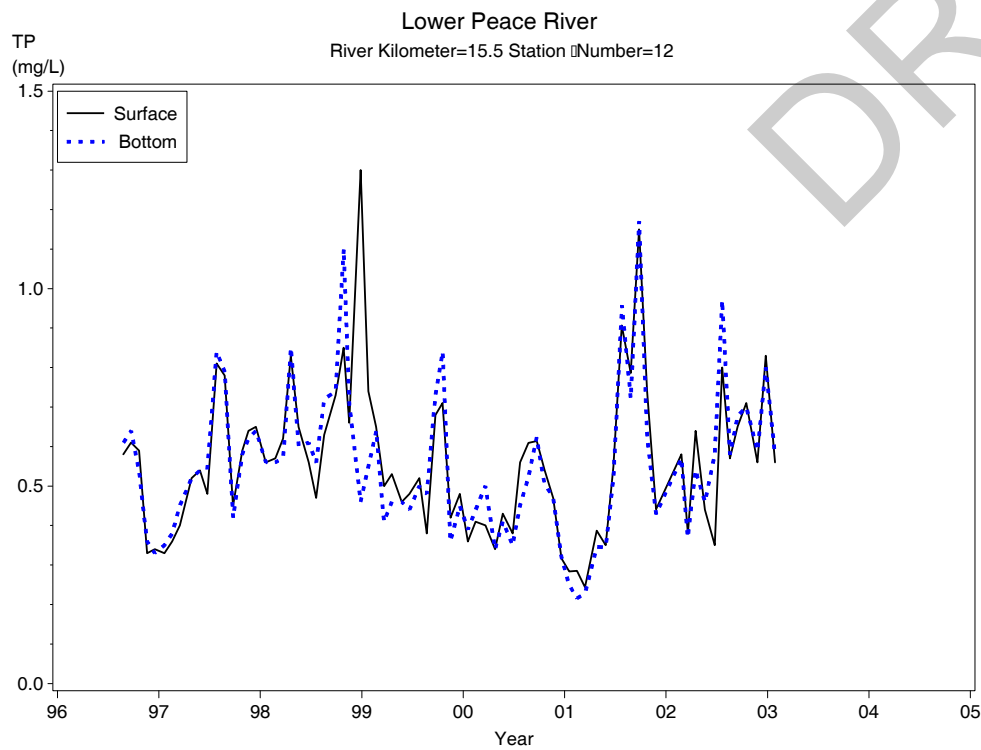
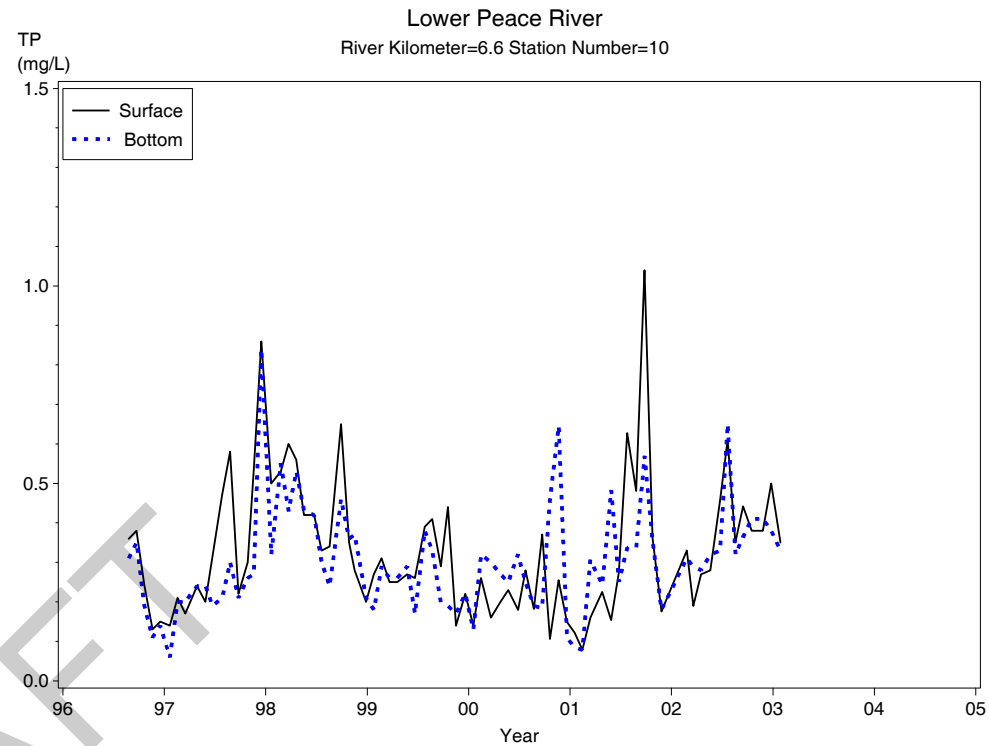
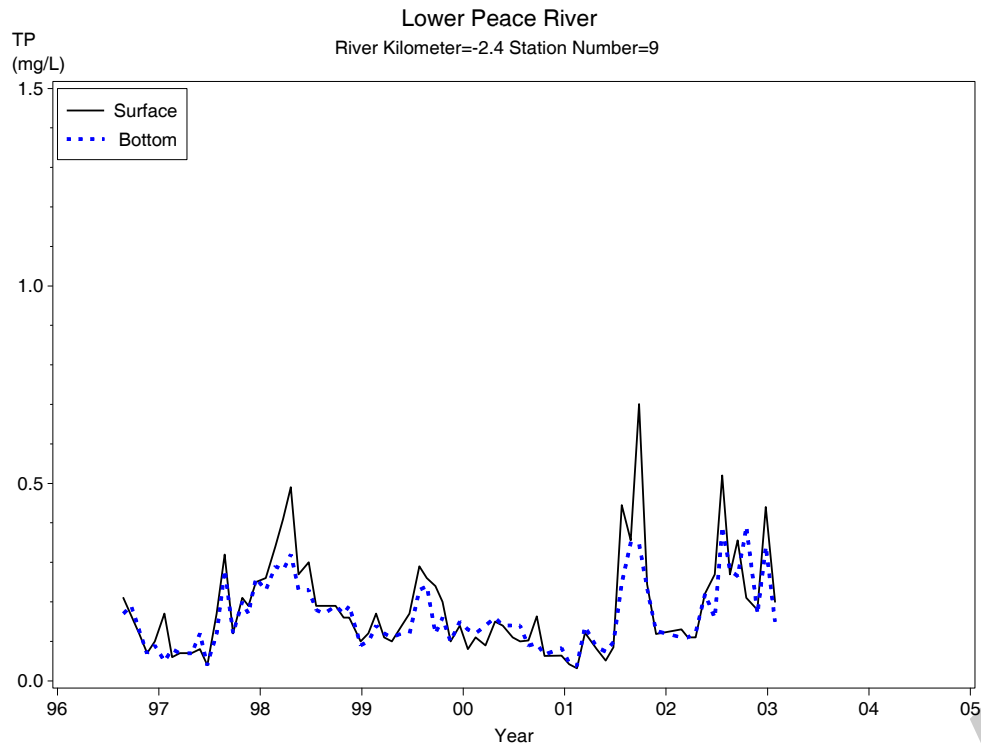




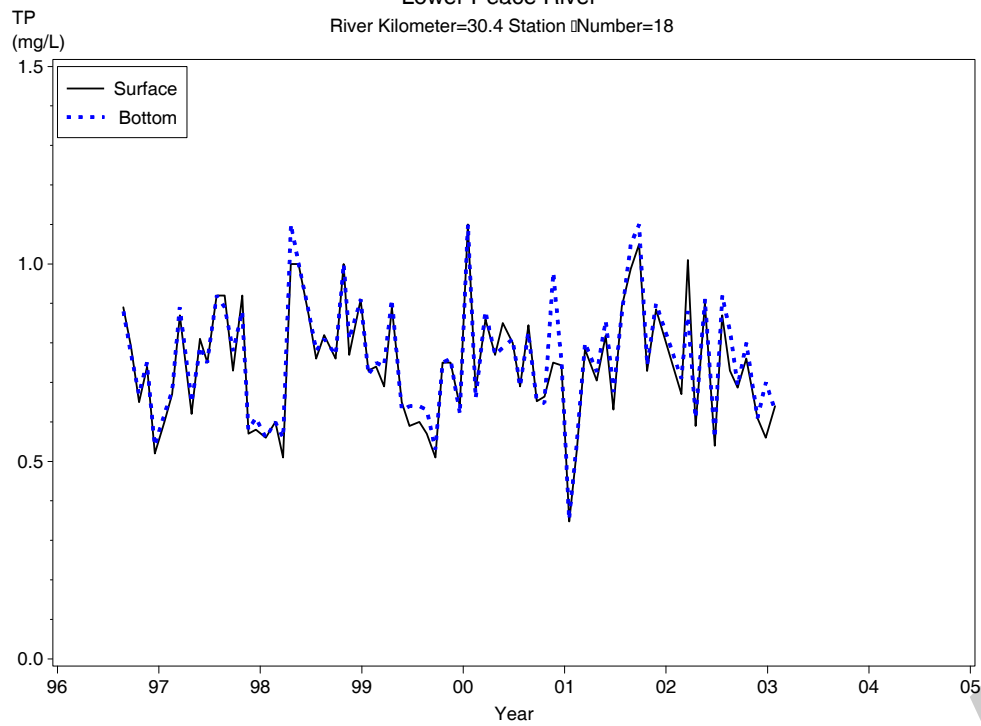








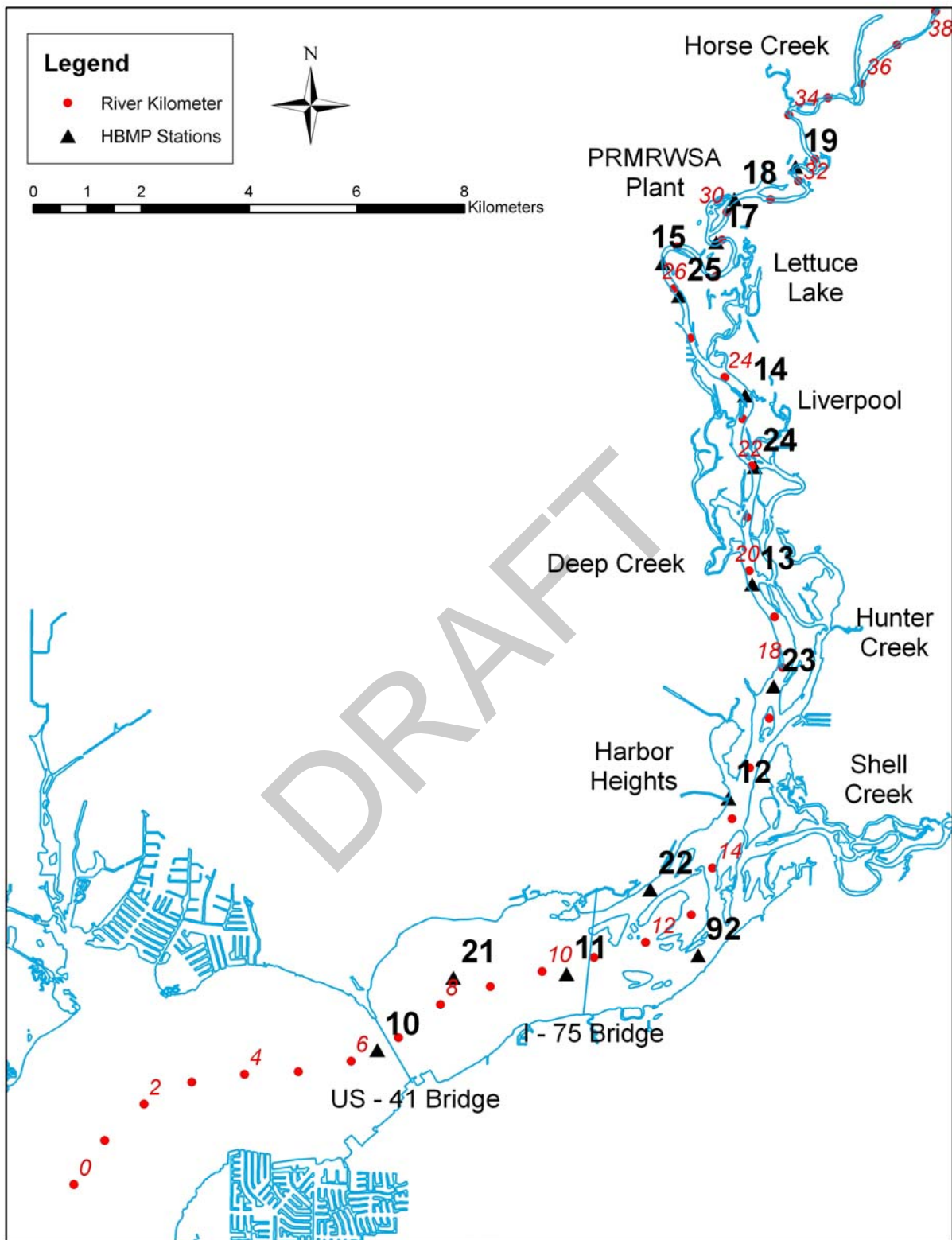
Lower Peace River
River Kilometer=30.4 Station Number=18

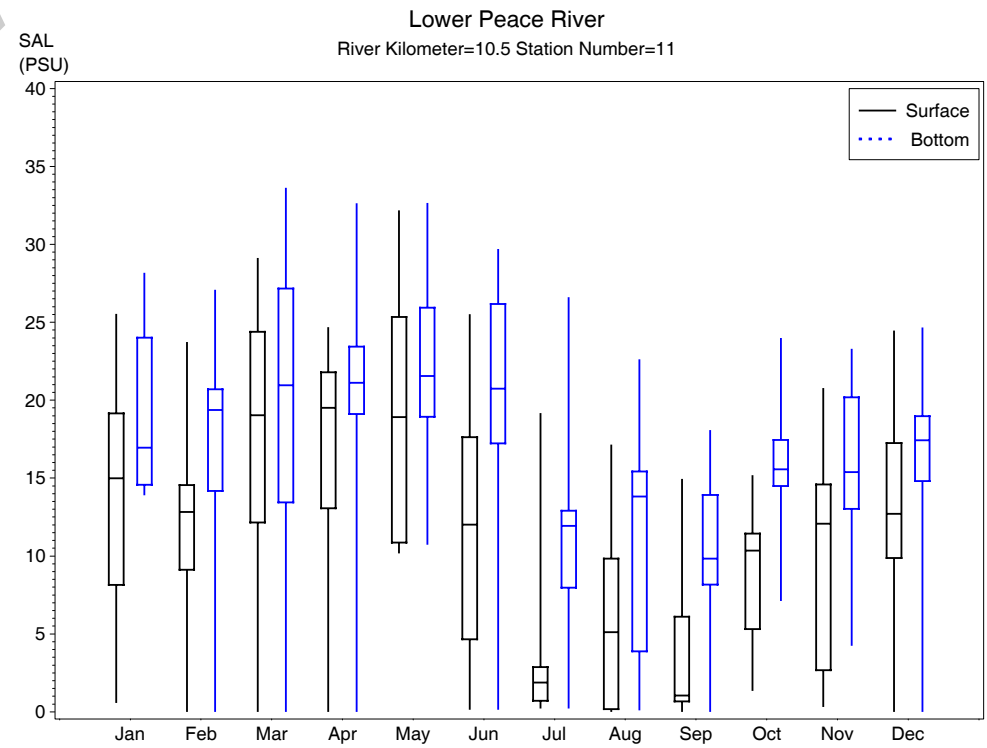
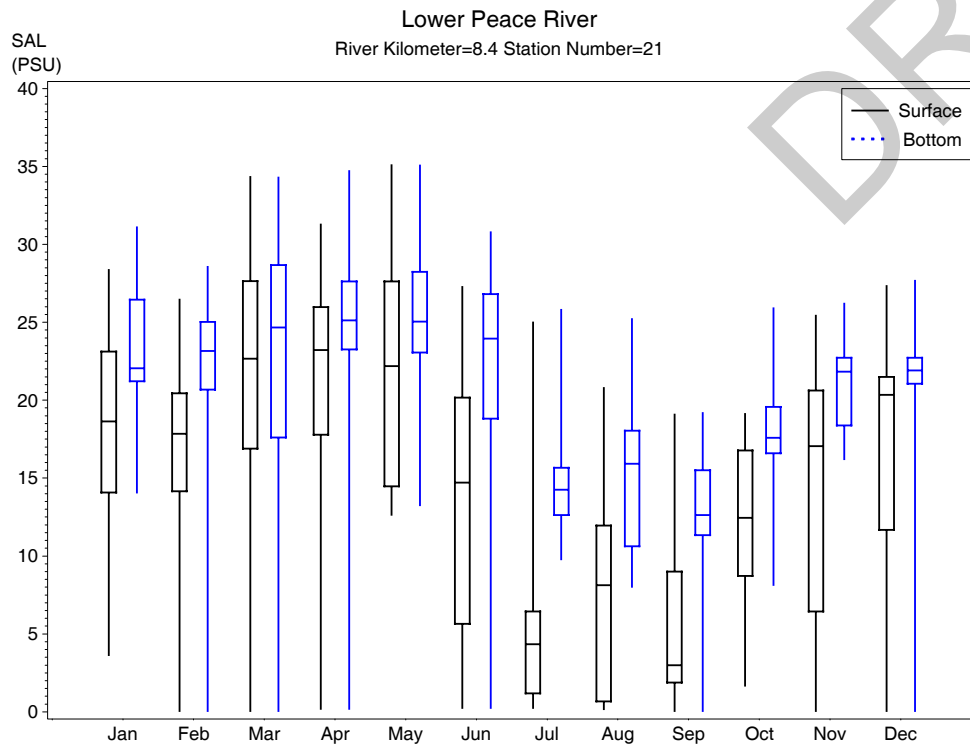
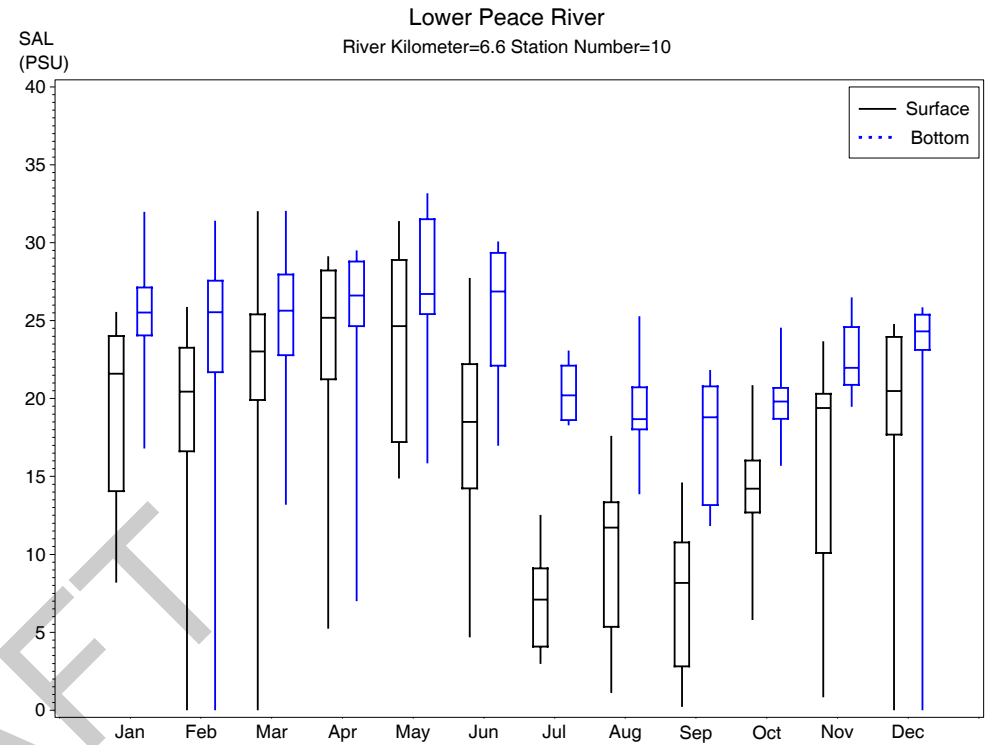
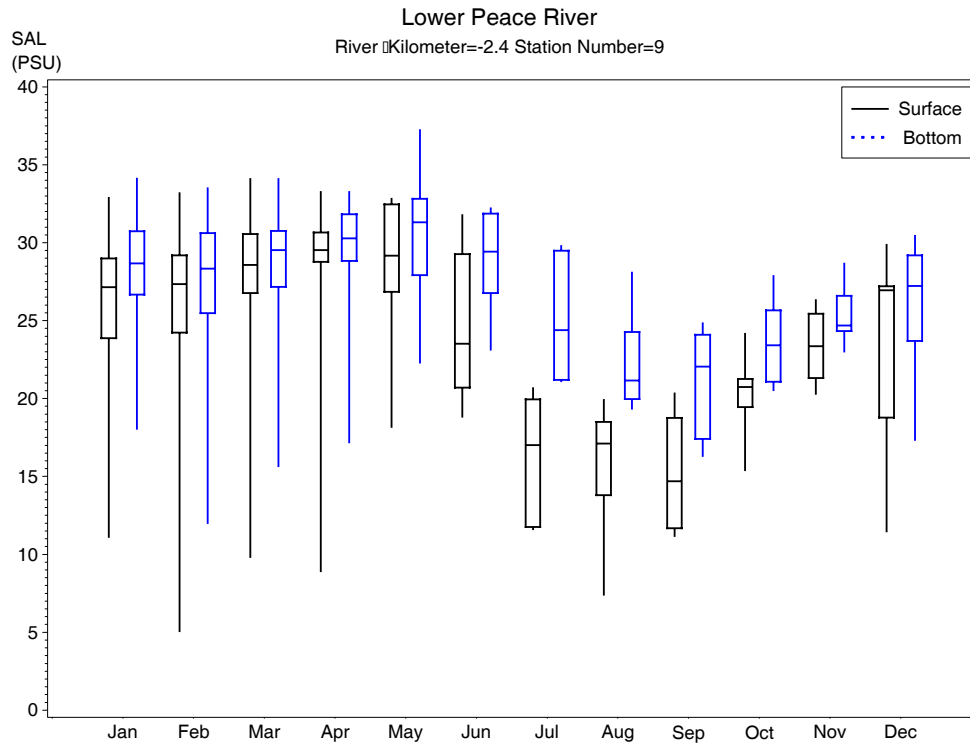


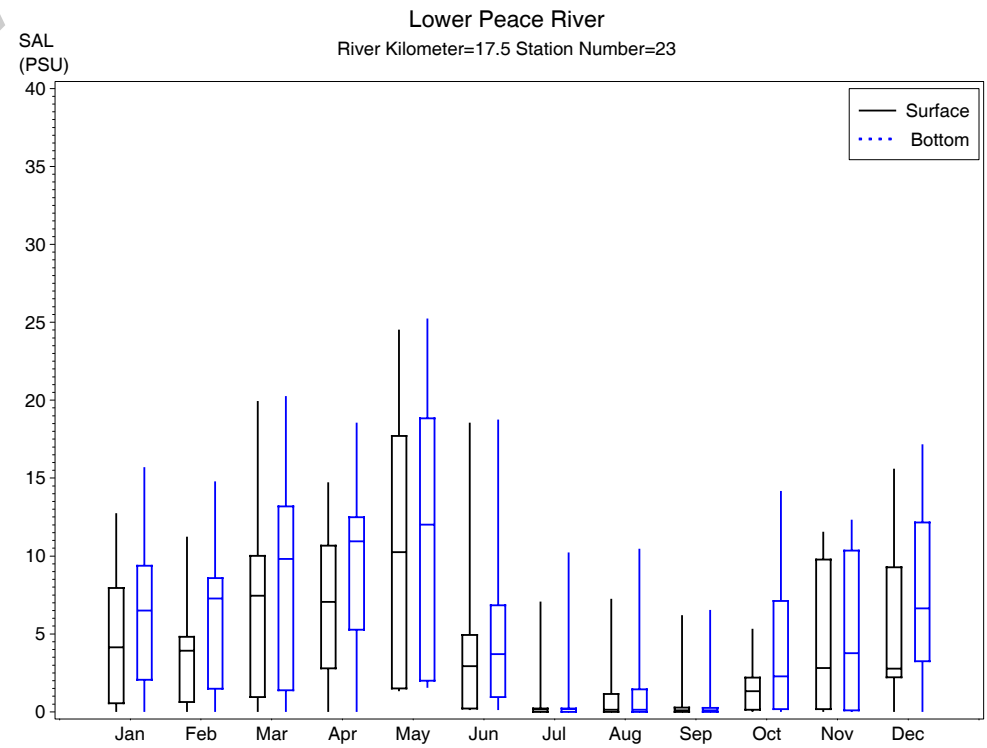
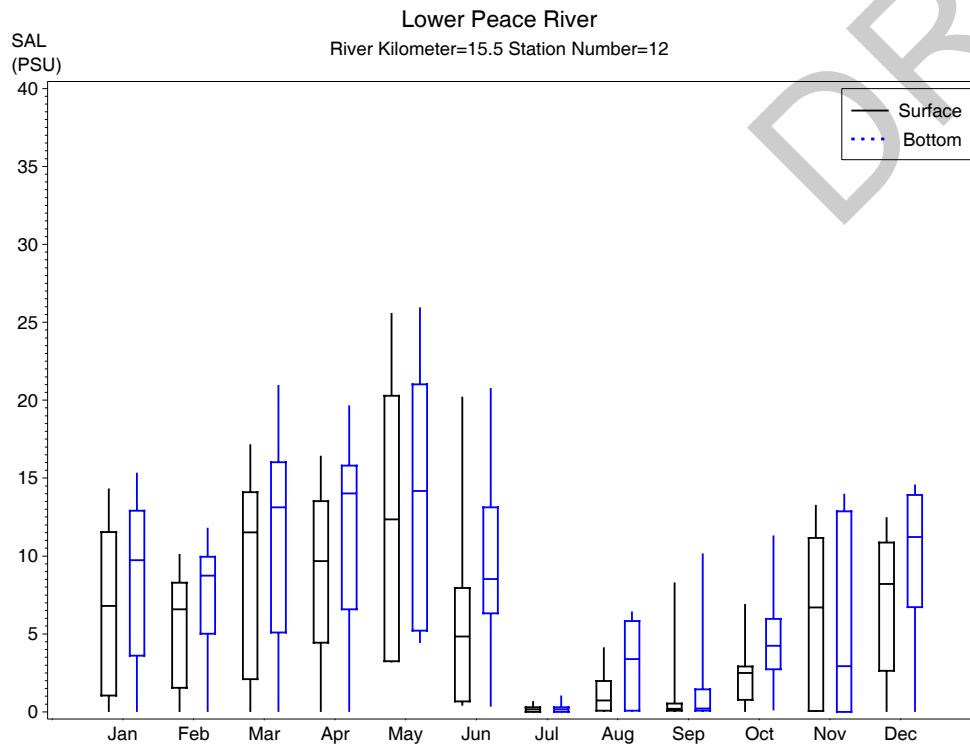
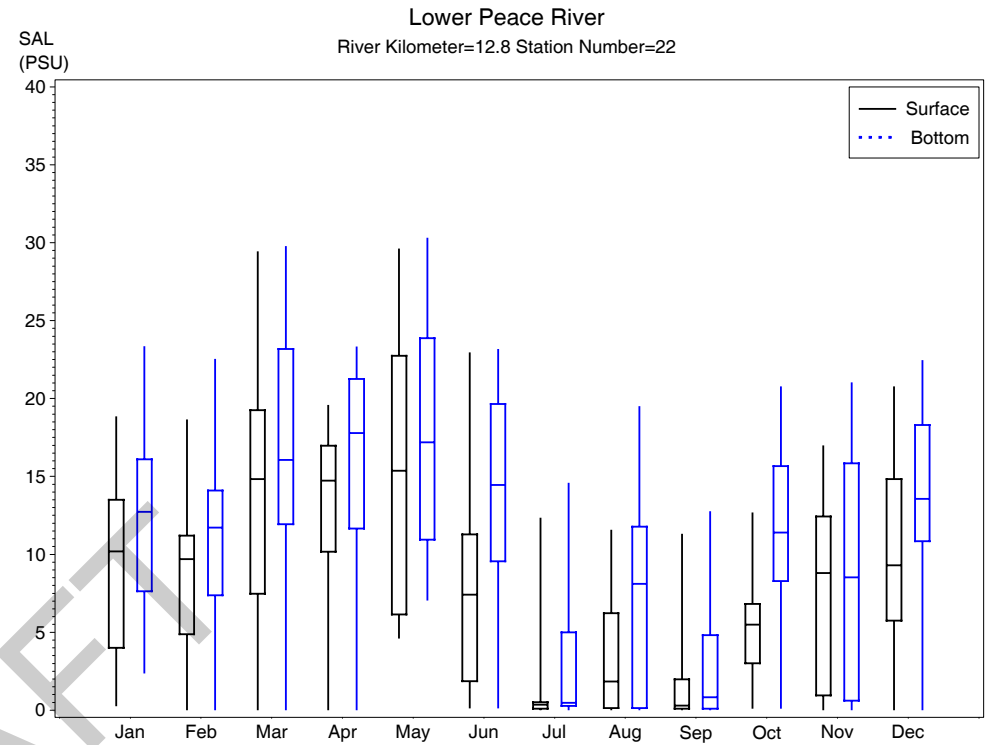
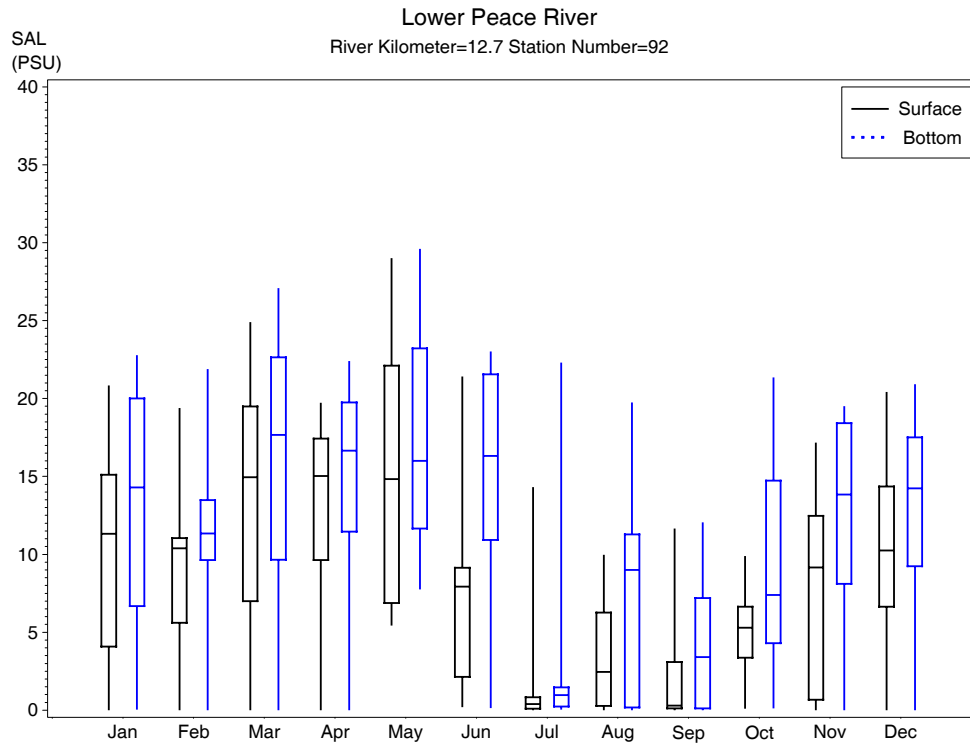
Appendix 3-2

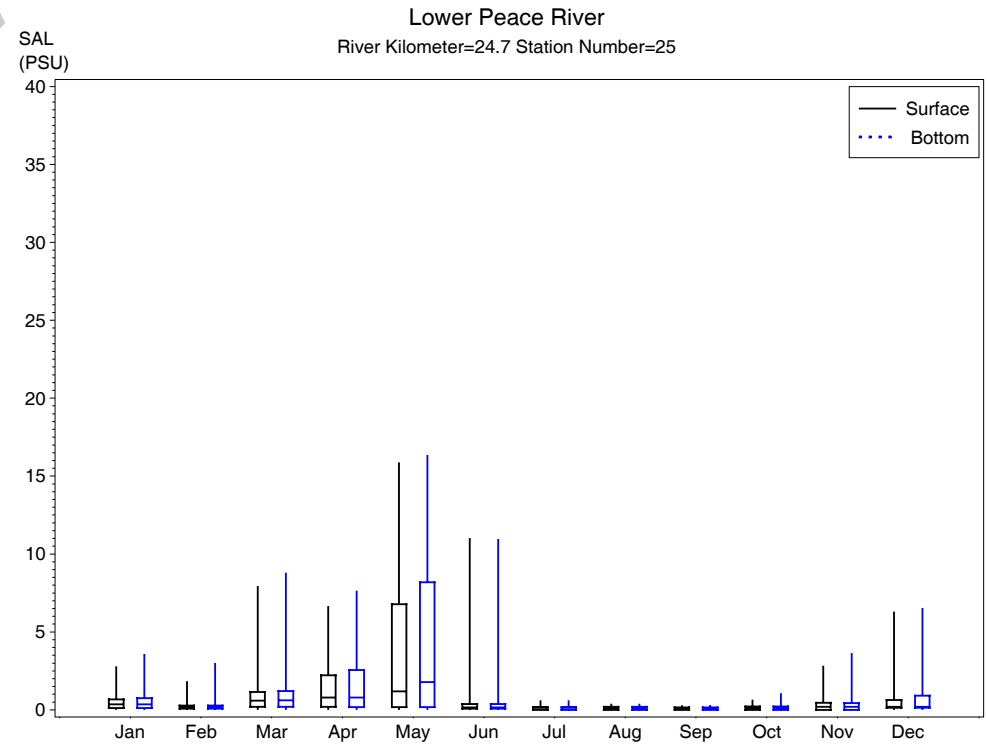
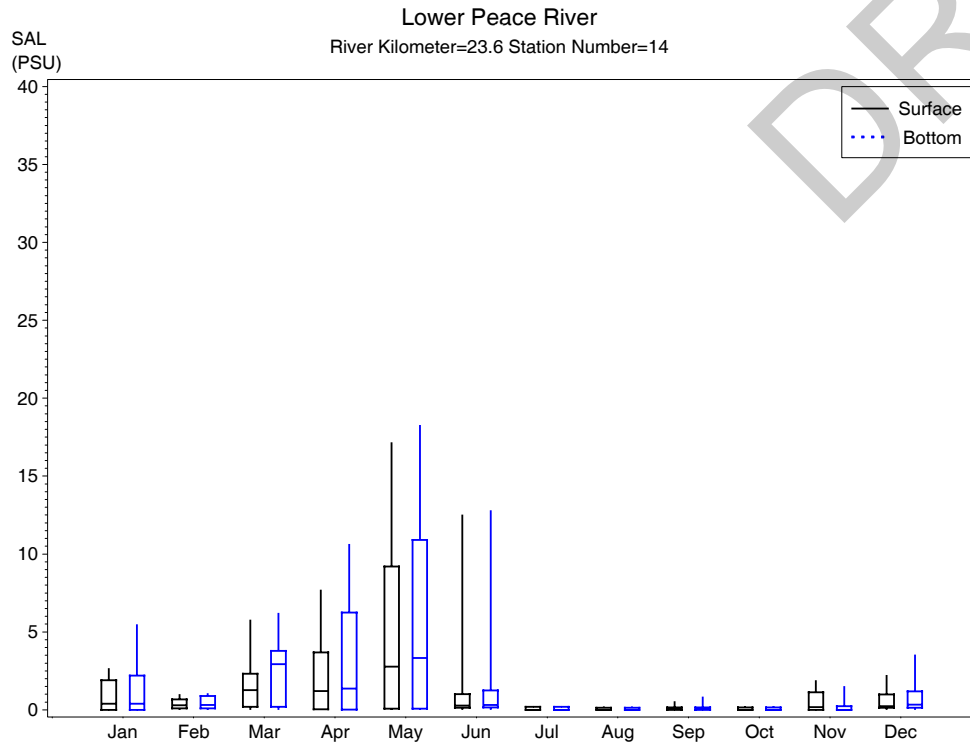
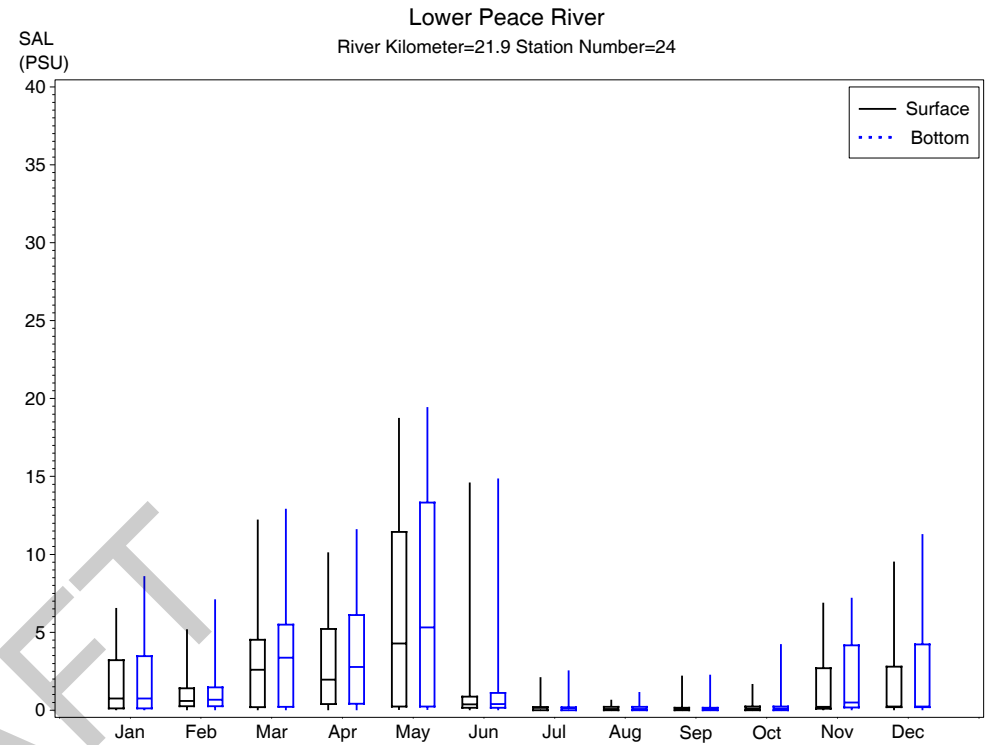
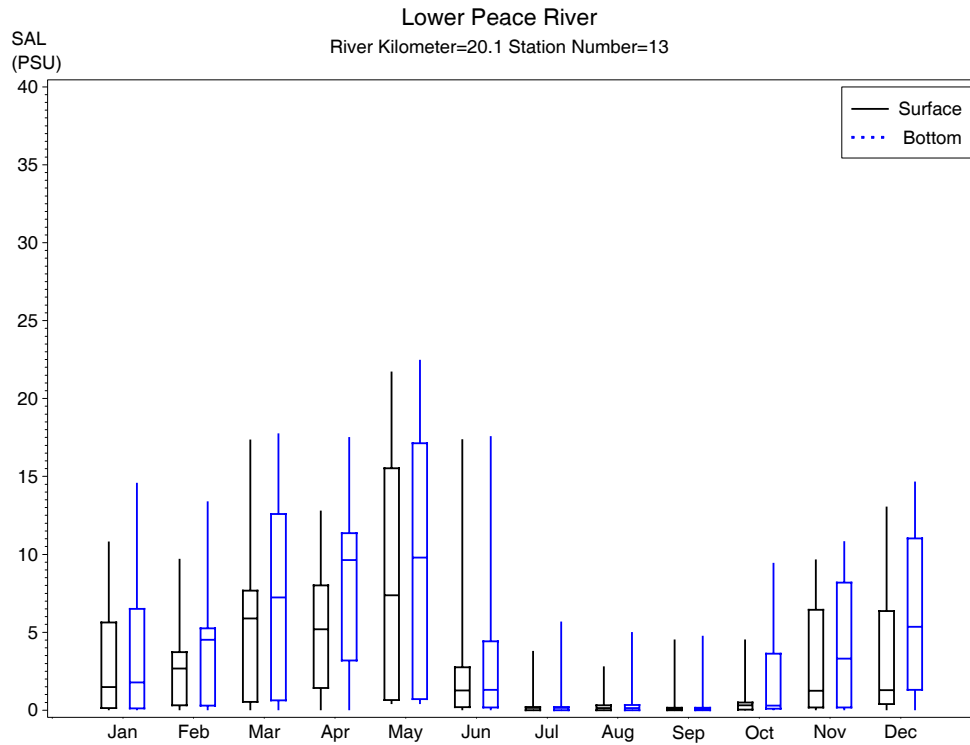
Within-Year Variation in Lower Peace River

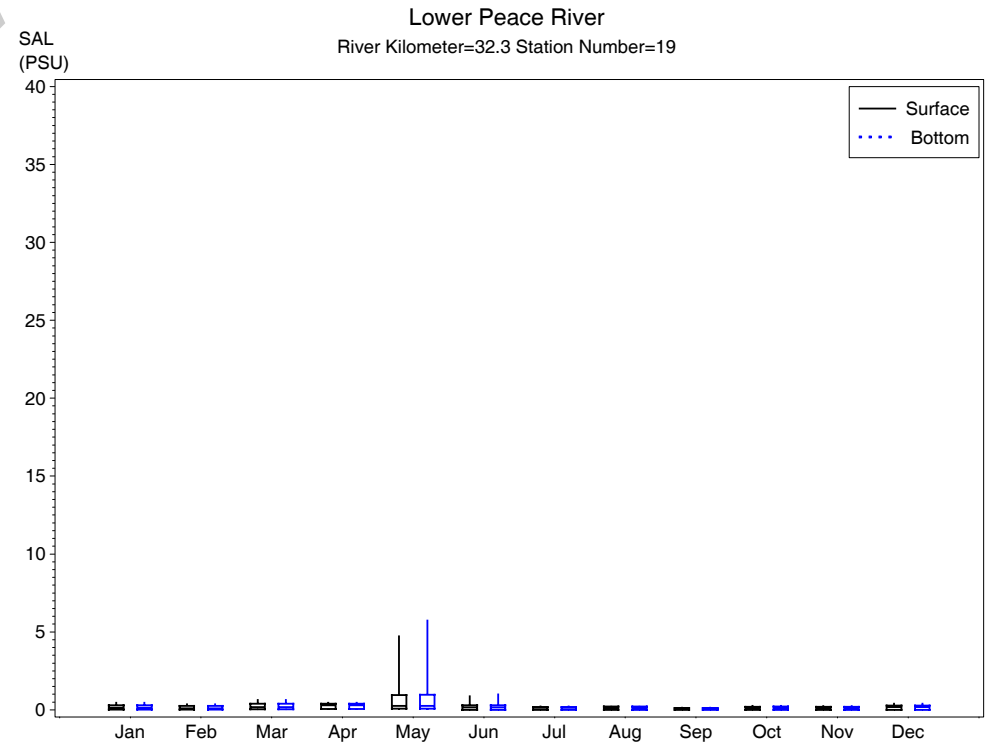
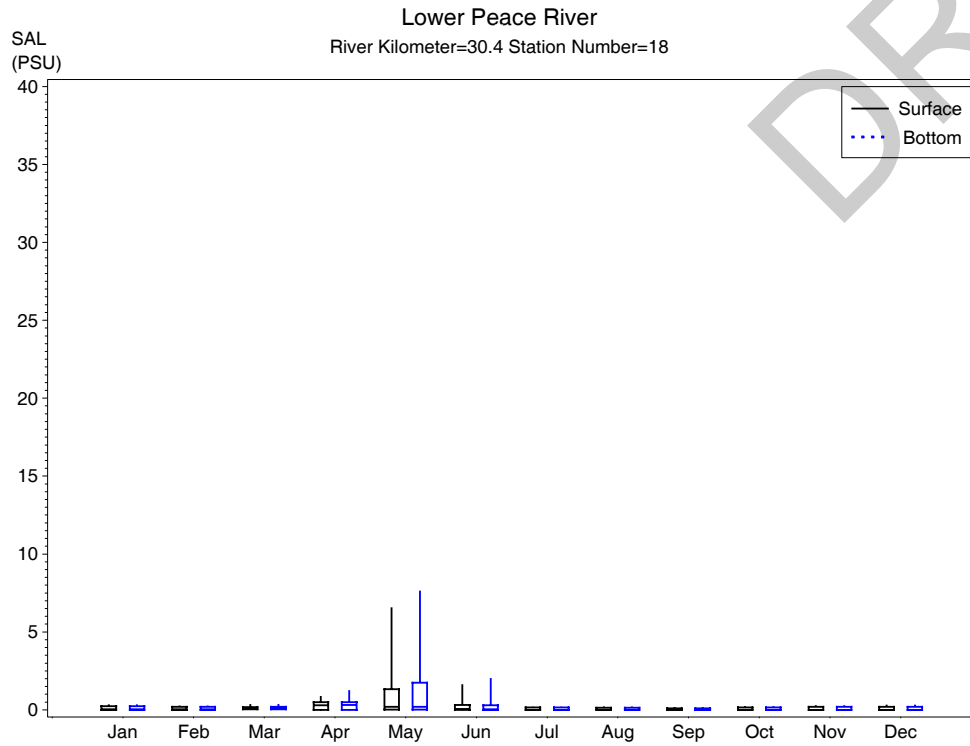
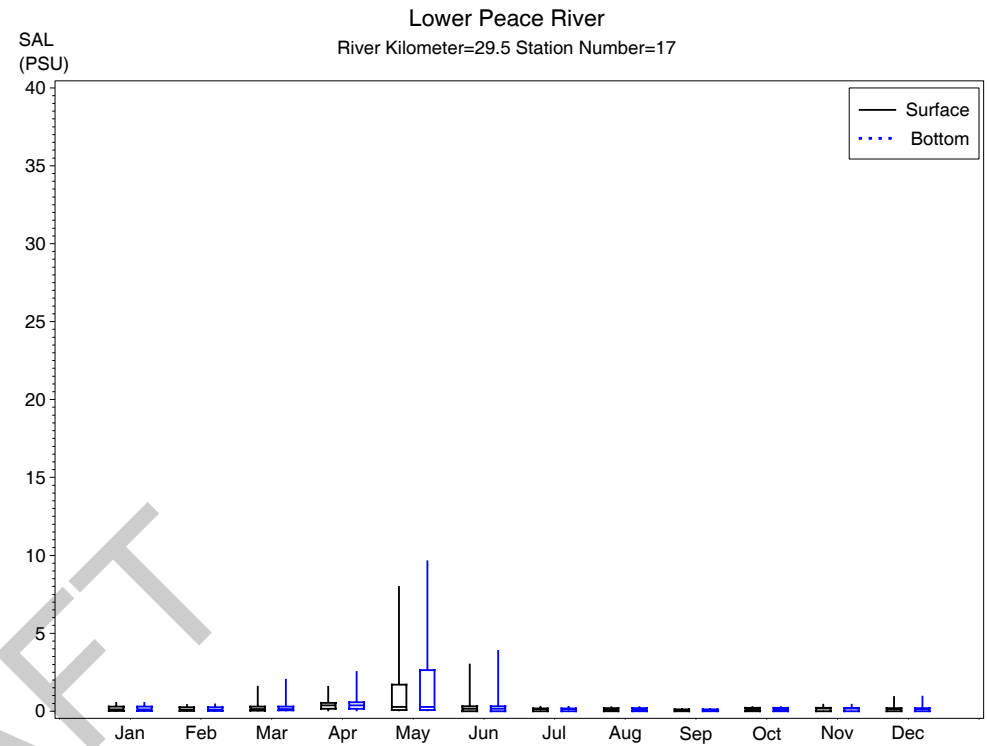
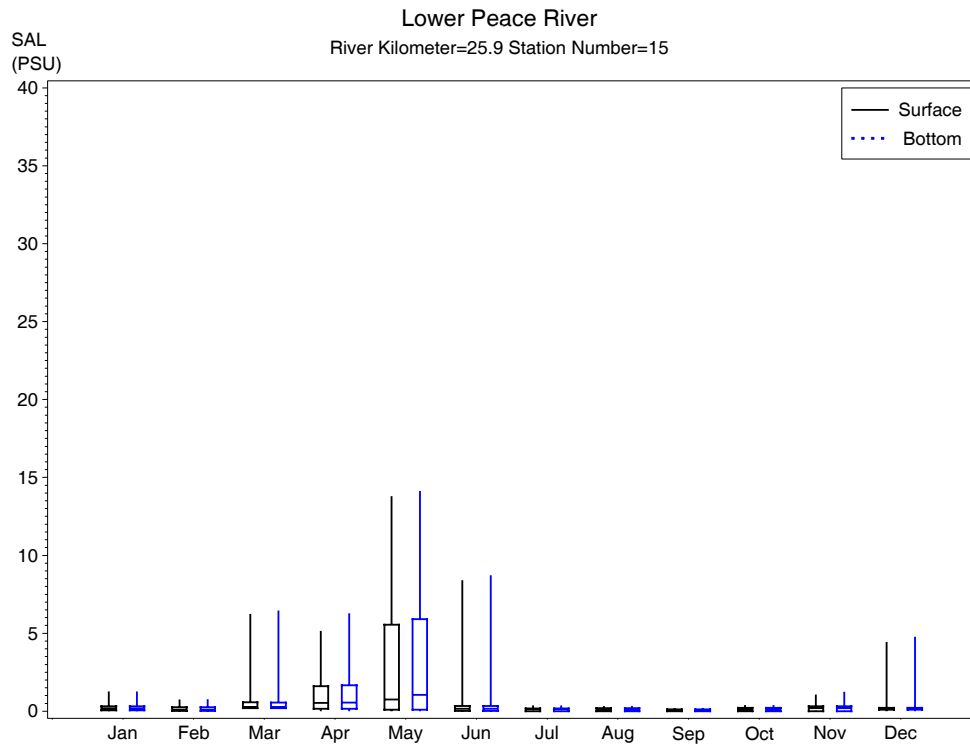
Water Quality Constituents

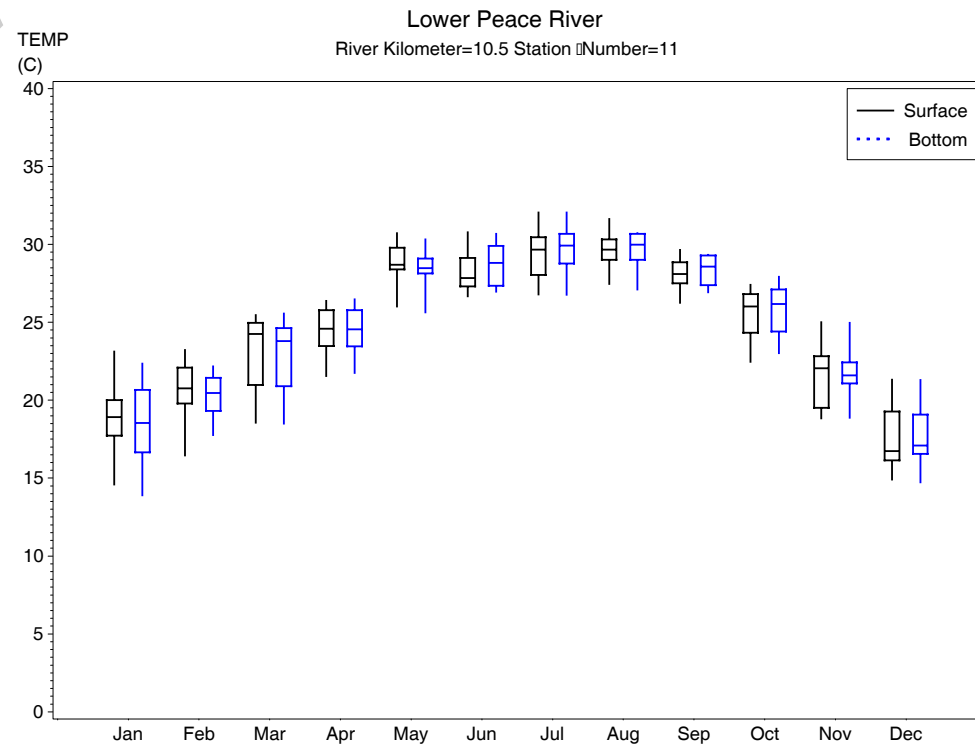
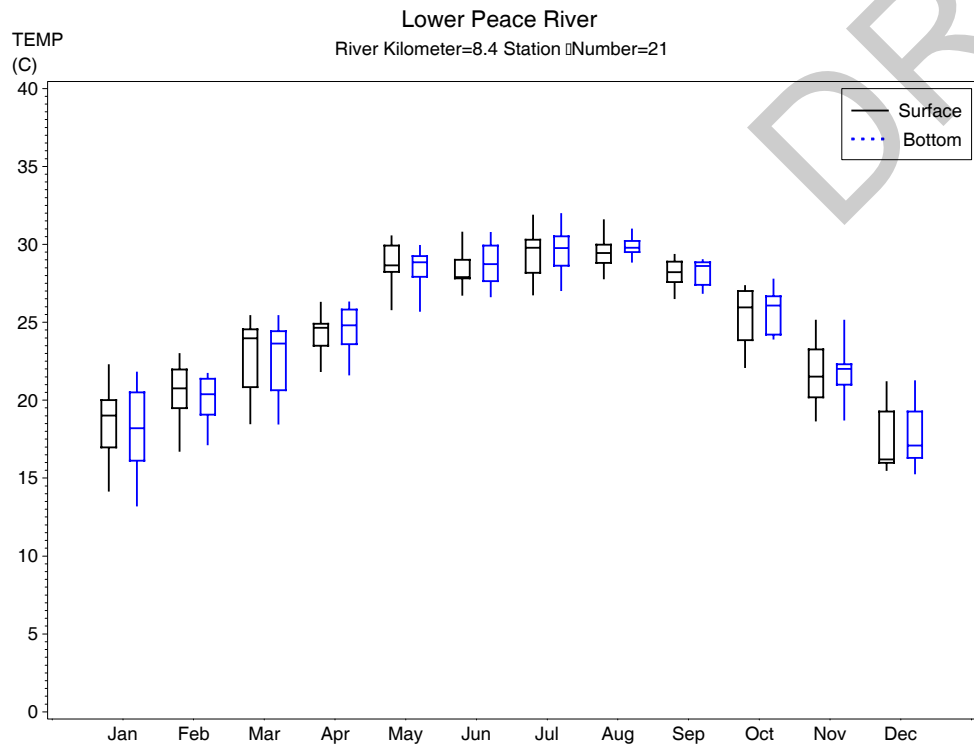
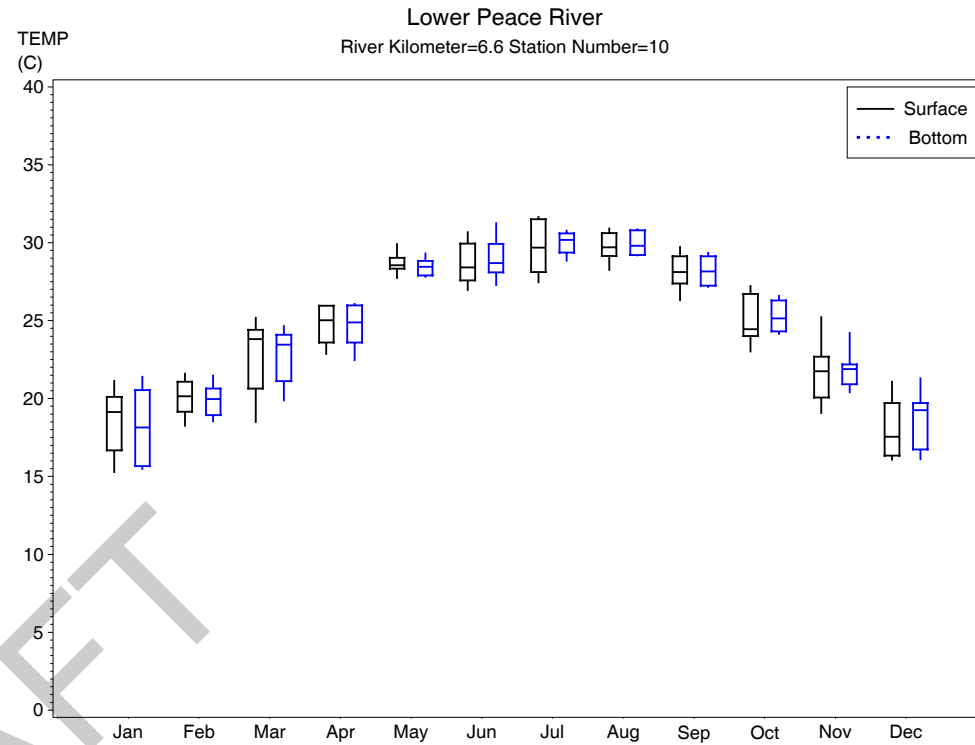
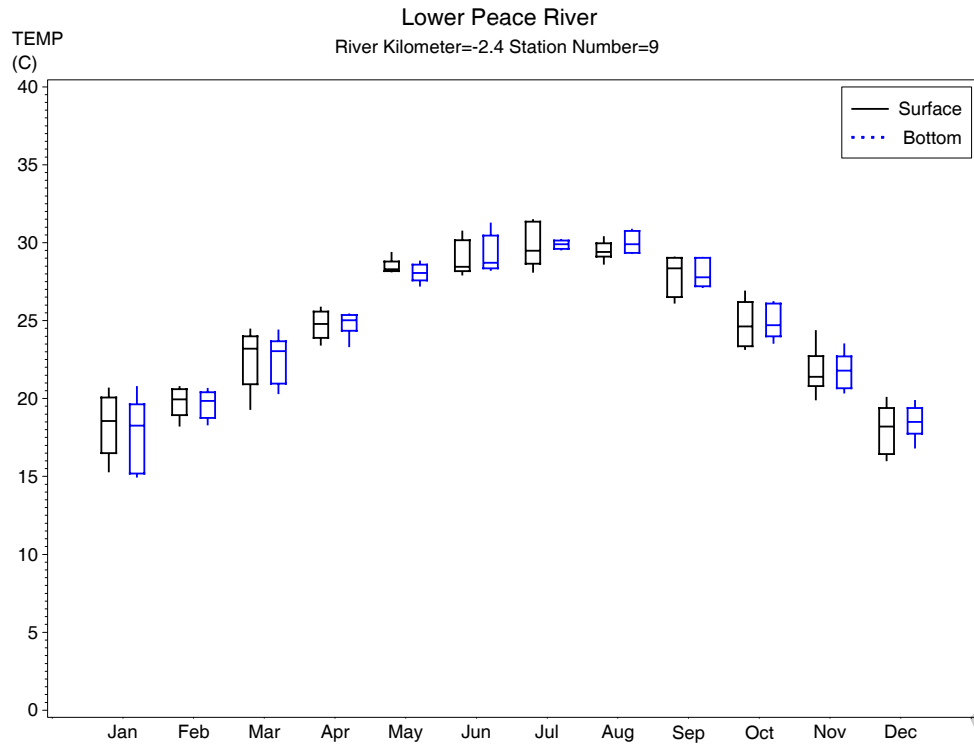


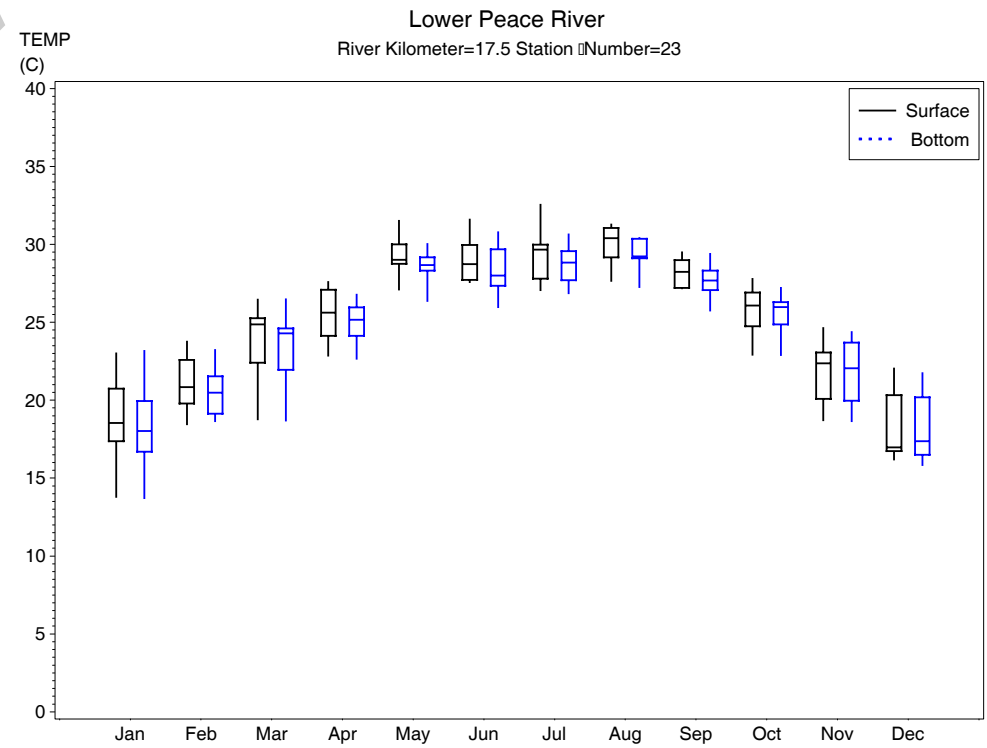
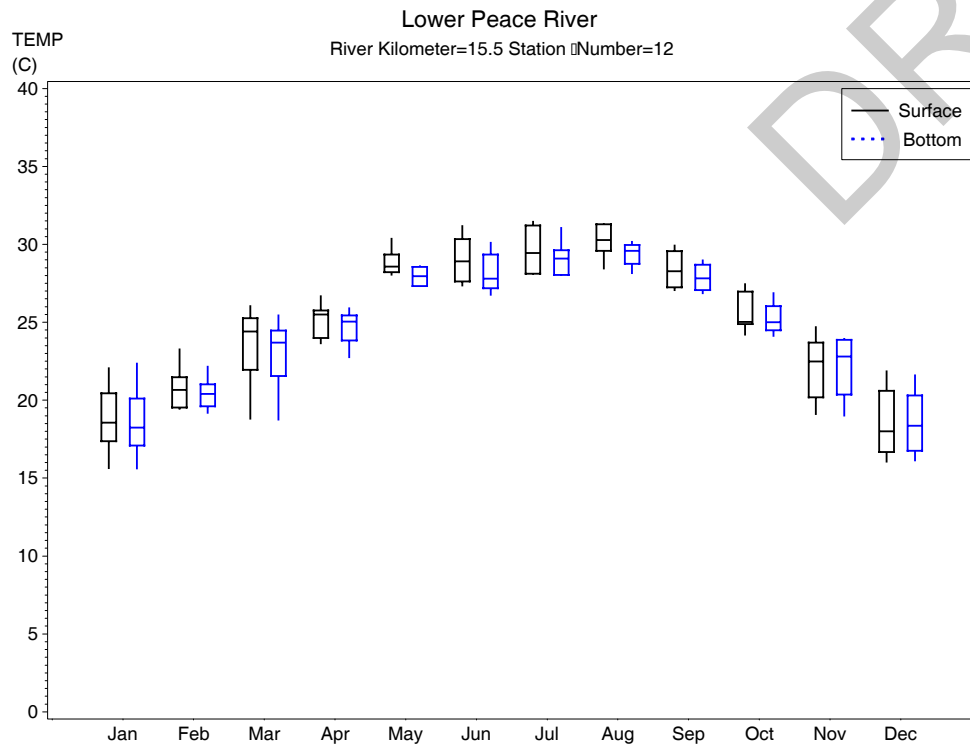
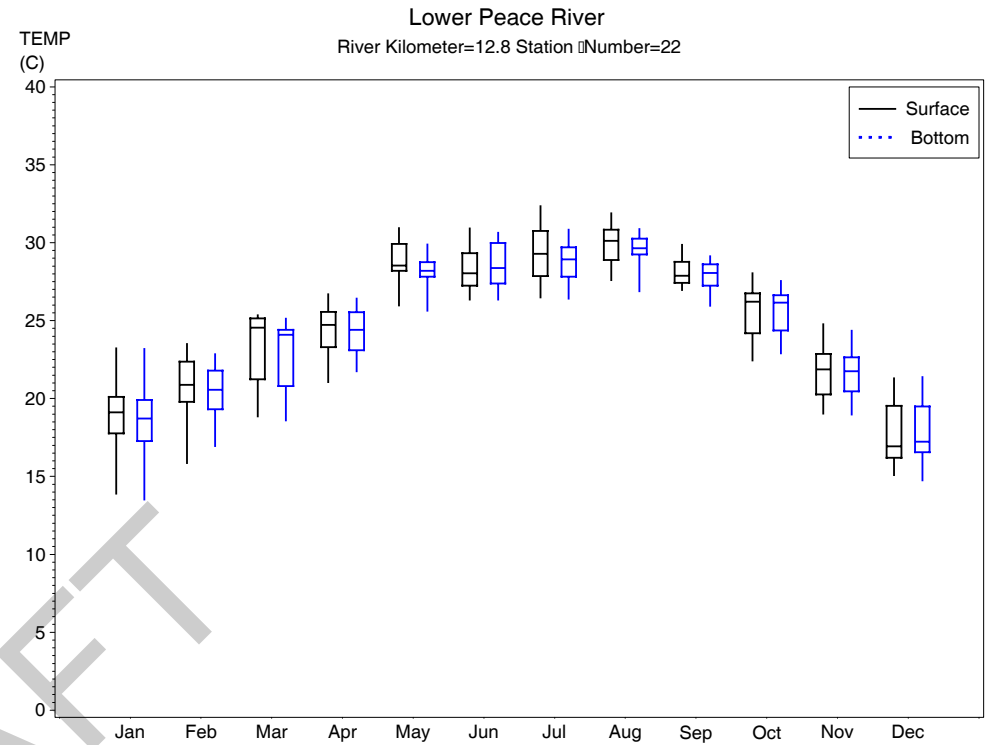
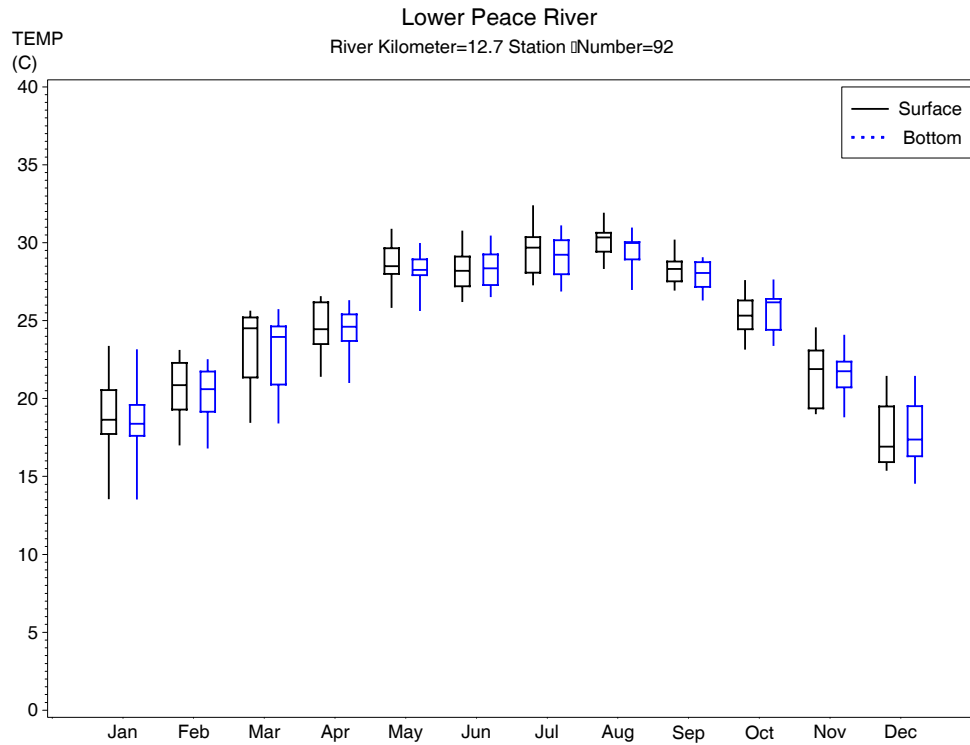


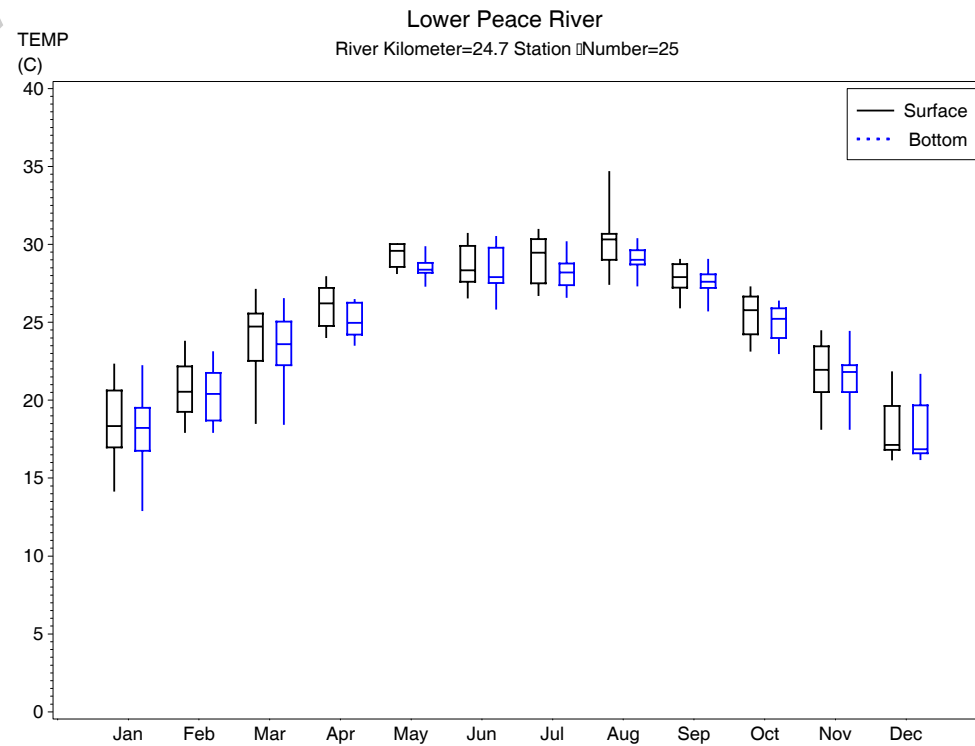
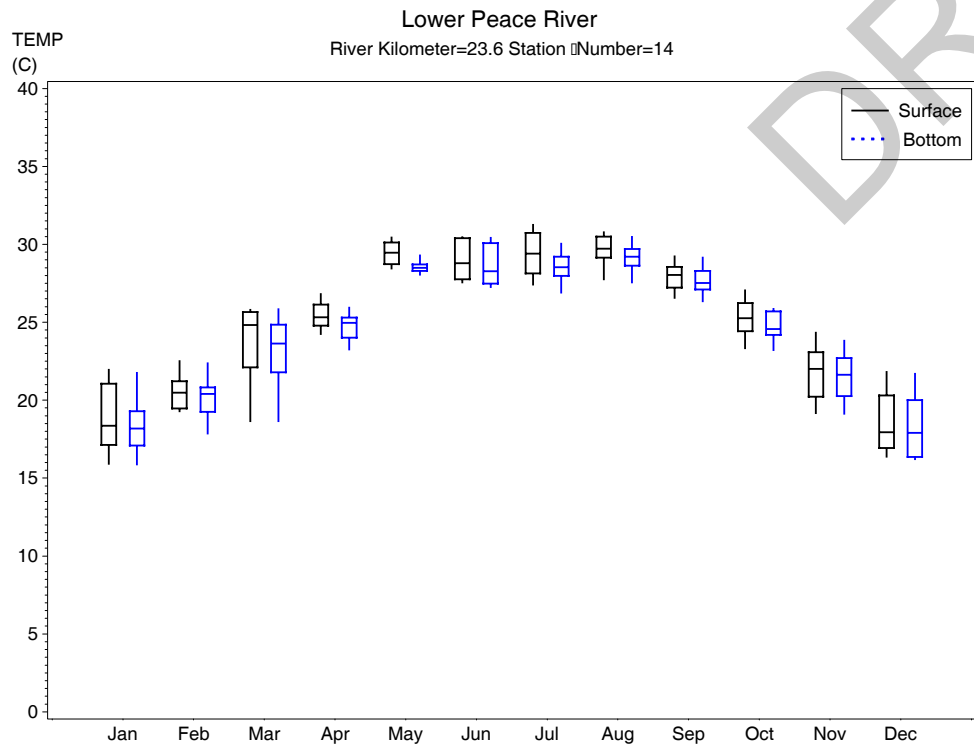
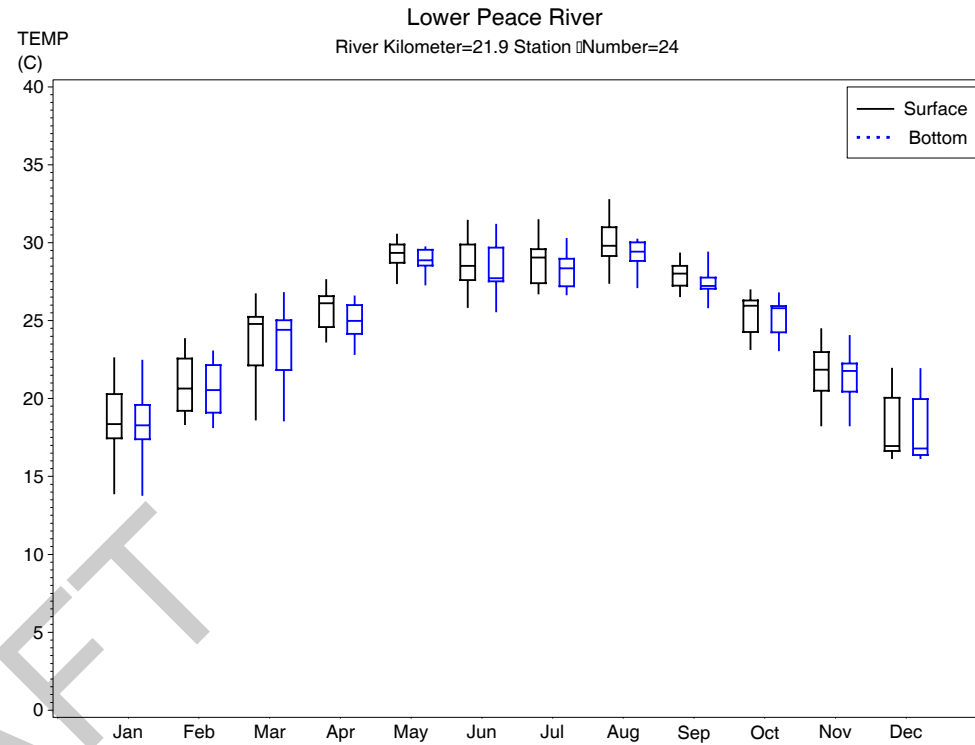
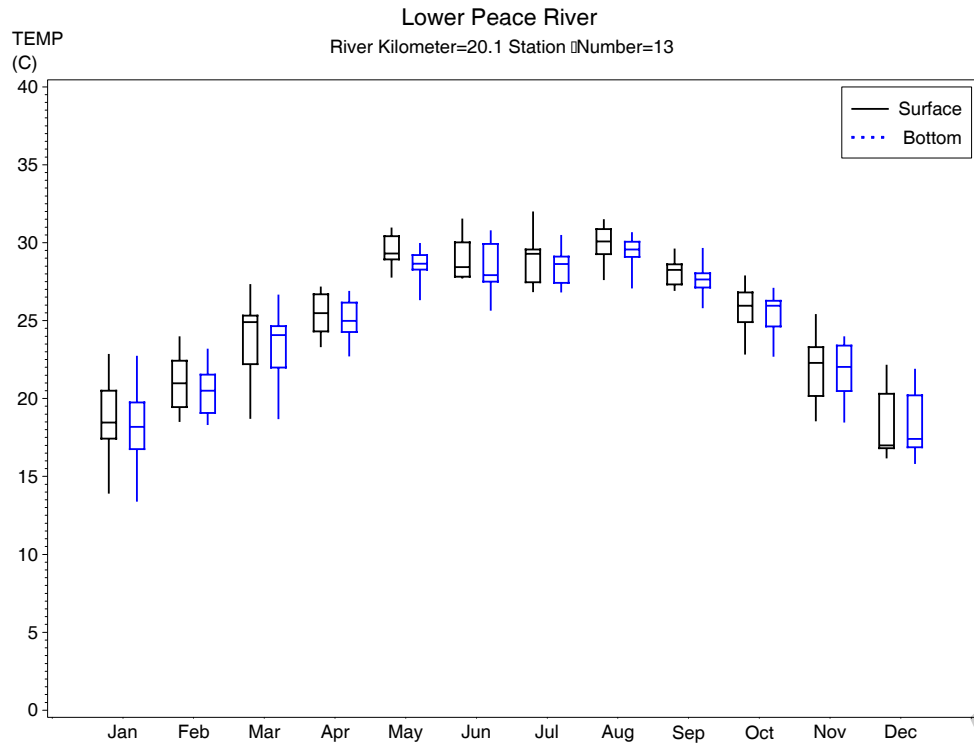


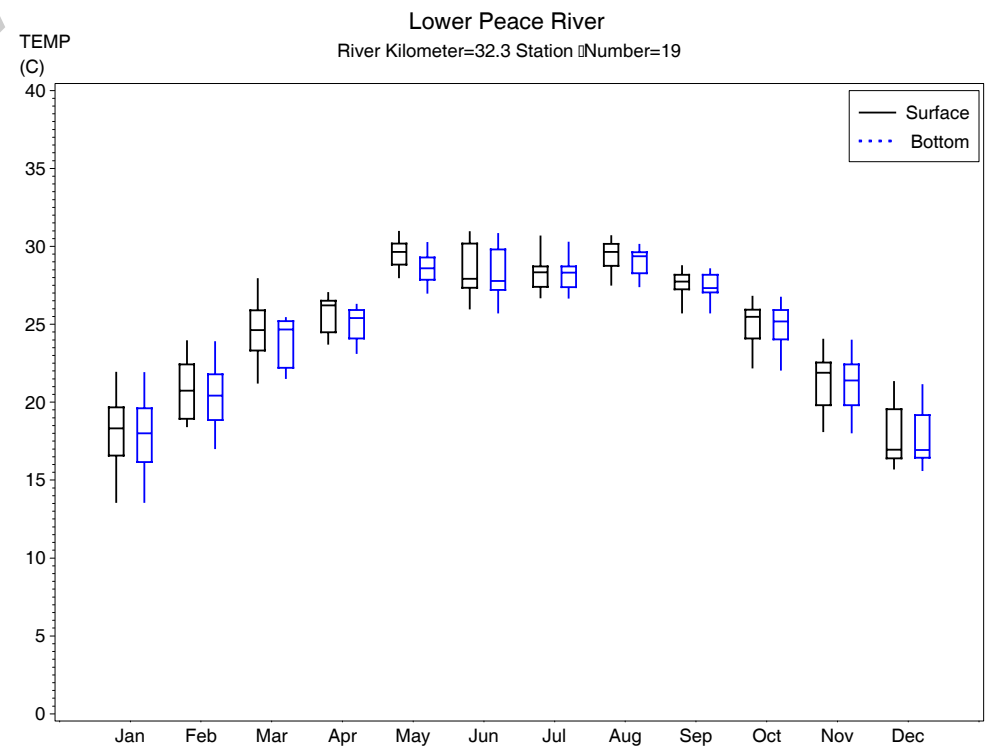
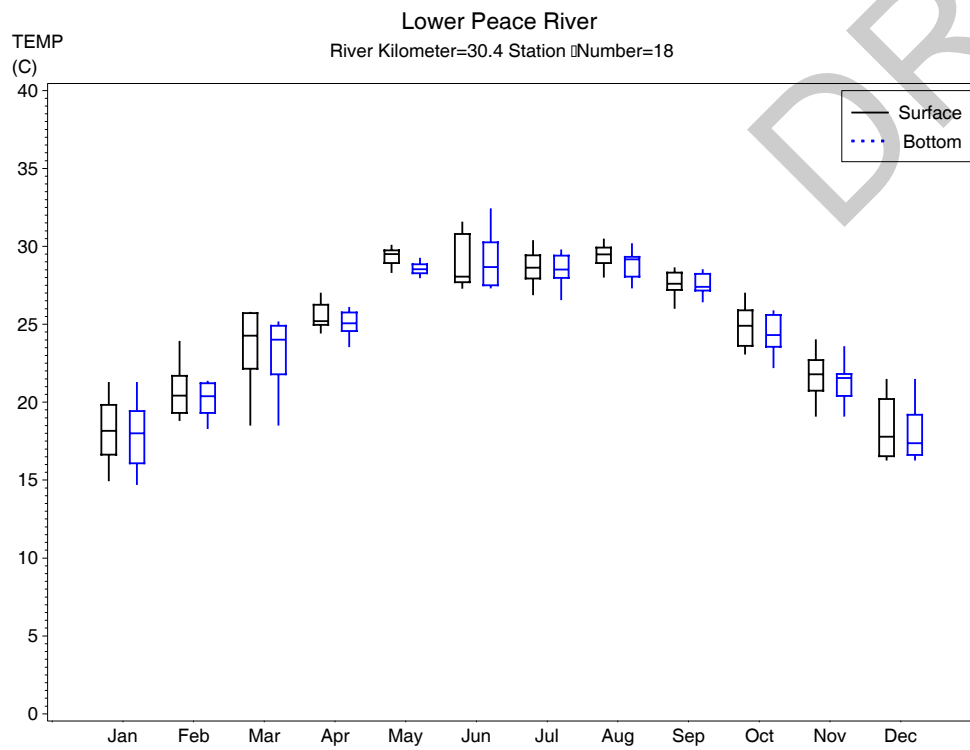
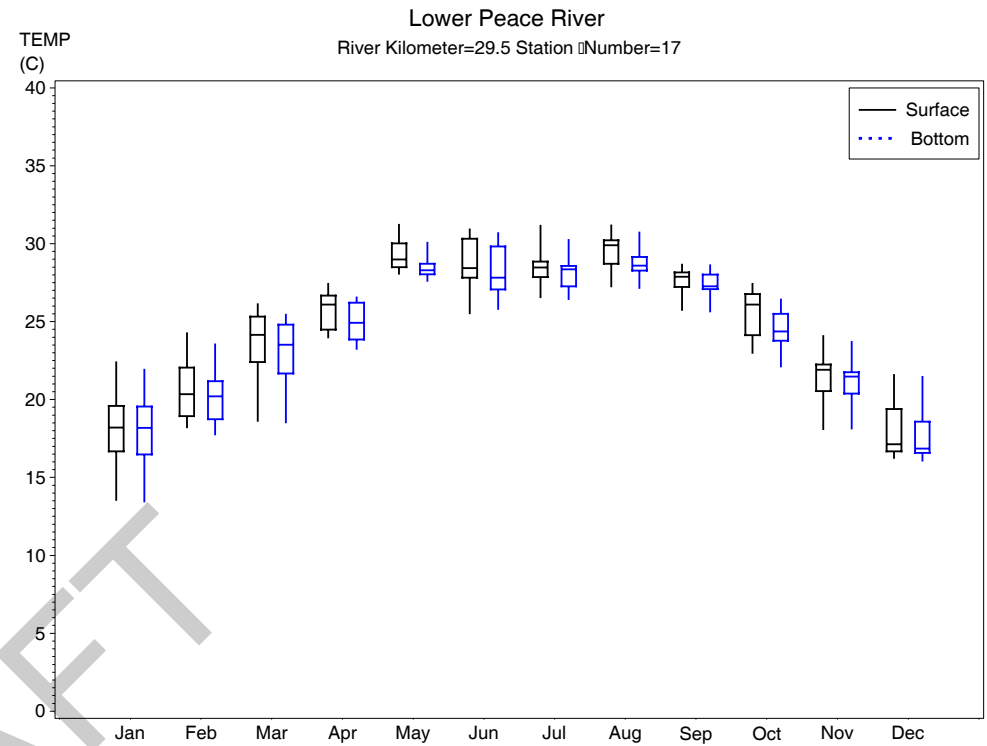
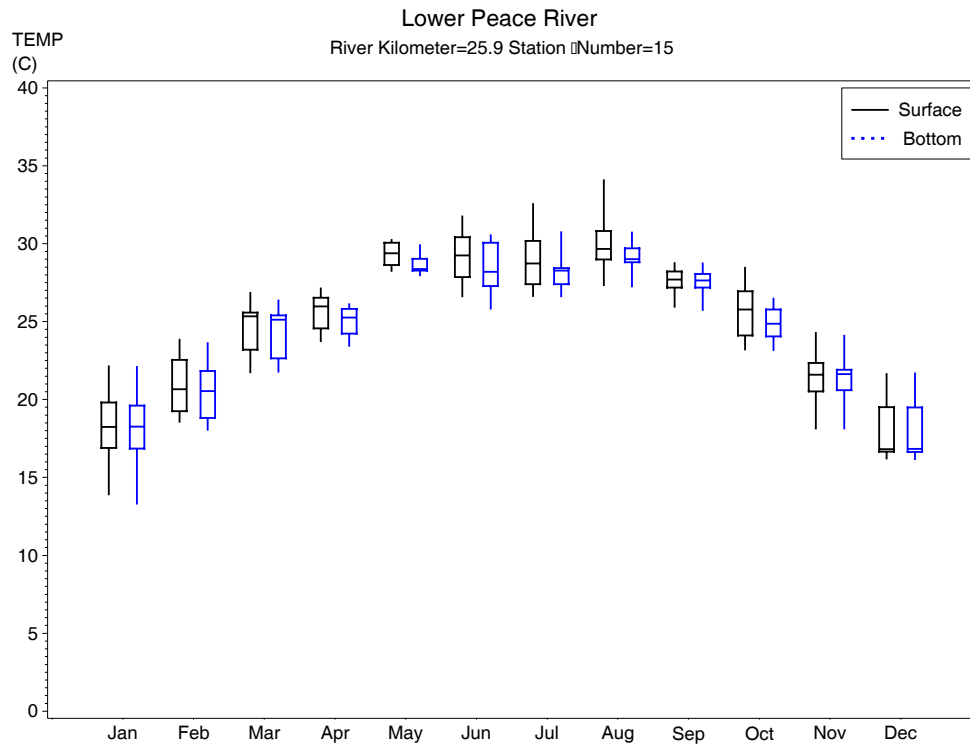


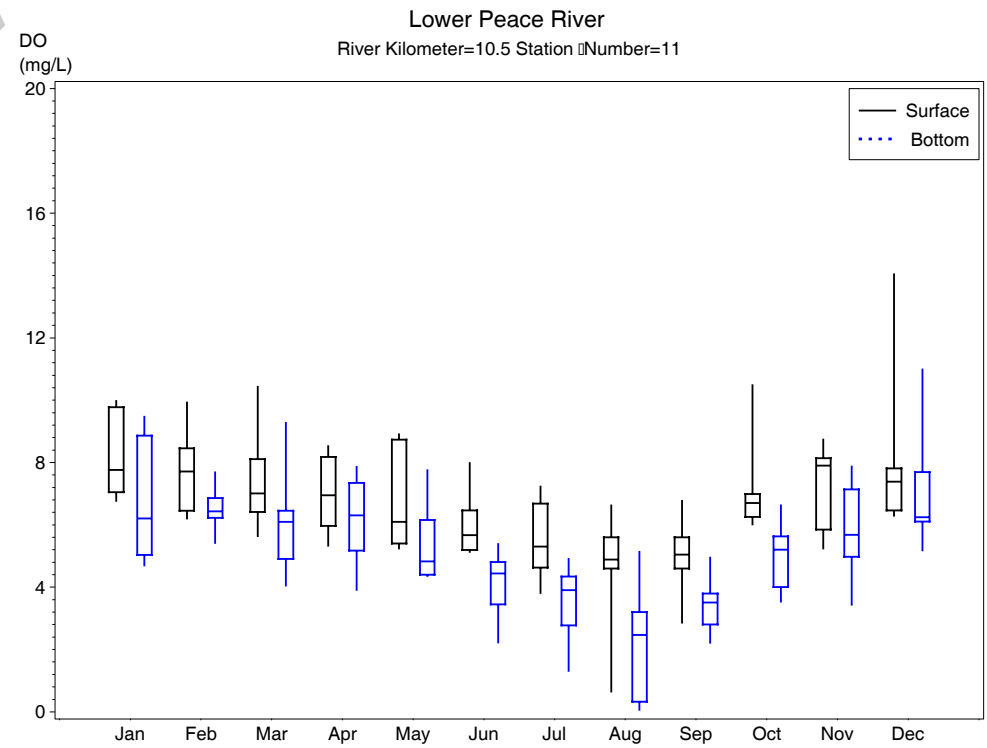
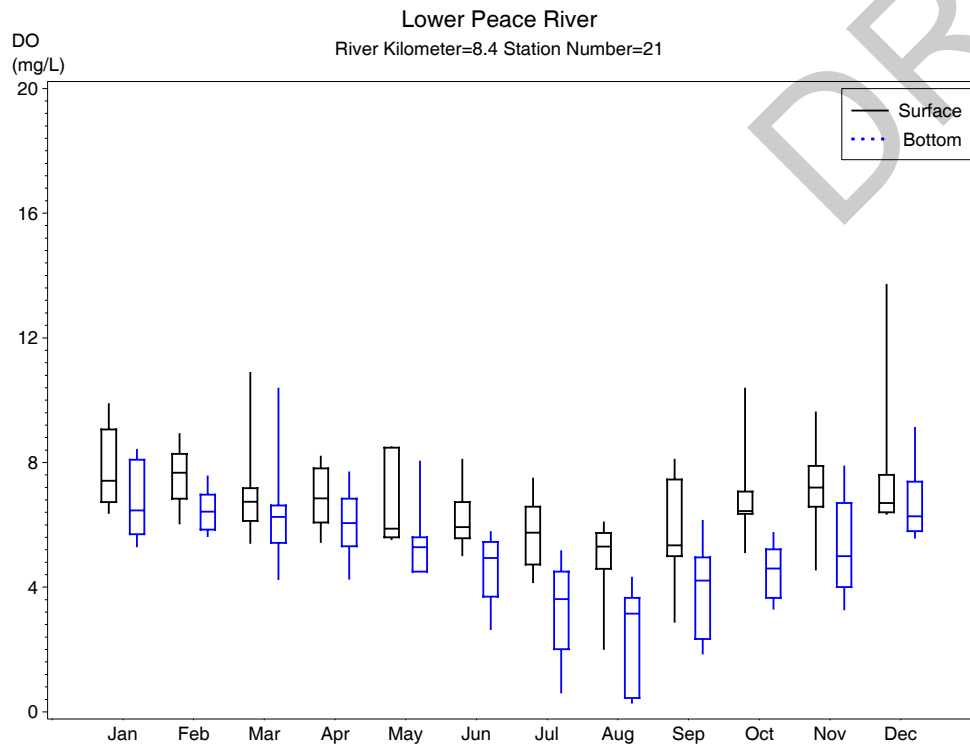
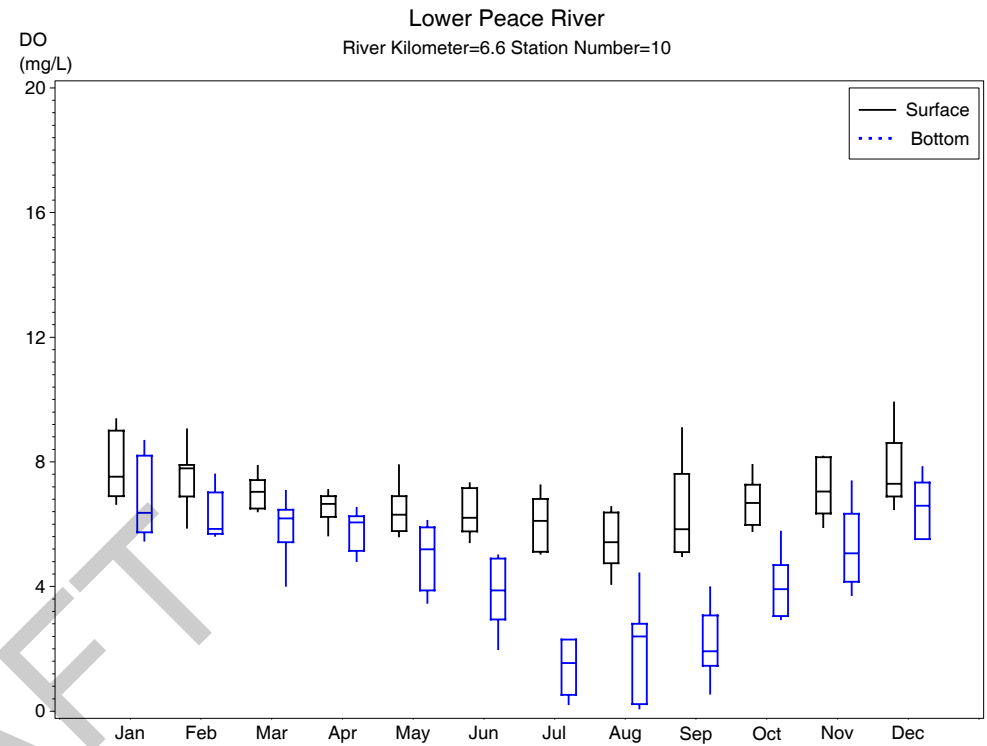
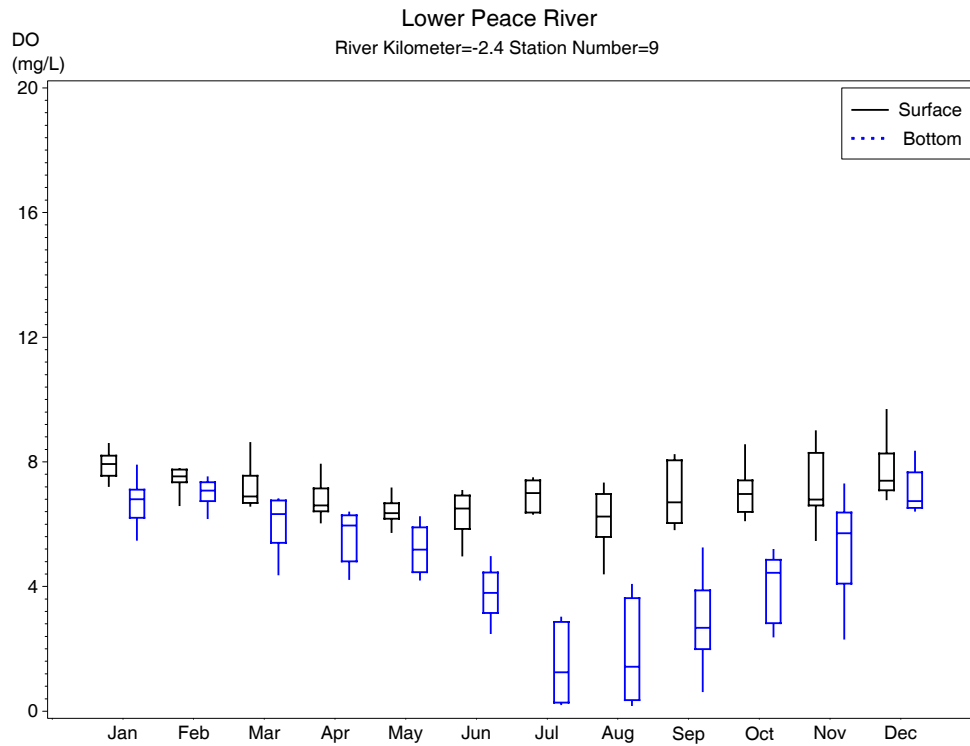


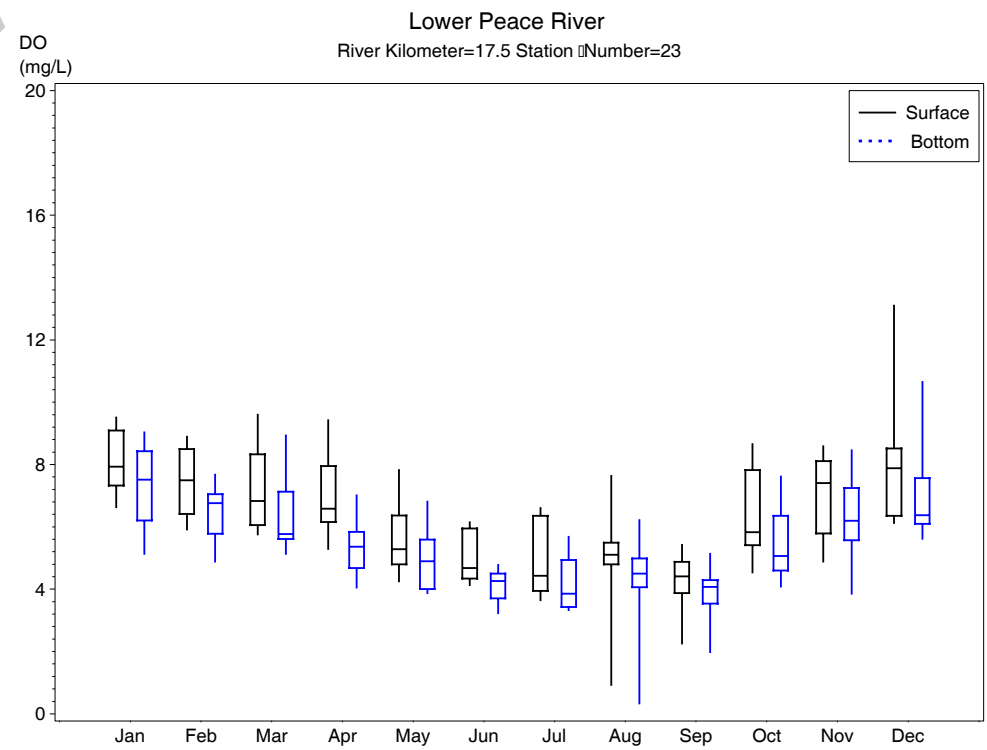
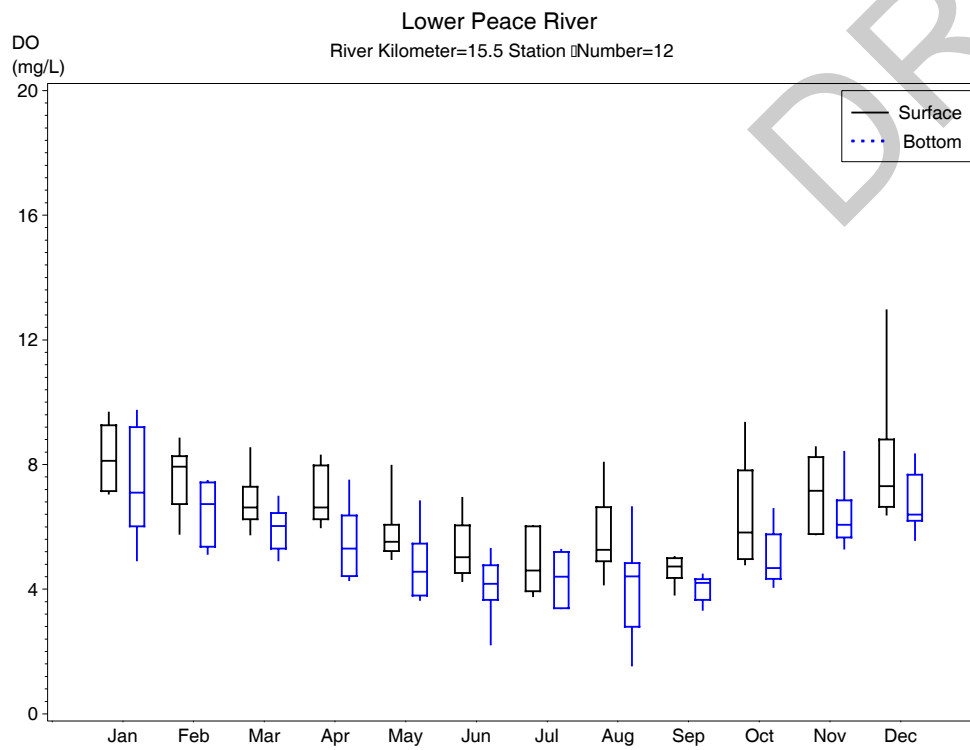
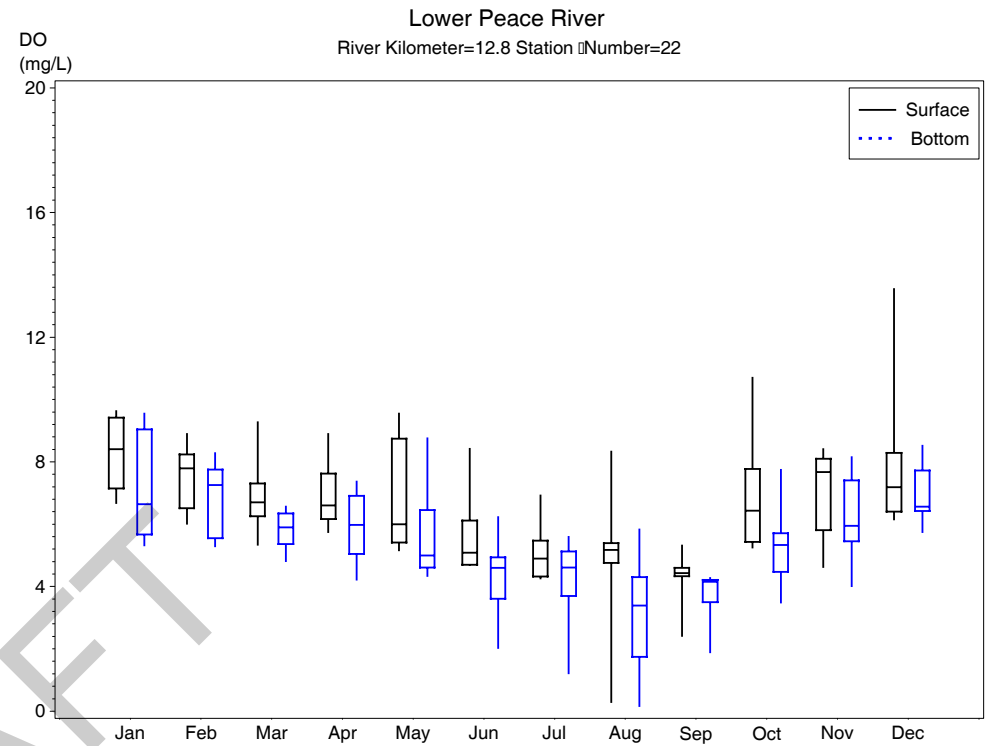
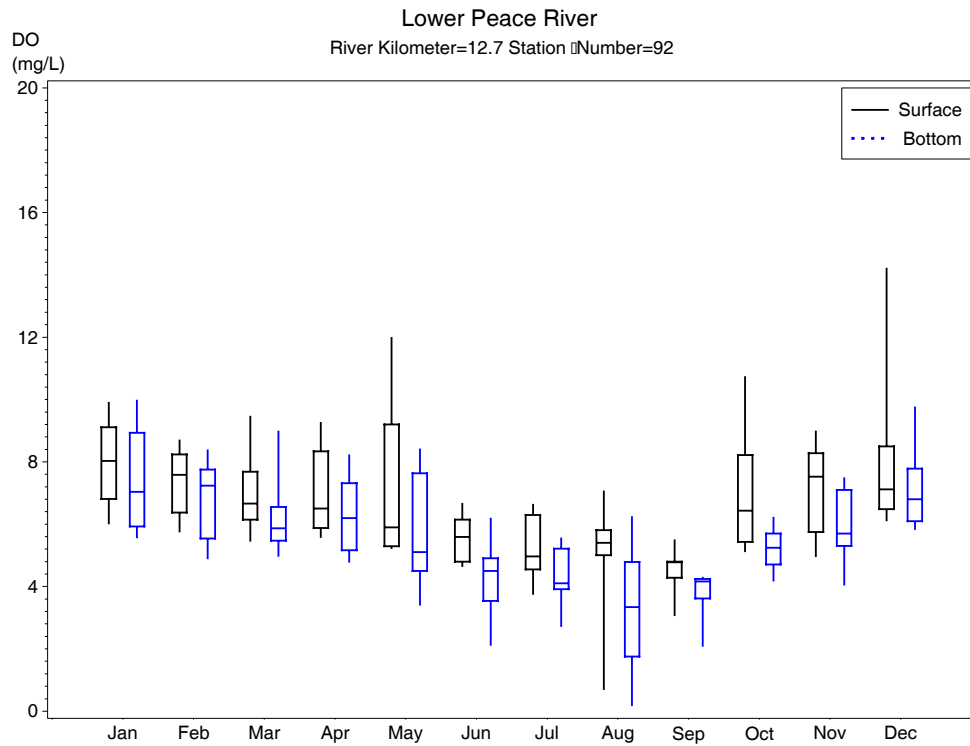


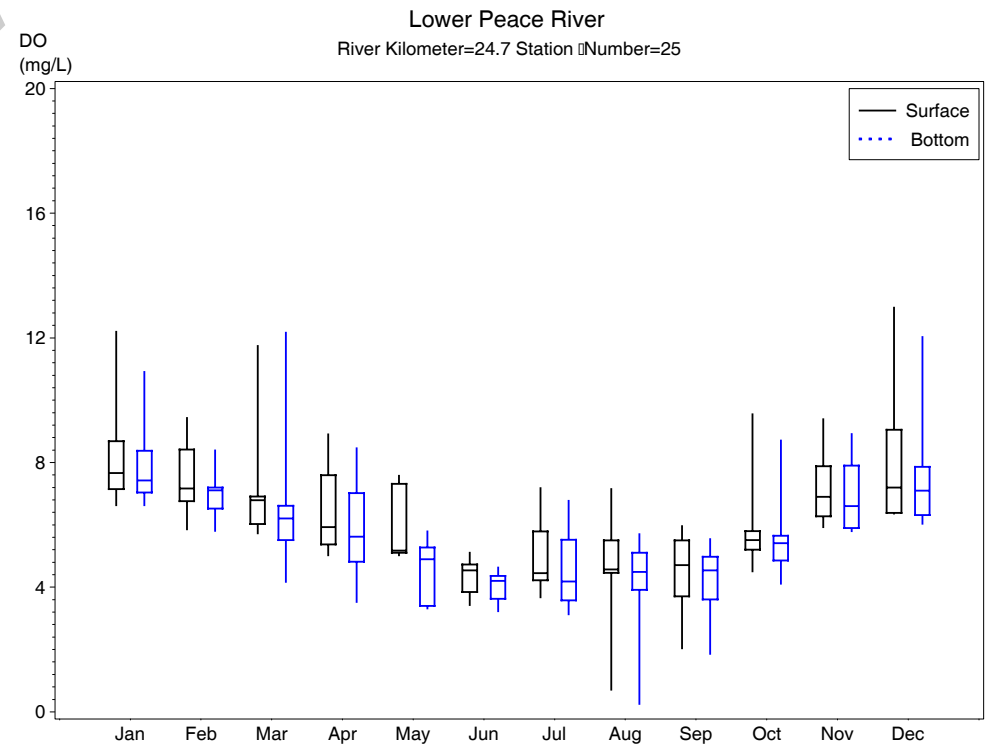
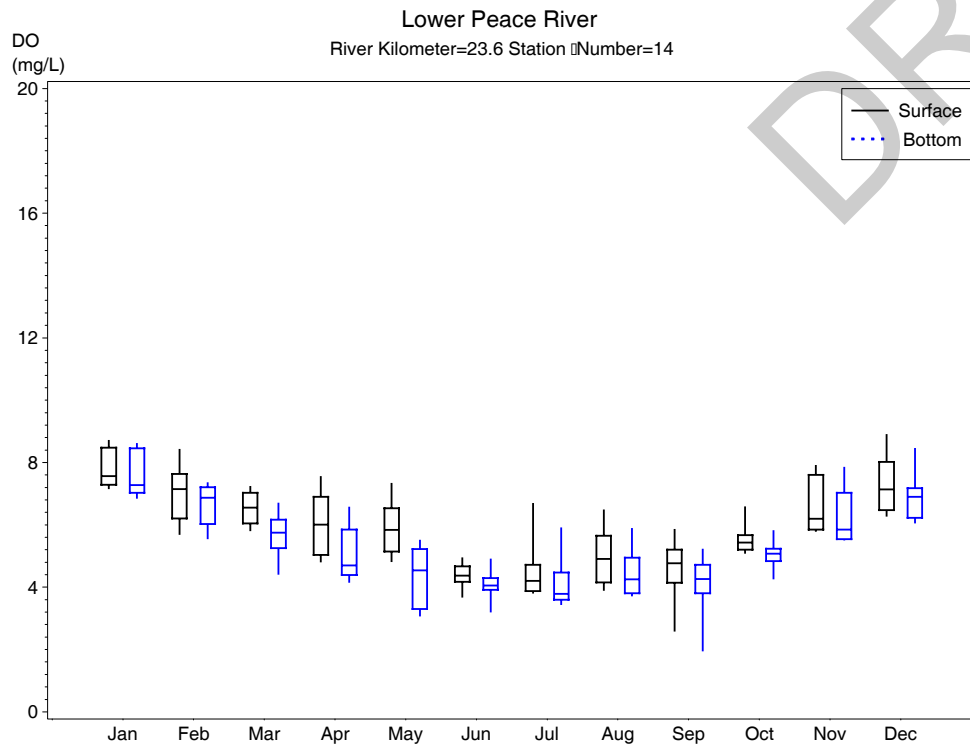
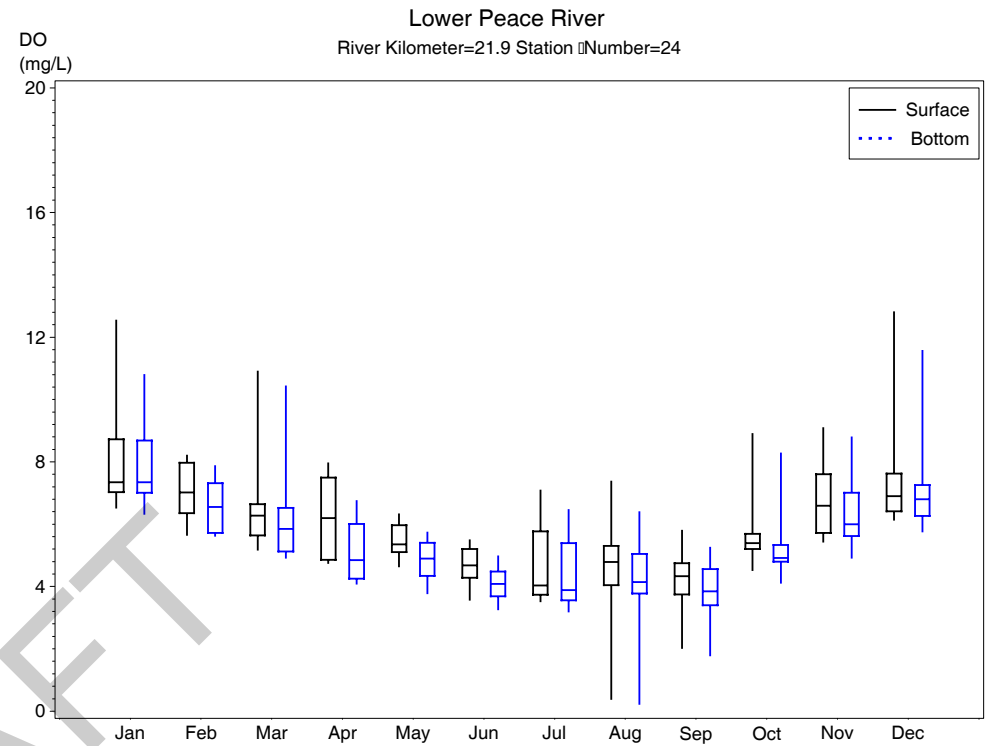
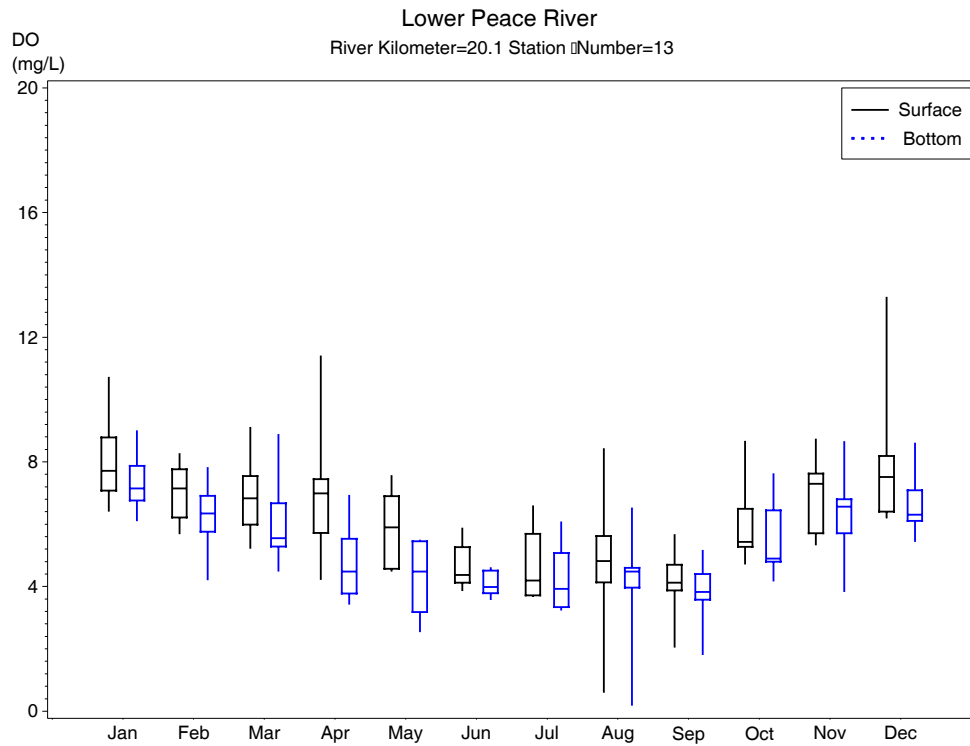


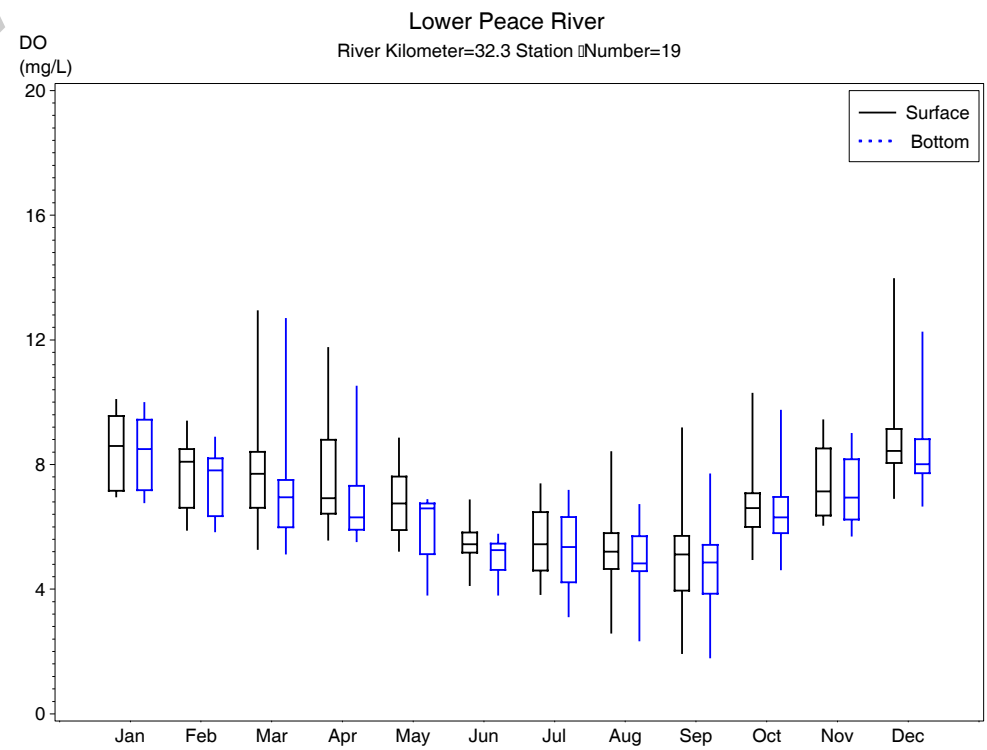
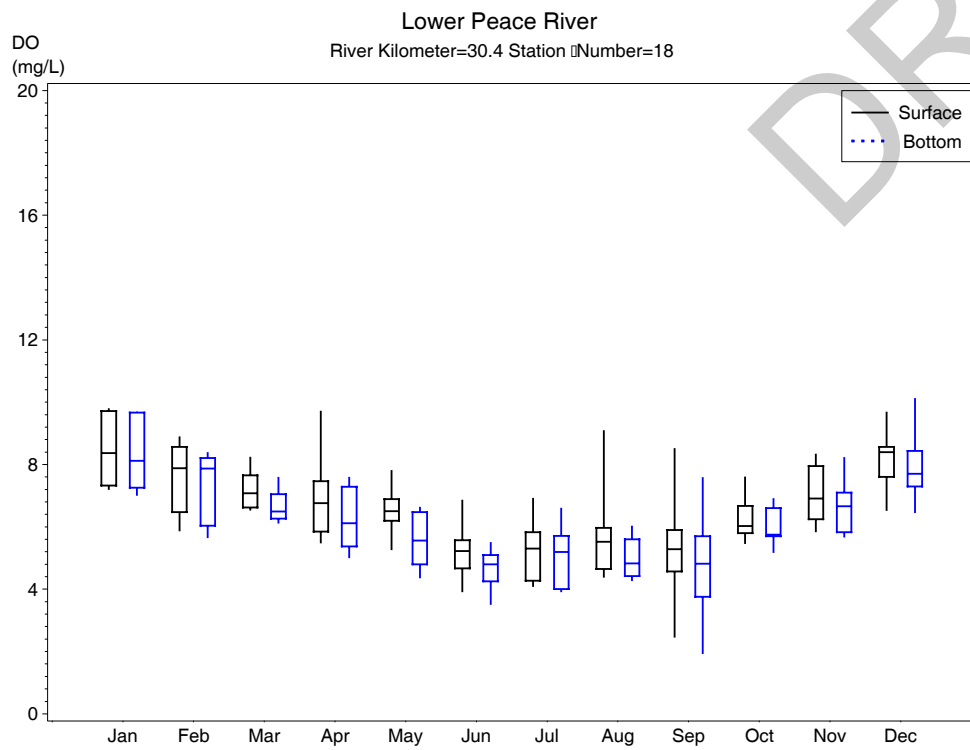
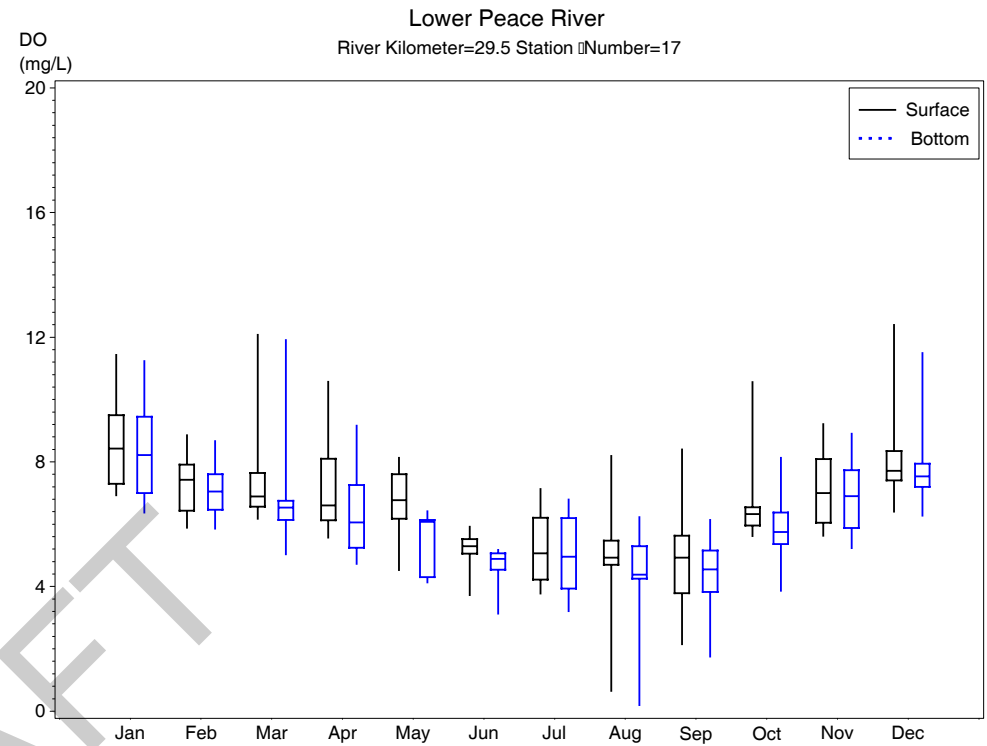
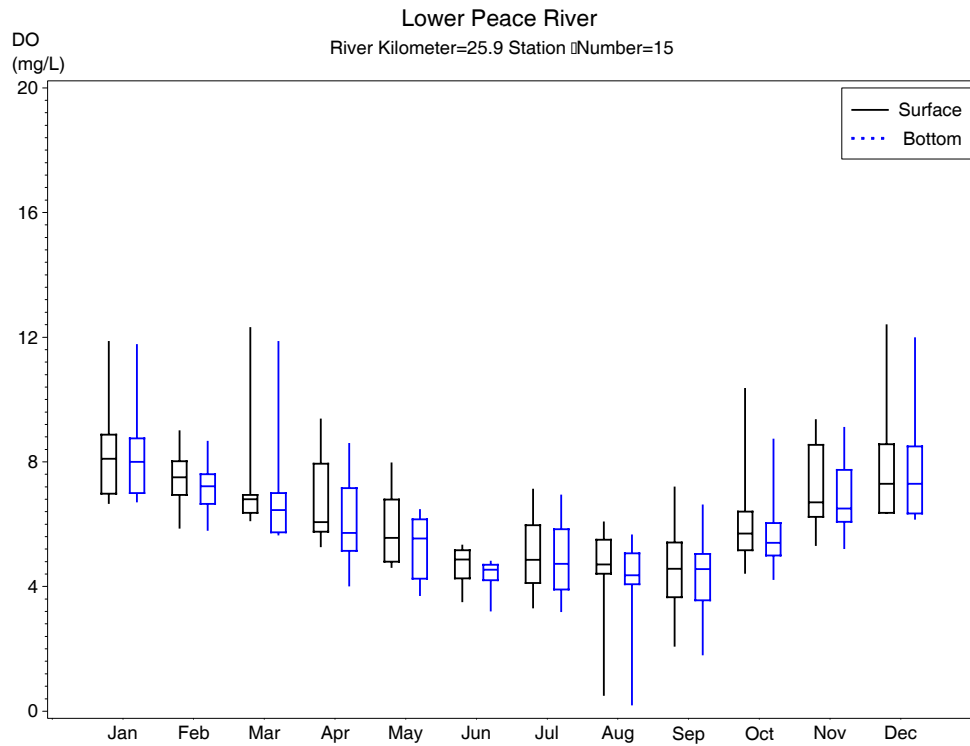


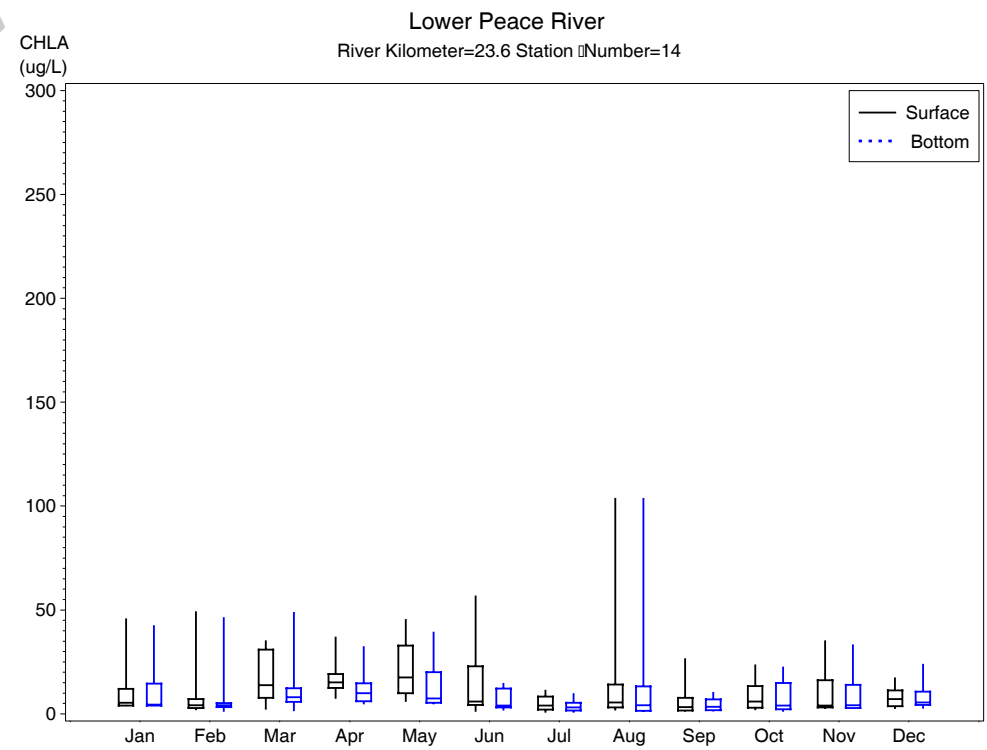
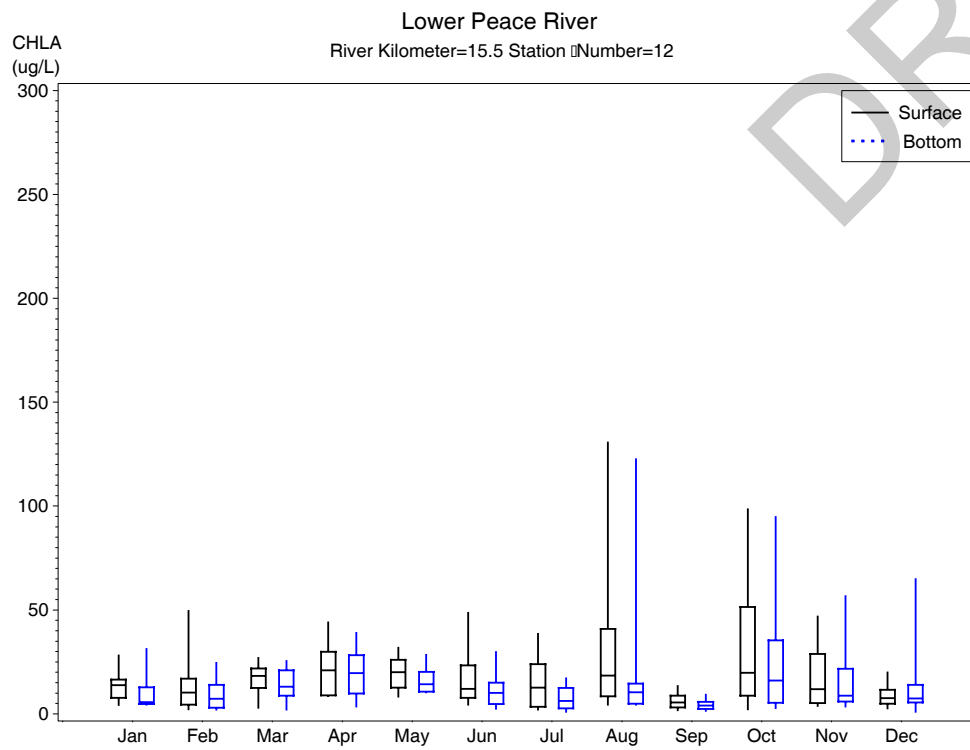
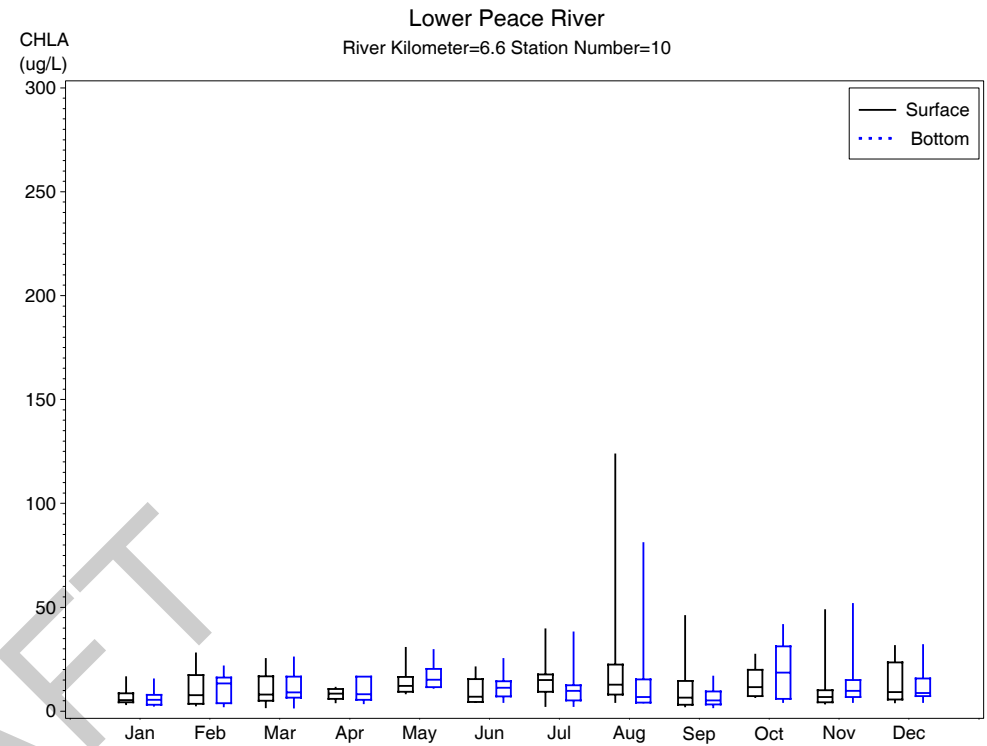
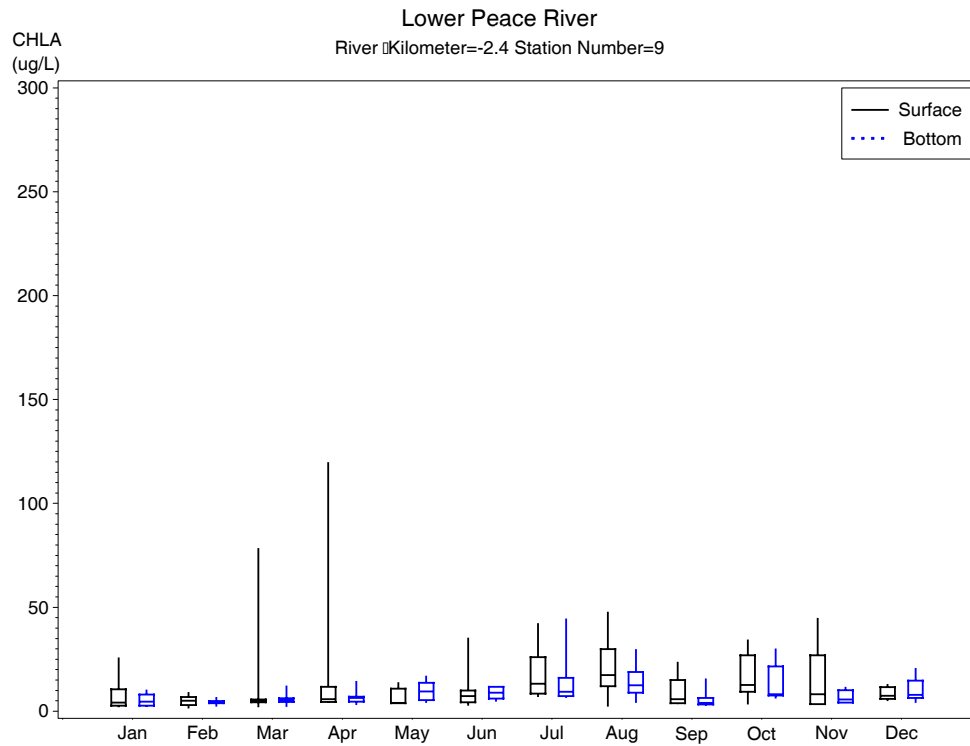


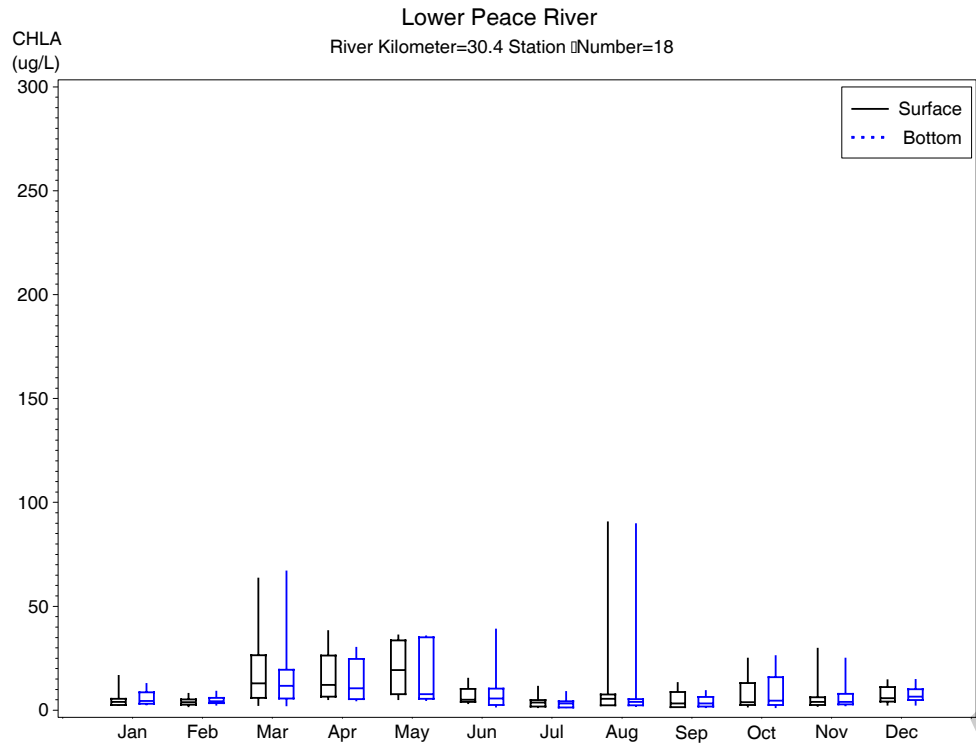


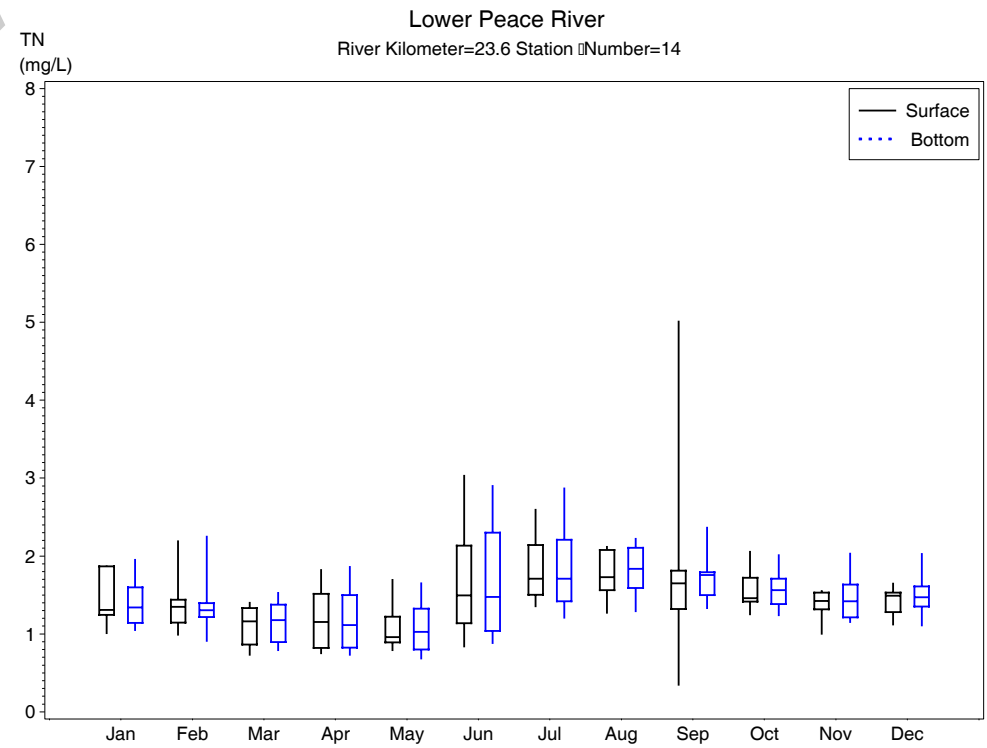
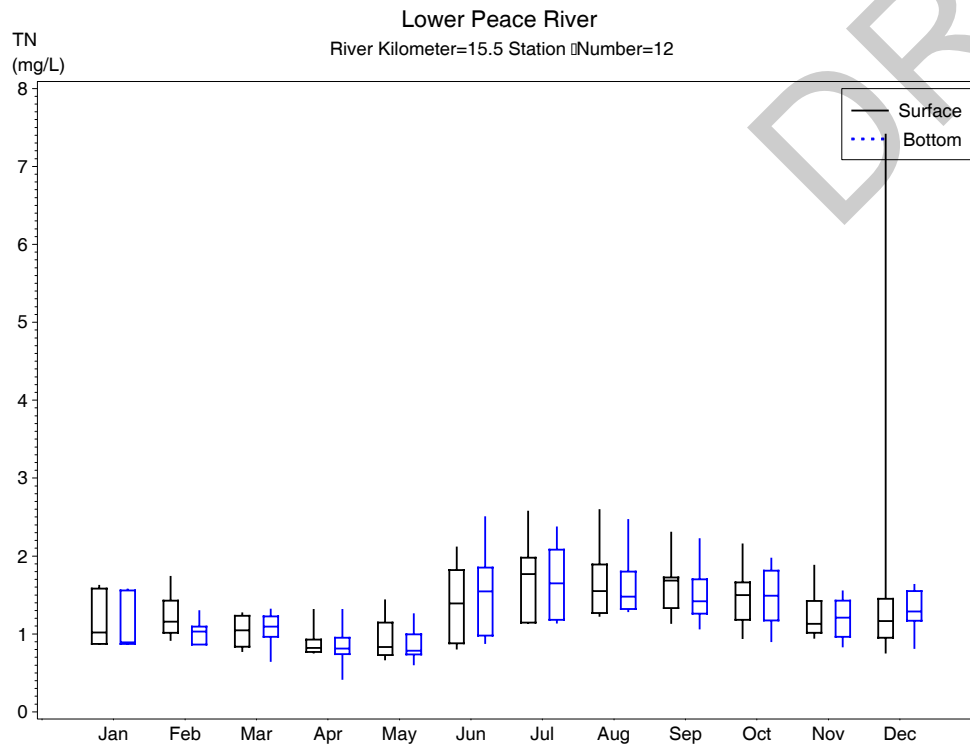
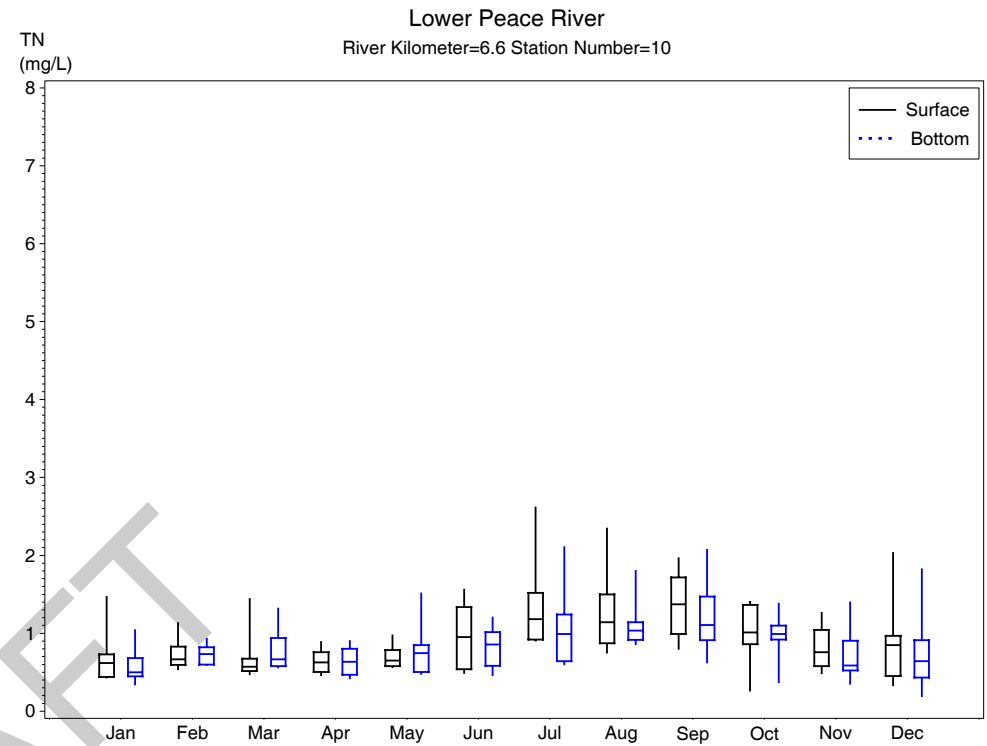
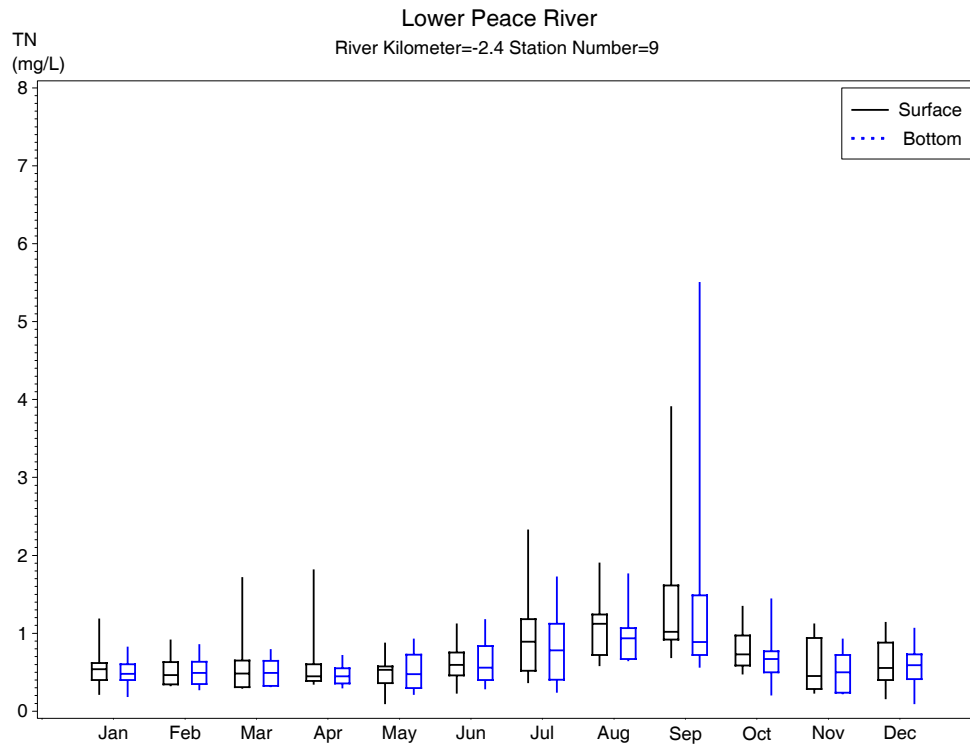


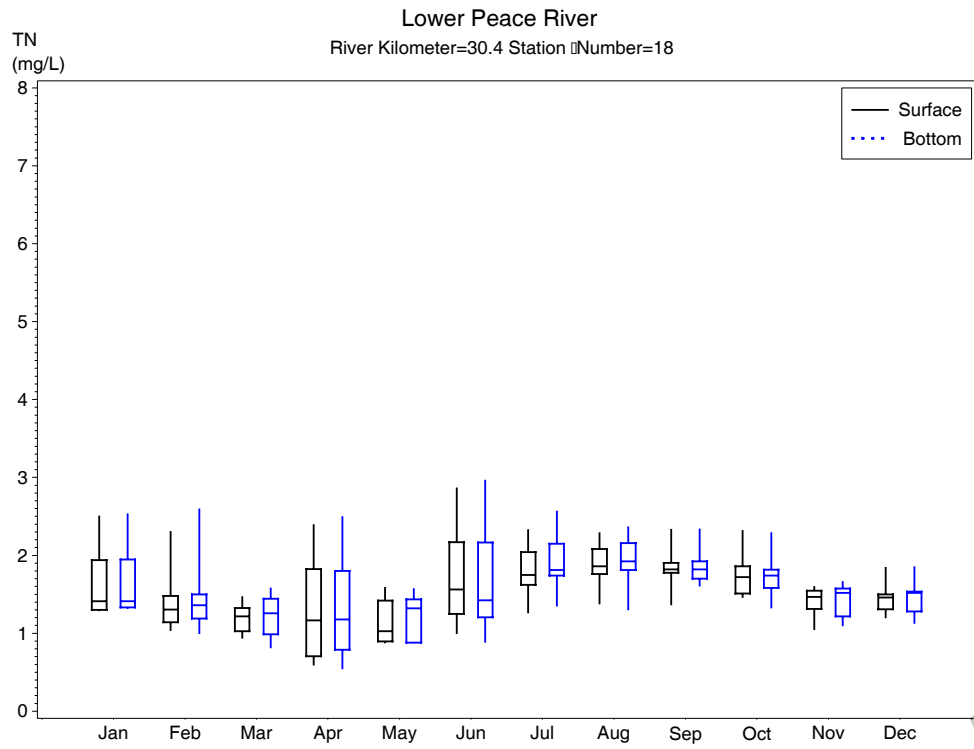


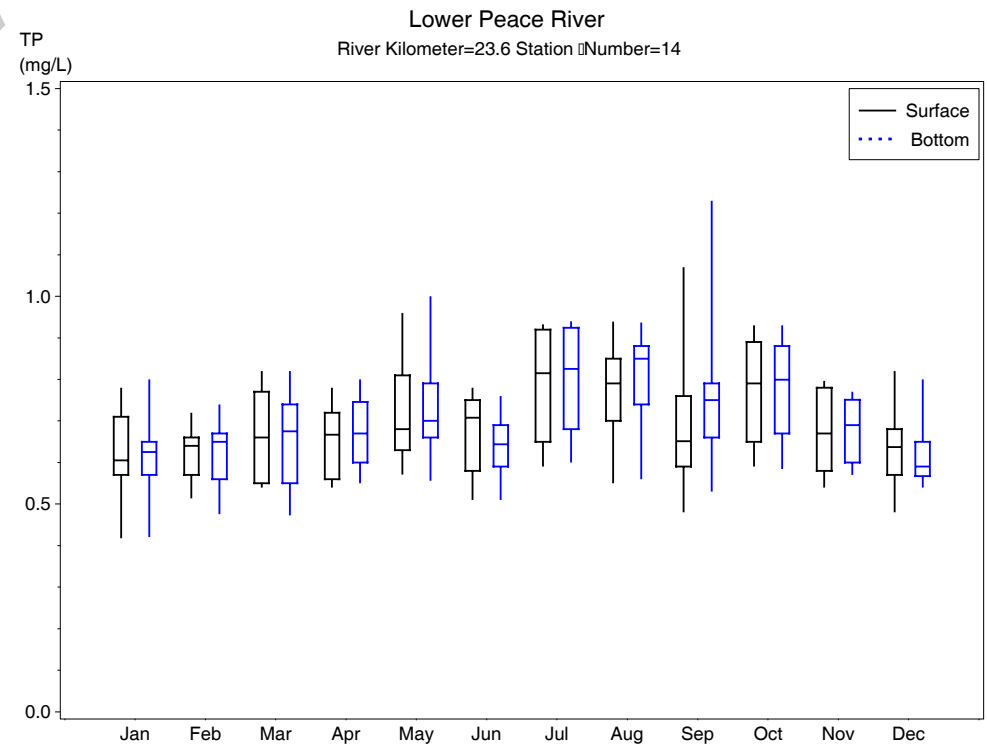
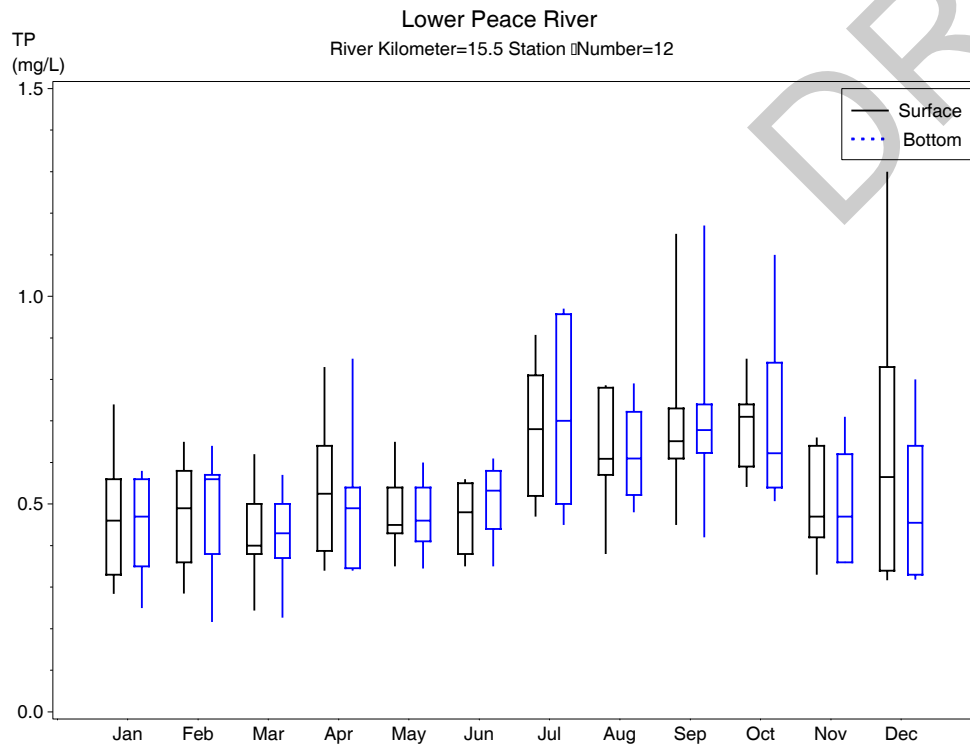
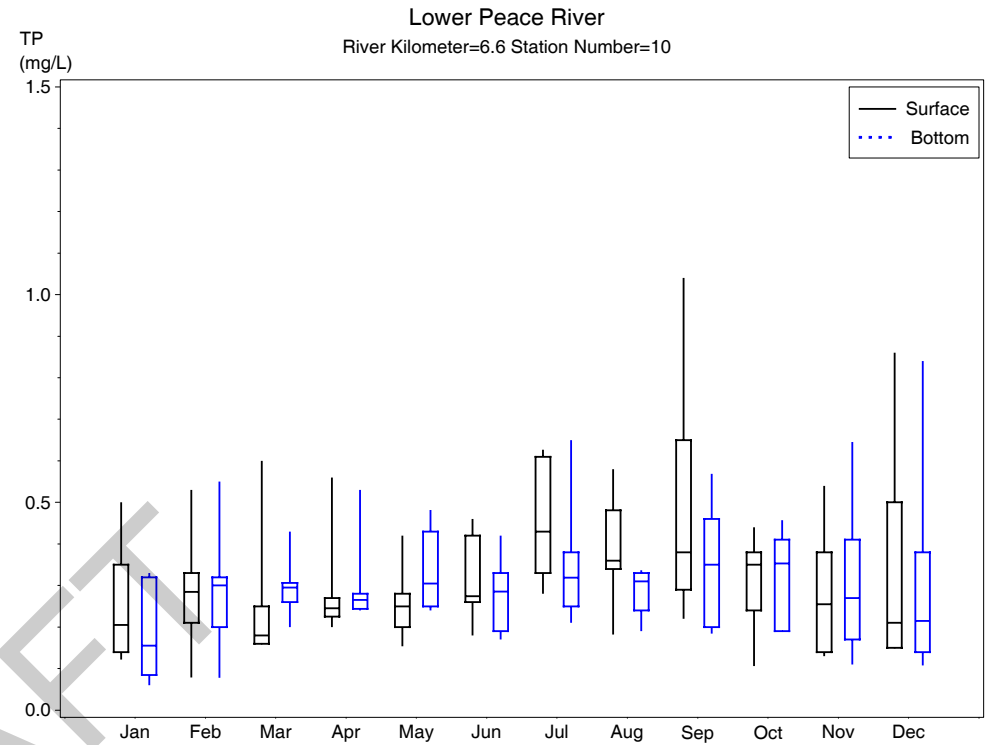
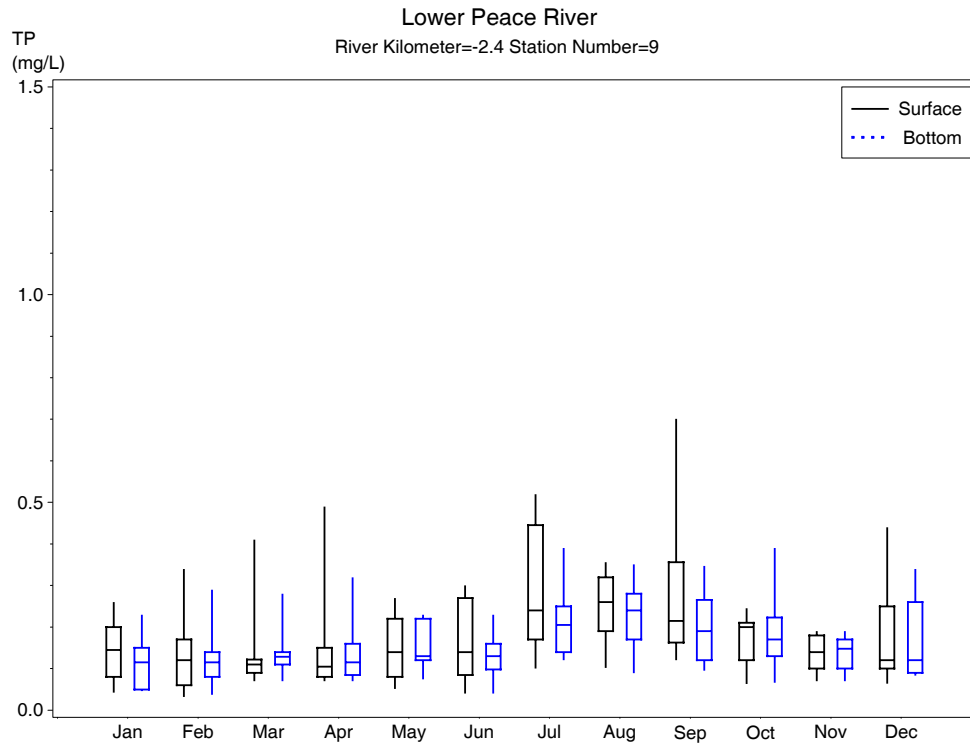


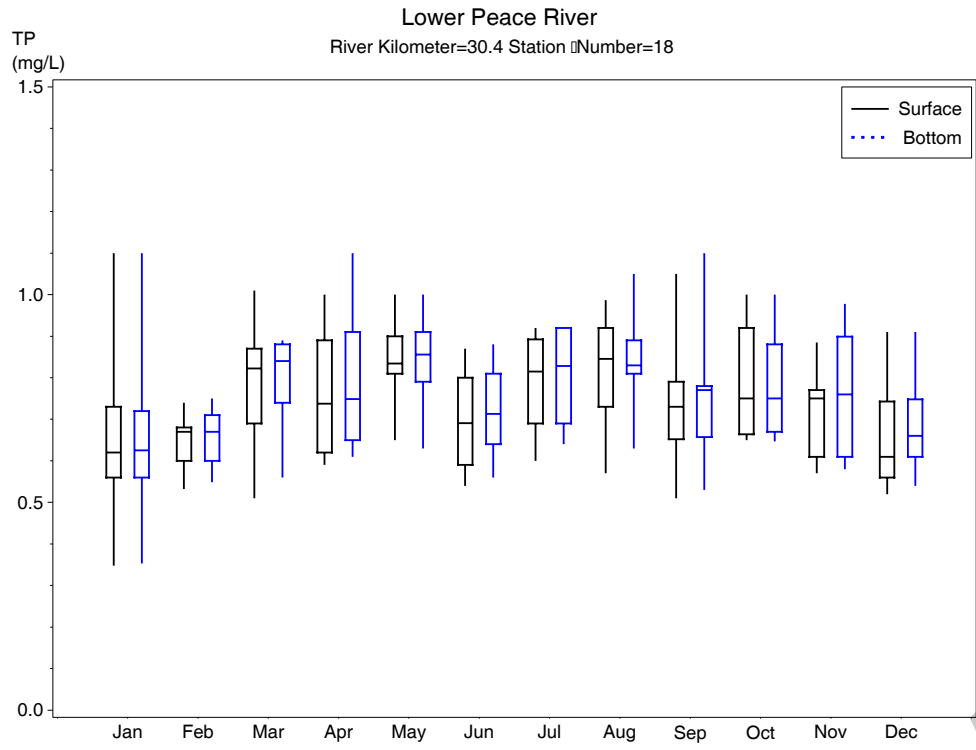










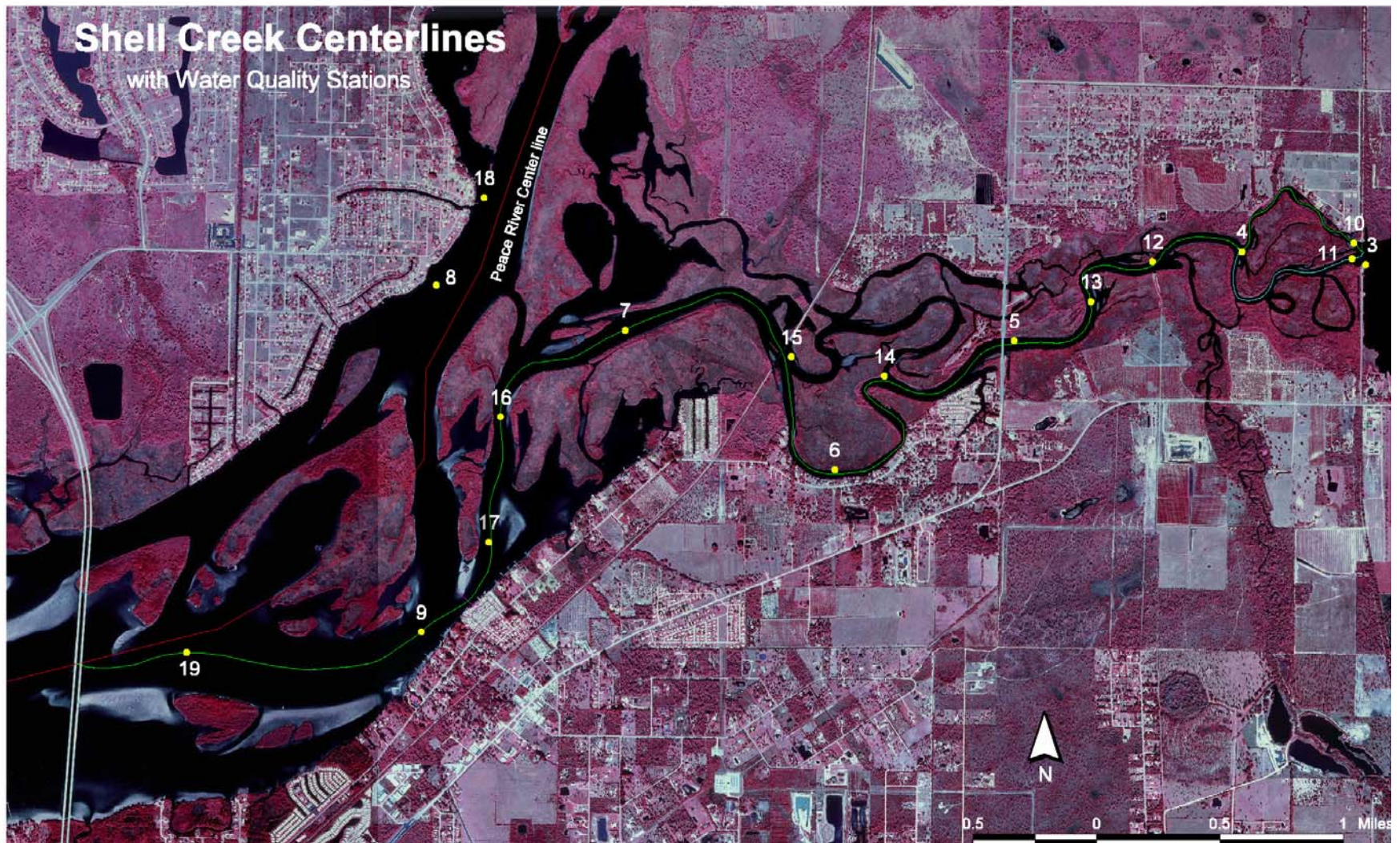


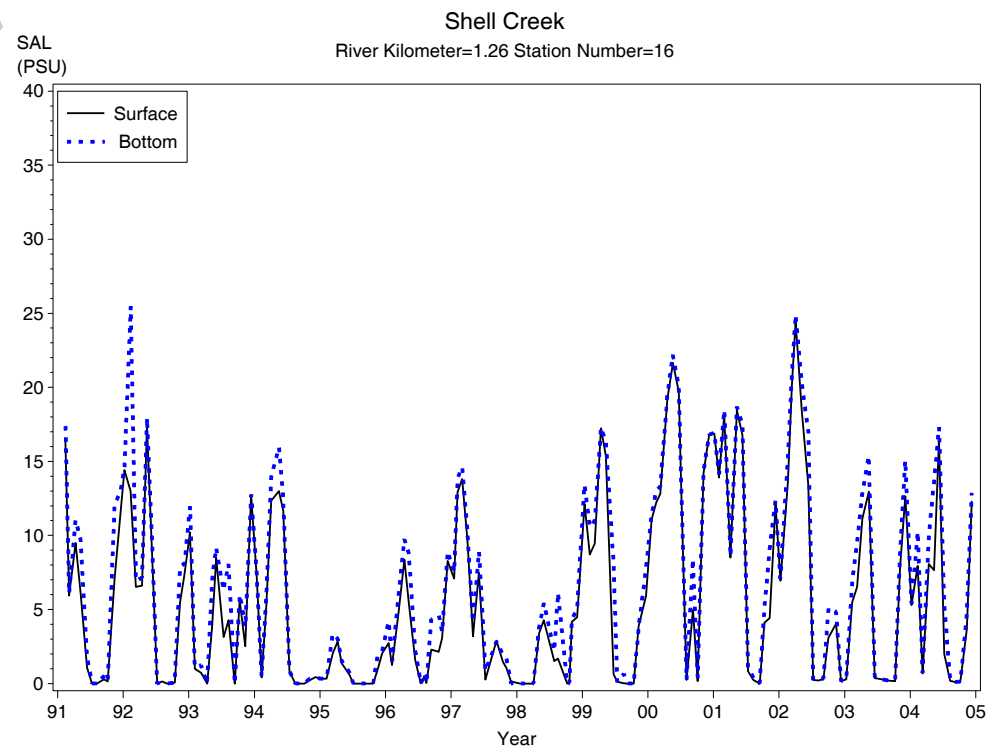
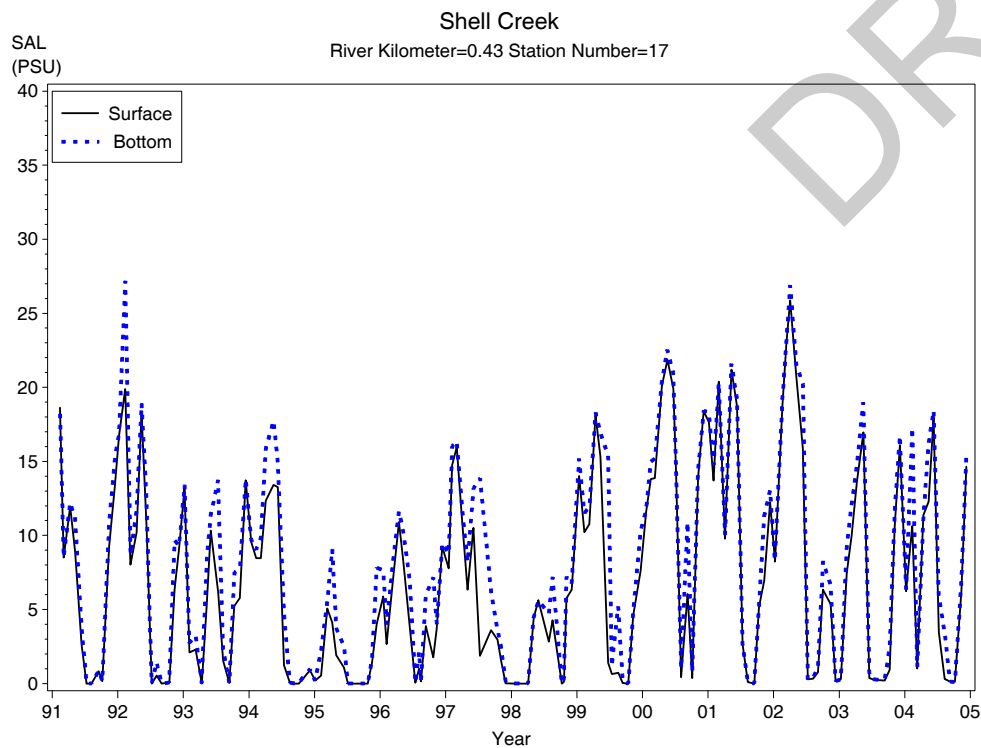
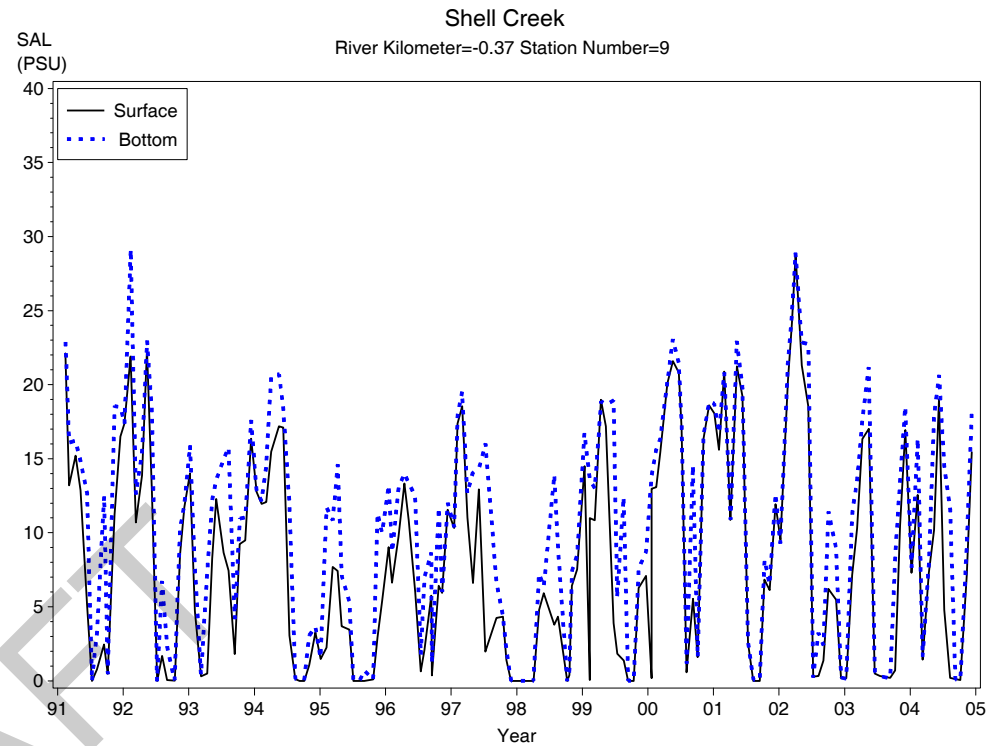
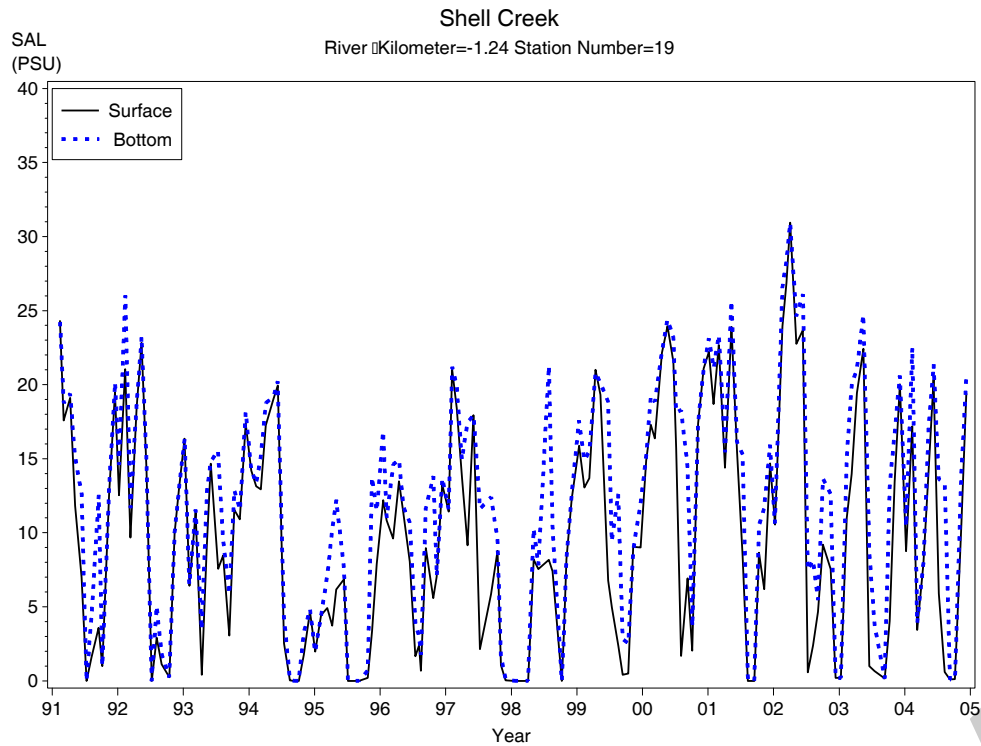
Appendix 3-3

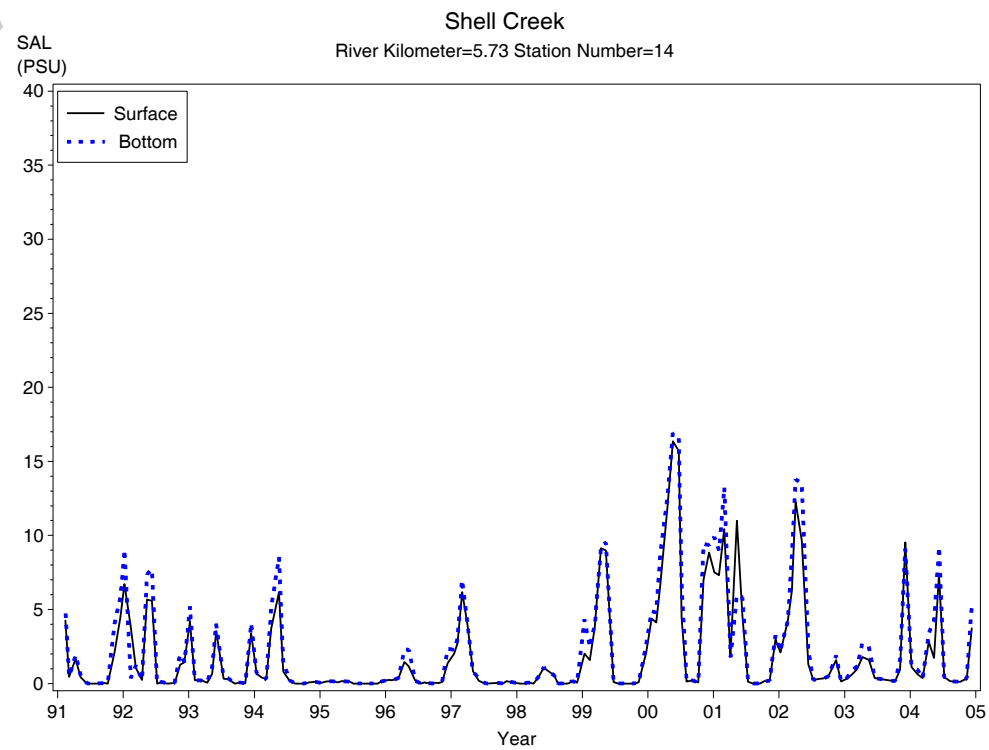
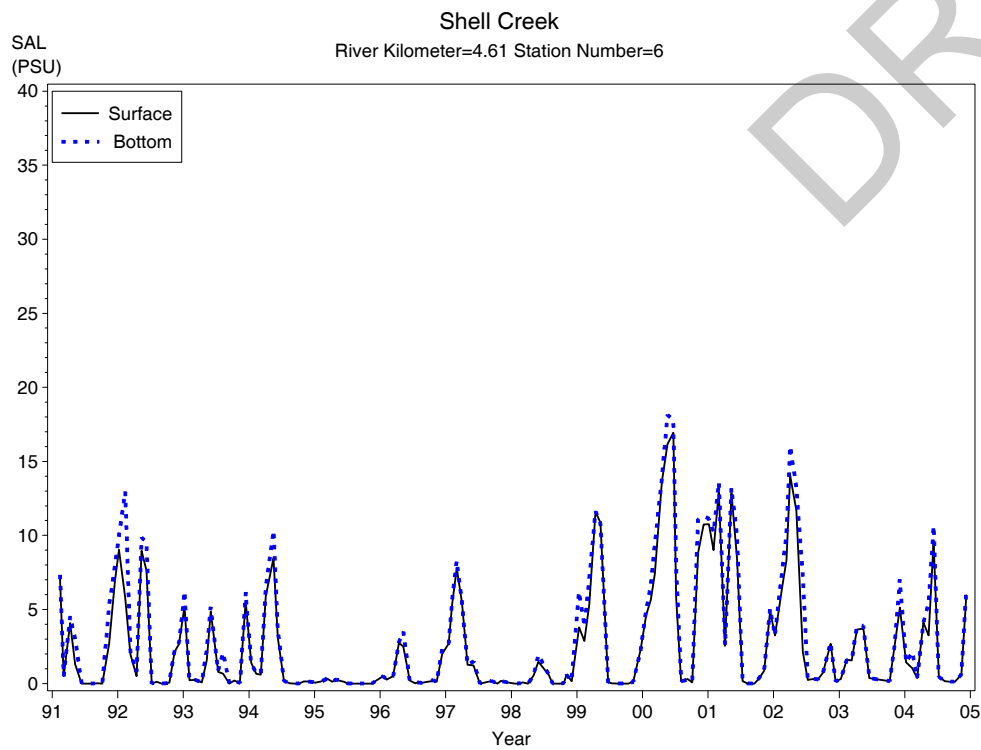
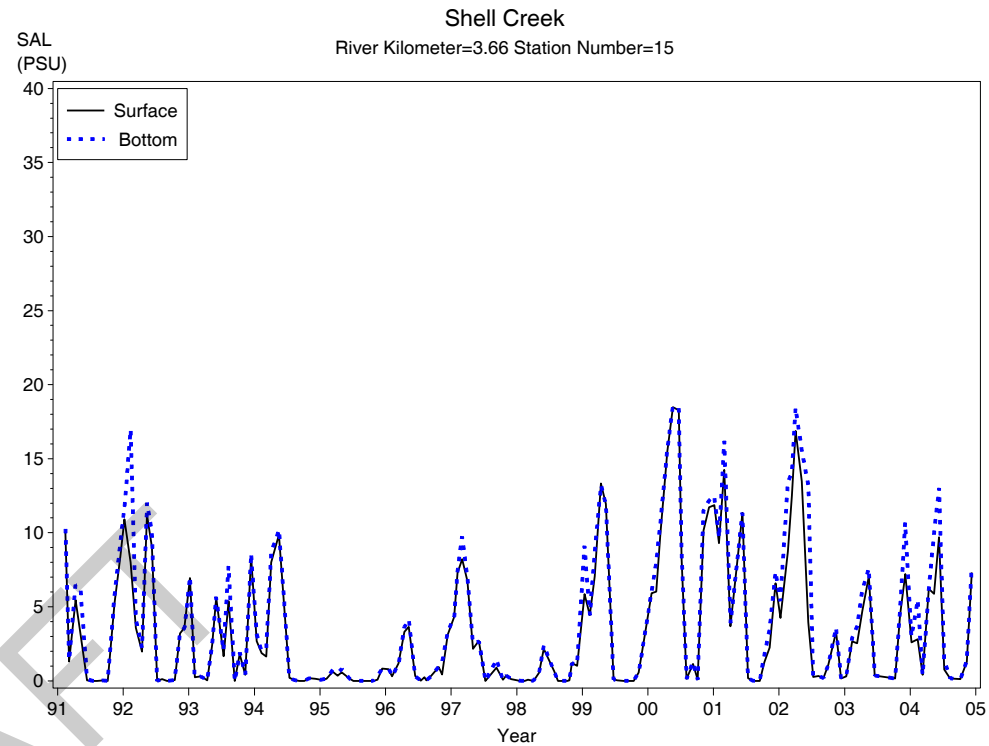
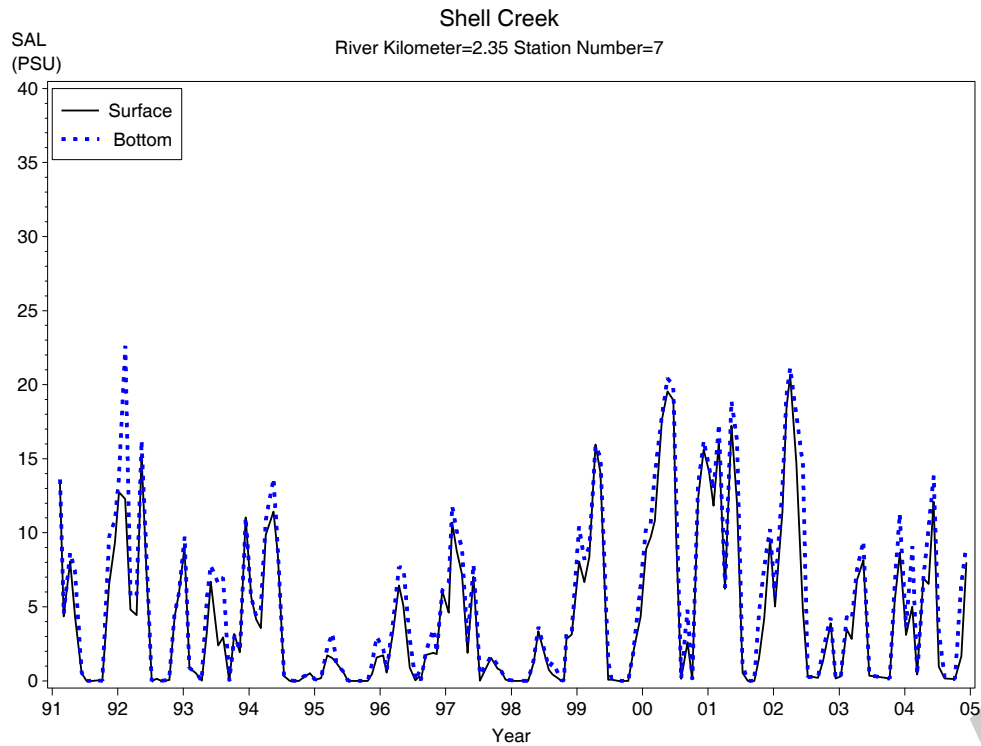
Annual Variation in Shell Creek Water Quality Constituents

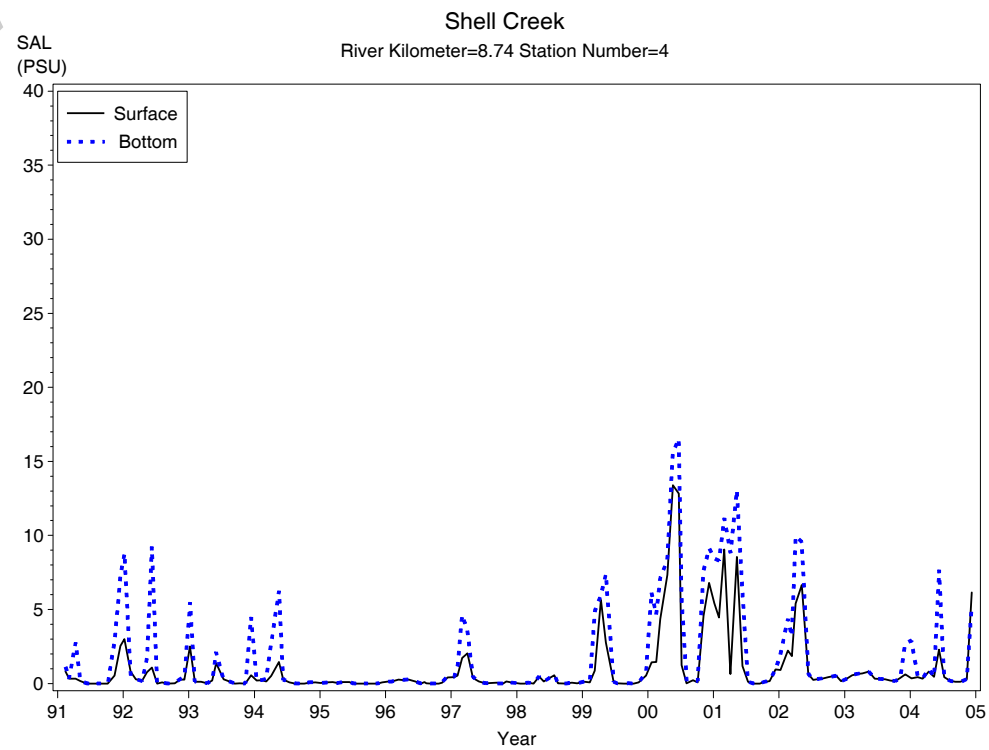
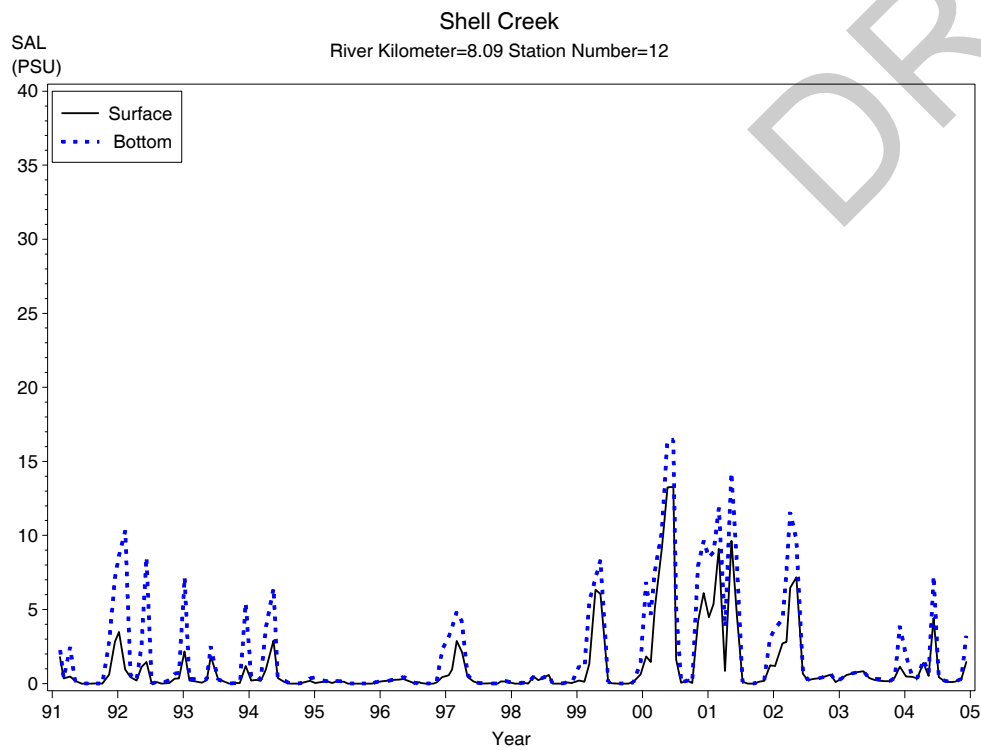
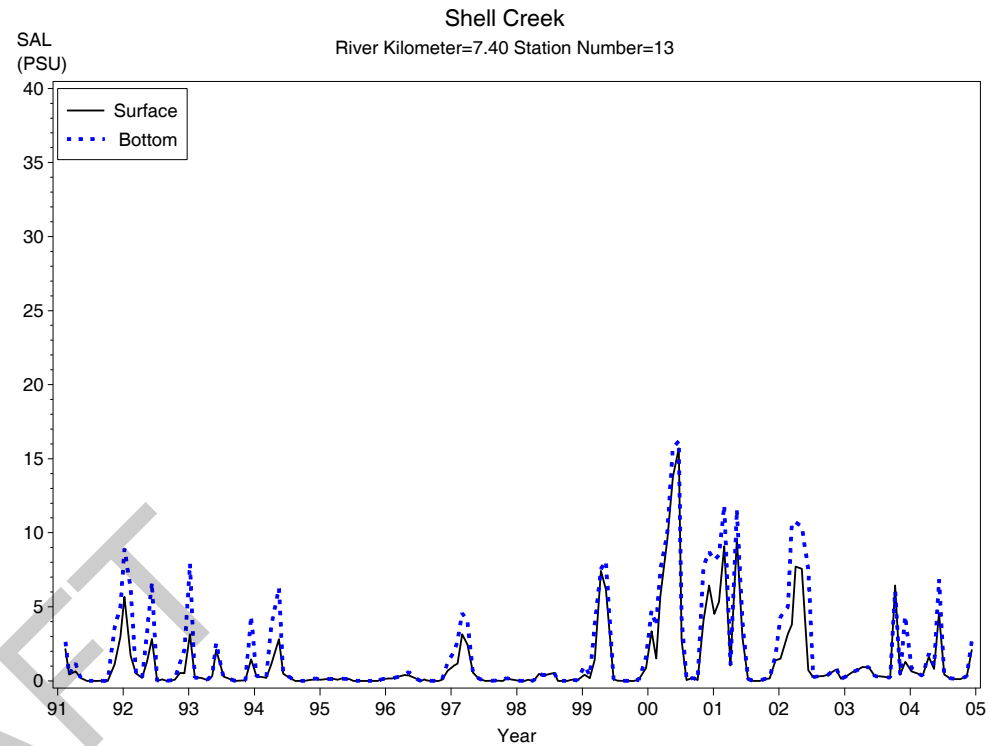
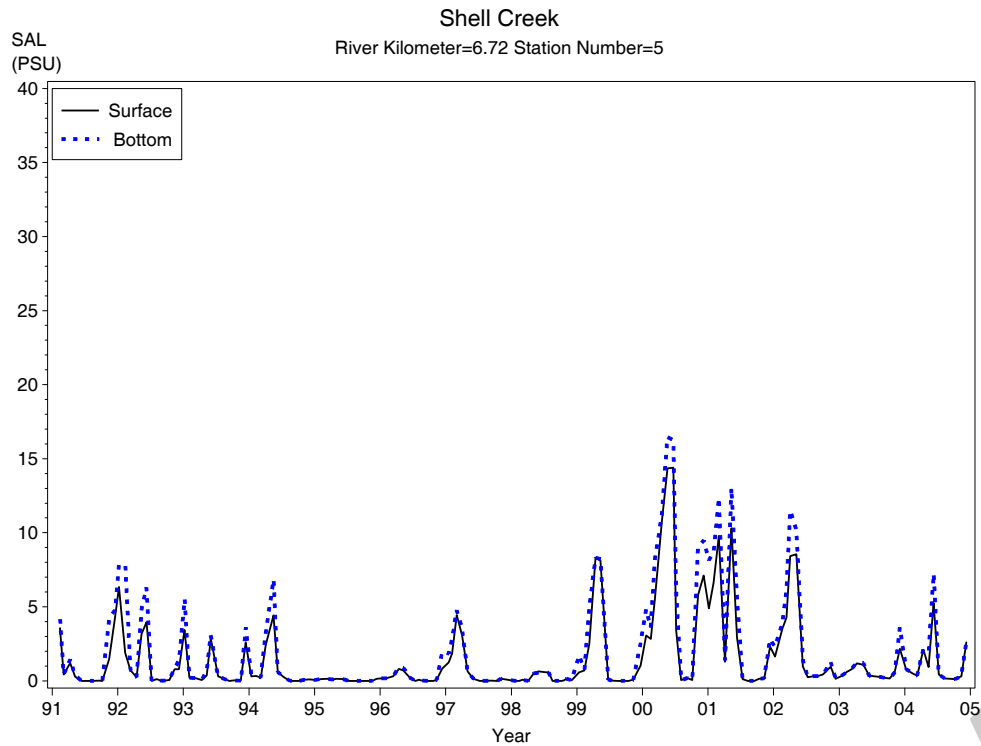
Shell Creek Centerlines

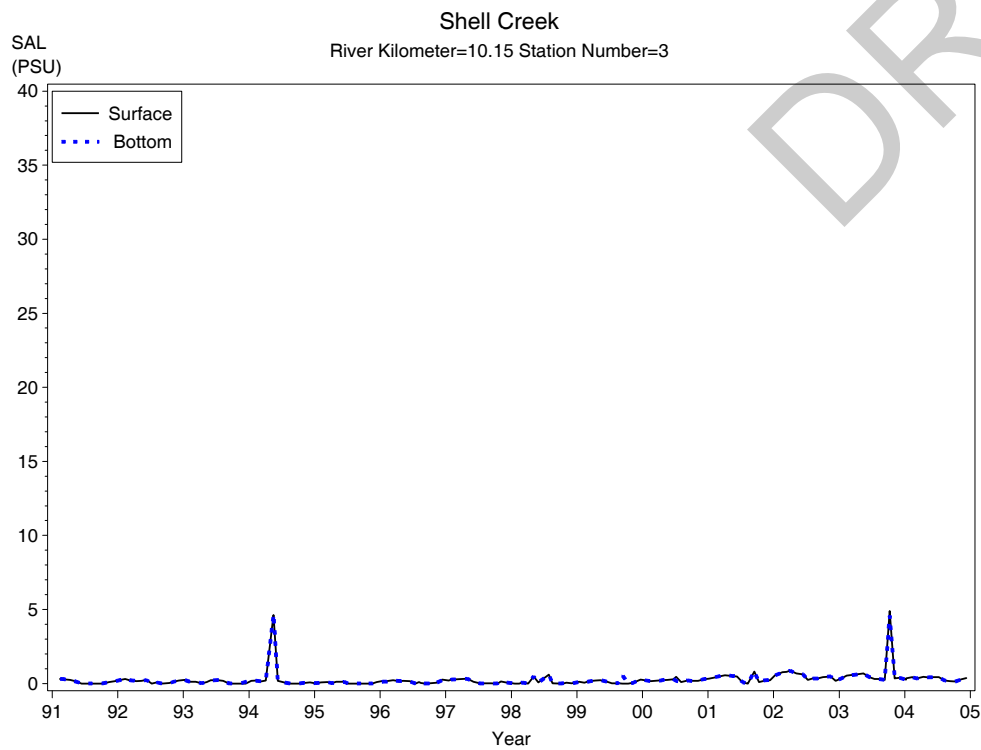
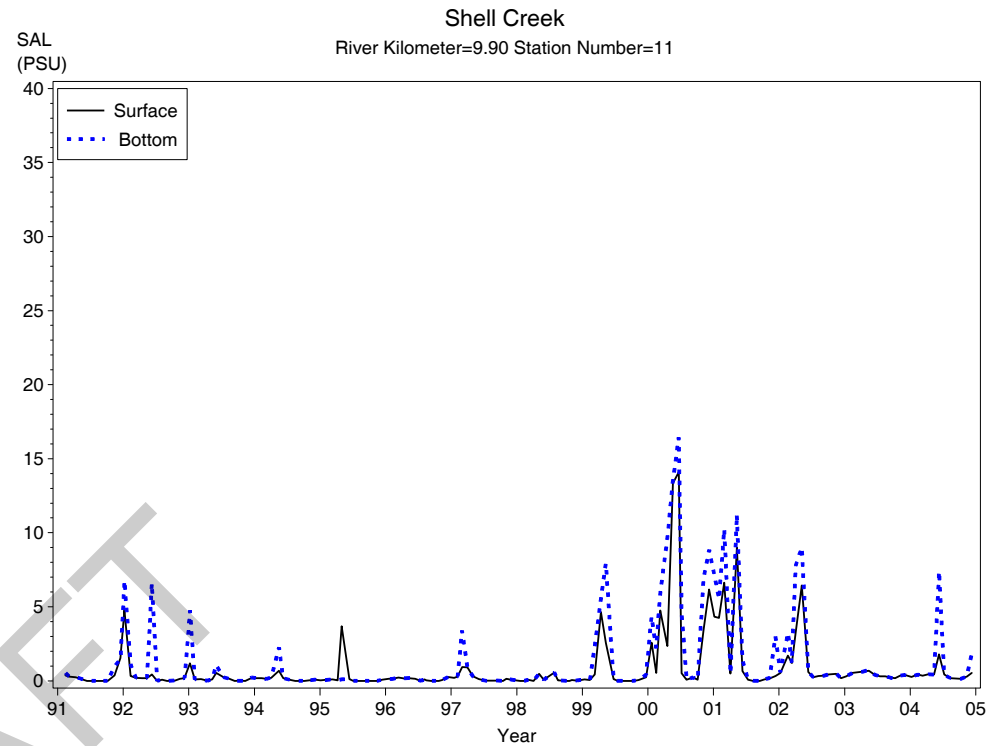
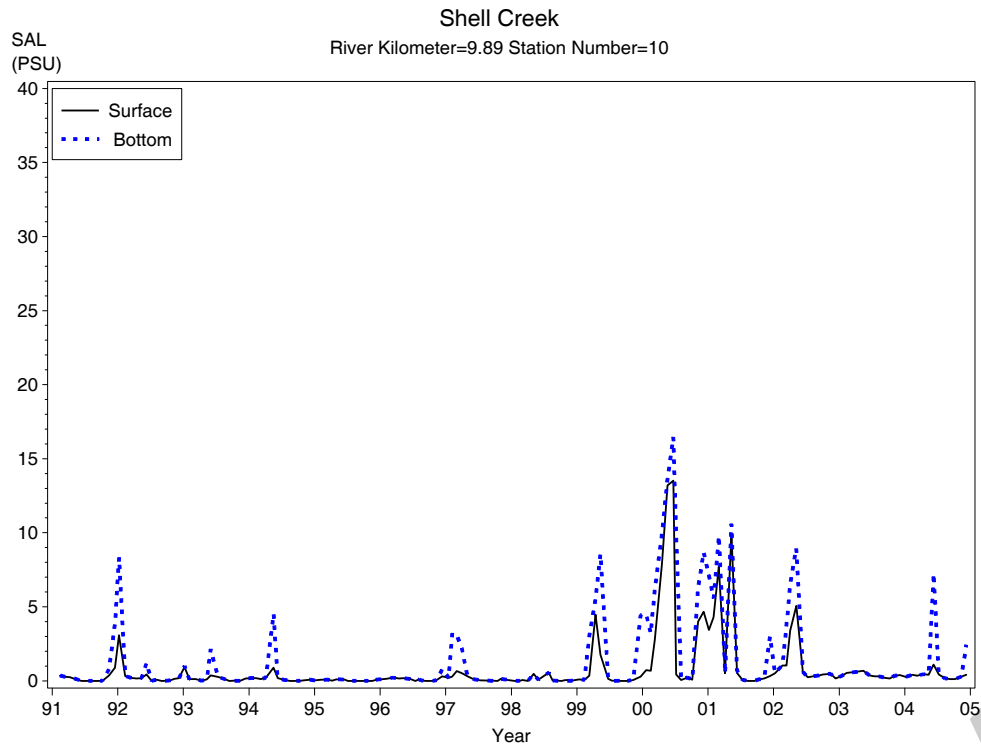
with Water Quality Stations

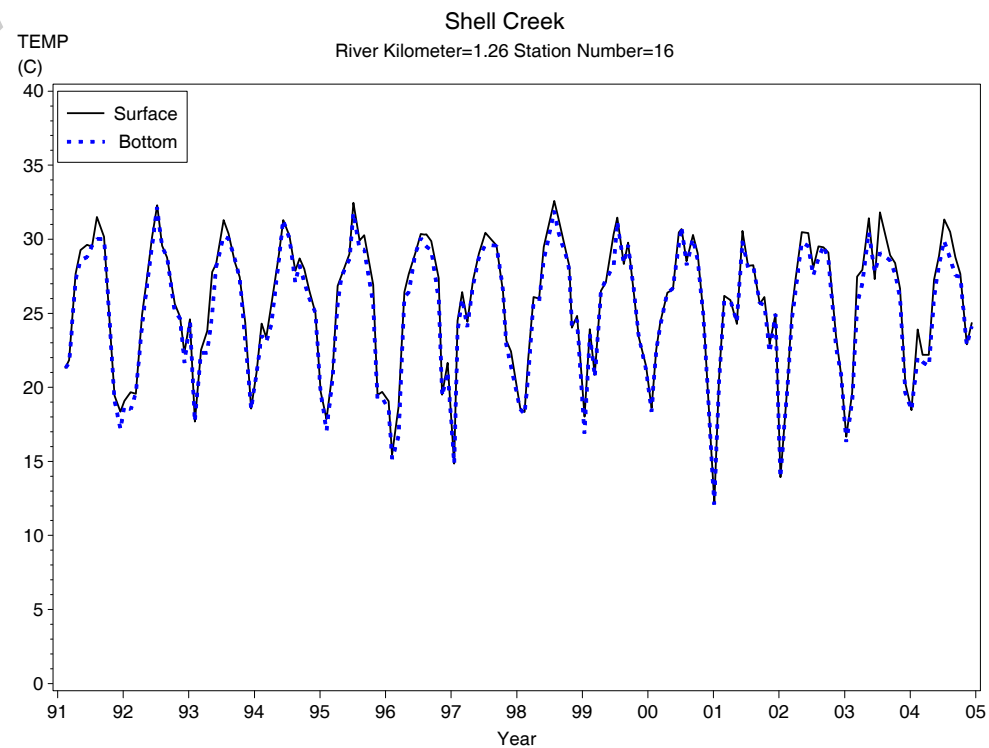
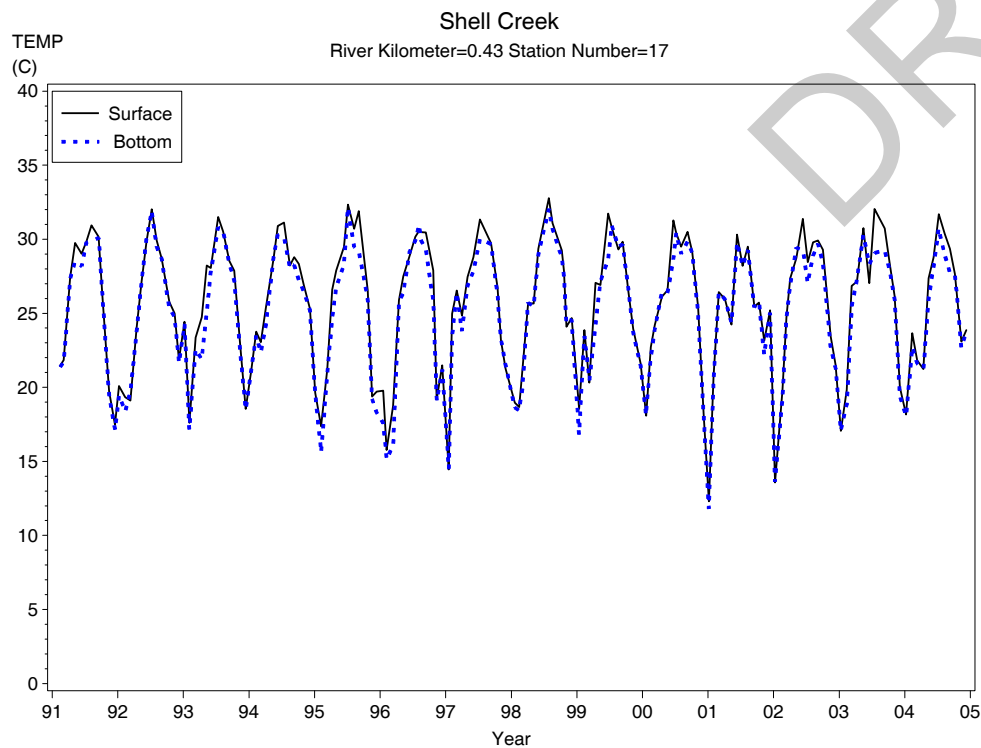
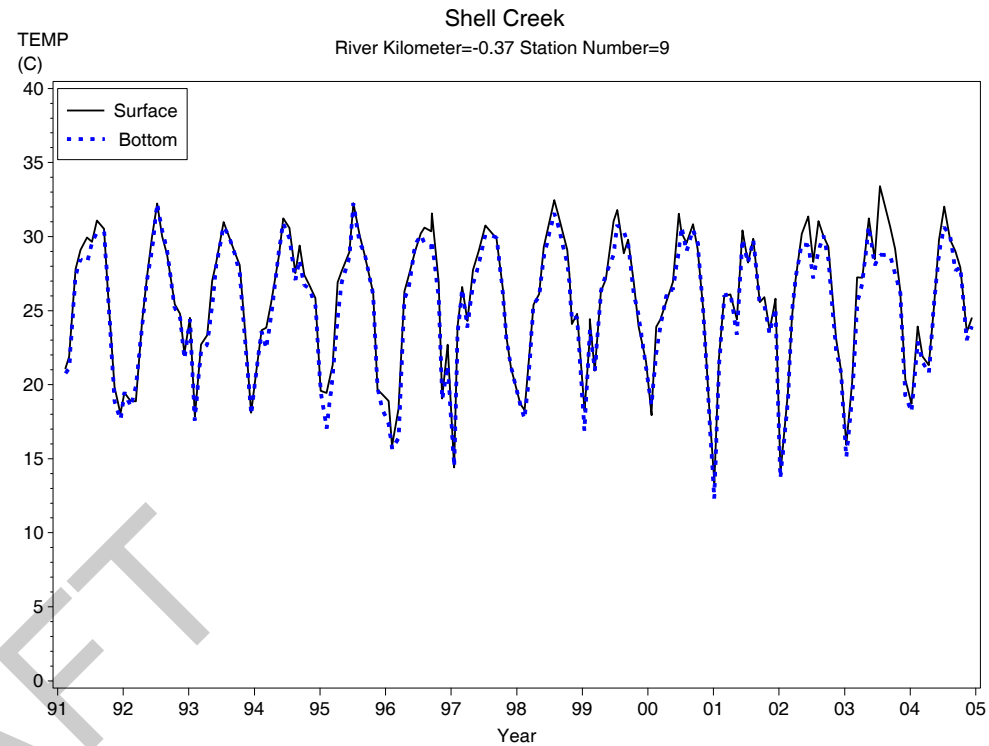
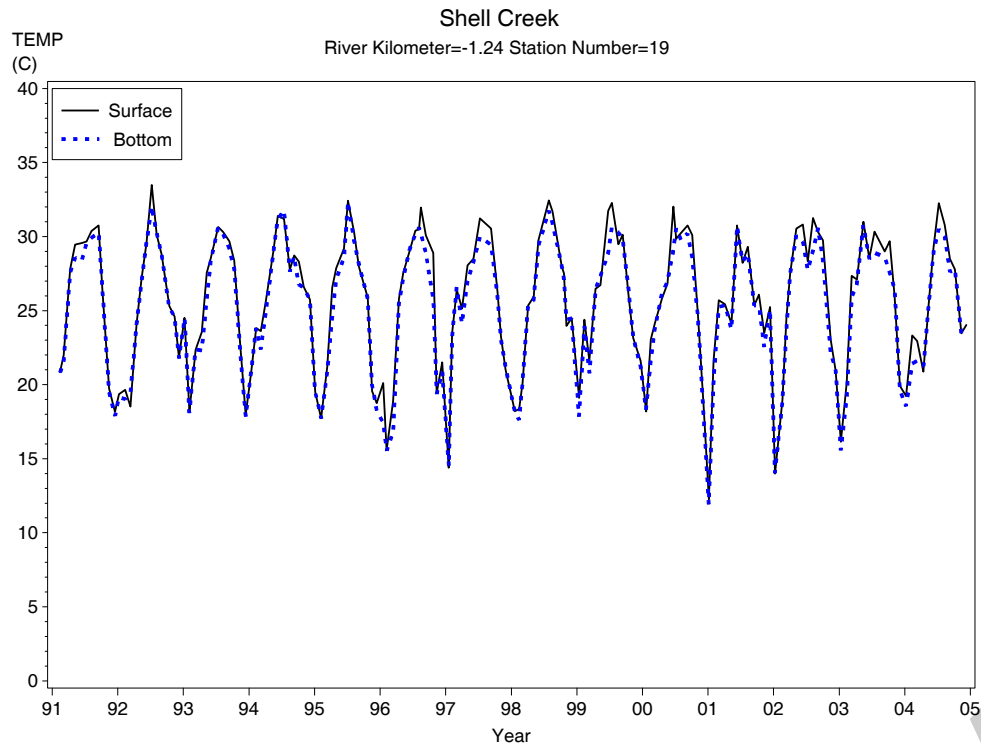


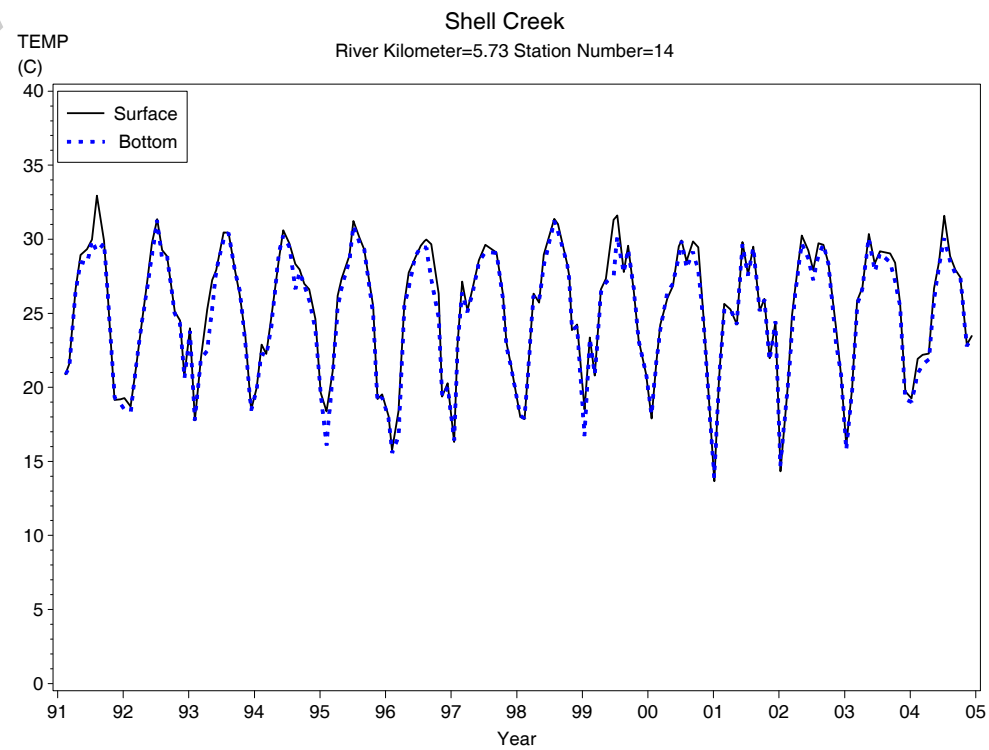
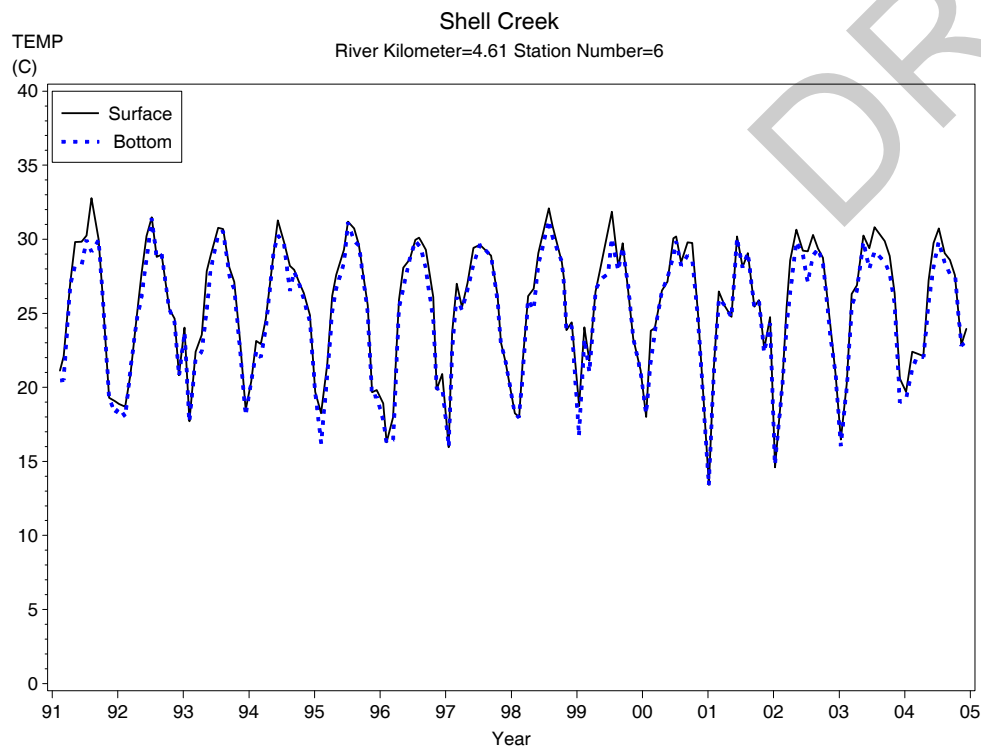
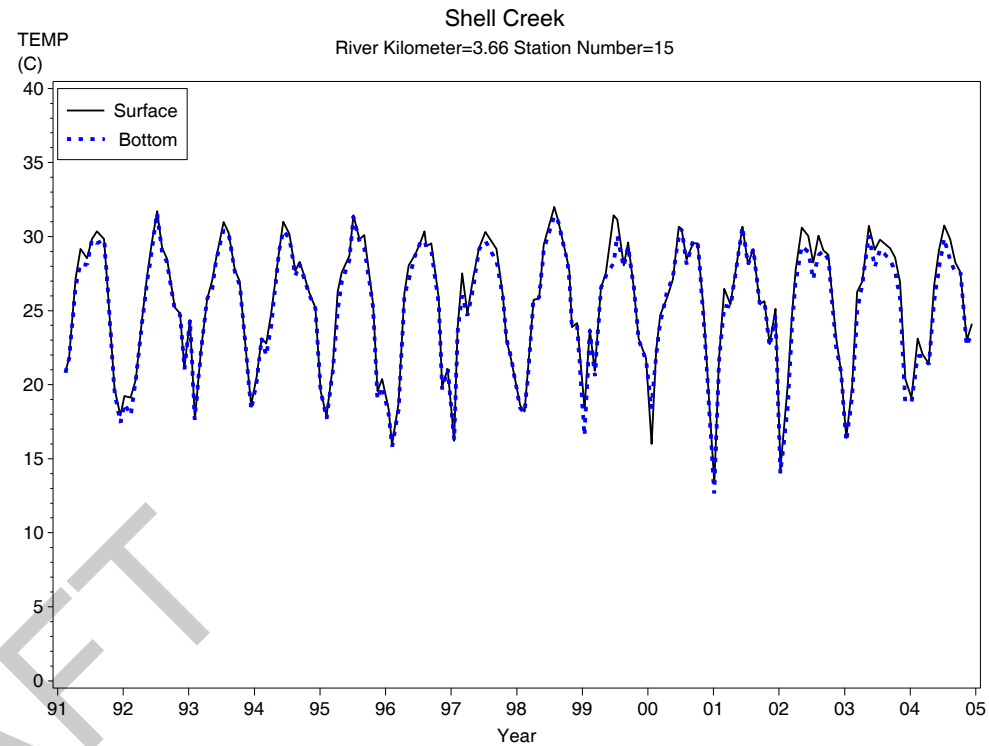
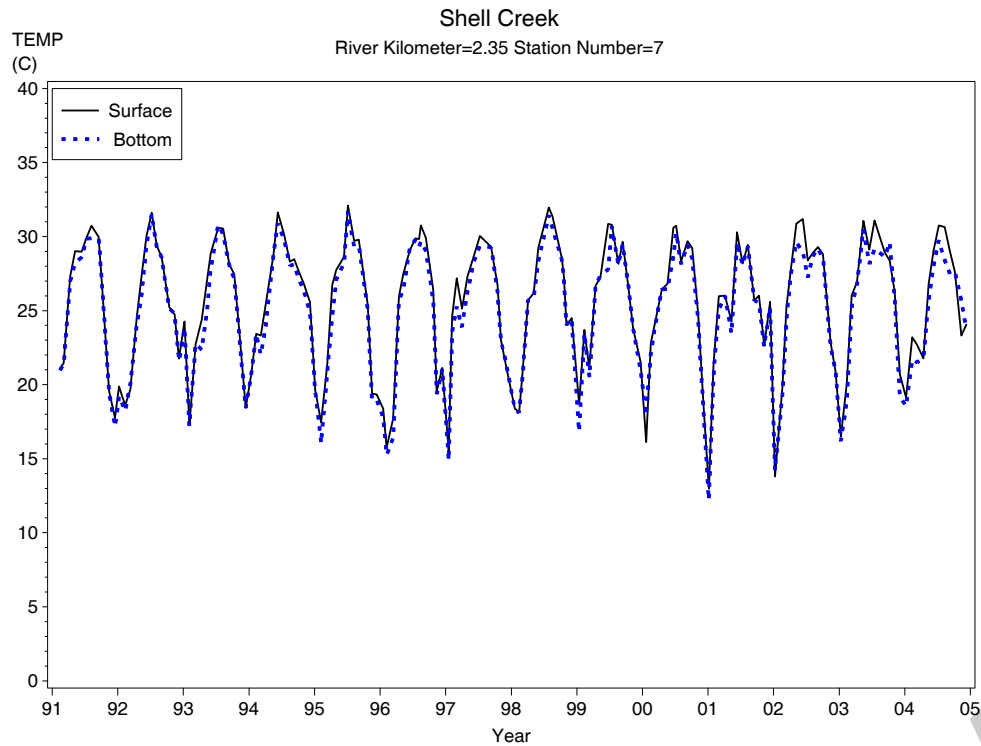


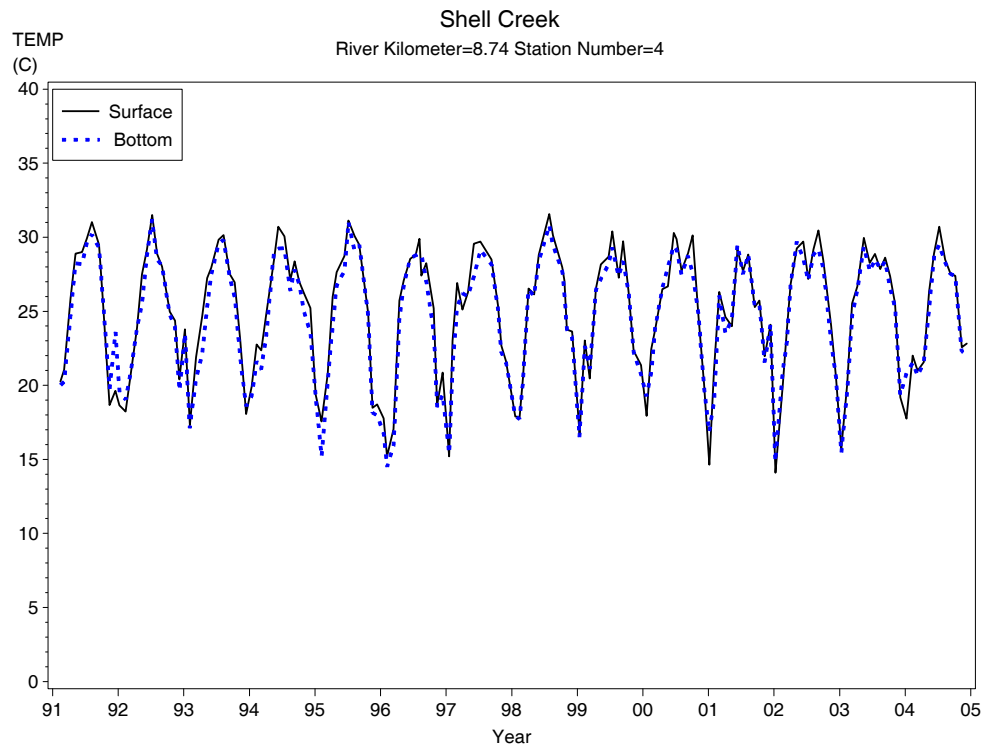
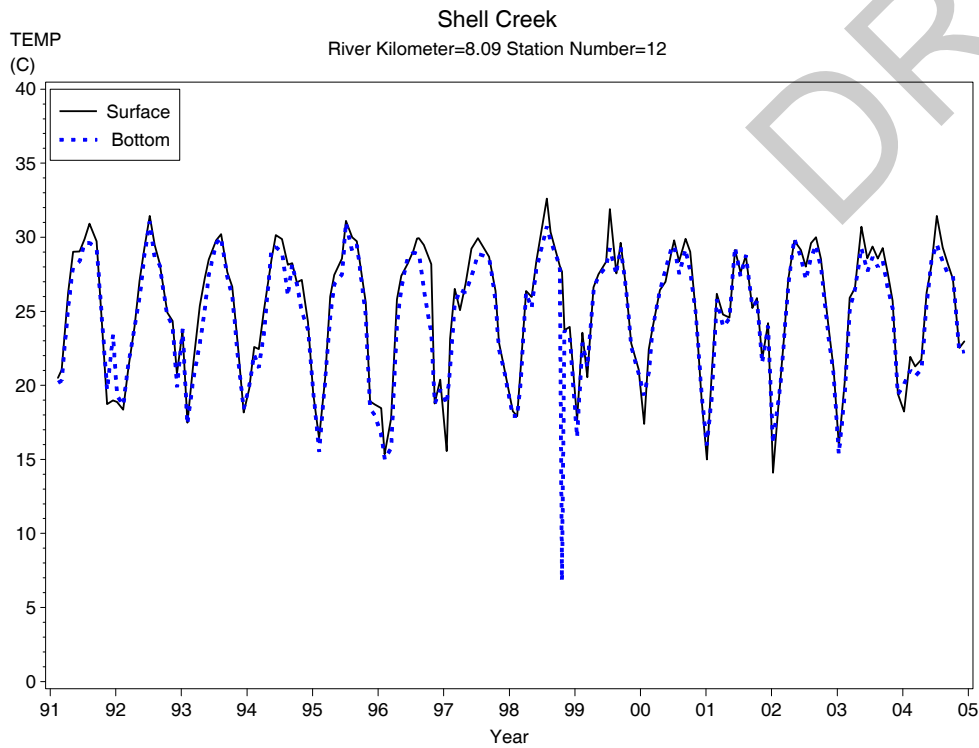
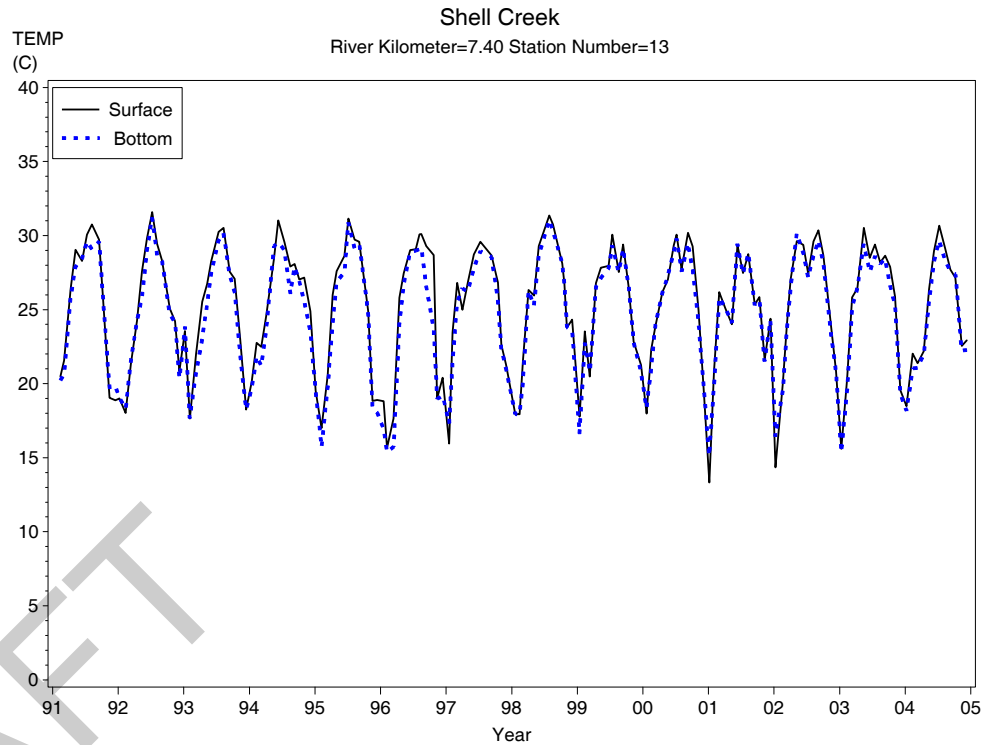
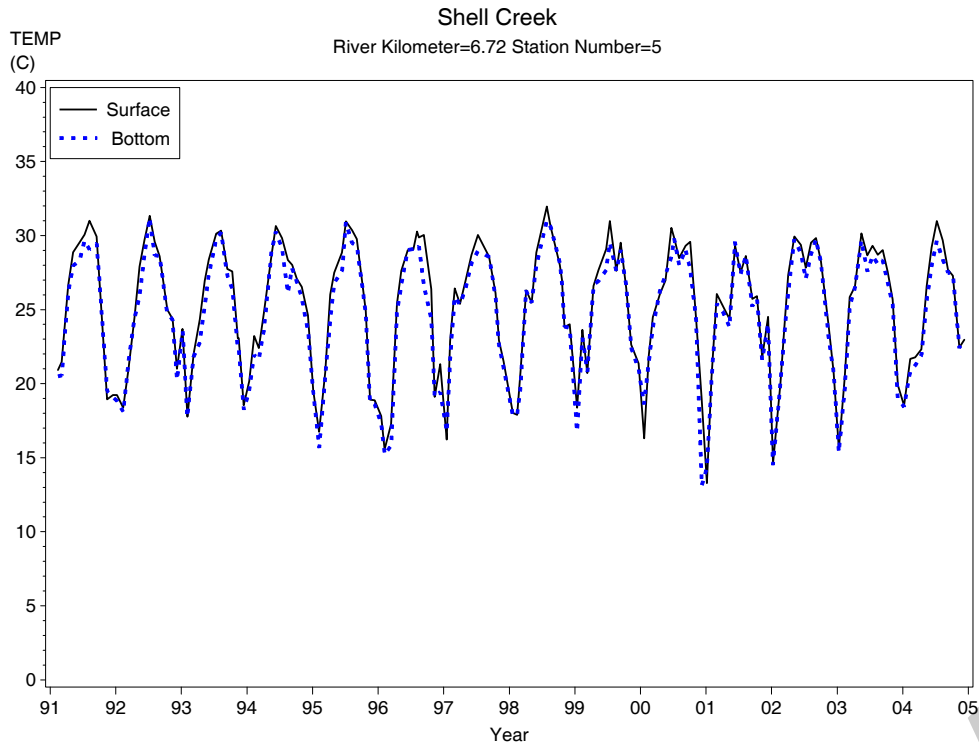


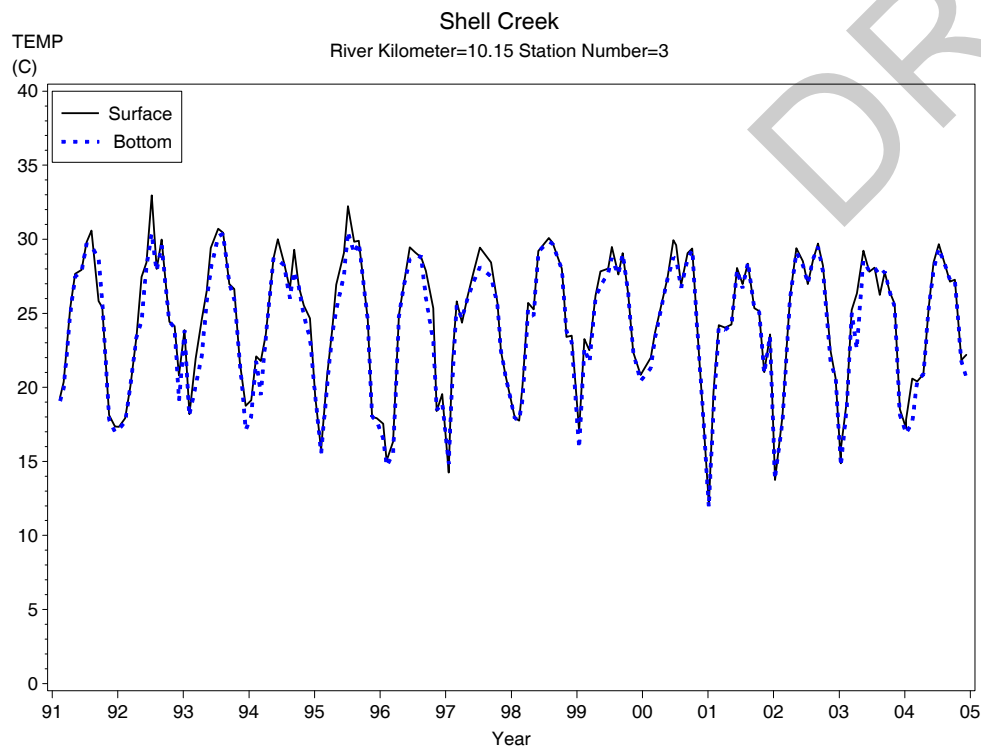
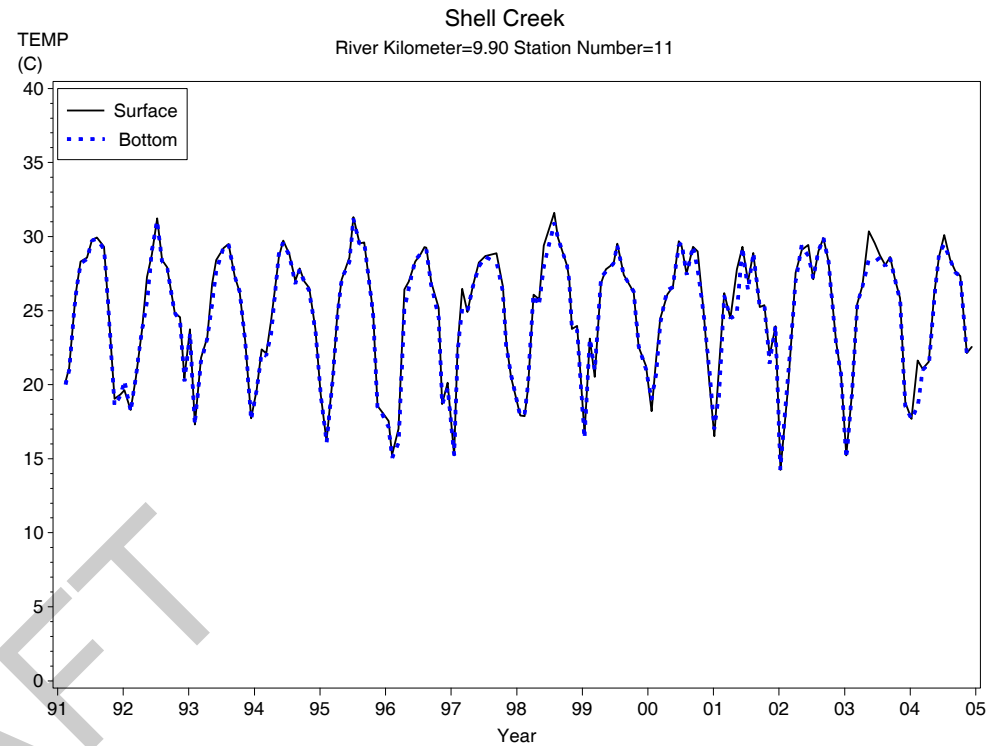
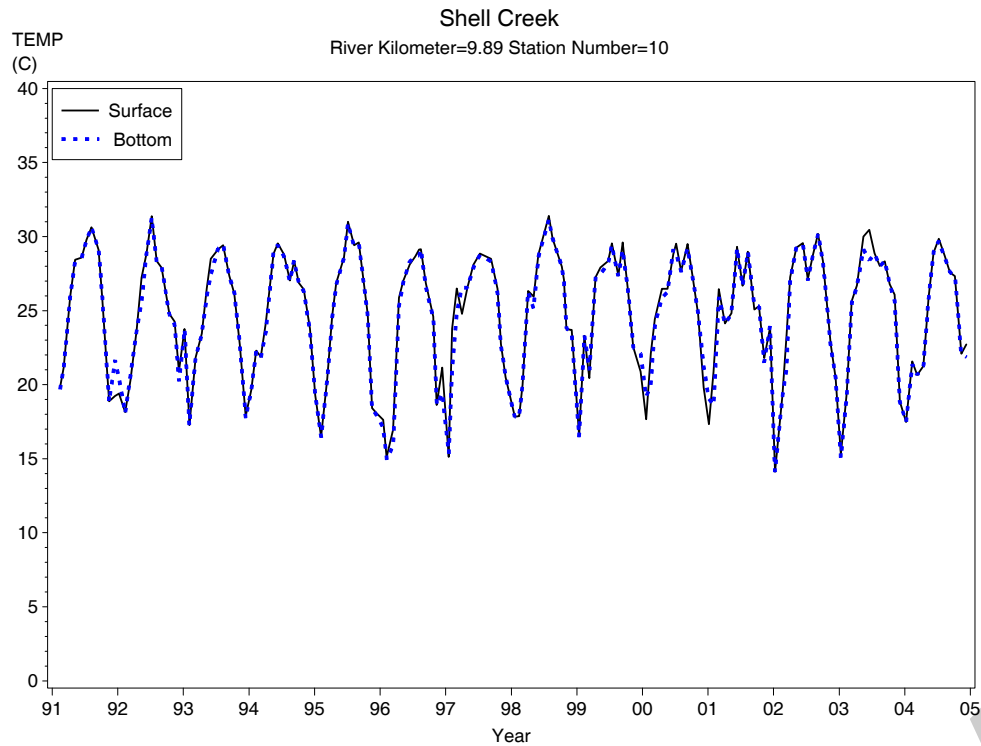


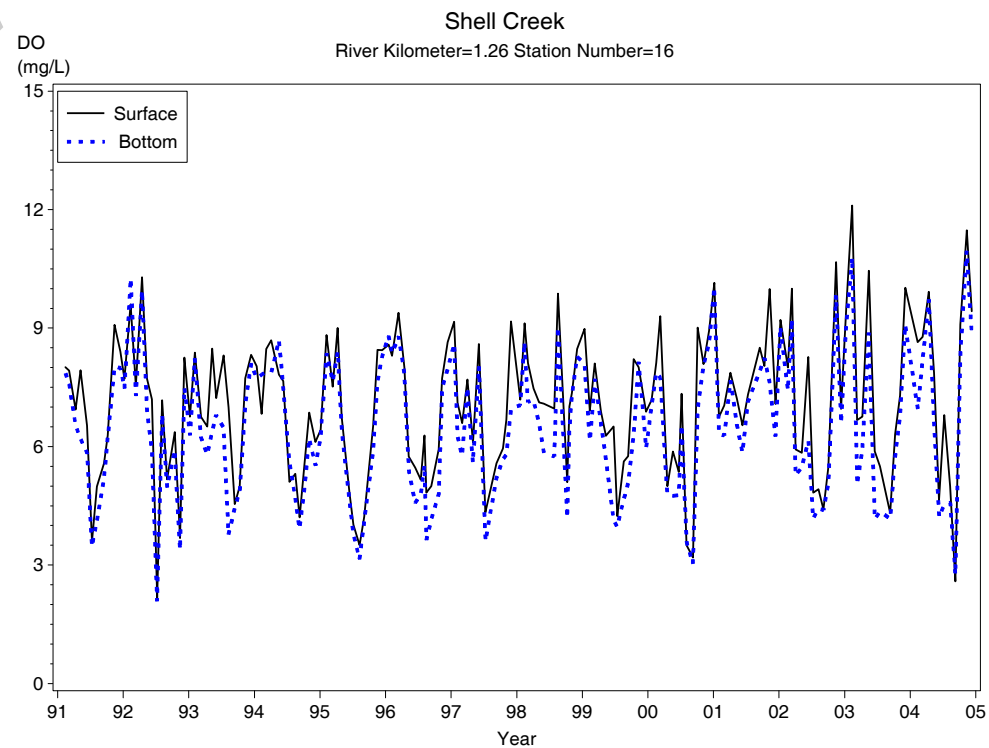
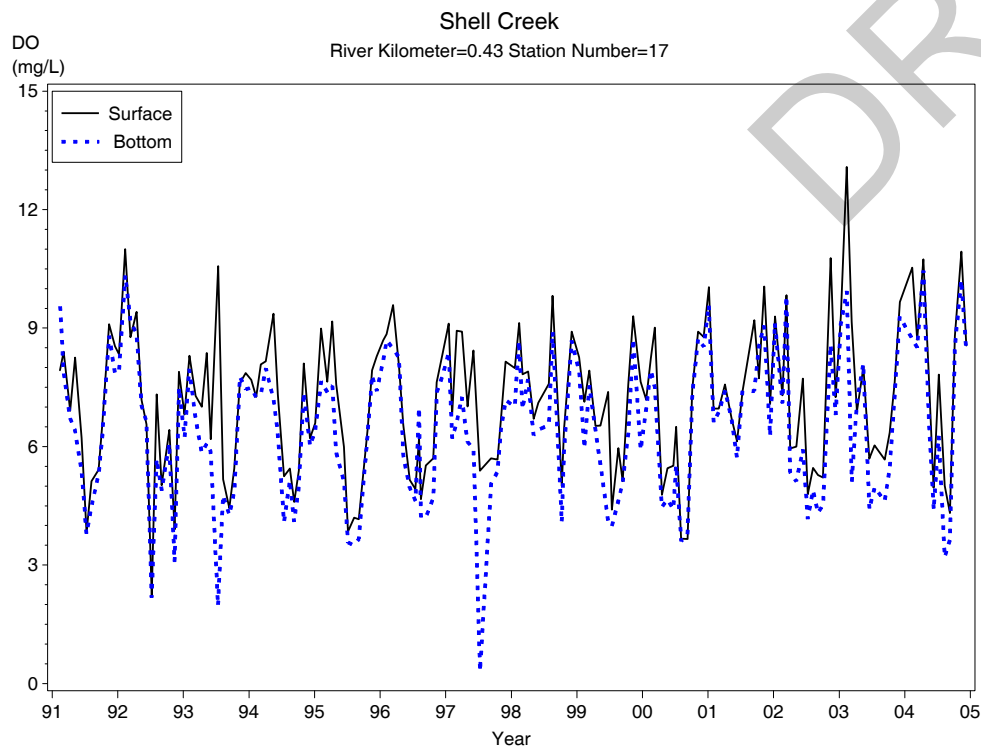
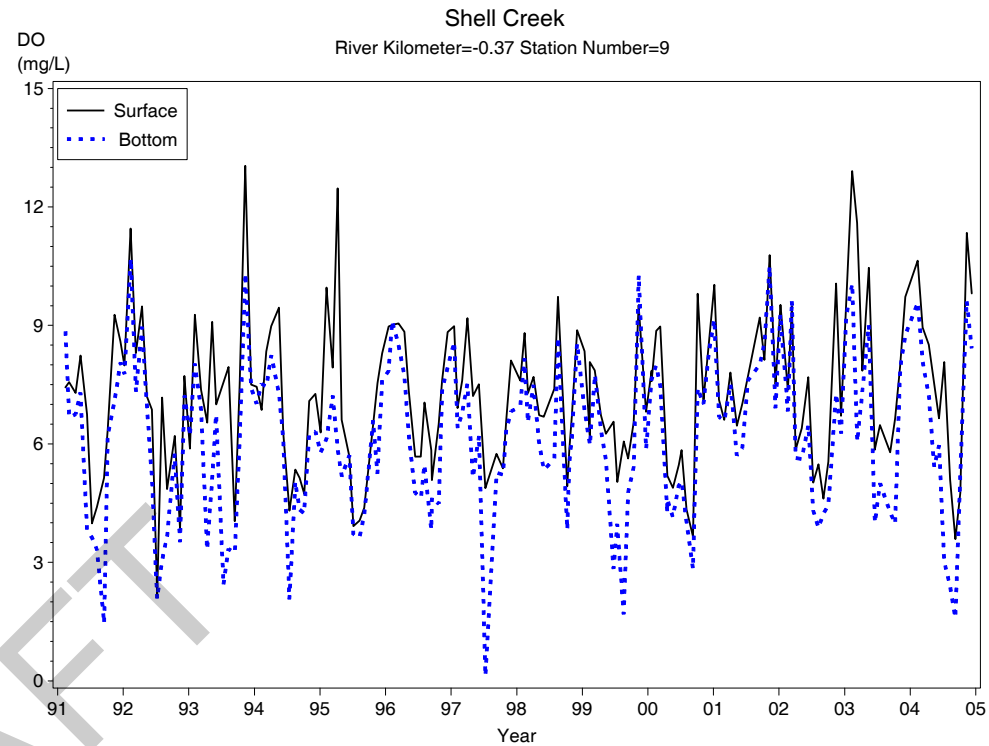
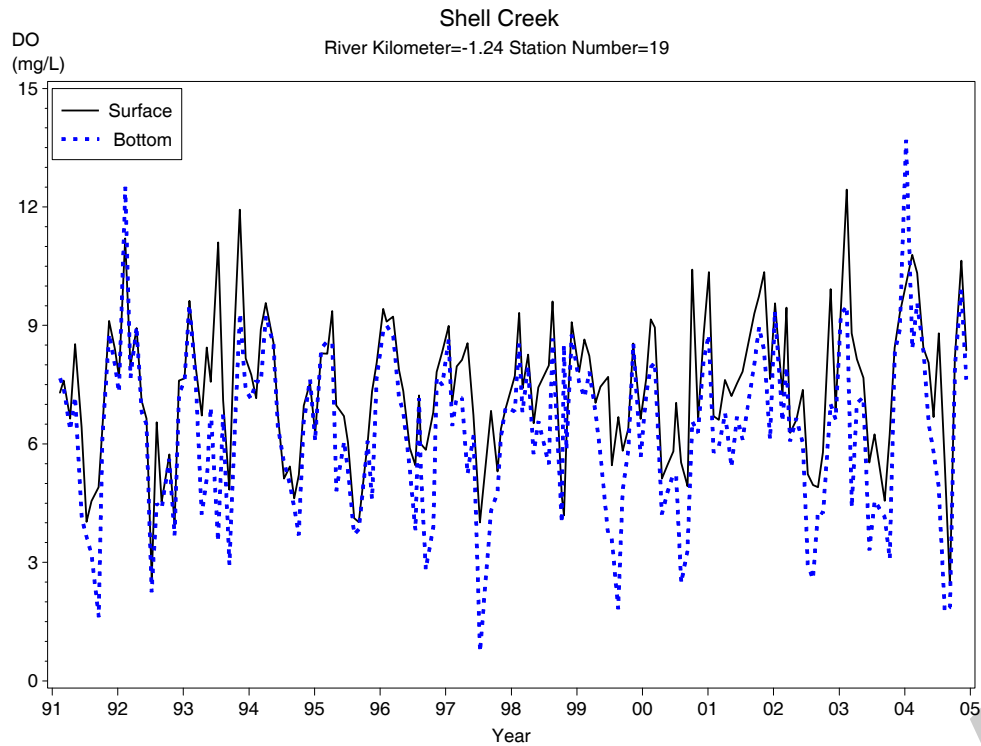


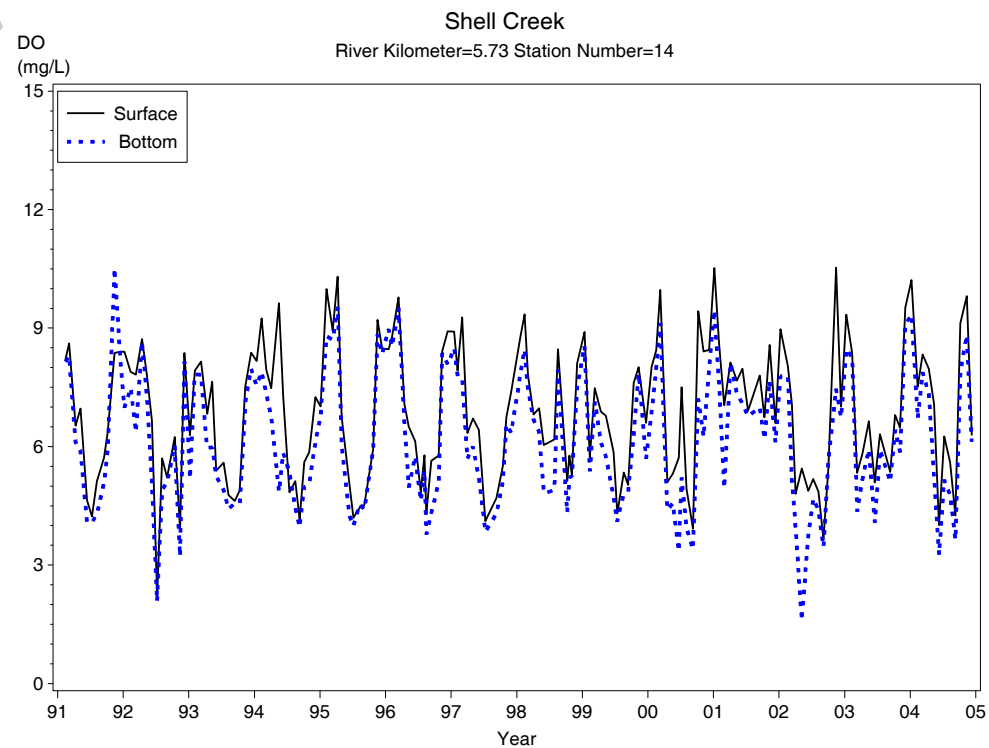
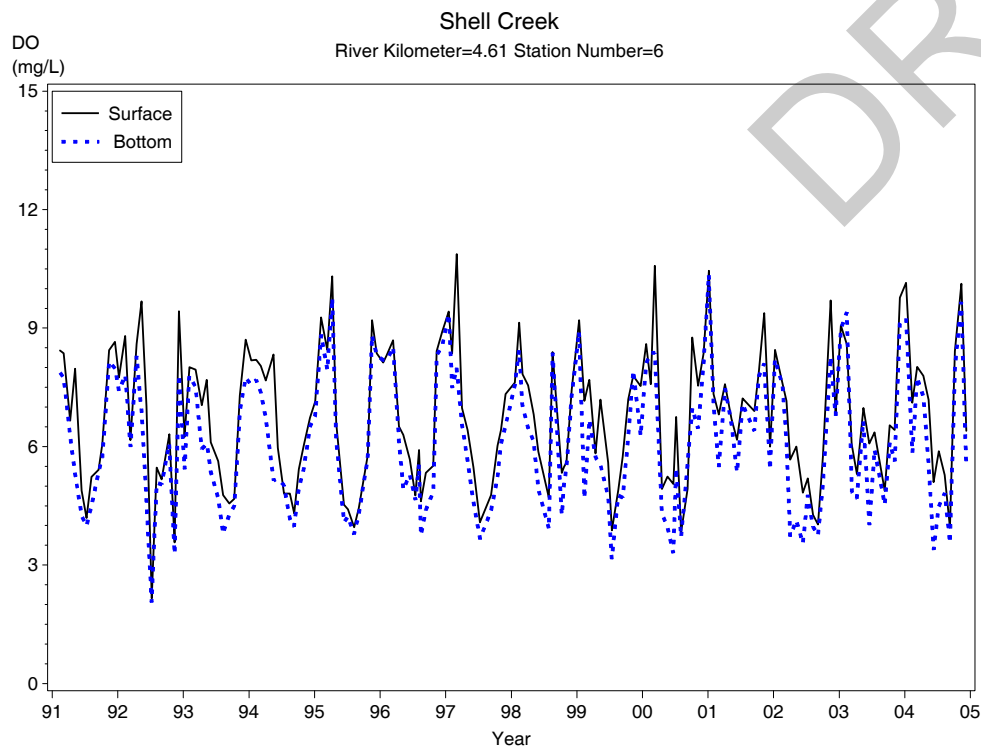
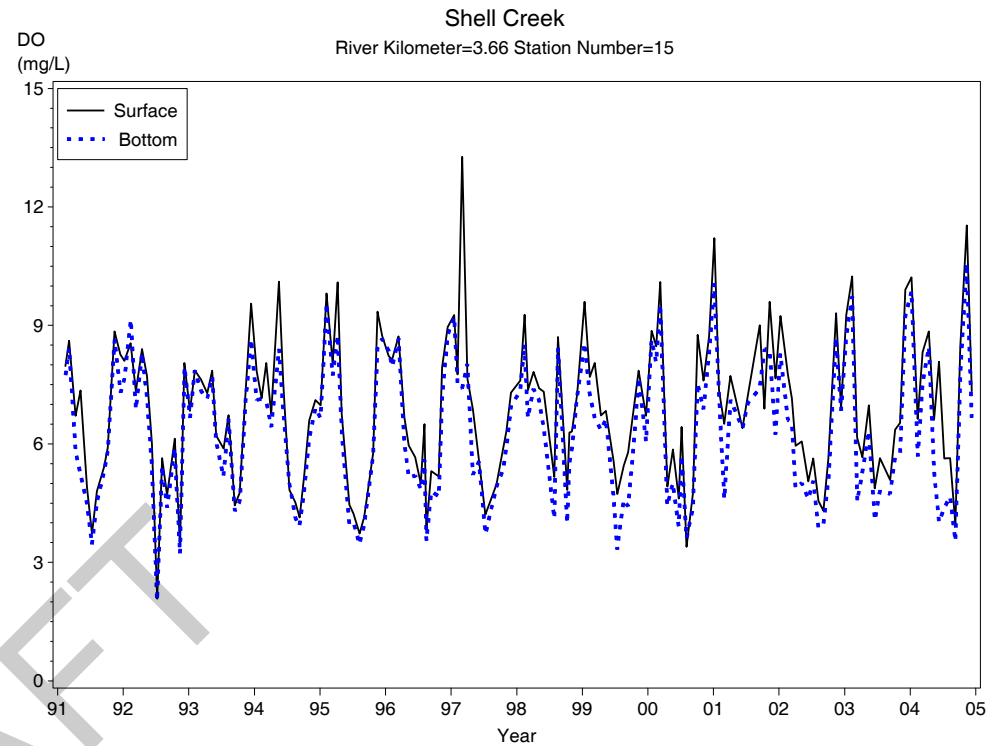
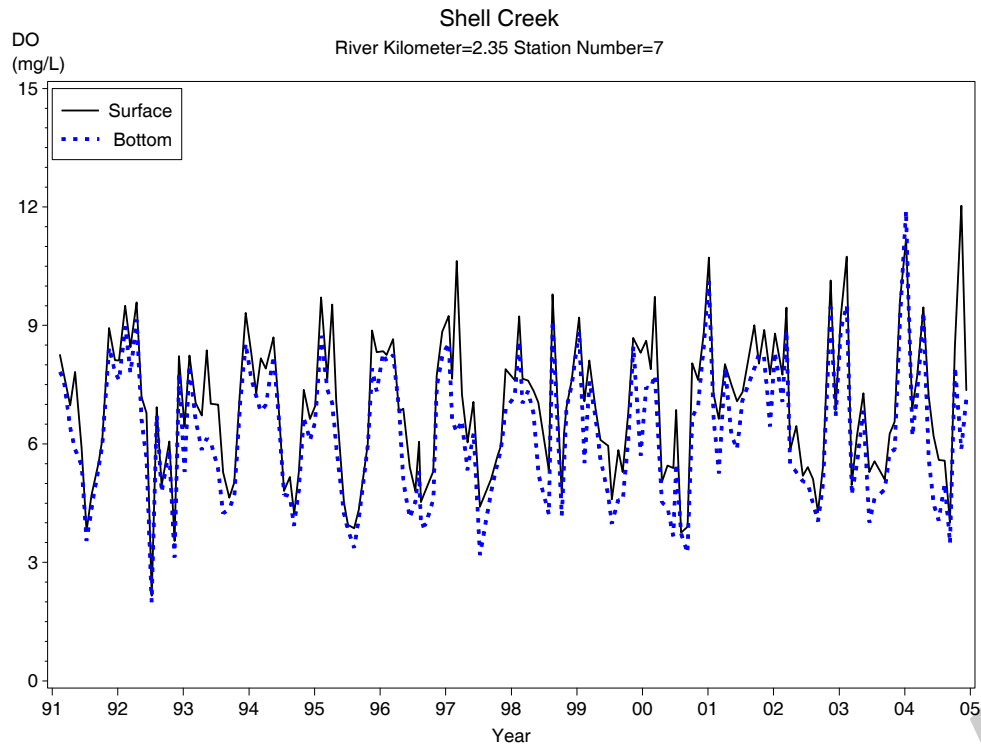


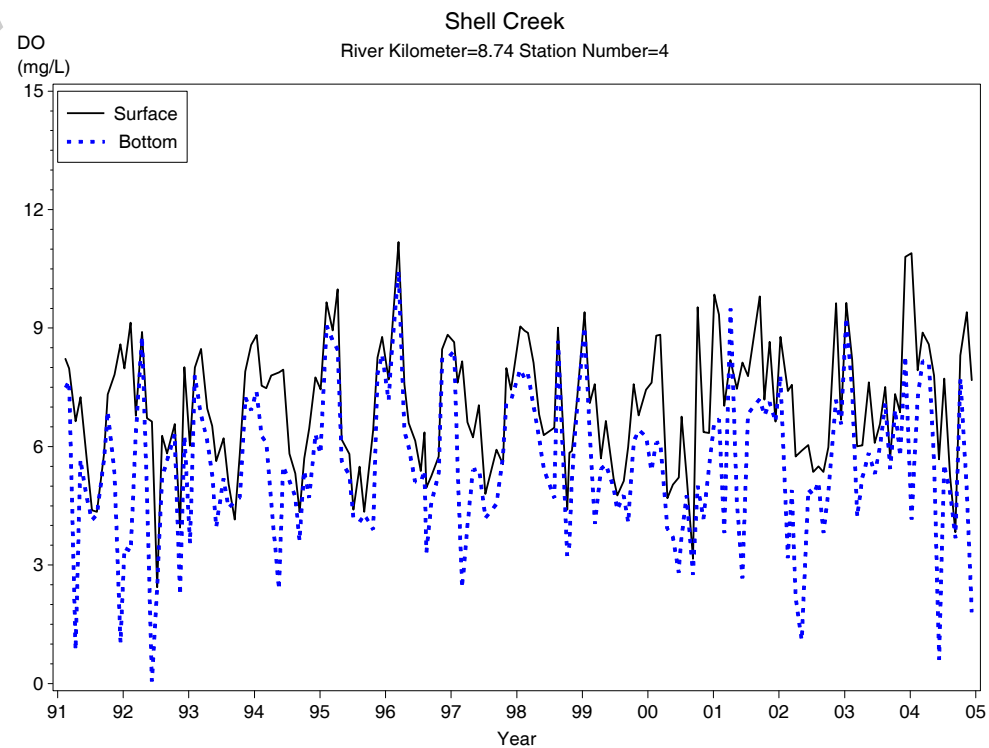
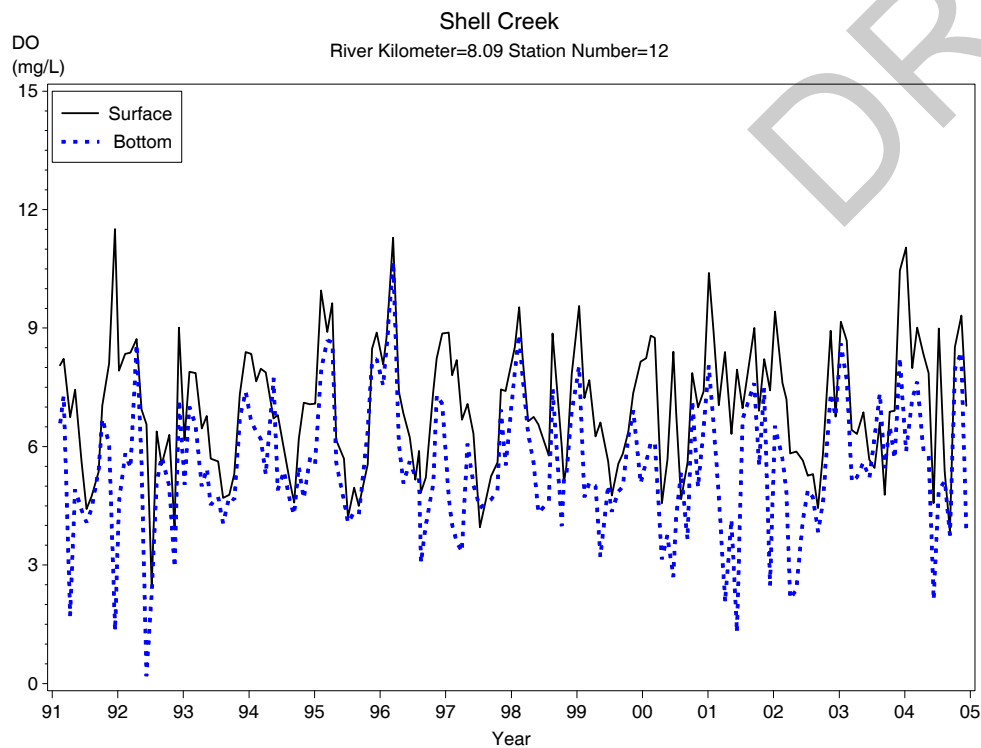
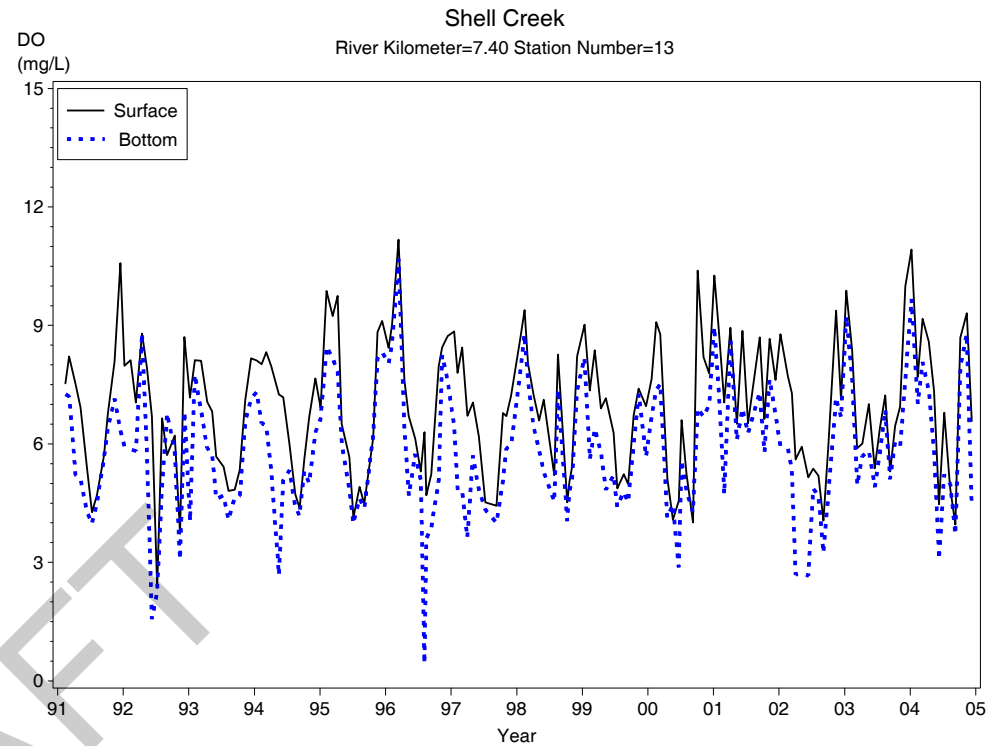
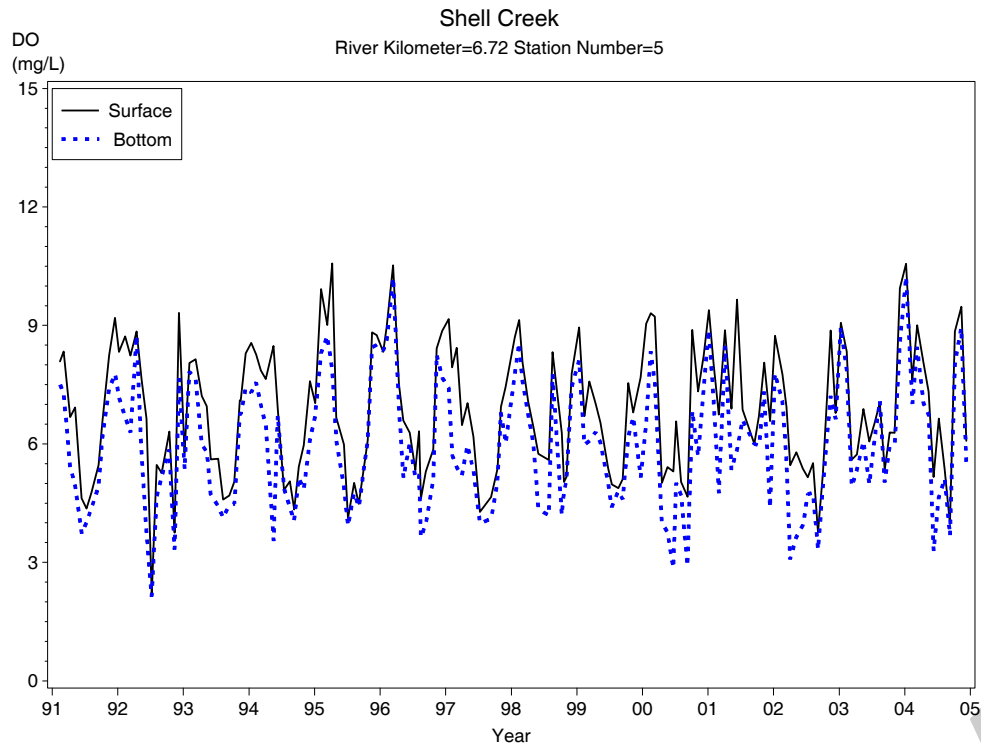


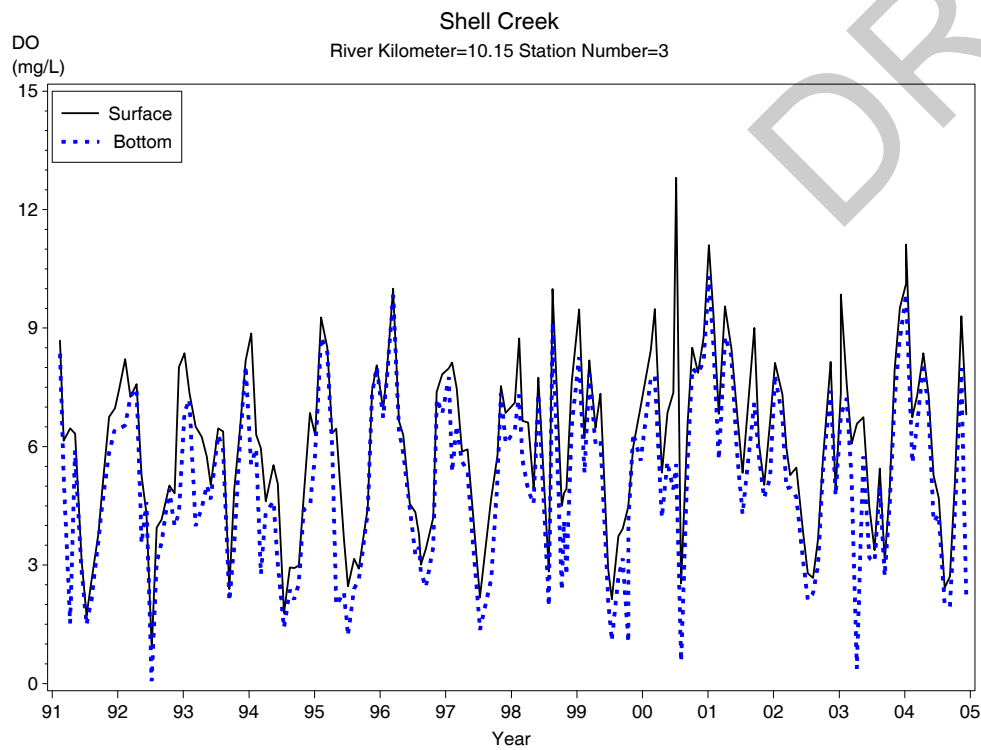
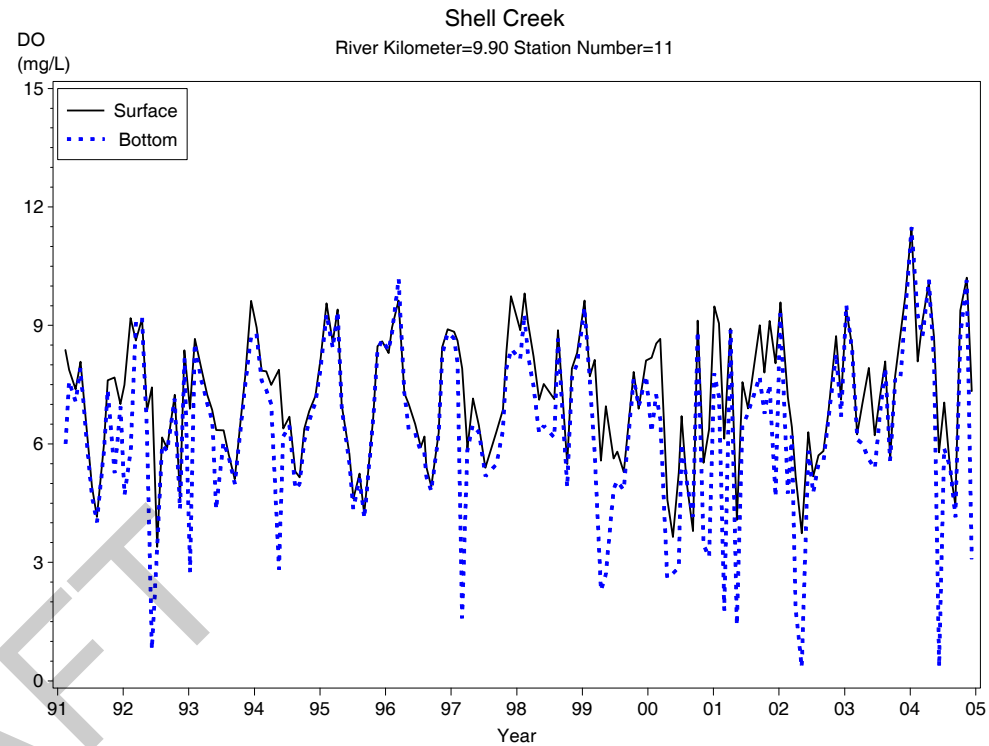
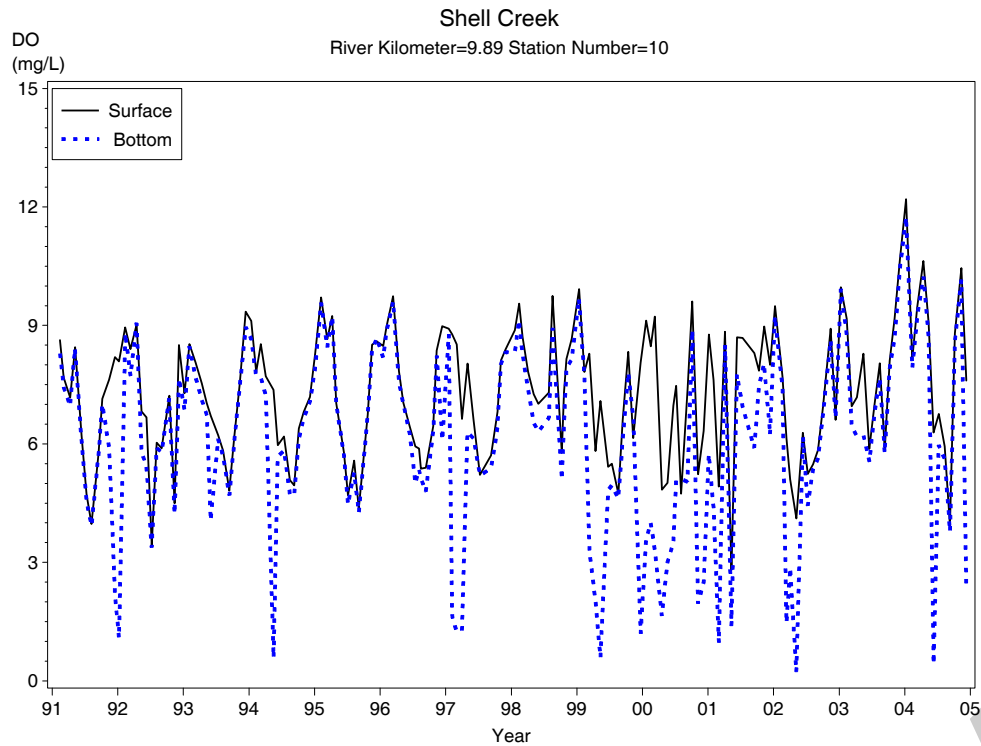




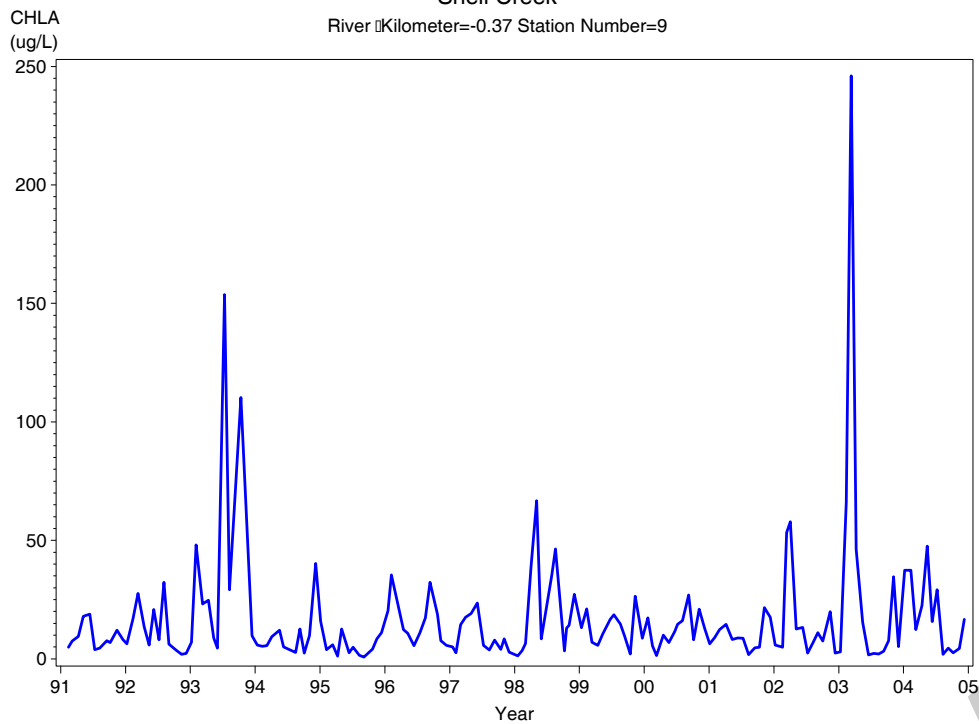




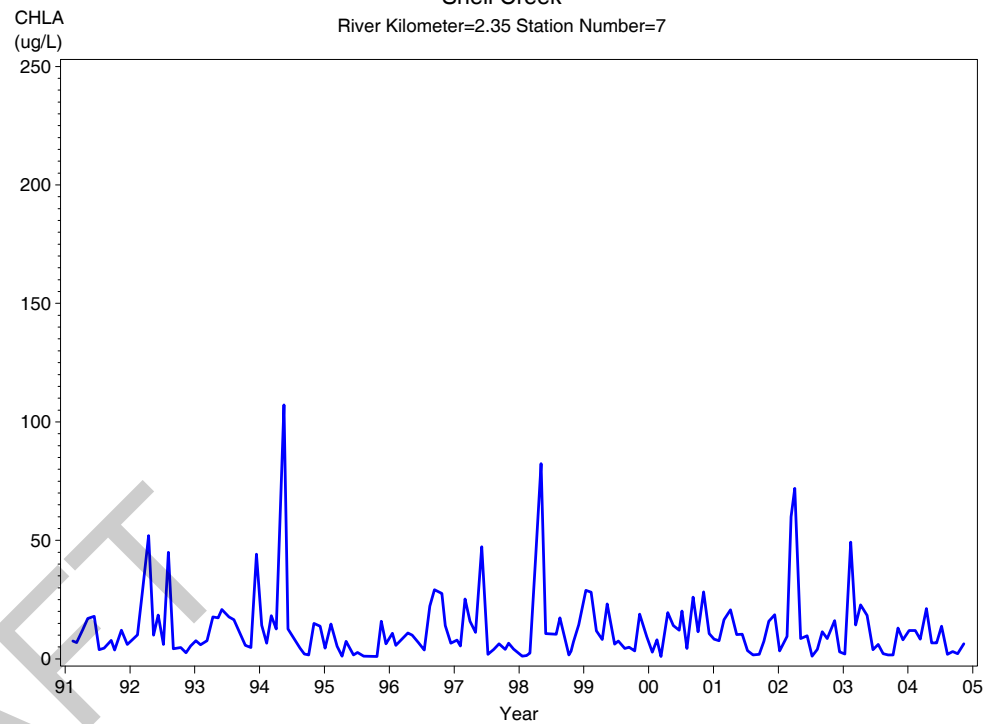




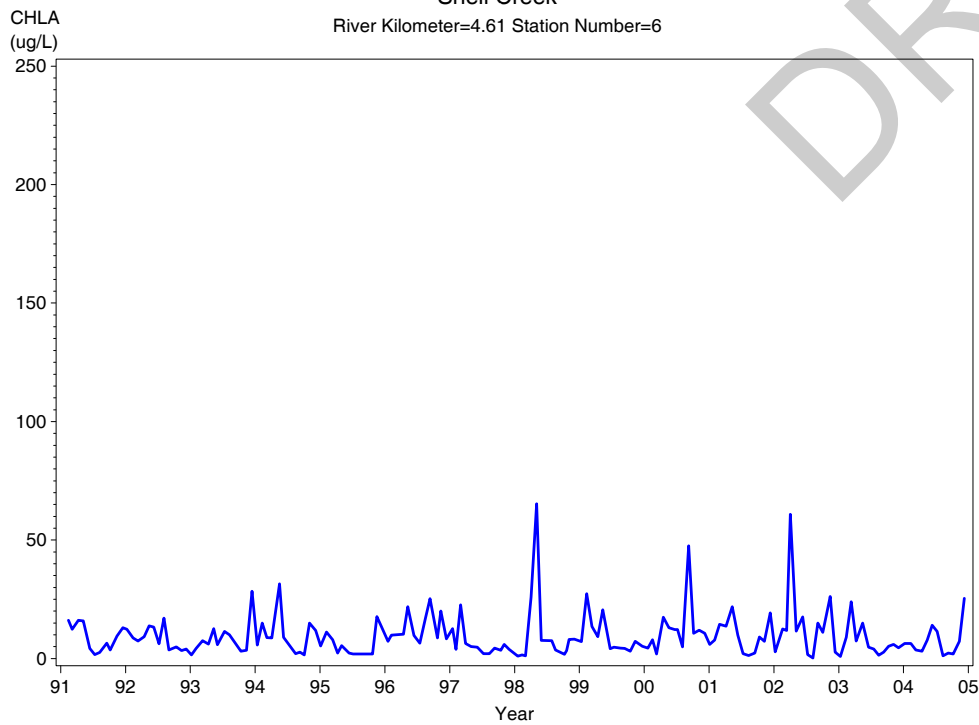
Shell Creek
River Kilometer=-0.37 Station Number=9



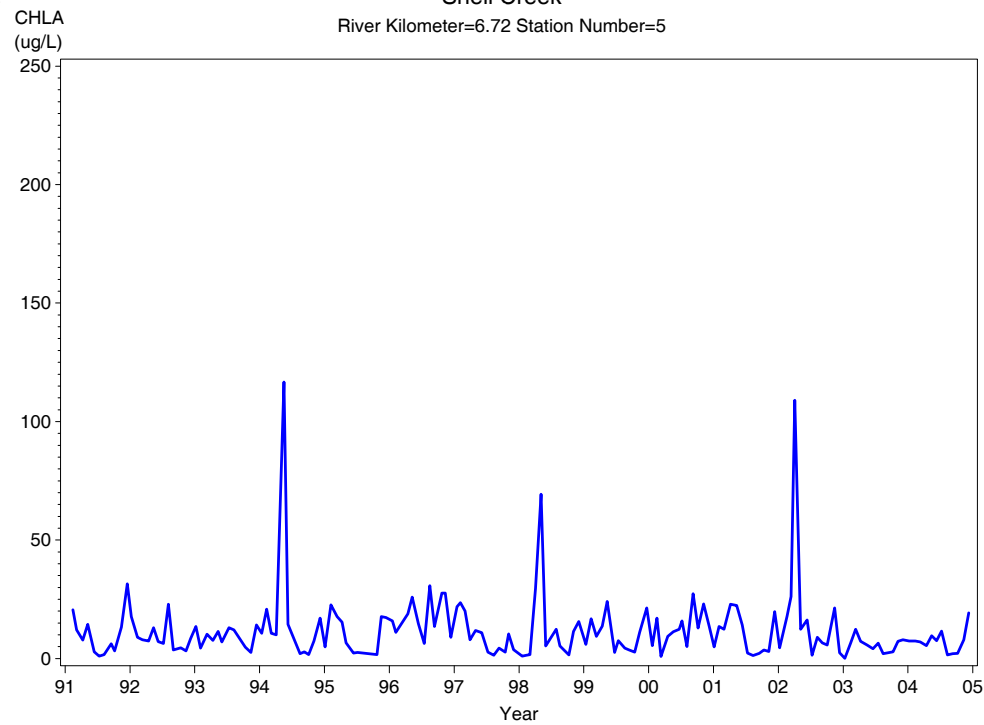
Shell Creek
River Kilometer=2.35 Station Number=7



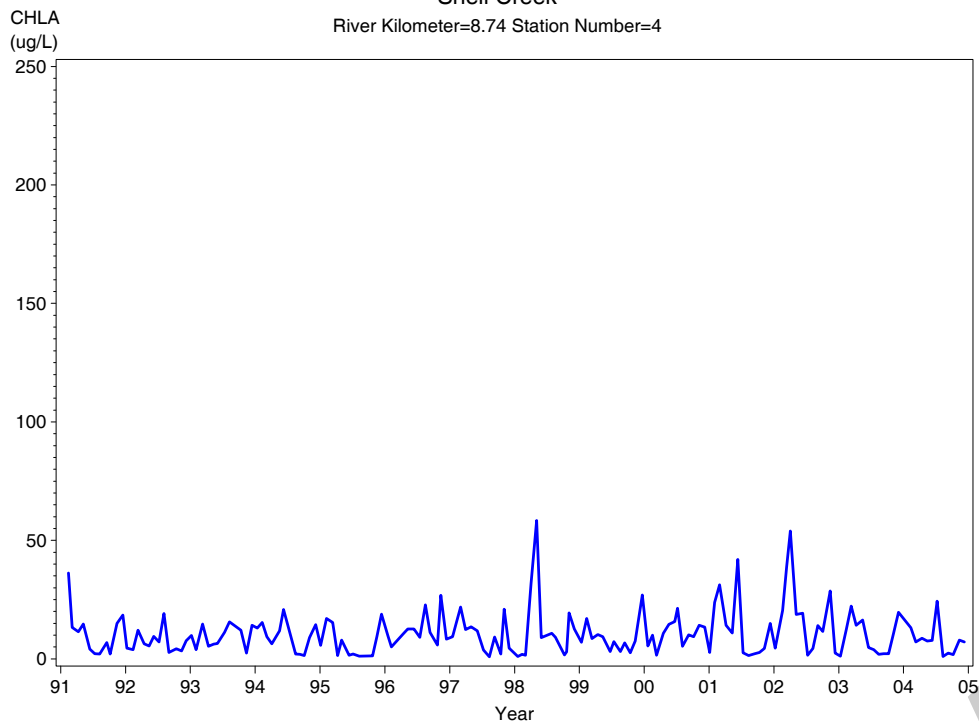
Shell Creek
River Kilometer=4.61 Station Number=6



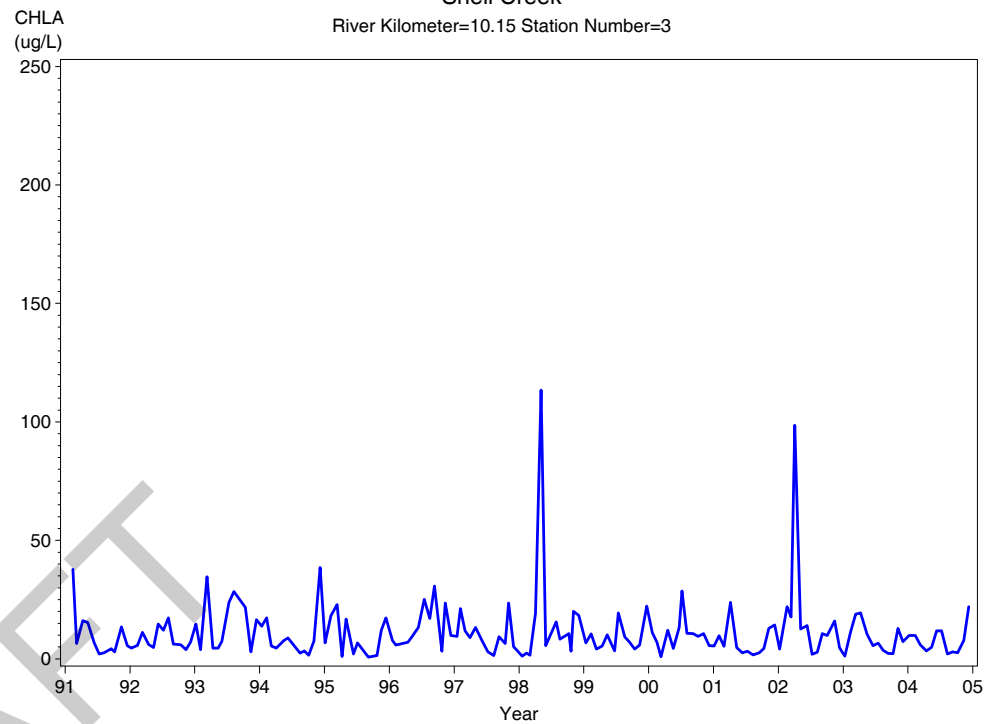
Shell Creek
River Kilometer=6.72 Station Number=5

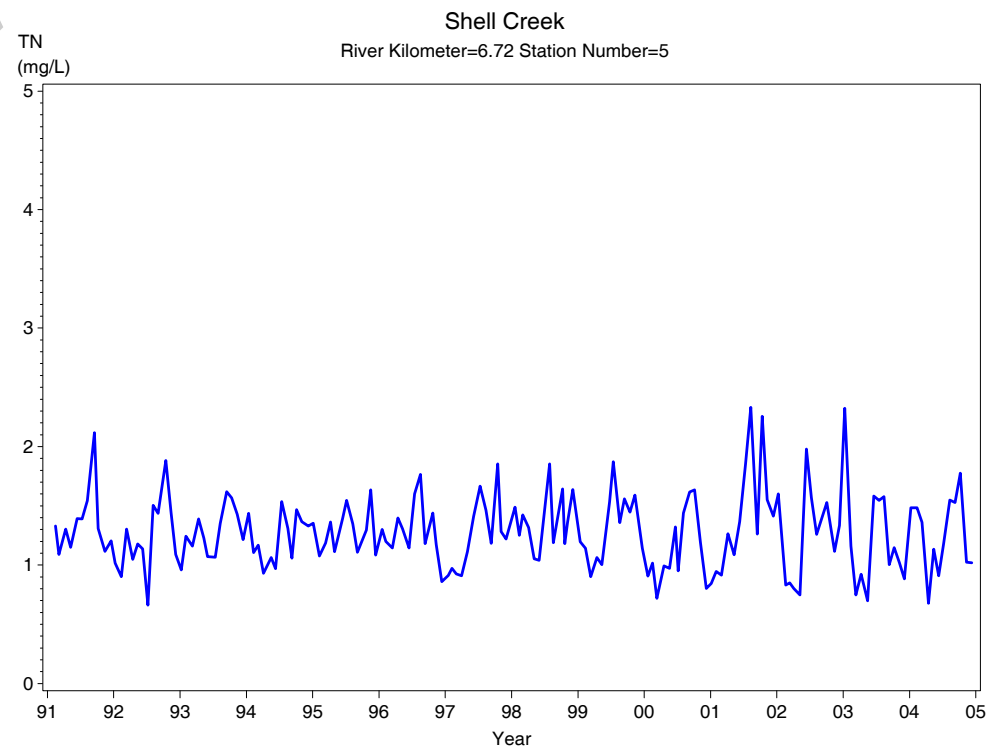
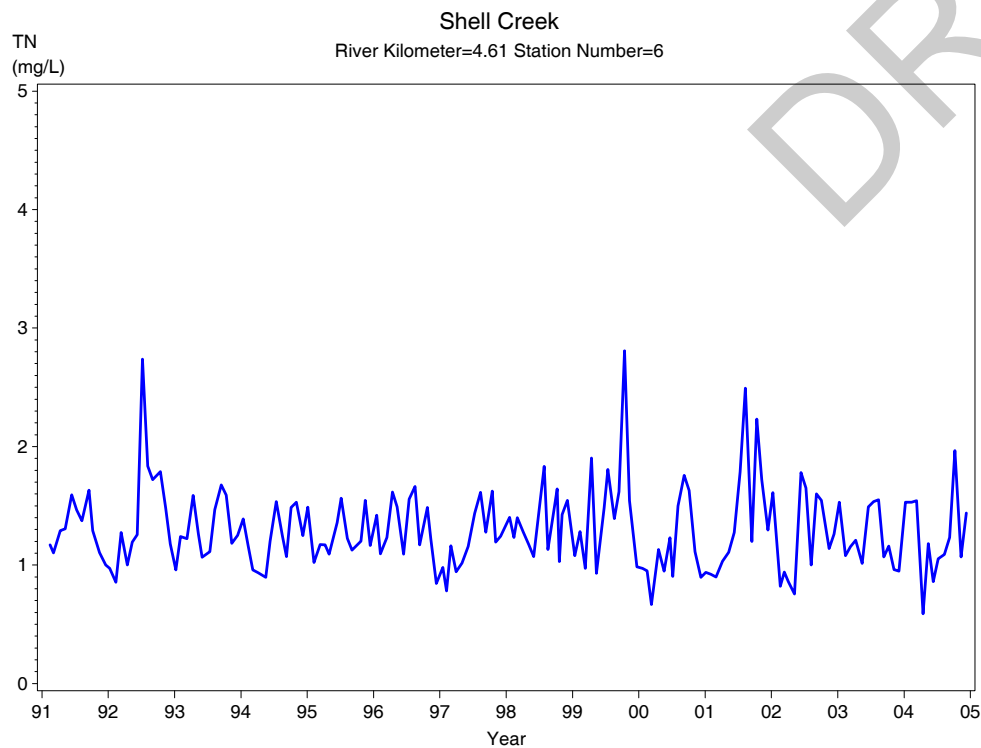
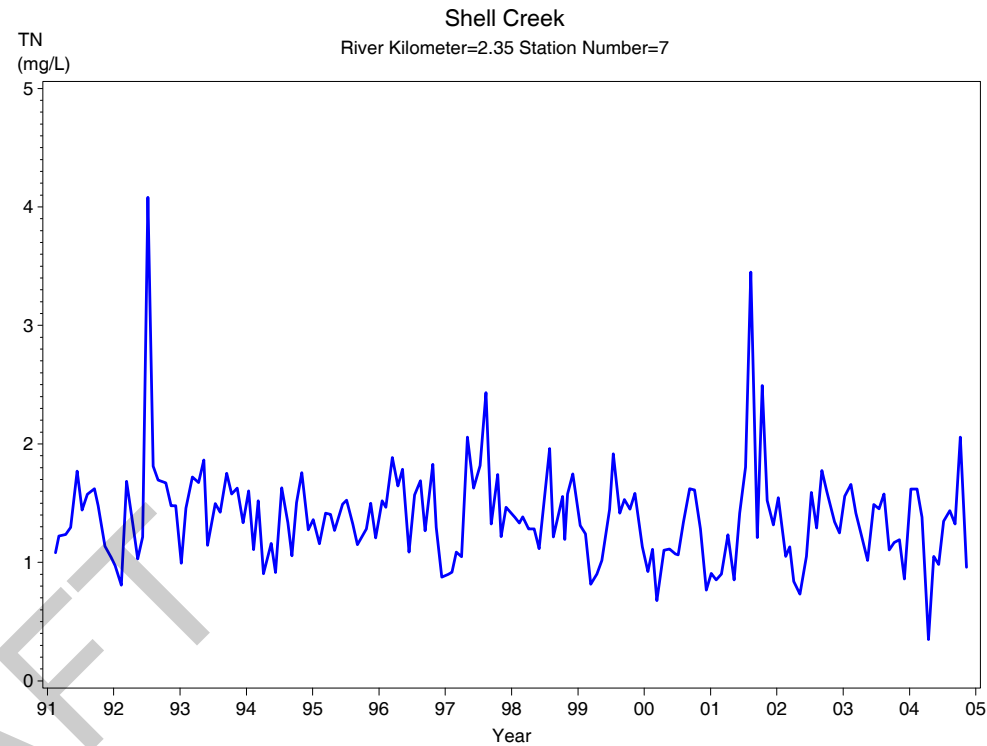
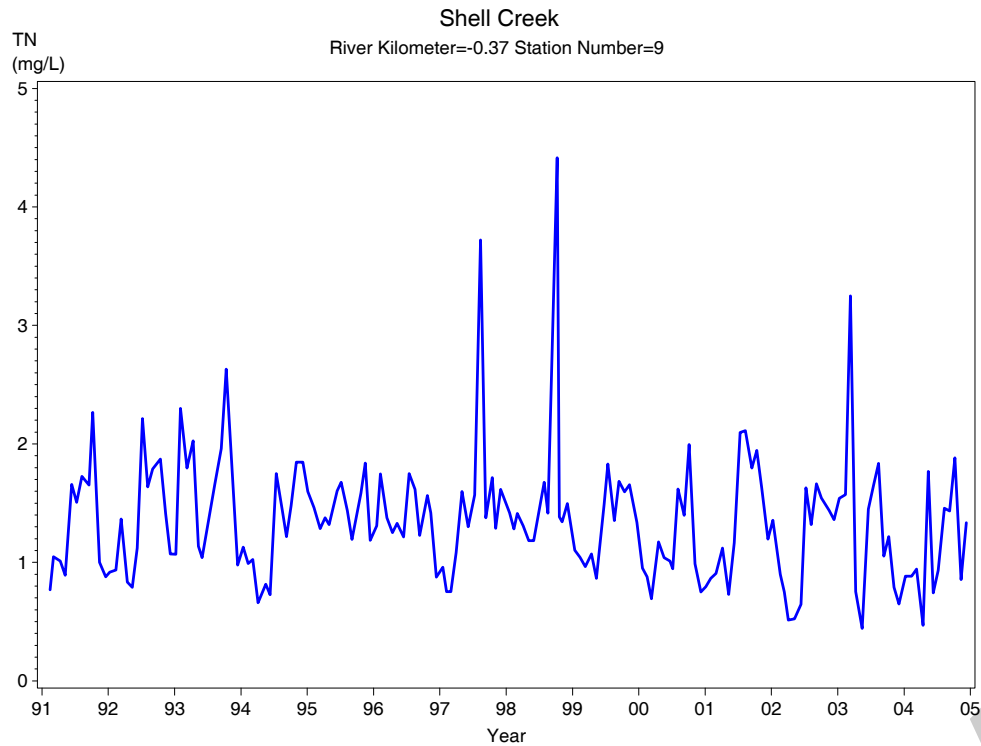


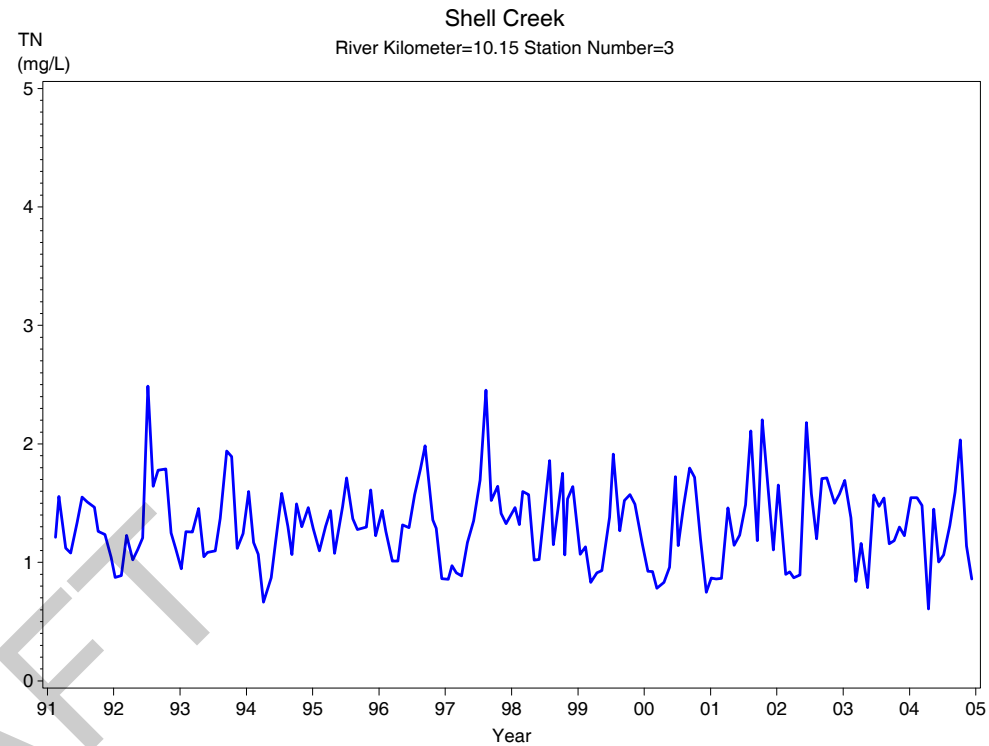
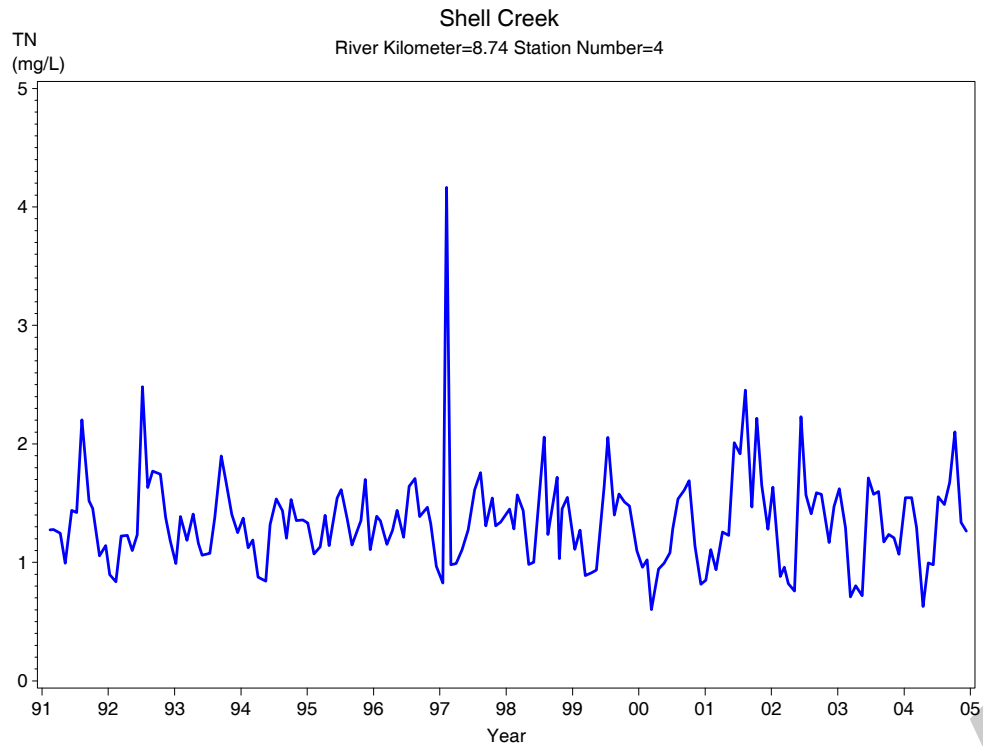
Shell Creek
River Kilometer=8.74 Station Number=4

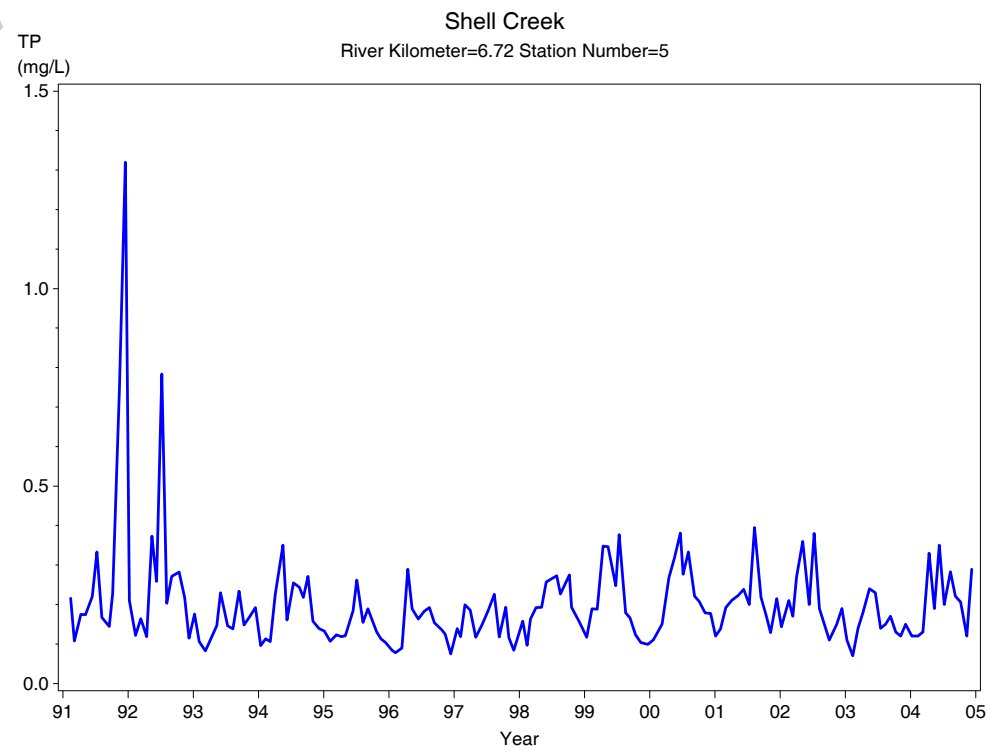
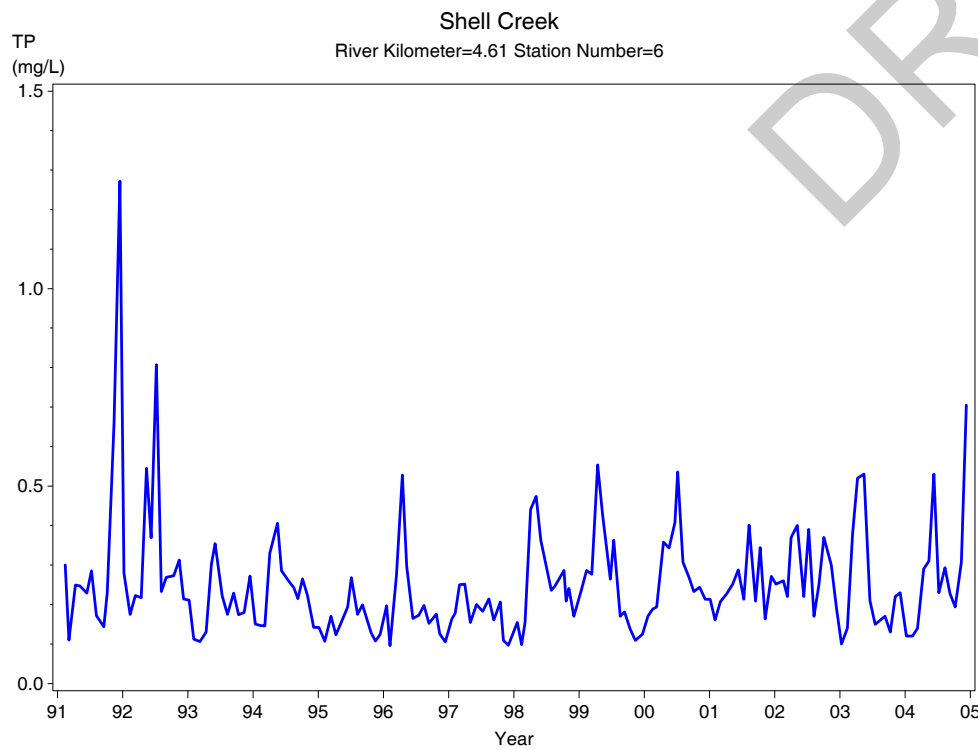
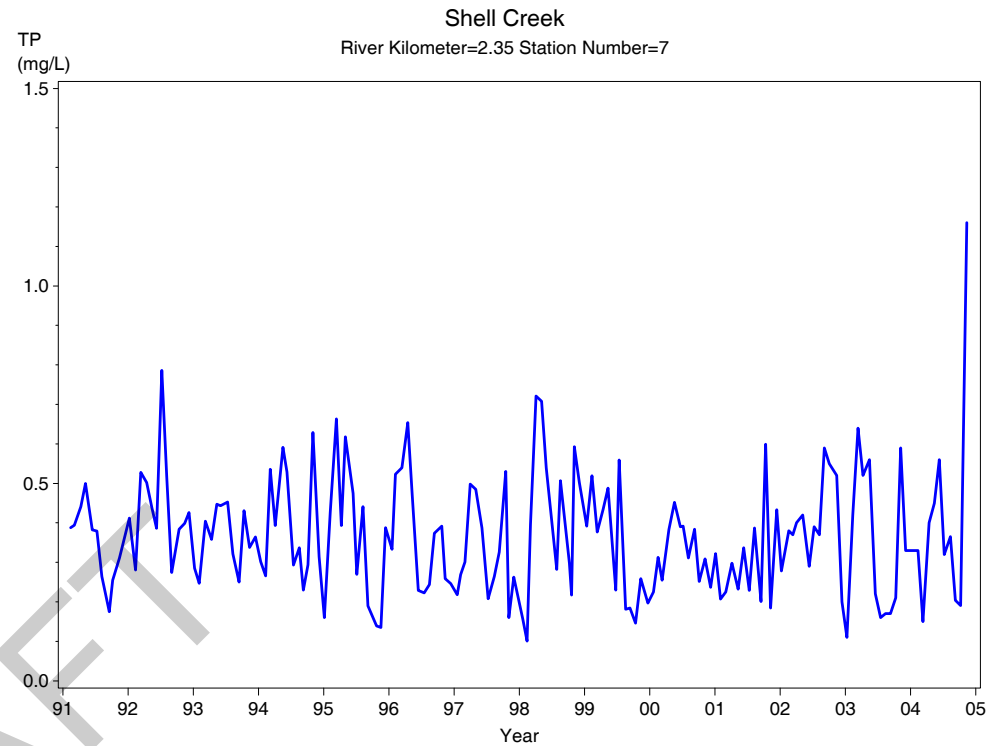
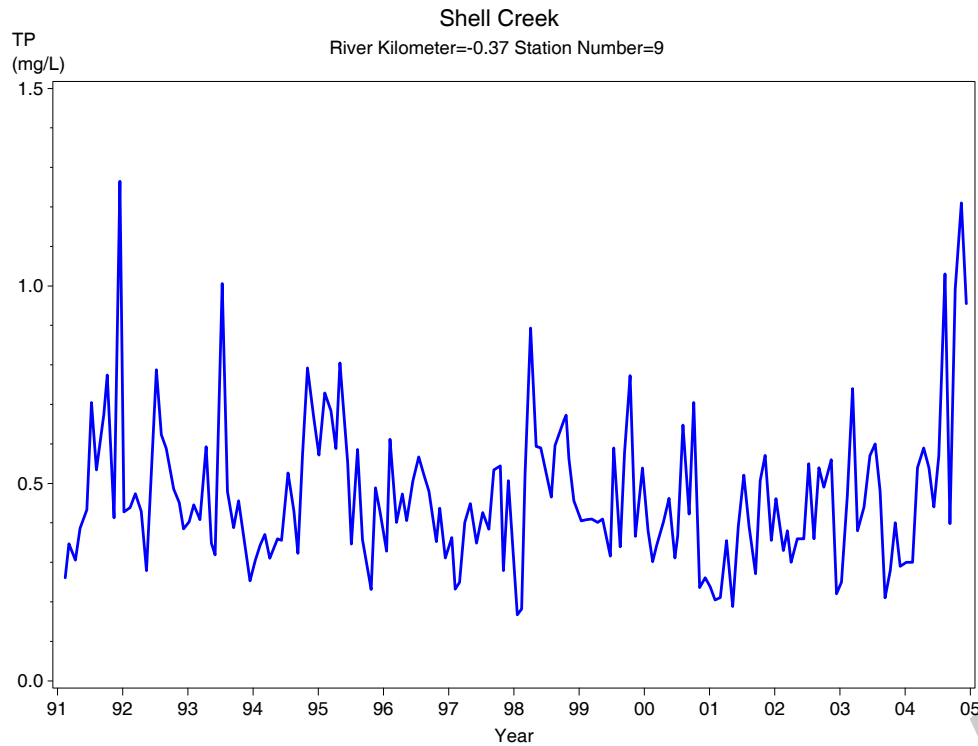


Shell Creek
River Kilometer=10.15 Station Number=3

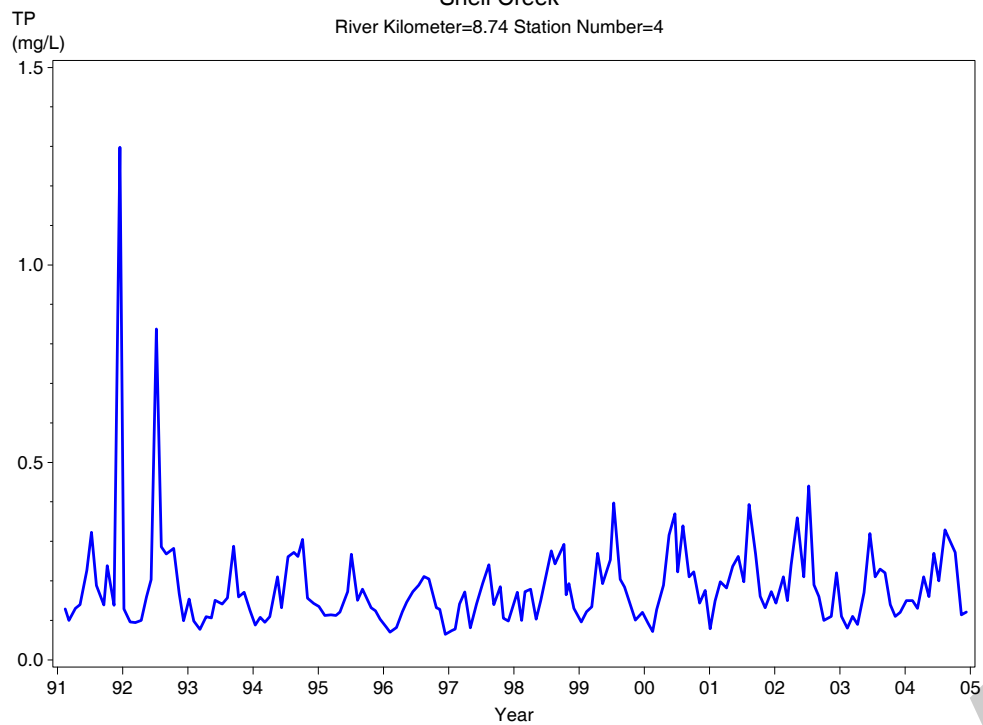




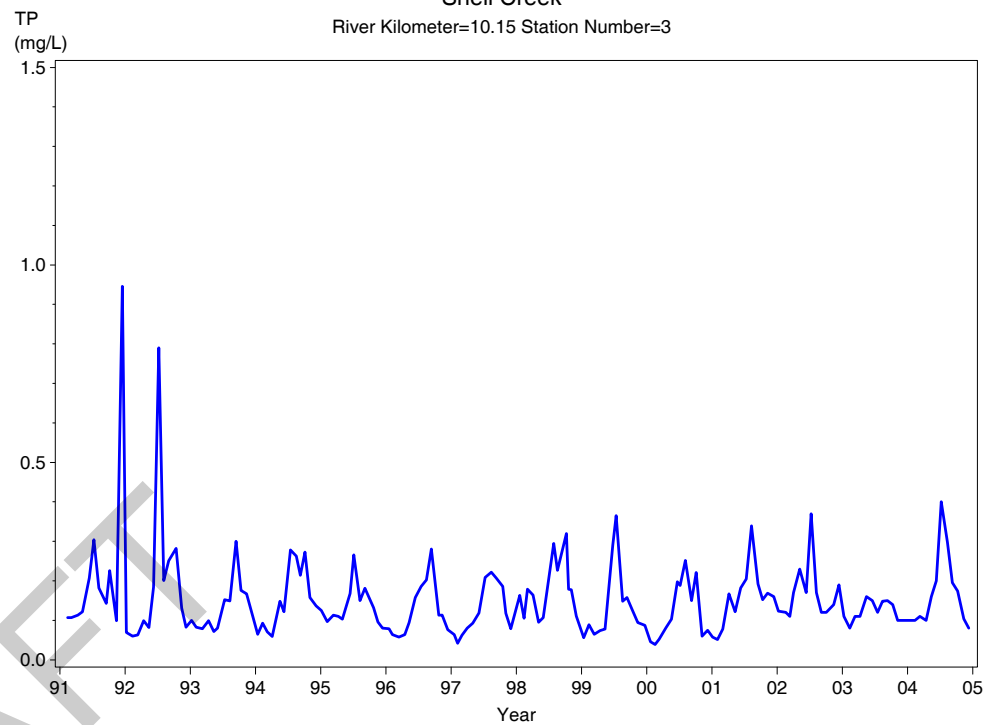




Shell Creek
River Kilometer=8.74 Station Number=4



Shell Creek
River Kilometer=10.15 Station Number=3



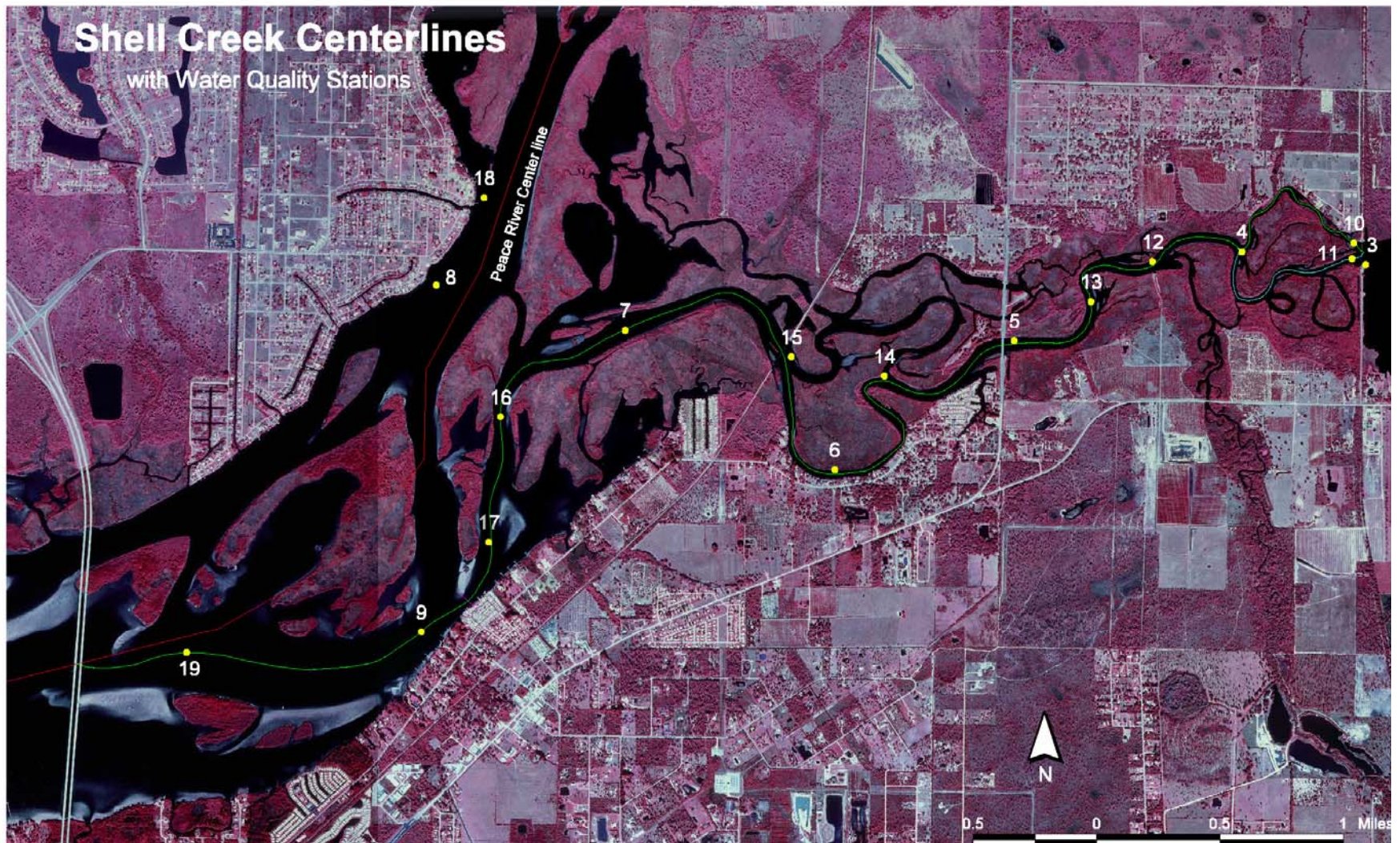
Appendix 3-4

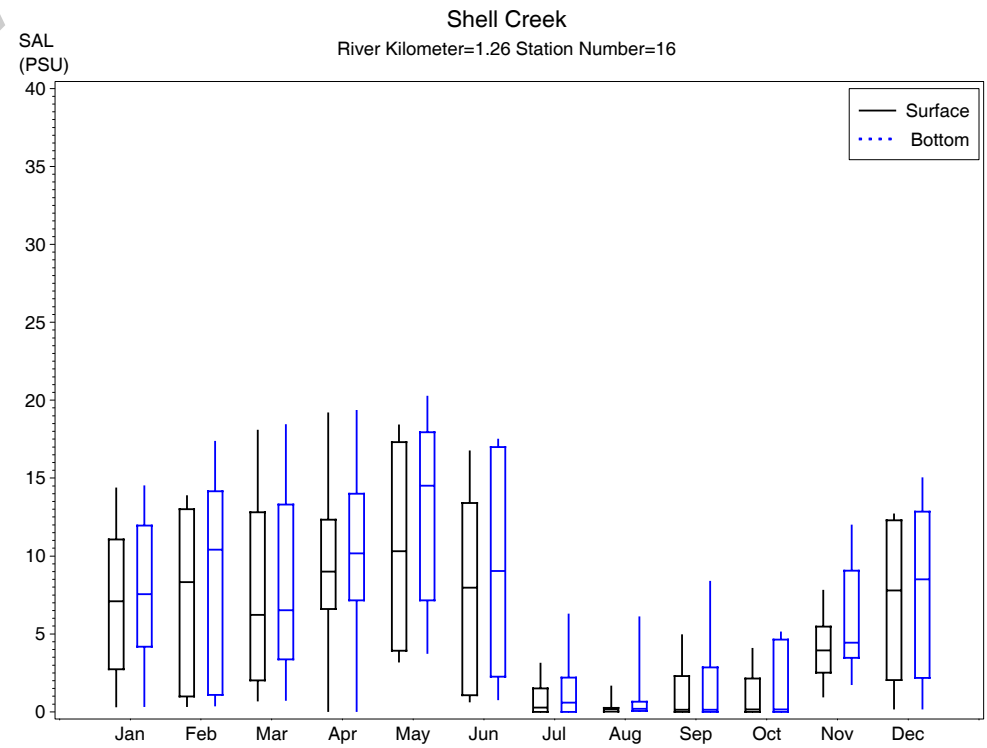
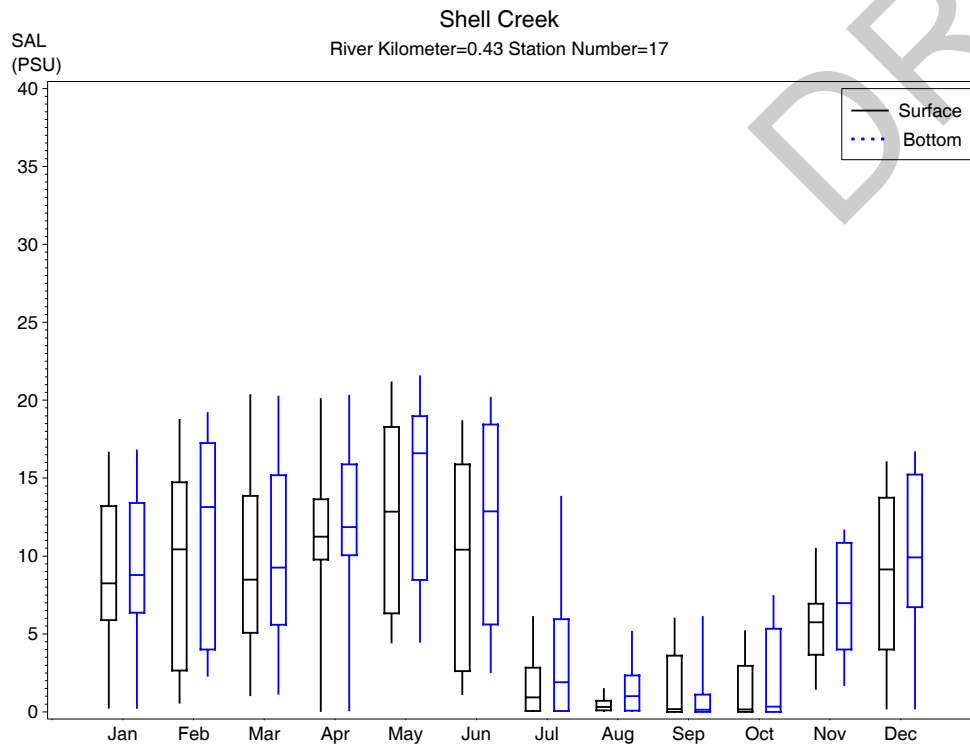
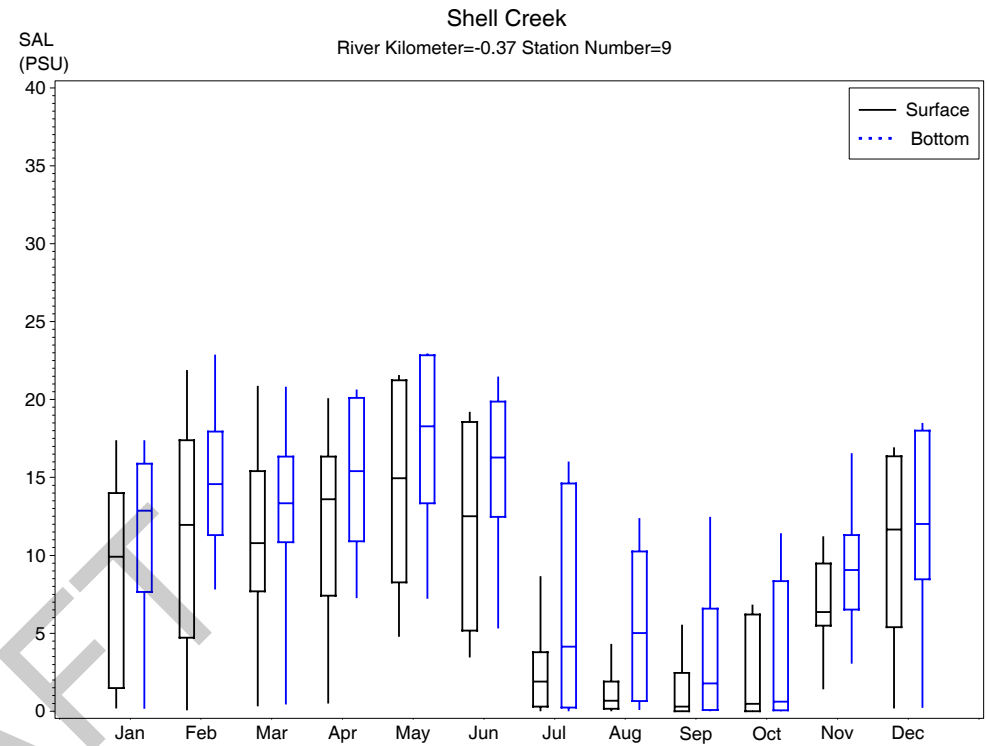
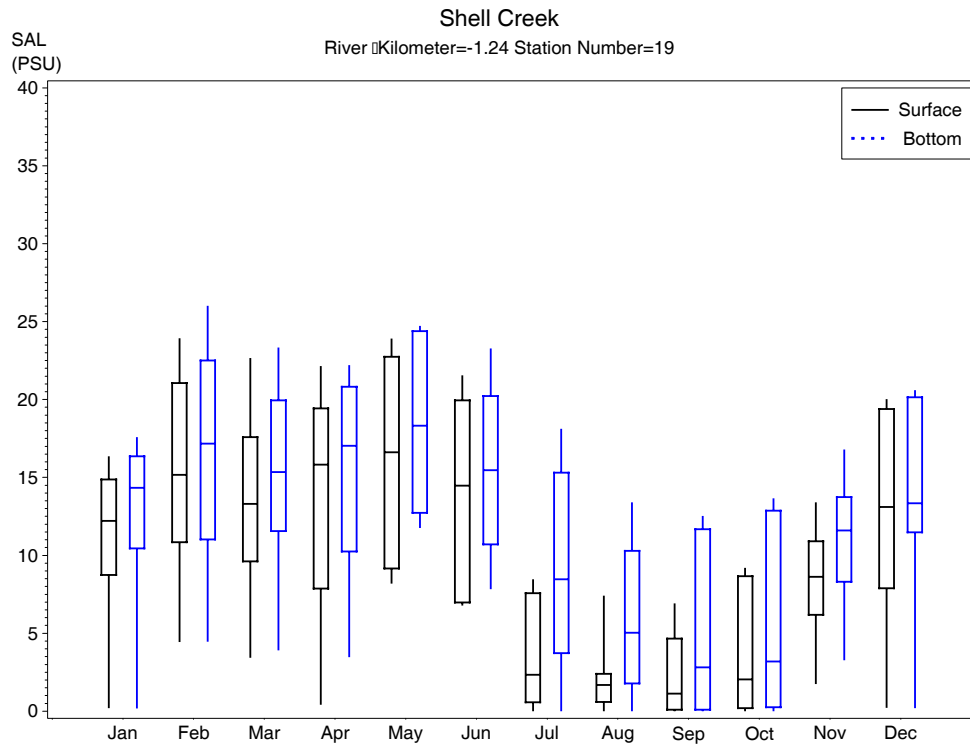
Within-Year Variation in Shell Creek

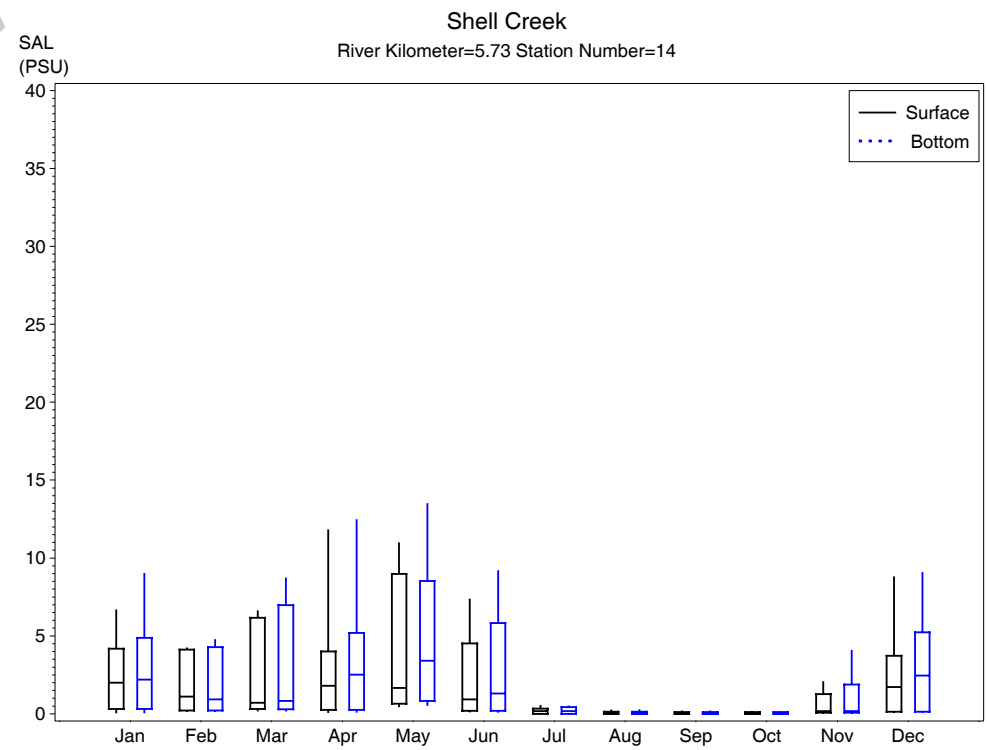
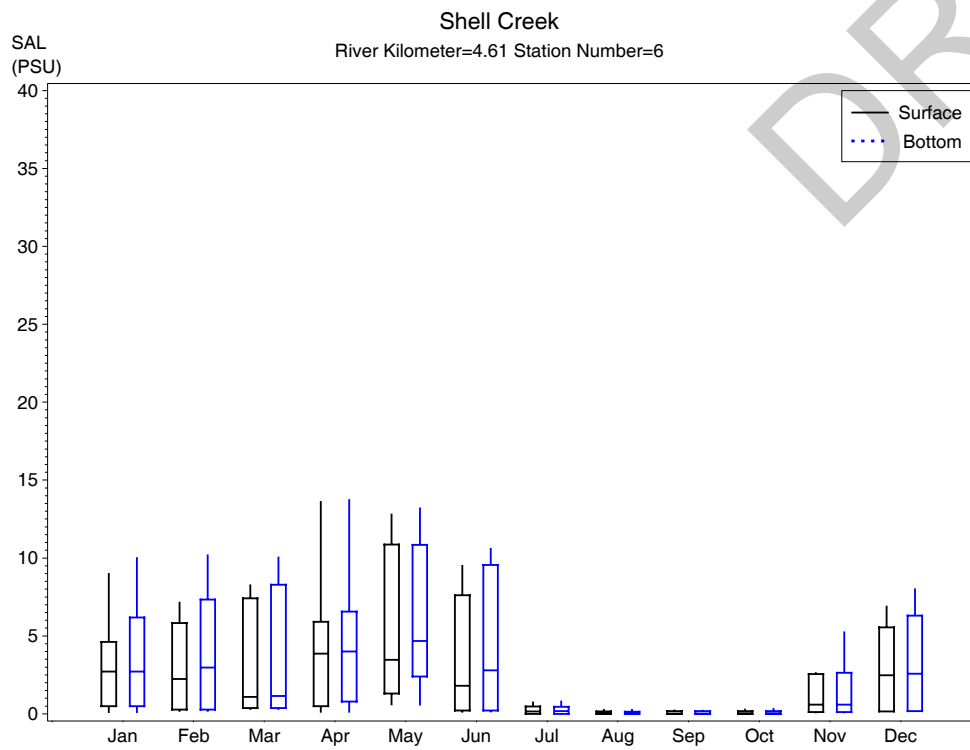
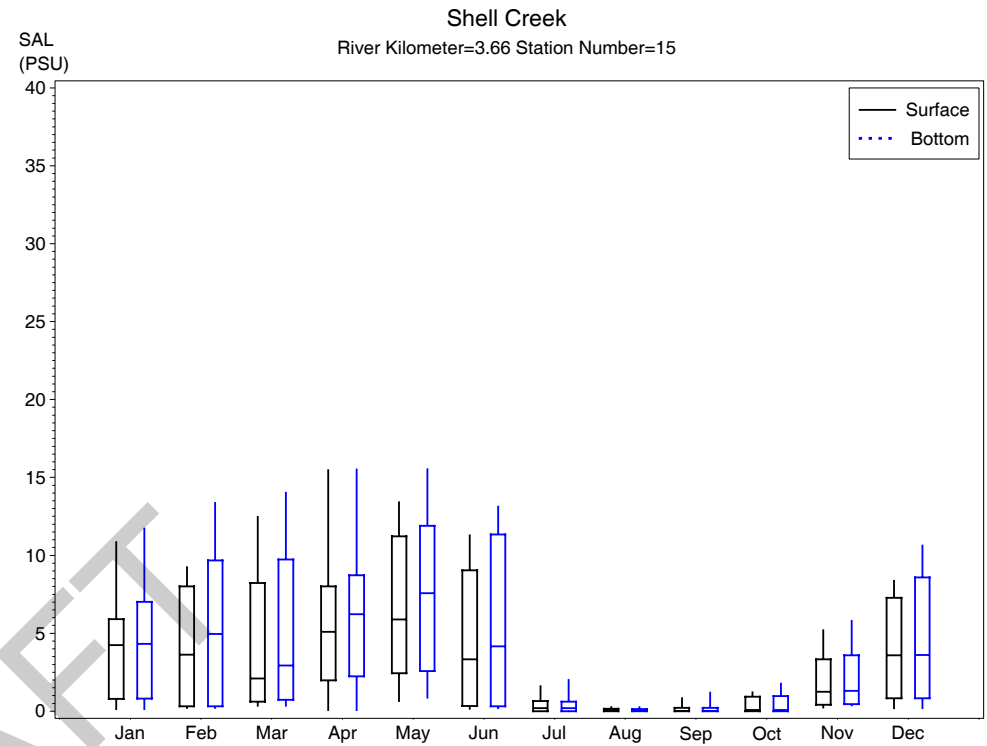
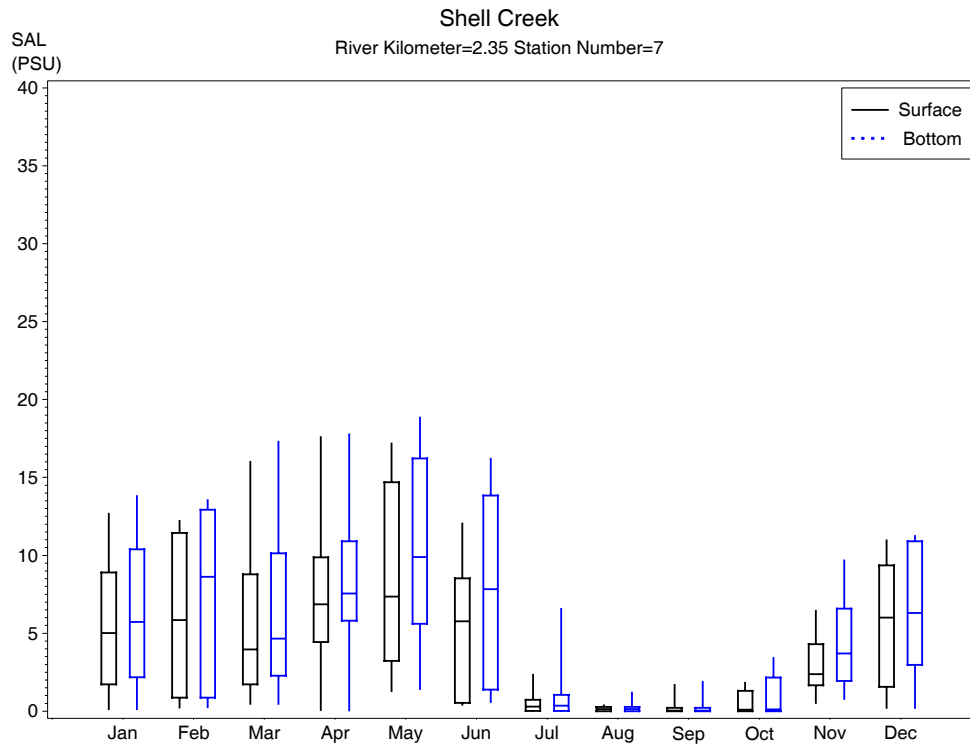
Water Quality Constituents

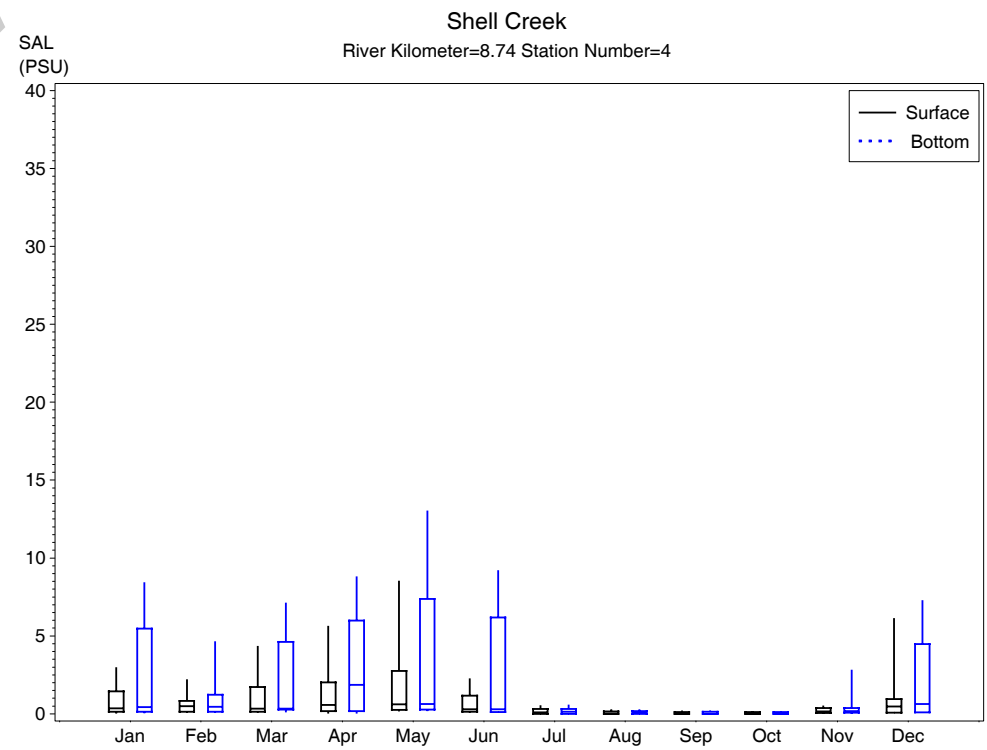
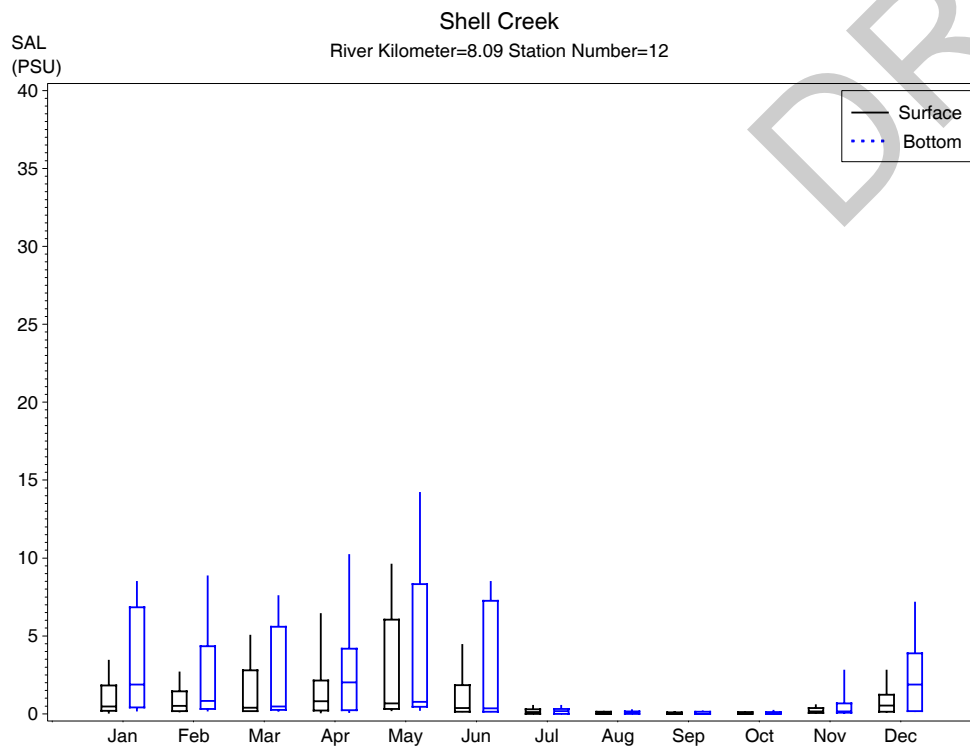
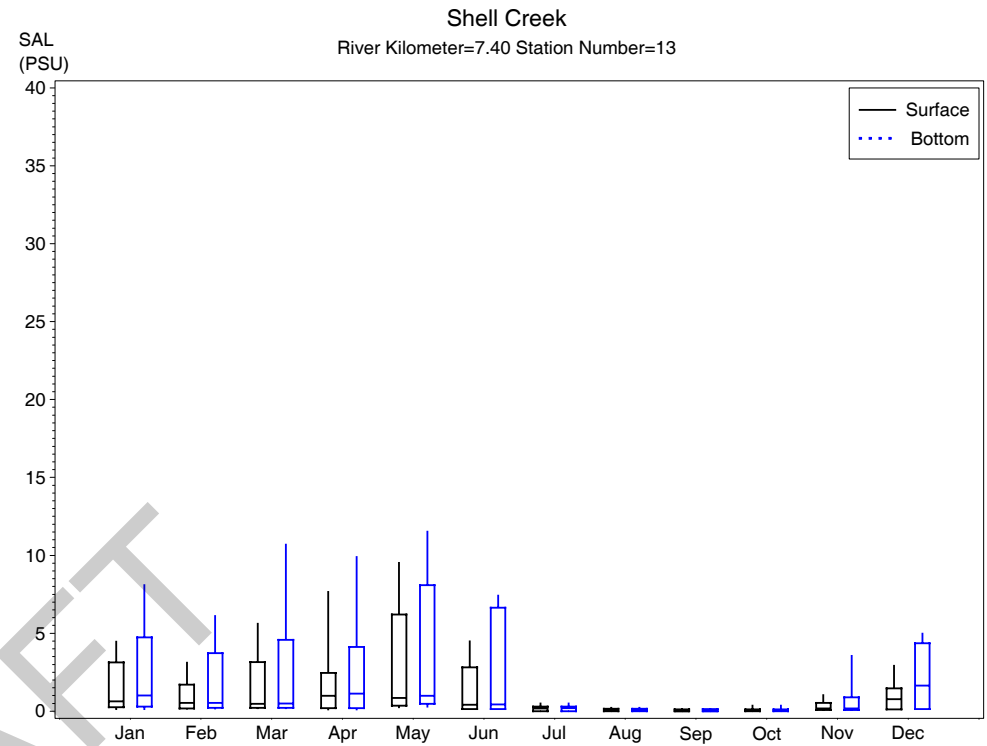
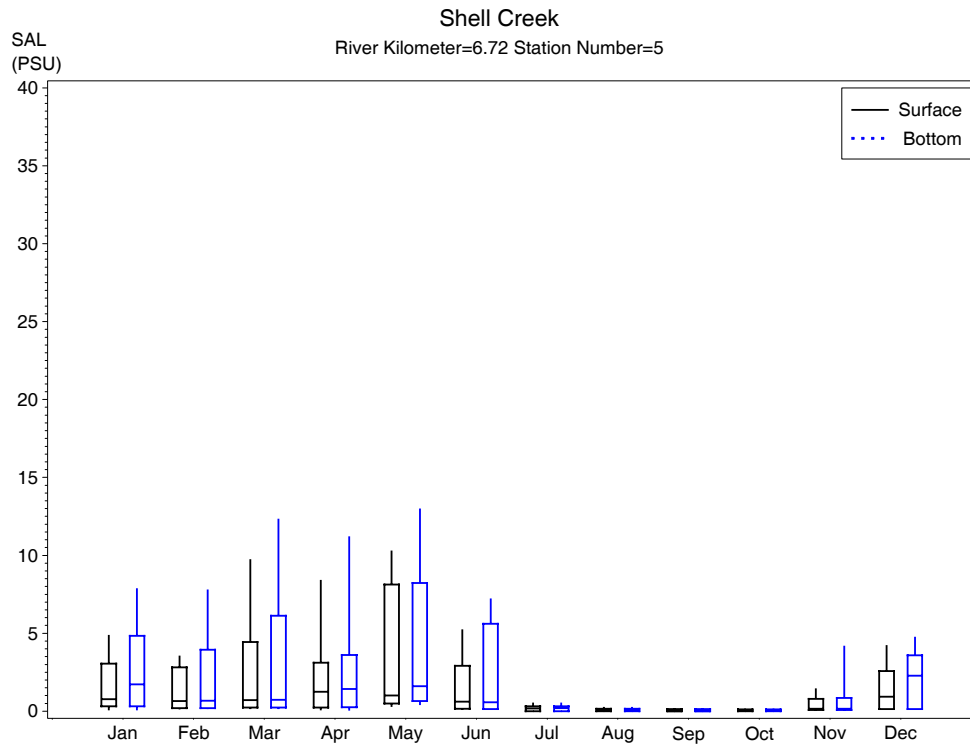
Shell Creek Centerlines

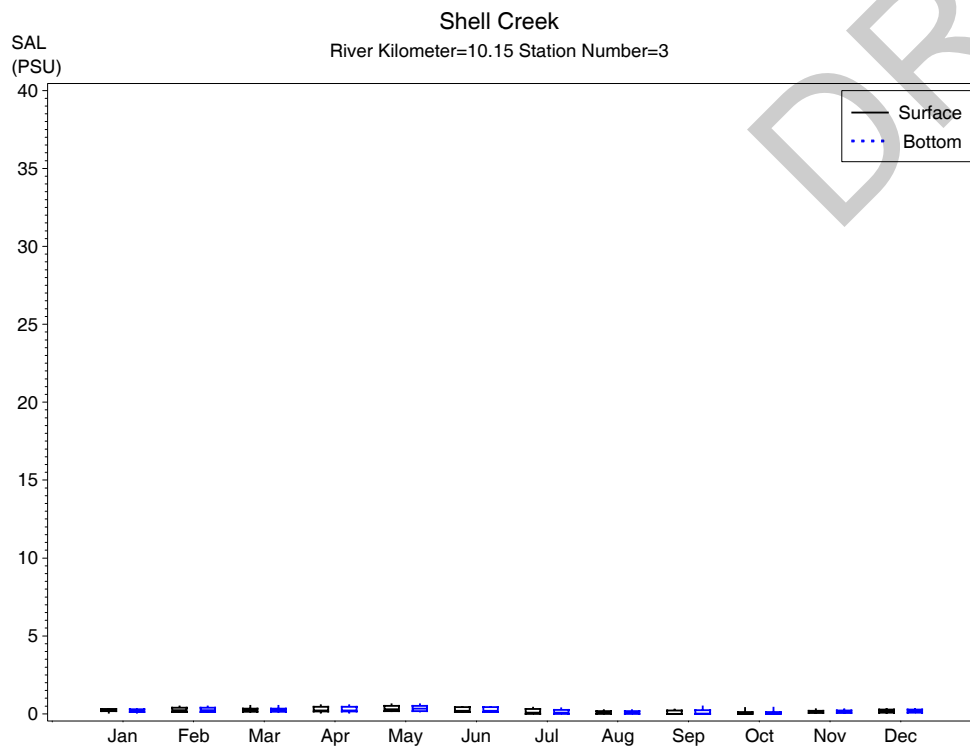
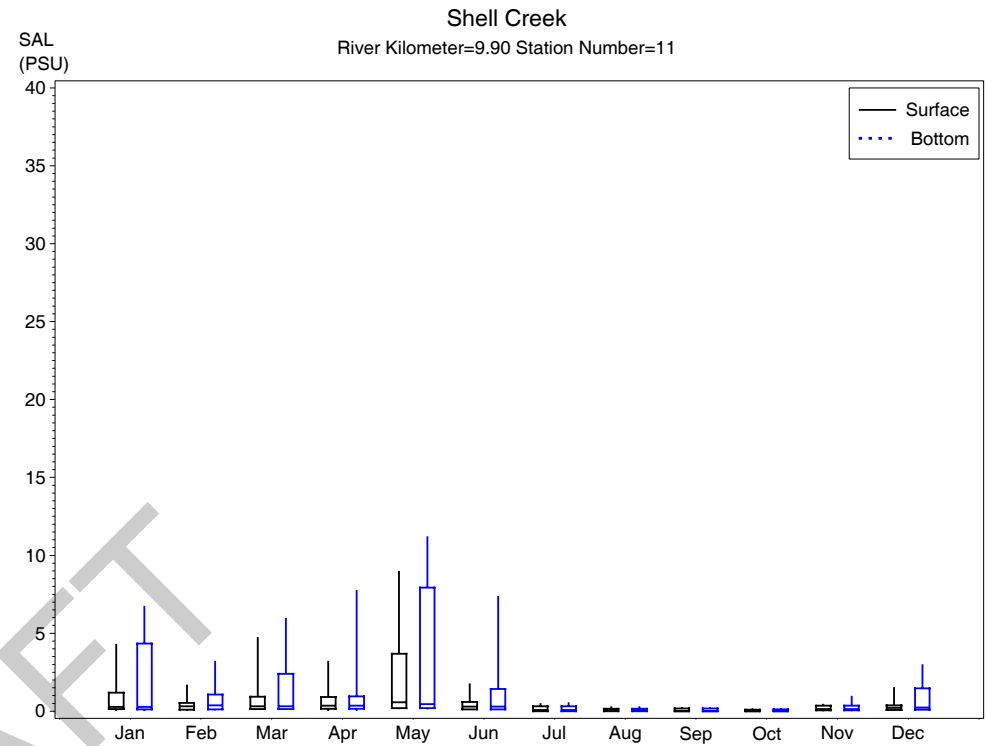
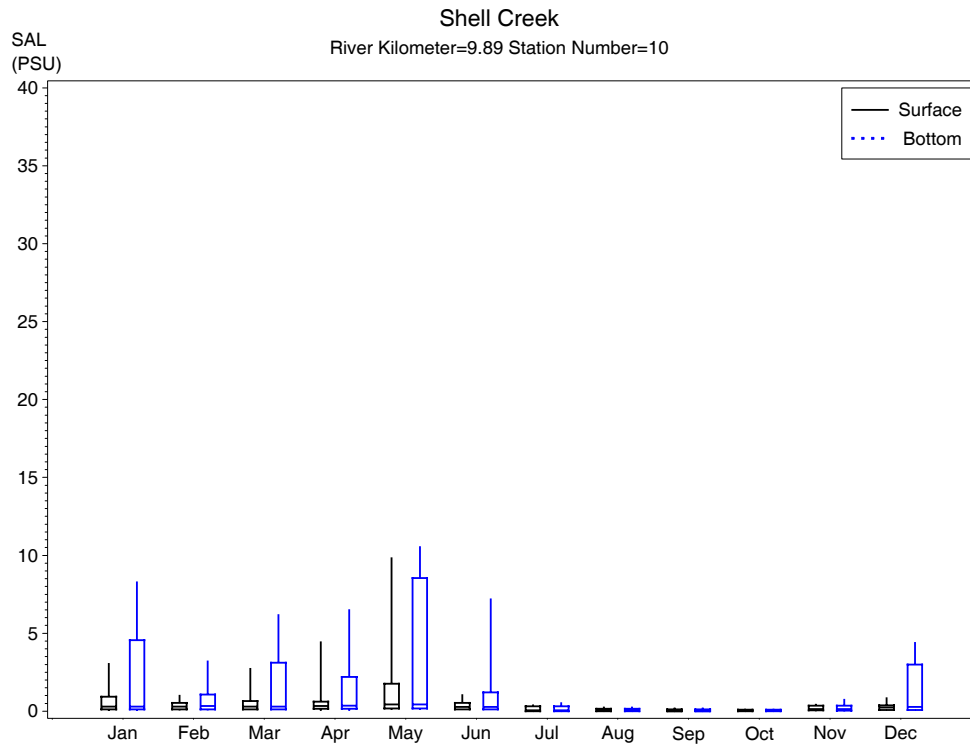
with Water Quality Stations

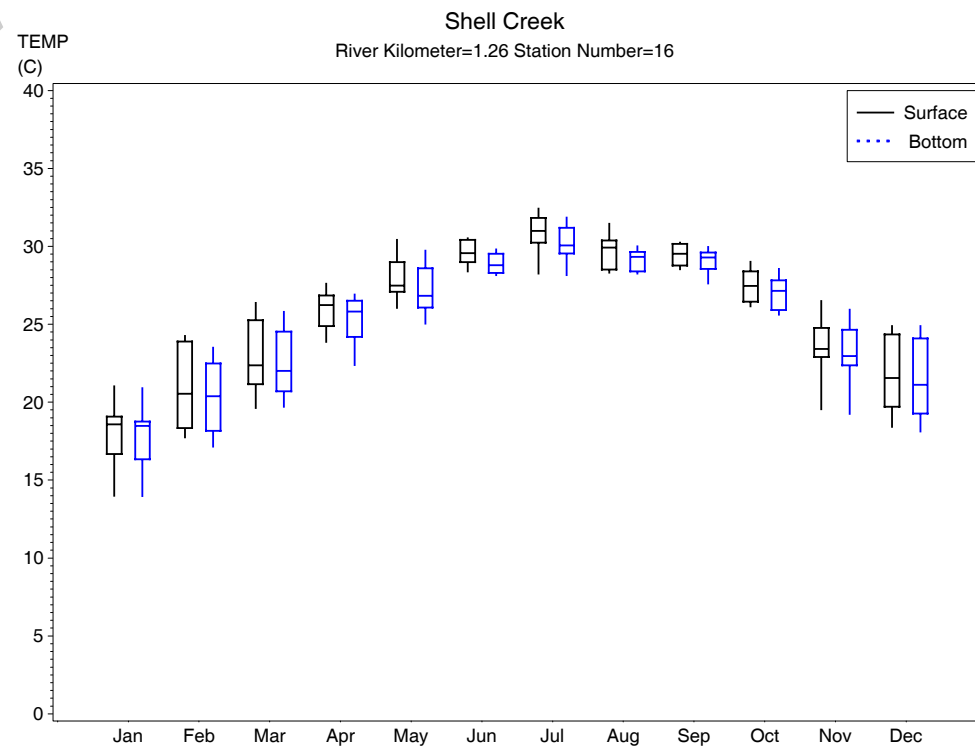
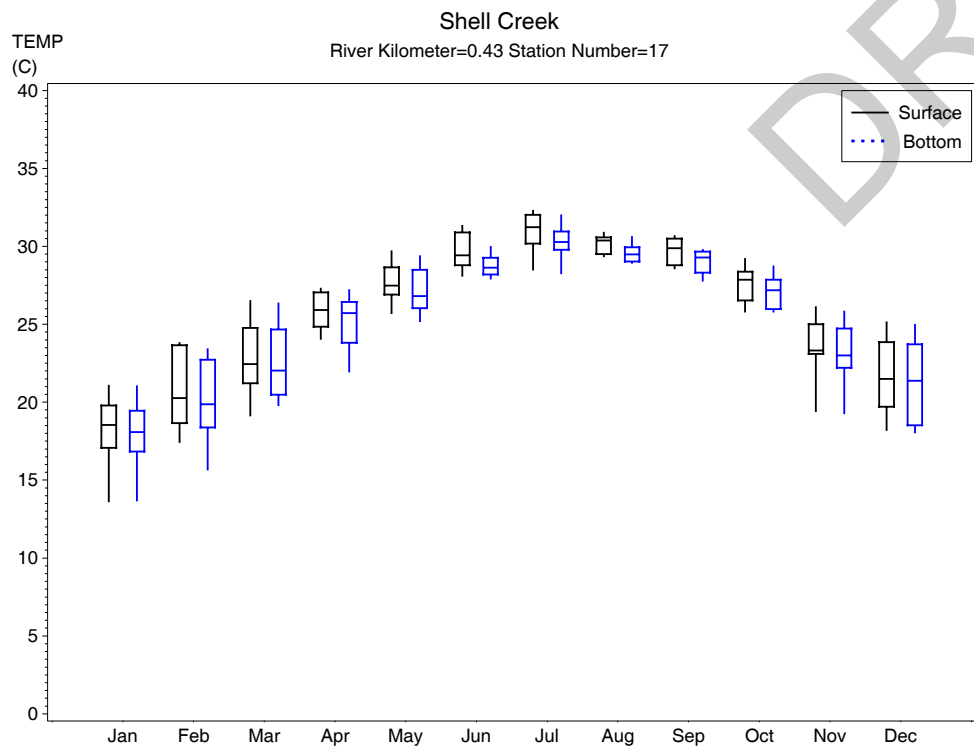
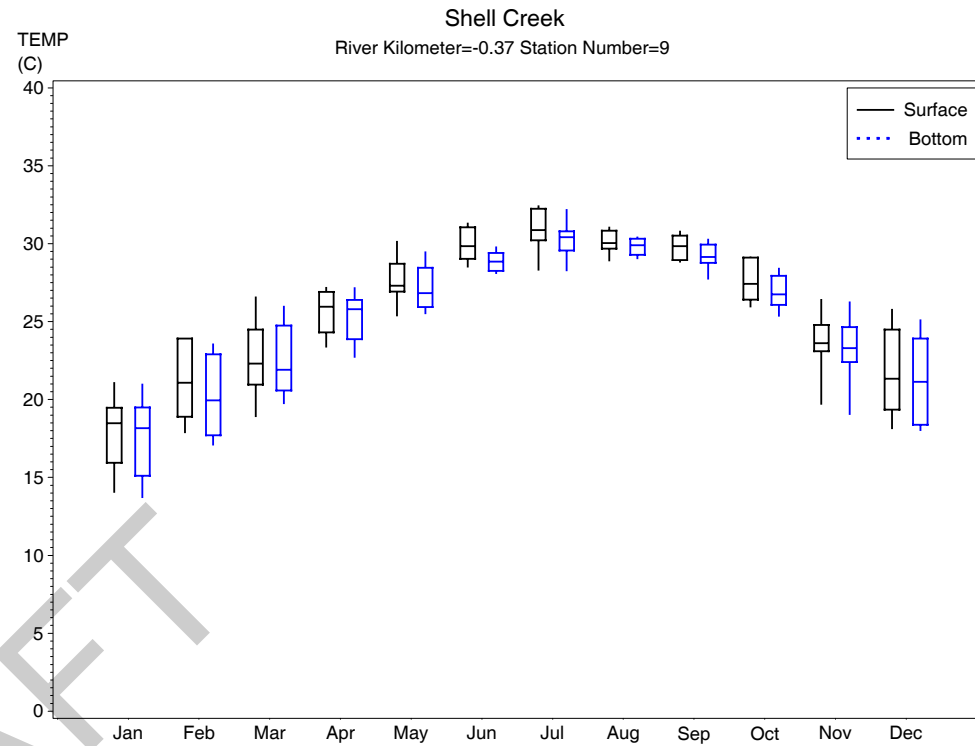
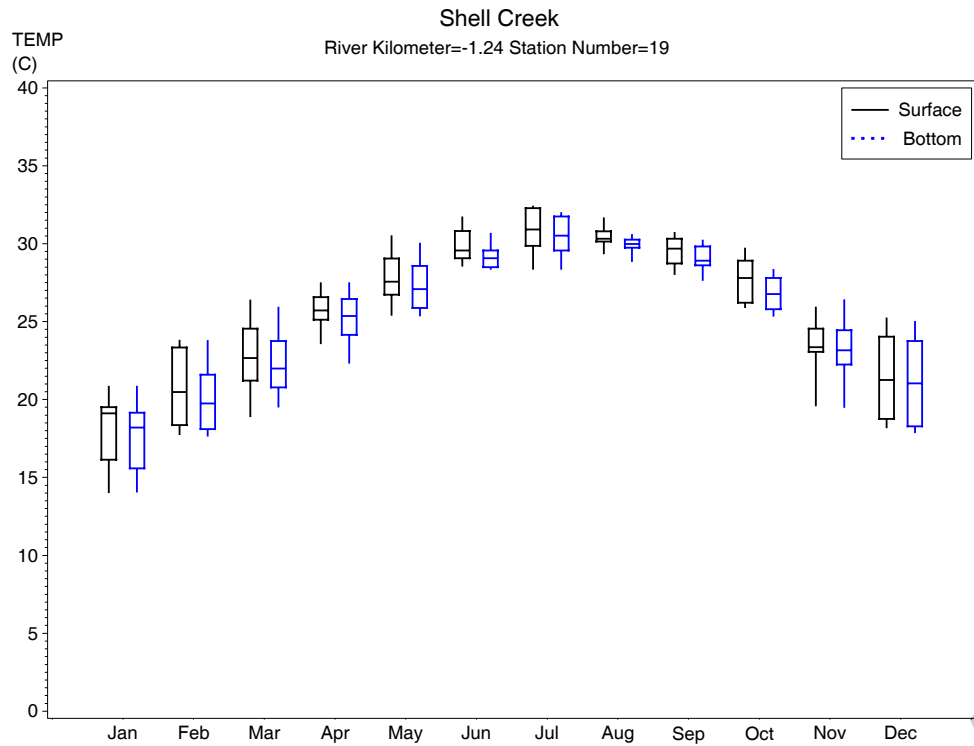


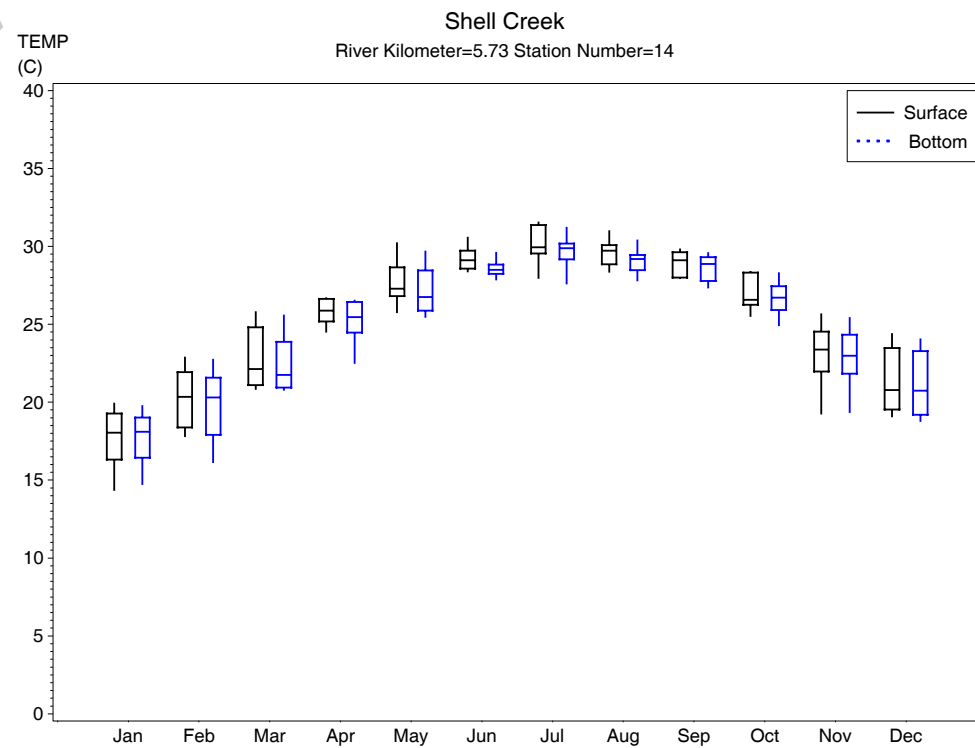
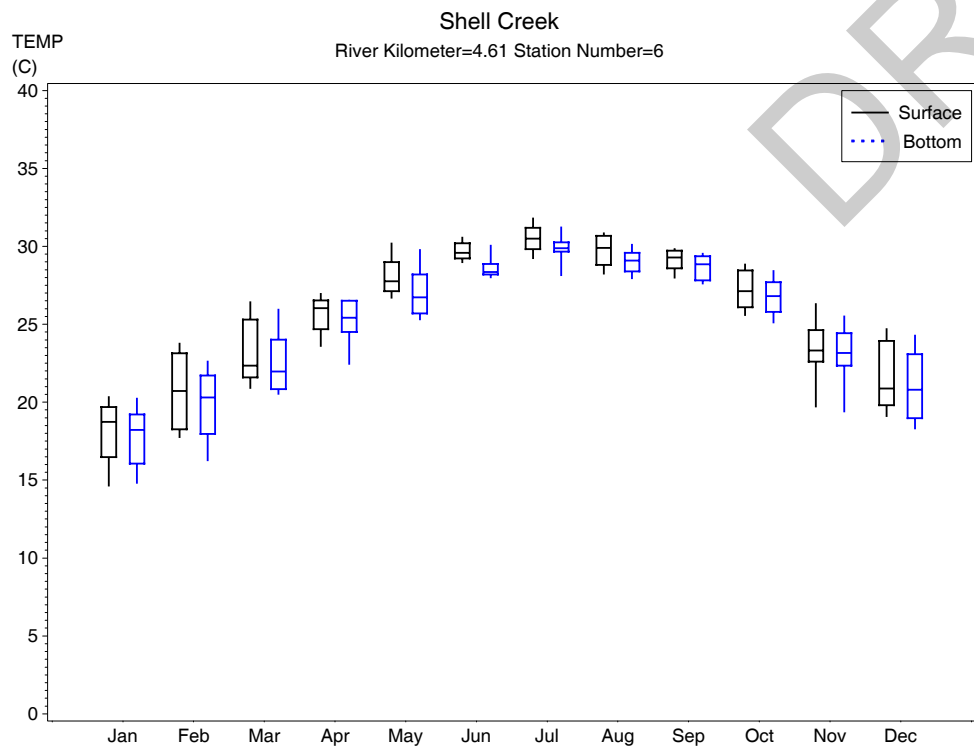
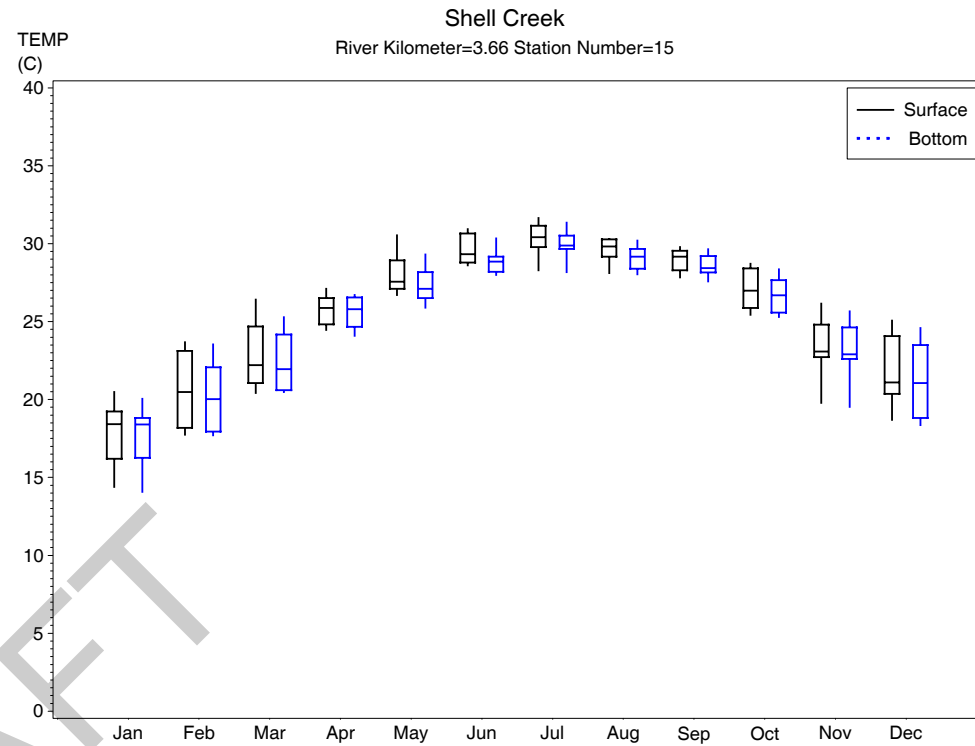
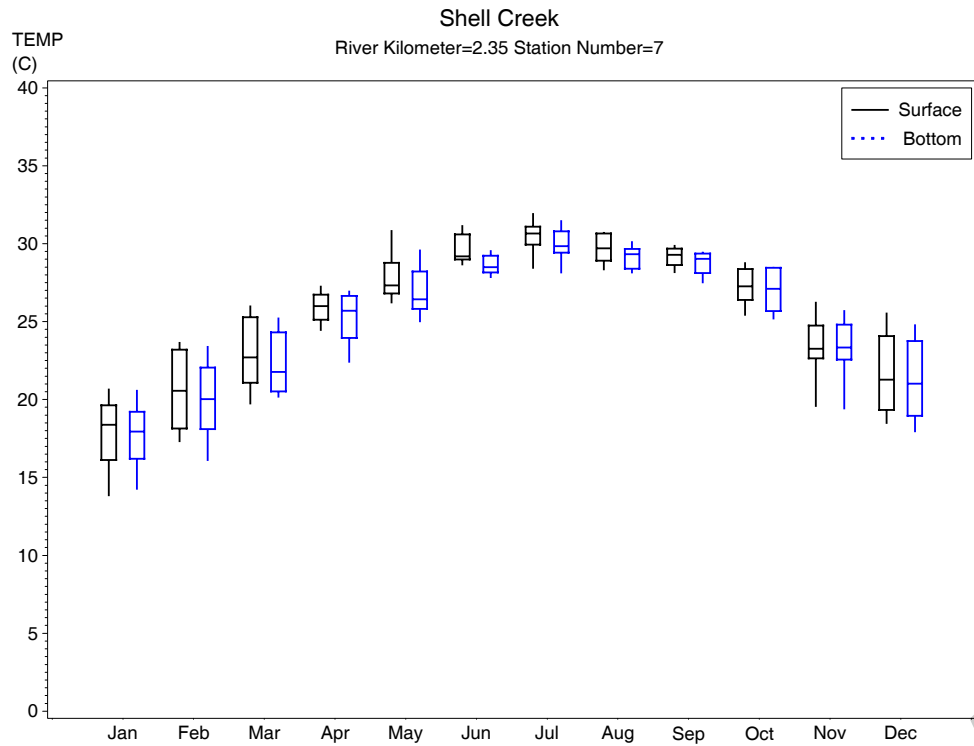


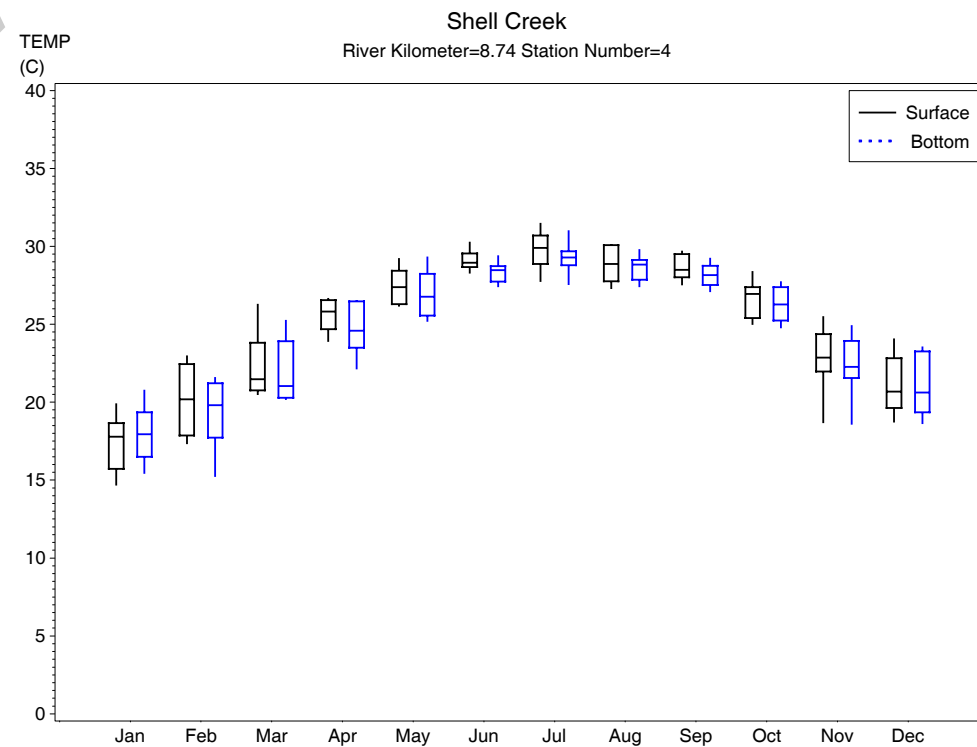
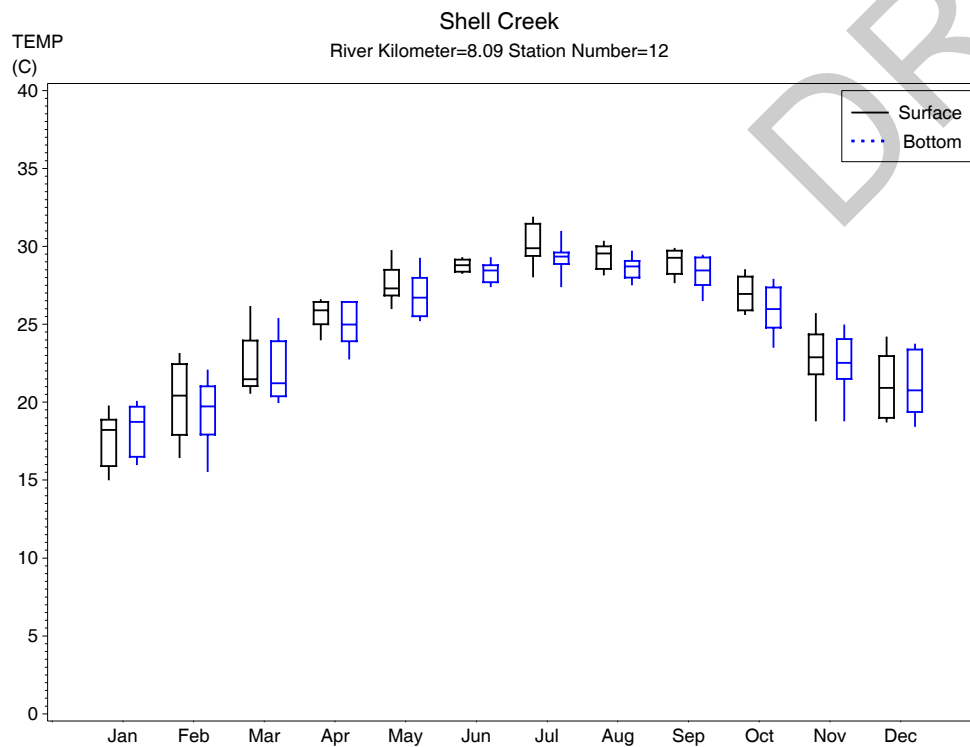
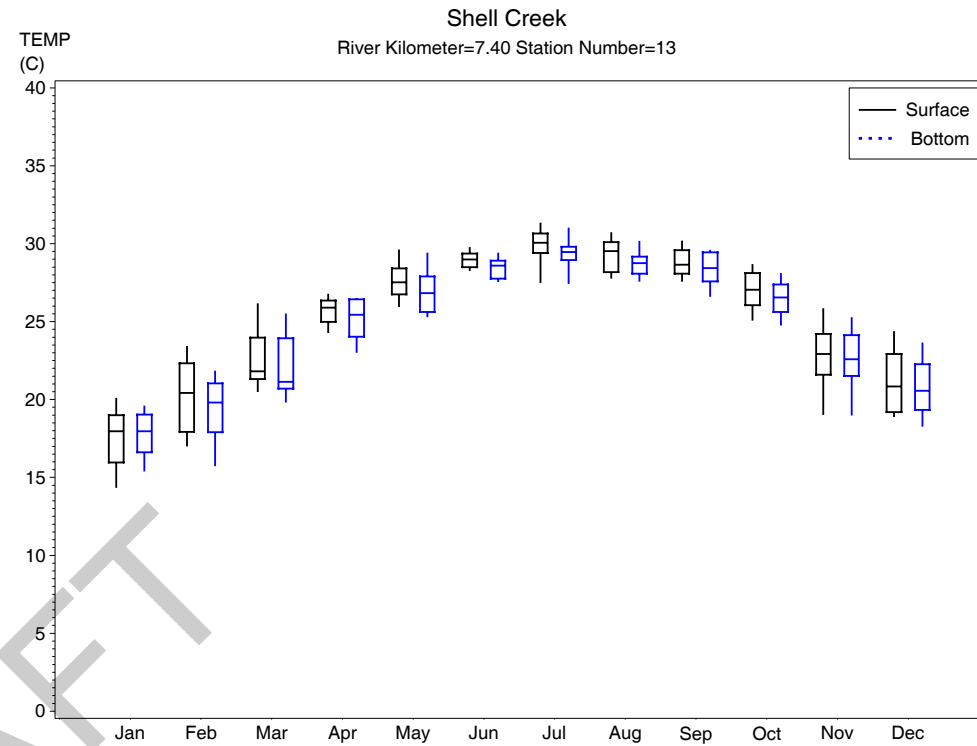
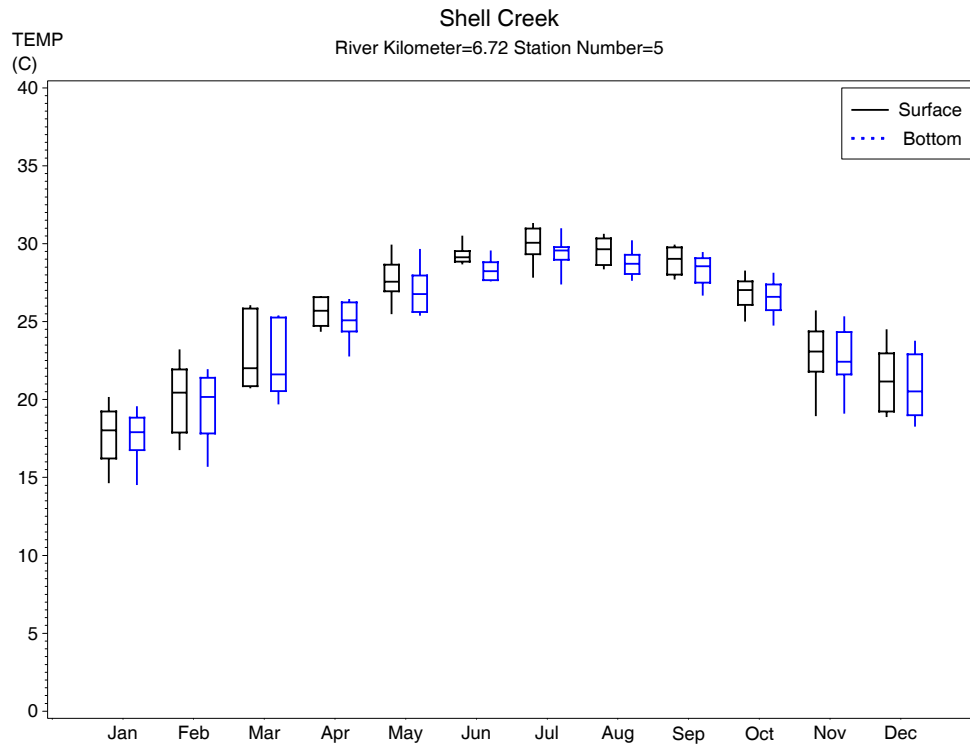


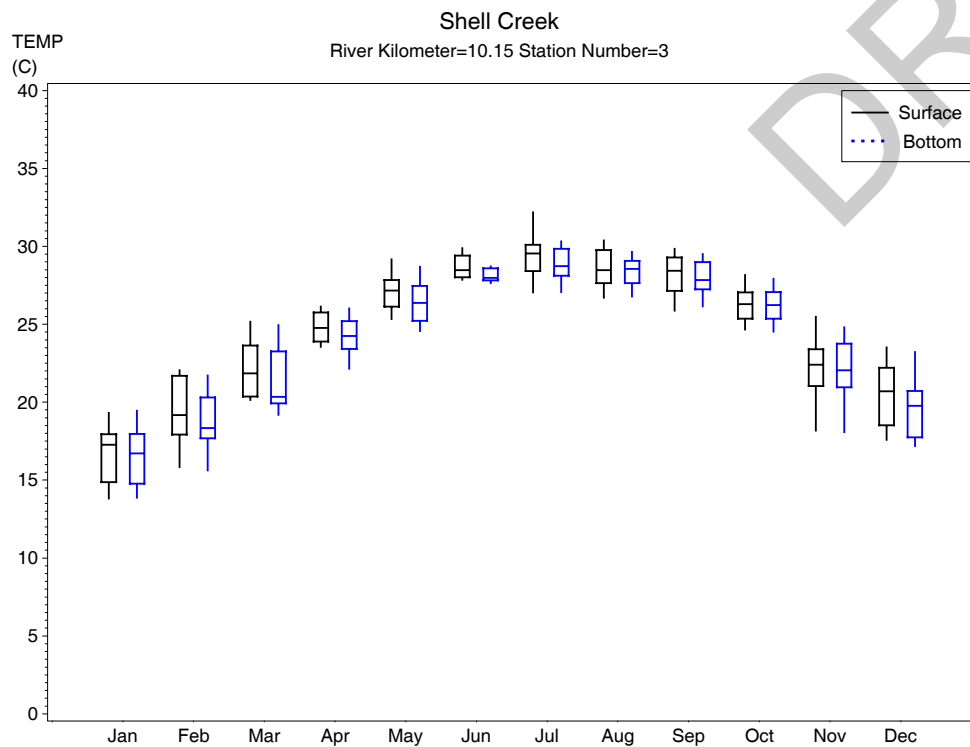
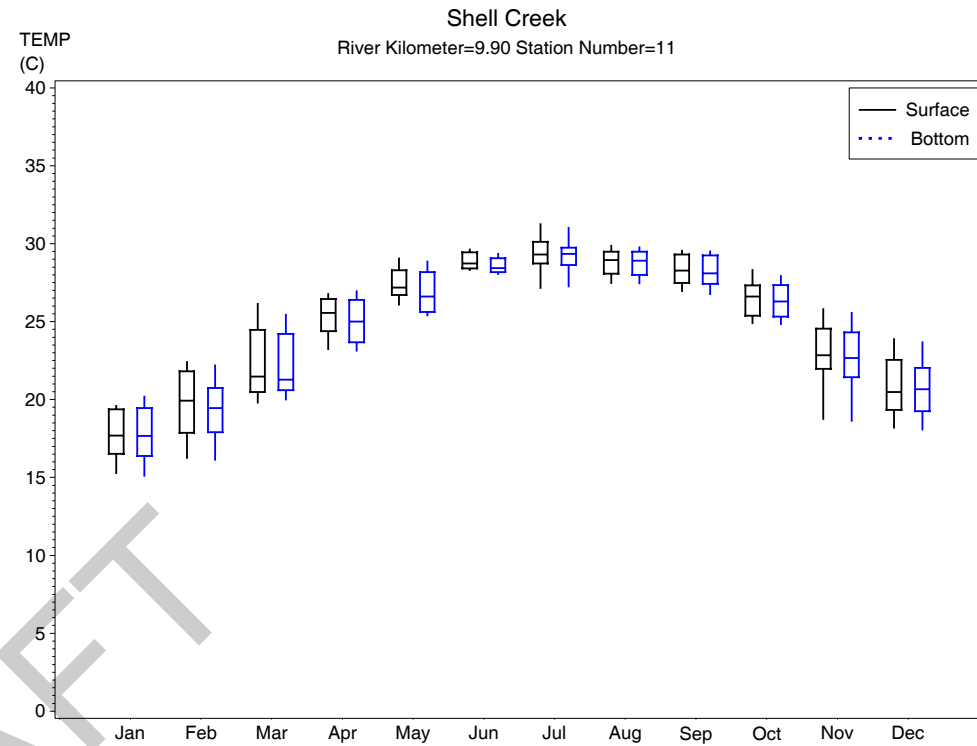
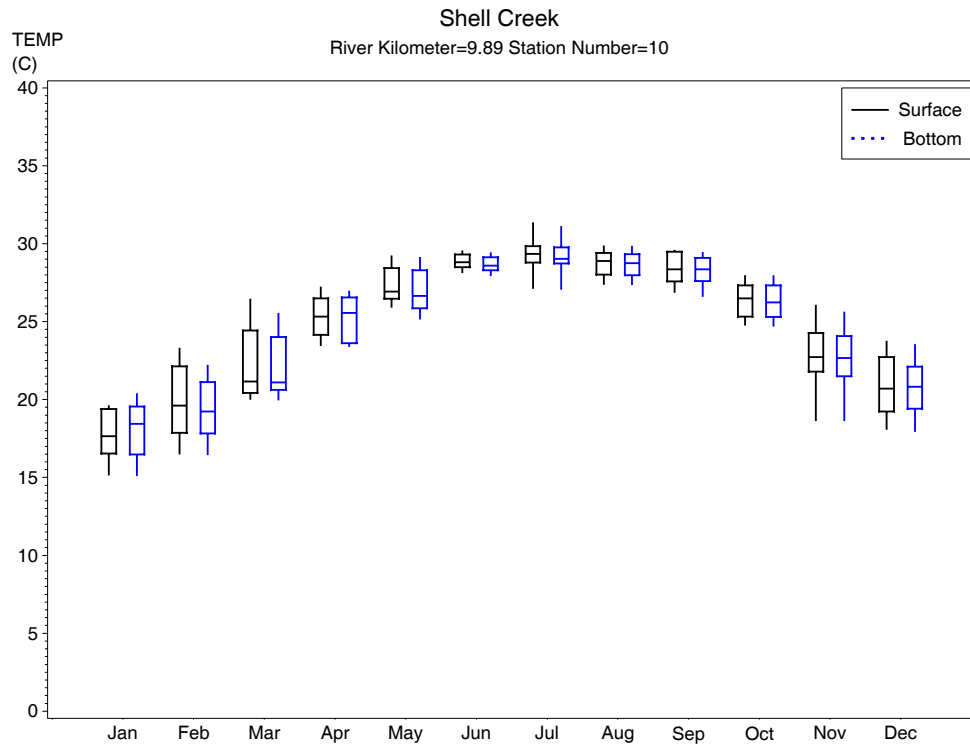


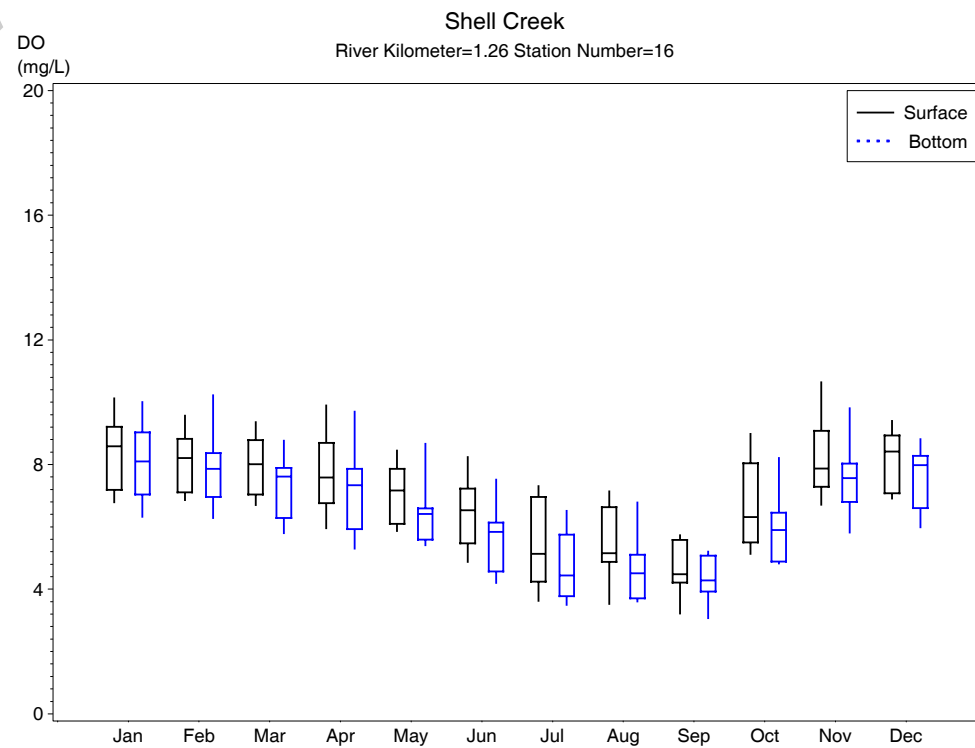
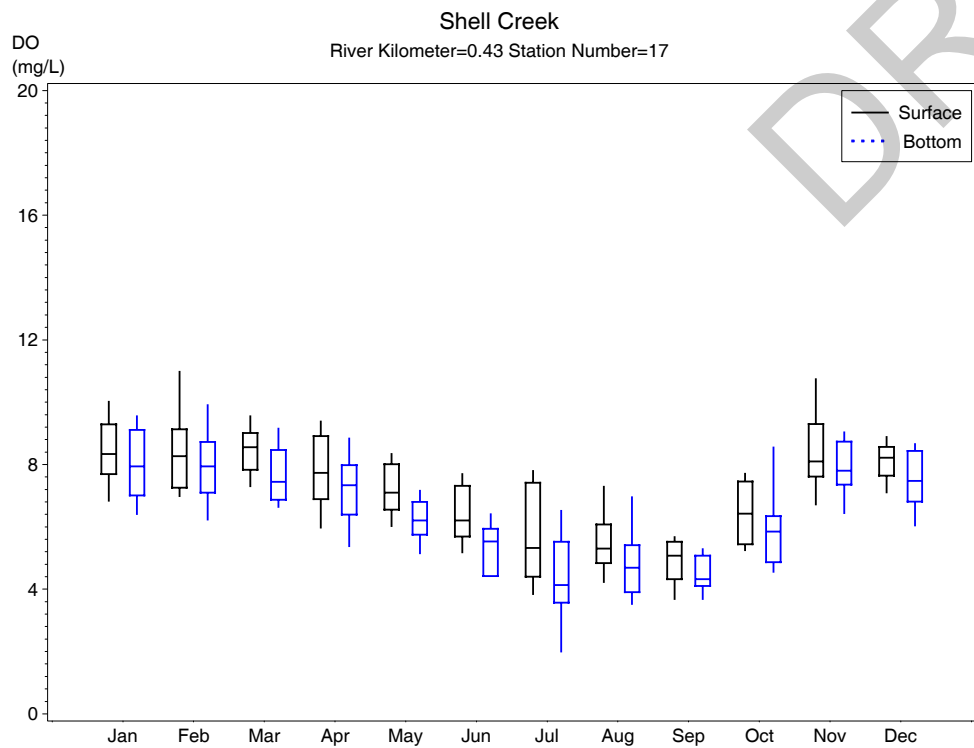
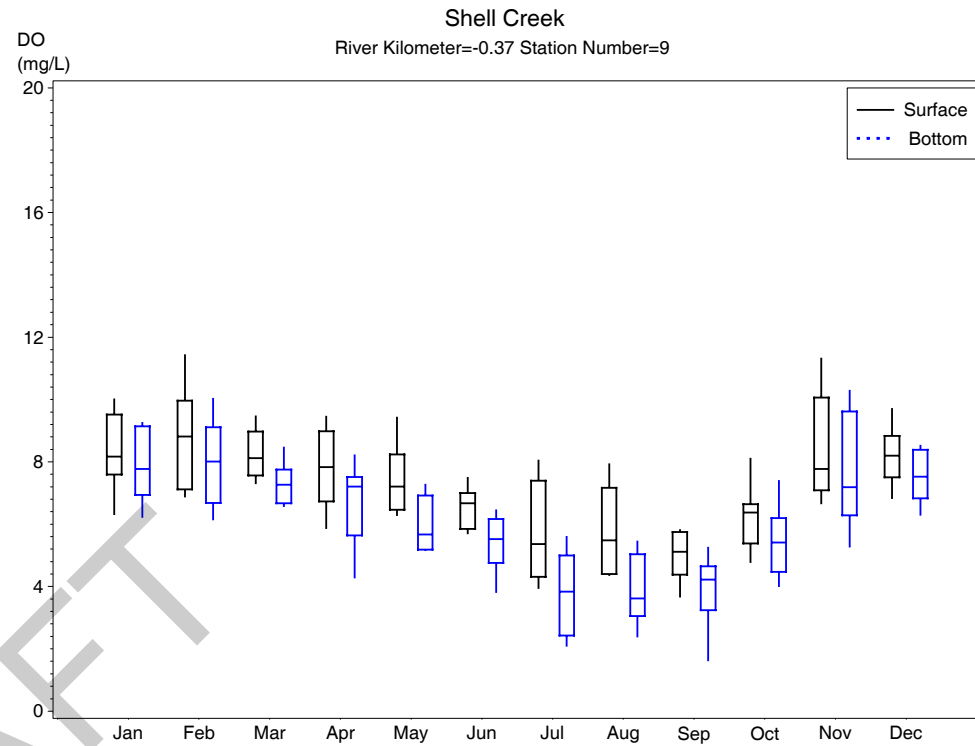
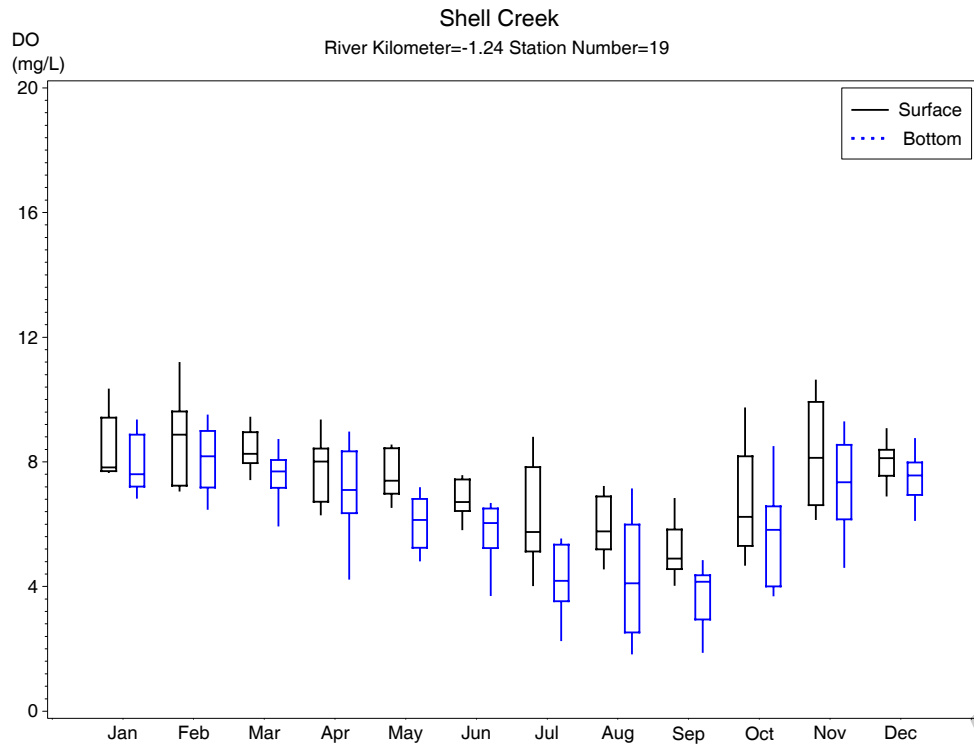


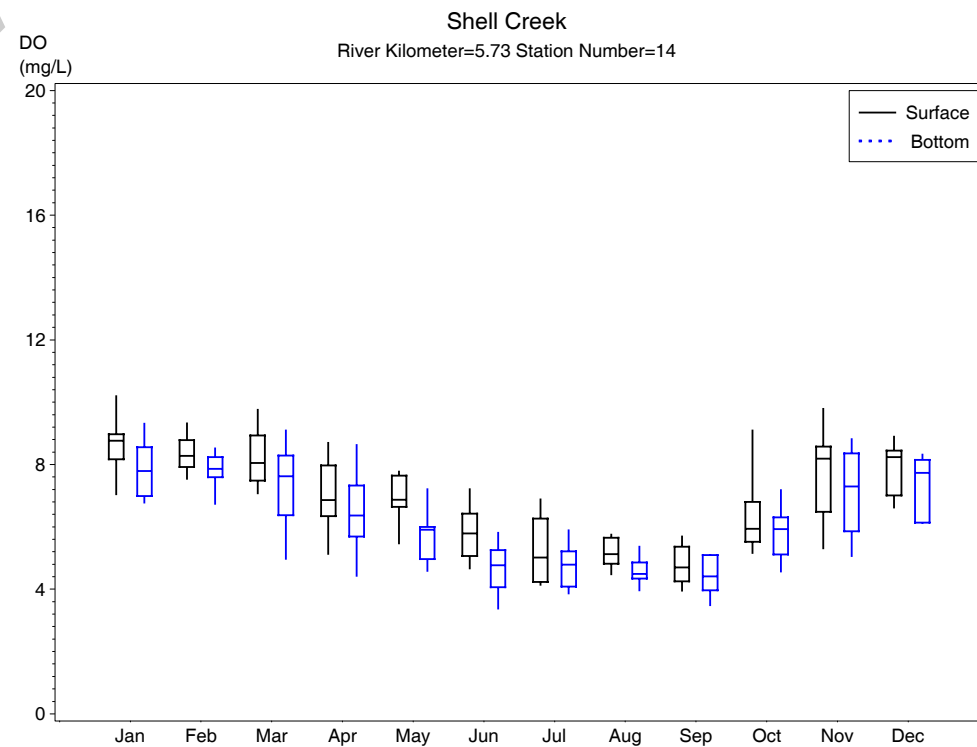
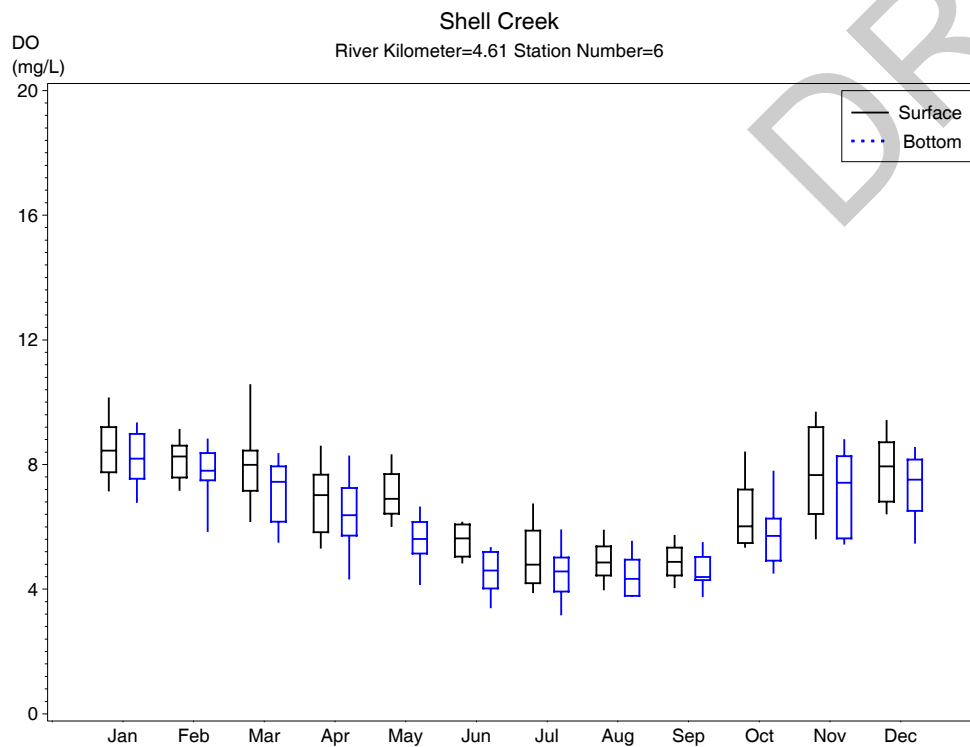
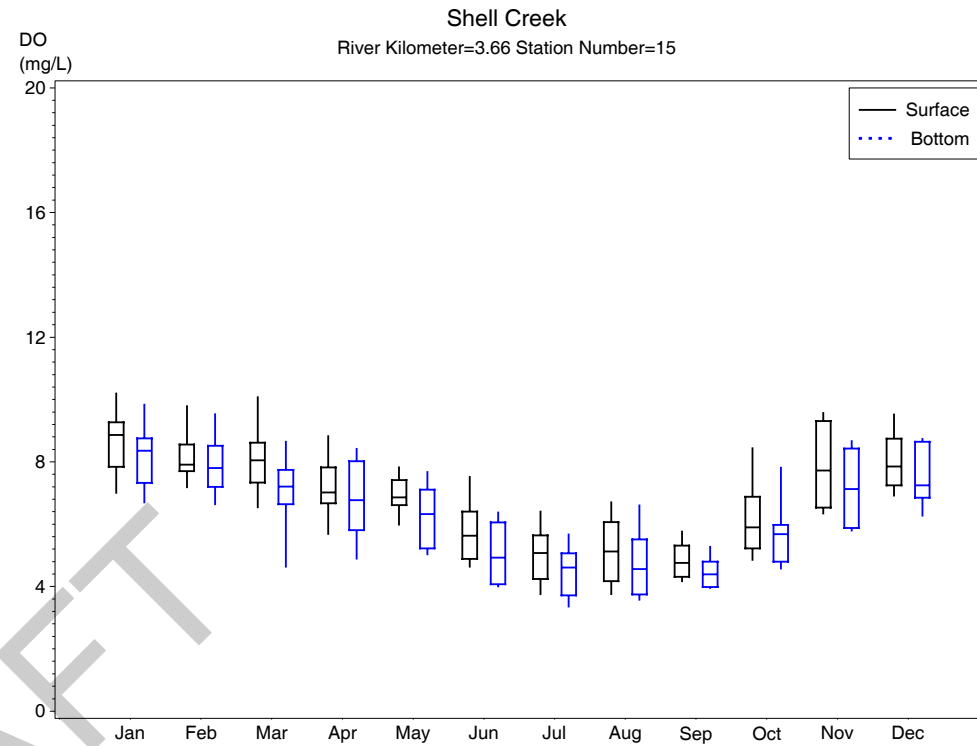
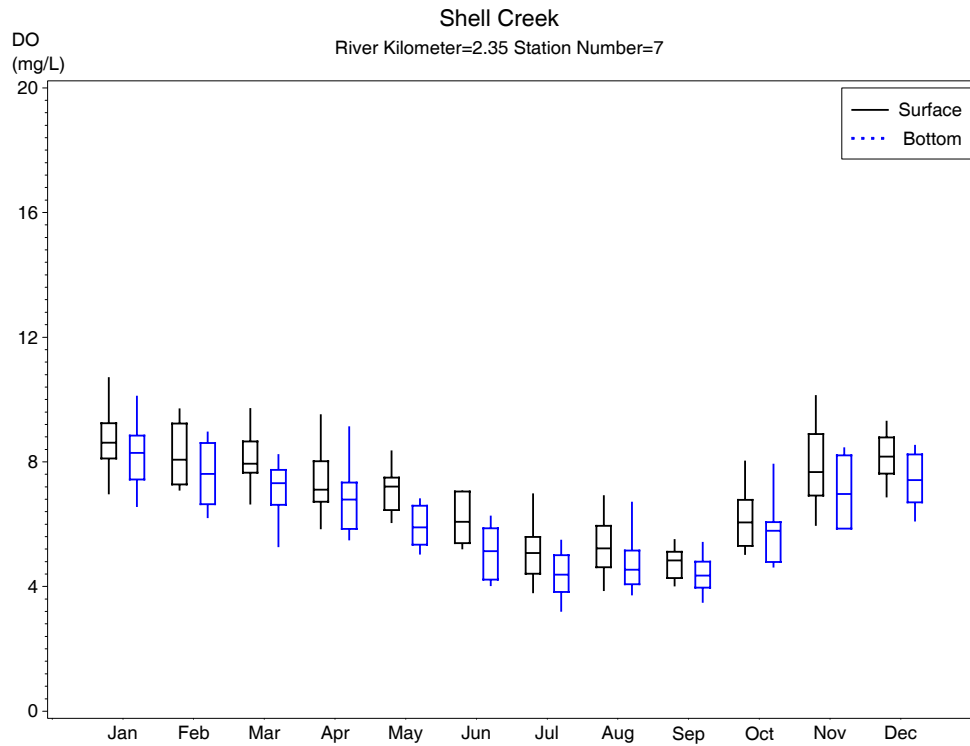


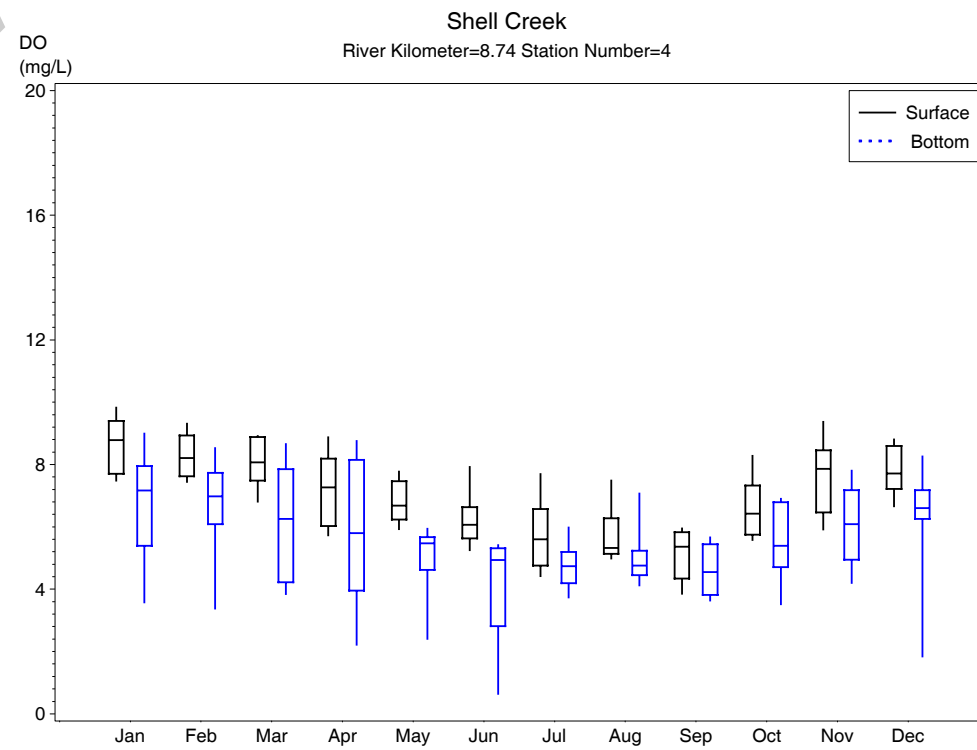
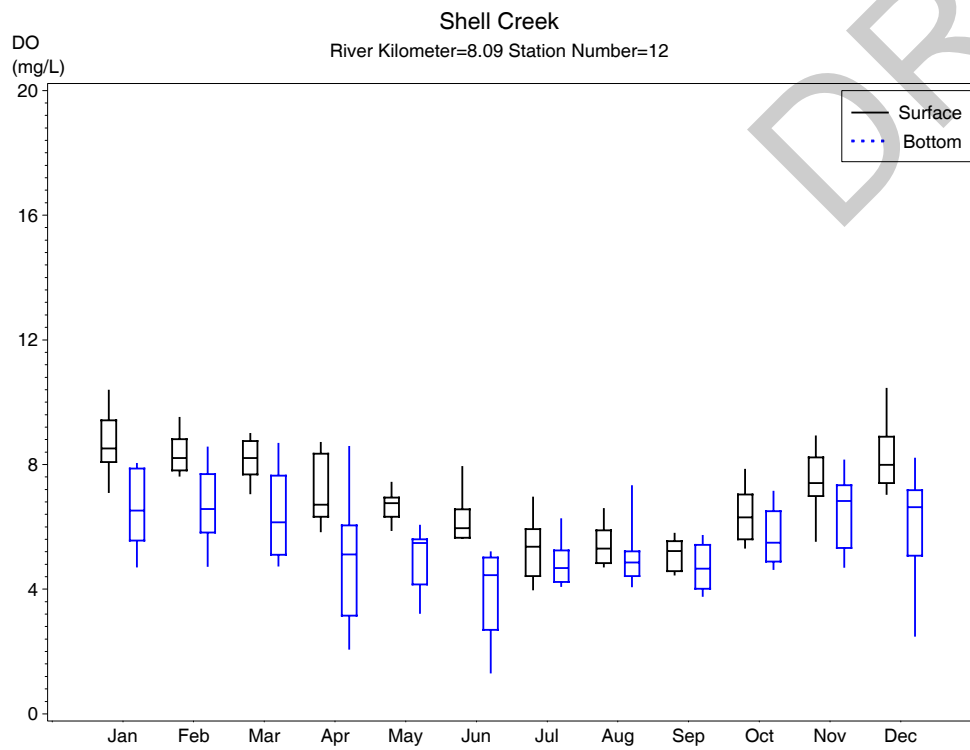
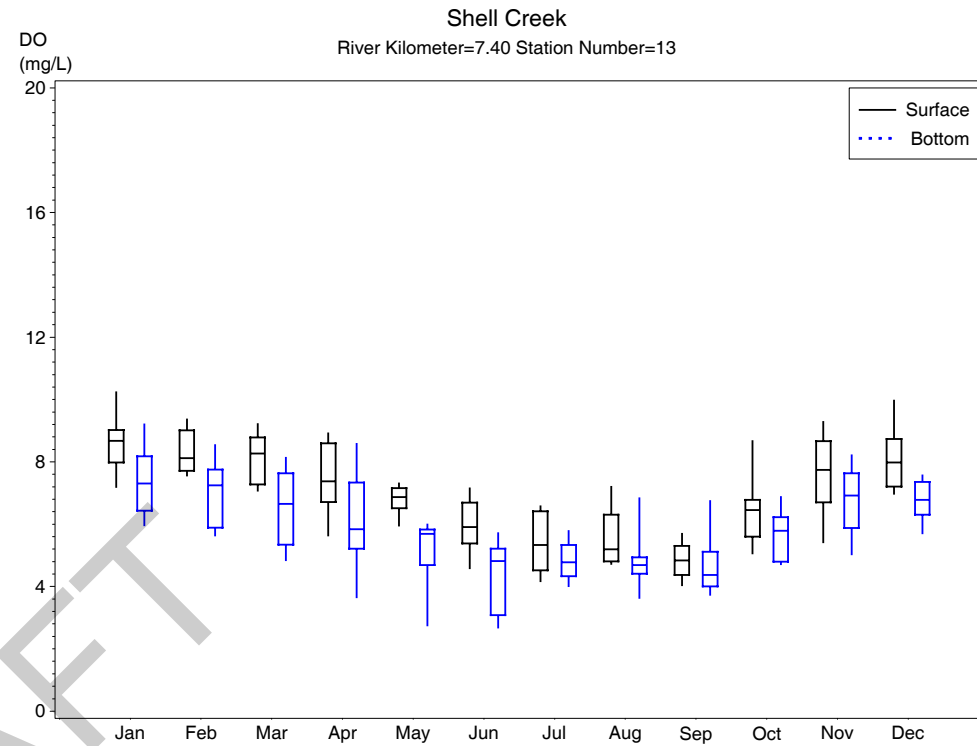
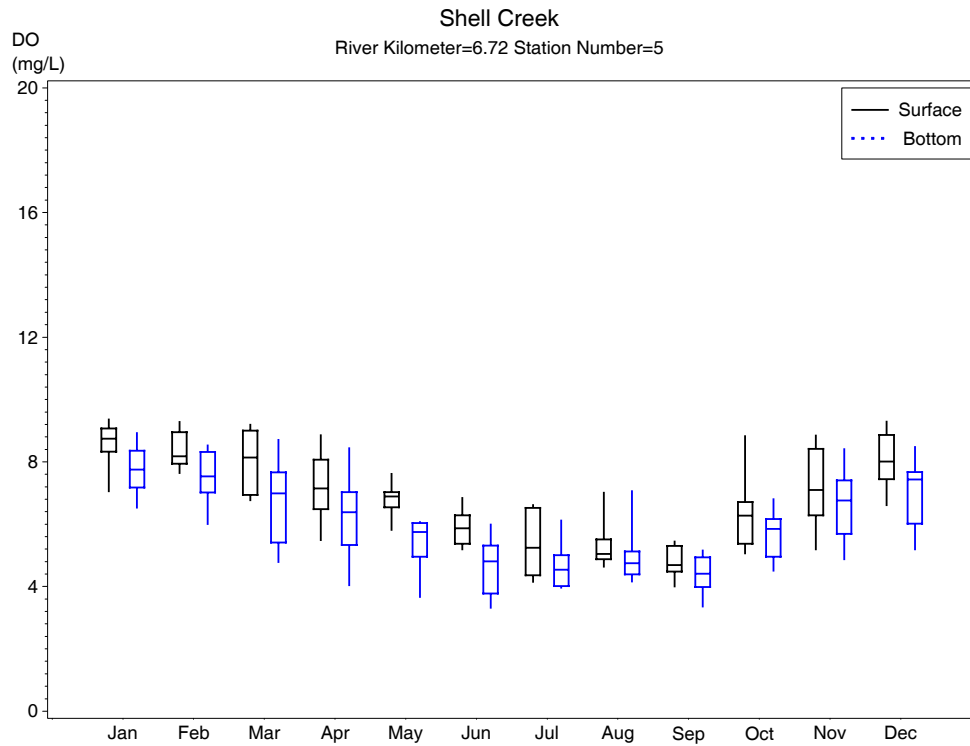


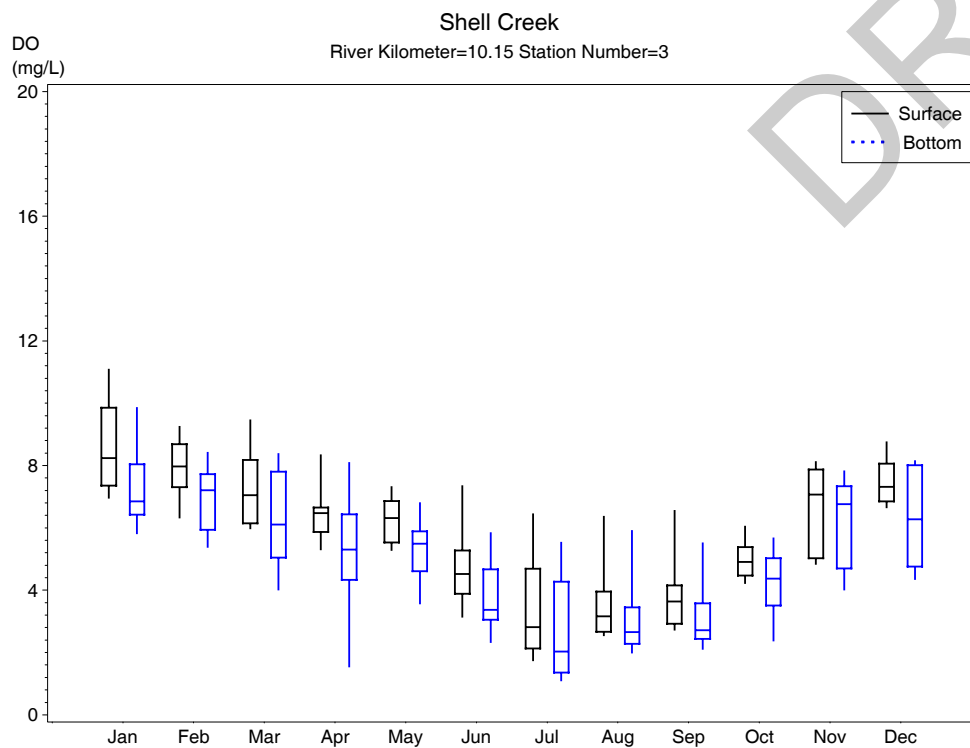
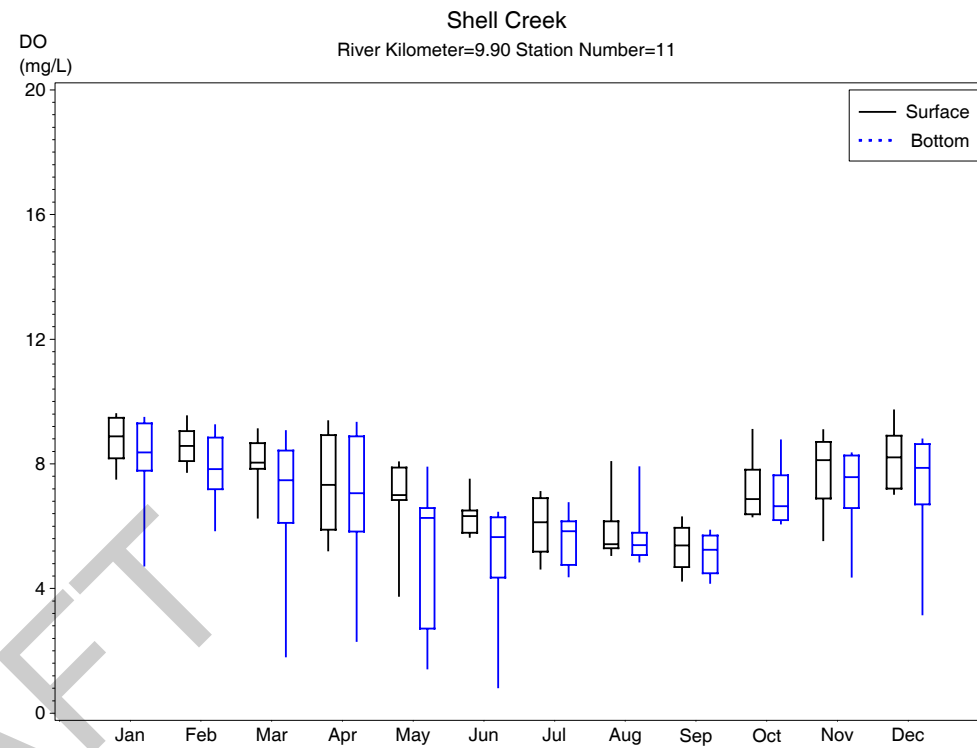
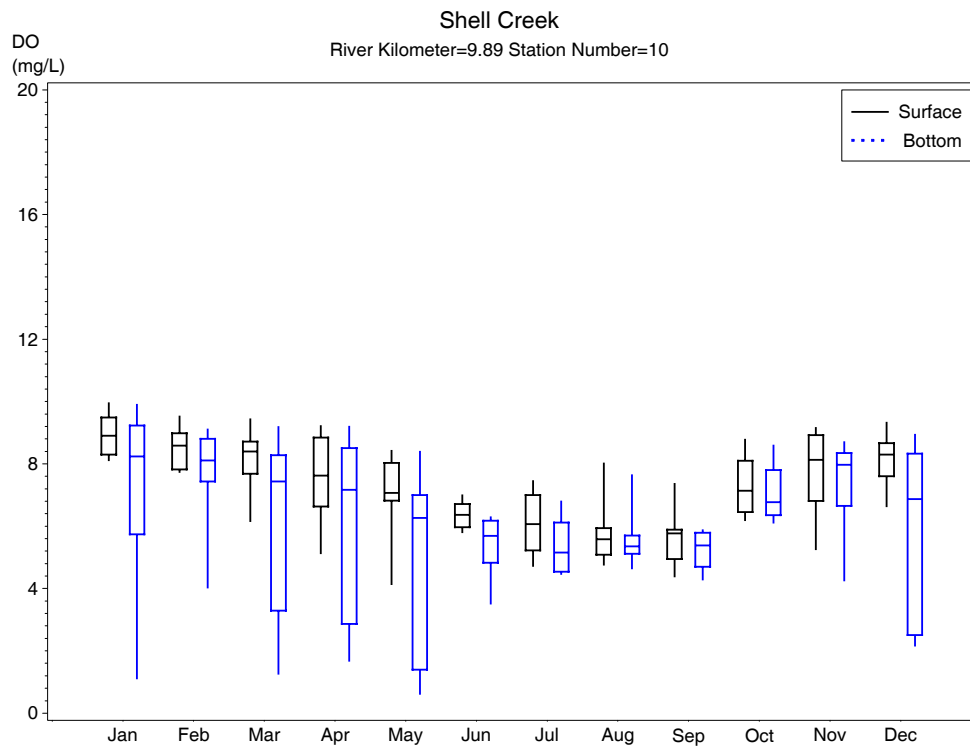


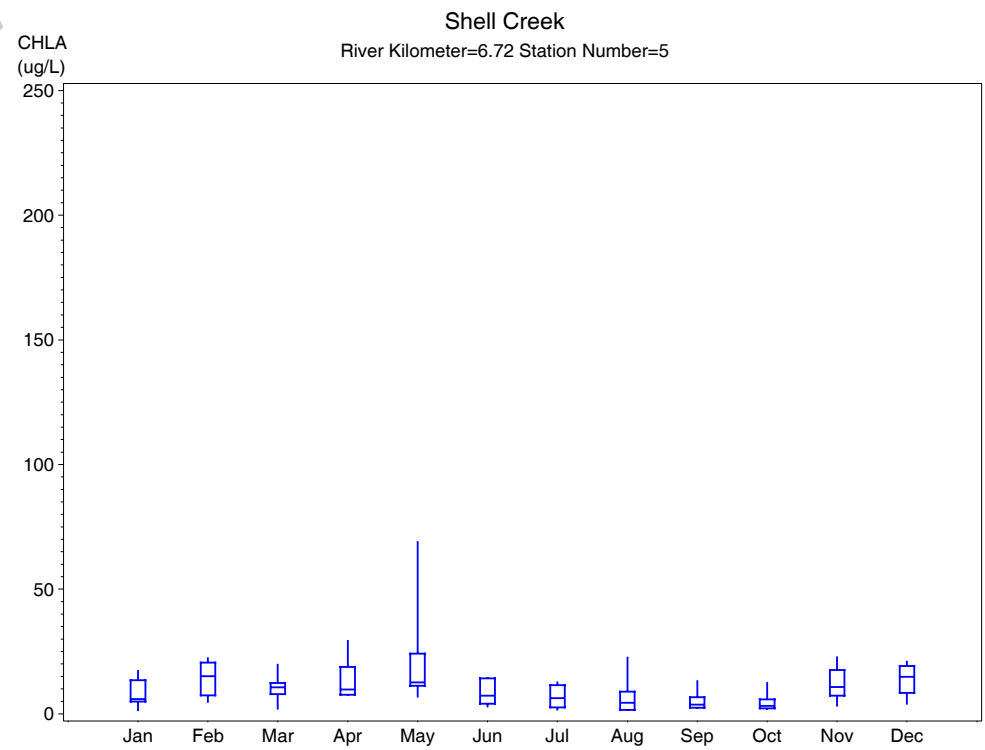
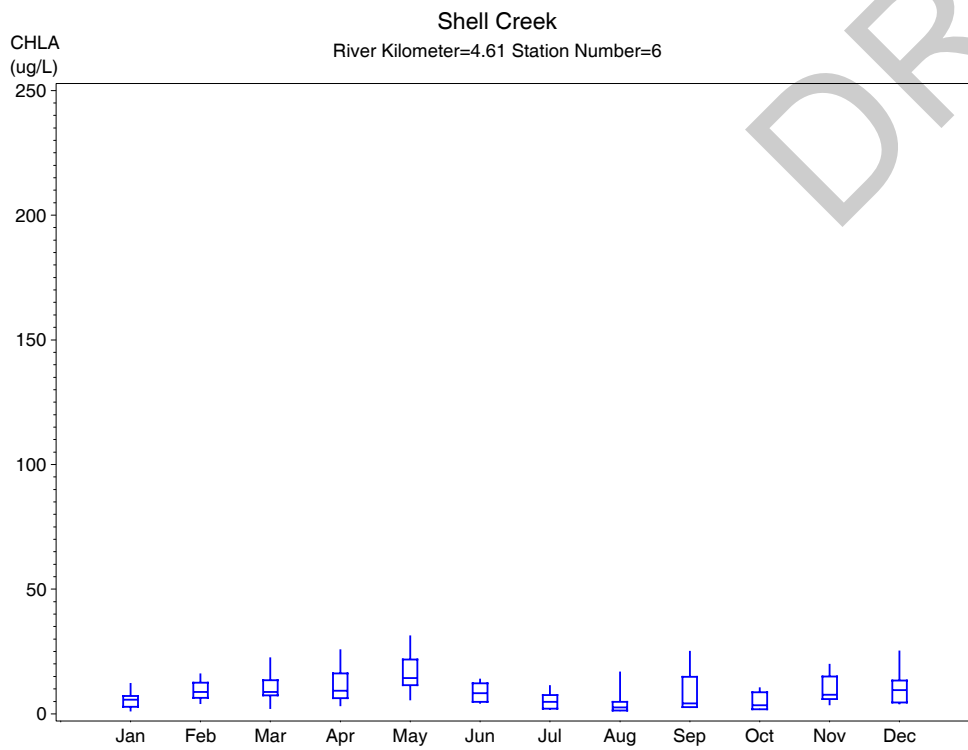
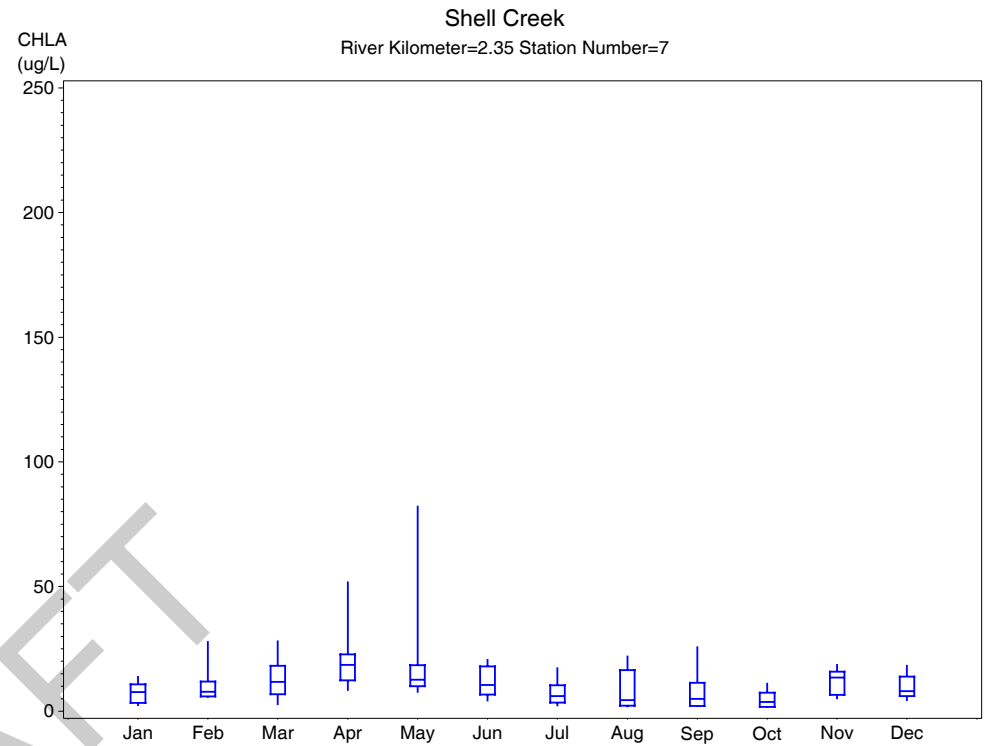
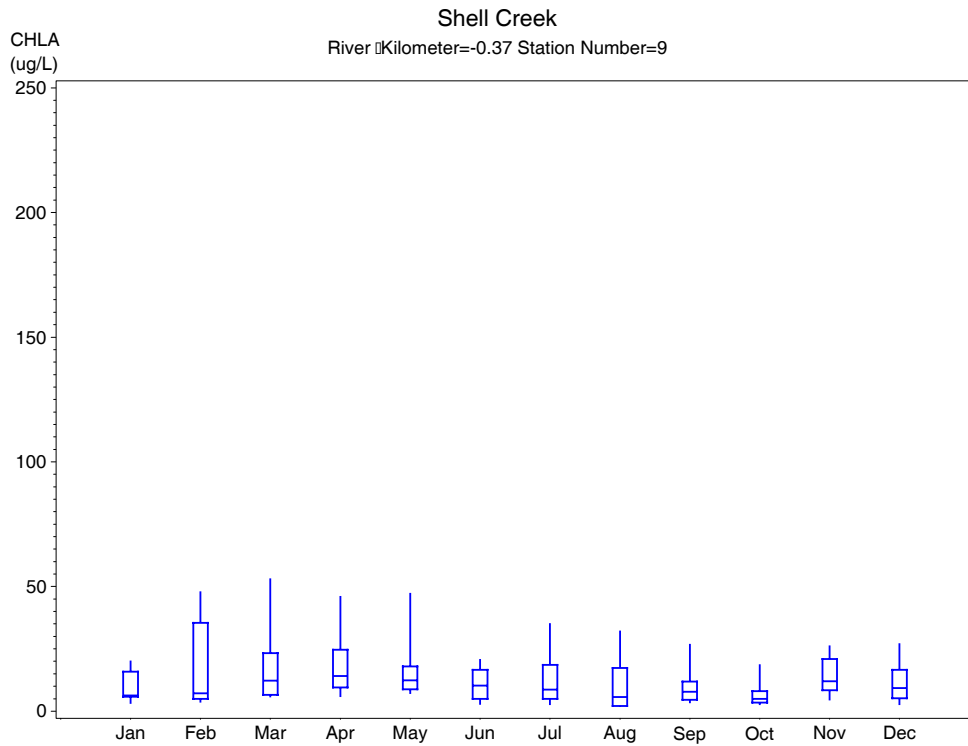




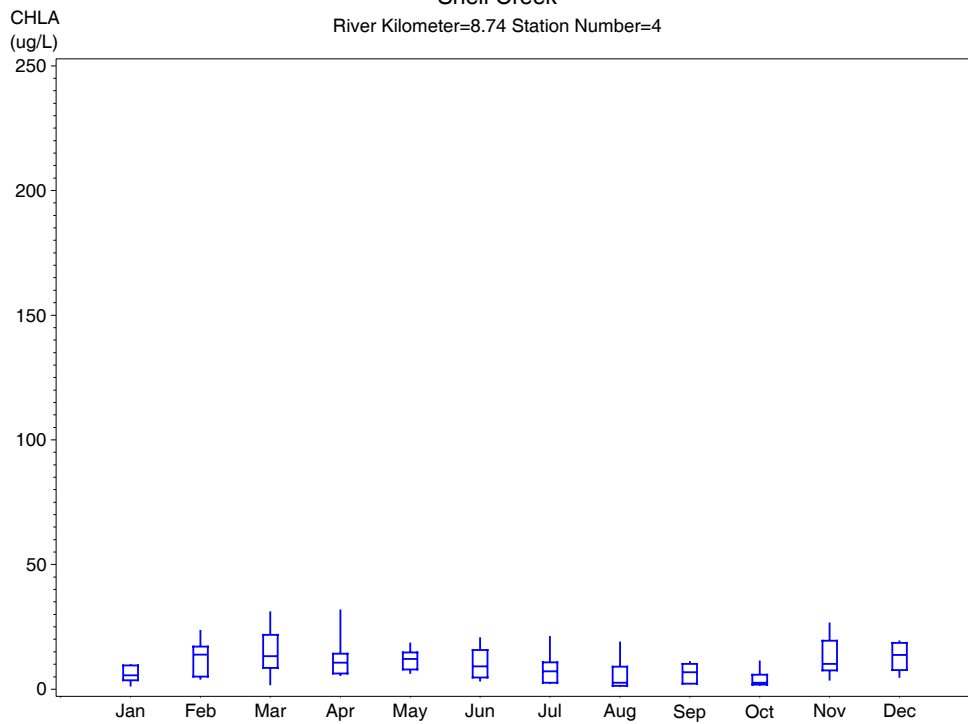




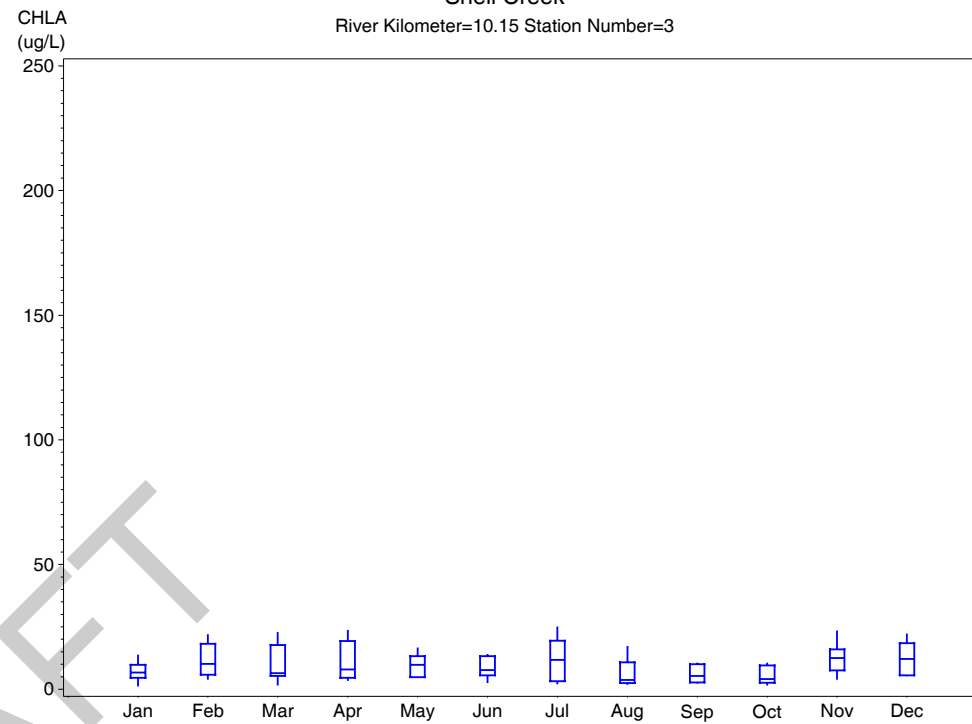


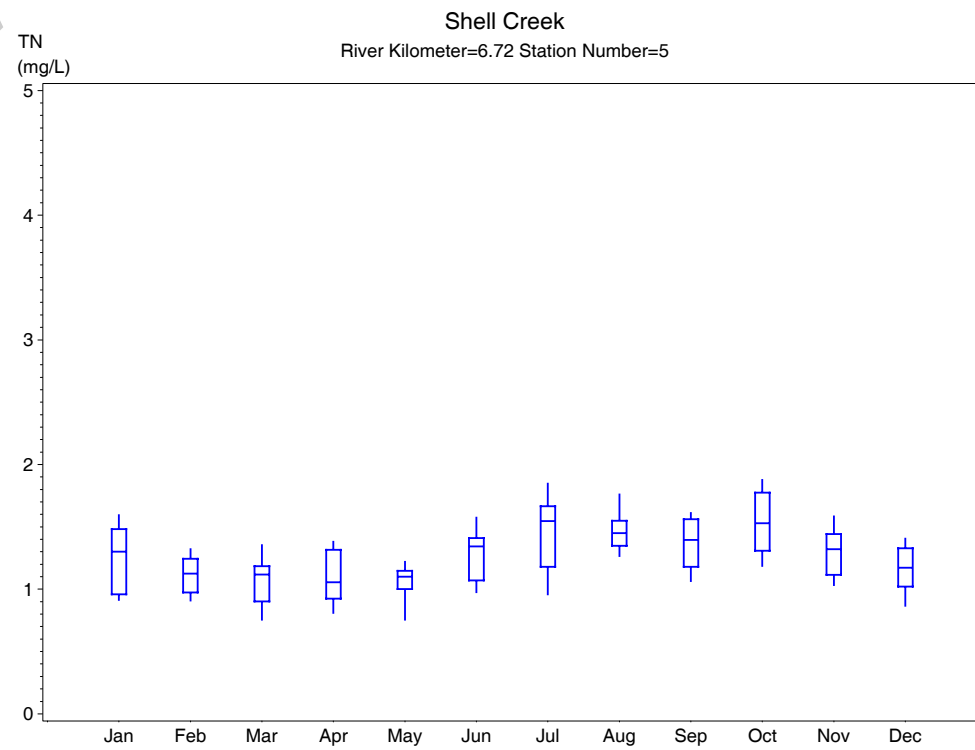
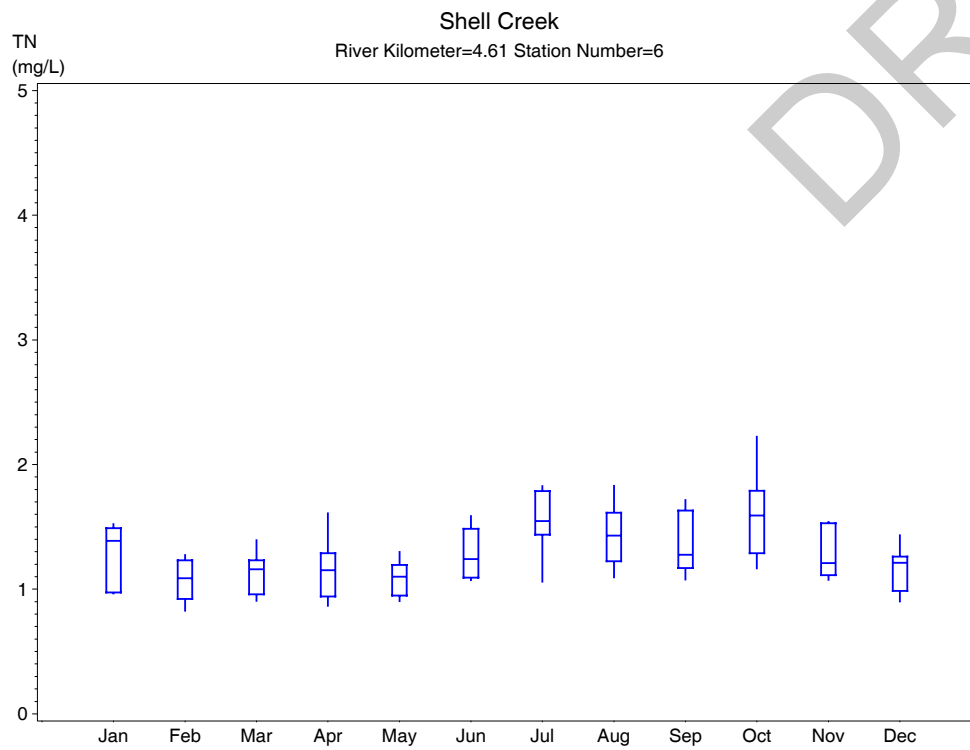
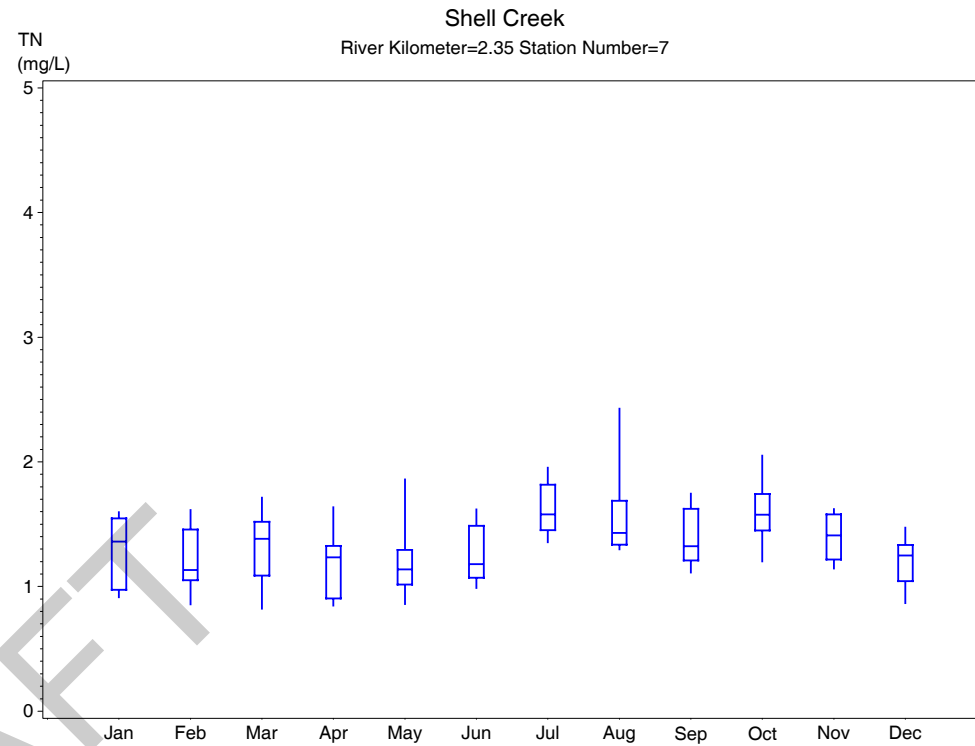
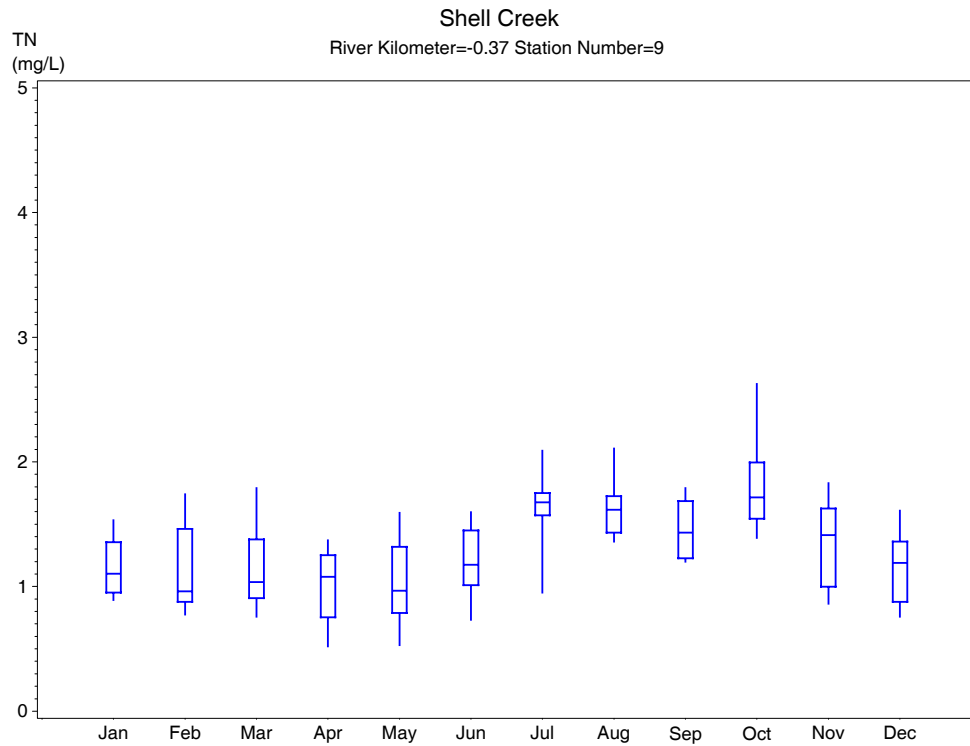


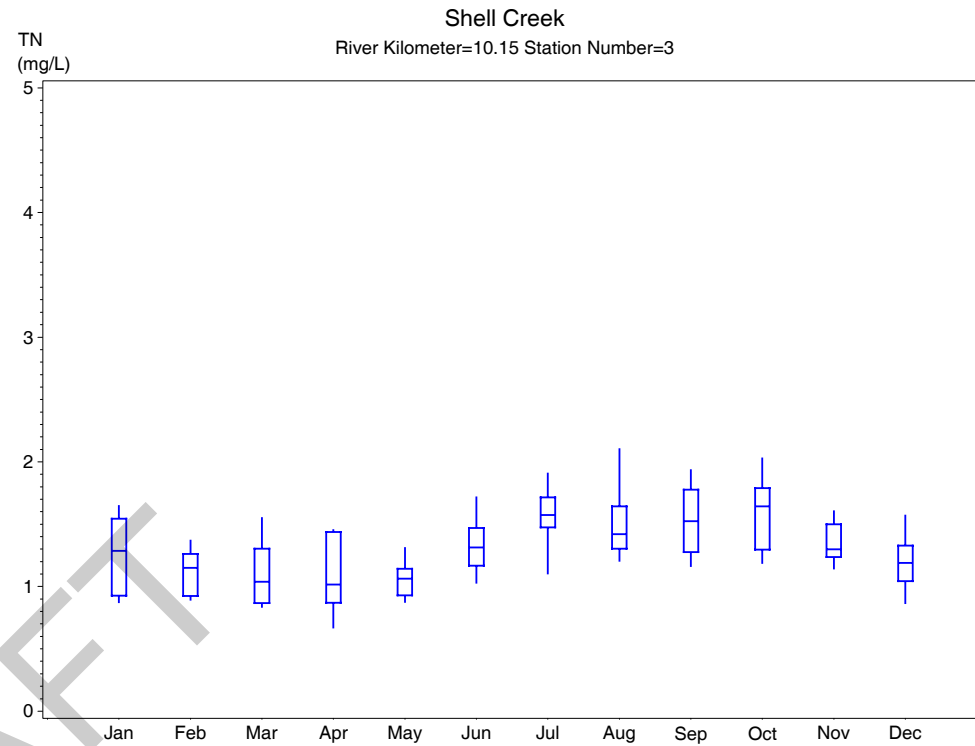
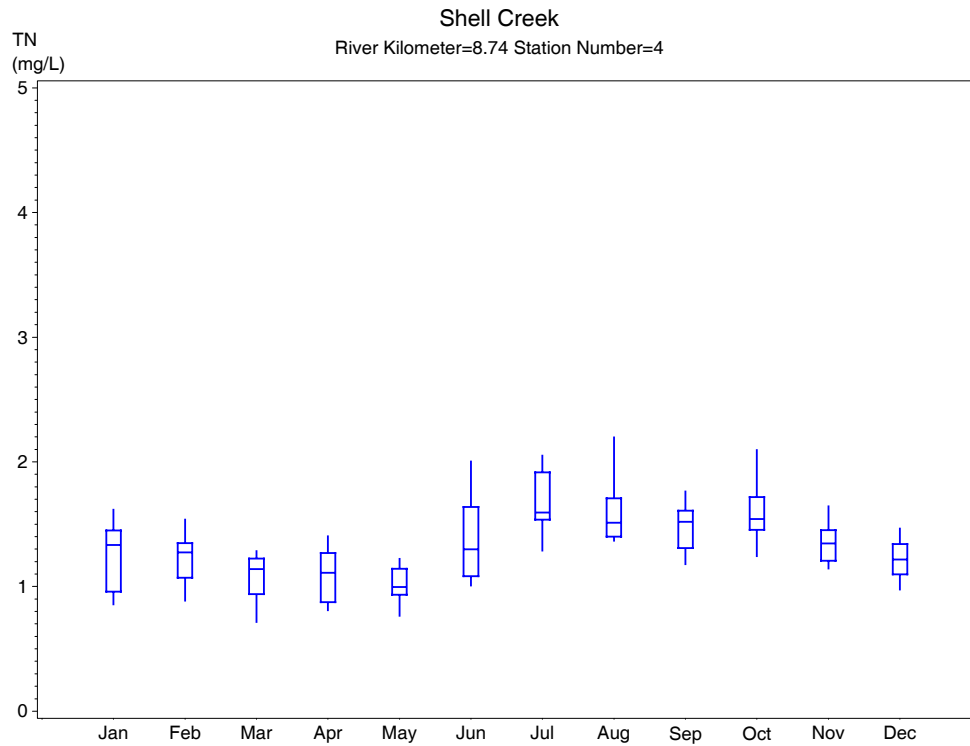
Shell Creek
River Kilometer=8.74 Station Number=4



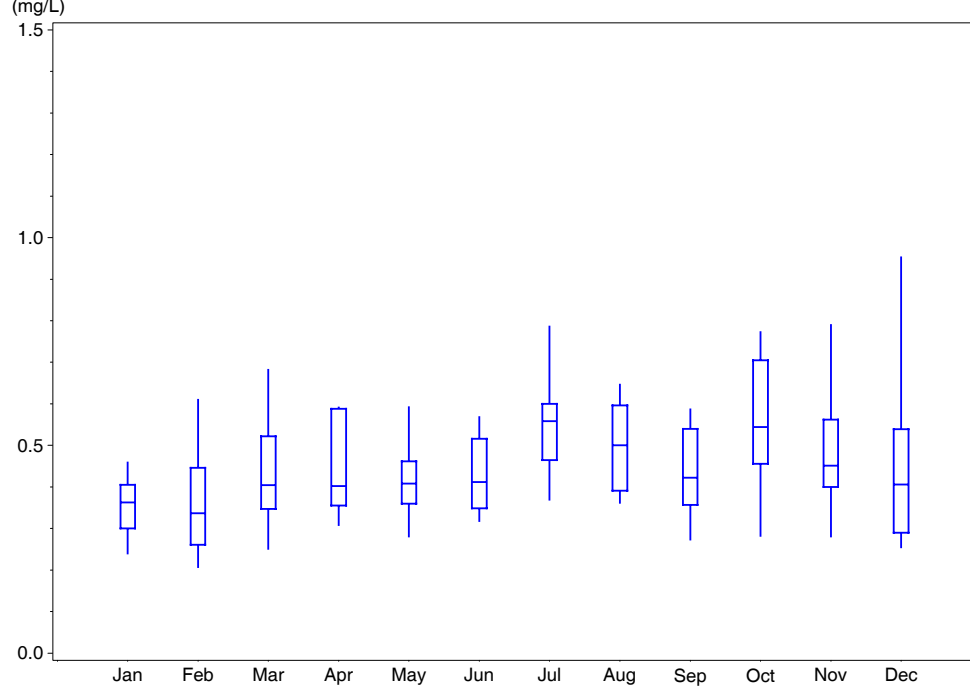
Shell Creek
River Kilometer=10.15 Station Number=3



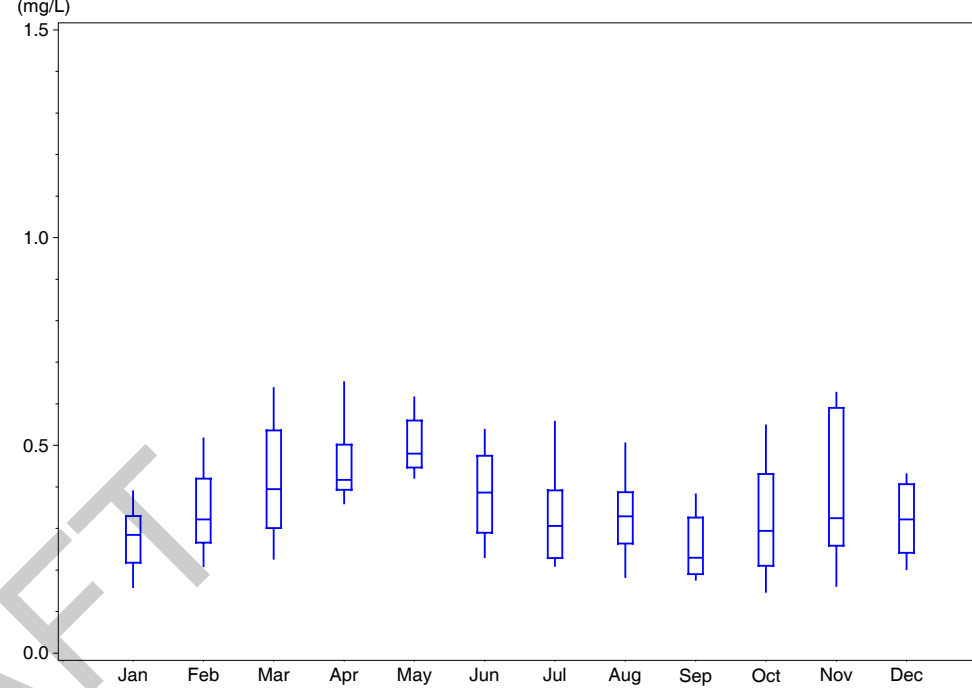




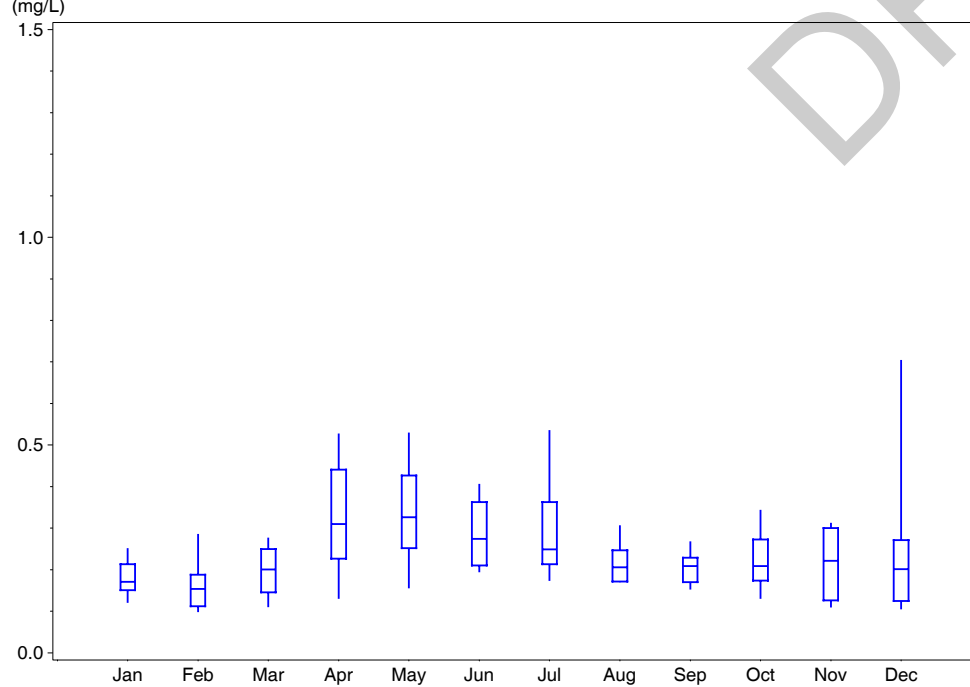
Shell Creek
River Kilometer=-0.37 Station Number=9



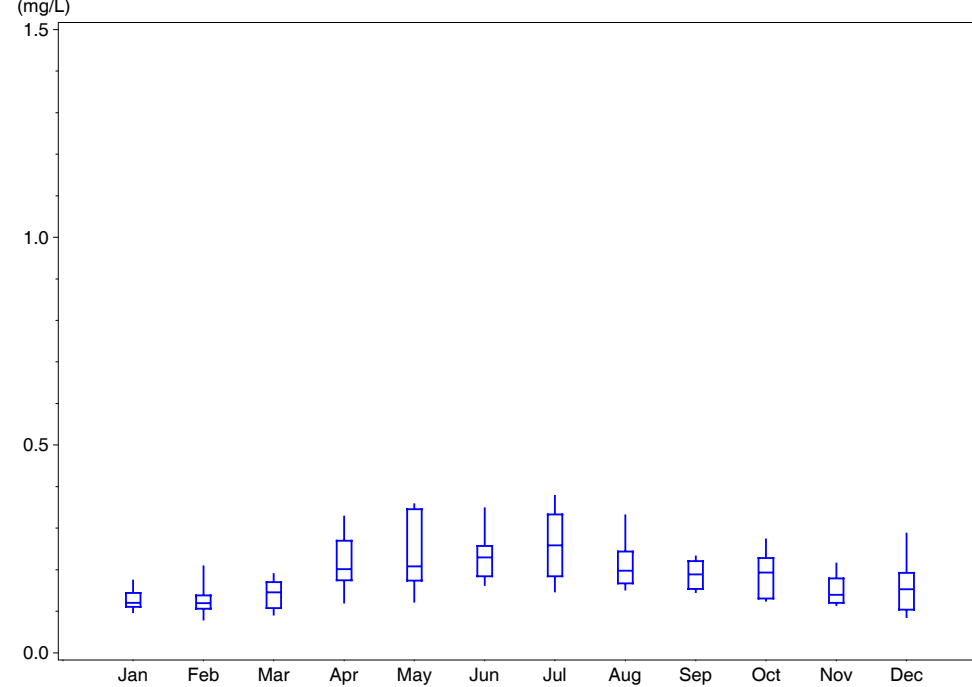
Shell Creek
River Kilometer=2.35 Station Number=7



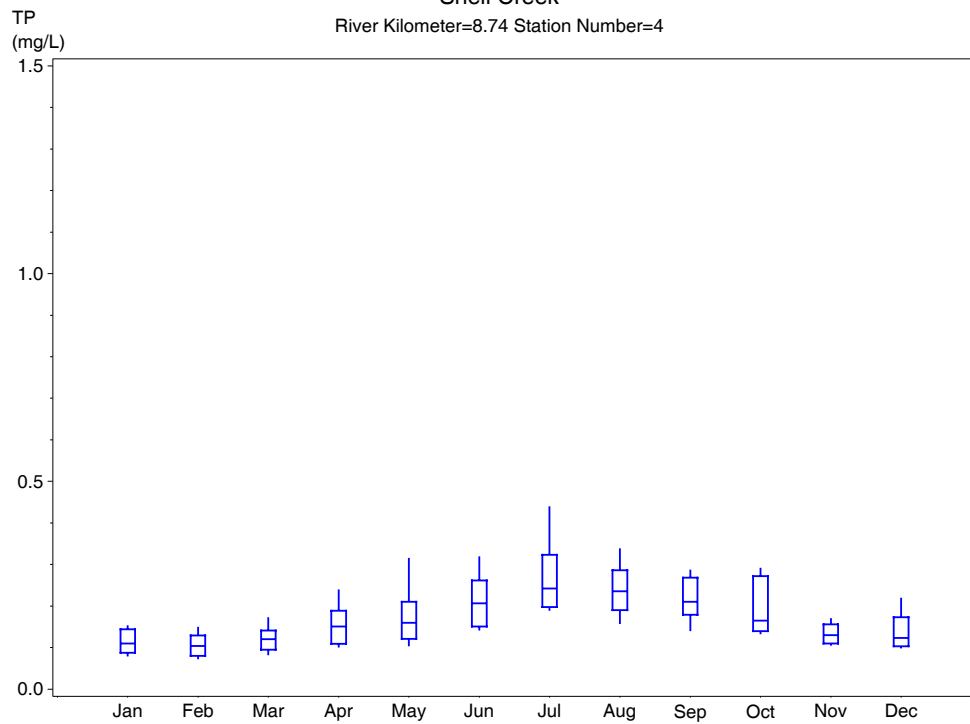
Shell Creek
River Kilometer=4.61 Station Number=6



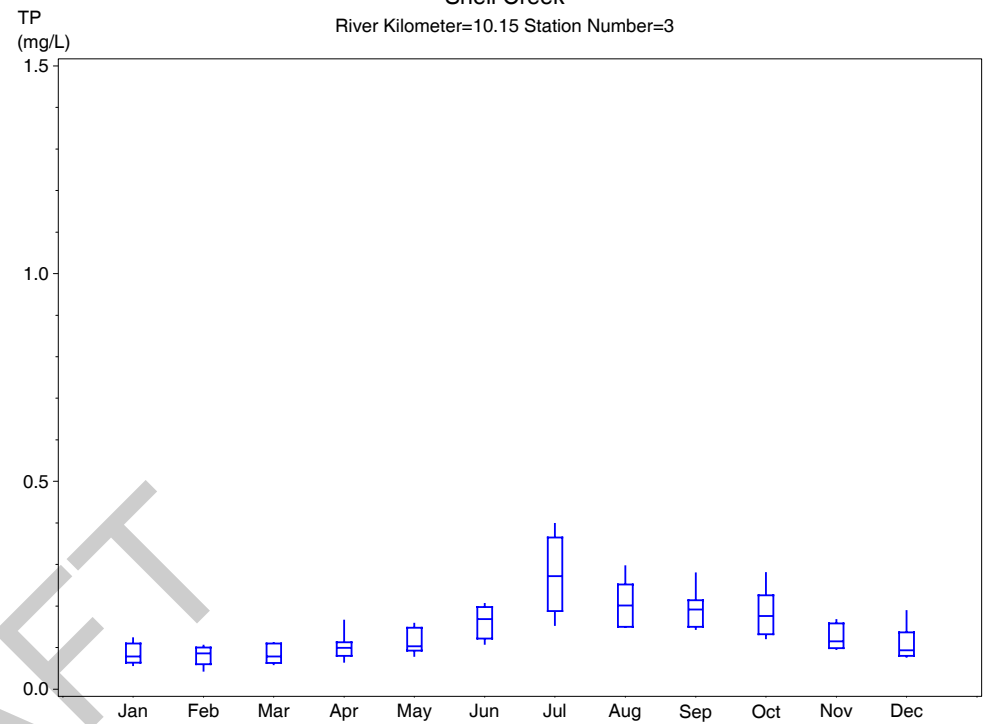
Shell Creek
River Kilometer=6.72 Station Number=5



Shell Creek
River Kilometer=8.74 Station Number=4



Shell Creek
River Kilometer=10.15 Station Number=3



Appendix 4-1

Alphabetical Taxonomic Inventory of Benthos Identified in the Lower Peace River (1998-1999) and Shell Creek (2003)

<i>Acteocina canaliculata</i>	<i>Cryptotendipes</i> spp	<i>Leitoscoloplos fragilis</i>	<i>Polydora ligni</i>
<i>Almyracuma proximoculi</i>	<i>Cyclaspis</i> cf <i>varians</i>	<i>Leitoscoloplos robustus</i>	<i>Polymesoda caroliniana</i>
<i>Amakusanthura magnifica</i>	<i>Cyclinella tenuis</i>	Leptoceridae	<i>Polypedilum halterale</i> grp
<i>Americamysis almyra</i>	<i>Cymadusa compta</i>	<i>Leptochela serratorbita</i>	<i>Polypedilum scalaenum</i> gp
<i>Americamysis bahia</i>	<i>Dicrotendipes</i> cf <i>neomodestus</i>	<i>Limulus polyphemus</i>	<i>Prionospio perkinsi</i>
<i>Americamysis bigelowi</i>	<i>Dicrotendipes</i> cf <i>tritonus</i>	<i>Lopescaldius</i> sp	<i>Pristinella</i>
<i>Ampelisca abdita</i>	<i>Dicrotendipes lobus</i>	<i>Macoma constricta</i>	<i>Processa</i>
<i>Amygdalum papyrium</i>	<i>Diopatra cuprea</i>	<i>Macoma tenta</i>	<i>Procladius</i>
<i>Anachis</i> sp	<i>Dipolydora socialis</i>	Mactridae	<i>Rangia cuneata</i>
<i>Anadara transversa</i>	<i>Djalmabatista pulchra</i>	<i>Mediomastus californiensis</i>	<i>Rhithropanopeus harrisii</i>
<i>Apocorophium lacustre</i>	<i>Edotea montosa</i>	<i>Mesanthura pulchra</i>	<i>Rictaxis punctostriatus</i>
<i>Apocorophium louisianum</i>	<i>Einfeldia natchitochaeae</i>	Mesovelia	Saldidae
<i>Argissa hamatipes</i>	<i>Elasmopus levis</i>	Molgulidae	<i>Scolecopsis texana</i>
<i>Aricidea philbinae</i>	Elmidae	<i>Monticellina dorsobranchialis</i>	Sigalionidae
Ascidacea	<i>Ensis minor</i>	<i>Mulinia lateralis</i>	<i>Sigambra bassi</i>
<i>Assimineia succinea</i>	<i>Epitonium</i> spp	<i>Mysella planulata</i>	<i>Sigambra tentaculata</i>
<i>Astysis lunata</i>	<i>Erichsonella attenuata</i>	<i>Mytilopsis leucophaea</i>	<i>Sipuncula</i>
<i>Asychis elongata</i>	<i>Erichthonius brasiliensis</i>	<i>Nassarius vibex</i>	Sminthuridae
<i>Axarus</i> sp	<i>Eteone heteropoda</i>	Nemertea a	<i>Sphaeroma quadridentata</i>
<i>Batea catharinensis</i>	<i>Exosphaeroma diminuta</i>	Nemertea b	<i>Sphaeroma terebrans</i>
<i>Bemlos</i> sp	<i>Fissimentum</i> sp	Nemertea sp f	<i>Spiochaetopterus costarum oculat</i>
<i>Boccardiella</i>	<i>Fittkauimyia</i>	<i>Nereis succinea</i>	<i>Stempellina</i>
<i>Bowmaniella portoricensis</i>	<i>Gammarus</i> cf <i>tigrinus</i>	<i>Neritina usnea</i>	<i>Stenochironomus</i> spp
<i>Brachidontes exustus</i>	<i>Gammarus mucronatus</i>	<i>Neverita duplicata</i>	<i>Stenothoe</i> sp
<i>Branchiostoma floridae</i>	<i>Genetyllis castanea</i>	Nudibranchia	<i>Sthenelais</i>
<i>Brania wellfleetensis</i>	<i>Glottidia pyramidata</i>	<i>Odostomia</i> spp	<i>Stictochironomus</i>
Caenidae	<i>Glycinde solitaria</i>	<i>Oecetis cinerascens</i>	<i>Streblosio gynobranchiata</i>
<i>Callinectes sapidus</i>	<i>Goeldichironomus</i> sp	Oeonidae	<i>Tagelus plebeius</i>
<i>Capitella capitata</i> complex	<i>Grandidierella bonnieroides</i>	<i>Ogyrides alphaerostris</i>	<i>Tanytarsus</i> sp g
<i>Caprella</i>	<i>Haminoea succinea</i>	Orchestia	<i>Tanytarsus</i> sp k
Ceratopogonidae	<i>Hargeria rapax</i>	<i>Oxyurostylis smithi</i>	<i>Tanytarsus</i> sp o
<i>Chironomini</i> genus a	<i>Hartmanodes nyei</i>	<i>Palaemonetes pugio</i>	<i>Tanytarsus</i> sp s
<i>Chironomus</i> sp	<i>Hemipodus roseus</i>	<i>Parachironomus carinatus</i>	<i>Taphromysis bowmani</i>
Cirratulidae	<i>Heteromastus filiformis</i>	<i>Paracladopelma</i> sp	<i>Tellina tampaensis</i>
<i>Cladopelma</i> spp	<i>Heteromysis formosa</i>	<i>Paramphionome</i> sp b	<i>Tellina texana</i>
<i>Cladotanytarsus</i>	<i>Hippolyte zostericola</i>	<i>Paraprionospio pinnata</i>	<i>Tozeuma carolinense</i>
<i>Cladotanytarsus</i> sp b	<i>Hobsonia florida</i>	<i>Paratendipes basidens</i>	Trichoptera
<i>Coelotanypus</i>	<i>Hourstonius laguna</i>	<i>Parvilucina multilineata</i>	<i>Tricorythodes albilineatus</i>
<i>Corbicula fluminea</i>	<i>Hydracarina</i>	<i>Pectinaria gouldii</i>	<i>Typosyllis</i> sp
Cordulegastridae	Hydrobiidae	<i>Phyllodoce arenae</i>	<i>Uromunna</i> sp
Corixidae	Hydroptila	<i>Pinnixa sayana</i>	Vitrinellidae
<i>Crassostrea virginica</i>	Isotomidae	Planorbidae	<i>Xenanthura brevitelson</i>
<i>Crepidula</i>	<i>Laeonereis culveri</i>	<i>Podarkeopsis levifusca</i>	<i>Zavreliella</i>
<i>Cryptochironomus</i>	<i>Laevicardium mortoni</i>	<i>Polydora caulleryi</i>	Zygoptera

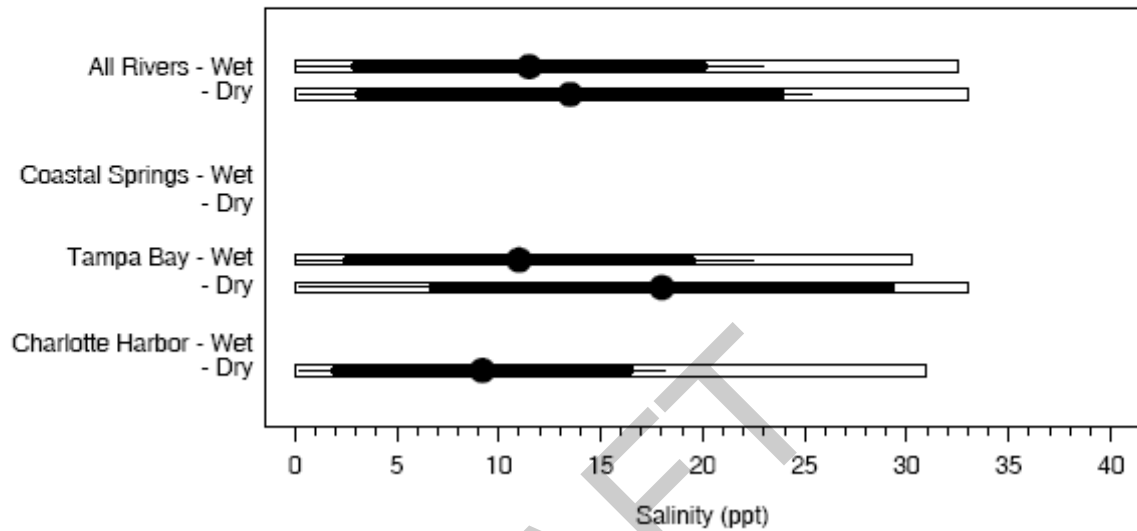
Appendix 4-2

**Logistic Regression Analysis Summary Plots:
Salinity Optima and Tolerance Ranges for Selected Taxa
Dominants in the Lower Peace River and Shell Creek**

Salinity Tolerance Compared Between River Groups

by Taxon and Season in the Order of Taxonomic Dominance

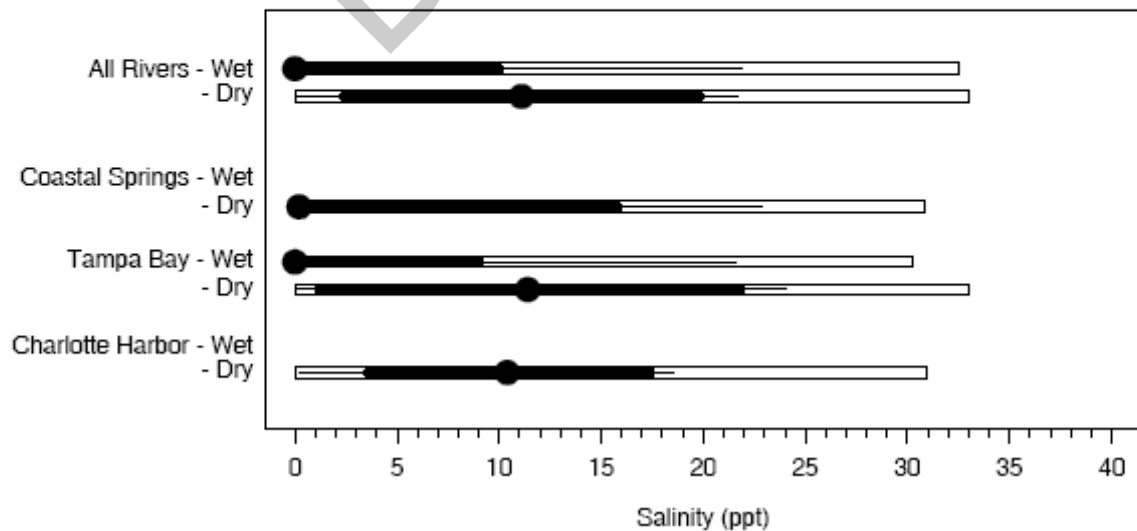
Dominance Rank=1 Taxon=*Grandidierella bonnieroides*



Salinity Tolerance Compared Between River Groups

by Taxon and Season in the Order of Taxonomic Dominance

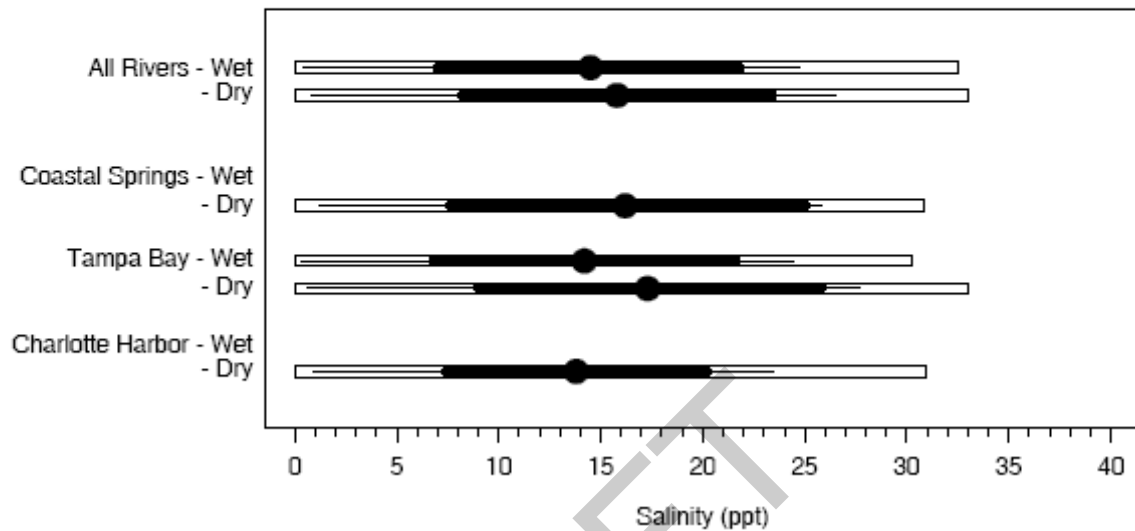
Dominance Rank=5 Taxon=*Laeonereis culveri*



Salinity Tolerance Compared Between River Groups

by Taxon and Season in the Order of Taxonomic Dominance

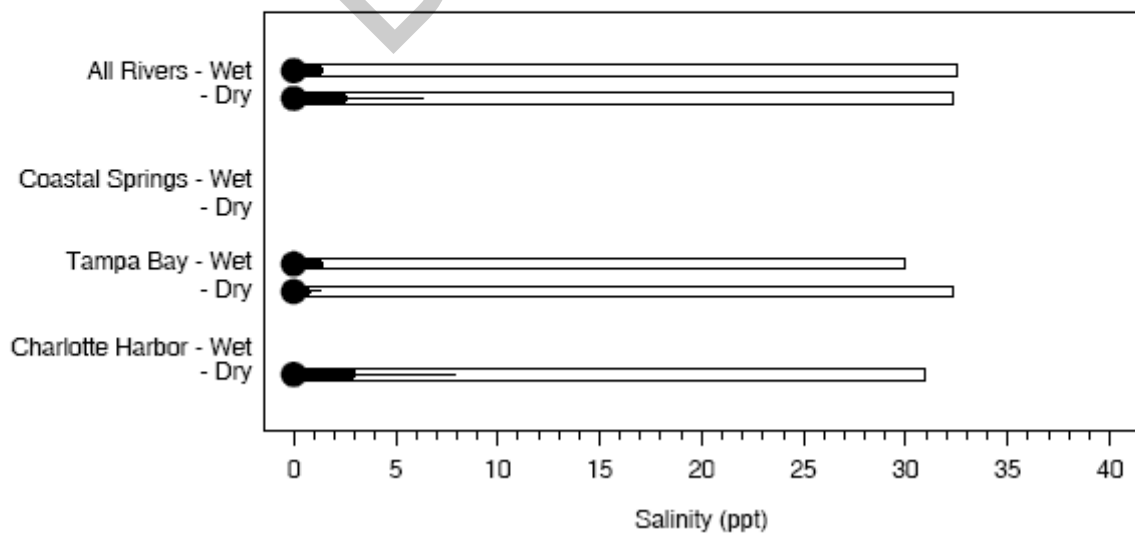
Dominance Rank=6 Taxon=*Streblospio gynobranchiata*



Salinity Tolerance Compared Between River Groups

by Taxon and Season in the Order of Taxonomic Dominance

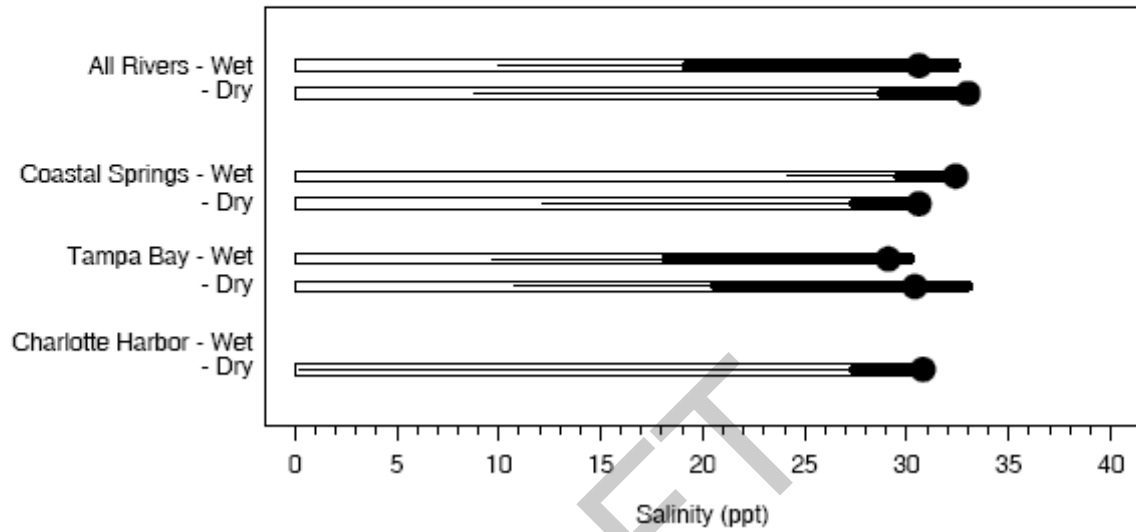
Dominance Rank=10 Taxon=*Corbicula fluminea*



Salinity Tolerance Compared Between River Groups

by Taxon and Season in the Order of Taxonomic Dominance

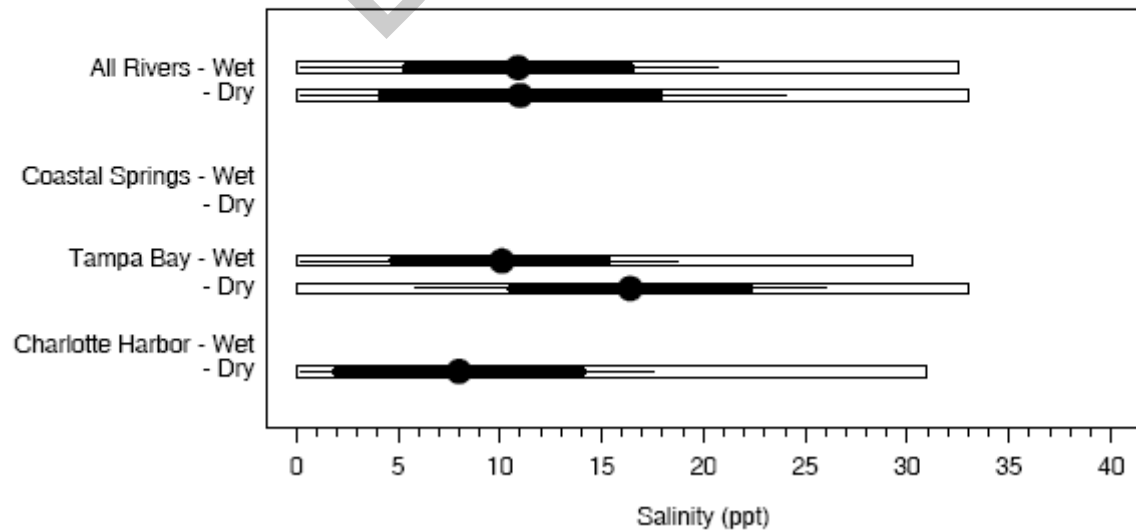
Dominance Rank=12 Taxon=*Paraprionospio pinnata*



Salinity Tolerance Compared Between River Groups

by Taxon and Season in the Order of Taxonomic Dominance

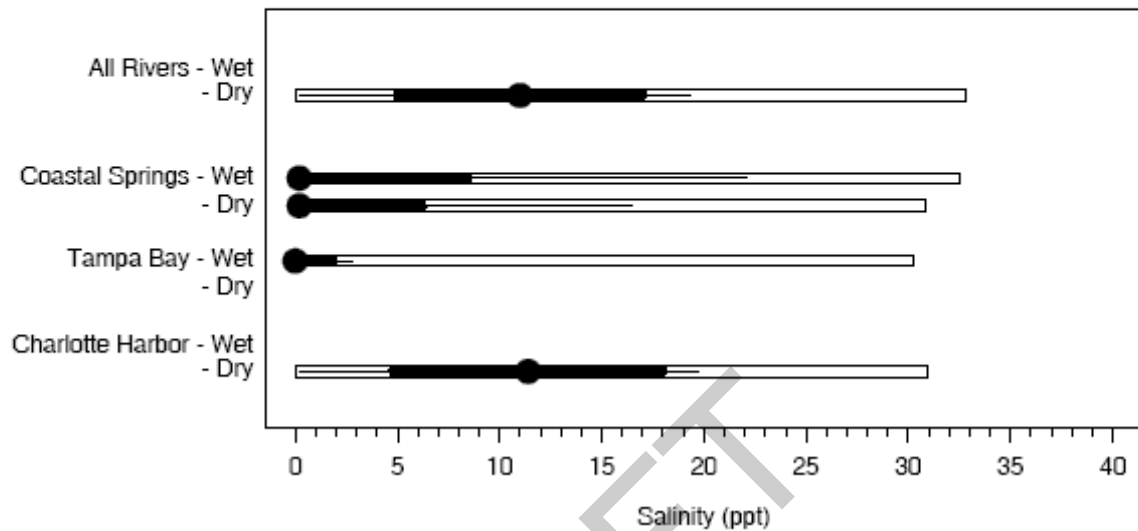
Dominance Rank=13 Taxon=*Apocorophium louisianum*



Salinity Tolerance Compared Between River Groups

by Taxon and Season in the Order of Taxonomic Dominance

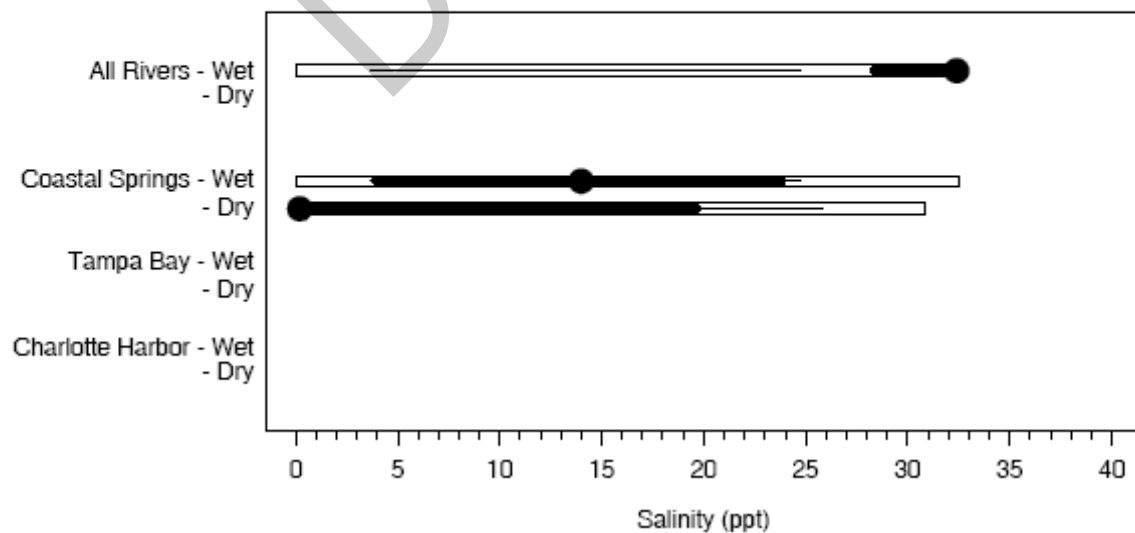
Dominance Rank=15 Taxon=*Polymesoda caroliniana*



Salinity Tolerance Compared Between River Groups

by Taxon and Season in the Order of Taxonomic Dominance

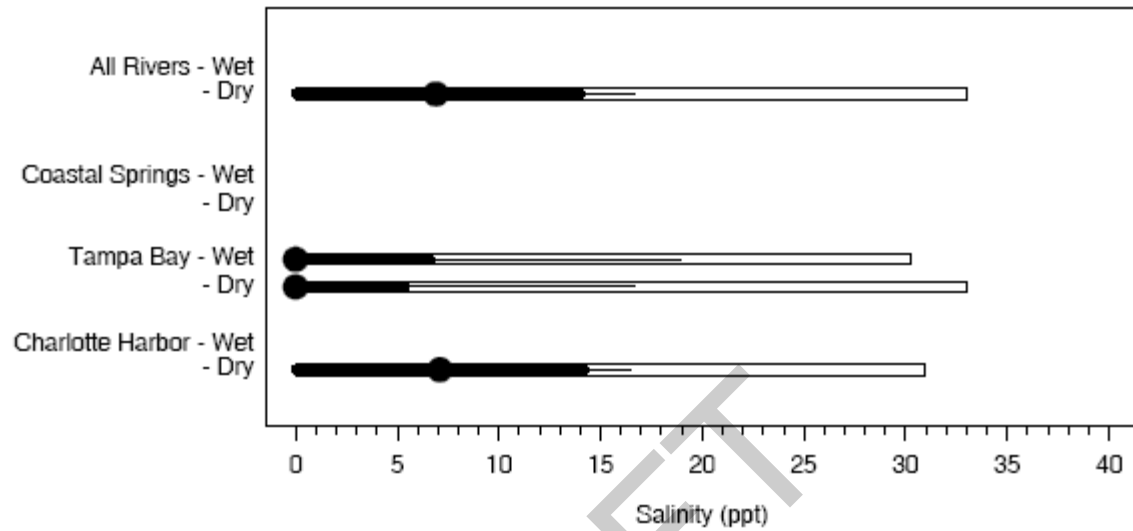
Dominance Rank=18 Taxon=*Mesanthura pulchra*



Salinity Tolerance Compared Between River Groups

by Taxon and Season in the Order of Taxonomic Dominance

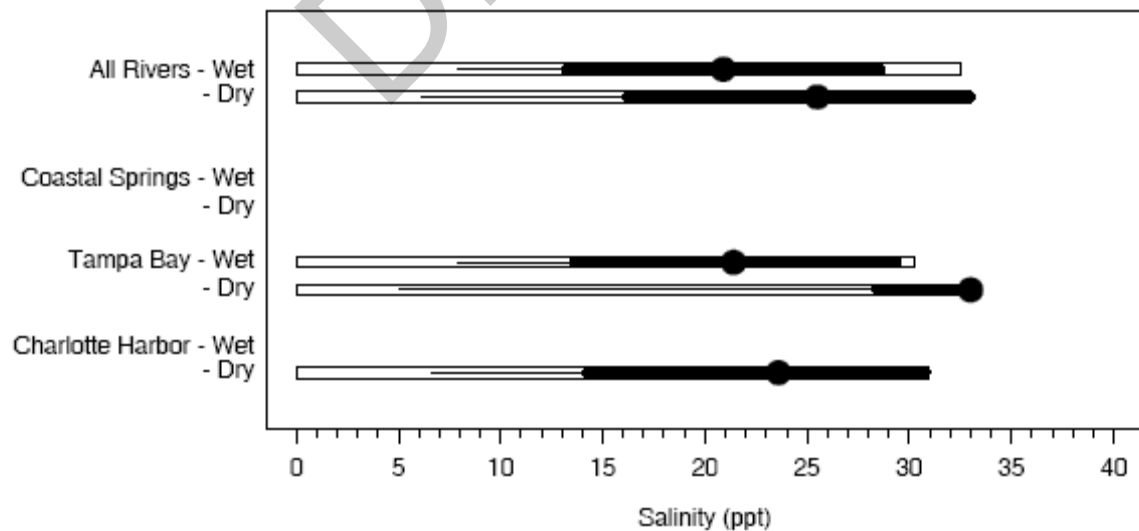
Dominance Rank=19 Taxon=Hydrobiidae



Salinity Tolerance Compared Between River Groups

by Taxon and Season in the Order of Taxonomic Dominance

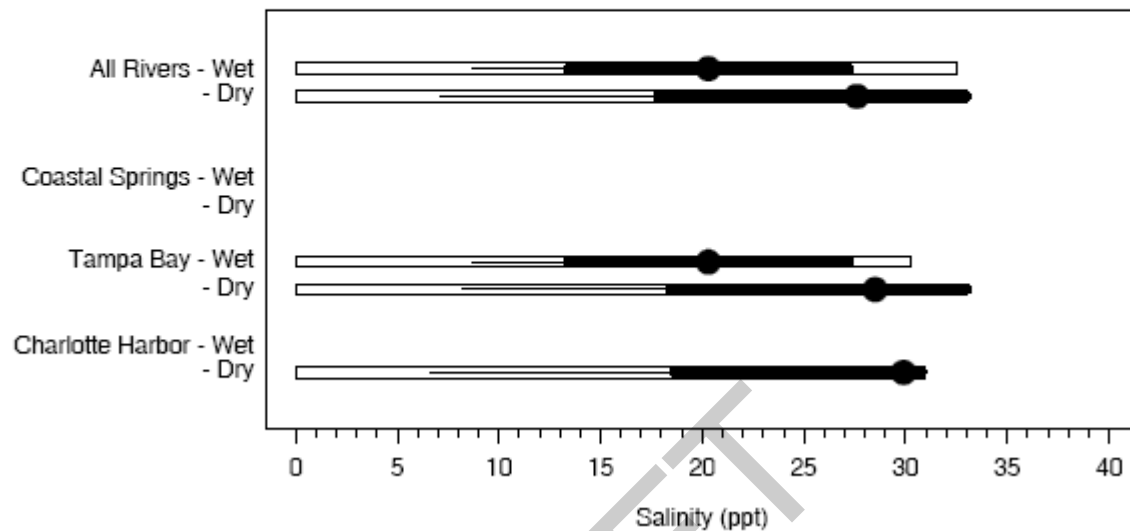
Dominance Rank=20 Taxon=Cyclaspis cf



Salinity Tolerance Compared Between River Groups

by Taxon and Season in the Order of Taxonomic Dominance

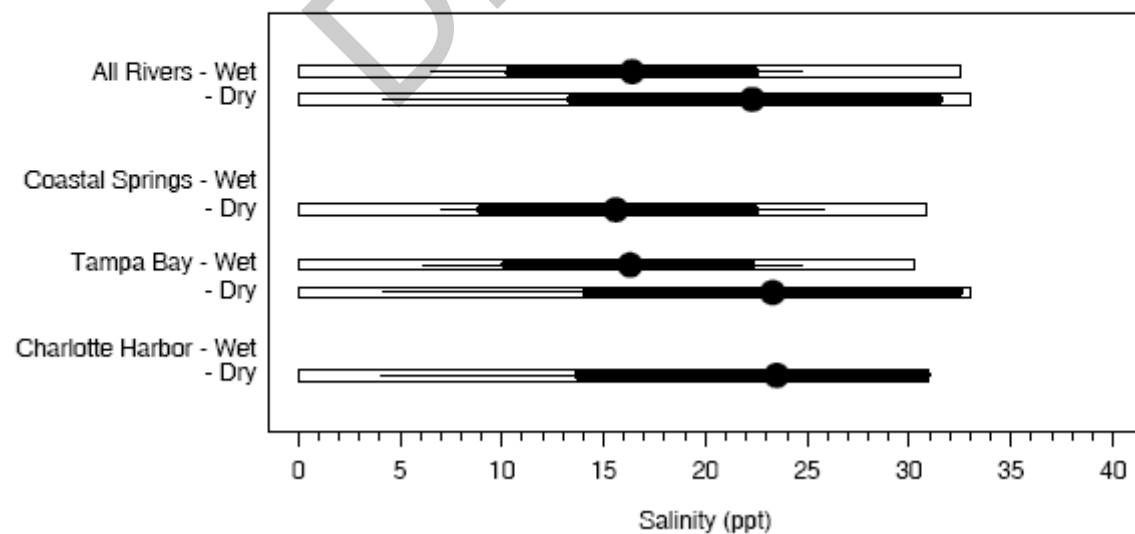
Dominance Rank=23 Taxon=*Mulinia lateralis*



Salinity Tolerance Compared Between River Groups

by Taxon and Season in the Order of Taxonomic Dominance

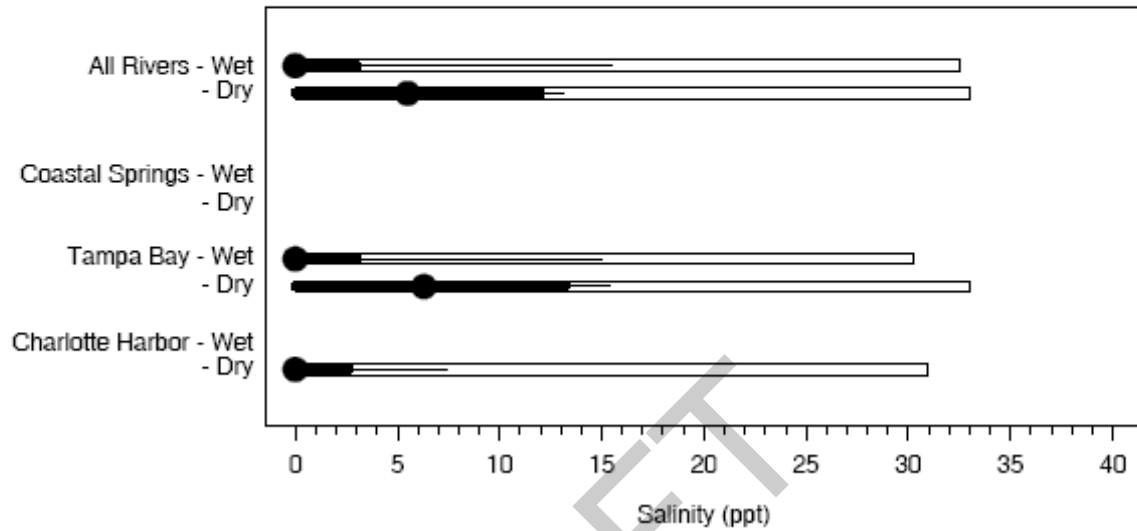
Dominance Rank=25 Taxon=*Amygdalum papyrium*



Salinity Tolerance Compared Between River Groups

by Taxon and Season in the Order of Taxonomic Dominance

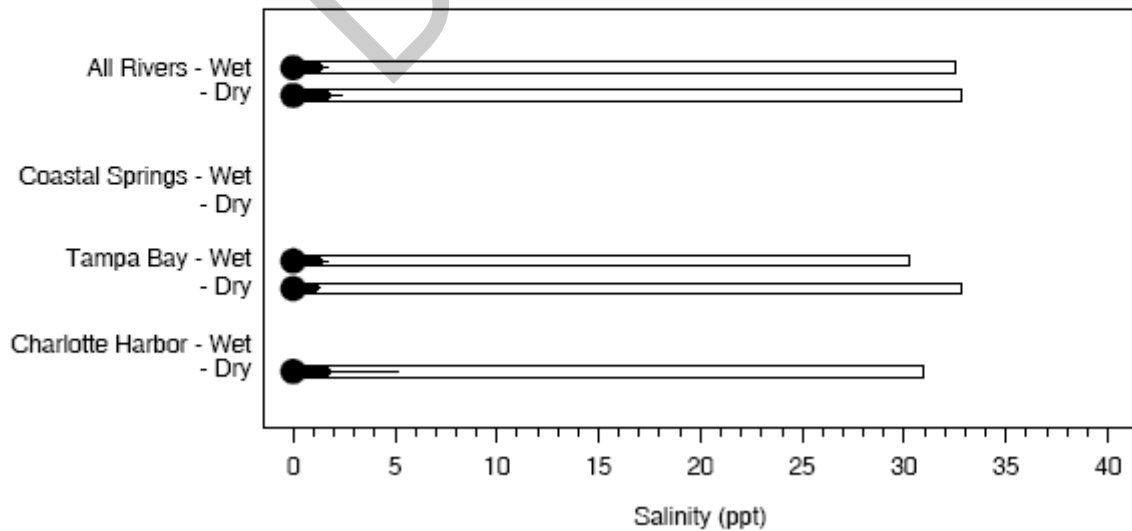
Dominance Rank=26 Taxon=Chironomus sp



Salinity Tolerance Compared Between River Groups

by Taxon and Season in the Order of Taxonomic Dominance

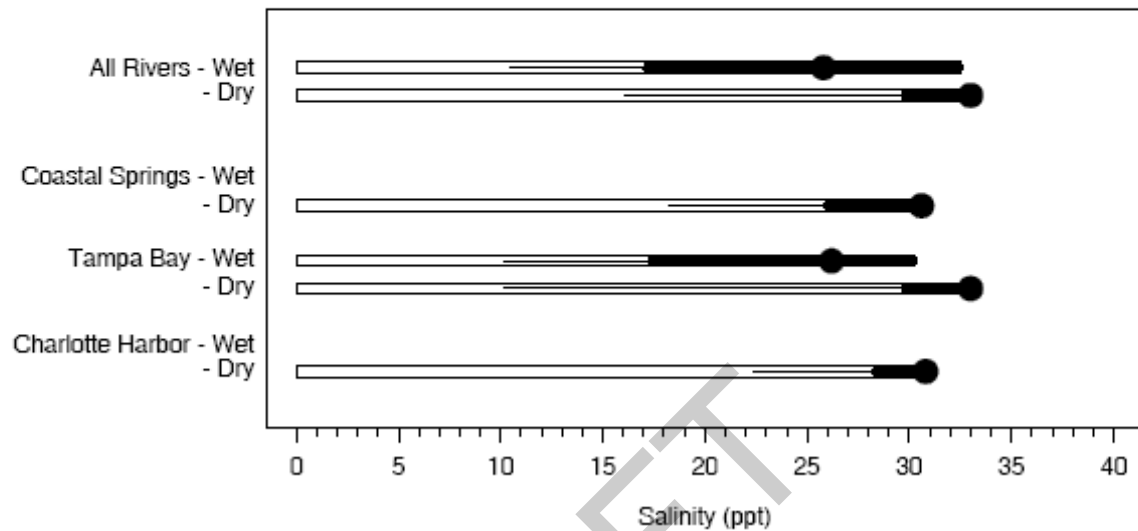
Dominance Rank=27 Taxon=Polypedilum halterale



Salinity Tolerance Compared Between River Groups

by Taxon and Season in the Order of Taxonomic Dominance

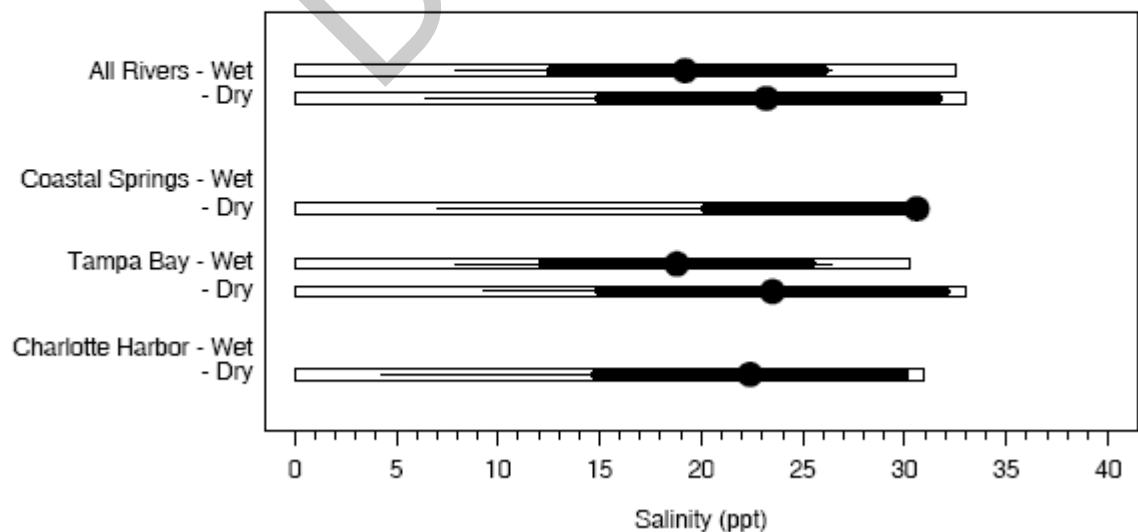
Dominance Rank=28 Taxon=*Mysella planulata*



Salinity Tolerance Compared Between River Groups

by Taxon and Season in the Order of Taxonomic Dominance

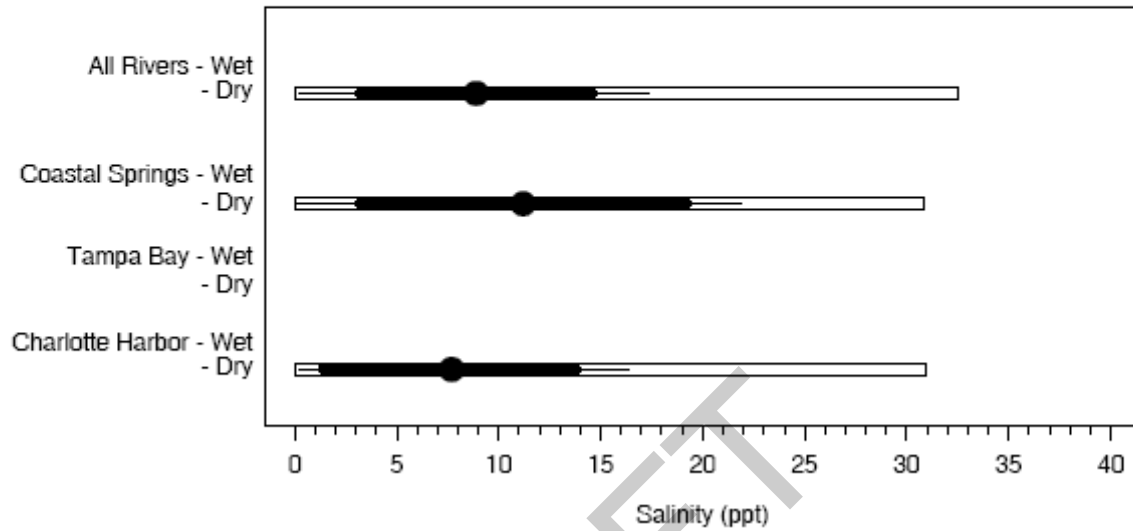
Dominance Rank=29 Taxon=*Capitella capitata*



Salinity Tolerance Compared Between River Groups

by Taxon and Season in the Order of Taxonomic Dominance

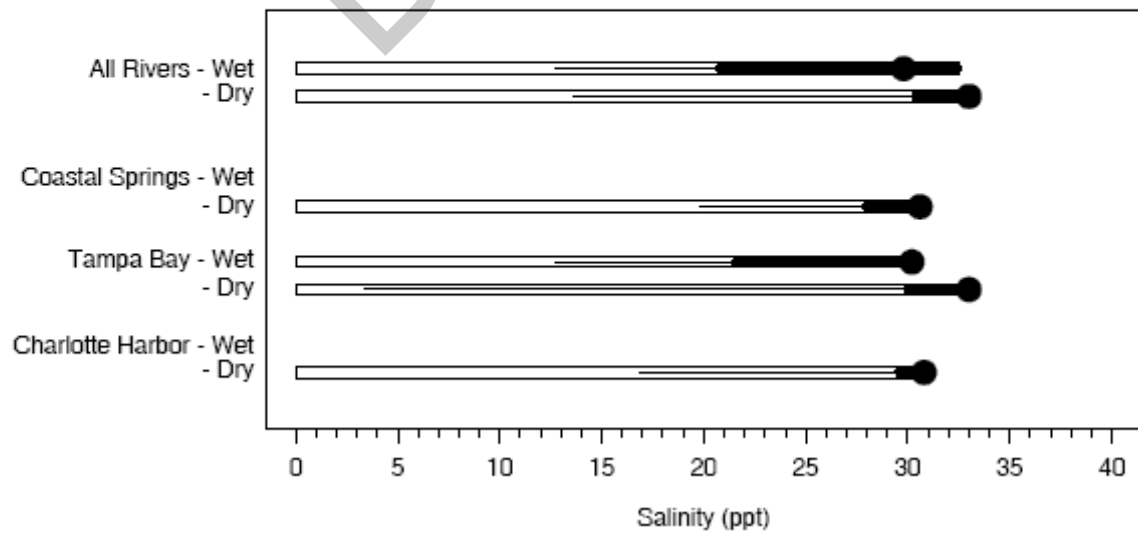
Dominance Rank=32 Taxon=*Apocorophium lacustre*



Salinity Tolerance Compared Between River Groups

by Taxon and Season in the Order of Taxonomic Dominance

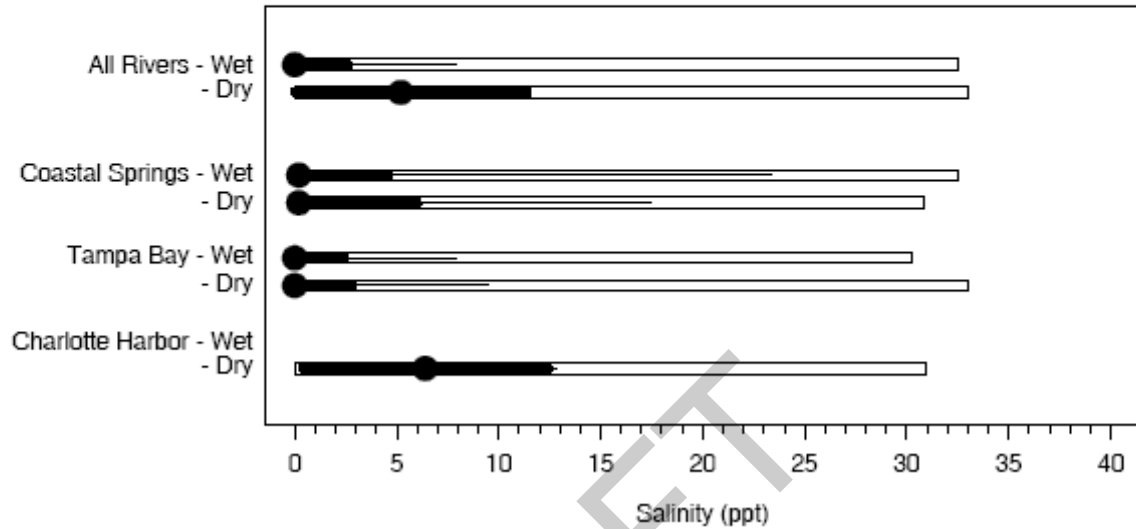
Dominance Rank=33 Taxon=*Glottidia pyramidata*



Salinity Tolerance Compared Between River Groups

by Taxon and Season in the Order of Taxonomic Dominance

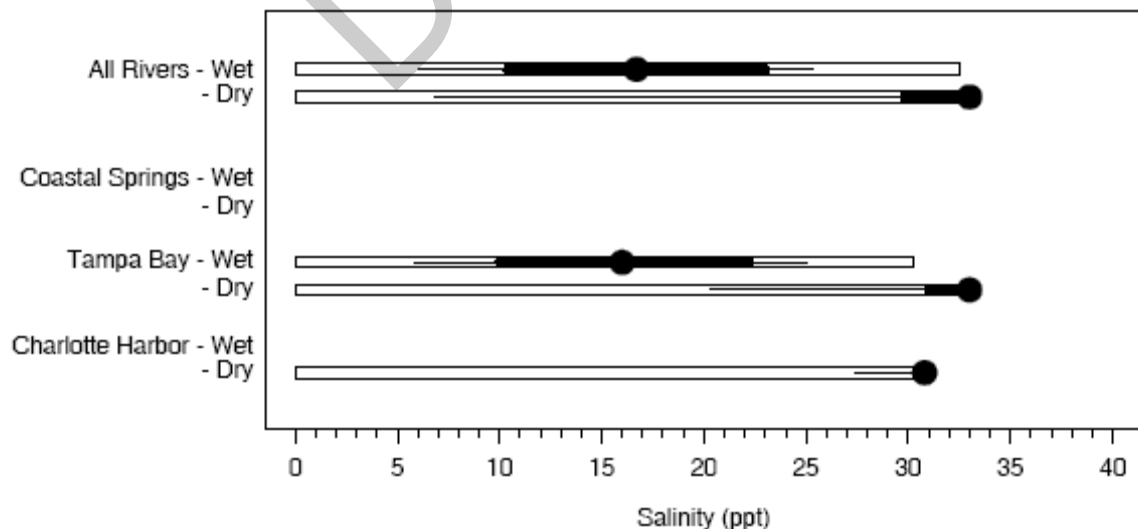
Dominance Rank=34 Taxon=*Polypedilum scalaenum*



Salinity Tolerance Compared Between River Groups

by Taxon and Season in the Order of Taxonomic Dominance

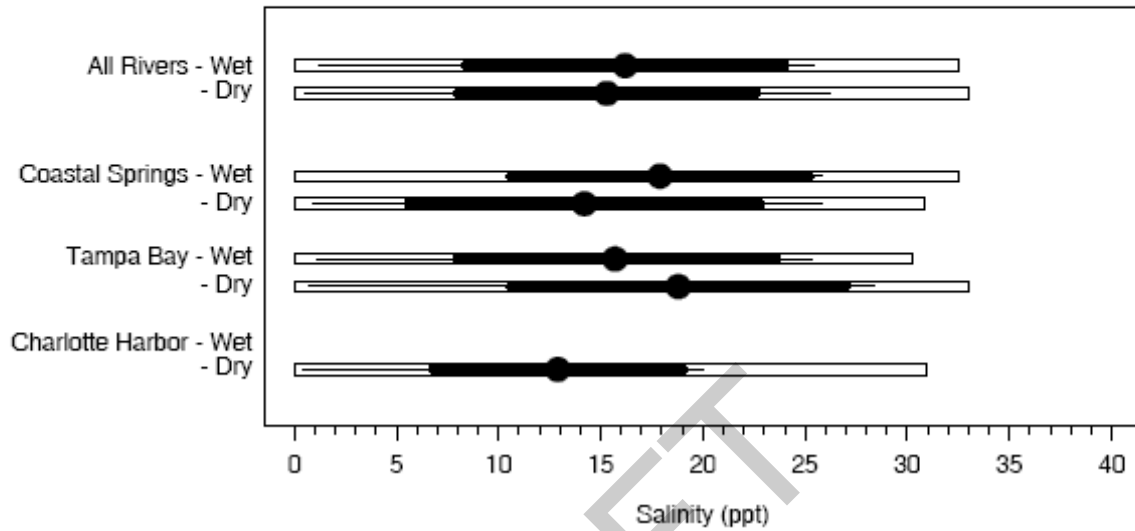
Dominance Rank=36 Taxon=*Xenanthura brevitelson*



Salinity Tolerance Compared Between River Groups

by Taxon and Season in the Order of Taxonomic Dominance

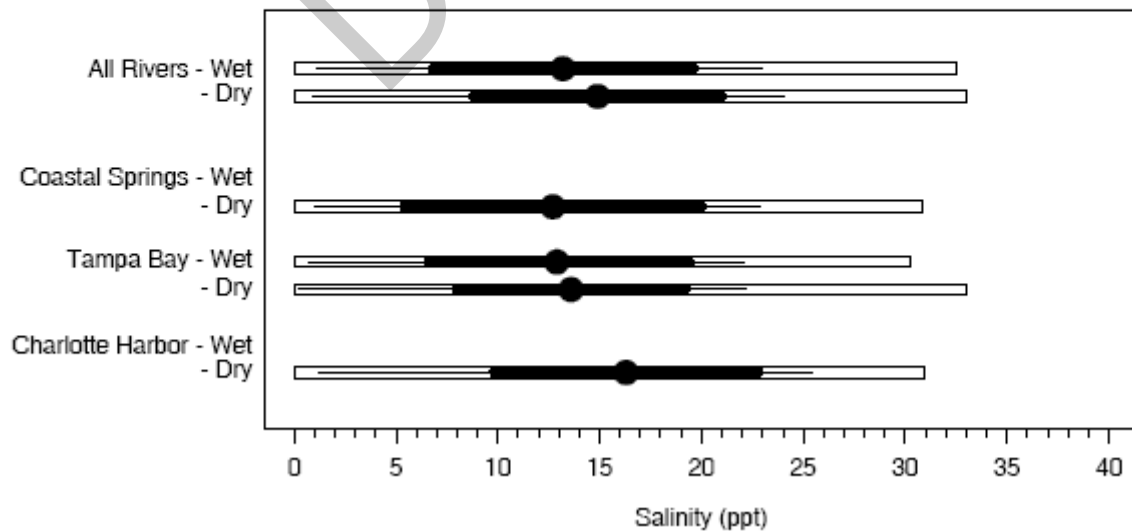
Dominance Rank=38 Taxon=*Edotea montosa*



Salinity Tolerance Compared Between River Groups

by Taxon and Season in the Order of Taxonomic Dominance

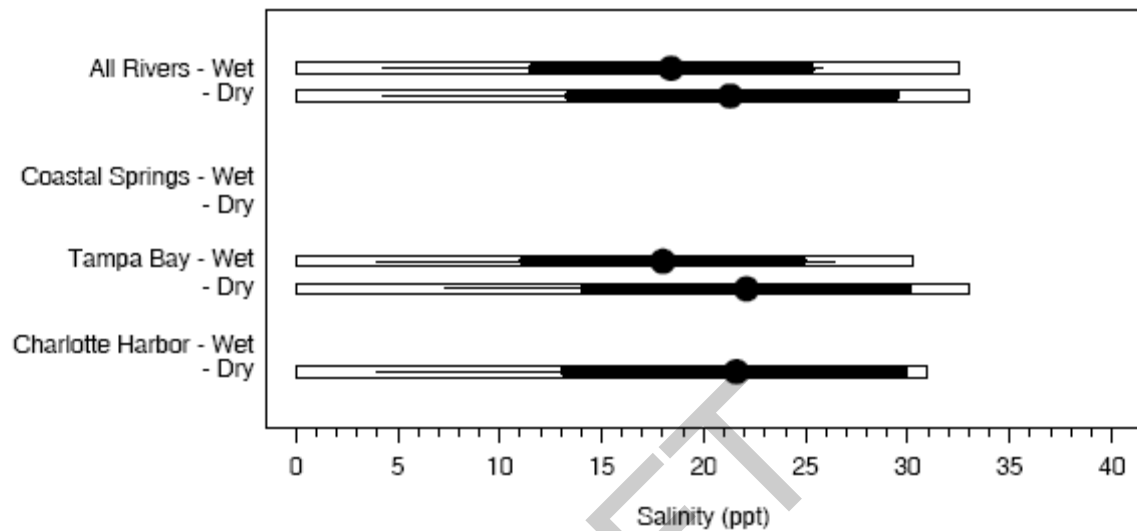
Dominance Rank=40 Taxon=*Tagelus plebeius*



Salinity Tolerance Compared Between River Groups

by Taxon and Season in the Order of Taxonomic Dominance

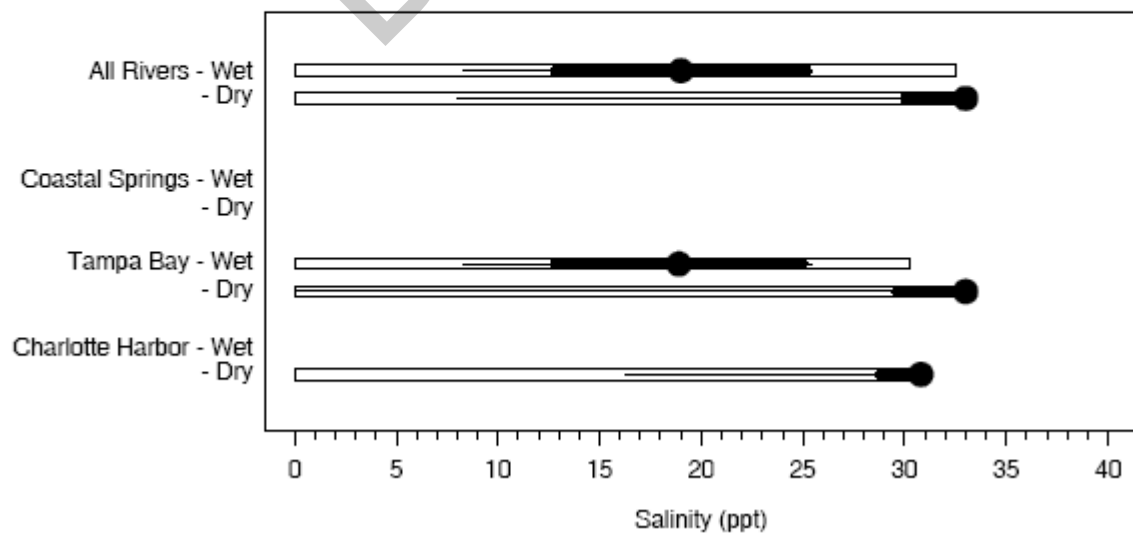
Dominance Rank=43 Taxon=*Nereis succinea*



Salinity Tolerance Compared Between River Groups

by Taxon and Season in the Order of Taxonomic Dominance

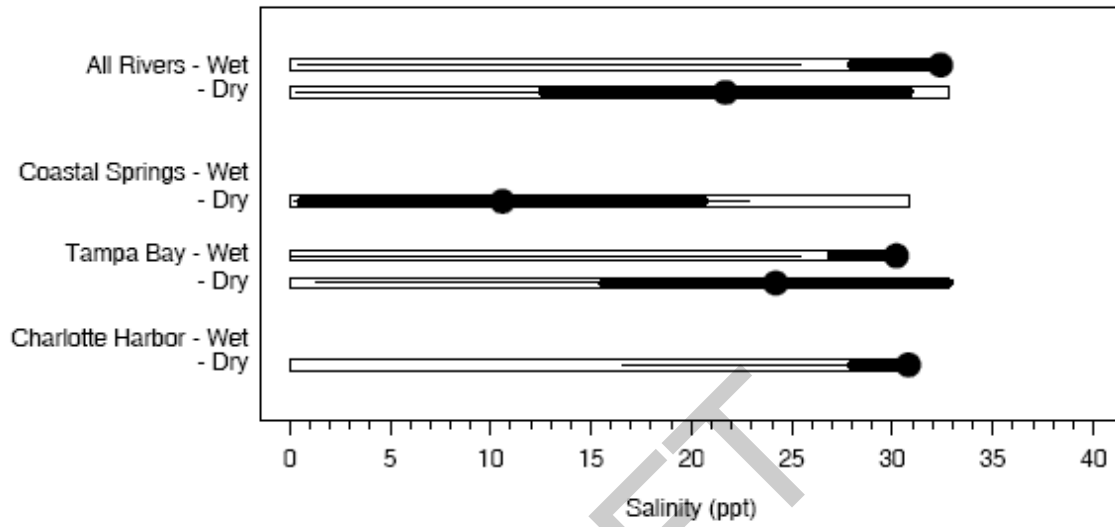
Dominance Rank=45 Taxon=*Acteocina canaliculata*



Salinity Tolerance Compared Between River Groups

by Taxon and Season in the Order of Taxonomic Dominance

Dominance Rank=49 Taxon=*Gammarus mucronatus*



Appendix 7-1

Shell Creek Whole River Regression

Whole River Regression Model:

Salinity in Shell Creek is affected by multiple forces including Shell Creek flow, Peace River flow, salinity in the Charlotte Harbor, tide, wind, etc. The Peace River Water Supply Authority has maintained a Hydro-Biological Monitoring Program (HBMP) in Shell Creek conducting fixed station profile and water chemistry samples since 1991. The HBMP station locations are spread throughout Shell Creek from the dam (rkm 10.15) to near the confluence of the Peace River (rkm 2.35). Profile data including salinity, temperature and dissolved oxygen measures were taken at surface, bottom and 1 meter intervals in the water column. Analysis of the surface, bottom, and water column average salinity by river km (Figure below) revealed that Shell Creek was well mixed, with a difference between average surface and bottom salinity generally less than one part per thousand. Therefore, water column average salinity was used for the regression analysis. Examination of scatter plots of salinity and flow revealed that at flows above 500cfs in Shell Creek, salinity at all fixed stations was nearly null (i.e., fresh water). Therefore, the regression analysis was censored to include only flows below 500cfs.

A whole river regression model was developed to predict water column average salinity in Shell Creek as a function of several physical variables. Several factors including missing time values for salinity data and lack of information on background salinity at station Black Marker #9 prior to 1997 restricted analysis to data from 1997-2004. Because the flows from Shell Creek and Peace River at Arcadia were not normally distributed, mathematical transformations of these variables were used to improve the fit of the predictors to the response variable. The natural log transformation was used for the Peace River flow. For Shell Creek, the flow was raised to the power of -0.05. For the purposes of fitting the regression model the river kilometer system was re-assigned such that the distance increases in the downstream direction by subtracting 10.15 from each fixed station and multiplying by -1; however, all results are reported (labeled) in their original scale. Further, the river kilometer was transformed to account for nonlinear increases in salinity with increasing distance downstream. As an indicator of the background salinity, the salinity in Charlotte Harbor at Black Marker #9 was used as a covariate in the regression model. Monthly intercepts were also used to capture variability in the response due to unmeasured factors such as prevailing wind direction and speed that was expressed as seasonality affecting the relationship between inflow and salinity. A Variance Inflation Factor (VIF) score was used to screen the predictor variables for multi-collinearity and no significant multi collinearity existed in the final model based on the VIF scores.

The whole river regression model was highly statistically significant ($\text{Pr}>F = < 0.0001$, $r^2 = 0.82$) and predicted water column average salinity adequately at all fixed stations. Plots comparing the predicted and observed salinities and box plots of the inter and intra-annual distribution of residuals (i.e., observed salinity – predicted salinity) for each fixed sampling station modeled in Shell Creek is provided along with the analysis of variance table and parameter estimates in the following pages of this appendix.

The final form of the regression model is:

$$\text{Salinity} = \alpha + \beta_{1-11} \text{Month} + \beta_{12} Q_{SC}^{-0.05} + \beta_{13} S_{BM} + \beta_{14} \text{Tide} + \beta_{15} (\ln Q_{PR}) + \beta_{16} RK^{1.5} + \beta_{17} Q_{SC} * RK$$

where:

Salinity	=	Water Column Average Salinity
Month ₁₋₁₁	=	January-November using December as a reference group
Q _{SC}	=	Shell Creek Flow (raised to the negative power of 0.05)
S _{BM}	=	Salinity - Black Marker
Tide	=	Tide Height at Boca Grande
Q _{PR}	=	Peace River Flow (Natural log transformed)
RK	=	River Kilometer
Q _{SC} *RK	=	Interaction term of Shell flow and River Kilometer
β ₁₋₁₇	=	Regression coefficients

DRAFT

Distribution of Depth-Integrated Salinity by Month

The GLM Procedure

Number of Observations Read	591
Number of Observations Used	582

DRAFT

Distribution of Depth-Integrated Salinity by Month

The GLM Procedure

Dependent Variable: mnsal Salinity

Source	DF	Sum of Squares	Mean Square	F Value	Pr > F
Model	17	10818.47010	636.38059	147.47	<.0001
Error	564	2433.81568	4.31528		
Corrected Total	581	13252.28578			

R-Square	Coeff Var	Root MSE	mnsal Mean
0.816347	54.67415	2.077324	3.799463

Source	DF	Type I SS	Mean Square	F Value	Pr > F
fpower_05m	1	7286.357847	7286.357847	1688.50	<.0001
rk_x	1	1516.900444	1516.900444	351.52	<.0001
bot_sal_blmk	1	802.345005	802.345005	185.93	<.0001
SHELL*rk1	1	31.160525	31.160525	7.22	0.0074
elev	1	216.806807	216.806807	50.24	<.0001
lpeace	1	639.044918	639.044918	148.09	<.0001
m2	1	71.750932	71.750932	16.63	<.0001
m1	1	1.973149	1.973149	0.46	0.4992
m3	1	13.532186	13.532186	3.14	0.0771
m4	1	18.011355	18.011355	4.17	0.0415
m5	1	17.992774	17.992774	4.17	0.0416
m6	1	105.960786	105.960786	24.55	<.0001
m7	1	10.840312	10.840312	2.51	0.1135
m8	1	6.363217	6.363217	1.47	0.2251
m9	1	12.278109	12.278109	2.85	0.0922

Distribution of Depth-Integrated Salinity by Month

The GLM Procedure

Dependent Variable: mnsal Salinity

Source	DF	Type I SS	Mean Square	F Value	Pr > F
m10	1	35.489015	35.489015	8.22	0.0043
m11	1	31.662718	31.662718	7.34	0.0070

Source	DF	Type III SS	Mean Square	F Value	Pr > F
fpower_05m	1	319.265189	319.265189	73.98	<.0001
rk_x	1	1407.051640	1407.051640	326.06	<.0001
bot_sal_blmk	1	129.831788	129.831788	30.09	<.0001
SHELL*rk1	1	141.852246	141.852246	32.87	<.0001
elev	1	23.007527	23.007527	5.33	0.0213
lpeace	1	438.554417	438.554417	101.63	<.0001
m2	1	56.988738	56.988738	13.21	0.0003
m1	1	3.779015	3.779015	0.88	0.3498
m3	1	5.865884	5.865884	1.36	0.2441
m4	1	18.517632	18.517632	4.29	0.0388
m5	1	1.673624	1.673624	0.39	0.5337
m6	1	72.931655	72.931655	16.90	<.0001
m7	1	9.272204	9.272204	2.15	0.1432
m8	1	9.763383	9.763383	2.26	0.1331
m9	1	7.777553	7.777553	1.80	0.1800
m10	1	6.589706	6.589706	1.53	0.2171
m11	1	31.662718	31.662718	7.34	0.0070

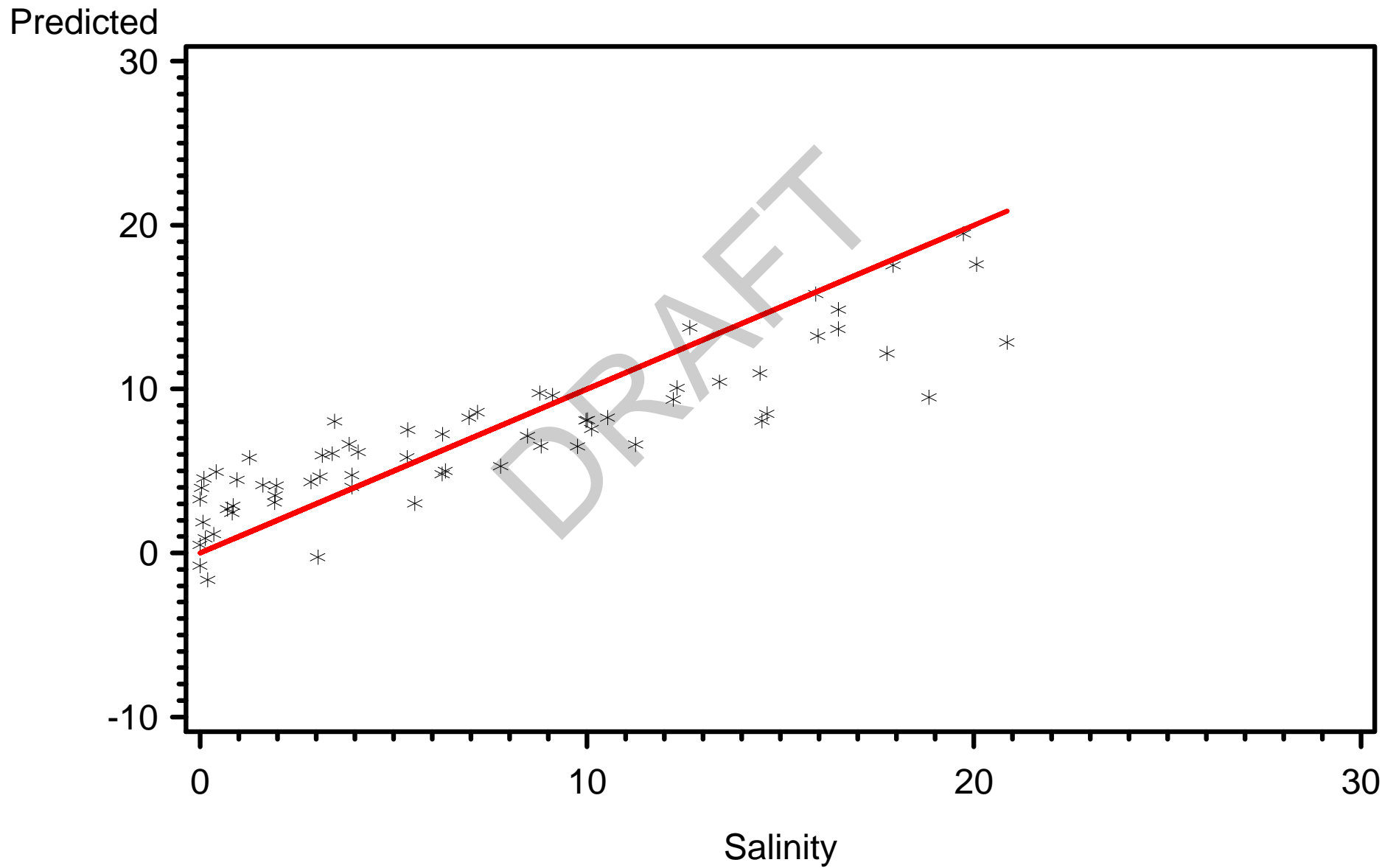
Distribution of Depth-Integrated Salinity by Month

The GLM Procedure

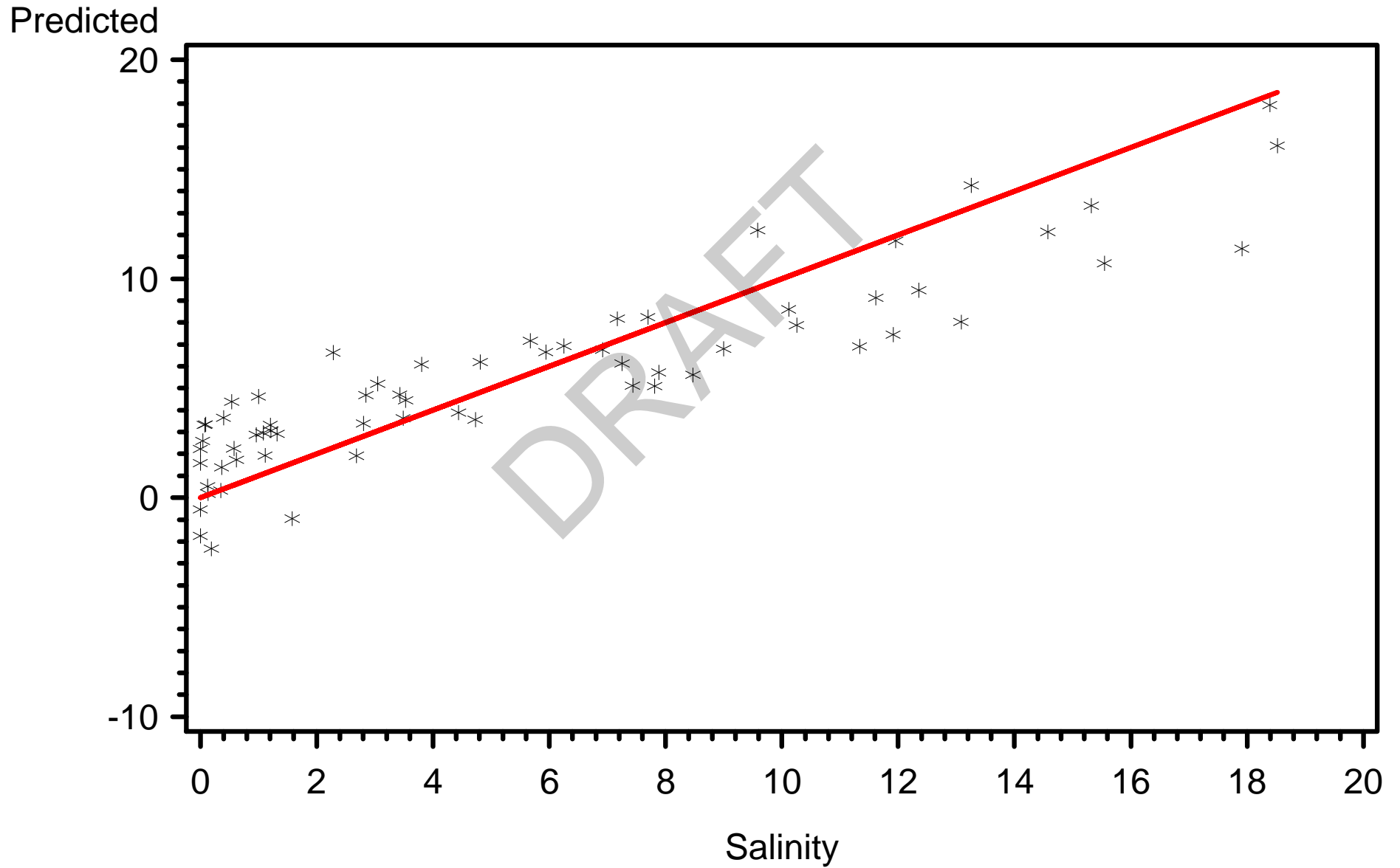
Dependent Variable: mnsal Salinity

Parameter	Estimate	Standard Error	t Value	Pr > t
Intercept	-12.40717646	3.03151701	-4.09	<.0001
fpower_05m	22.69300848	2.63827815	8.60	<.0001
rk_x	0.29157160	0.01614710	18.06	<.0001
bot_sal_blmk	0.12356416	0.02252715	5.49	<.0001
SHELL*rk1	-0.00132505	0.00023111	-5.73	<.0001
elev	0.60967040	0.26403678	2.31	0.0213
lpeace	-1.47377952	0.14619249	-10.08	<.0001
m2	-1.44253769	0.39695104	-3.63	0.0003
m1	-0.39873146	0.42608423	-0.94	0.3498
m3	-0.45960712	0.39420699	-1.17	0.2441
m4	0.81065421	0.39133366	2.07	0.0388
m5	-0.25258403	0.40558442	-0.62	0.5337
m6	1.70346190	0.41436082	4.11	<.0001
m7	-0.83128481	0.56710392	-1.47	0.1432
m8	0.95172737	0.63272747	1.50	0.1331
m9	0.67116598	0.49993407	1.34	0.1800
m10	0.51411462	0.41603629	1.24	0.2171
m11	-1.01206124	0.37362591	-2.71	0.0070

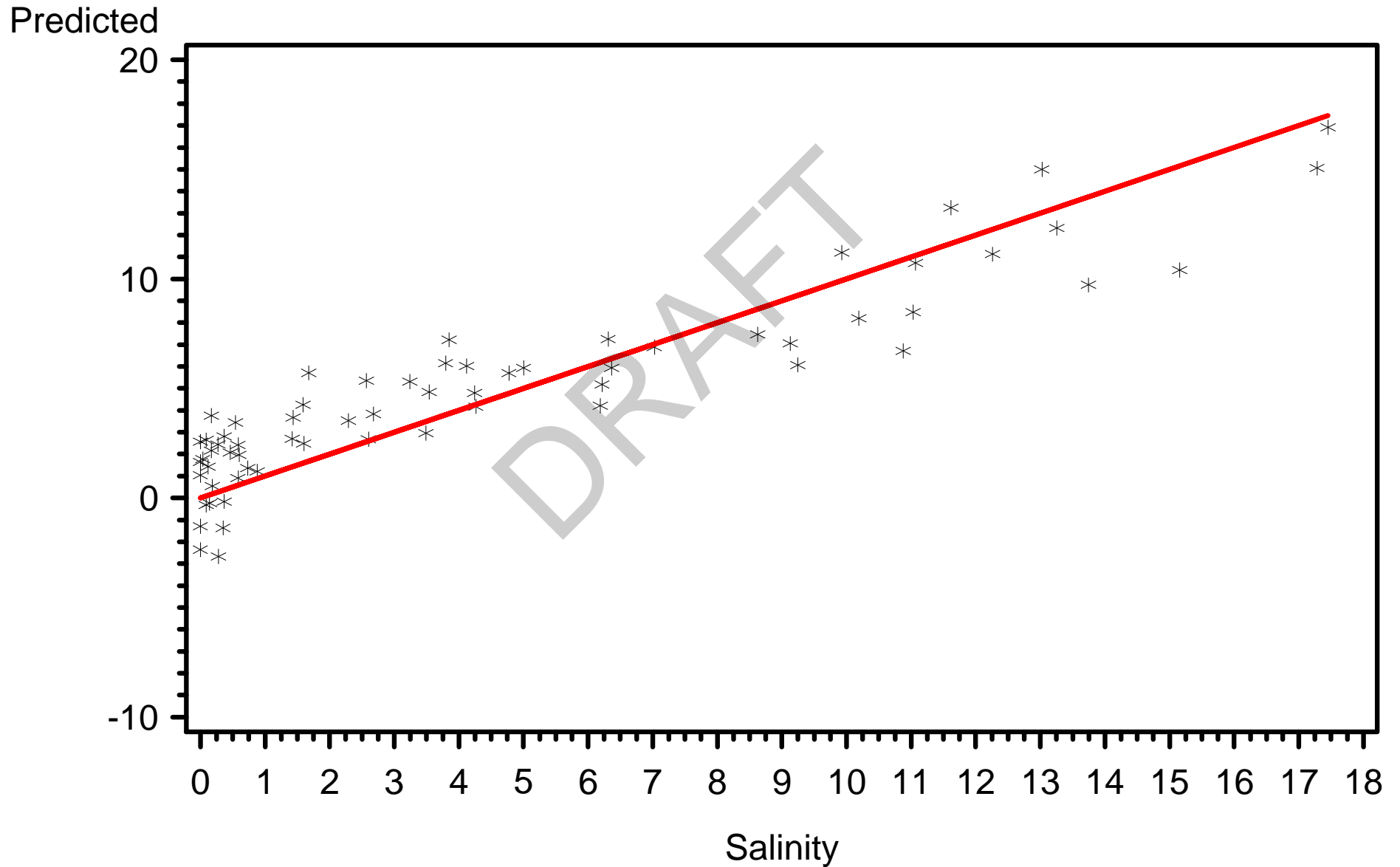
Shell Creek 1997-2004
Predicted vs Observed Salinity by Station
River Kilometer=2.35



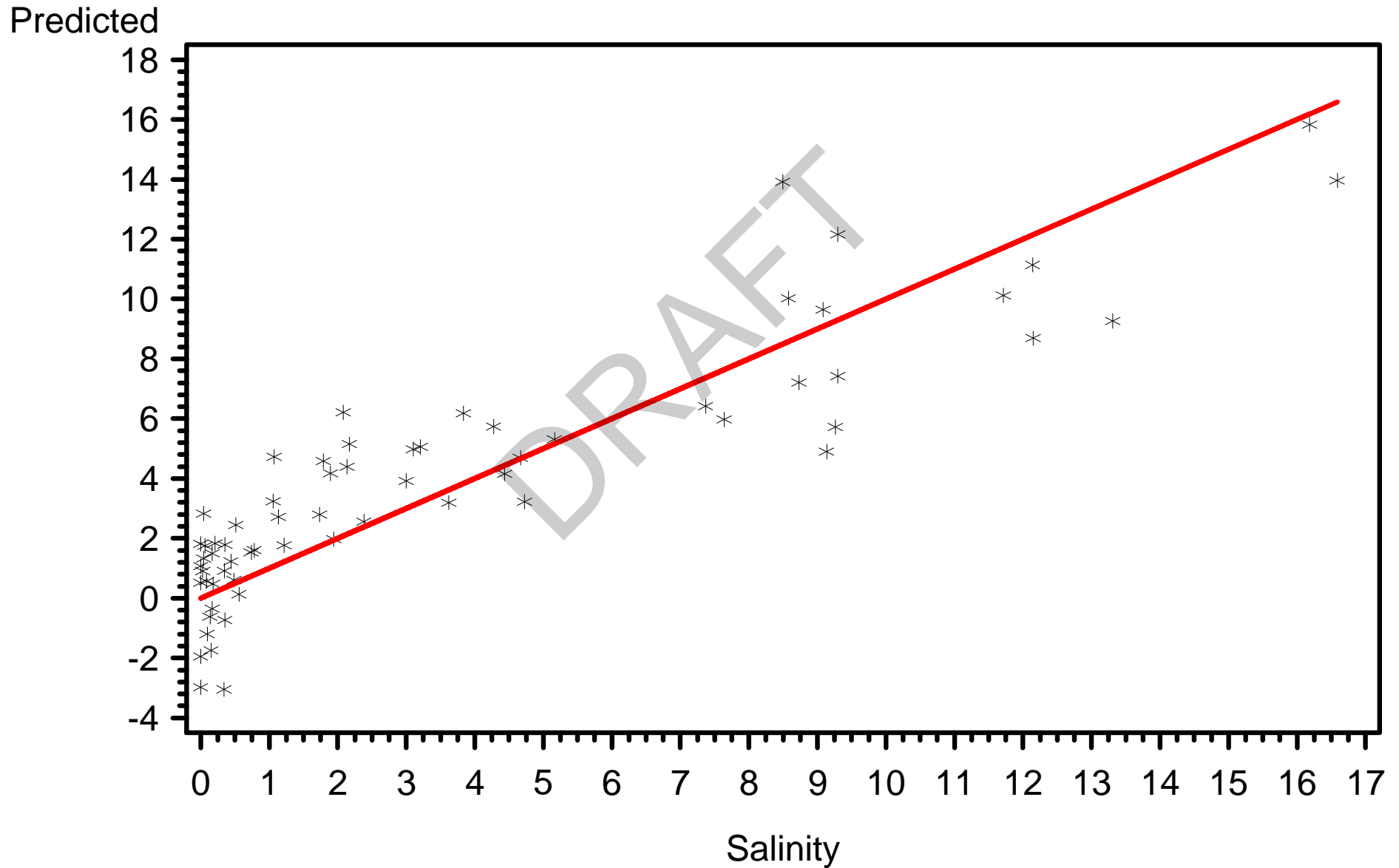
Shell Creek 1997-2004
Predicted vs Observed Salinity by Station
River Kilometer=3.66



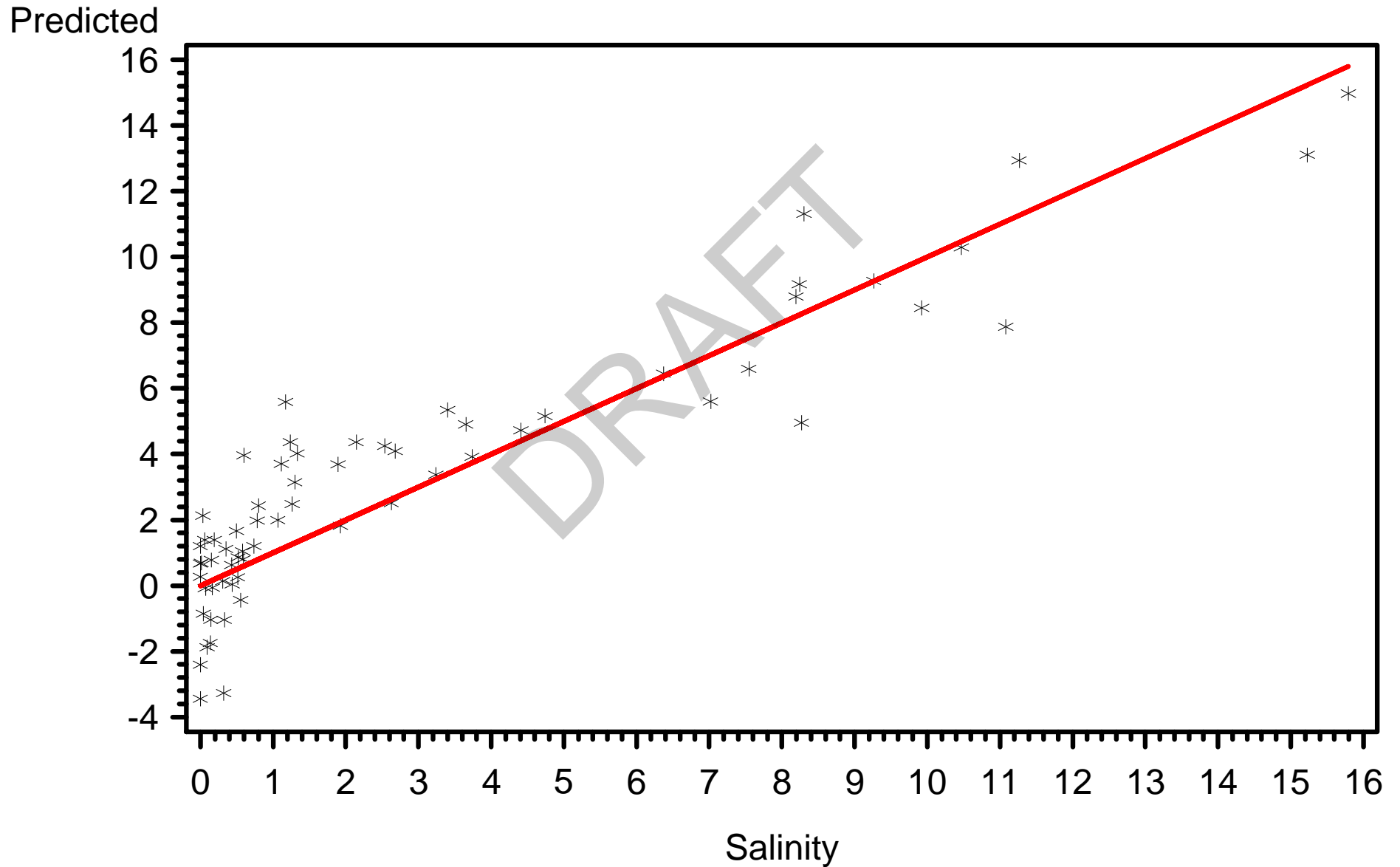
Shell Creek 1997-2004
Predicted vs Observed Salinity by Station
River Kilometer=4.61



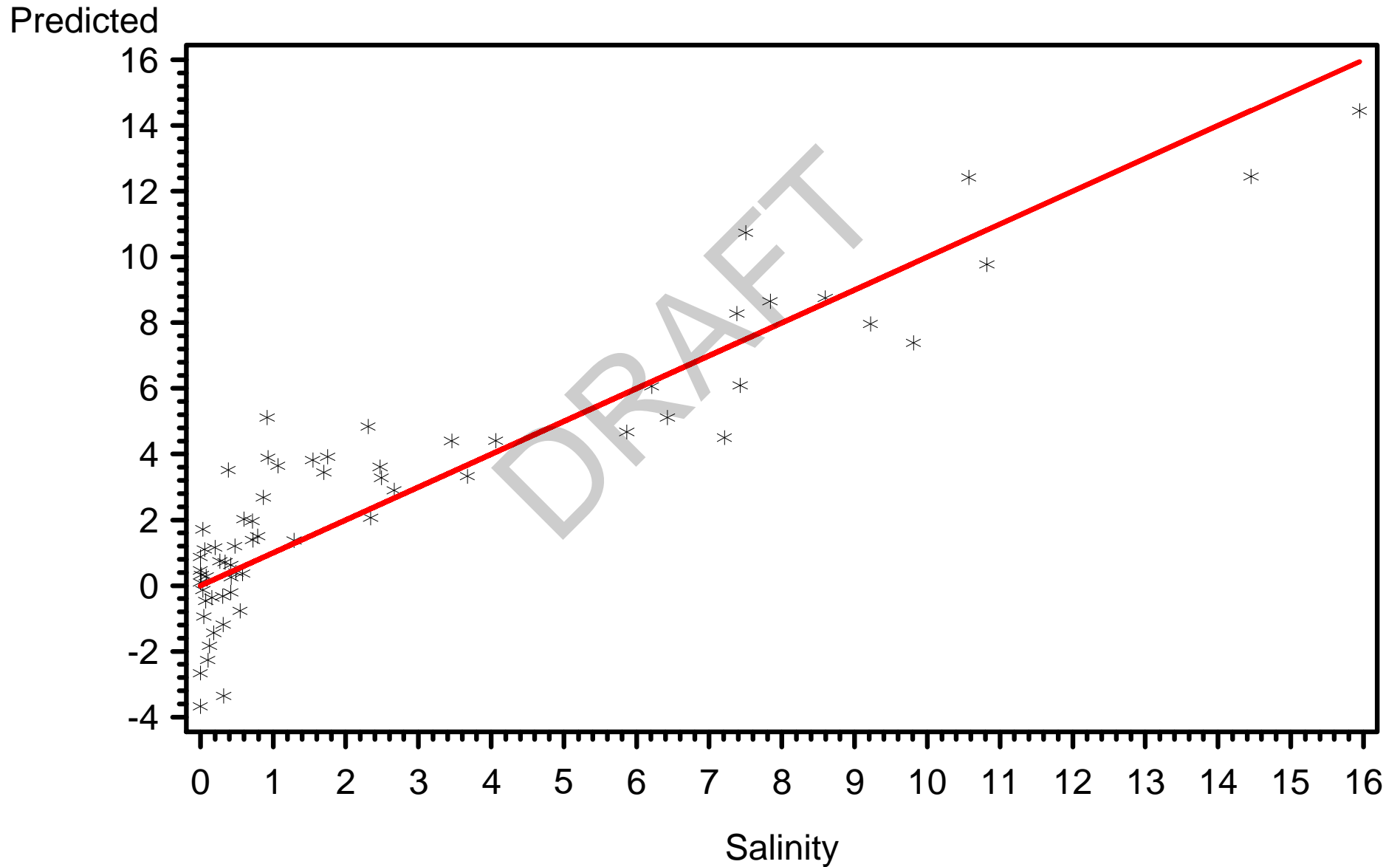
Shell Creek 1997-2004
Predicted vs Observed Salinity by Station
River Kilometer=5.73



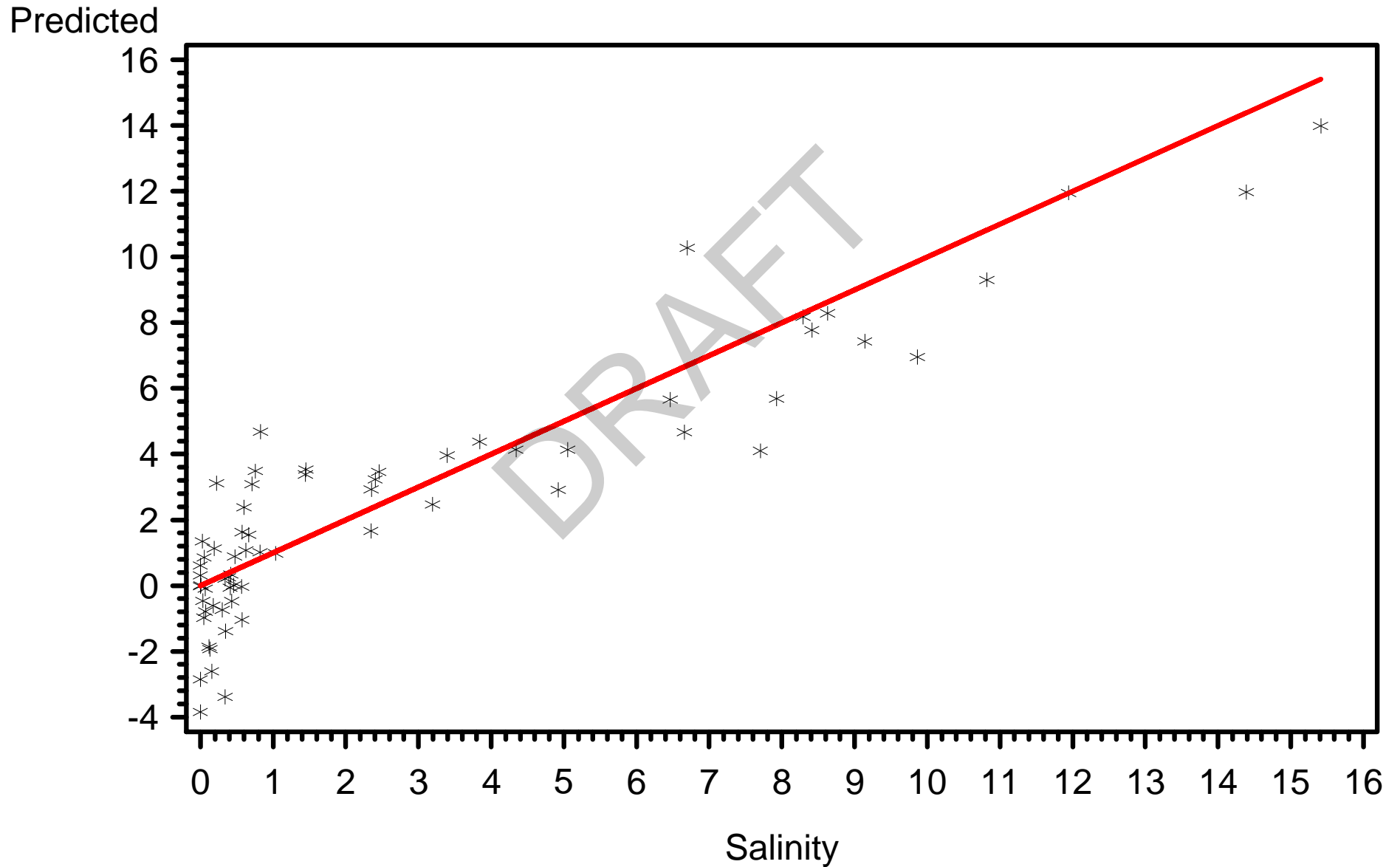
Shell Creek 1997-2004
Predicted vs Observed Salinity by Station
River Kilometer=6.72



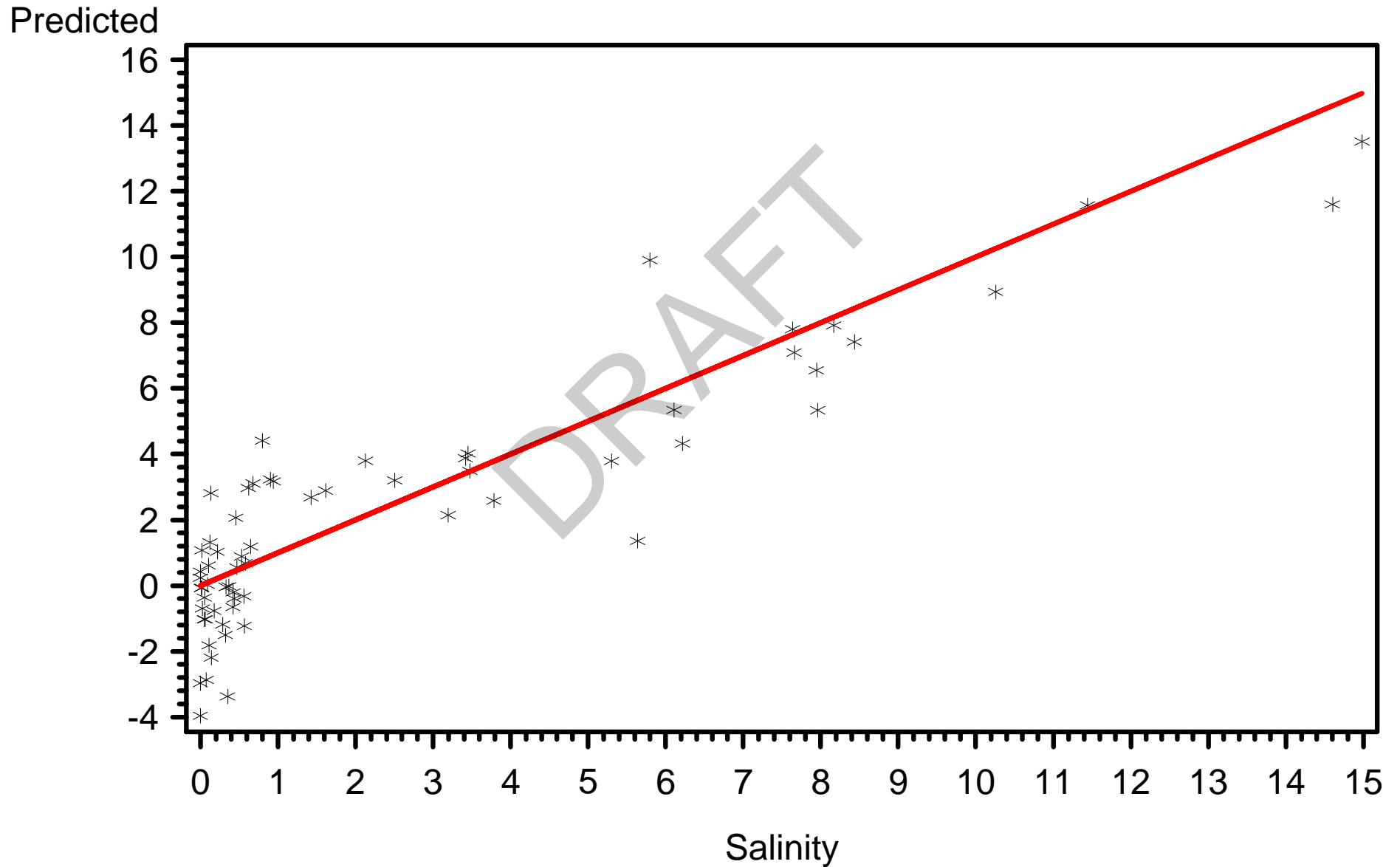
Shell Creek 1997-2004
Predicted vs Observed Salinity by Station
River Kilometer=7.40



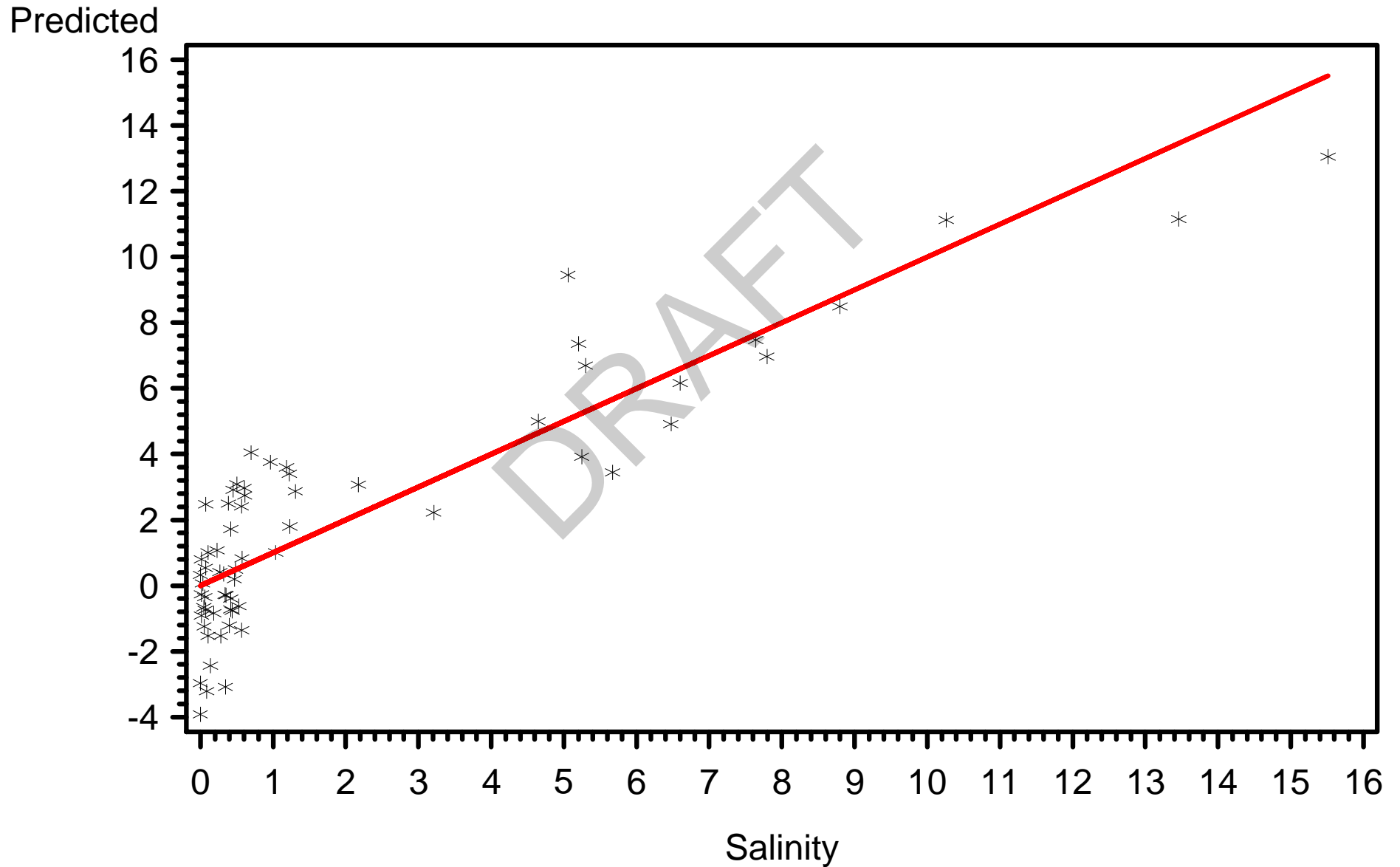
Shell Creek 1997-2004
Predicted vs Observed Salinity by Station
River Kilometer=8.09



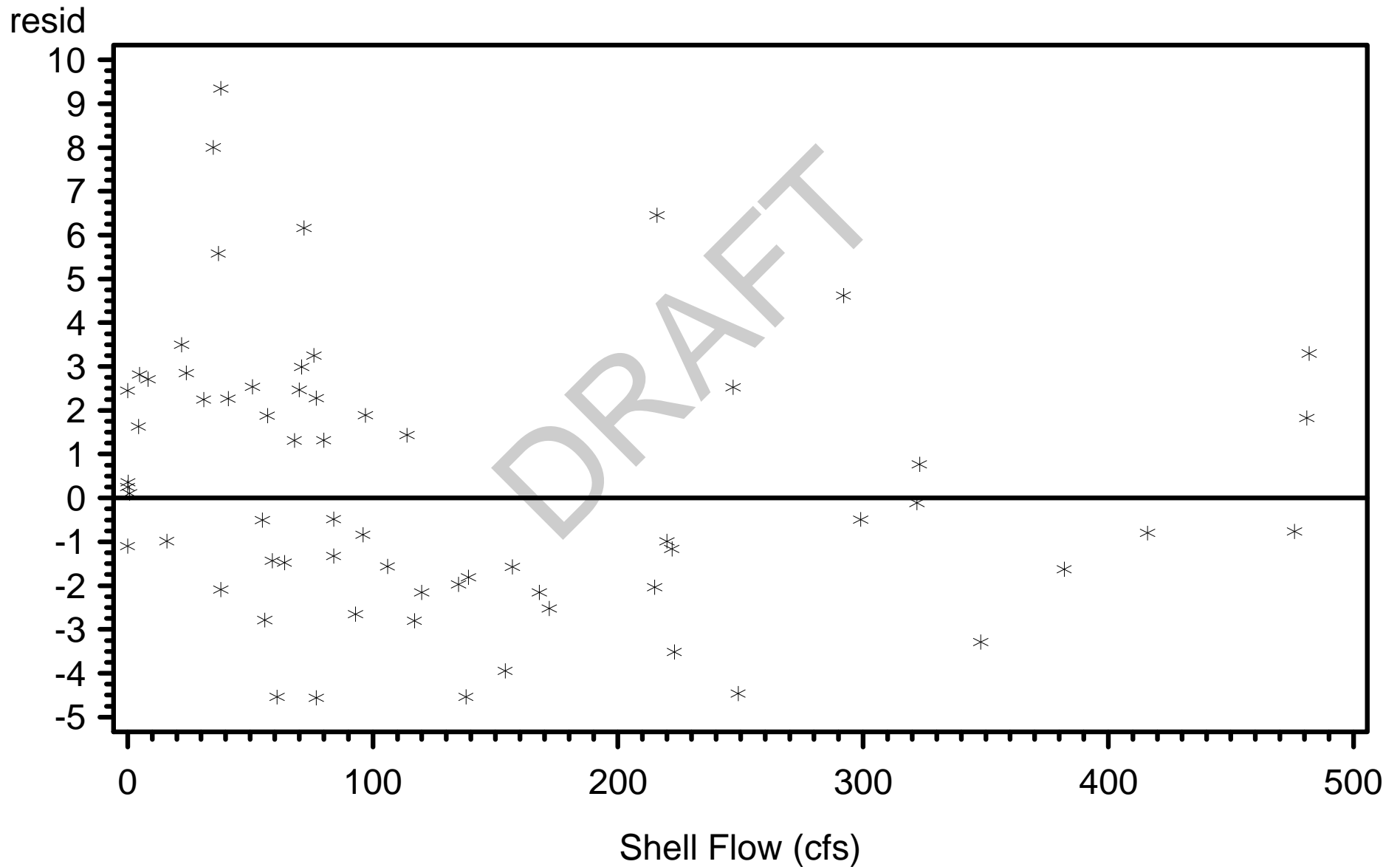
Shell Creek 1997-2004
Predicted vs Observed Salinity by Station
River Kilometer=8.74



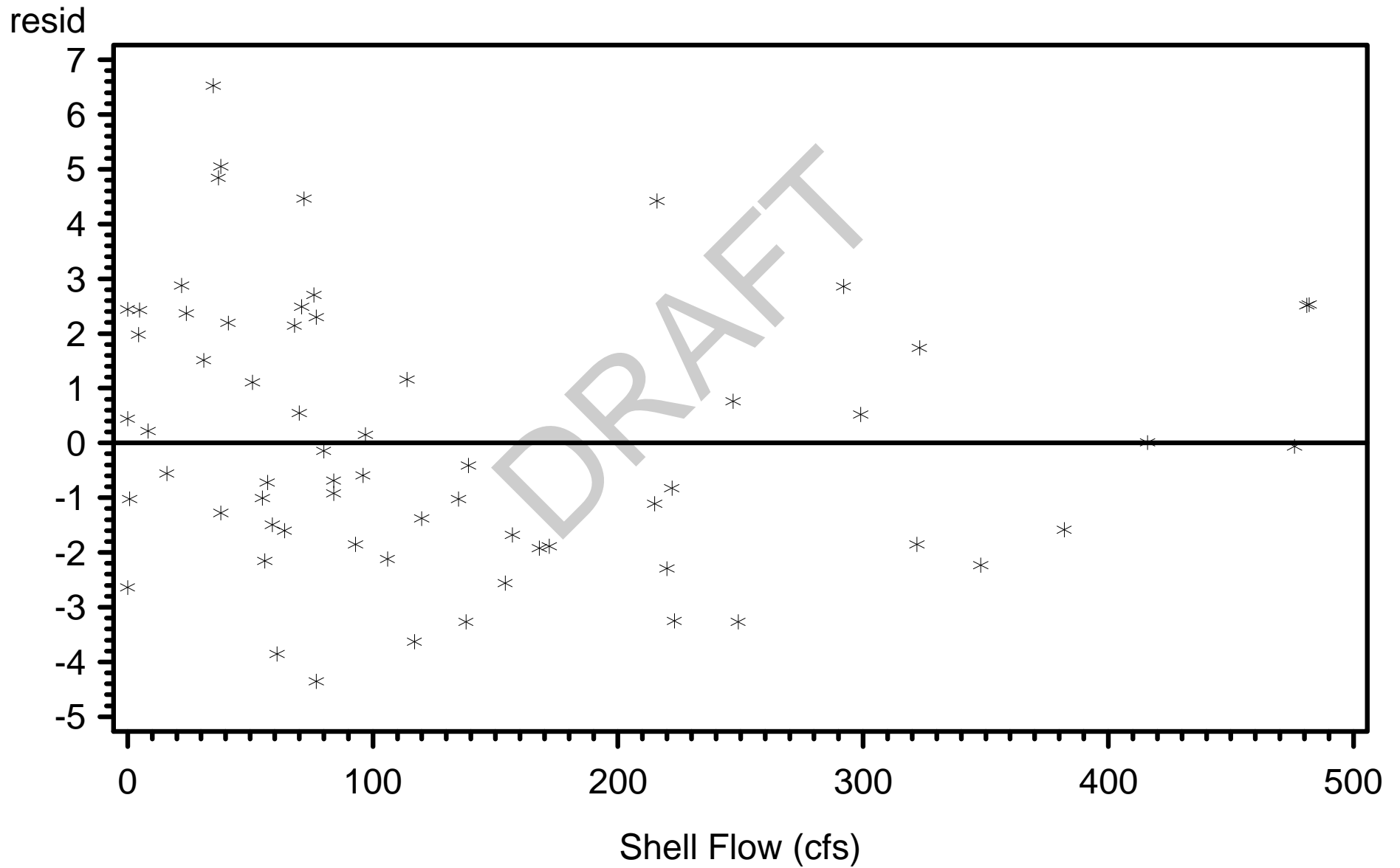
Shell Creek 1997-2004
Predicted vs Observed Salinity by Station
River Kilometer=9.90



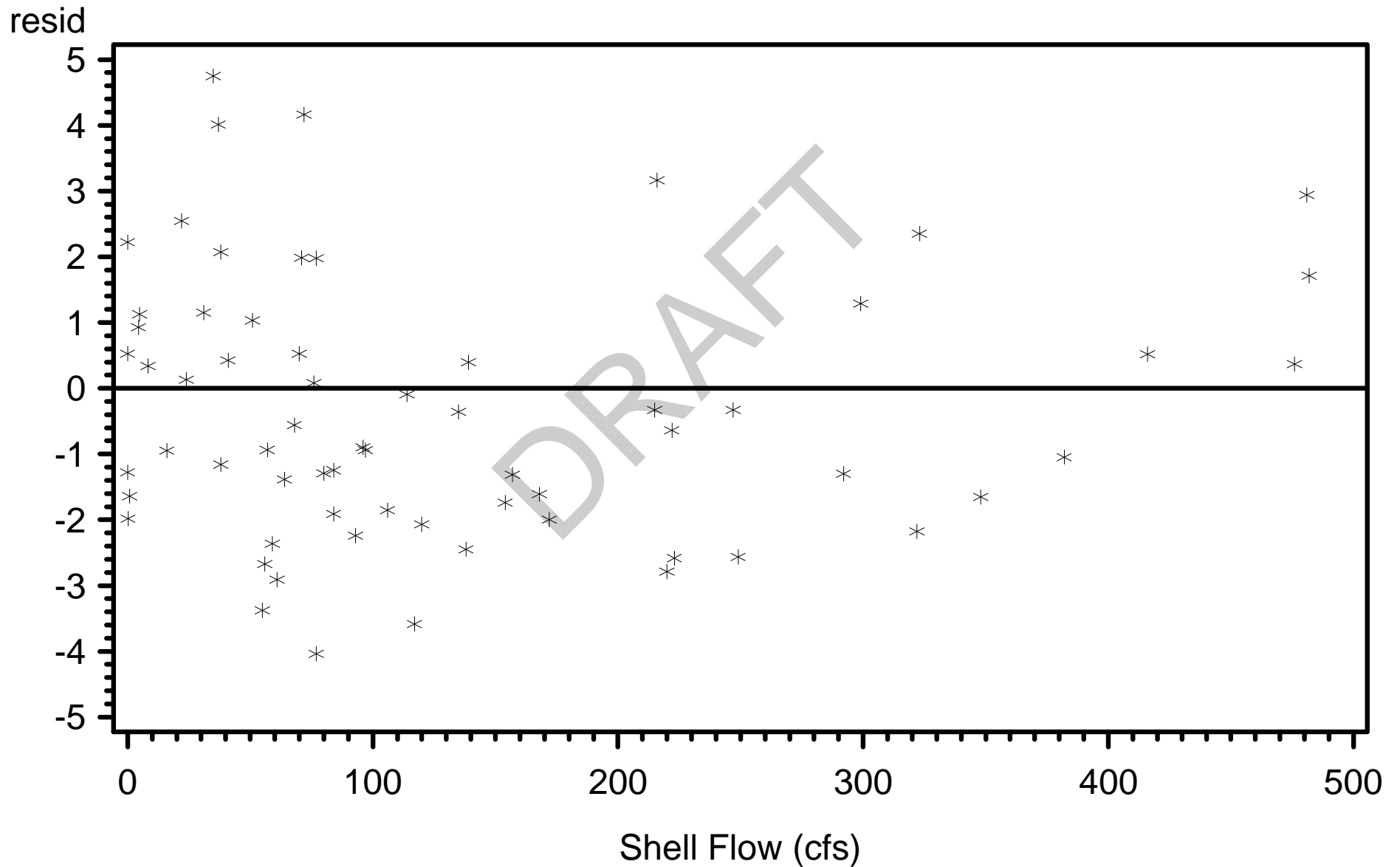
Shell Creek 1997-2004
Residuals vs Shell Creek Flow (cfs)
River Kilometer=2.35



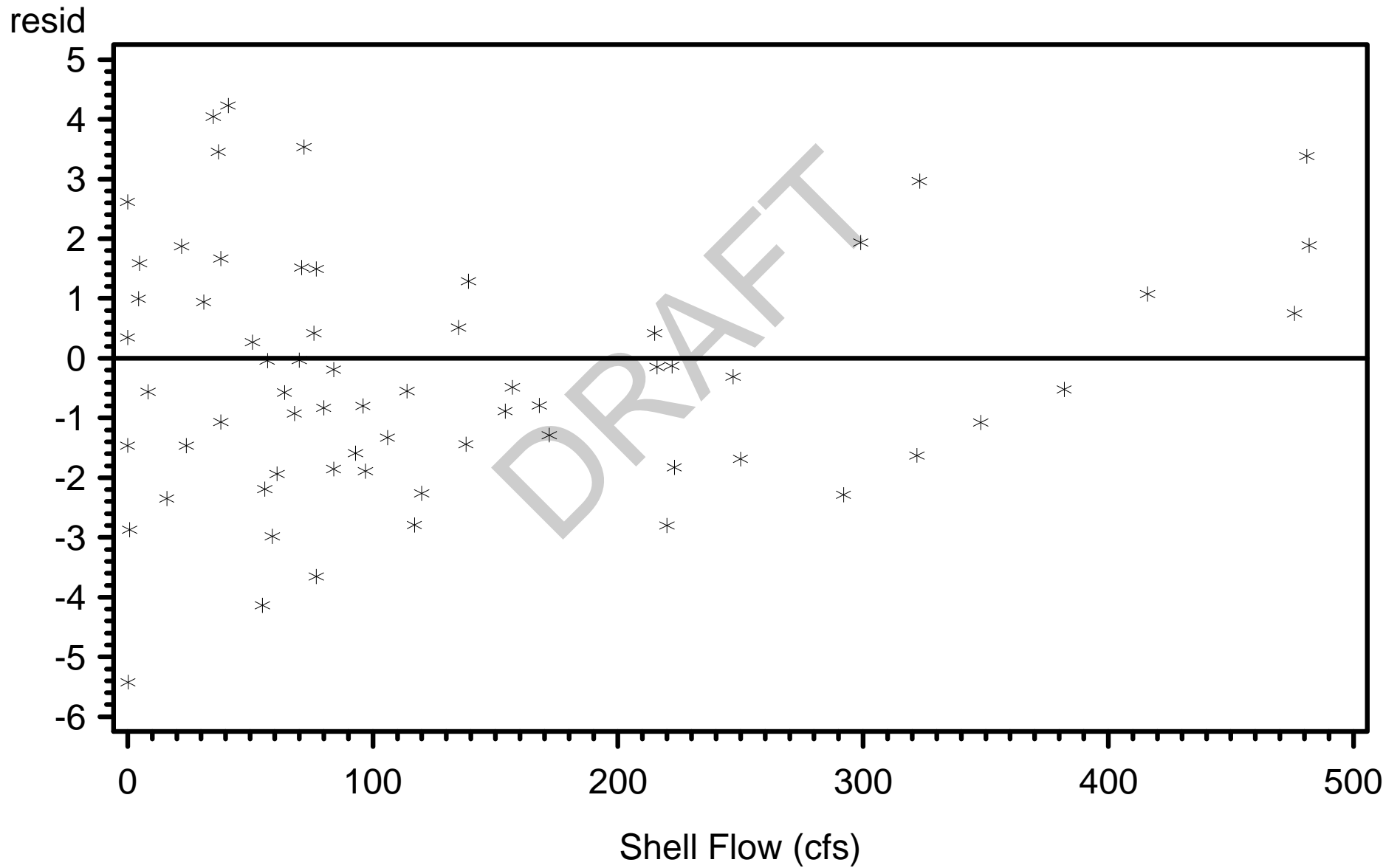
Shell Creek 1997-2004
Residuals vs Shell Creek Flow (cfs)
River Kilometer=3.66



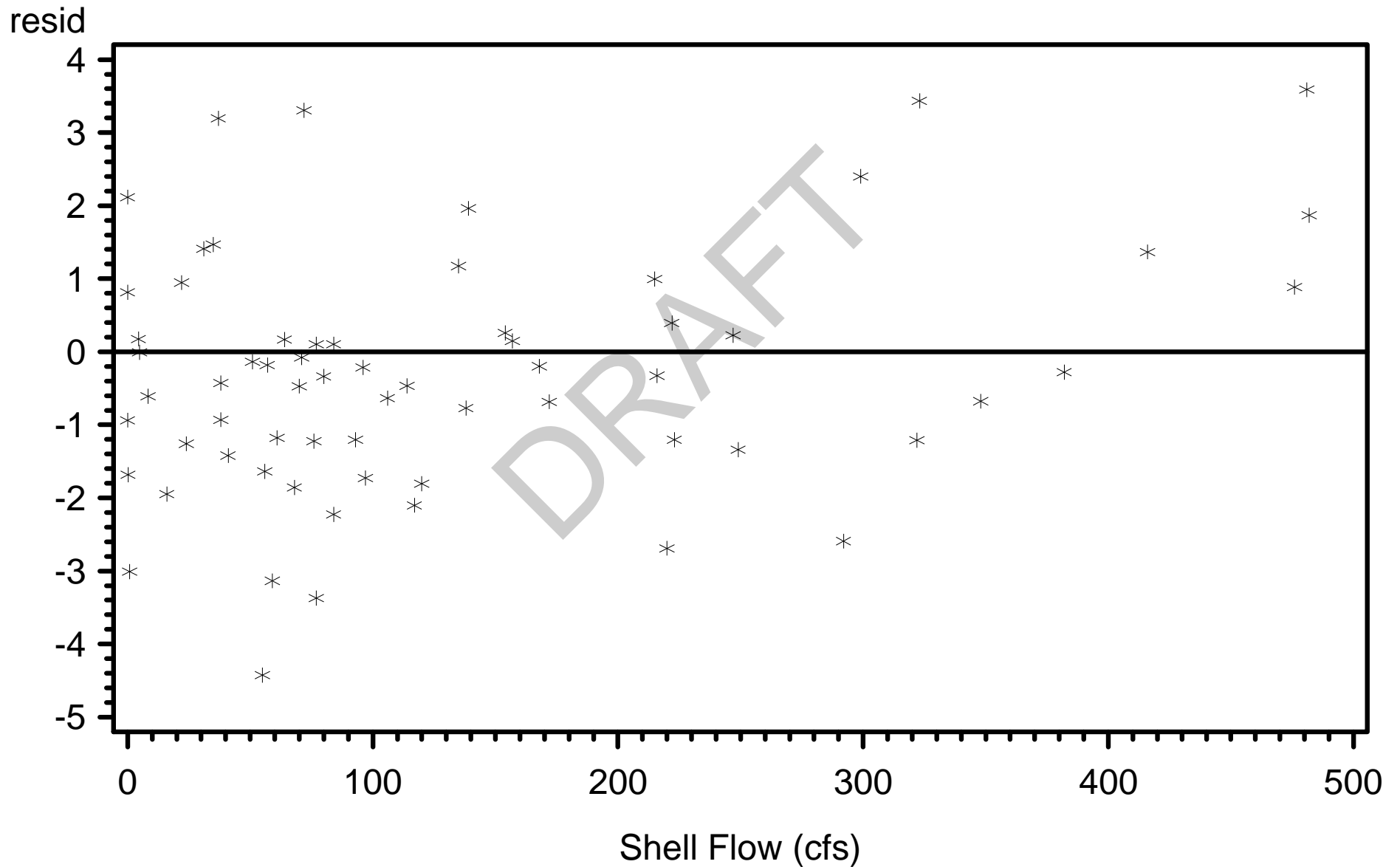
Shell Creek 1997-2004
Residuals vs Shell Creek Flow (cfs)
River Kilometer=4.61



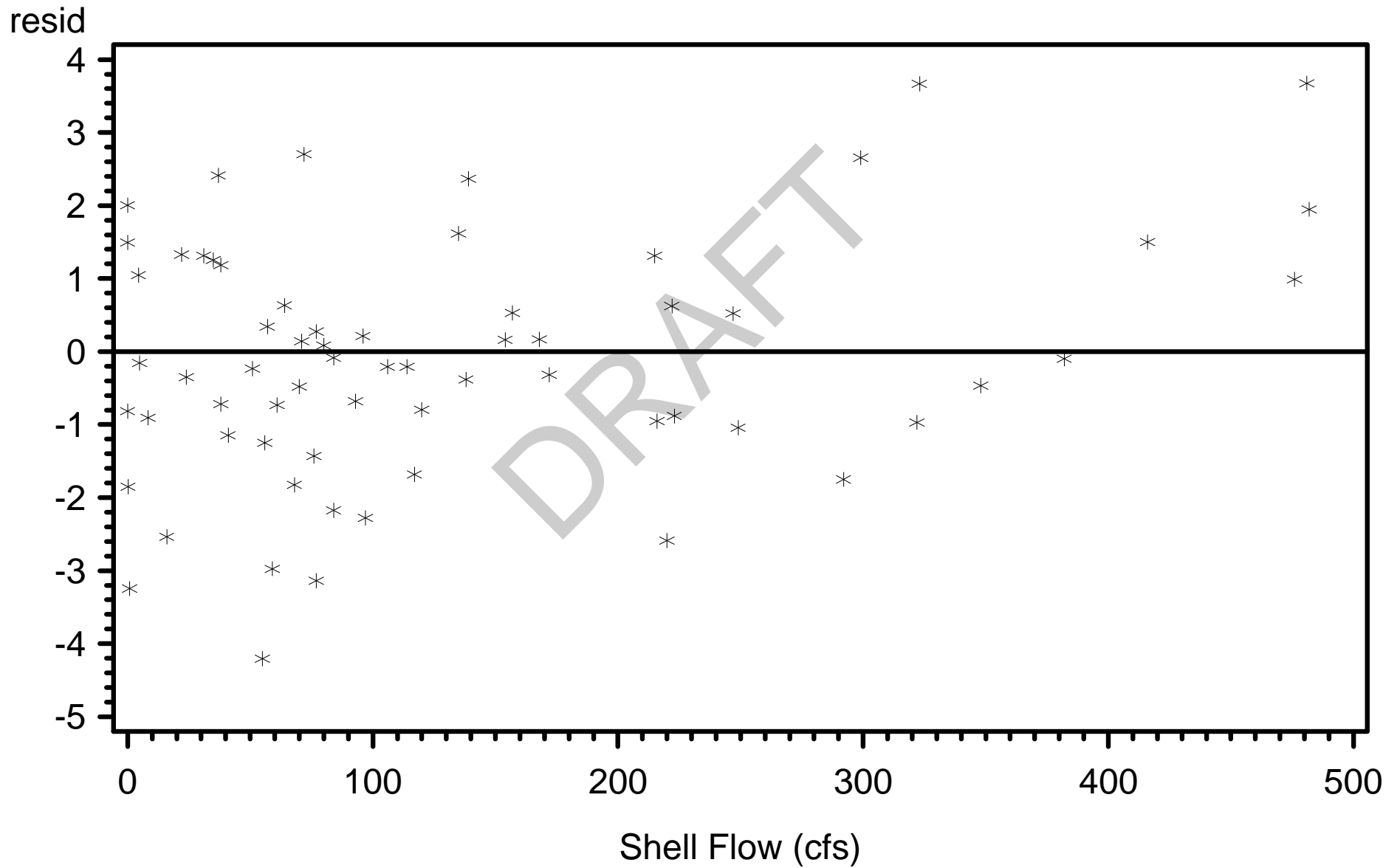
Shell Creek 1997-2004
Residuals vs Shell Creek Flow (cfs)
River Kilometer=5.73



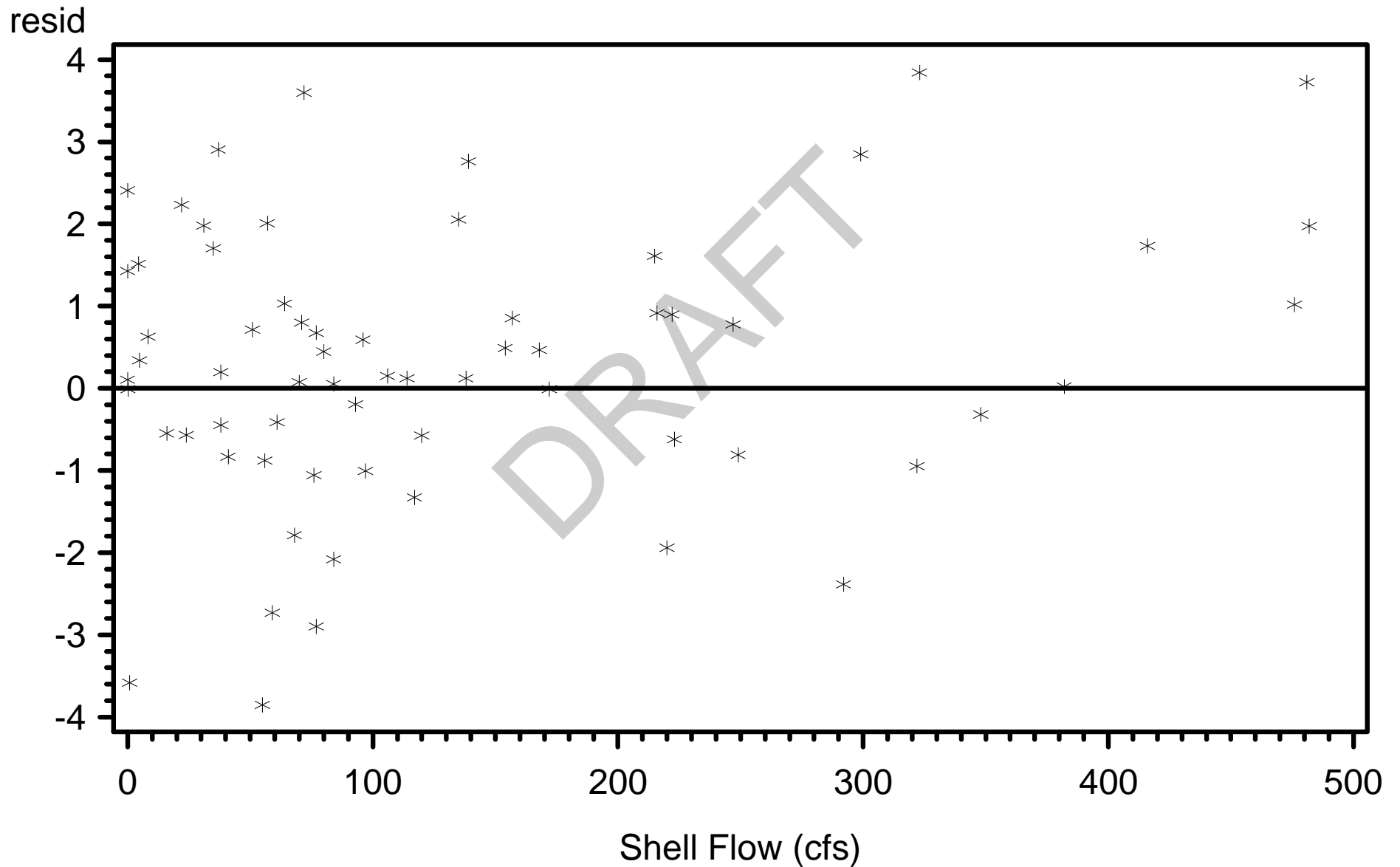
Shell Creek 1997-2004
Residuals vs Shell Creek Flow (cfs)
River Kilometer=6.72



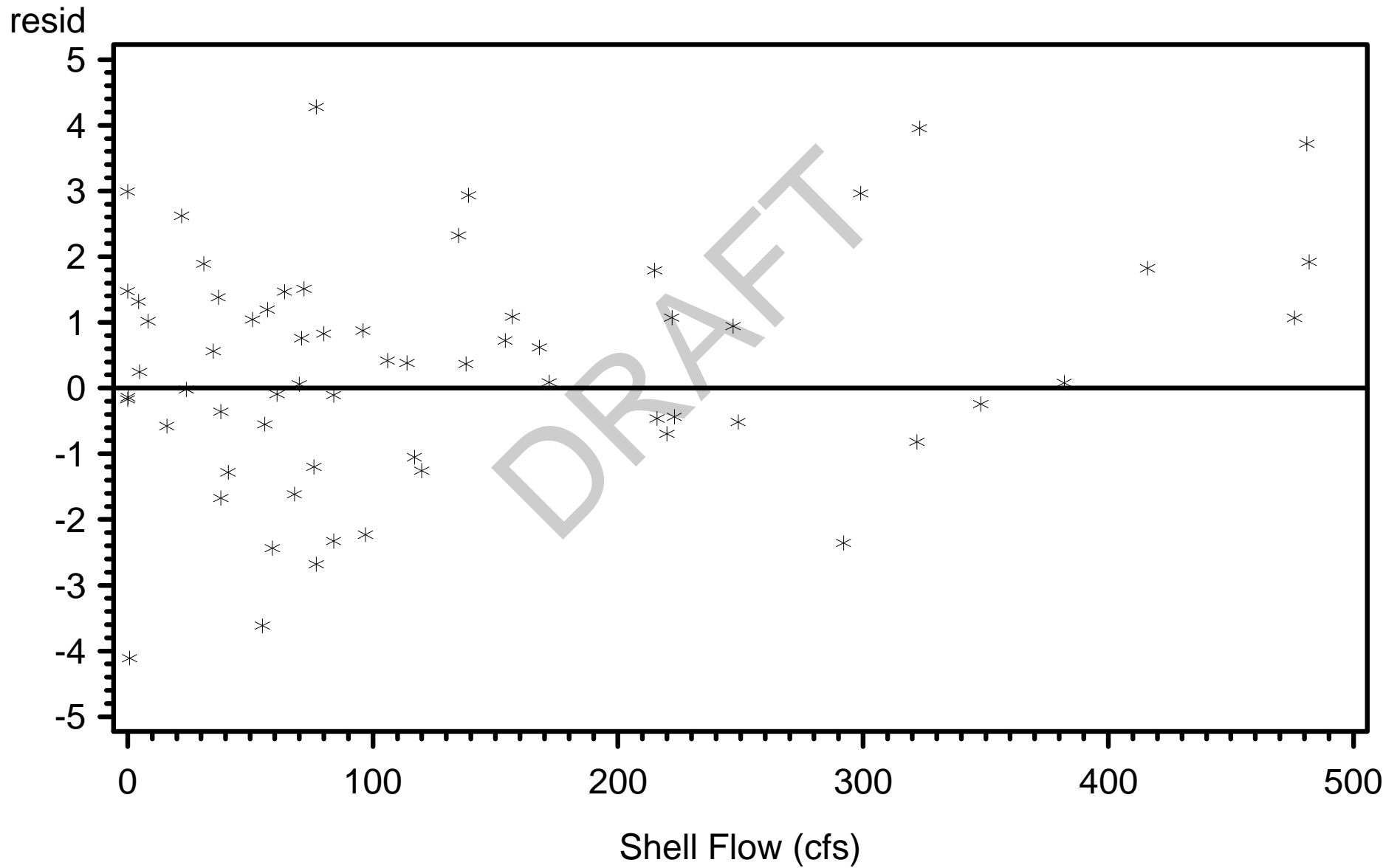
Shell Creek 1997-2004
Residuals vs Shell Creek Flow (cfs)
River Kilometer=7.40



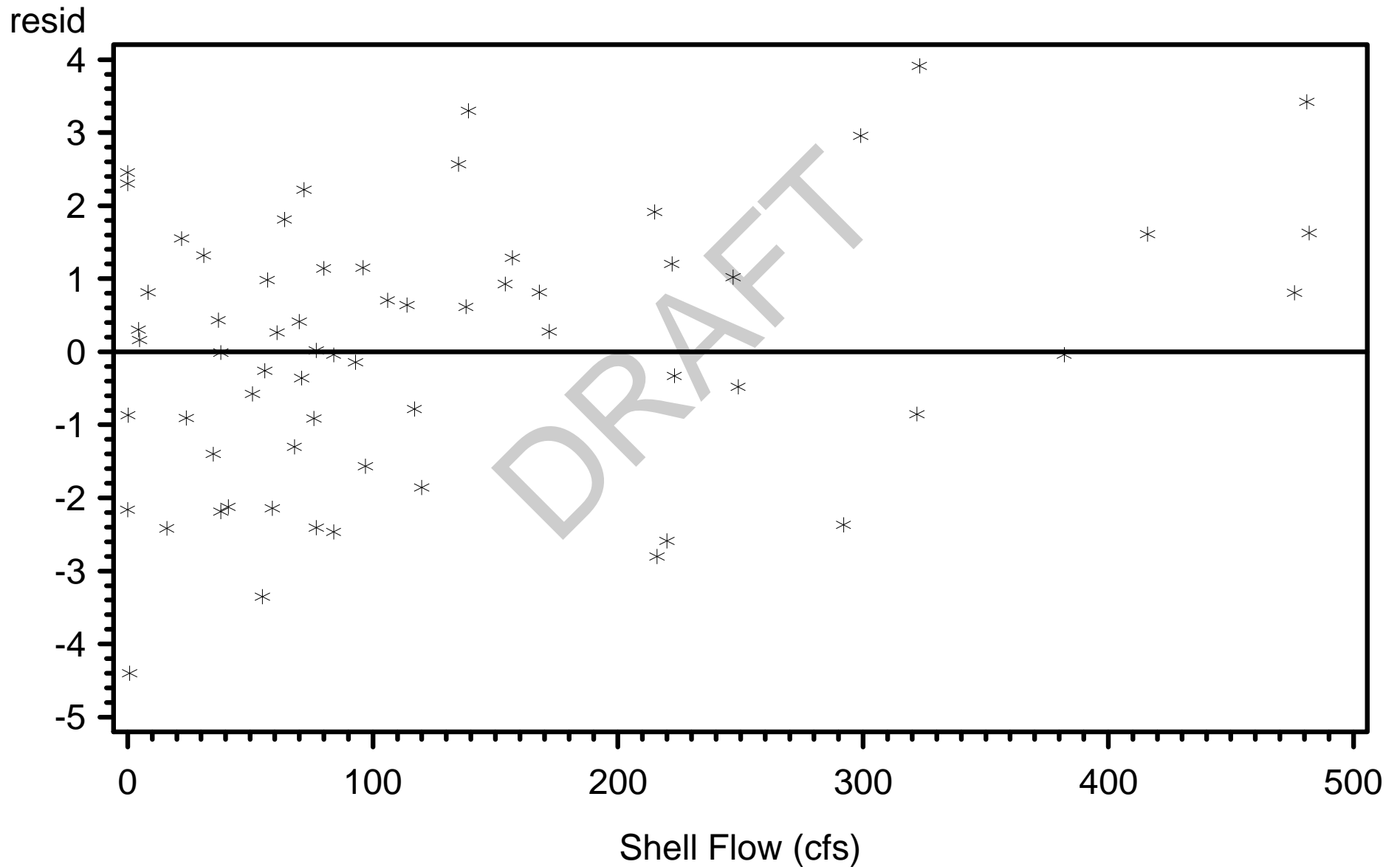
Shell Creek 1997-2004
Residuals vs Shell Creek Flow (cfs)
River Kilometer=8.09



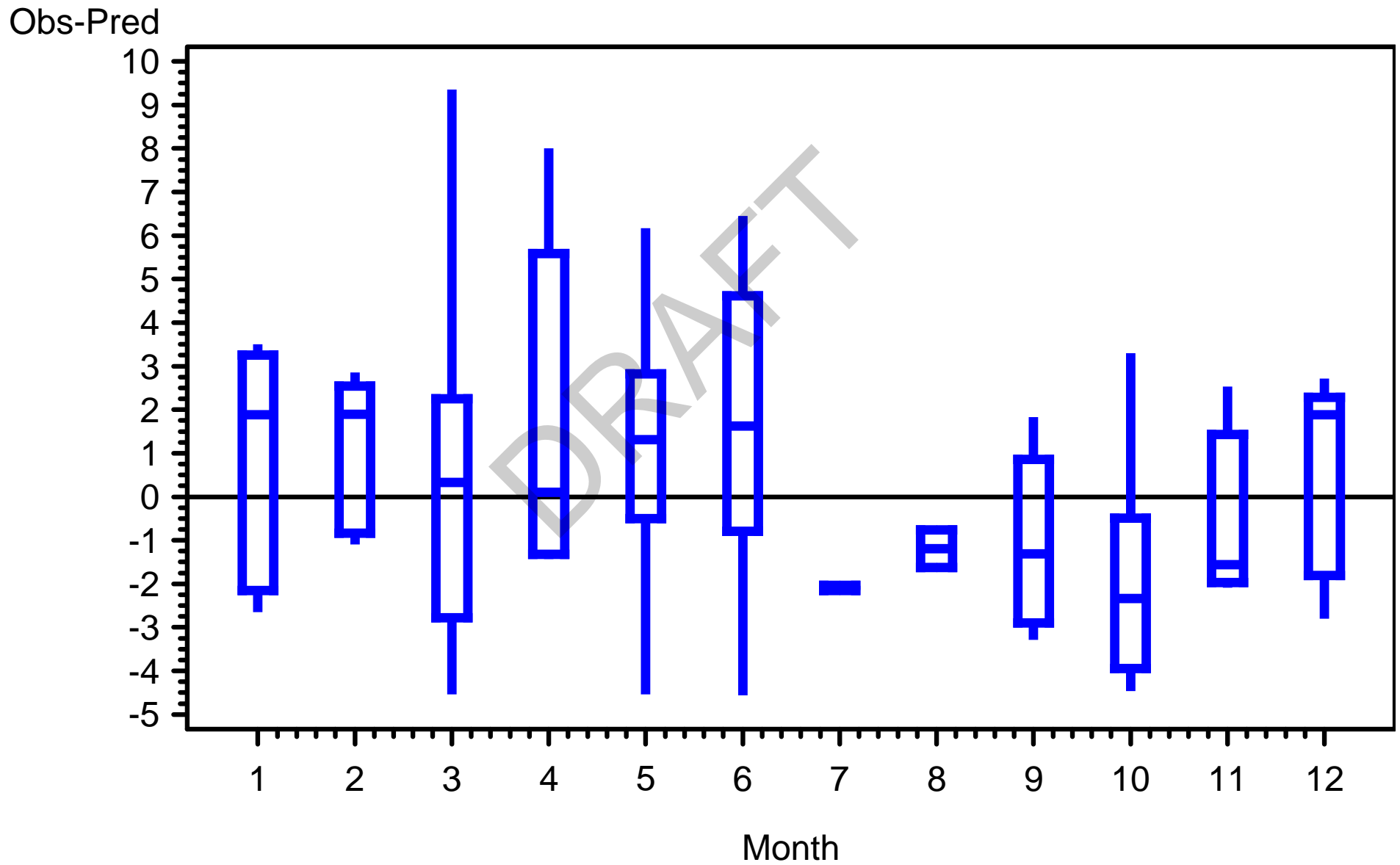
Shell Creek 1997-2004
Residuals vs Shell Creek Flow (cfs)
River Kilometer=8.74



Shell Creek 1997-2004
Residuals vs Shell Creek Flow (cfs)
River Kilometer=9.90

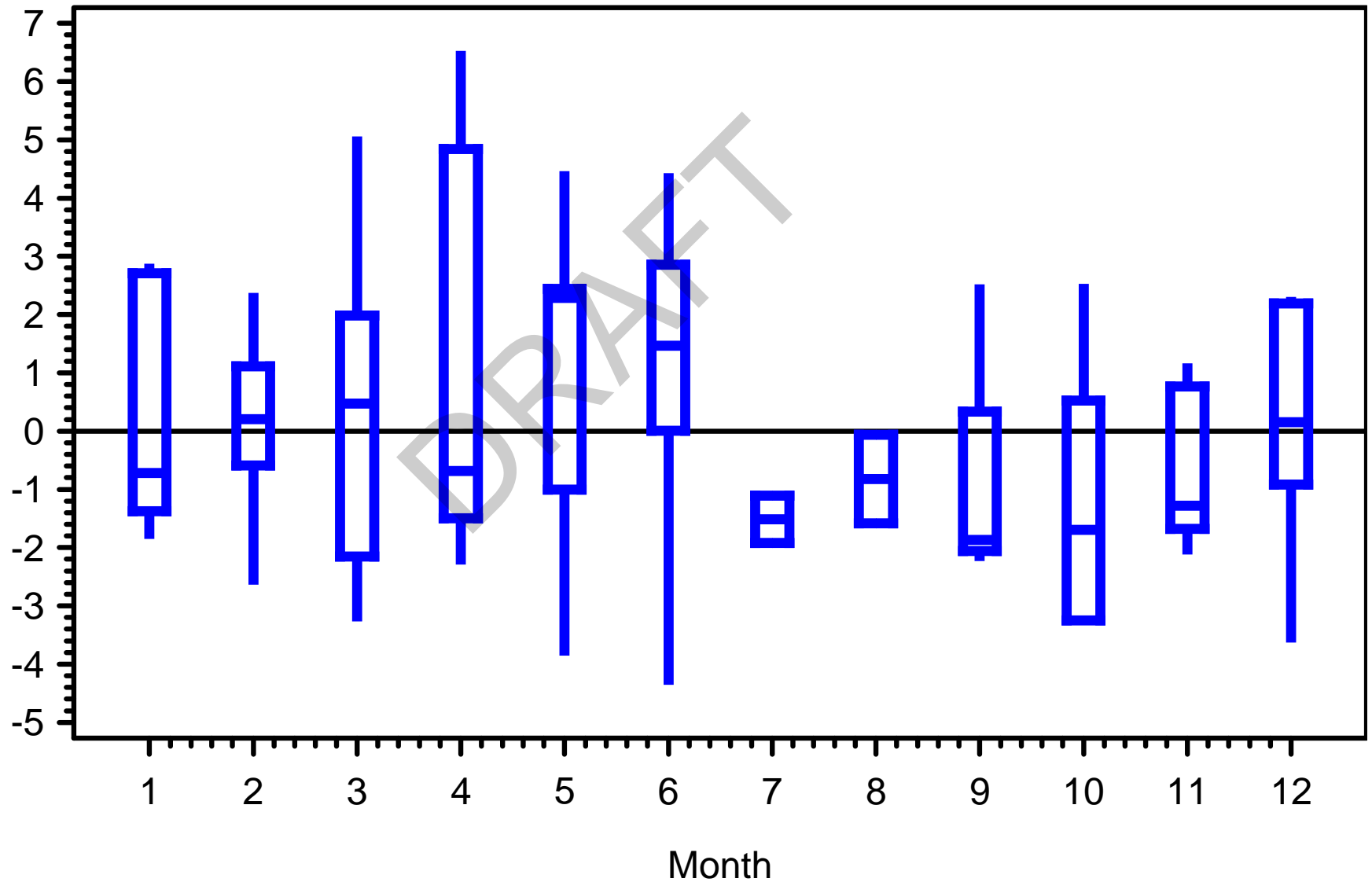


Shell Creek 1997-2004
Residuals by Month
River Kilometer=2.35



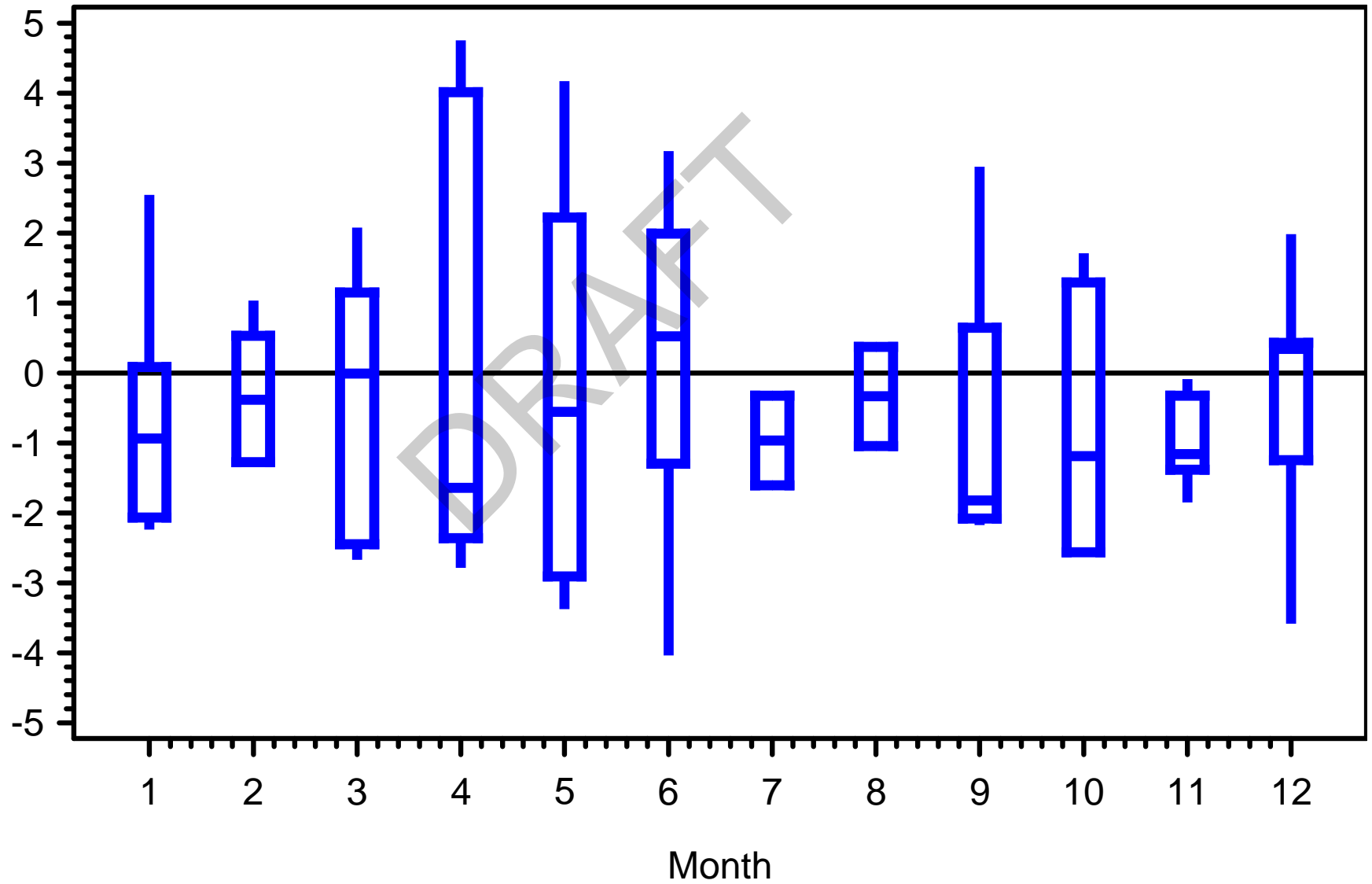
Shell Creek 1997-2004
Residuals by Month
River Kilometer=3.66

Obs-Pred



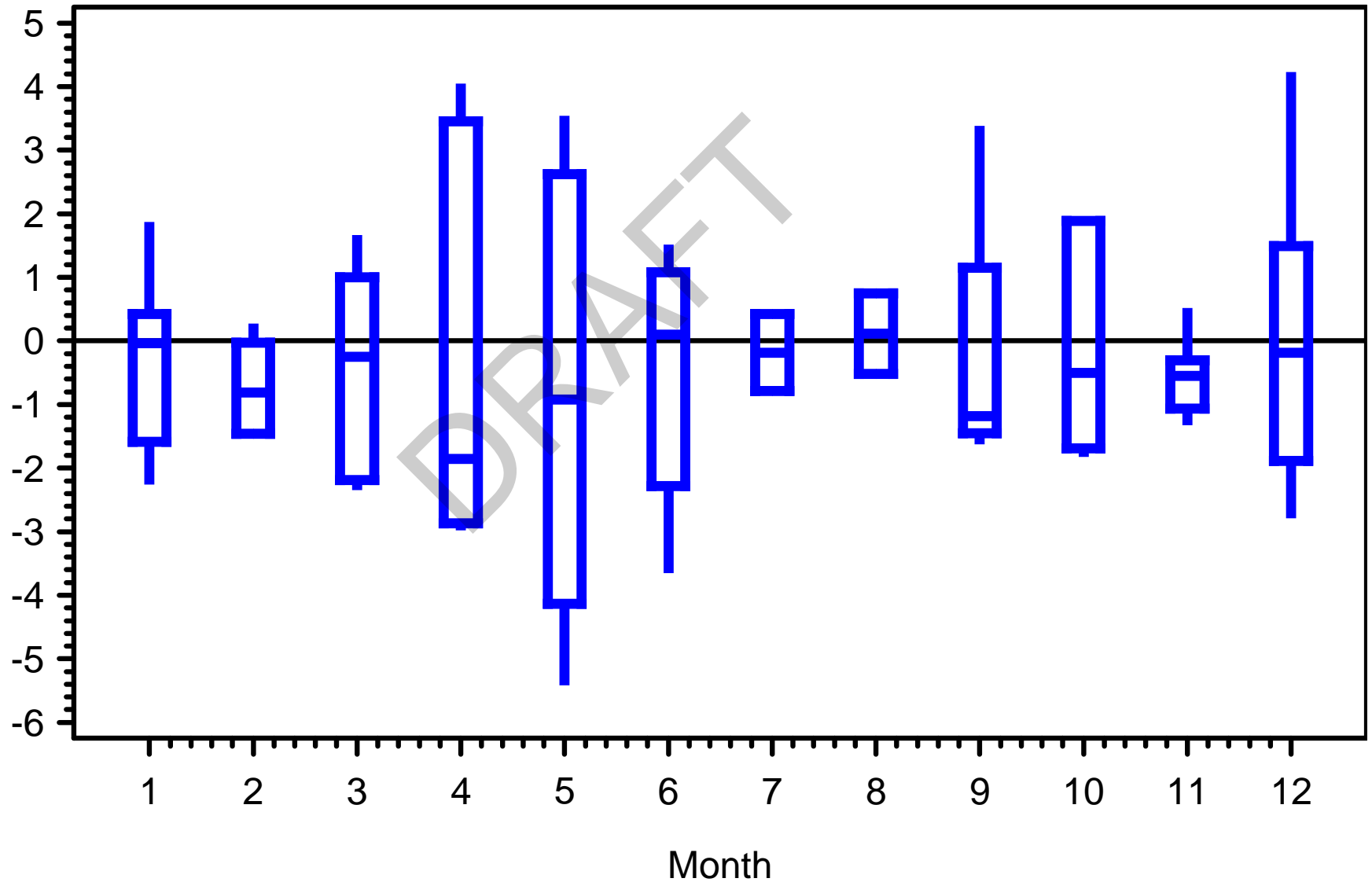
Shell Creek 1997-2004
Residuals by Month
River Kilometer=4.61

Obs-Pred

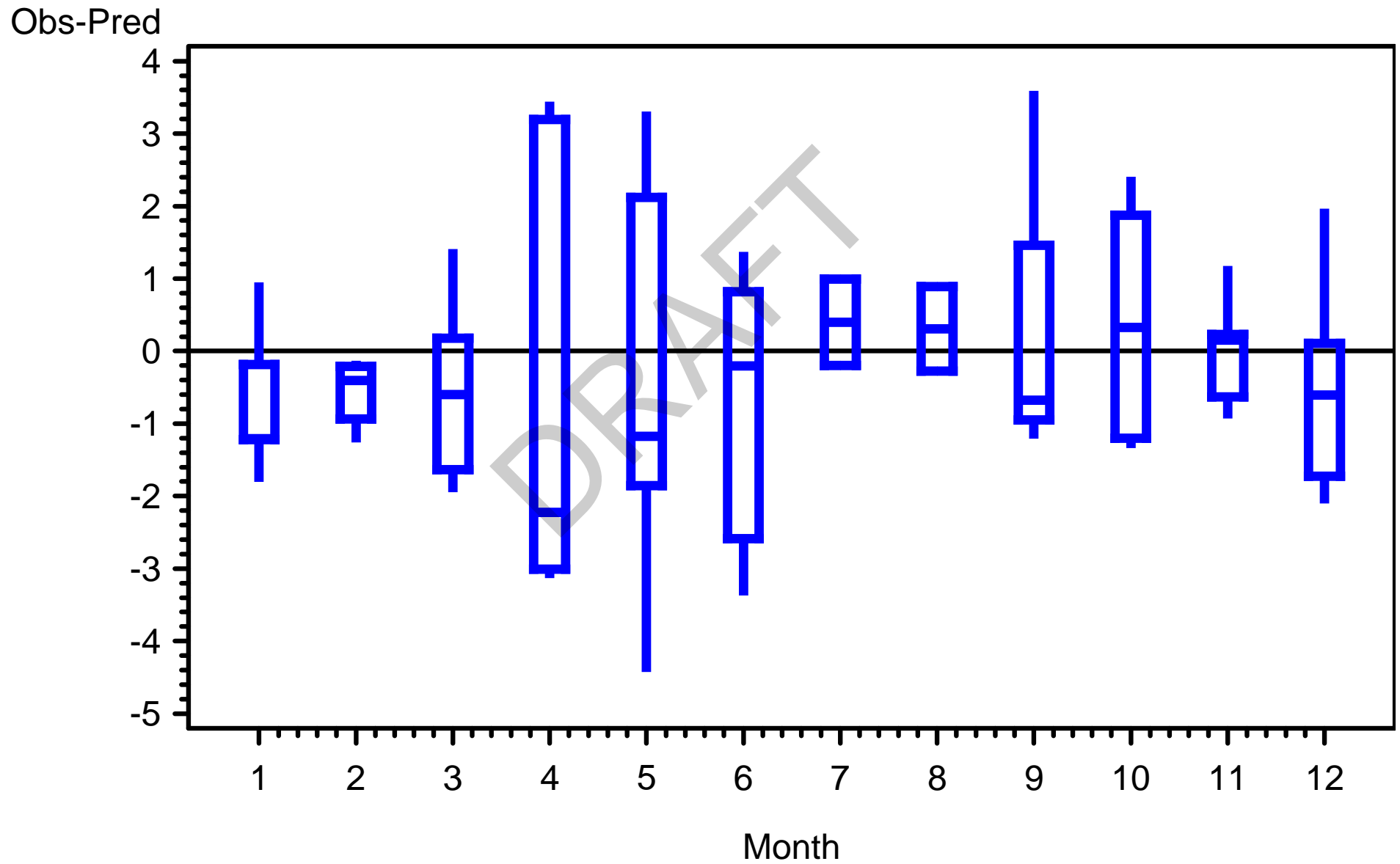


Shell Creek 1997-2004
Residuals by Month
River Kilometer=5.73

Obs-Pred

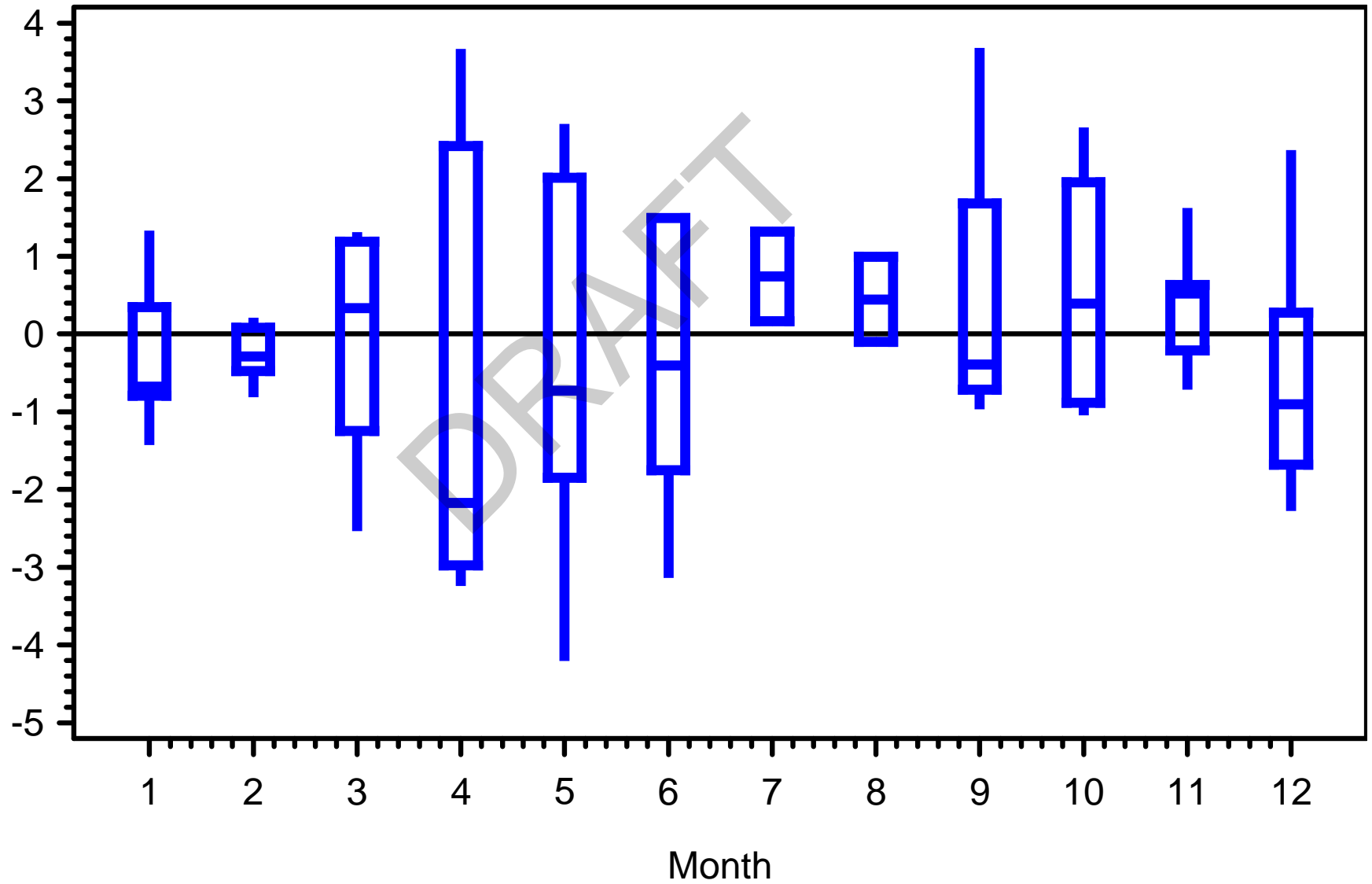


Shell Creek 1997-2004
Residuals by Month
River Kilometer=6.72



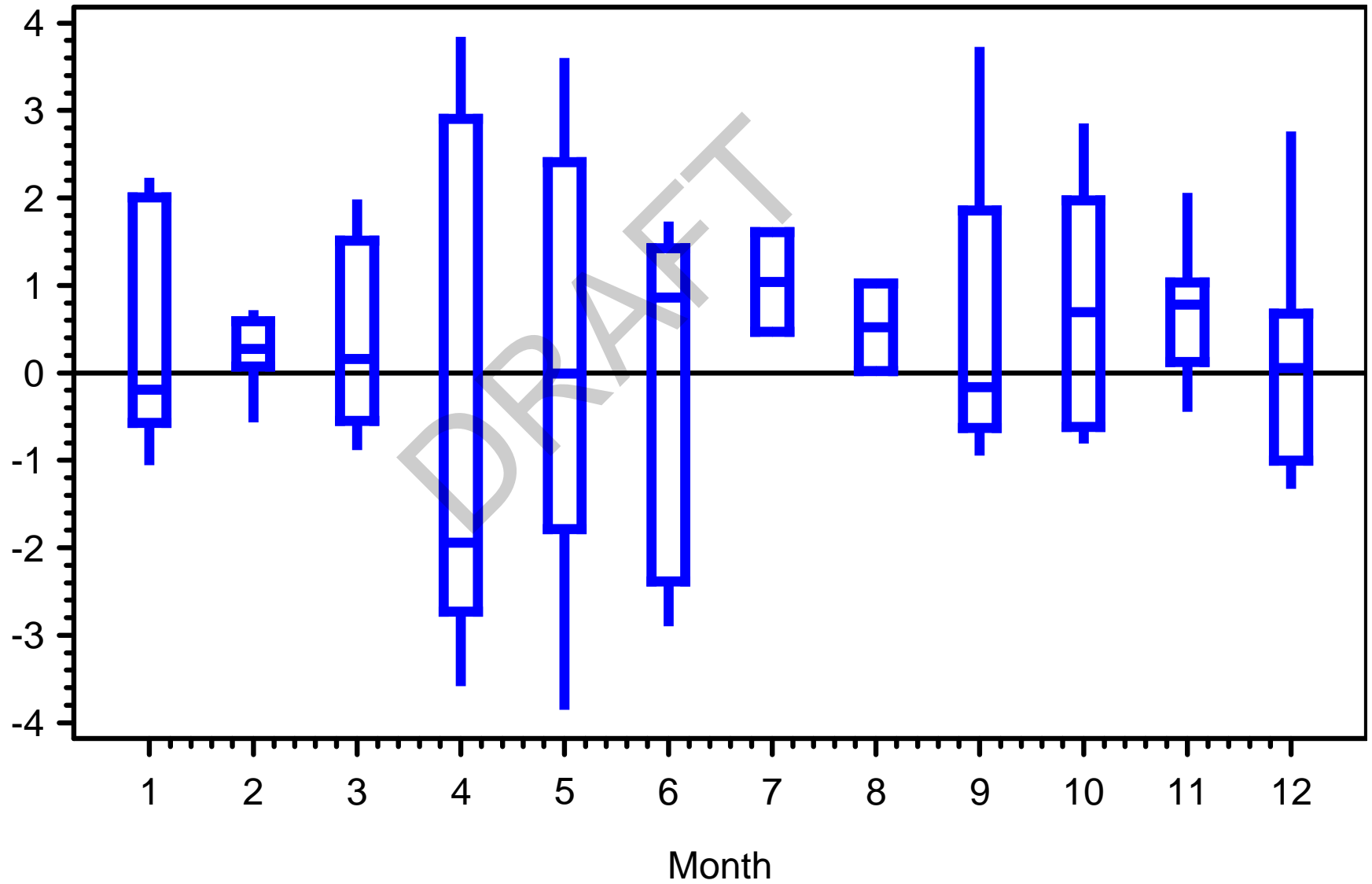
Shell Creek 1997-2004
Residuals by Month
River Kilometer=7.40

Obs-Pred



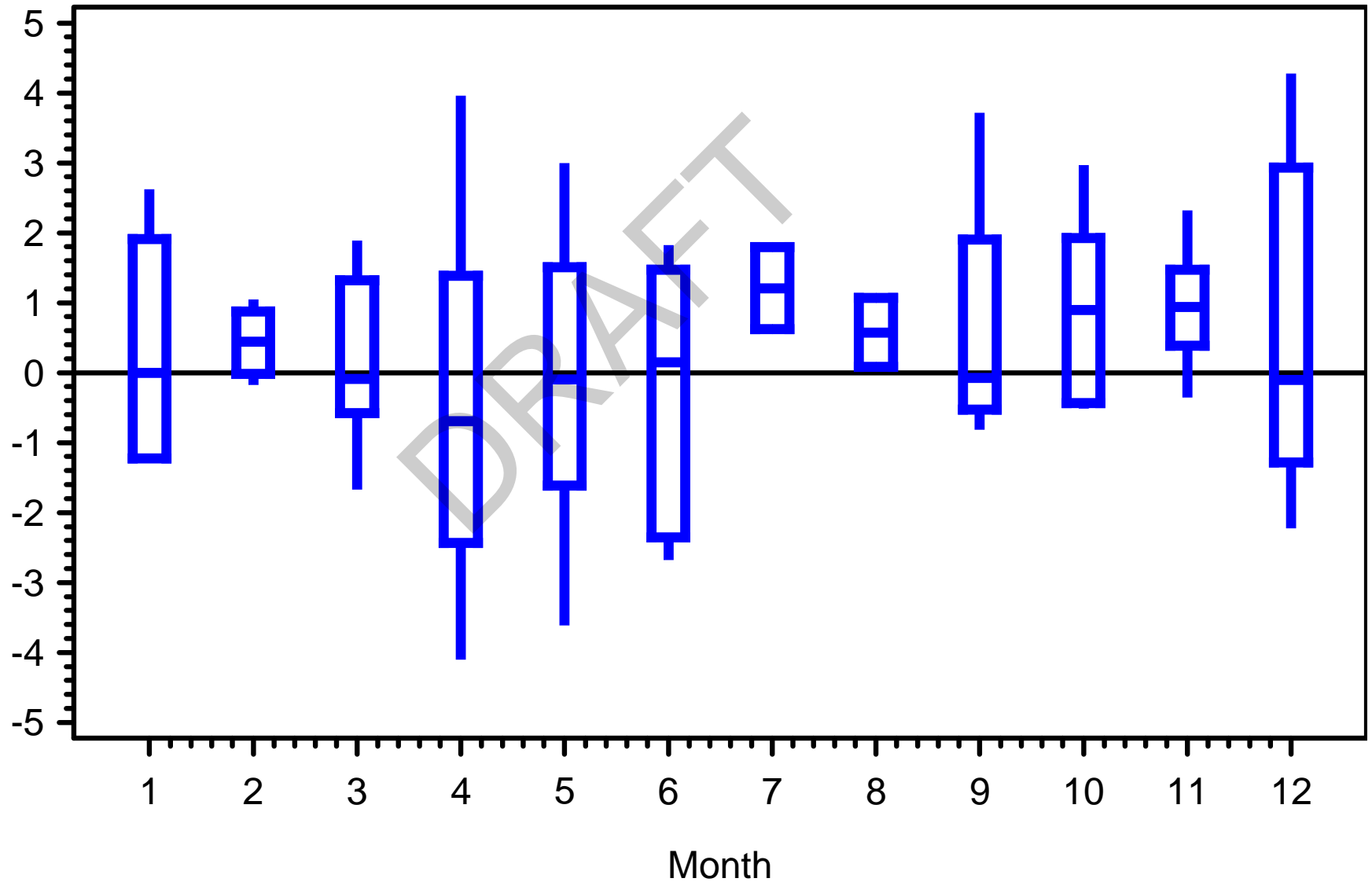
Shell Creek 1997-2004
Residuals by Month
River Kilometer=8.09

Obs-Pred



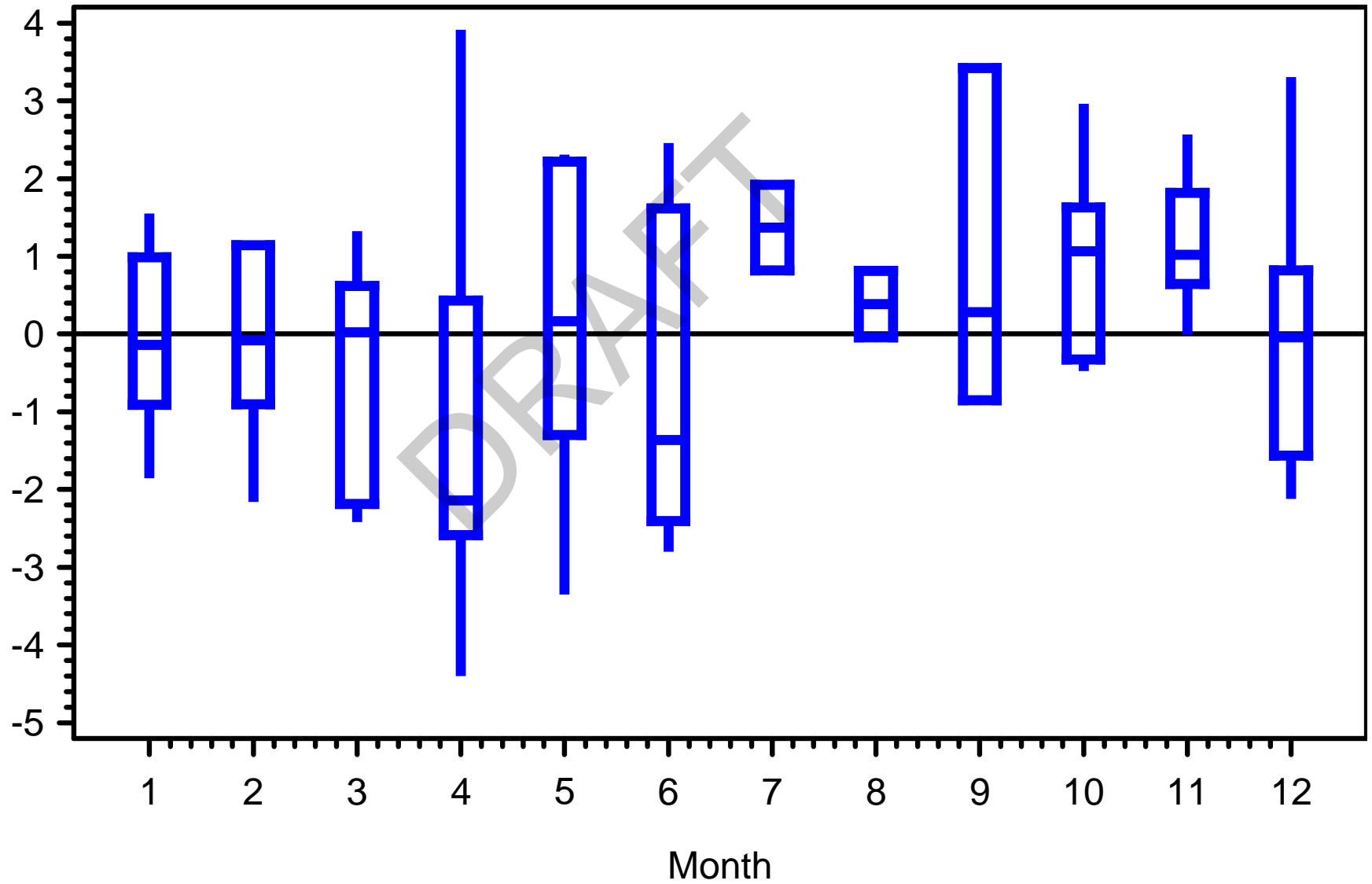
Shell Creek 1997-2004
Residuals by Month
River Kilometer=8.74

Obs-Pred

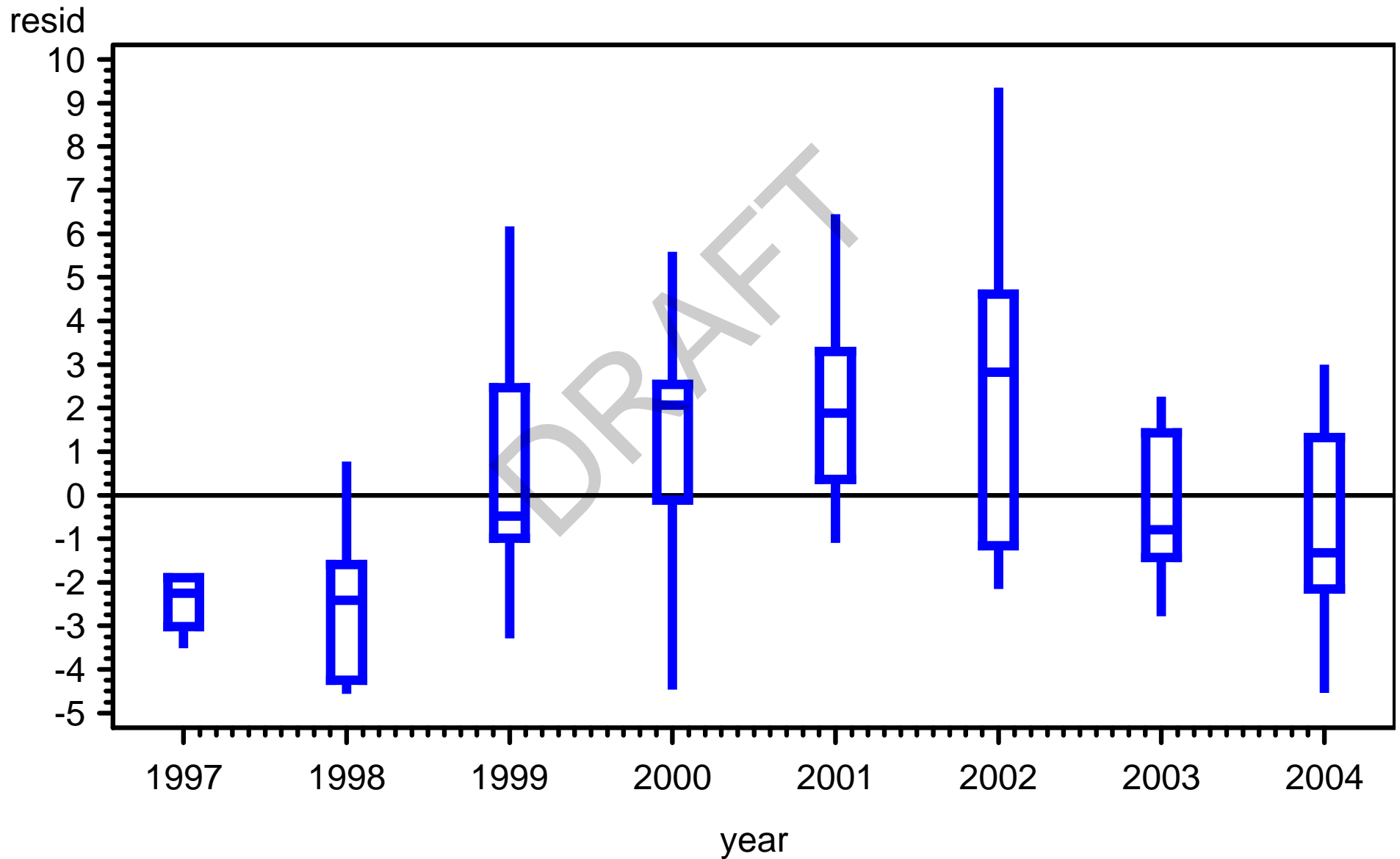


Shell Creek 1997-2004
Residuals by Month
River Kilometer=9.90

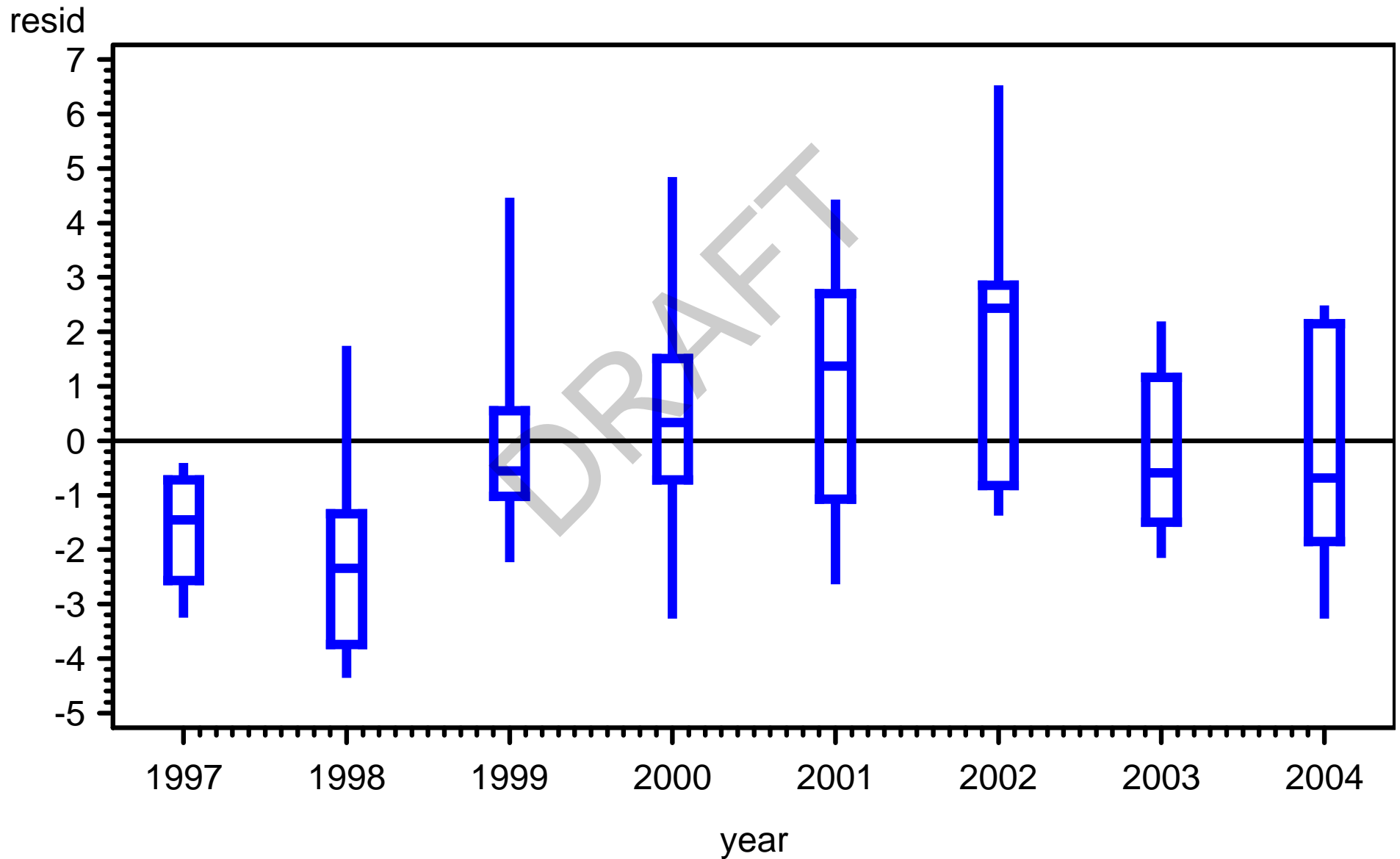
Obs-Pred



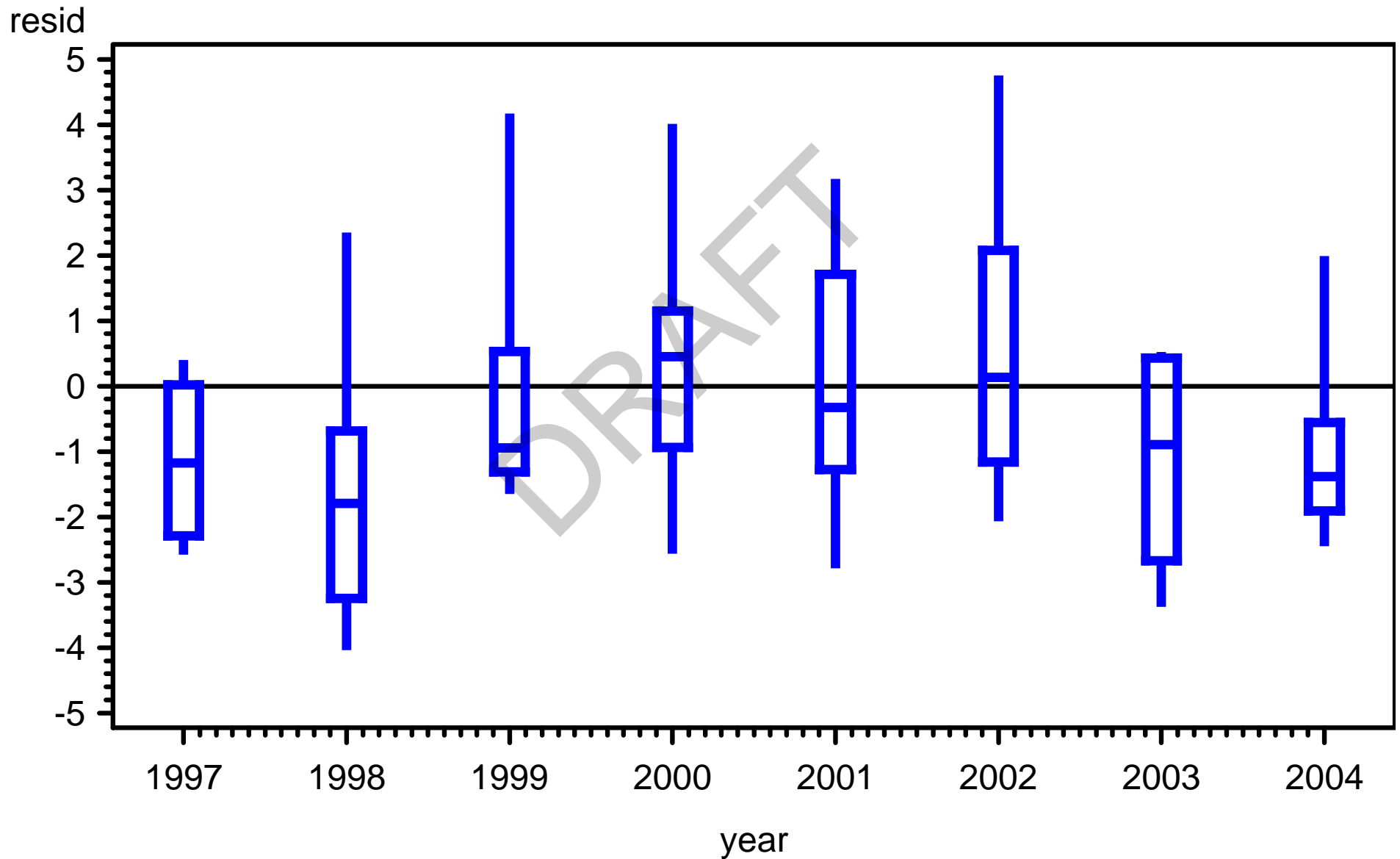
Shell Creek 1997-2004
Residuals by Year
River Kilometer=2.35



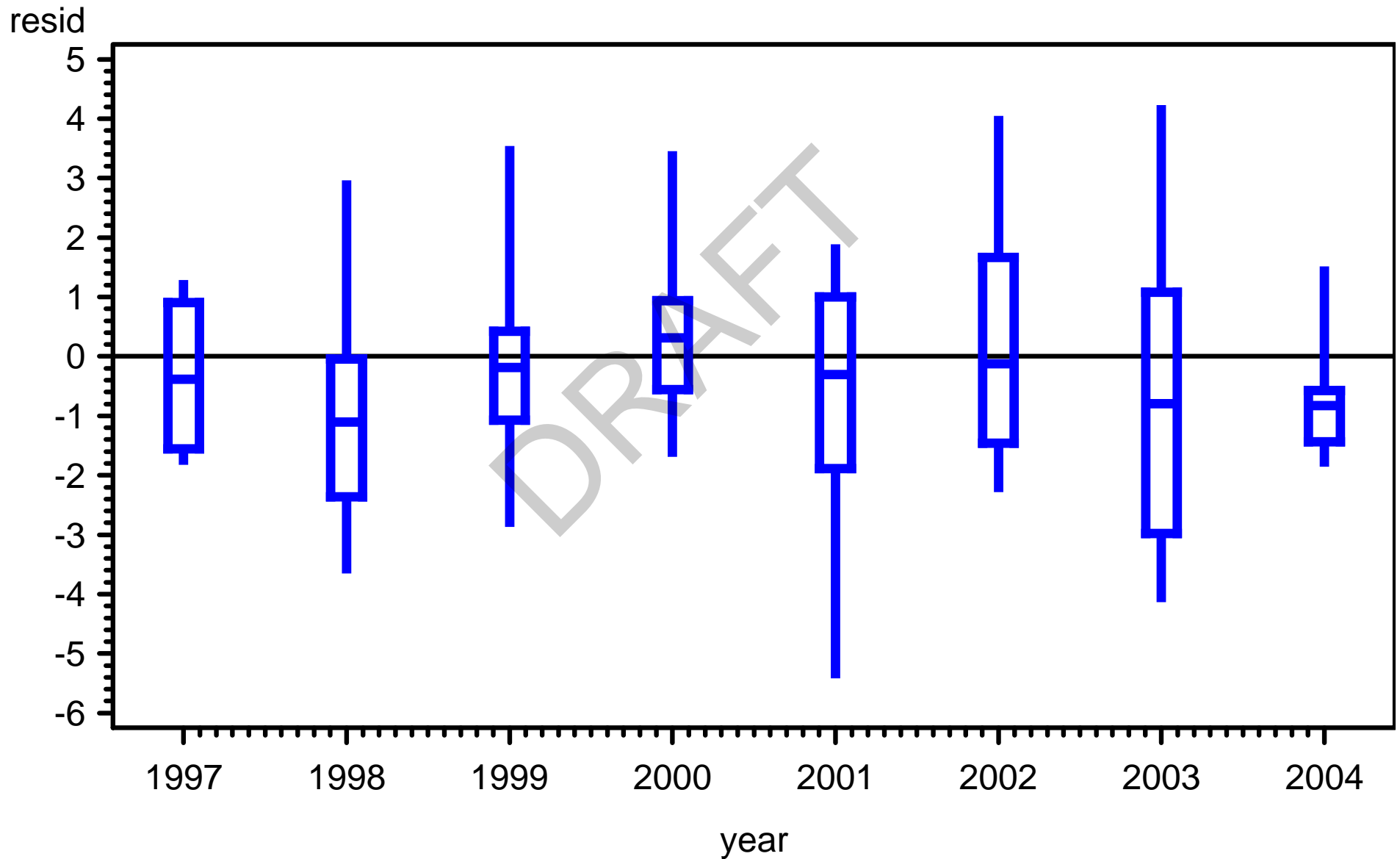
Shell Creek 1997-2004
Residuals by Year
River Kilometer=3.66



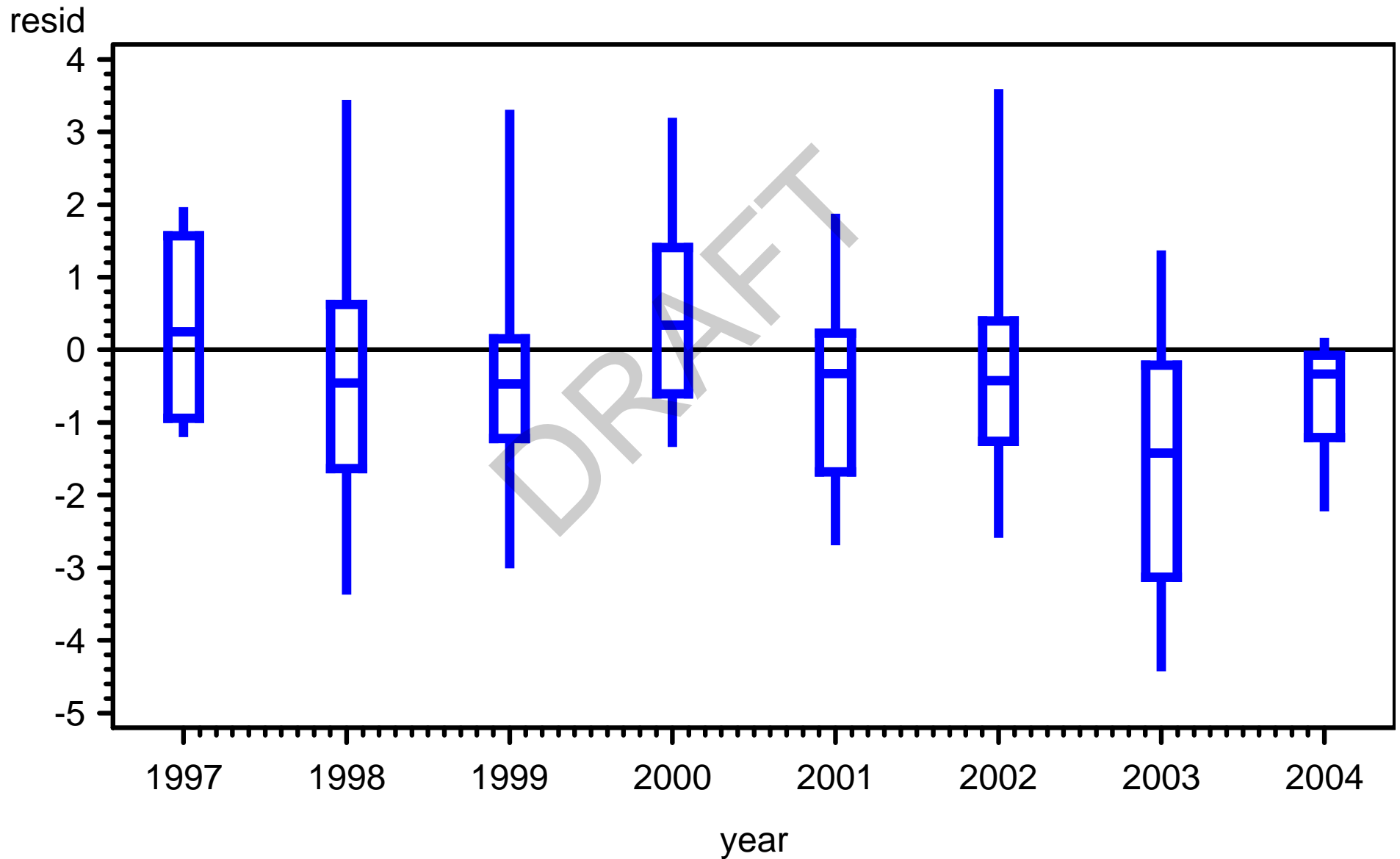
Shell Creek 1997-2004
Residuals by Year
River Kilometer=4.61



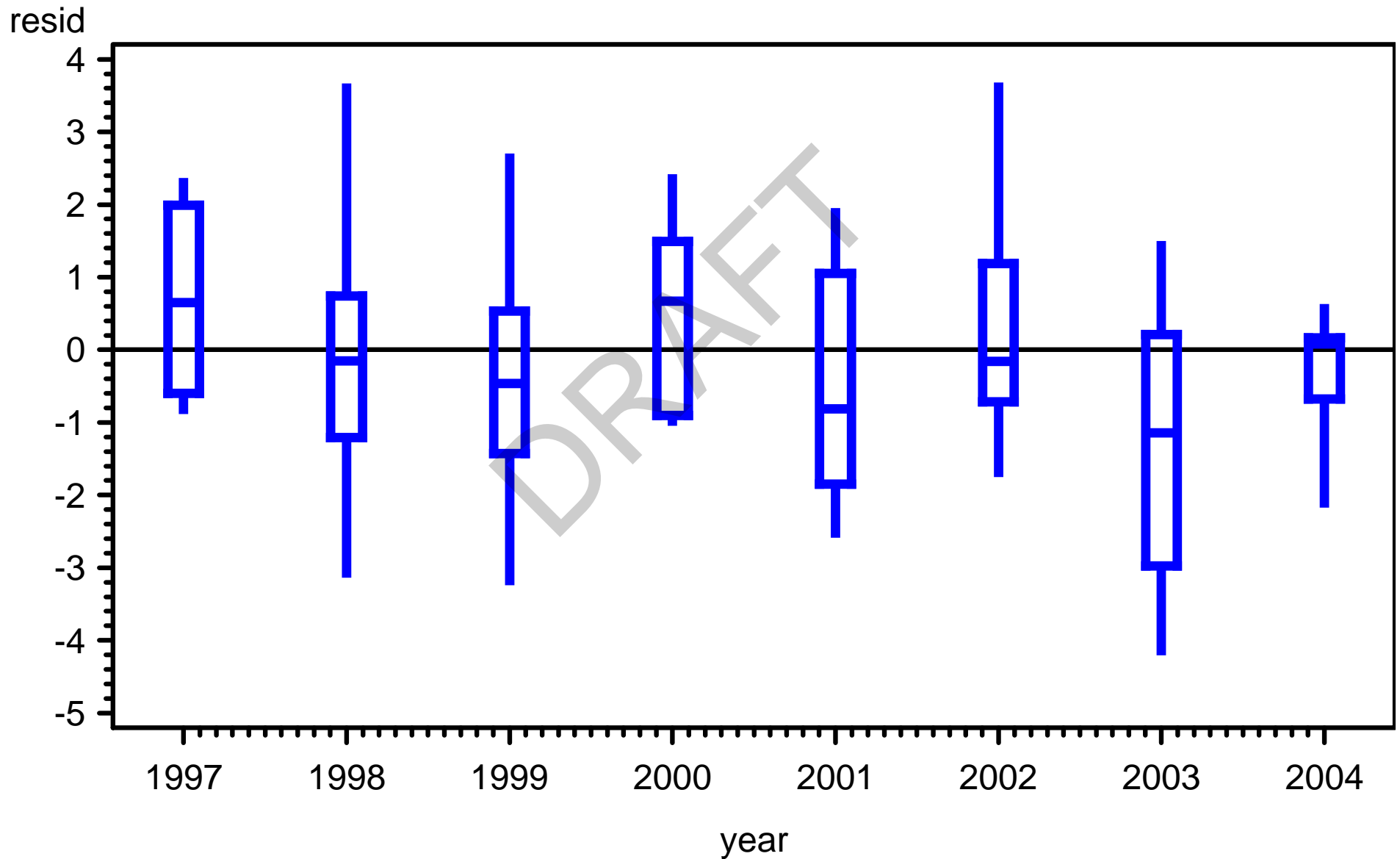
Shell Creek 1997-2004
Residuals by Year
River Kilometer=5.73



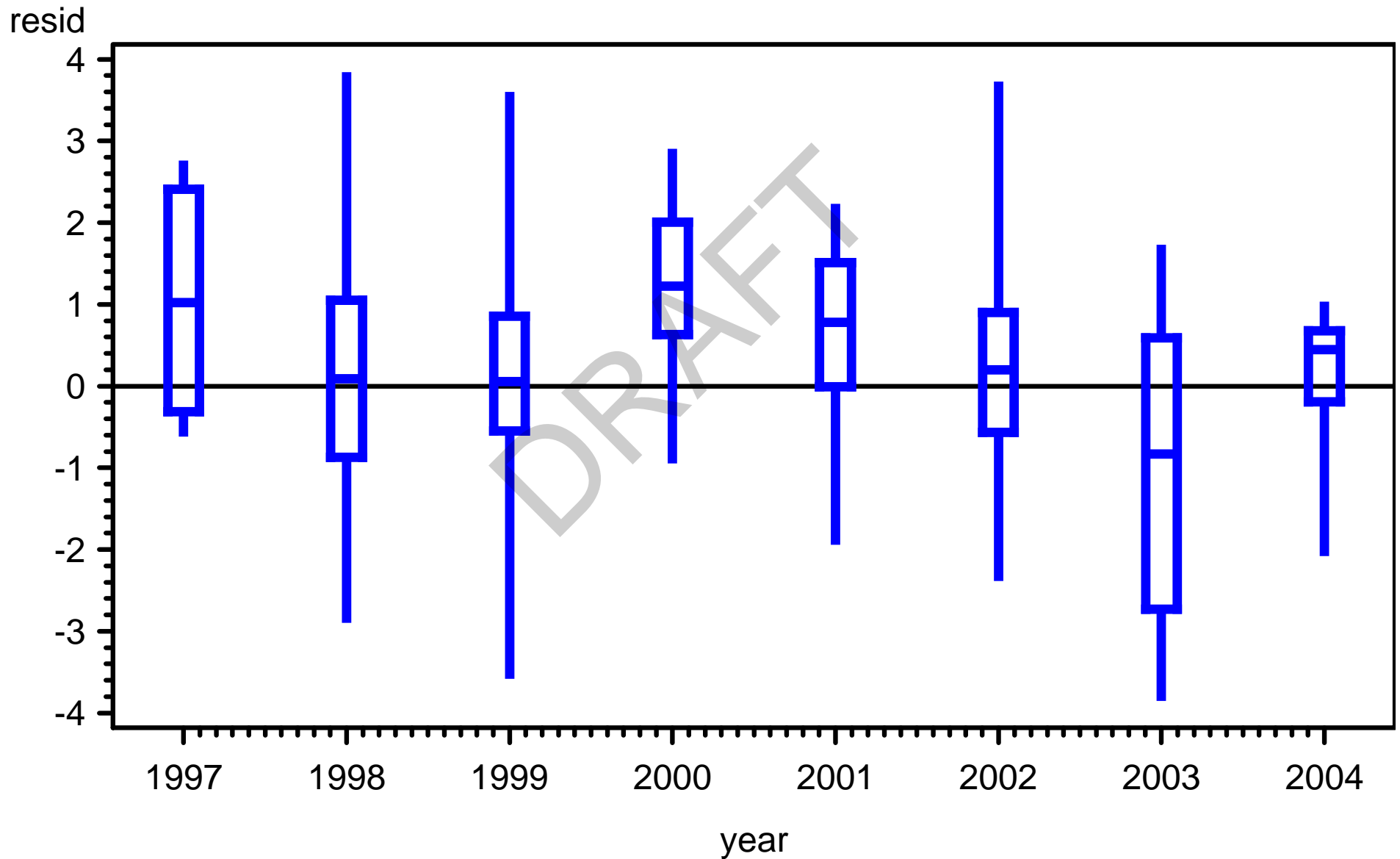
Shell Creek 1997-2004
Residuals by Year
River Kilometer=6.72



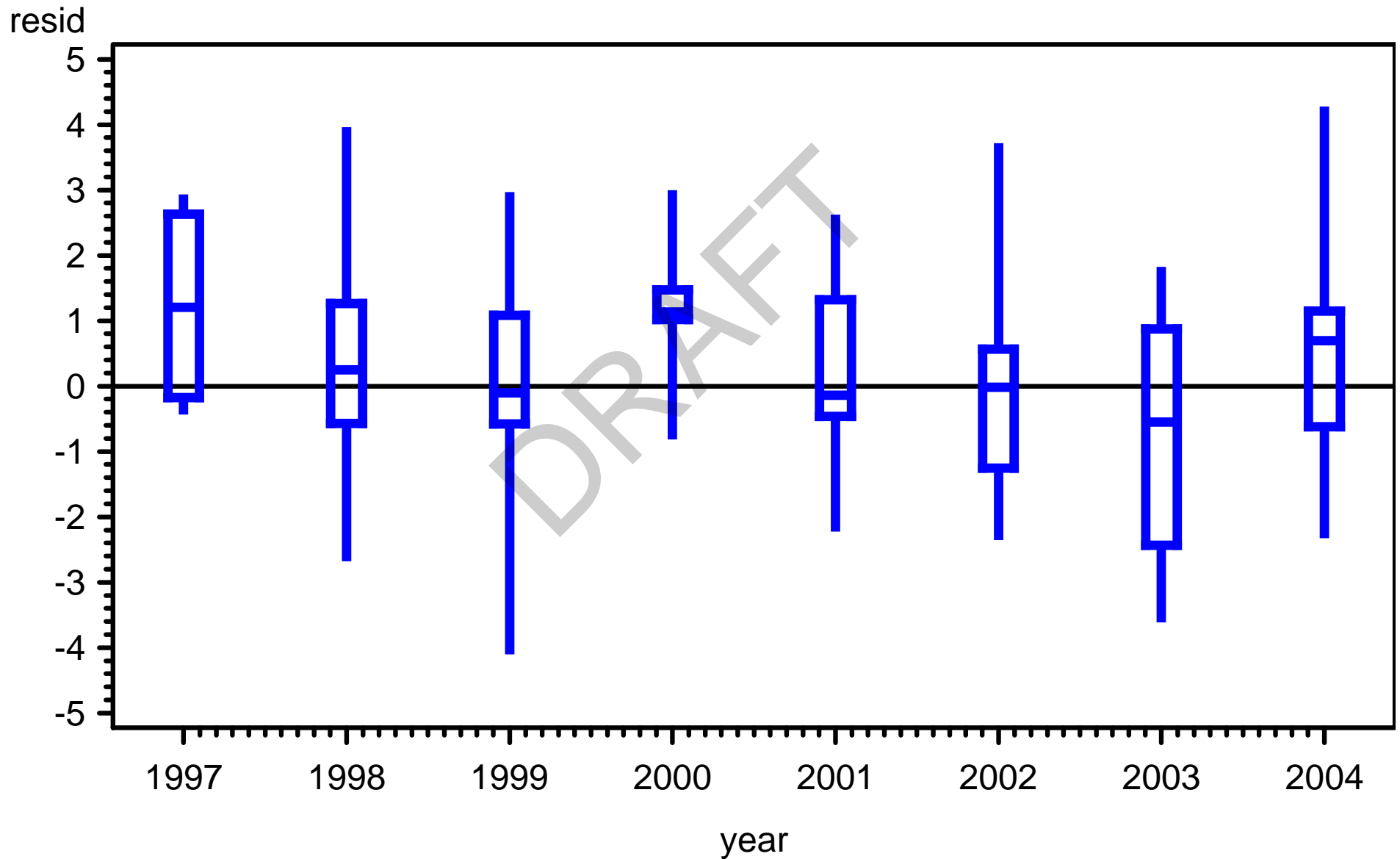
Shell Creek 1997-2004
Residuals by Year
River Kilometer=7.40



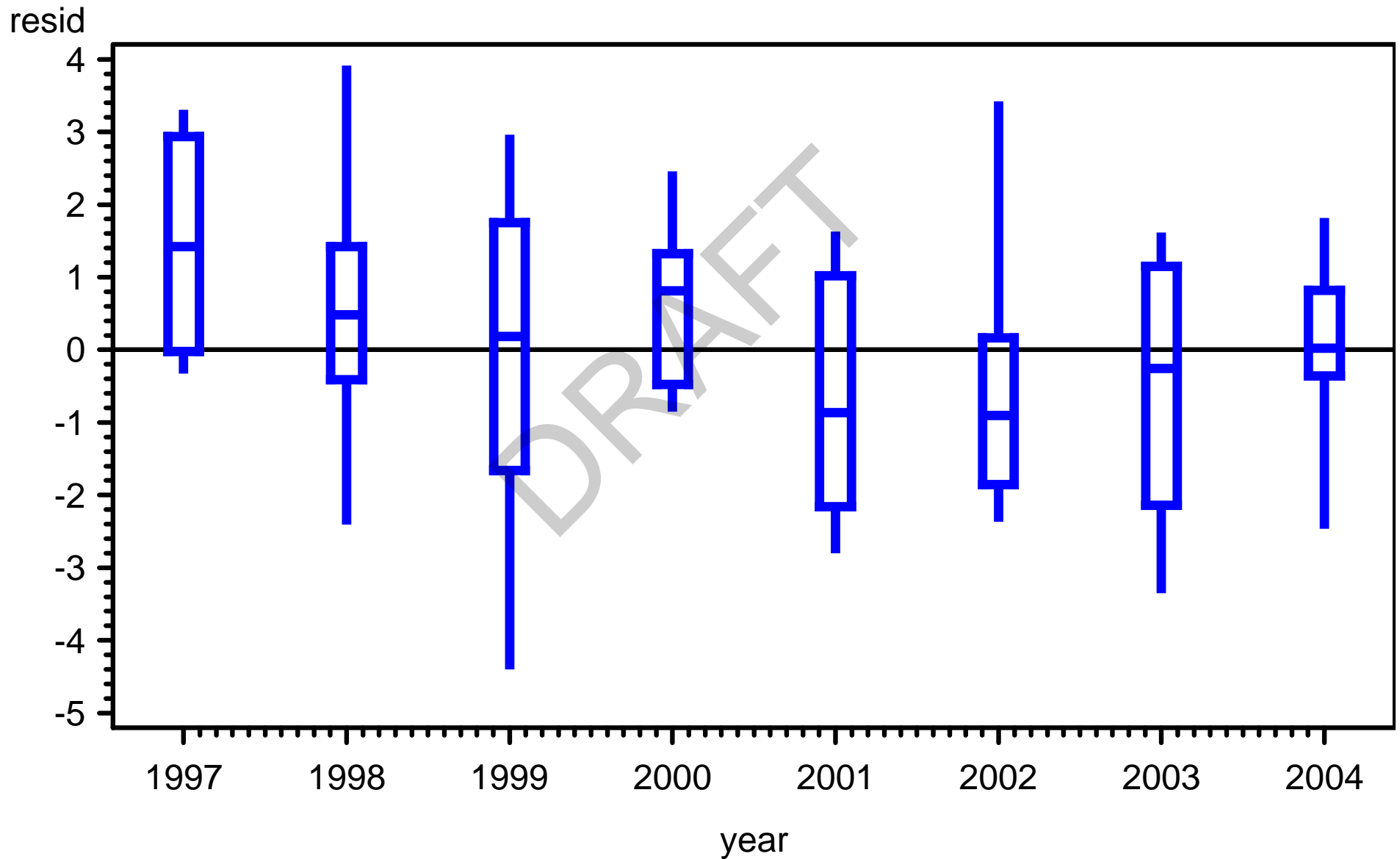
Shell Creek 1997-2004
Residuals by Year
River Kilometer=8.09



Shell Creek 1997-2004
Residuals by Year
River Kilometer=8.74



Shell Creek 1997-2004
Residuals by Year
River Kilometer=9.90



Distribution of Depth-Integrated Salinity by Month

The UNIVARIATE Procedure

Variable: resid

Moments			
N	582	Sum Weights	582
Mean	0	Sum Observations	0
Std Deviation	2.04670748	Variance	4.18901149
Skewness	0.45199117	Kurtosis	0.83877232
Uncorrected SS	2433.81568	Corrected SS	2433.81568
Coeff Variation	.	Std Error Mean	0.08483875

Basic Statistical Measures			
Location		Variability	
Mean	0.00000	Std Deviation	2.04671
Median	-0.11574	Variance	4.18901
Mode	.	Range	14.77015
		Interquartile Range	2.69203

Tests for Location: Mu0=0				
Test	Statistic		p Value	
Student's t	t	0	Pr > t 	1.0000
Sign	M	-17	Pr >= M 	0.1713
Signed Rank	S	-2871.5	Pr >= S 	0.4797

Distribution of Depth-Integrated Salinity by Month

The UNIVARIATE Procedure

Variable: resid

Tests for Normality				
Test	Statistic		p Value	
Shapiro-Wilk	W	0.987846	Pr < W	<0.0001
Kolmogorov-Smirnov	D	0.039537	Pr > D	0.0251
Cramer-von Mises	W-Sq	0.161193	Pr > W-Sq	0.0183
Anderson-Darling	A-Sq	0.931159	Pr > A-Sq	0.0195

Quantiles (Definition 5)	
Quantile	Estimate
100% Max	9.350552
99%	5.583082
95%	3.438479
90%	2.567972
75% Q3	1.312504
50% Median	-0.115745
25% Q1	-1.379526
10%	-2.445263
5%	-3.134682
1%	-4.424244
0% Min	-5.419602

Distribution of Depth-Integrated Salinity by Month

The UNIVARIATE Procedure

Variable: resid

Extreme Observations			
Lowest		Highest	
Value	Obs	Value	Obs
-5.41960	225	6.16430	26
-4.55708	32	6.45287	34
-4.54027	25	6.52864	88
-4.53521	17	8.00335	22
-4.45803	49	9.35055	15

Missing Values			
Missing Value	Count	Percent Of	
		All Obs	Missing Obs
.	9	1.52	100.00

+--+---+--+---+--+---+--+---+--+---+--+---

y represent up to 3 counts

+--+---+--+---+--+---+--+---+

y represent up to 3 counts

DRAFT

97
60
20
11
1

+--+---+--+---+--+---+--+---+

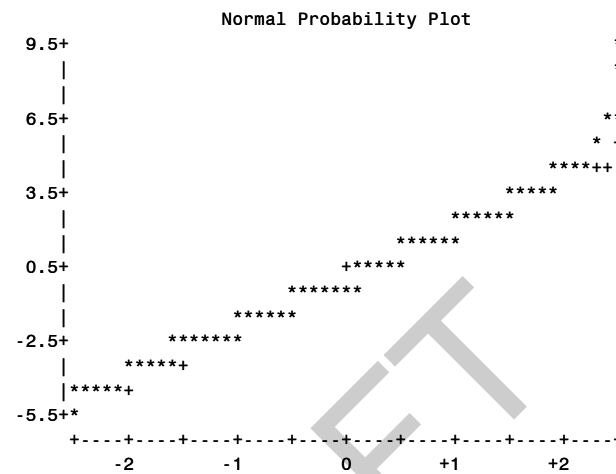
y represent up to 3 counts

[illegible]

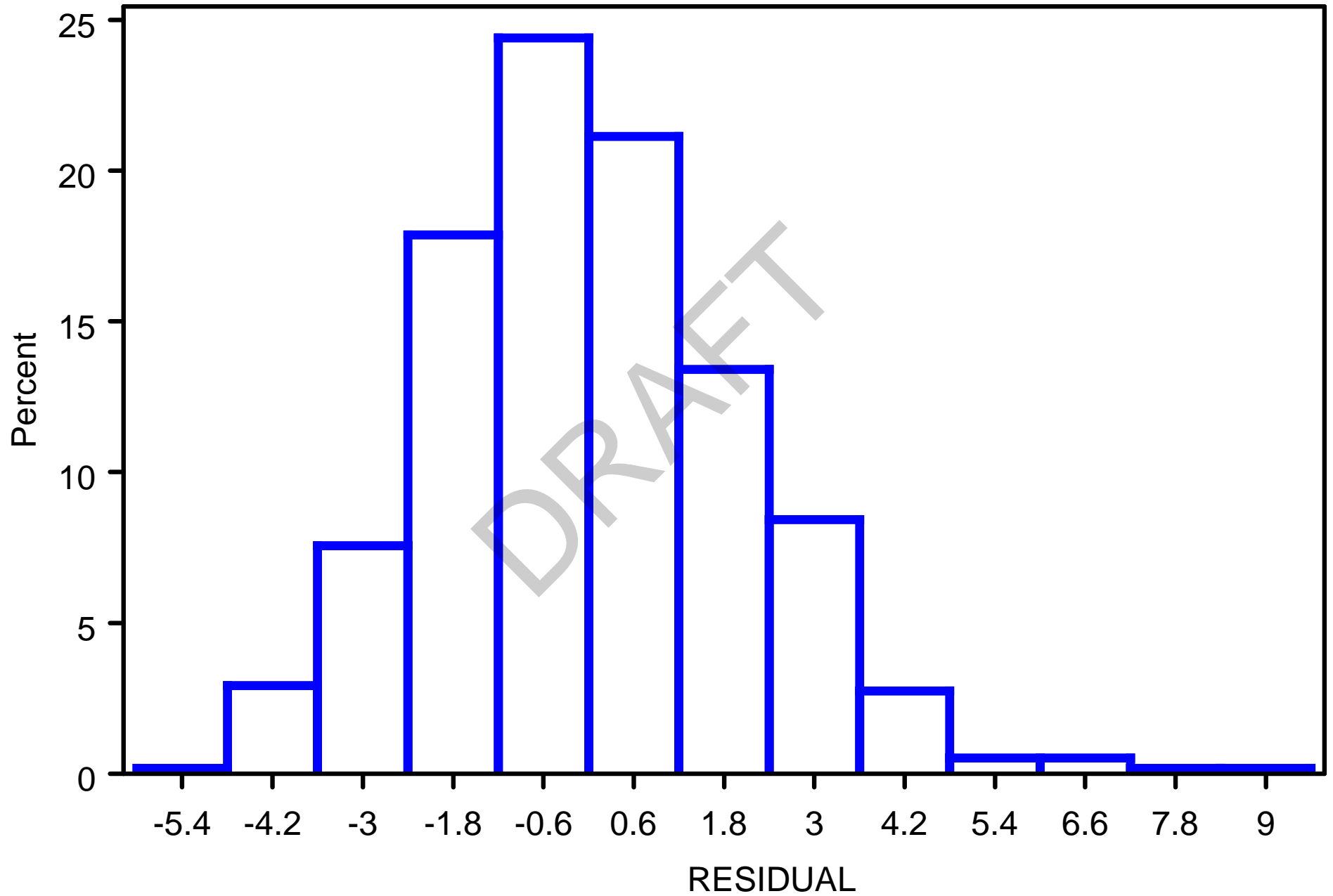
Distribution of Depth-Integrated Salinity by Month

The UNIVARIATE Procedure

Variable: resid



Distribution of Residuals



Appendix 7-2

Hydrodynamic Model Description

Simulating Hydrodynamics in the Lower Peace River – Lower Myakka River – Upper Charlotte Harbor System

XinJian Chen, Ph.D., P.E.

Ecological Evaluation Section
Resource Conservation & Development Department



April 2007

Summary

In an effort to determine the regulatory minimum freshwater inflows to the lower Peace River (LPR) and the lower Myakka River (LMR), a sophisticated hydrodynamic model has been developed that simulates circulations, salt transport processes, and thermal dynamics in a simulation domain that comprises not only the LPR and LMR, but also the upper portion of the Charlotte Harbor (UCH) and Shell Creek. The numerical model developed for this complex LPR - LMR - UCH system is a coupled 3D – 2DV model name LESS that dynamically links a laterally averaged two-dimensional hydrodynamic model (LAMFE) with a three-dimensional hydrodynamic model (LESS3D).

Model simulations were conducted for a 13-month period from June 13, 2003 to July 11, 2004, during which the first 30 days of the simulation (June 13 – July 12, 2003) were used for model spin-up. Data used to drive the model included measured freshwater inflows at upstream boundaries, wind speed near the mouth of the Myakka River in UCH, meteorological data (rain, solar radiation, air temperature, air humidity) at a SWFWMD SCADA station near the Peace River/Manasota Regional Water Supply Authority, estimated un-gauged flows, and the downstream boundary conditions of tides, salinity, and temperature that came from another model simulation effort that included the entire Charlotte Harbor and a coastal area extending almost 45km off-shore.

The LESS model was calibrated and verified against measured real-time data at a total of eight stations inside the simulation domain, including a University of Florida (UF) station in the UCH, an USGS station in Shell Creek, three USGS stations in the LPR, and three USGS stations in the LMR. The calibration of the model was conducted for a 3-month period between January 10 and April 9, 2004, while the verification of the model was done for a 6-month period between July 13, 2003 and January 9, 2004 and a 3-month period between April 10 and July 11, 2004.

After the model was calibrated and verified, it was used to evaluate estuarine residence times for 16 flow scenarios for the LPR. It was found that the estuarine residence time (ERT) in the LPR is related to the sum of gauged USGS flows (Q) in the Joshua Creek, the Horse Creek, and in the Peace River at the Arcadia station through a power function, with its coefficient and exponent depending on what percentage (L) of remaining conservative mass is used in defining the ERT. An analysis of the estuarine residence times using different L values in the 16 flow scenarios has concluded that ERT in the LPR can be expressed as a function of Q and L :

$$ERT = [1747.3 - 375.53 \ln(L)] Q^{-(0.54 + 0.00088L)}.$$

The calibrated model was used to evaluate minimum flows for both the LPR and LMR, in conjunction with the minimum flow evaluation of the Shell Creek. Various model runs were conducted for a 4-year period from January 1996 to December 1999 under various flow reduction scenarios of the LPR, the LMR, and the Shell Creek. Details on the scenario runs for the LPR are described in a report by Janicki Environmental, Inc. (2007), while those for the LMR are reported in Chen (2007b).

1. Introduction

The Peace and Myakka Rivers (Figure 1) are major tributaries to the Charlotte Harbor, one of the largest estuaries in Florida that was identified by the US Environmental Protection Agency as an estuary with national significance. The Peace River has a length of approximately 120km and runs southwestward into the northeast portion of the Charlotte Harbor, while the Myakka River is about 106km long and flows first southwestward and then southeastward into the northwest portion of the Charlotte Harbor. The entire Peace River watershed is about 6213km². The most downstream segment of the Peace River, from Arcadia to the mouth, is the lower Peace River (LPR) that is about 58km long. About 84% of the Peace River watershed is gauged by the United States Geological Survey (USGS) at the Peace River at Arcadia station and in two tributaries downstream of Arcadia: Joshua and Horse Creeks (SWFWMD, 2001). The remaining 16% of the Peace River watershed is un-gauged with unknown freshwater contribution to the Charlotte Harbor. The lower Peace River is generally narrow and meandering, except for areas near the mouth where the river becomes wider with islands. Majority of the 58km long Lower Peace River is tidally influenced, and the tidal limit extends to roughly 50km upstream from the mouth.

On the Myakka River side, the lower Myakka River (LMR) is about 40km long and starts at the downstream side of the lower Myakka Lake (Downs' Dam) in the Myakka River State Park. The Myakka River watershed is approximately 608km². Only about 50% of the Myakka River watershed is gauged at the USGS Myakka Head station and a few tributary stations downstream of the Downs' Dam, and thus the un-gauged area is about half the watersheds for the Myakka River. Similar to the Peace River, the Myakka River is also narrow and meandering, except for its very downstream portion where the river is wider and has several islands. The entire lower Myakka River is tidally influenced, as tides can reach to the base of Downs' Dam.

Although they are often treated as three individual water bodies in many cases, the LPR, LMR, and the UCH are interconnected with different degrees of interactions among them. On one hand, the LPR and LMR provide the UCH freshwater inflows that are ecologically critical for the health of the harbor. On the other hand, hydrodynamics and salinity in the UCH play a very important role in keeping the ecosystems of the LPR and LMR in balance as both rivers are tidally influenced. Tides and salinity transport in the downstream estuary directly affect habitat distributions in both rivers. To manage the water resources and protect the ecosystems of the LPR and LMR, it is important to understand the hydraulic interactions among the LPR, the LMR, and the UCH. As such, it is necessary to develop a numerical model that can provide detailed information of circulations and salinity and temperature distributions in all three segments of the LPR - LMR - UCH system with the same degree of accuracy.

Because the flow pattern in the Charlotte Harbor is general three-dimensional, a 3D hydrodynamic model is needed to accurately simulate hydrodynamics in the estuary. To include the Lower Peace River and the Lower Manatee River in the simulation, one can extend the 3D model domain upstream to cover the entire reach of the LPR and LMR. However, this way of including the tributary in the simulation is apparently not efficient. In addition, it is also difficult to correctly represent the cross section of the LPR and LMR in a 3D model because only limited number of grids (usually five or less grids, sometimes just one grid) are used to discretize the width of the river (e.g., Johnson et al, 1991; Sucsy et al, 1997; Mendelsohn et al, 1997). For example, it is impossible to accurately resolve the cross section shown in Figure 2 with just three grids in the latitudinal direction of the tributary (perpendicular to the tributary).

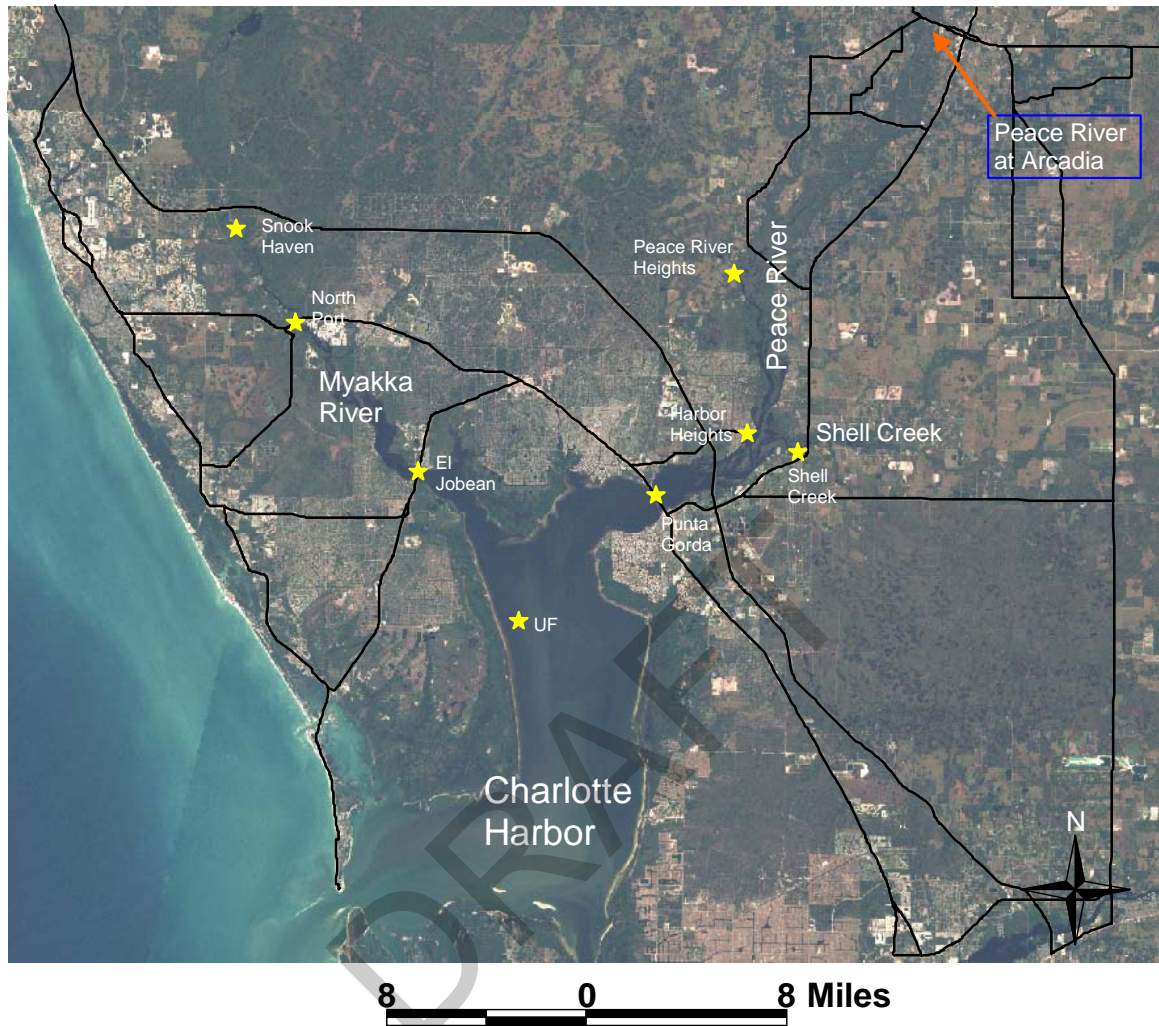


Figure 1 An aerial photo of the LPR - LMR - UCH system. Yellow stars denote the locations where real-time data were collected.

Although the flow pattern in upper Charlotte Harbor is three-dimensional, it is generally vertically two-dimensional in most segments of the LPR and LMR because the rivers are narrow. It is much efficient to use a laterally averaged 2D (2DV) model for the narrow and meandering portions of the LPR and LMR than to use a 3D model. With enough number of vertical layers (generally eight or more), a 2DV model resolves the bathymetry of a tributary better than a 3D model that has only a limited number of grids in the latitudinal direction. Also, a 2DV model automatically handles the wetting/drying phenomenon in the tributary, while a 3D model often needs a lot of computational efforts to deal with the temporal shoreline change in the narrow and meandering tributary. The cross section shown in Figure 2 is quite typical in the narrow portions of the LPR and LMR. As can be seen from the figure, the cross section is composed of a main channel and two flood plains at both sides of the river. While the main channel can be very narrow and in the order of 10 – 20 m, the flood plain can be as wide as a few kilometers. When flow is low, water only exists in the main channel. However, during a major storm event, the

flood plains will be submerged and used as conveyance for the flood. For a better understanding of the ecological system in the rivers, it is critical to accurately simulate emerging/submerging feature of the flood plain. In this circumstance, what one needs is information about the total flow rate and the water elevation, not the detailed velocity distribution in the narrow portions of the LPR and LMR. Evidently, it is much harder for a 3D model to handle these areas of the rivers even if it has the ability to do so. The emerging/submerging feature of the cross section can be automatically simulated in a laterally averaged 2D model without any special treatment often seen in a 3D model, simply because the river width is included in the governing equations for the 2DV model (see Section 3).

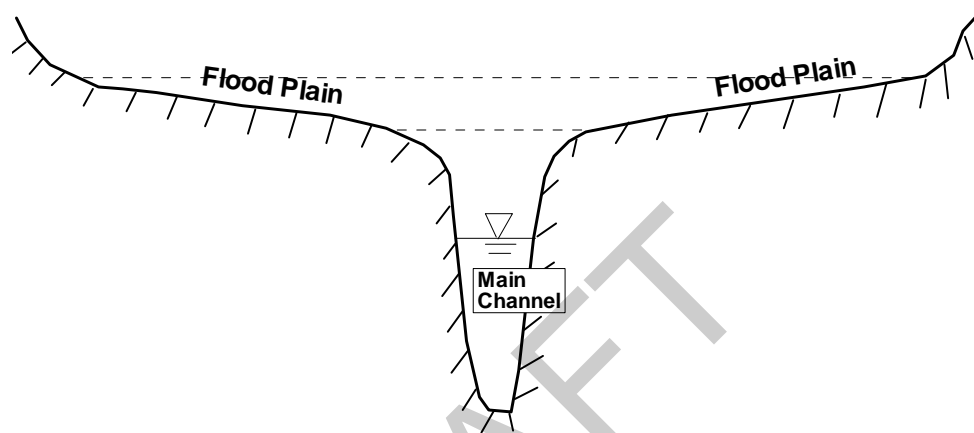


Figure 2 A typical cross section of the narrow part of the Peace (or Myakka) River. It is comprised of a main channel and two flood plains at both sides. Most of the time, flow only exists in the main channel. During a major storm event, the flood plains can be submerged to convey the flood.

It is apparent that the effective way to simulate the interactions among the upper Charlotte Harbor and the lower Peace and Myakka Rivers is a coupled 3D-2DV model. For this purpose, this study developed and used a dynamically coupled 3D-2DV model to simulate hydrodynamics in the lower Peace River – lower Manatee River - upper Charlotte Harbor system. In the following sections, a dynamically coupled 3D-2DV hydrodynamic model developed for the LPR – LMR - UCH system is briefly presented, followed by a description of available field data used by the model as boundary conditions and for model calibration/verification. The use of the coupled model to simulate hydrodynamics in the LPR – LMR – UCH system is then described. Model results are presented and discussed before conclusions of the study are drawn.

2. A Dynamically Coupled 3D-2DV Model

The coupled 3D-2DV model (Chen, 2003c, 2005, 2007a) involves a dynamic, two-way coupling of a laterally averaged 2D hydrodynamic model named LAMFE (Chen and Flannery, 1997; Chen et al., 2000; Chen, 2003a and 2004a) and a 3D hydrodynamic model named LESS3D (Chen, 1999, 2003b, 2004b). In the LAMFE model, the following governing equations are solved:

$$\frac{\partial ub}{\partial x} + \frac{\partial wb}{\partial z} = v \quad (1)$$

$$\begin{aligned} \frac{\partial u}{\partial t} + u \frac{\partial u}{\partial x} + w \frac{\partial u}{\partial z} = & -\frac{\tau_{wx}}{\rho_o b} - g \frac{\partial \eta}{\partial x} - \frac{g}{\rho_o} \int_z^\eta \frac{\partial \rho}{\partial x} d\zeta + \frac{1}{b} \frac{\partial}{\partial x} (b A_h \frac{\partial u}{\partial x}) \\ & + \frac{1}{b} \frac{\partial}{\partial z} (b A_v \frac{\partial u}{\partial z}) \end{aligned} \quad (2)$$

$$b \frac{\partial c}{\partial t} + \frac{\partial ubc}{\partial x} + \frac{\partial wbc}{\partial z} = \frac{\partial}{\partial x} (b B_h \frac{\partial c}{\partial x}) + \frac{\partial}{\partial z} (b B_v \frac{\partial c}{\partial z}) + v c_t + S_s \quad (3)$$

where t is time; x is the horizontal coordinate along the river/estuary, z is the vertical coordinate, u and w denote velocity components in x - and z -directions, respectively; v is the lateral velocity from lateral inputs (sheet flow of direct runoff, tributary, etc.); b , p , g , and η denote the width, pressure, gravity acceleration, and the free surface elevation, respectively; ρ_o is the reference density; τ_{wx} represents the shear stress due to the friction acting on the side wall ($= \rho C_w u [u^2 + w^2]^{1/2}$, where C_w is a non-dimensional frictional coefficient for side walls); A_h and A_v are kinetic eddy viscosities in the x - and z -directions, respectively; c is concentration (can be temperature, salinity, suspended sediment concentrations, nutrient concentrations, etc.); c_t is concentration in lateral inputs; B_h and B_v are eddy diffusivities in the x - and z -directions, respectively; S_s denotes source/sink terms; and ρ is density which is a function of salinity and temperature (UNESCO, 1983). In the above transport equation, if the material simulated involves settling, w in the advective term includes the settling velocity of the material.

In the LESS3D model, the governing equations are

$$\frac{\partial u}{\partial x} + \frac{\partial v}{\partial y} + \frac{\partial w}{\partial z} = 0 \quad (4)$$

$$\begin{aligned} \frac{\partial u}{\partial t} + \frac{\partial uu}{\partial x} + \frac{\partial vu}{\partial y} + \frac{\partial wu}{\partial z} = & f v - \frac{1}{\rho_o} \frac{\partial p}{\partial x} + \frac{\partial}{\partial x} (A_h \frac{\partial u}{\partial x}) + \frac{\partial}{\partial y} (A_h \frac{\partial u}{\partial y}) + \frac{\partial}{\partial z} (A_v \frac{\partial u}{\partial z}) \\ \frac{\partial v}{\partial t} + \frac{\partial uv}{\partial x} + \frac{\partial vv}{\partial y} + \frac{\partial wv}{\partial z} = & -f u - \frac{1}{\rho_o} \frac{\partial p}{\partial y} + \frac{\partial}{\partial x} (A_h \frac{\partial v}{\partial x}) + \frac{\partial}{\partial y} (A_h \frac{\partial v}{\partial y}) + \frac{\partial}{\partial z} (A_v \frac{\partial v}{\partial z}) \end{aligned} \quad (5)$$

$$p = g \int_z^\eta \rho d\zeta \quad (6)$$

$$\frac{\partial c}{\partial t} + \frac{\partial uc}{\partial x} + \frac{\partial vc}{\partial y} + \frac{\partial wc}{\partial z} = \frac{\partial}{\partial x} (B_h \frac{\partial c}{\partial x}) + \frac{\partial}{\partial y} (B_h \frac{\partial c}{\partial y}) + \frac{\partial}{\partial z} (B_v \frac{\partial c}{\partial z}) + S_s \quad (7)$$

where x , y , and z are Cartesian coordinates (x is from west to east, y is from south to north, and z

is vertical pointing upward); u , v , and w are velocities in the x -, y -, and z -directions, respectively; f denotes Coriolis parameter; and A_h and A_v represent horizontal and vertical eddy viscosities, respectively; and B_h and B_v are horizontal and vertical eddy diffusivities, respectively. Again, if the material simulated in Equation (7) involves settling, w in the advective term includes the settling velocity of the material.

Both the LAMFE and LESS3D models use a semi-implicit scheme called the free-surface correction (FSC) method (Chen, 2003a, 2003b) to solve the governing equations. The FSC method is a very efficient scheme that is unconditionally stable with respect to gravity waves, wind and bottom shear stresses, and vertical eddy viscosity terms. The FSC method in the 2DV model involves the solution of the following FSC equation

$$\mathbf{r}\Delta\boldsymbol{\eta}_{2DV} = \Delta\boldsymbol{\eta}_{2DV}^* \quad (8)$$

where $\Delta\boldsymbol{\eta}_{2DV}$ and $\Delta\boldsymbol{\eta}_{2DV}^*$ are respectively the final and intermediate surface elevation changes over the time step Δt in the 2DV domain

$$\begin{aligned} \Delta\boldsymbol{\eta}_{2DV} &= [\Delta\eta_1 \quad \Delta\eta_2 \quad \dots \quad \Delta\eta_{N-1} \quad \Delta\eta_N]^T \\ \Delta\boldsymbol{\eta}_{2DV}^* &= [\Delta\eta_1^* \quad \Delta\eta_2^* \quad \dots \quad \Delta\eta_{N-1}^* \quad \Delta\eta_N^*]^T \end{aligned} \quad (9)$$

and \mathbf{r} is a sparse matrix that can be split into two parts: $\mathbf{r} = \mathbf{r}_0 + \mathbf{r}'$. The first part is a three-diagonal matrix

$$\mathbf{r} = \begin{bmatrix} r_{11} & r_{12} & & & & \\ r_{21} & r_{22} & r_{23} & & & \\ & \cdot & \cdot & \cdot & & \\ & & \cdot & \cdot & \cdot & \\ & & & \cdot & \cdot & \cdot \\ & & & & r_{(N-1)(N-2)} & r_{(N-1)(N-1)} & r_{(N-1)N} \\ & & & & \cdot & r_{N(N-1)} & r_{NN} \end{bmatrix} \quad (10)$$

where $r_{i(i-1)} = -R_i^w$, $r_{i(i+1)} = -R_i^e$, $r_{ii} = 1 - r_{i(i-1)} - r_{i(i+1)}$, R_i^w and R_i^e are simply functions of the cross-sectional area and the grid size, and N is the total number of grids in the 2DV domain. The second part (\mathbf{r}') is a very sparse matrix in which only several rows representing connections among the main river stem and its branches have one or two non-zero elements locating outside the three-diagonal block.

In the FSC method for the 3D model, the FSC equation is as follows

$$\mathbf{q}\Delta\boldsymbol{\eta}_{3D} = \Delta\boldsymbol{\eta}_{3D}^* \quad (11)$$

where $\Delta\boldsymbol{\eta}_{3D}$ and $\Delta\boldsymbol{\eta}_{3D}^*$ are respectively the final and intermediate surface elevation changes over the time step Δt in the 3D domain

$$\begin{aligned} \Delta\boldsymbol{\eta}_{3D} &= [\Delta\eta_1 \quad \Delta\eta_2 \quad \dots \quad \Delta\eta_{M-1} \quad \Delta\eta_M]^T \\ \Delta\boldsymbol{\eta}_{3D}^* &= [\Delta\eta_1^* \quad \Delta\eta_2^* \quad \dots \quad \Delta\eta_{M-1}^* \quad \Delta\eta_M^*]^T \end{aligned} \quad (12)$$

and

$$\mathbf{q} = \begin{bmatrix} q_{11} & q_{12} & & & & q_{1(L+1)} & & & \\ q_{21} & q_{22} & q_{23} & & & & q_{2(L+2)} & & \\ & \cdot & \cdot & \cdot & & & & \cdot & \\ & & \cdot & \cdot & \cdot & & & & \cdot \\ & & & \cdot & \cdot & \cdot & & & \\ & & & & \cdot & \cdot & \cdot & & \\ & & & & & \cdot & \cdot & \cdot & \\ & & & & & & \cdot & \cdot & \\ & & & & & & & \cdot & \\ & & & & & & & & q_{(M-1)(M-L-1)} & q_{11} & q_{11} & q_{11} \\ & & & & & & & & q_{M(M-L)} & q_{M(M-1)} & q_{MM} \end{bmatrix} \quad (13)$$

where $q_{l(l-L)} = -R_{i,j}^s$, $q_{l(l-1)} = -R_{i,j}^w$, $q_{l(l+1)} = -R_{i,j}^e$, $q_{l(l+L)} = -R_{i,j}^n$, $q_{ll} = 1 - q_{l(l-L)} - q_{l(l-1)} - q_{l(l+1)} - q_{l(l+L)}$, $R_{i,j}^s$, $R_{i,j}^w$, $R_{i,j}^e$, $R_{i,j}^n$ are functions of the total side area of the grid cell and the grid sizes in x - and y -directions, and M is the total number of grids in the 3D domain.

Equation (13) is a five-diagonal matrix and can be saved in five 1D arrays. However, because a Cartesian model often involves many land grids that are not included in the computation, it is more efficient to compress the matrix, so that it only contains those grids that have water in them. If it is assumed that only m grids in the 3D domain have water in them, then renumbering these 3D grids will result in a new and compressed matrix (let us call it \mathbf{q}') of order $m \times m$, which sometimes could be much smaller than the original size of in Equation (13).

The compressed form of Equation (13) takes the following form

$$\mathbf{q}' \Delta \boldsymbol{\eta}'_{3D} = \Delta \boldsymbol{\eta}^*_{3D} \quad (14)$$

where $\Delta \boldsymbol{\eta}'_{3D}$ and $\Delta \boldsymbol{\eta}^*_{3D}$ are compressed forms of $\Delta \boldsymbol{\eta}_{3D}$ and $\Delta \boldsymbol{\eta}^*_{3D}$, respectively.

By numbering all grids that possess water in the 3D together with 2DV grids, Equations (8) and (14) can be merged together as follows

$$\begin{bmatrix} \mathbf{q}' & \mathbf{p} \\ \mathbf{s} & \mathbf{r} \end{bmatrix} \begin{bmatrix} \Delta \boldsymbol{\eta}'_{3D} \\ \Delta \boldsymbol{\eta}_{2DV} \end{bmatrix} = \begin{bmatrix} \Delta \boldsymbol{\eta}^*_{3D} \\ \Delta \boldsymbol{\eta}^*_{2DV} \end{bmatrix} \quad (15)$$

Where \mathbf{p} and \mathbf{s} are rectangular matrices of orders $m \times N$ and $N \times m$, respectively. They are needed to ensure a proper modeling of the two-way interaction between the 3D and 2DV domains. Both \mathbf{p} and \mathbf{s} only have a limited number of non-zero elements. In fact, the number of non-zero elements in \mathbf{p} and \mathbf{s} is the same as the number of grids that are connected to the 2DV domain (Chen, 2005).

The sparse matrix system shown in Equation (15) is similar to those in Equations (8) and (14). It has a three-diagonal block with each row having a maximum of one non-zero element on each side of the three diagonals. Equation (15) can be efficiently solved using the bi-conjugate gradient method of Van der Vorst (1992). After Equation (15) is solved, the final free surface location is found for the entire simulation area, including both the 3D and 2DV domains.

Final velocities at the new time step can be calculated after the final free surface elevations in both the 3D and 2DV domains are found. The transport equations are then solved to update distributions of simulated constituents (salinity, temperature, suspended sediment concentration etc.). Details on the numerical schemes for calculating velocities and concentrations can be found in Chen (2003a, 2003b, and 2007a).

3. Field Data

This section presents measured field data used in modeling hydrodynamics and salinity and thermal transport processes in the LPR – LMR - UCH system. As will be described in the next section, the simulation period is a 13-month period from the middle of June 2003 to the middle of July 2004. As such, the focus of the section is only on measured field data during this 13-month period.

Flow Data

Freshwater inflows are critical to the health of an estuary, as they directly affect salinity distributions in the estuary. The purpose of the hydrodynamic simulation of the LPR – LMR - UCH system is to use a hydrodynamic model to find the relationship between freshwater inflows and salinity distributions in the system, so that minimum freshwater inflows for the LPR and LMR can be determined to prevent the two riverine estuaries from significant harms. Therefore, flow data are the most important piece of information needed in every steps of the process of determining minimum flows, including the hydrodynamic modeling.

The USGS has been gauging flow rates at several locations in the Peace and Myakka River watersheds for many years. These USGS stations include (1) Peace River at Arcadia (02296750), (2) Joshua Creek at Nocatee (02297100), (3) Horse Creek near Arcadia (02297310), (4) Shell Creek near Punta Gorda (02298202), (5) Big Slough Canal at Tropicair (02299450), (6) Myakka River near Sarasota (02298830), (7) Deer Prairie Slough near Myakka City (02299060), and (8) Blackburn Canal near Vnice (02299692). The gauged USGS flow data were used, either directly or indirectly, as freshwater inputs to the hydrodynamic model described in the next section. In addition to gauged USGS flows, there are also un-gauged flows that contribute a significant portion of the total freshwater budget to the upper Charlotte Harbor. As mentioned before, for the Peace River watershed, the un-gauged area is about 16% of the total watershed, while for the Myakka River, about one half of the watershed is un-gauged. In this study, freshwater flows from the un-gauged sub-basins of the watershed were estimated by Ross et al (2005) using the Hydrological Simulation Program - FORTRAN (HSPF) (Bicknell, 1997). Some of the USGS gauge stations are located at the boundary of the simulation domain of the HSPF model, and gauged flow rates at these stations were used as boundary fluxes in the HSPF model.

Figure 3 shows flow data gauged during the 13-month period from June 2003 to July 2004 at four locations on the Peace River side of the watershed, including Peace River at Arcadia (black solid line), Horse Creek (green solid line), Joshua Creek (red solid line), and Shell Creek (blue solid line). Also shown in the figure is the withdrawal (black dashed line) from the Peace River by the Peace River/Manasota Regional Water Supply Authority. The withdrawal point of the regional water supply authority is located roughly 3.5 km upstream of USGS Peace River Heights station (Figure 1). Withdrawal by the City of Punta Gorda from the upstream of the Shell Creek dam is included in the Shell Creek flow shown in the figure. Figure 4 shows gauged flow rates at the USGS Myakka River near Sarasota station (black solid line) and the USGS Myakkahatchee (Big Slough Canal) at North Port station (blue solid line). The black dashed line shown in Figure 4 is the flow in the Blackburn Canal that connects the Donna/Roberts Bay on the Florida Gulf Coast to the Myakka River at about 3.8 km upstream of the USGS Myakka

River at Snook Haven station. The period of available gauged flow data for the Blackburn Canal at the time of this modeling study was a 209-day period from March 6, 2004 to September 30, 2004. It was found that water in the Blackburn Canal can flow either to or away from the Myakka River, depending on the water levels in the Myakka River and in the Donna/Roberts Bay. Although it drains the Myakka River most of the time, the Blackburn Canal occasionally flows to Myakka River. Figure 5 is a plot of the flow leaving Myakka River through the Blackburn Canal versus the Myakka River flow gauged at the USGS Myakka River near Sarasota station. From the figure, it can be seen that the two flow rates are fairly correlated. Therefore, water leaving the Myakka River through Blackburn Canal can be roughly estimated using the following equations:

$$\begin{aligned} Q_b &= 0.057Q_m, & Q_m &\leq 457 \\ Q_b &= 0.169Q_m - 51.2, & Q_m &> 457 \end{aligned} \quad (16)$$

where Q_b is the flow rate that drains Myakka River through the Blackburn Canal, and Q_m is the Myakka River flow at the USGS station near Sarasota. The units in the above equation are cubic feet per second. It should be noted that the above equation only estimates flow leaving the Myakka River, as Q_b calculated from in the equation is always positive. From the available Blackburn Canal flow data shown in Figure 5, the negative flow rate is generally very small in magnitude (≤ 2.2 cfs) and occurs only infrequently.

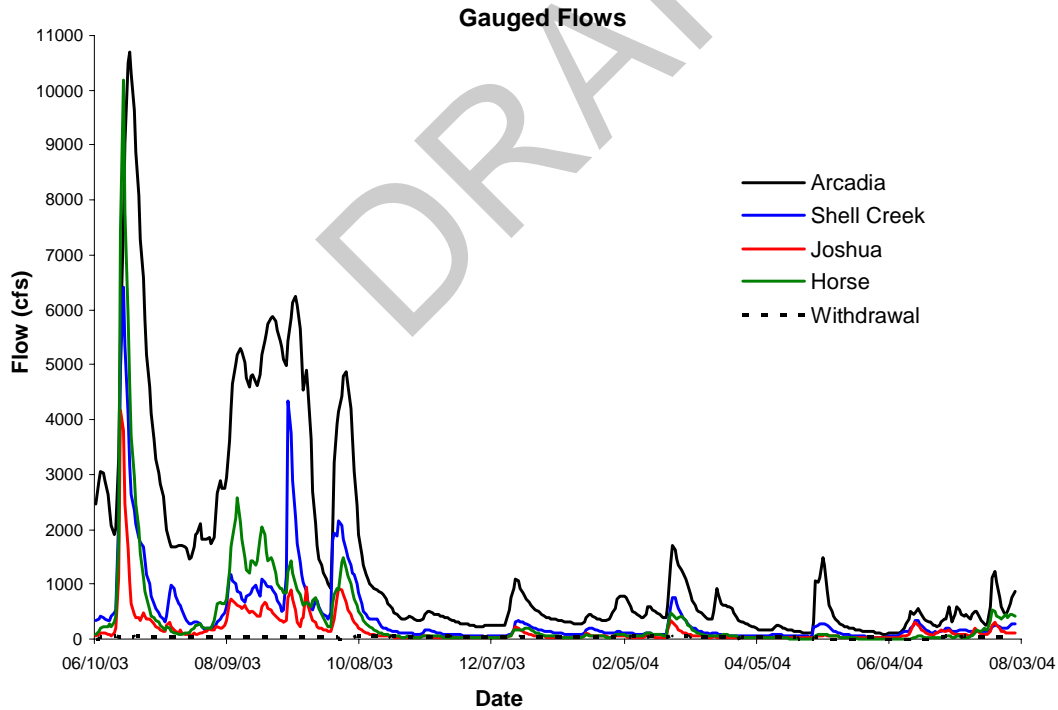


Figure 3 Gauged flow rates on the Peace River side, including USGS gauges at Arcadia, Joshua, Horse, and Shell Creek. The withdrawal by the Peace River/Manasota Regional Water Supply Authority is also shown.

From Figures 3 and 4, several things can be quickly discerned. First, during the 13-month period, the LPR – LMR - UCH received majority of its freshwater inflows during a 100-day

period from June 20, 2003 to the end of September 2003. Second, all gauged flows have the their highest peaks around June 24, 2003, with Arcadia, Horse and Myakka flows having similar peak values that are larger than 10,000cfs. Rainfall data collected at a SWFWMD rain station close to the Peace River/Manasota Regional Water Supply Authority (Figure 6) indicated that a major storm event passed through the region and dumped about 10 inches of rain during a 3-day period on June 20 - 22, 2003. It is interesting that although the Horse Creek and the Myakka River near Sarasota stations gauged much smaller areas than that of the Peace River Arcadia station, they had almost the same peak discharge as the Arcadia station. This might be caused by a relatively low surface water yield with significant buffer areas in the upstream portion of the Peace River watershed after a long period of dry months. A close look of the flow data measured at these stations revealed that the time of concentration for the Arcadia station is much longer than those at the Horse Creek station and the Myakka River near Sarasota station.

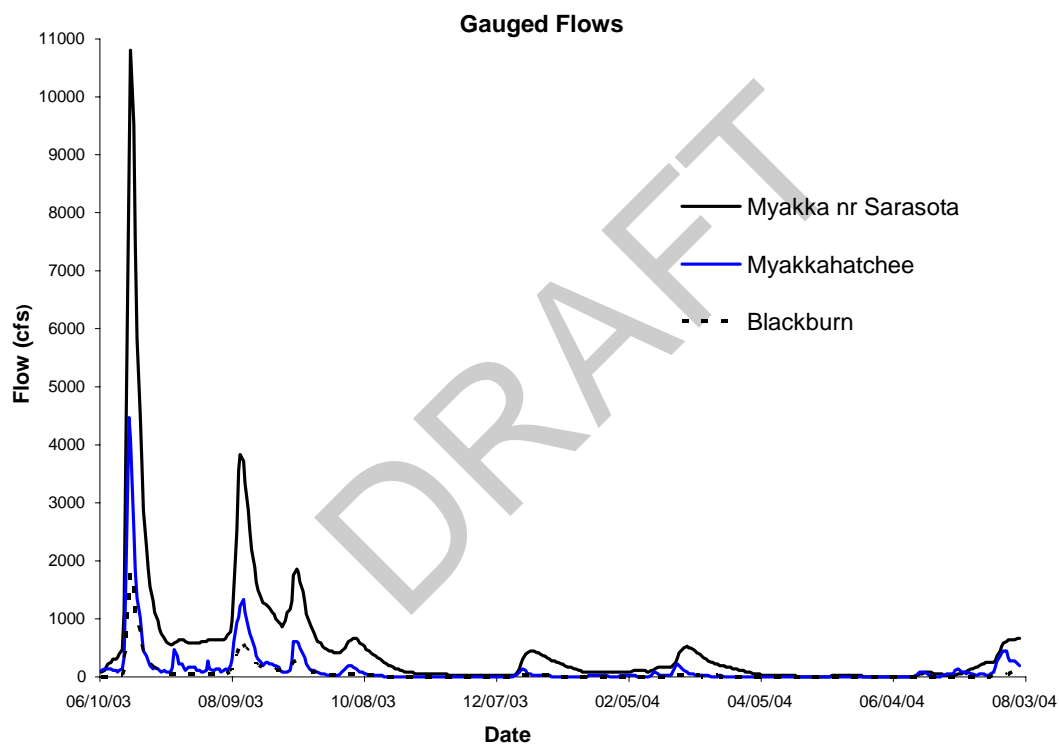


Figure 4 Gauged flow rates on the Peace River side, including USGS gauges at Arcadia, Joshua, Horse, and Shell Creek. The withdrawal by the from the Peace River/Manasota Regional Water Supply Authority is also shown.

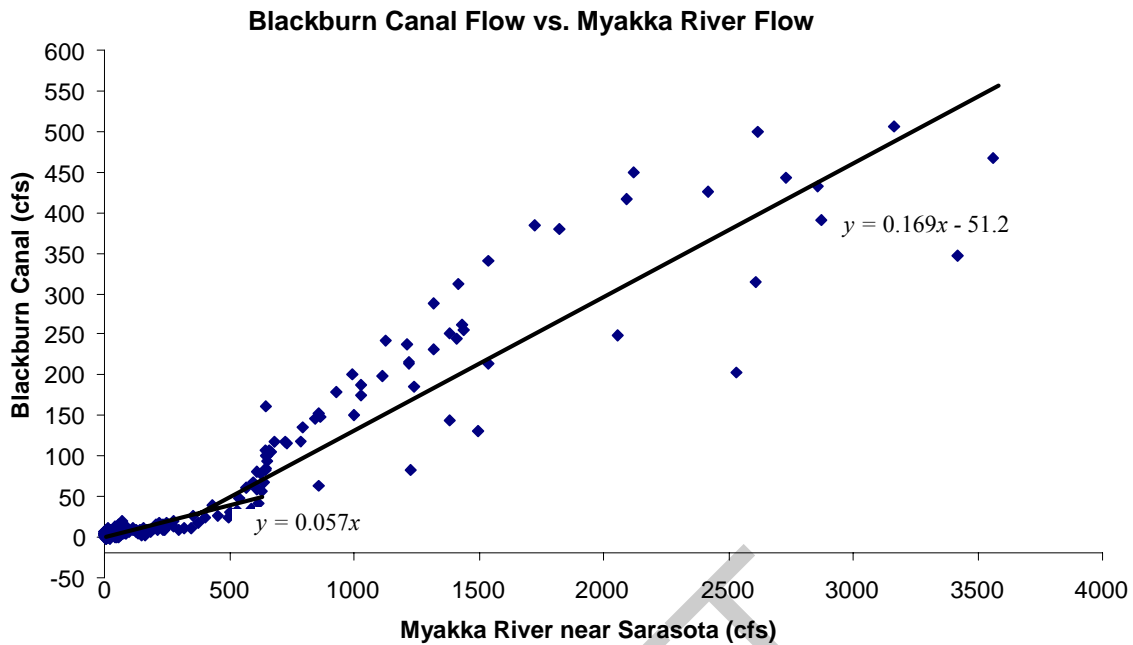


Figure 5 Blackburn Canal flow versus Myakka River flow gauged at the USGS station near Sarasota. Positive Blackburn Canal flow leaves the Myakka River.

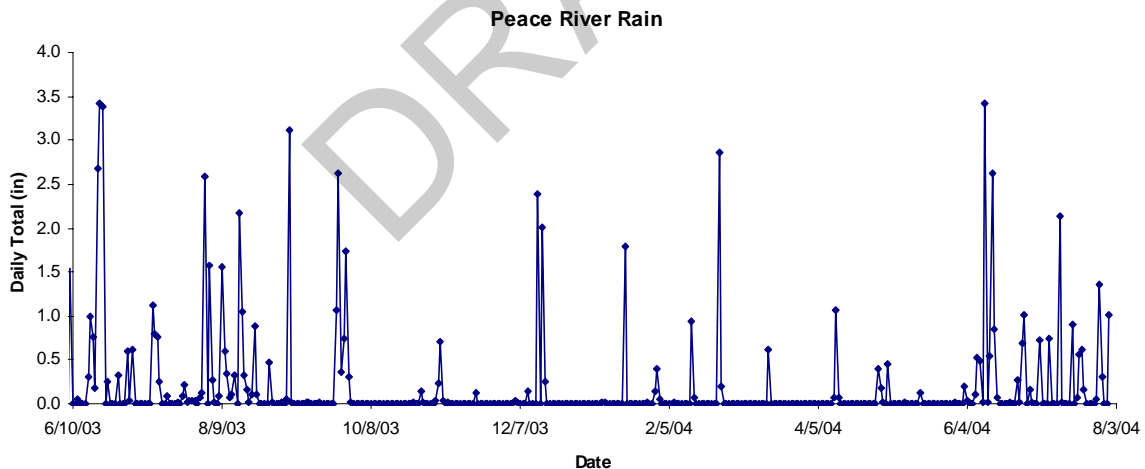


Figure 6 Daily rainfall total measured at location close to the Peace River/Manasota Regional Water Supply Authority

Water Level, Salinity, Temperature, and Velocity

Real-time data of water level, salinity, and temperature were collected by the University of Florida (UF) and the USGS at the several fixed stations noted with stars in Figure 1. These stations included (1) UF station in the upper Charlotte Harbor near the mouth of the Myakka River, (2) USGS Peace River at Punta Gorda (02298300), (3) USGS Peace River at Harbor Heights (02297460), (4) USGS Peace River at Peace River Heights, (5) USGS Myakka River at

El Jobean (02299496), (6) USGS Myakka River at North Port (02299230), (7) USGS Myakka River at Snook Haven (02298955), and (8) USGS Shell Creek Tidal near Punta Gorda (02298208). The USGS real-time data were collected with a time interval of 15 minutes, while the UF data had a time interval of 30 minutes. For salinity and temperature, data were collected at three water depths at the UF station, but only at two depths at the USGS stations. Table 1 lists elevations of the salinity and temperature sensors at all eight stations.

Real-Time Measurement Stations	Sensors	Elevations (ft, NGVD29)
UF in the UCH	Top Middle Bottom	-1.31 -4.14 -7.4
Punta Gorda	Top Bottom	-1.1 -8.0
Harbor Height	Top Bottom	-1.0 -3.0
Peace River Heights	Top Bottom	-1.0 -3.0
El Jobean	Top Bottom	-2.0 -8.0
North Port	Top Bottom	-2.5 -10.0
Snook Haven	Top Bottom	-0.85 -6.0
Shell Creek	Top Bottom	-1.0 -3.0

Table 1 Elevations of salinity/temperature sensors in the eight stations in the LPR - LMR - UCH system. Units in the table are ft, NGVD29.

Figure 7 shows measured water levels during a 14-month period from June 2003 to July 2004 at the Punta Gorda, Harbor Heights, Peace River Heights, Shell Creek Tidal (for simplicity, this station is also called Shell Creek hereafter), El Jobean, North Port, Snook Haven, and UF stations. Water levels at all eight stations have strong tidal signals that are mainly semi-diurnal tides with a range of 50 – 60cm. Unlike downstream stations, upstream stations in both the LPR (Peace River Heights and Harbor Heights) and the LMR (Snook Haven and North Port) recorded considerable water level increases caused by major storm events occurred in 2003 as the tributaries are narrow in these areas. For the downstream stations, including Punta Gorda, El Jobean, and UF stations, although measured water level data do not contain distinctive storm signals, it does appear that average water levels were higher in the wet season than in the dry season. Of course, this kind of seasonal variation in water level is not only caused by storm events, but also caused by other factors, such as the general wind pattern, loop current in the Gulf of Mexico, and the seasonal water temperature variation.

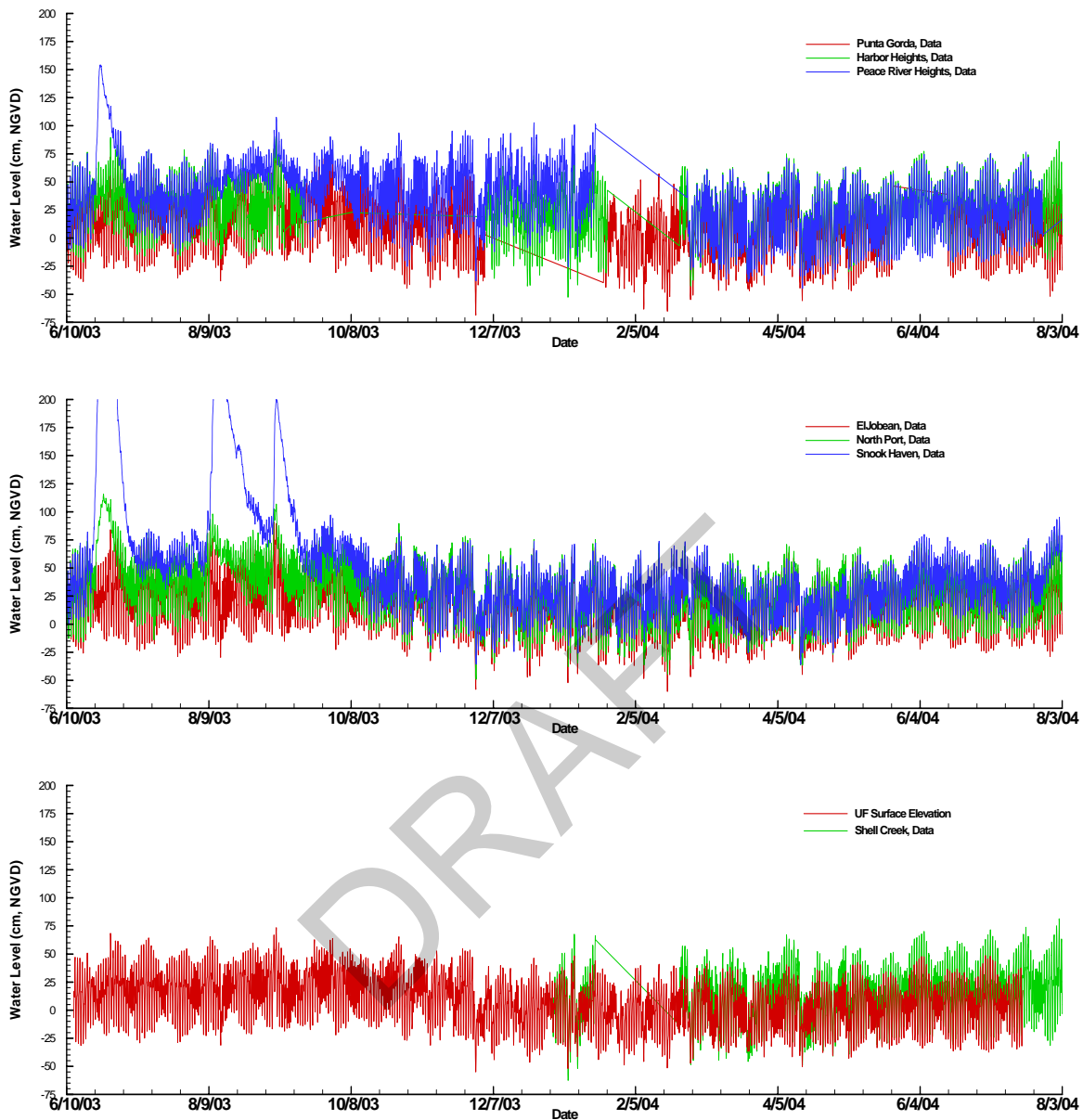


Figure 7 Measured water levels during June 2003 through July 2004 at three Lower Peace River stations (top graph), three Lower Myakka River stations (middle graph), one Shell Creek station (bottom graph), and one Upper Charlotte Harbor station (bottom graph).

Figure 8 shows top- and bottom-layer salinity time series measured at the three LPR stations, while Figure 9 presents top- and bottom-layer salinity time series measured at the three LMR stations. Measured salinity time series in Shell Creek and the UF station in the Upper Charlotte Harbor are plotted in Figure 10. Generally speaking, the vertical salinity stratification is not very strong for upstream narrow channels in the LPR – LMR - UCH system. Measured top- and bottom layer salinities were almost the same for Peace River Heights, Harbor Heights, Shell Creek, North Port, and Snook Haven. The three downstream stations (UF, El Jobean, and Punta Gorda) did show some vertical salinity stratification, especially during the time periods

when there were major storm events. The horizontal salinity gradients along the LPR and LMR are quite evident with the salt wedge being located between the Punta Gorda and Harbor Heights stations in the LPR and between the El Jobean and North Port stations in the LMR during the wet season. The salt wedge migrated upstream during the dry season and passed the Harbor Heights and North Port stations in the LPR and LMR, respectively. During the driest time period of the year 2004, the salt edge moved passed the Peace River Heights station in the LPR and the Snook Haven station in the LMR.

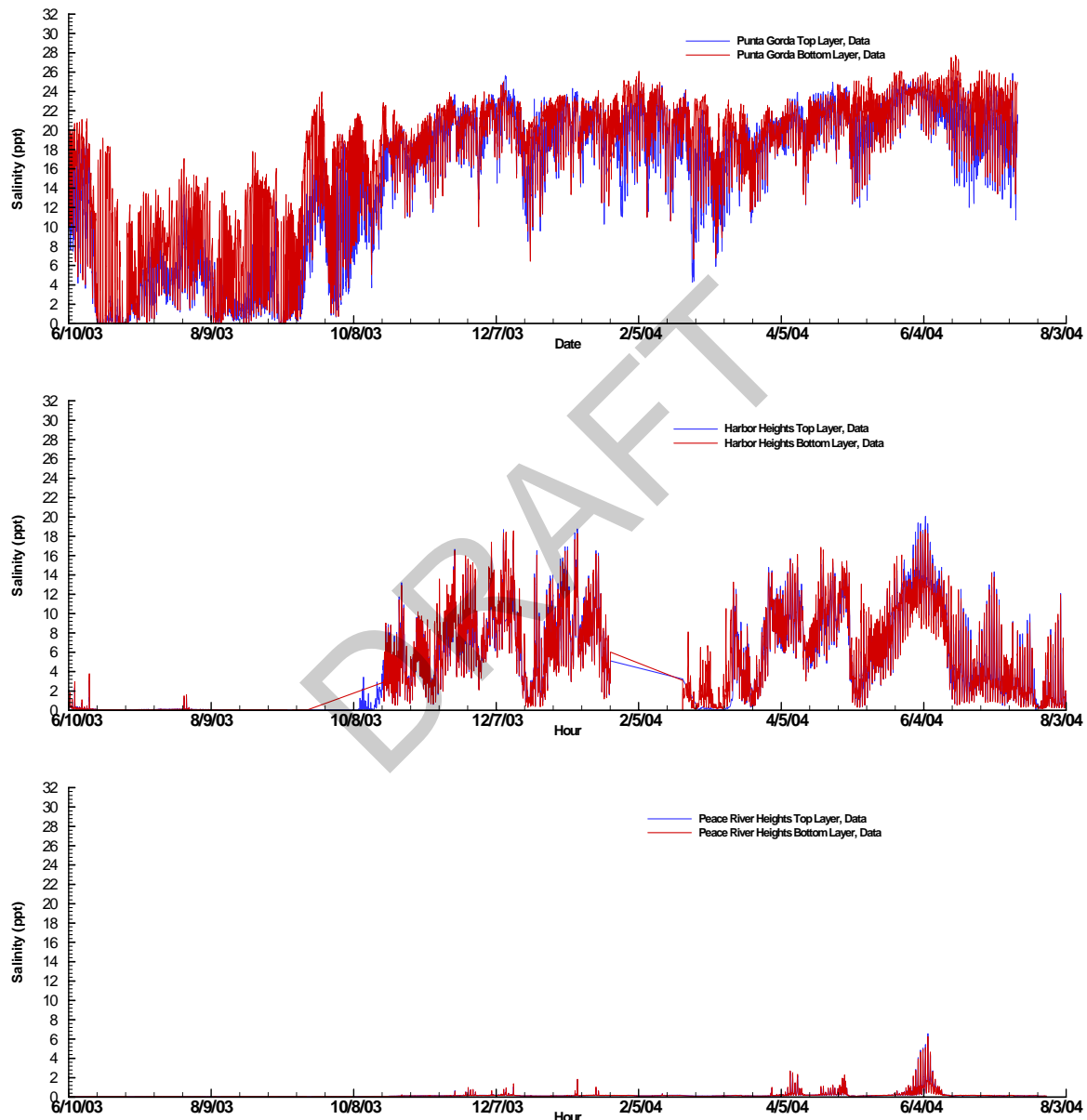


Figure 8 Measured salinity time series at three Lower Peace River stations during June 2003 – July 2004.

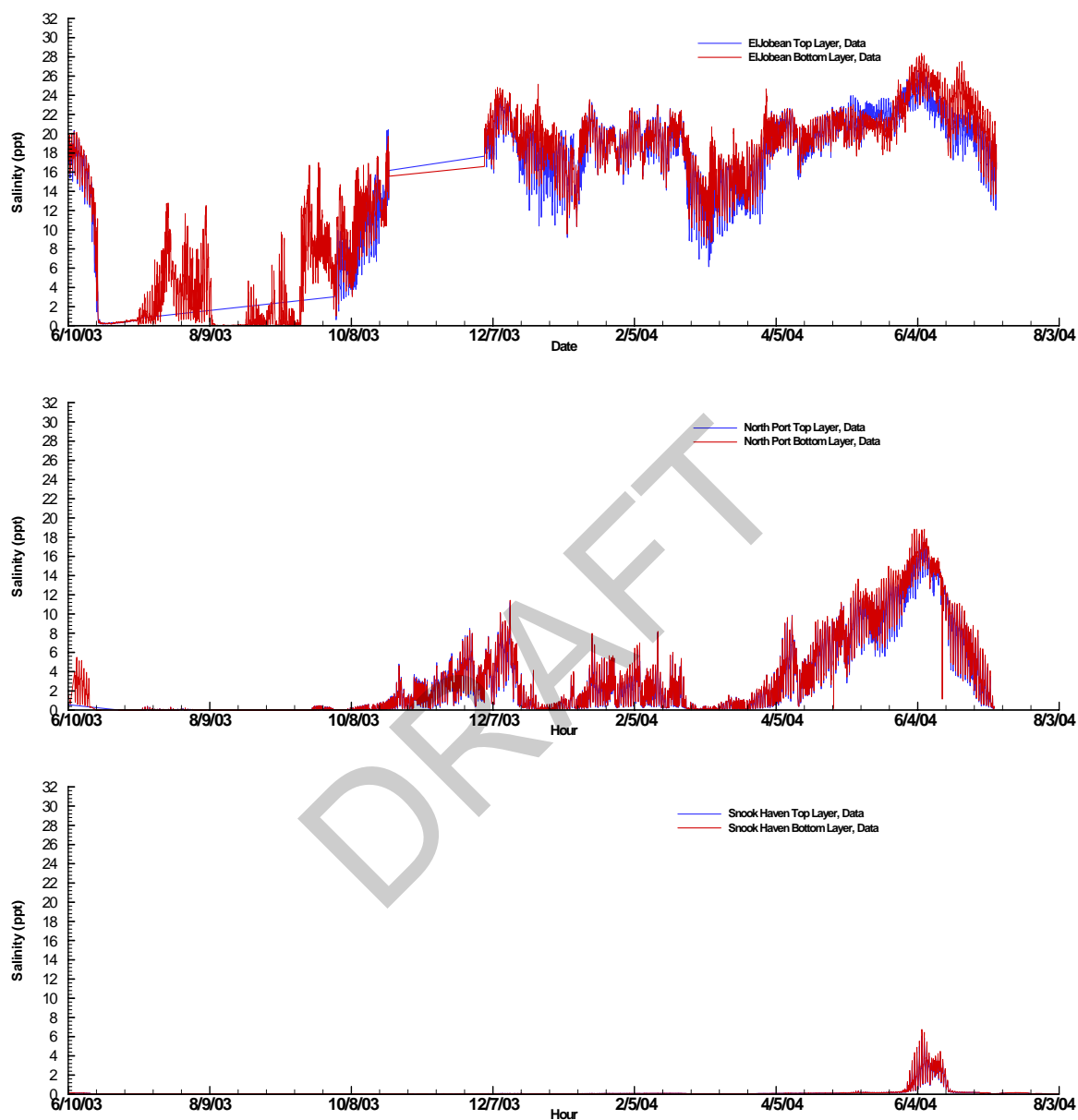


Figure 9 Measured salinity time series at three Lower Myakka River stations during June 2003 – July 2004.

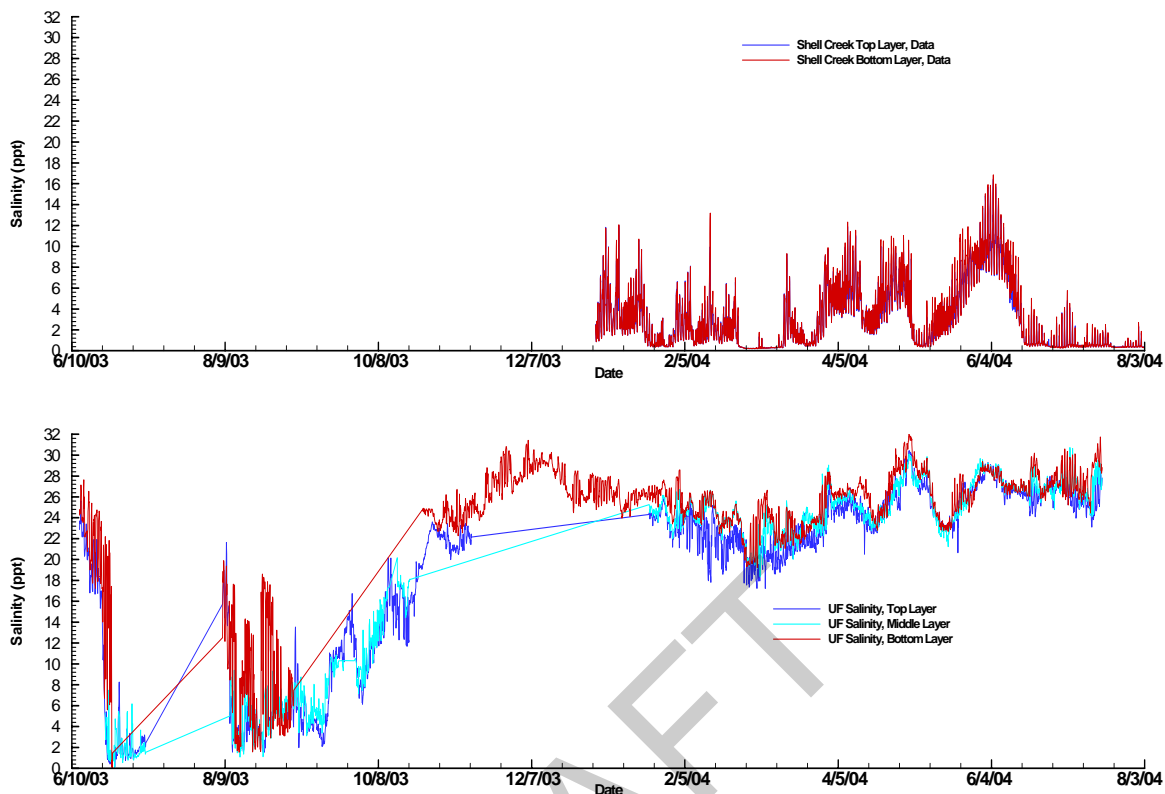


Figure 10 Measured salinity time series in Shell Creek (top graph) and Upper Charlotte Harbor (UF station, bottom graph) during June 2003 – July 2004.

Figures 11 – 13 are measured water temperature time series at the eight measurement stations in the LPR – LMR - UCH system in the same order as those of Figures 8 – 10. Figures 11 – 13 clearly show that water temperature does not exhibit much stratification in the LPR – LMR - UCH system. Except for the UF station in the UCH, all other seven stations exhibited only slight temperature differences between the top and bottom layers. The abnormality observed in top-layer temperature at the Peace River Heights station might be due to an equipment failure occurred in the measurement. The only measurement station that had shown temperature stratification is the UF station. However, the quality of the UF temperature data is questionable. One obvious problem is that the top-layer temperature was consistently higher than the middle- and bottom-layer temperatures during February – June 2004, while the middle-layer temperature was consistently lower than the bottom-layer temperature during the same period. Therefore, it is not certain whether the temperature stratification shown in UF data is real or not.

Overall, the quality of the available real-time water level, salinity, and temperature data measured at the eight stations is just average. Several stations had many missing data. Some of the salinity and temperature data do not make sense. For example, beside the problems involved in the UF temperature data, salinity data collected by the USGS had some problems in April and May 2004 at the Punta Gorda and El Jobean stations, respectively. While the daily high of the top-layer salinity is always higher than that of the bottom-layer salinity in April 2004 at the Punta Gorda station, the similar thing occurred in May 2004 at the El Jobean station. Obviously, salinity sensors malfunctioned at the two stations in April – May 2004. At the Peace River

Heights station, there appeared to have a datum problem before the missing data period around 2/5/04.

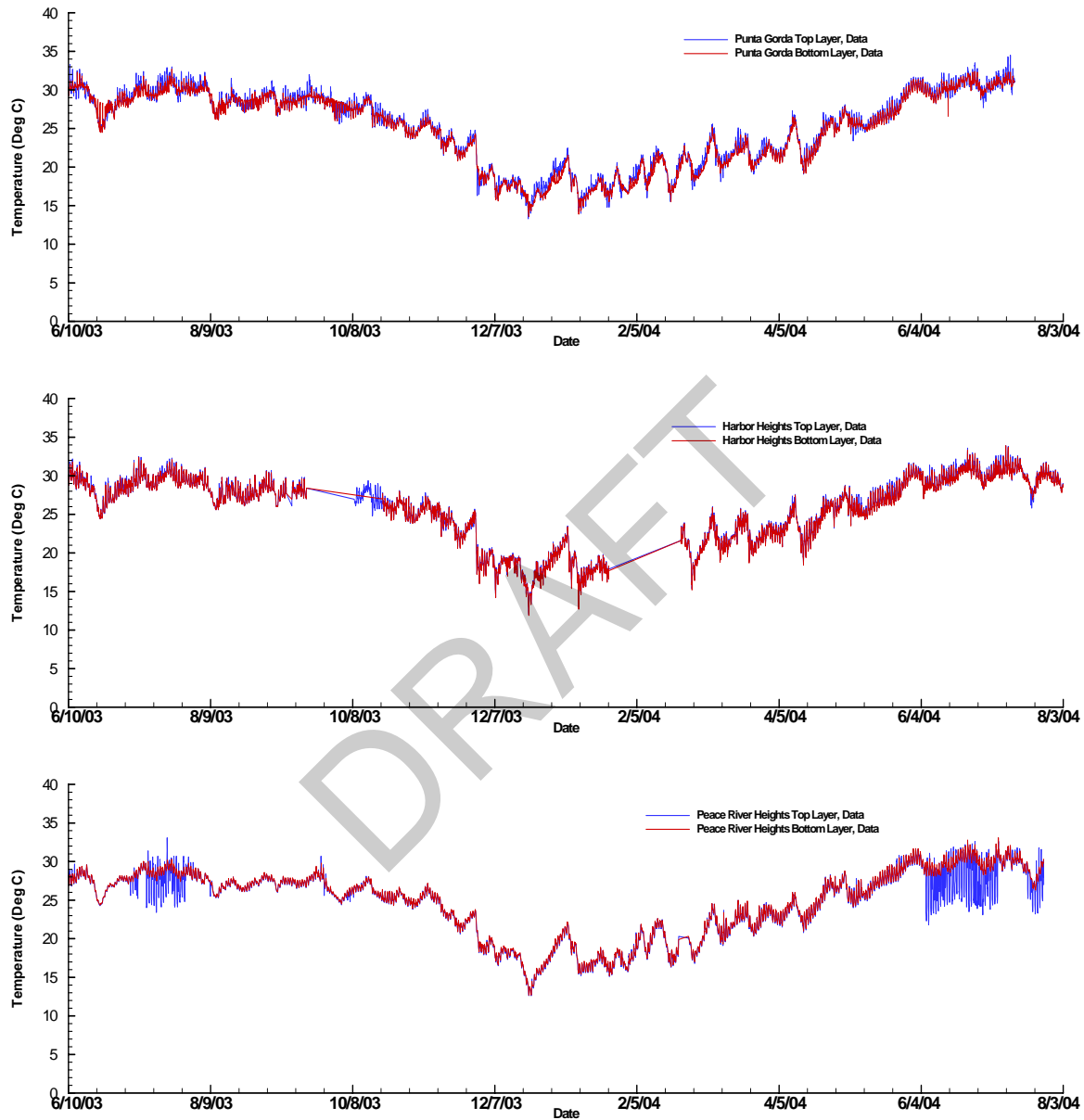


Figure 11 Measured temperature time series at three Lower Peace River stations during June 2003 – July 2004.

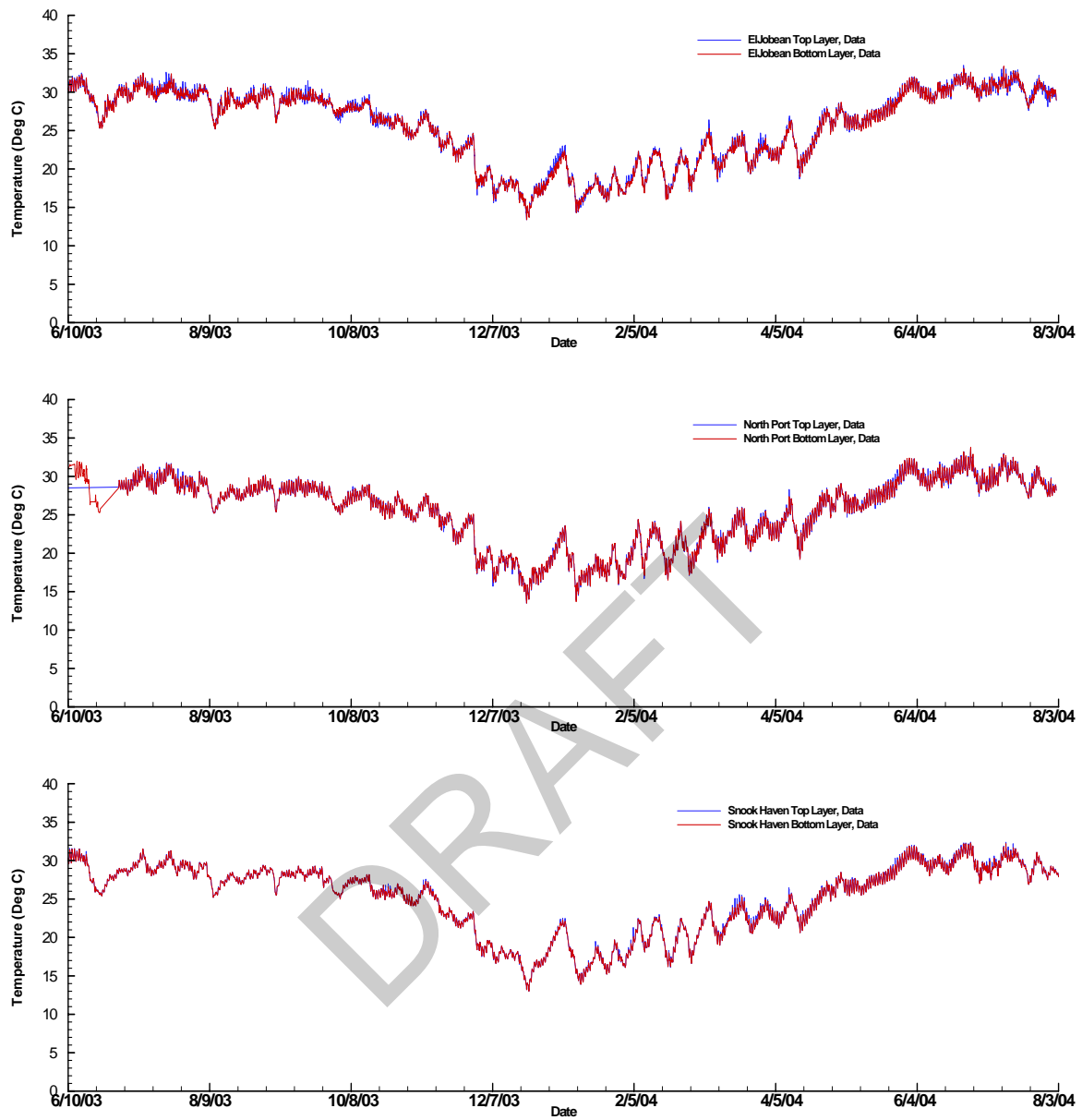


Figure 12 Measured temperature time series at three Lower Myakka River stations during June 2003 – July 2004.

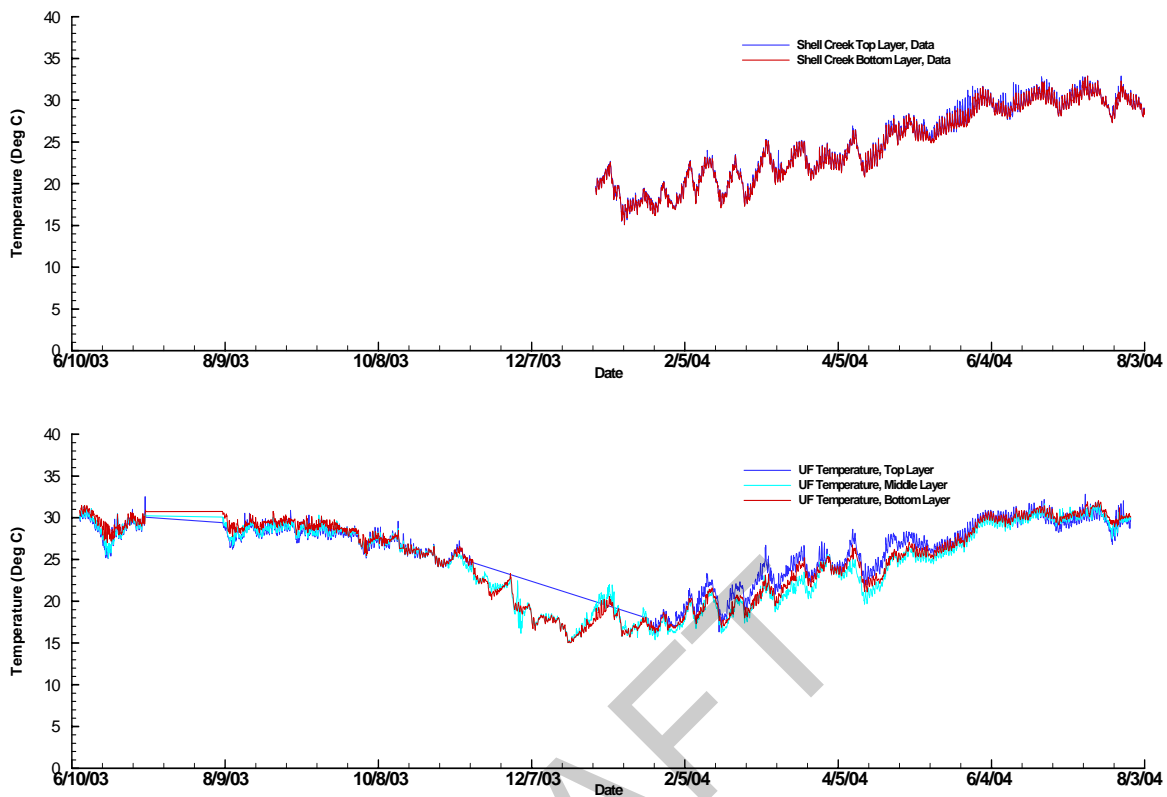


Figure 13 Measured temperature time series in Shell Creek (top graph) and Upper Charlotte Harbor (UF station, bottom graph) during June 2003 – July 2004.

Real-time water velocity data were measured only at the UF station in the Charlotte Harbor (Figure 1). An Acoustic Doppler Current Profiler (ADCP) was deployed to measure velocities at six vertical layers. Unfortunately, current data at the top two layers are not useful because the water level often dropped below these two layers (Sheng et al., 2007). Figure 14 shows measured velocities in the two depths that were always below the water surface. The u -velocity is the water velocity component in the x -direction that runs from west to east (a positive u -velocity means that water particle moves eastward), while the v -velocity is the water velocity component in the y -direction that points from south to north (a positive v -velocity means that water particle moves northward). Because of the physical configuration of the Charlotte Harbor, the magnitude of the v -component of the current is generally much larger than that of the u -component at the UF station. During the dry season when the current was predominantly tidal driven, the magnitude of the v -component was about twice of that of the u -component. However, during the wet season, the magnitude of the v -velocity was as large as three times of that of the u -component because fresh water coming from the Peace and Myakka Rivers turns south when it exits the Upper Charlotte Harbor. Due to the Coriolis effect and the way the Peace River flowing to the UCH, fresh water exits the harbor mainly near the west bank, resulting in a negative, long-term averaged v -velocity of 4 - 5 cm s^{-1} during the wet season and only about 1 cm s^{-1} during the dry season. On the other hand, although the long-term average of the u -velocity component is generally very small (about 0.75 cm s^{-1} in the wet season and about 0.4 cm s^{-1} in the dry season), it is always positive due to the proximity of the UF station to the mouth of the Myakka River.

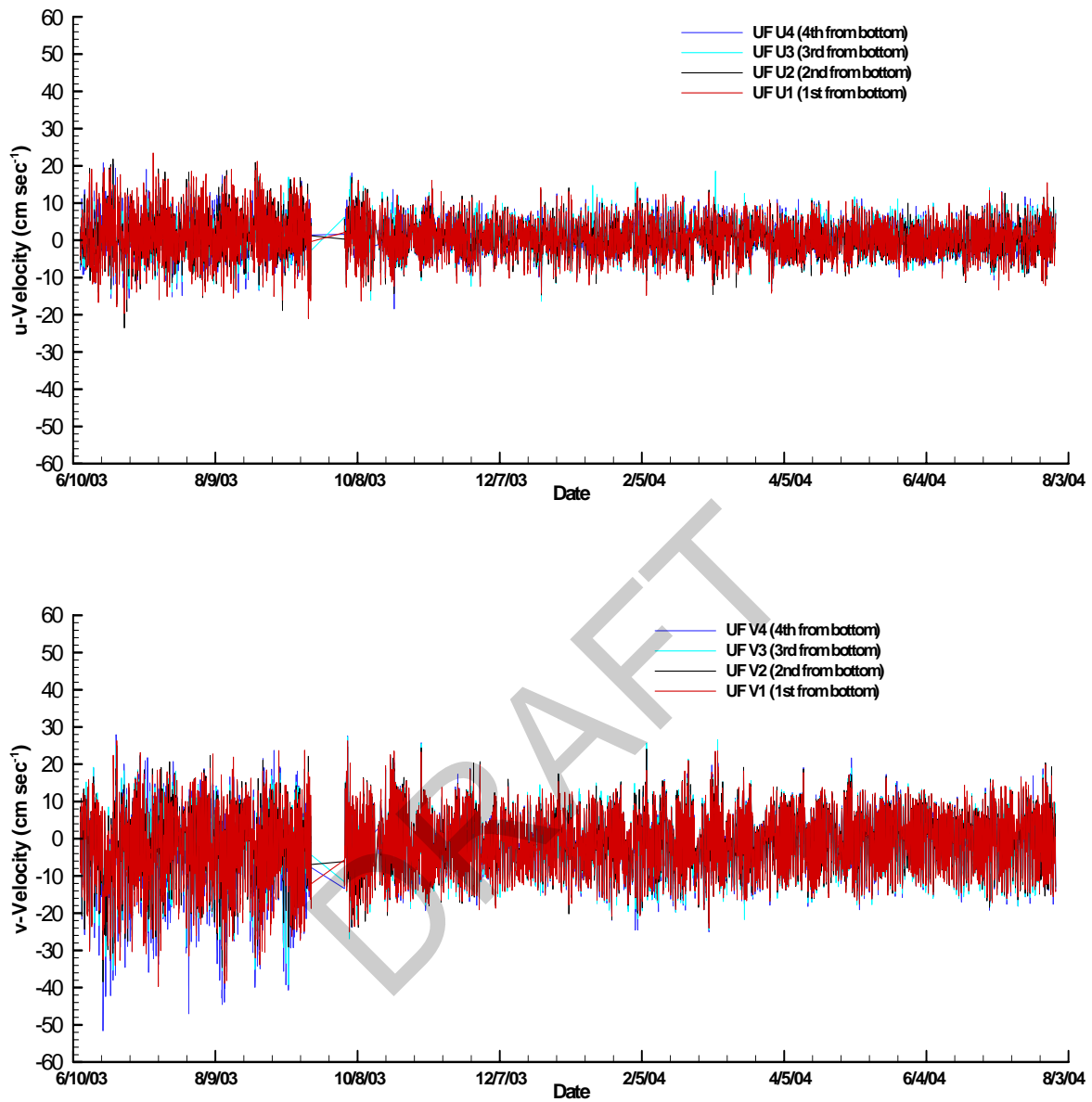


Figure 14 Measured u- (top graph) and v-velocities (bottom graph) in four depths at the UF station in the Upper Charlotte Harbor during June 2003 – July 2004.

Other Field Data

Other field data used in this modeling study of hydrodynamics in the LPR - LMR - UCH system included wind data measured at the UF station, air temperature, solar radiation, and air humidity data collected at a SWFWMD station near the Peace River/Manasota Regional Water Supply Authority.

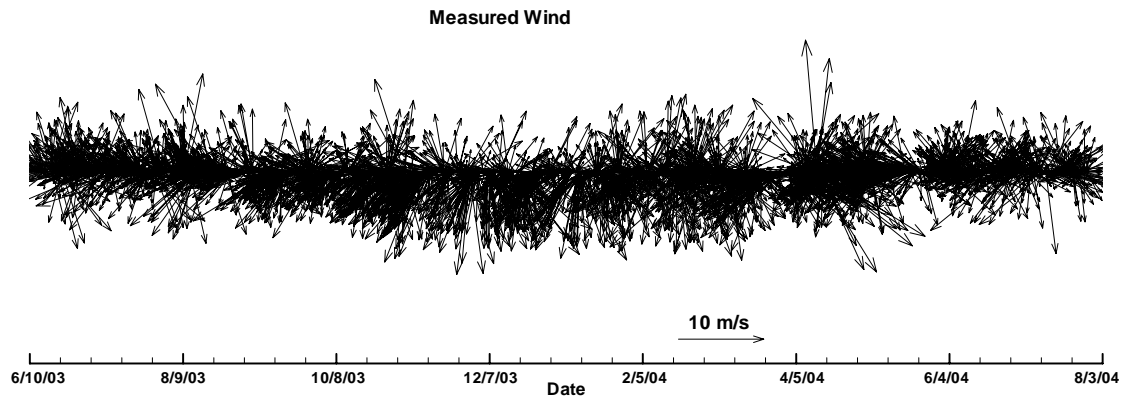


Figure 15 Measured wind at the UF station in the Upper Charlotte Harbor during June 2003 – July 2004.

Figure 15 shows vector plots of measured wind at the UF station in the UCH. The figure shows a quite dynamic wind pattern blowing over the UCH during the period from June 2003 to July 2004. It appears that there is not a dominant direction in which the wind would blow all the time or for a significant period of time; however, it does appear that the harbor often experienced either a northwest or a northeast wind during the 14 month period.

Measured solar radiation, relative air humidity, and air temperature collected at a SWFWMD station near the Peace River/Manasota Regional Water Supply Authority are plotted in Figure 16: the top graph is measured solar radiation in kilowatts per square meter (kw m^{-2}), the middle graph is the relative air humidity in percentage, and the bottom graph is the air temperature in degrees Celsius. All these meteorological parameters follow their general patterns for the southwest part of Florida, i.e.: summer is hotter and more humid with stronger solar radiation than winter.

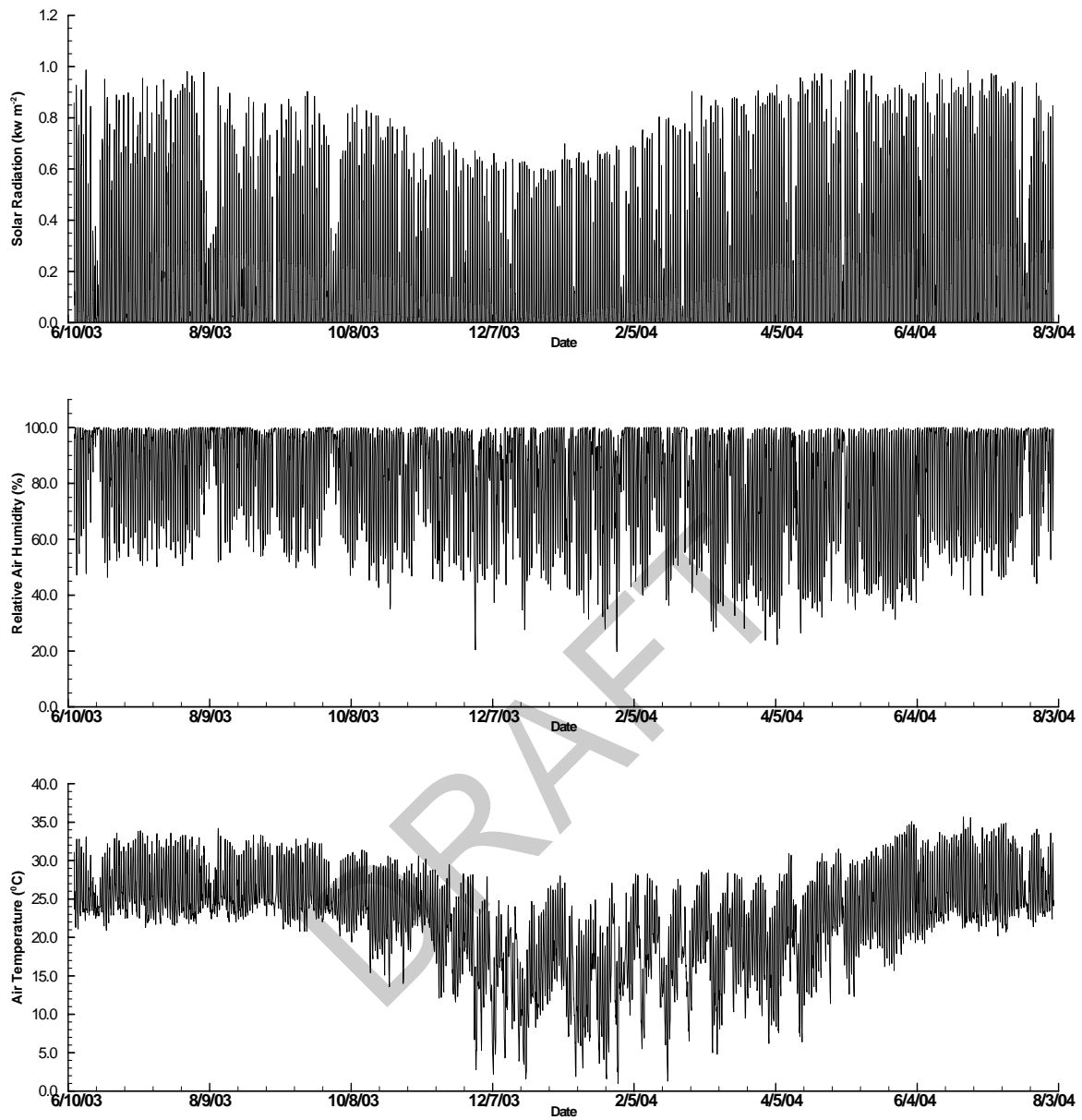


Figure 16 Measured solar radiation, relative air humidity, and air temperature a SWFWMD station near the Peace River/Manasota Regional Water Supply Authority.

4. Model Applications to the LPR - LMR - UCH System

The dynamically coupled model LESS was applied to simulate hydrodynamics in the LPR - LMR - UCH system in support of the determination of the regulatory minimum freshwater inflow rates for the LPR and the LMR. The 3D domain includes the entire upper Charlotte Harbor, the downstream 15.5 kilometers of the lower Peace River, the downstream 13.8 kilometers of the lower Myakka River, and the most downstream 1.74km portion of the Shell Creek. A Cartesian grid system was used to discretize the 3D simulation domain with 108 grids in the x -direction, 81 grids in the y -direction, and 13 layers in the z -direction. The grid size in the 3D domain varies from 100m to 500m in both the x - and y -directions, while the spacing varied between 0.3m and 1.0m in the vertical direction. The 2DV domain includes three main sub-domains: (1) the LPR from river-km 15.5 to Arcadia, (2) the LMR from river-km 13.8 to river-km 38.4, and (3) and the Shell Creek from river-km 1.74 to the dam. Also included in the 2DV domain were the downstream 4.16km of the Myakkahatchee Creek and major branches of the LPR and the Shell Creek. The 2DV domain was discretized with 356 longitudinal grids and 17 vertical layers. The longitudinal length for 2DV grids varied between 200m and 400m. To make the 3D-2DV coupling simple, the first 13 layers for the 2DV domain is set to be the same as the 13 layers used for the 3D domain. Table 2 lists the vertical spacing in both the 3D and 2DV domains. The layer number is counted from the bottom upward, with the first layer being the lowest layer. Also included in Table 2 are the elevations of the layer centers. The bottom of the first layer is located at the elevation of -6.766m. NGVD29. Basically, the first 10 layers discretize the water column below the NGVD29 datum, while Layers 11 and above discretize the water column above the NGVD29 datum. Because the vertical layers are fixed in space, many grid cells may not contain water all the times. Although these cells are included in the model, they are excluded in the computation.

Layer No.	DZ for 3D Domain (m)	DZ for 2DV Domain (m)	Layer Center Elevation (m, NGVD29)
17	0.8		3.434
16	0.8		3.034
15	0.7		2.284
14	0.6		1.634
13	0.5	0.5	1.084
12	0.4	0.4	0.634
11	0.3	0.3	0.284
10	0.3	0.3	-0.016
9	0.4	0.4	-0.366
8	0.6	0.6	-0.866
7	0.6	0.6	-1.466
6	0.8	0.8	-2.166
5	0.8	0.8	-2.966
4	0.8	0.8	-3.766
3	0.8	0.8	-4.566
2	0.8	0.8	-5.366
1	1.0	1.0	-6.266

Table 2. Layer thicknesses and layer center elevations for the 3D and 2DV domains.

The reason to have extra four layers for the 2DV domain is to allow the model to simulate major storm events when very high flows can cause the water surface in the narrow channel areas of the 2DV domain to have a significant rise. Another reason for have some extra layers for the 2DV domain is that the riverbed near the USGS Peace River at Arcadia station is more than 1m above the NGVD 29 datum, which is about 8km upstream of the tidal limit.

Figure 17 is the mesh of the LPR - LMR - UCH model, including model grids for both the 3D and 2DV domains. The red portion of the mesh represents land grids in the 3D domain, while the black portion represents water grids. Only water grids are included in the computation at each time step. Land grids are kept inactive and not included in the computation. As the water level rises, the shoreline also changes. As a result, some land grids may become water grids and will be treated as active grids in the computation at the new time step.

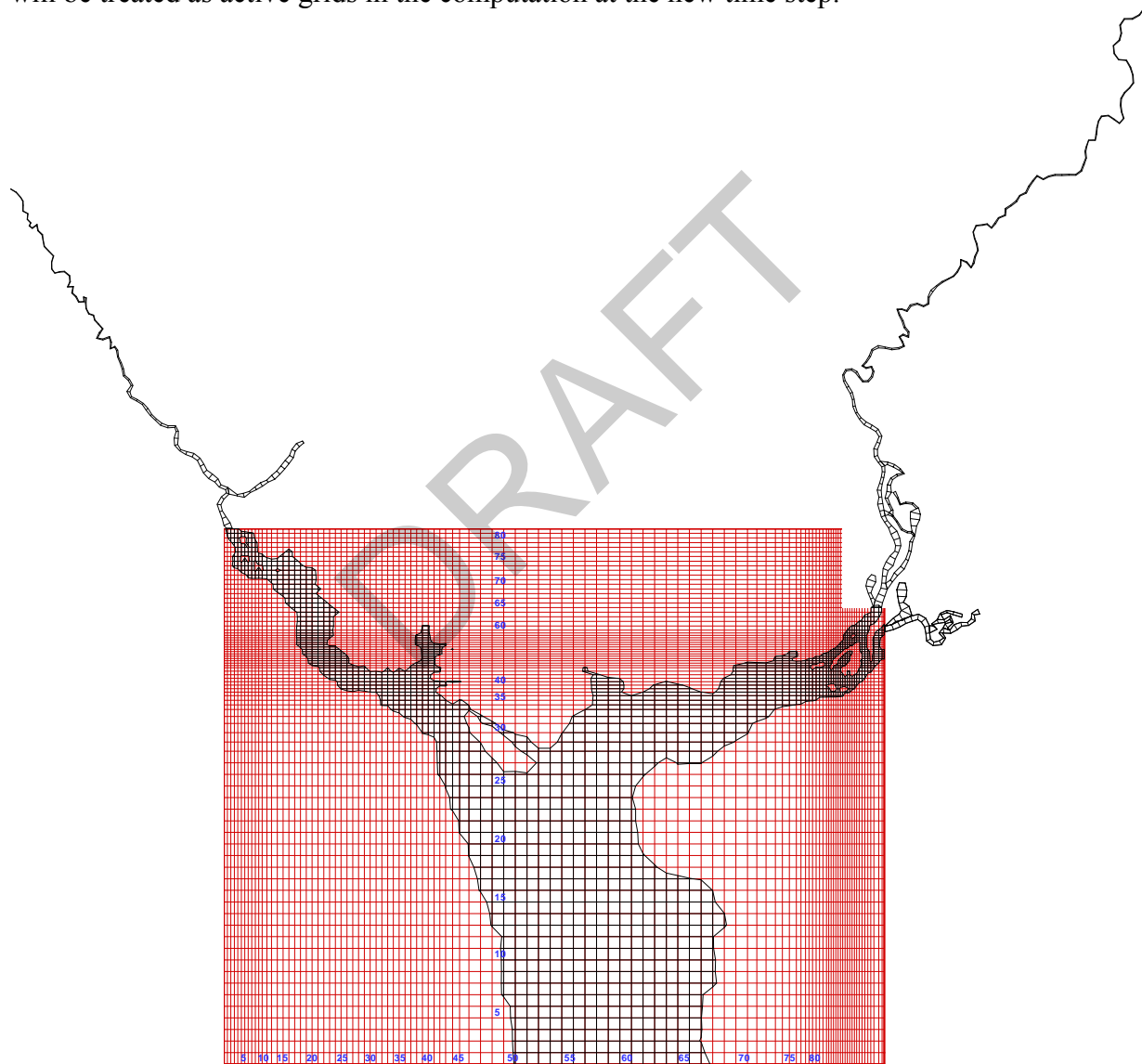


Figure 17 Model grids used in the LPR - LMR - UCH model. The red portion of the mesh represents land grids that are inactive in the computation in the 3D domain.

The model was used to simulate hydrodynamics in the complex LPR - LMR - UCH system for a period of 395 days from June 13, 2003 through July 12, 2004, with a variable time step between 90 and 180 seconds. The dynamically coupled 3D-2DV model was driven by boundary conditions specified at free surface (wind shear stresses and heat fluxes), at the open boundary at the southern side of the 3D domain, and at the upstream boundaries of the LPR, the LMR, and the Myakkahatchee and Shell Creeks of the 2DV domain. At the upstream boundaries of the 2DV domain, measured daily flow rates were uniformly distributed over the cross sections with zero salinity and zero temperature gradient in the longitudinal direction. At the open boundary on the southern side of the 3D domain, the boundary conditions were given using simulated results of water elevation, salinity and temperature by another hydrodynamic model (Sheng, et al., 2007) that covered the entire Charlotte Harbor and a coastal area almost 45km offshore into the Gulf of Mexico (Figure 18). Wind data measured at the UF station were used to calculate shear stresses at the free surface. The heat exchange with the atmosphere at the free surface was calculated based on measured solar radiation, wind, and air temperature data at the UF station and the SWFWMD station near the Peace River/Manasota Regional Water Supply Authority.

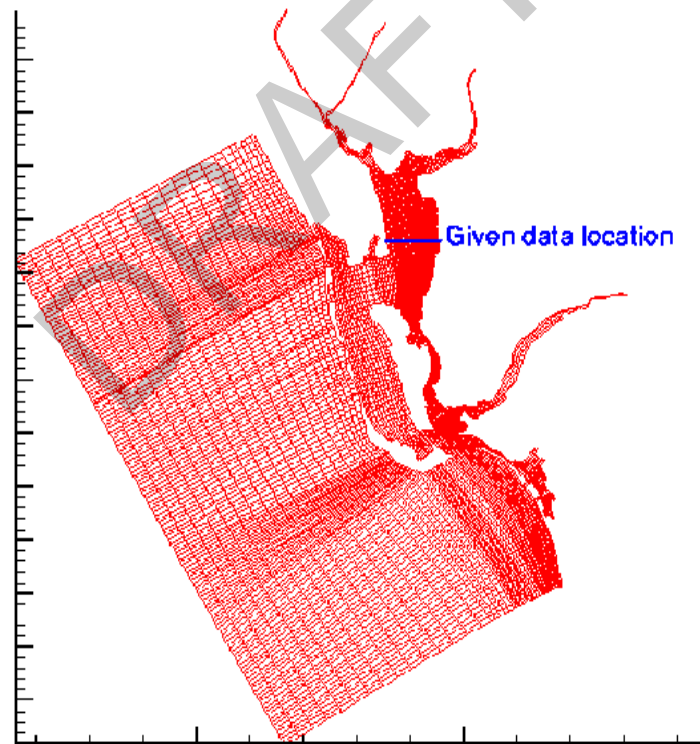


Figure 18 The boundary conditions at the southern boundary of the LPR - LMR - UCH model were provided by another hydrodynamic model by Sheng et al. (2005). The blue bar represents the southern boundary of the LPR - LMR - UCH model.

As mentioned above, because about 16% of the Peace River sub-basin and almost 50% of the Myakka River sub-basin are un-gauged, freshwater inflows from these un-gauged areas comprise a great deal of the total freshwater budget to the Charlotte Harbor and have significant

effects on salinity distributions in the LPR – LMR - UCH system. However, it is very challenging to obtain reasonable estimates of un-gauged flows from a very complex system such as the Peace - Myakka River watershed. Although the HSPF model (Bicknell et al., 1997) is a popular model that has been used in many areas of the country, including Florida, it can not guarantee good model results, especially when it is used as an interpolation tool for an area that is quite different from the gauged areas in terms of land-use and hydro-geological properties. Moreover, due to the unavailability of freshwater flow data to the tidal reaches, it is impossible to determine the severity of the errors and the confidence interval of the simulated un-gauged flows. The unknown errors in the estimated un-gauged flow will inevitably cause errors in model results of the coupled 3D-2DV model. Unfortunately, without a better way to estimate un-gauged flows, simulated results using the HSPF model by Ross et al. (2005) appeared to be the only choice available for a rough estimate of the freshwater contribution from the un-gauged areas of the watershed. During the calibration process of the model, it was found that the model under-predicted salinity during the wet months of the simulation period (see below), suggesting that un-gauged flows by Ross et al. (2005) could be over-estimated. As such, this study compared the HSPF results to those estimated by Janicki Environmental using a simple method developed by SDI Environmental Services (SWFWMD, 2007). It turned out that the estimated un-gauged flows using the SDI method are generally 50 – 60% lower than the HSPF results, except for the few peak flows in the first couple of months of the simulation period which are much higher than HSPF peak flows. Based on this comparison, the daily un-gauged flow values generated by the HSPF model were multiplied by constant coefficients (0.39 for the Peace, and 0.51 for the Myakka) to produce the final adjusted un-gauged flow values that were input to the coupled model.

Model Calibration and Verification

During the 13-month simulation period from June 13, 2003 to July 11, 2004, the first 30 days, from June 13m to July 12, were used for spinning up the LESS model because no initial conditions on June 13, 2003 were available. Considering the quality of available data and errors associated with the estimation of un-gauged flows during extreme conditions, a three-month period from January 10, 2004 to April 9, 2004 was chosen for model calibration. During the model calibration process, key model parameters (e.g., bottom roughness, background vertical eddy viscosity and diffusivity, various advection schemes, etc.) were adjusted to obtain the best fit between model results and measured data at the eight stations in the LPR - LMR - UCH system. Because the initial conditions for the calibration period were also unknown, a 30-day spin-up period was included in the model calibration. Therefore, the calibration run was actually performed for a four-month period from December 12, 2003 to April 9, 2004, with the model results during the first 30 days being excluded in calibrating the model. After the model was calibrated, it was verified against field data measured at the eight stations during a six-month period before the calibration period (July 12, 2003 – January 9, 2004) and a three-month period after the calibration period (April 19 – July 11, 2004).

Figures 19 and 20 are comparisons of simulated water levels with measured field data during the 91-day calibration period from January 10, 2004 to April 9, 2004. While Figure 19 compares at the four stations in the 3D domain (UF, Punta Gorda, El Jobean, and Harbor Heights), Figure 20 compares at the four stations in the 2DV domain (Peace River Heights, Shell Creek, North Port, and Snook Haven). Comparisons of simulated water levels to measured field

data at all eight stations during the two verification periods are shown in figures A-1 through A-6 in Appendix A. As can be seen from these figures, simulated water levels match with data very well, with the exception that the model under-predicts flooding at the Peace River Heights and the Snook Haven stations during extremely high flow events. The under-prediction of the water levels at these two stations is mainly due to the inaccurate bathymetric data for the flood plains of the upstream portions of the LPR and LMR. For the Peace River Heights station, it is also partially due to the datum problem mentioned in Section 2.

Figures 21 and 22 compare simulated u - and v -velocities with measured data at the UF station during the 91-day calibration period. Simulated u - and v -velocities during the two verification periods were plotted and compared with measured data in Figures B-1 through B-6 in Appendix B. For simplicity, comparisons were made only at three depths (second to fourth from the bottom), instead of all four depths, in the figures. The reason for this is that the spatial resolution ($500\text{m} \times 500\text{m}$) used near the UF station was quite coarse and the actual bottom elevation at the UF station can not be accurately represented in the model. Therefore, in Figures 21-22, "Near Bottom", "Middle Depth", and "Near Surface" are respectively the second, third, and fourth layers from the bottom in Figure 14. From Figures 21 – 22, as well as those shown in Appendix B, it is evident the model worked well in simulating currents in the harbor (at least near the UF station). Both the short-term (semi-diurnal) and long-term variations of the current in the x - and y -directions have been successfully simulated by the model.

Simulated salinities during the calibration period at all eight measurement station are also plotted against measured real-time data for comparison. Figures 23 – 26 are plots of simulated and measured salinities at UF, Punta Gorda, El Jobean, and Harbor Heights, respectively, while Figure 27 - 30 are those of simulated and measured salinities at Peace River Heights, Shell Creek, North Port, and Snook Haven, respectively. These plots suggest that the dynamically coupled model has been successfully calibrated against measured real-time salinities in the LPR - LMR - UCH system, except for the North Port station, where model under-predicted salinities at both the top and bottom layers during the calibration period. There are many factors that could cause the under-prediction of salinity at the North Port station, including the un-gauged flow from the Myakka River watershed, the Myakka River bathymetry data used in the model, flow estimated for Blackburn Canal, etc. A careful comparison of the bathymetric used in the model with those surveyed in the Myakka River showed that many deep areas in the river were not correctly represented in the model because of the use of model grids ranging from a $200\text{m} \times 100\text{m}$ resolution to a $200\text{m} \times 200\text{m}$ resolution in the Myakka River portion of the 3D sub-domain. Adjusting the bathymetry data in these areas by lowering the bottom elevations a bit, the simulated salinity results at the North Port station did show some degree of improvement. Although one can continue to adjust the bathymetry data to further improve simulated salinity results at North Port, one should only do it within a certain extent. This study decided to adjust the bathymetry data in the downstream portions of the Peace and Myakka Rivers only slightly to ensure that downstream water volumes of the two rivers have no obvious increases and important physical characteristics in the regions are preserved (e.g., islands are not noticeably shrunk or eliminated).

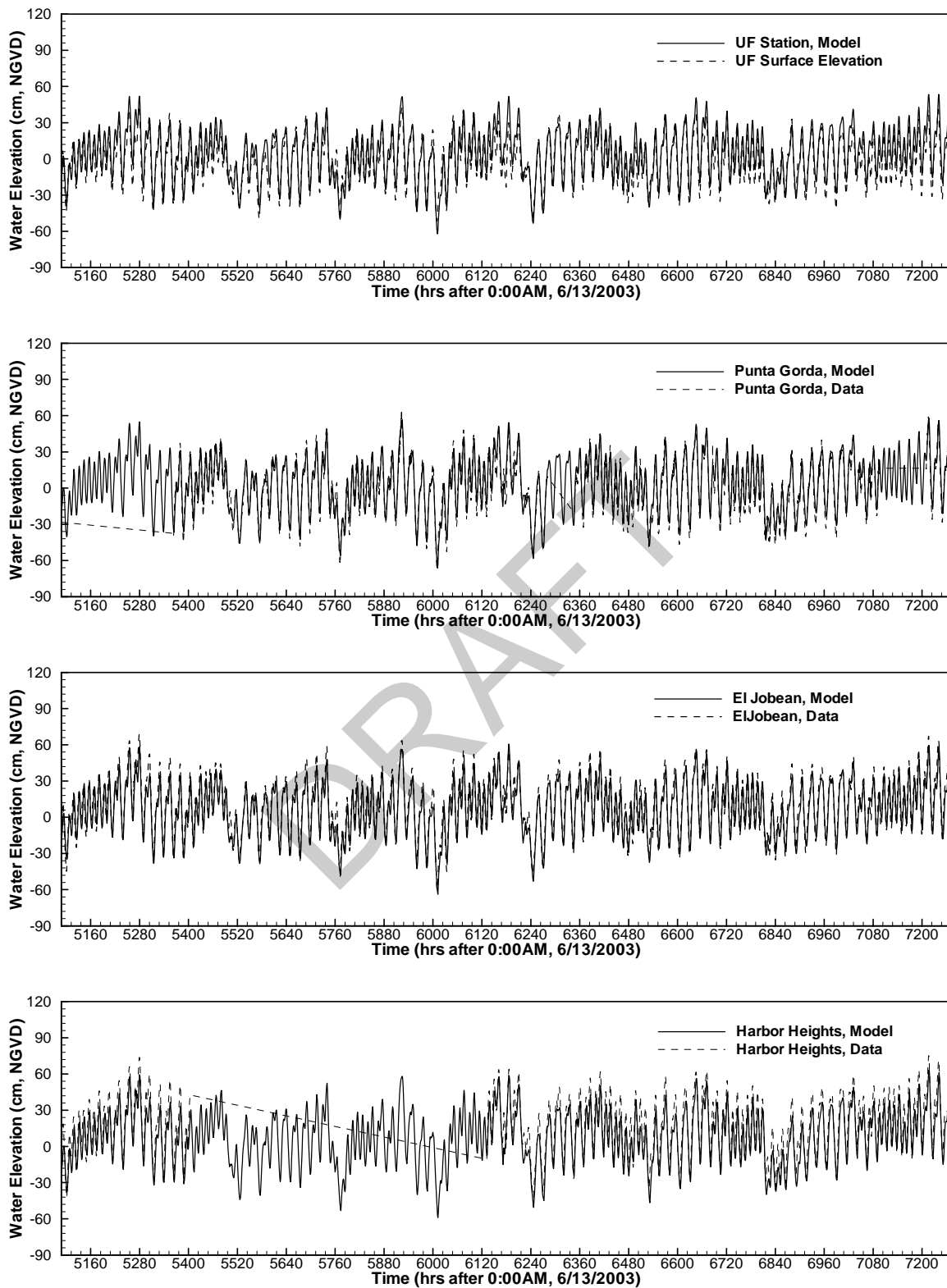


Figure 19 Comparisons of simulated and measured water elevations at UF, Punta Gorda, El Jobean, and Harbor Heights during January 10 – April 9, 2004.

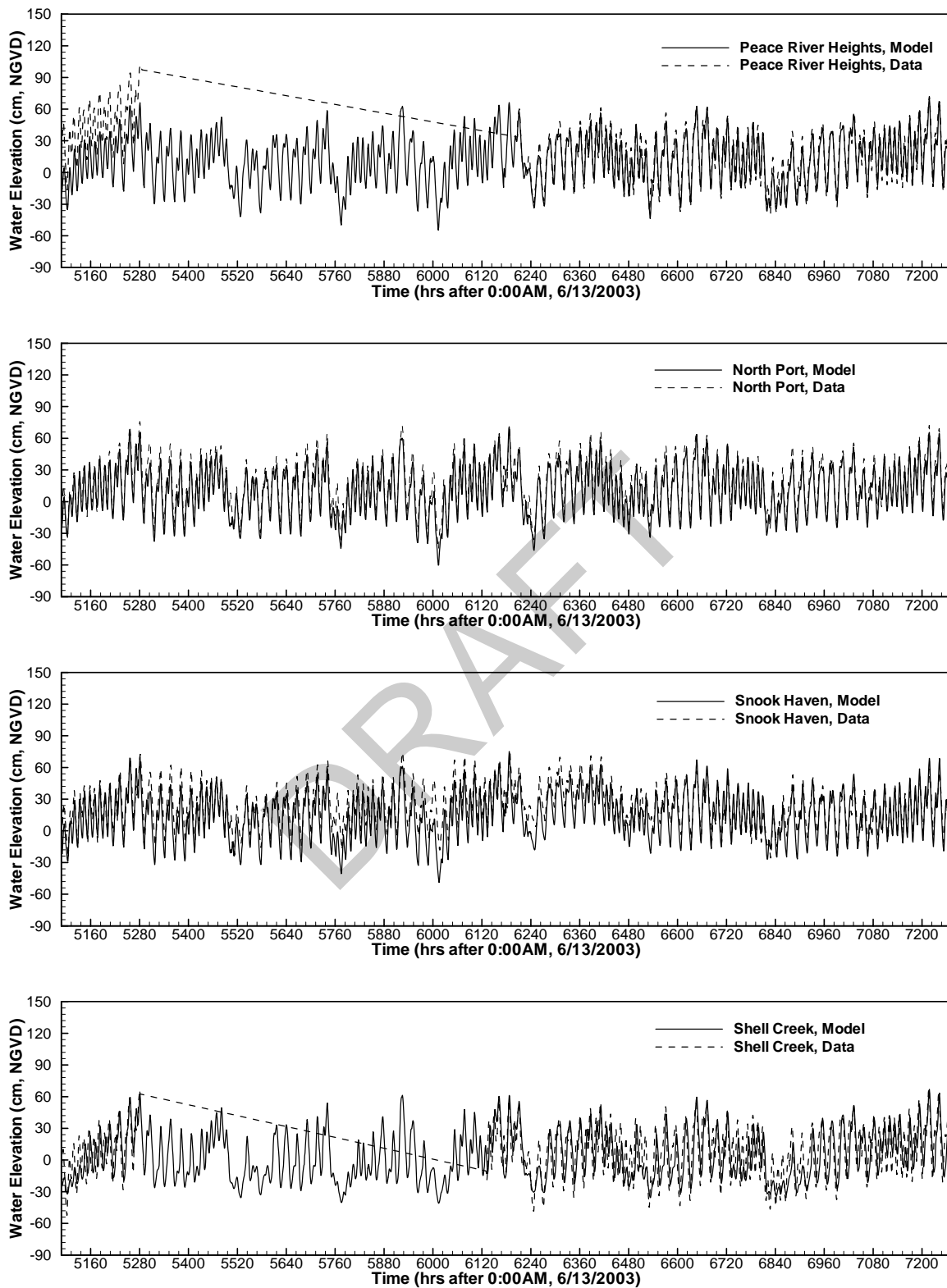


Figure 20 Comparisons of simulated and measured water elevations at Peace River Heights, North Port, Snook Haven, and Shell Creek during January 10 – April 9, 2004.

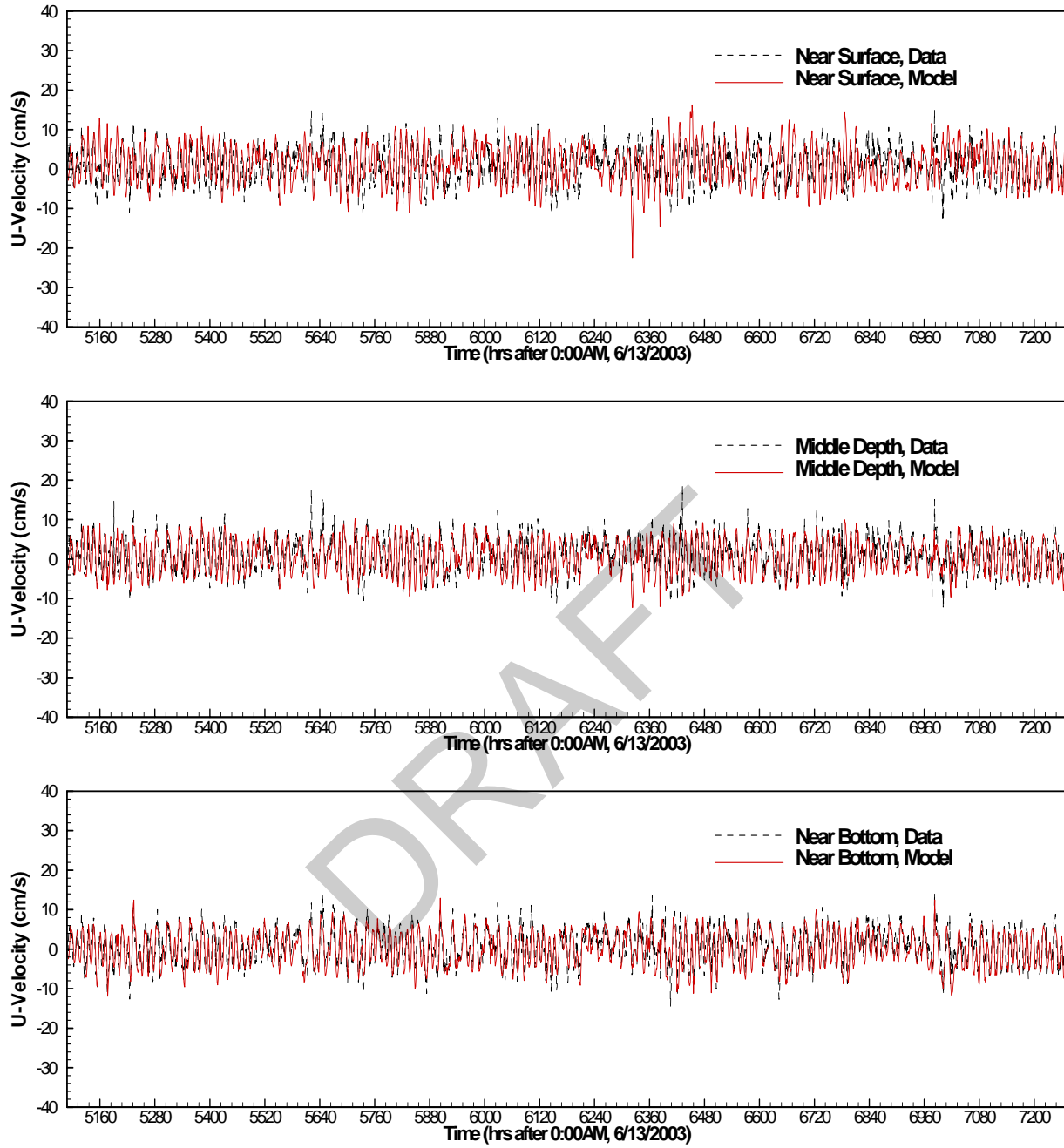


Figure 21 Comparisons of simulated and measured u-velocities at three depths at the UF station during January 10 – April 9, 2004.

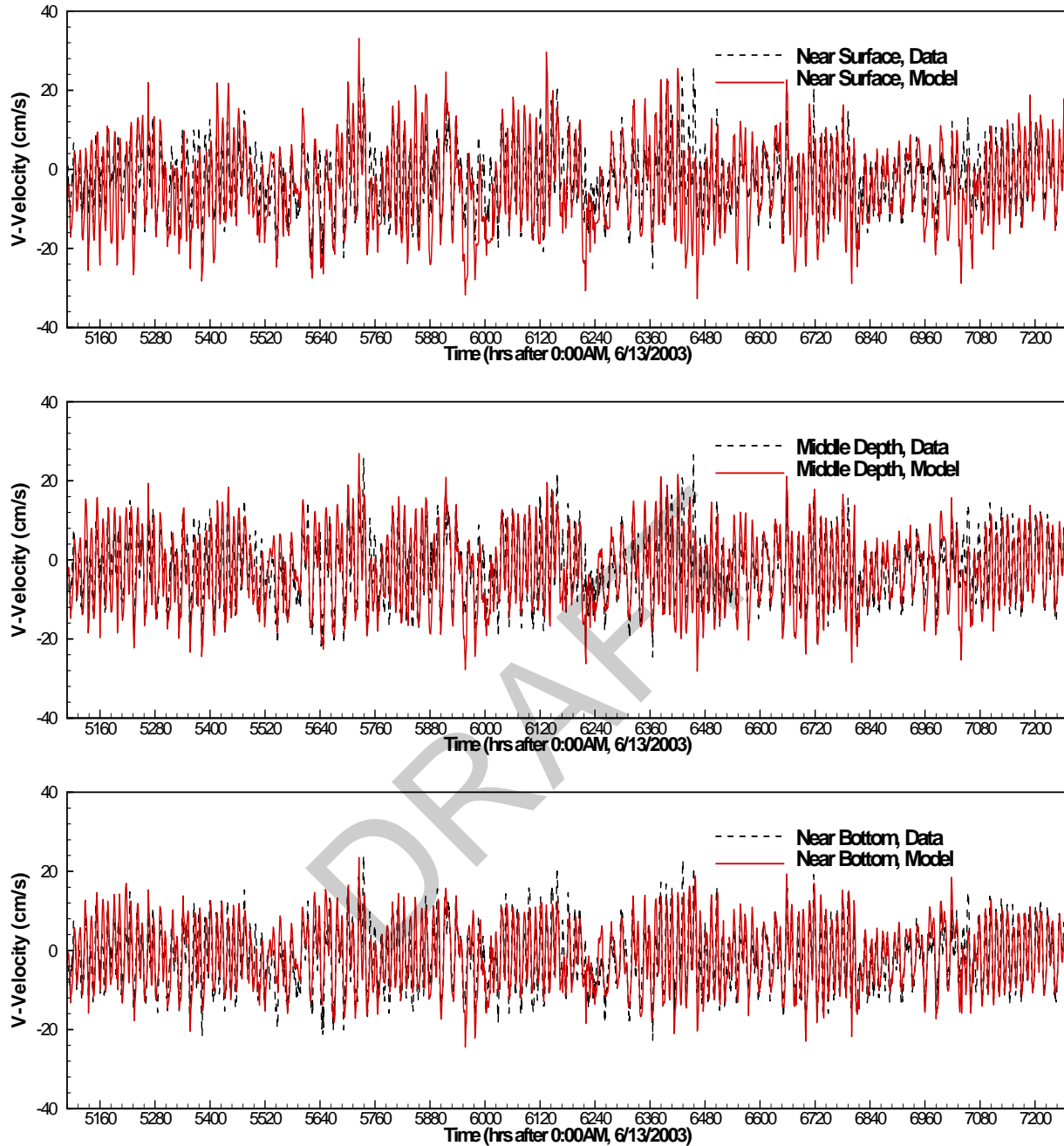


Figure 22 Comparisons of simulated and measured v-velocities at three depths at the UF station during January 10 – April 9, 2004.

Comparisons of model results and measured salinities at the eight stations for the two verification periods are presented in Figures C-1 through C-23 in Appendix C. Overall, the agreement between simulated and measured salinities at all eight stations in the LPR - LMR - UCH system is marginally. In the wet season before the calibration period, the coupled model generally under-predicts salinities; however, in the driest months after the calibration period, the model slightly over-predicts salinities. The best agreement between simulated and measured salinities occurred in last couple weeks of the second verification period when simulated

salinities in all eight stations match with data very well. Again, many factors could have caused the not-so-good agreement between simulated salinities and measured data, including the bathymetry data read to the model, un-gauged flow estimates, the boundary conditions provided by another model (Sheng et al., 2007).

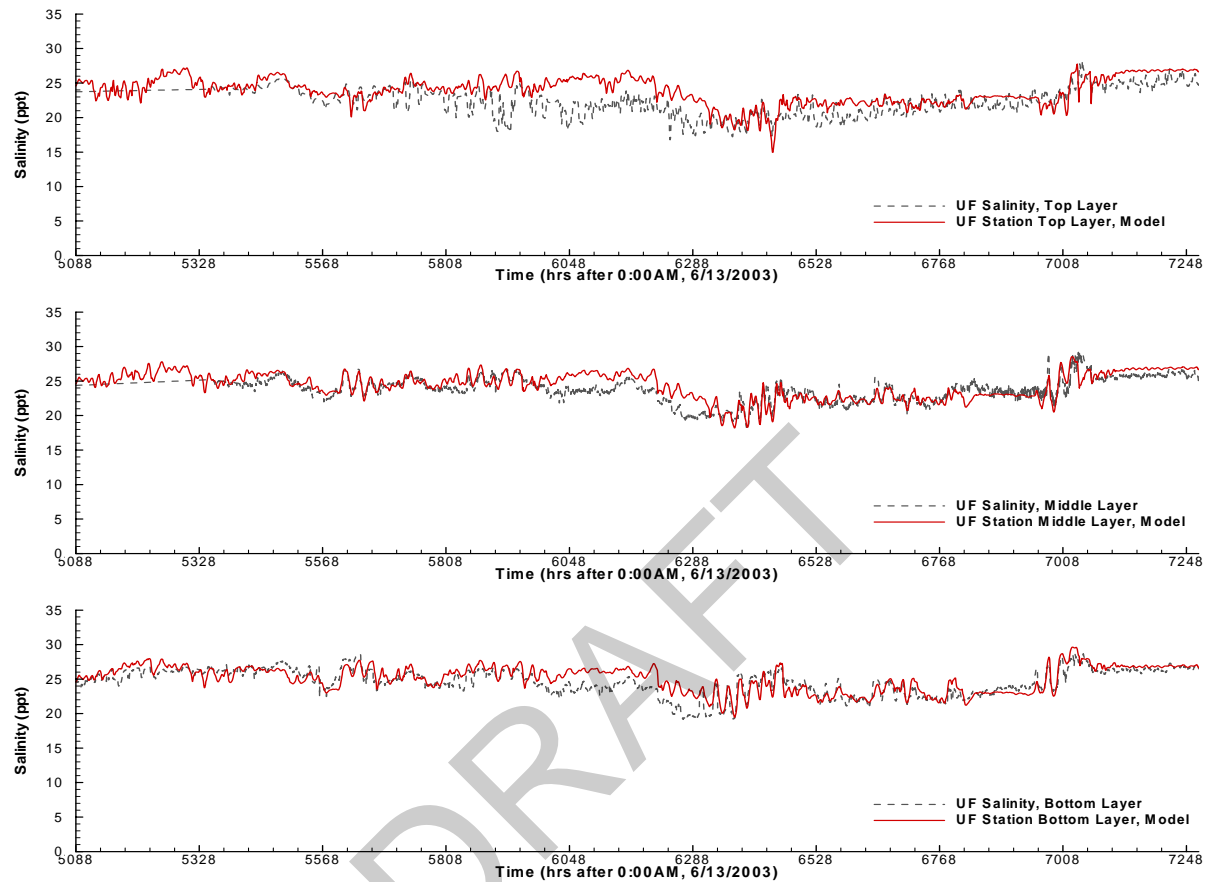


Figure 23 Comparisons of simulated and measured salinities at three depths at the UF station during January 10 – April 9, 2004.

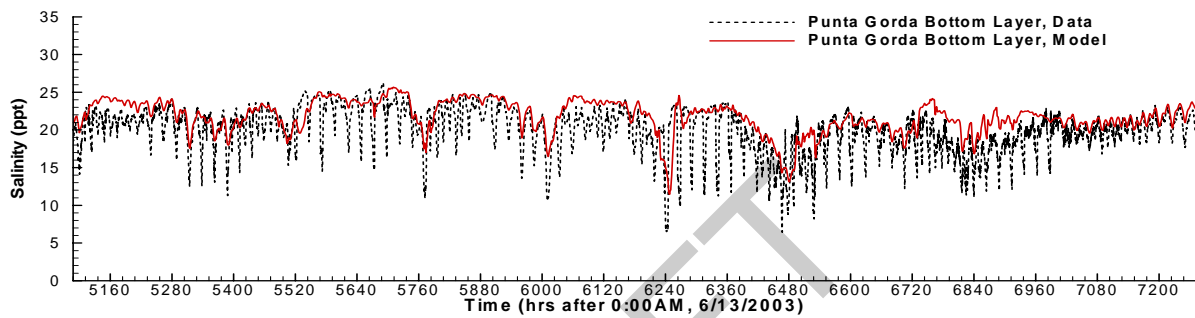
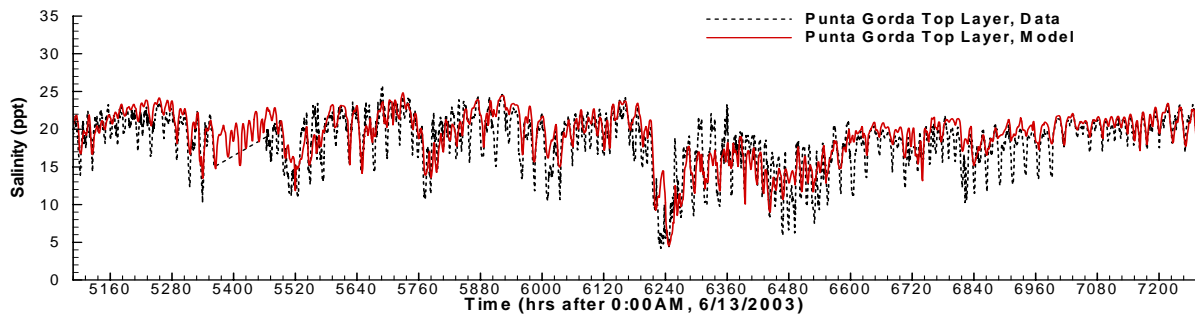


Figure 24 Comparisons of simulated and measured salinities at two depths at the Punta Gorda station during January 10 – April 9, 2004.

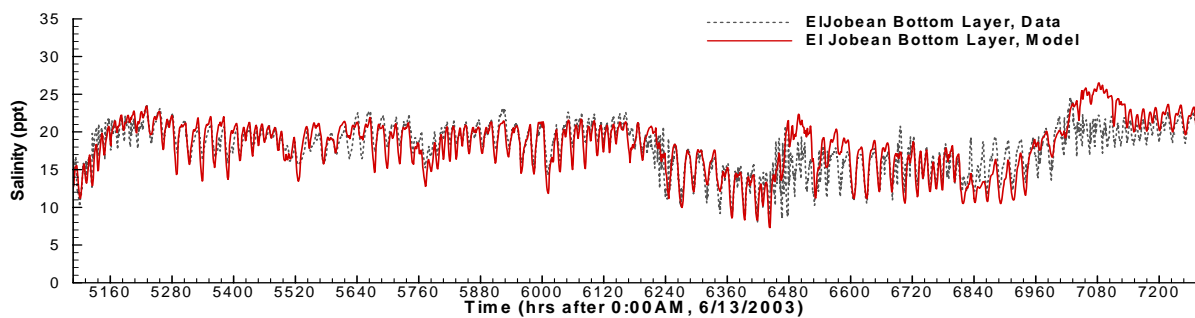
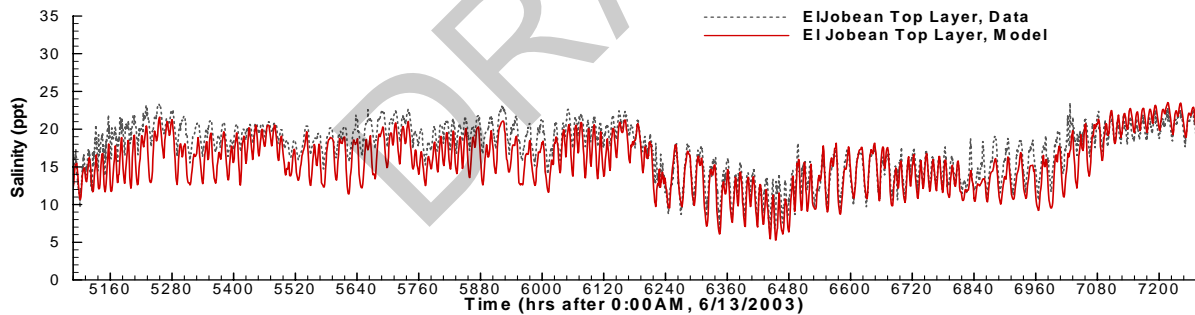


Figure 25 Comparisons of simulated and measured salinities at two depths at the El Jobean station during January 10 – April 9, 2004.

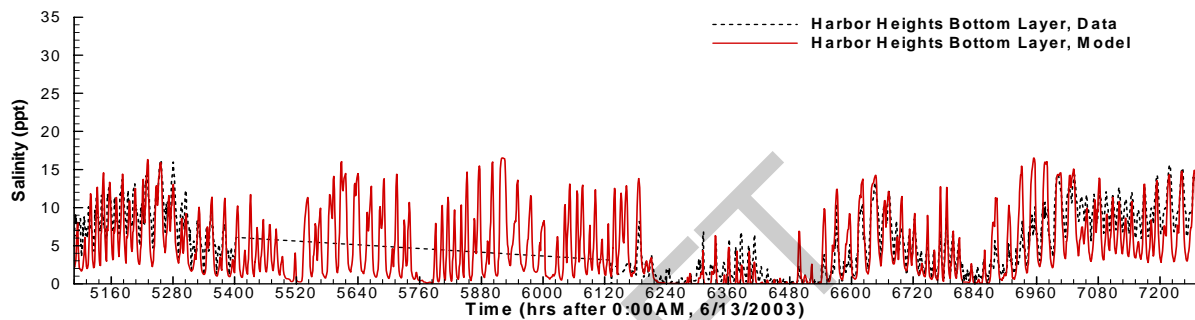
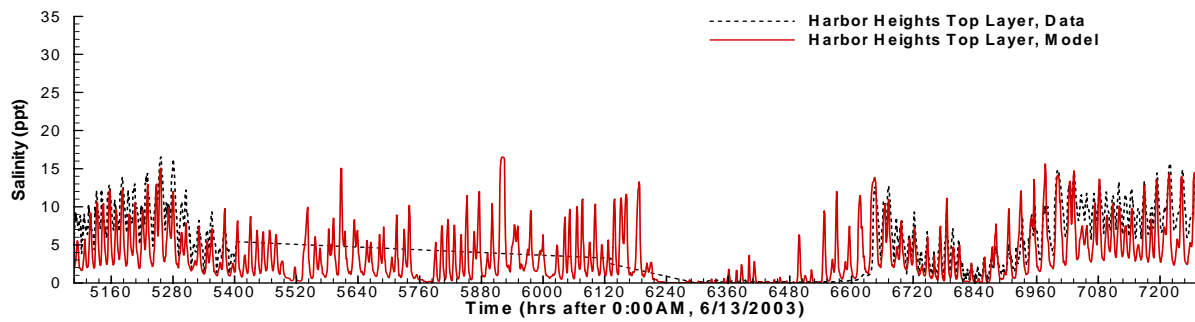


Figure 26 Comparisons of simulated and measured salinities at two depths at the Harbor Heights station during January 10 – April 9, 2004.

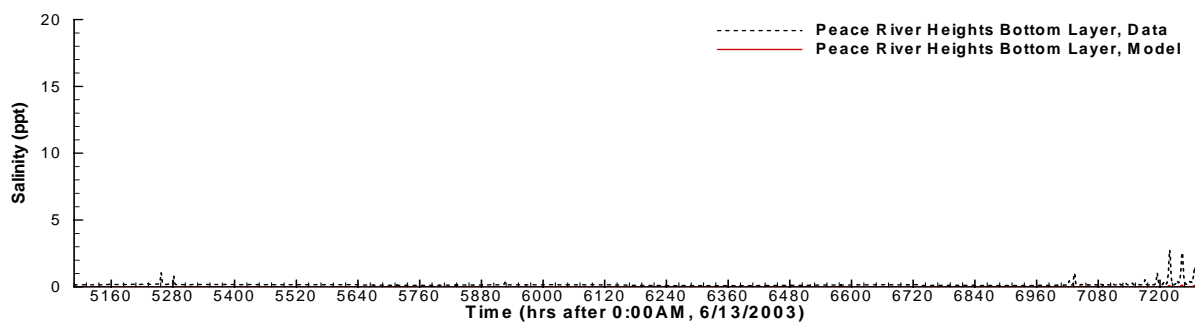
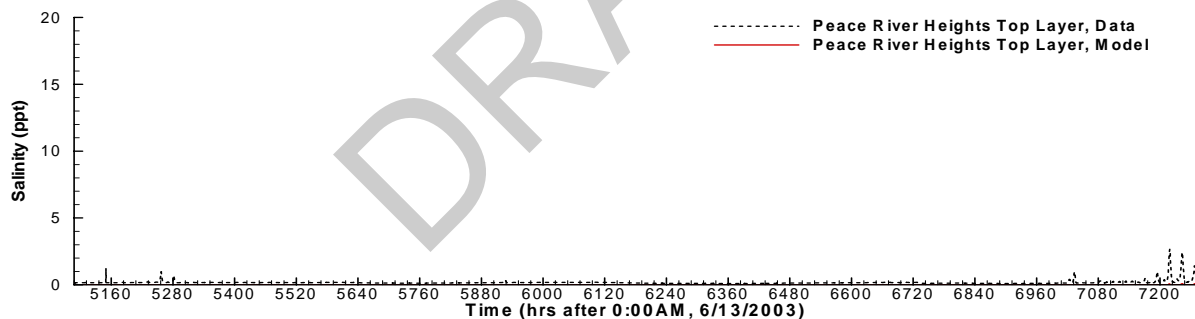


Figure 27 Comparisons of simulated and measured salinities at two depths at the Peace River Heights station during January 10 – April 9, 2004.

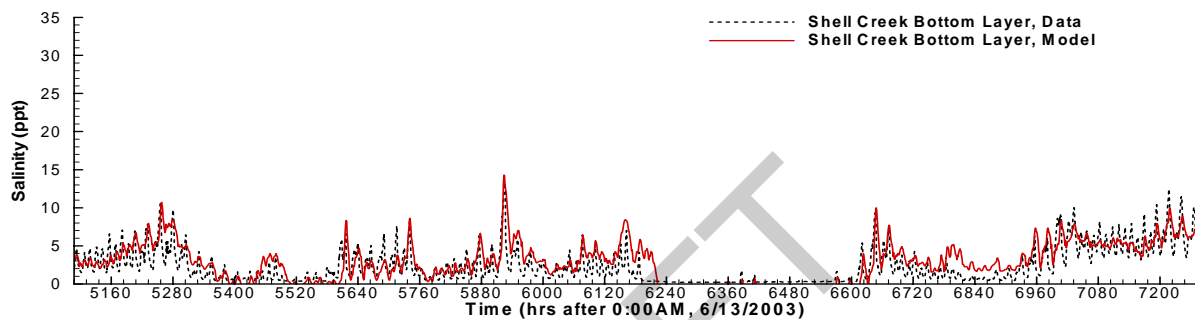
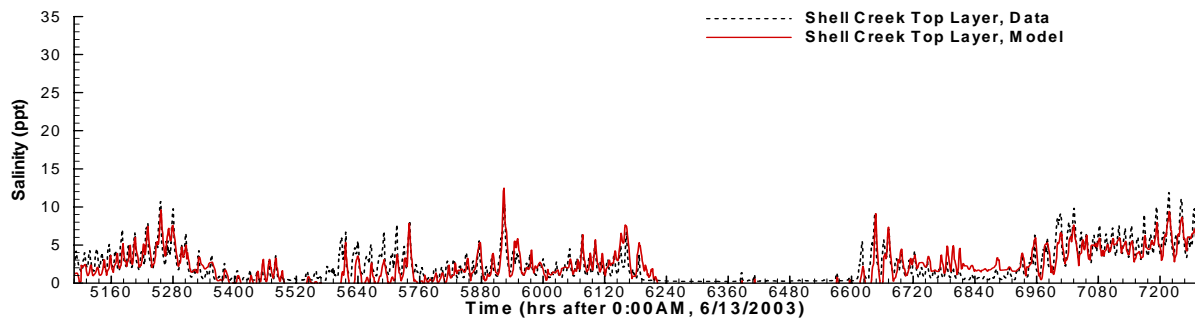


Figure 28 Comparisons of simulated and measured salinities at two depths at the Shell Creek station during January 10 – April 9, 2004.

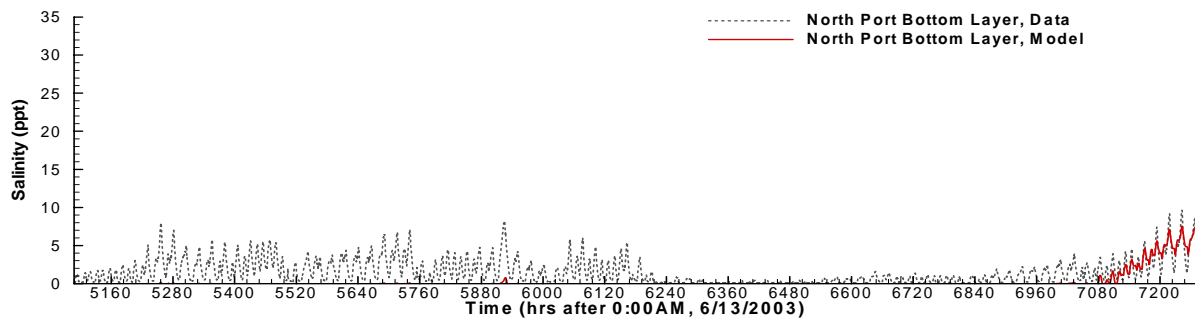
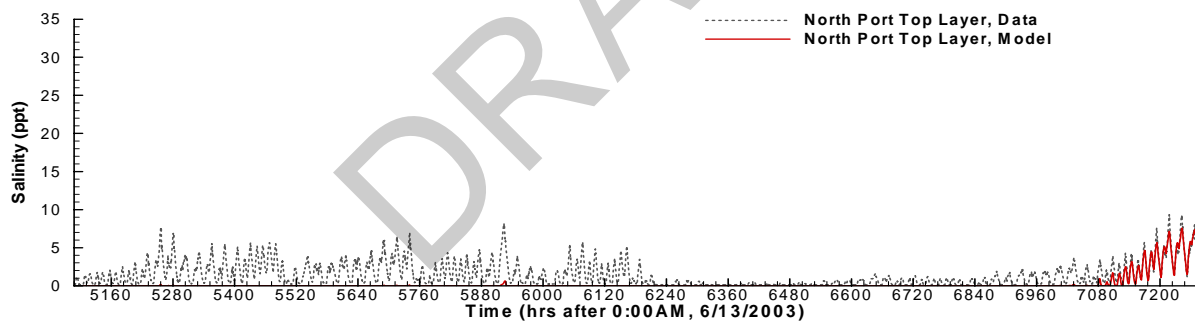


Figure 29 Comparisons of simulated and measured salinities at two depths at the North Port station during January 10 – April 9, 2004.

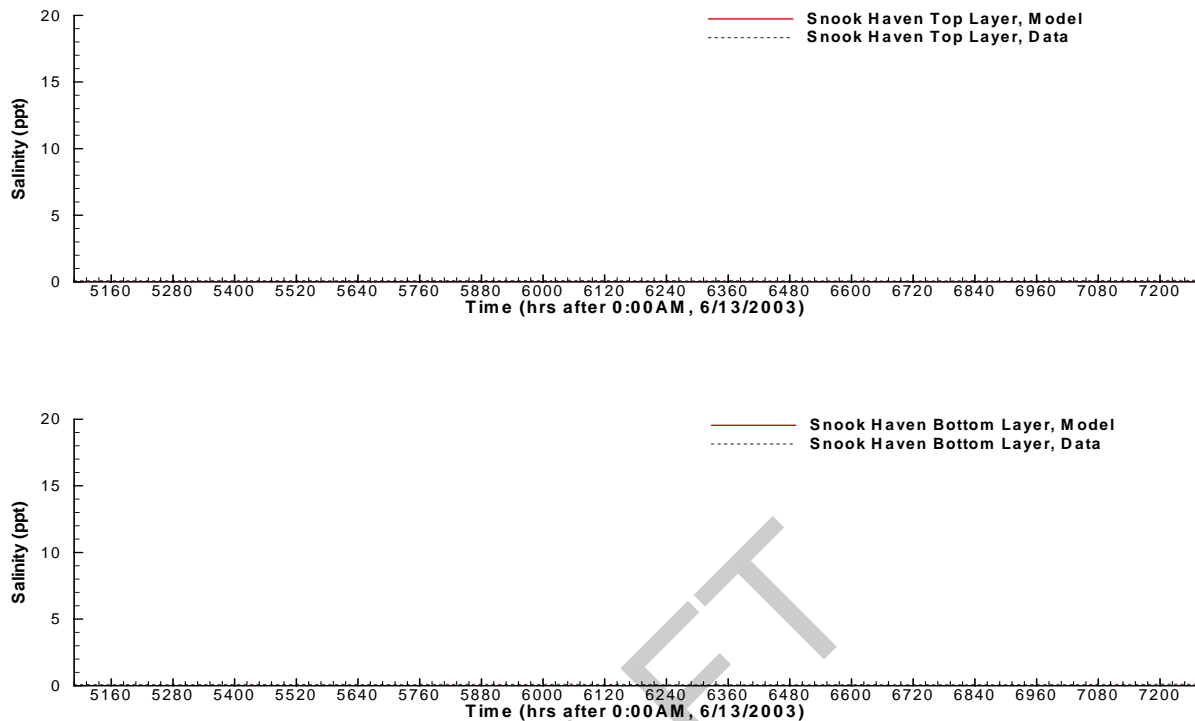


Figure 30 Comparisons of simulated and measured salinities at two depths at the Snook Haven station during January 10 – April 9, 2004.

Figure 31 – 35 are time series of simulated and measured temperatures during the calibration period at the UF, Punta Groda, El Jobean, Peace River Heghts, and Snook Haven stations. Because the purpose of this modeling study is to study effects of freshwater inflows on salinity distributions in the LPR and LMR in support of the establishments of the minimum freshwater flows for the two riverine estuaries, emphasis was placed on calibrating/verifying model results against measured salinity data instead of measured temperature data. Although no special effort was made to calibrate the model for temperature, Figures 31 - 35 illustrate that the agreement between simulated and measured temperatures in the LPR - LMR - UCH system is still good. For simplicity, only five stations during the calibration are included in this report. Comparisons of simulated and measured temperatures during the two verification periods and at the remaining three stations during the calibration period are omitted. As mentioned before, although measured temperature data in the simulation domain show large temporal variations, they exhibit only very small spatial variations. As a result, temperature has only minor effects on circulations and salt transport processes in the LPR - LMR - UCH system. Model runs confirmed that simulated water level, velocity, and salinity results are almost the same with or without including temperature in the simulations.

The dynamically coupled model LESS was used to estimate the estuarine residence time in the LPR system. By assuming an evenly distributed conservative tracer concentration of 10 mg L⁻¹ in the main stem of the LPR only, from Arcadia to its mouth, at time = 0, the model was run for 16 combined Arcadia – Joshua - Horse flow scenarios. Table 3 lists the 16 flow rates (Q) used in the ERT simulations, and they are sums of gauged USGS flows in the Joshua Creek, the Horse Creek, and the Peace River at the Arcadia station. These flow rates were partitioned among Arcadia, Joshua, and Horse according to their long-term averages. Their corresponding un-gauged flows for each un-gauged sub-basins used in the ERT runs were obtained using ratios of long-term averages of un-gauged flow estimates to that of the Arcadia flow. During the 16 model runs, the total mass of the conservative tracer remained in the LPR was calculated and book-kept at each time step. Time series of the remaining conservative tracer mass were analyzed. Figures D-1 through D-16 in Appendix D are plots of these time series. Time series of the percentage of the remaining conservative mass in the LPR are also shown in Figures D-1 through D-16. It is evident that strong tidal signals are contained in these time series. To filter out the tidal signals, trend lines in the form of exponential decade can be drawn to approximate the curves:

$$L = a \exp(-Kt) \quad (17)$$

where L is the percentage of the remaining conservative mass, a is a coefficient, K is the rate of the exponential decade in hour⁻¹, and t is time in hour. Parameters a and K for trend lines of the percentage remaining curves are listed in Table 3. As shown in the figures in Appendix D, all trend lines fit the percentage remaining curves well, with R^2 values being larger than 0.9. Some of the R^2 values are larger than 0.97.

No.	Q (cfs)	a	K
1	55	94.291	0.00119
2	106	95.316	0.00127
3	154	95.316	0.00136
4	199	86.390	0.00117
5	240	87.266	0.00256
6	281	71.633	0.00265
7	332	71.783	0.00247
8	391	83.899	0.00293
9	455	77.685	0.00301
10	544	108.858	0.00352
11	644	93.268	0.00379
12	939	78.729	0.00396
13	1443	95.558	0.00463
14	2256	63.996	0.00559
15	4036	66.788	0.00977
16	9340	100.238	0.01727

Table 3 Flow rates and values of a and K in Equation (17) for the 16 LPR ERT runs.

Equation (17) can be used to calculate the ERT for each of the flow scenarios with a given L :

$$t = -\frac{1}{K} \ln\left(\frac{L}{a}\right) \quad (18)$$

One may define ERT using different L values. For example, if the ERT is defined as the time when 95% of the conservative mass is flushed out of the system, then $L = 5$. Therefore, for different L values, one can obtain different ERTs for the same flow scenario. In the table below, ERT values (in days) were calculated for 16 flow rates using $L = 1, 2, 5, 10, 15, 20, 25, 30, 35$, and 36.79.

Q (cfs)	% Remaining L									
	1	2	5	10	15	20	25	30	35	36.79
55	159.32	135.03	102.92	78.63	64.42	54.34	46.52	40.13	34.73	32.98
106	149.75	126.97	96.86	74.09	60.76	51.31	43.98	37.99	32.92	31.28
154	139.93	118.65	90.51	69.23	56.78	47.94	41.09	35.49	30.76	29.23
199	158.25	133.65	101.13	76.53	62.14	51.93	44.01	37.54	32.07	30.30
240	72.62	61.36	46.47	35.20	28.62	23.94	20.31	17.35	14.85	14.04
281	67.21	56.31	41.89	30.98	24.60	20.08	16.56	13.70	11.27	10.48
332	72.24	60.52	45.03	33.32	26.46	21.60	17.83	14.75	12.14	11.30
391	63.04	53.17	40.13	30.27	24.50	20.40	17.23	14.63	12.44	11.73
455	60.35	50.74	38.04	28.43	22.80	18.81	15.72	13.19	11.06	10.36
544	55.60	47.38	36.52	28.30	23.49	20.08	17.44	15.28	13.45	12.86
644	49.84	42.22	32.15	24.54	20.08	16.92	14.47	12.46	10.77	10.22
939	45.96	38.66	29.02	21.72	17.45	14.43	12.08	10.16	8.53	8.01
1443	41.05	34.81	26.56	20.32	16.67	14.08	12.07	10.43	9.04	8.59
2256	30.99	25.82	19.00	13.83	10.81	8.67	7.00	5.65	4.50	4.12
4036	17.92	14.96	11.05	8.10	6.37	5.14	4.19	3.41	2.76	2.54
9340	11.11	9.44	7.23	5.56	4.58	3.89	3.35	2.91	2.54	2.42

Table 4 ERT values in days for 16 flow rates using 10 different L values ranging from 1 to 36.79.

From Table 4, one can find the relationship between ERT and Q for each L . These ERT- Q relationships are illustrated in Figures 31 – 33. For any L value, the ERT – Q relationship can be fitted to a power function:

$$ERT = bQ^n \quad (19)$$

where b is a coefficient and n is the exponent. The above equation has a R^2 value varying between 0.91 and 0.94. Furthermore, the coefficient b and the exponent n in the above equation are related to L , the percentage of remaining conservative mass, with the following functions (see Figure 34):

$$b = 1747.3 - 375.53 \ln(L) \quad (20)$$

$$n = -0.00088L - 0.54 \quad (21)$$

As can be seen from the R^2 values shown in Figure 34, the logarithm function in Equation (20) is a perfect fit to the b - L relationship with a R^2 of 1, while the linear relationship in Equation (21) also fit the n – L relationship very well with a R^2 of 0.987.

Replacing b and n in Equation (19) with the right hand sides of Equations (20) – (21), the final relationship among ERT, Q , and L is expressed as follows

$$ERT = [1747.3 - 375.53 \ln(L)] Q^{-(0.54 + 0.00088L)} \quad (22)$$

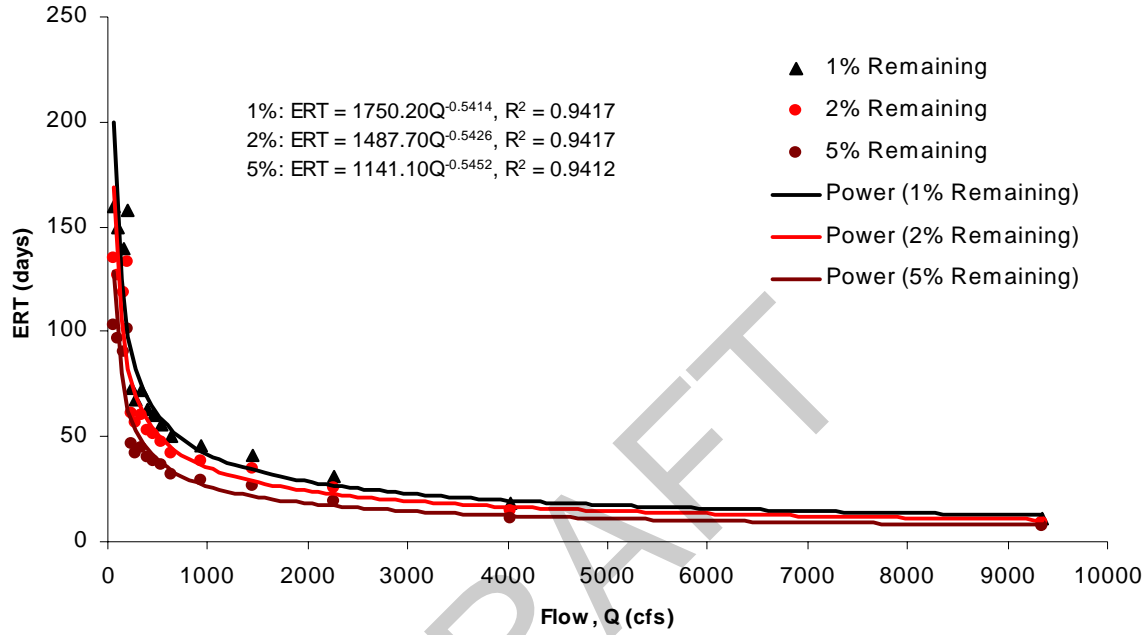


Figure 31 Relationships between ERT and Q for 1%, 2%, and 5% remaining of conservative mass in the LPR.

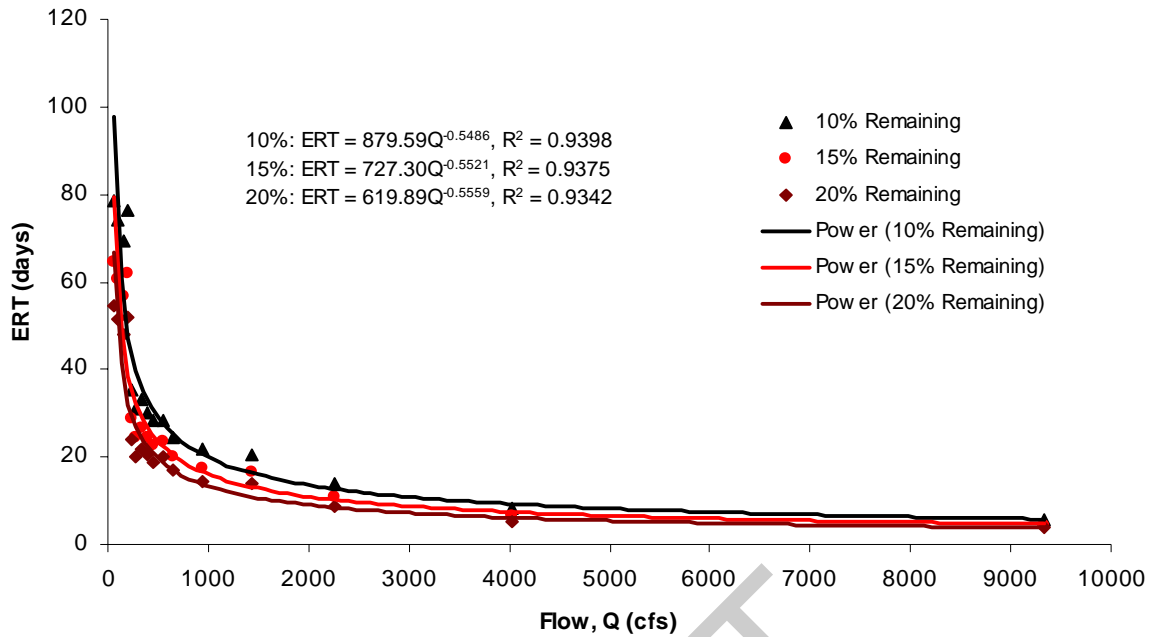


Figure 32 Relationships between ERT and Q for 10%, 15%, and 20% remaining of conservative mass in the LPR.

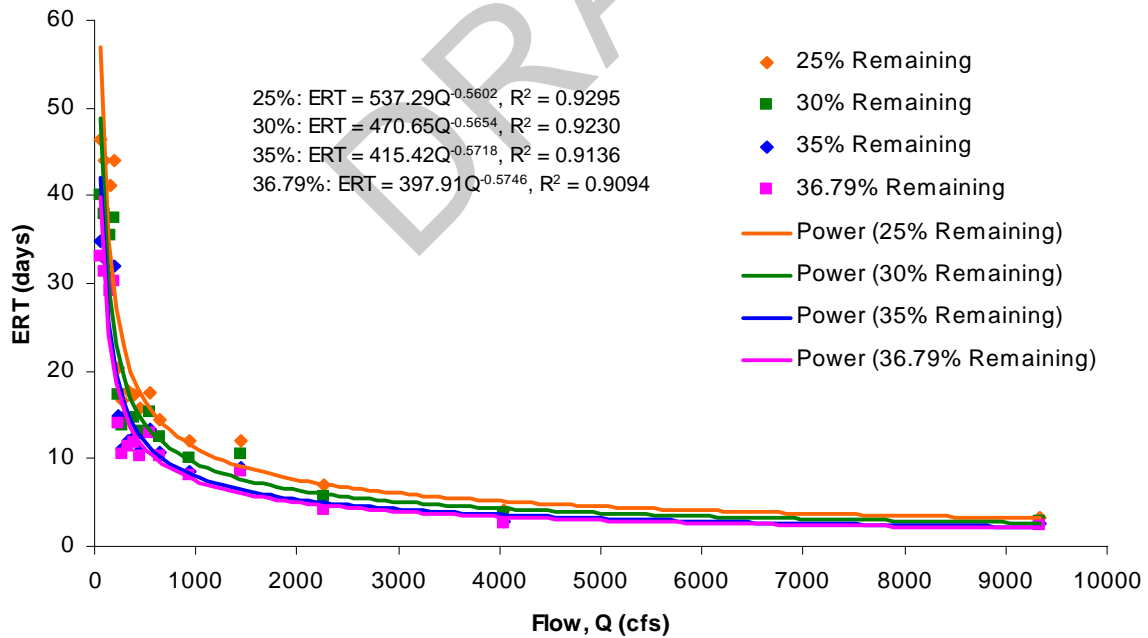


Figure 33 Relationships between ERT and Q for 25%, 30%, 35%, and 36.79% remaining of conservative mass in the LPR.

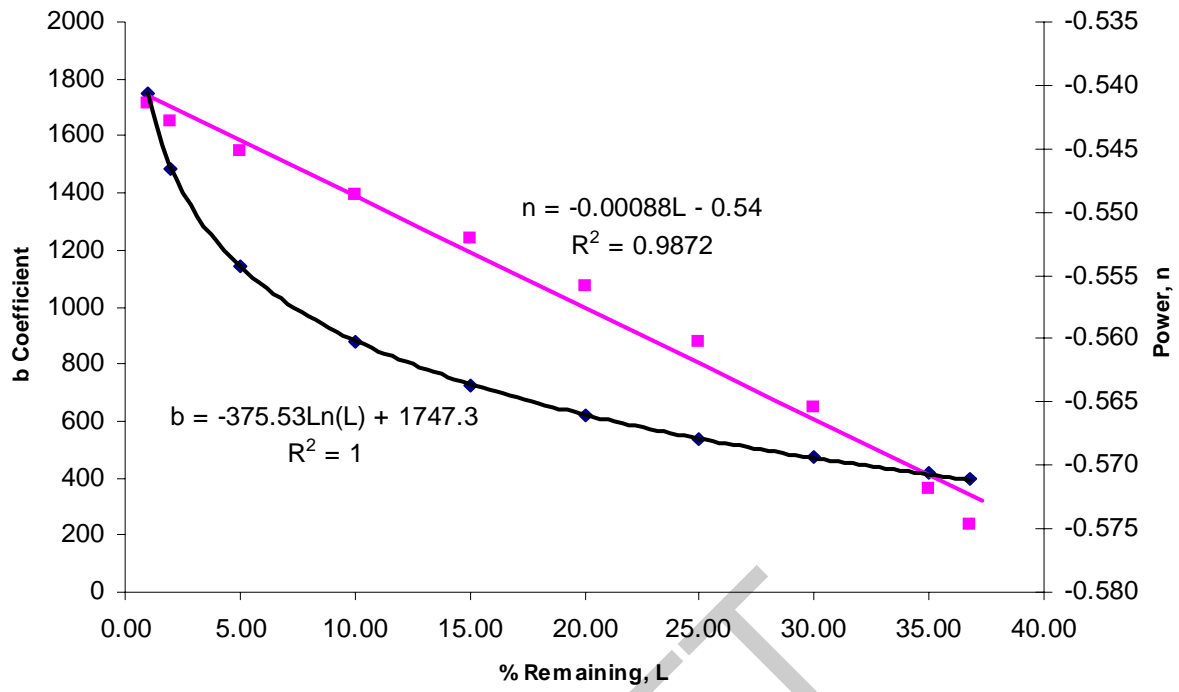


Figure 34 Relationship between b and L and relationship between n and L .

5. Conclusions

The purpose of this modeling study is to support the determinations of minimum freshwater inflows to the LPR and LMR to prevent the two riverine estuaries from significant harm. Because of the interactions among the LPR, the LMR, and the UCH, it is logical to develop a hydrodynamic model that includes all three water bodies. To efficiently deal with the complex geometry of the LPR – LMR - UCH system, this study developed a dynamically coupled 3D-2DV model by coupling a 3D model (LESS3D) with a 2DV model (LAMFE), so that both the large downstream water body and the narrow upstream tributaries can be simulated with the same degree of resolution. The dynamically coupling of the two models is facilitated with a free-surface correction (FSC) method that is unconditionally stable with respect to gravity waves, wind and bottom shear stresses, and vertical eddy viscosity terms. The use of the FSC method allows a simultaneous solution of the free-surface elevation in both the 3D sub-domain and the 2DV sub-domain, and thus avoids any problems associated with the internal boundary. The coupled model solves laterally averaged RANS equations for the narrow open channel. For the larger water body, it solves 3D RANS equations. This kind of a coupled model is especially desirable when the narrow open channel has a large flood plain that can be submerged during a major storm event.

To apply the coupled model to the LPR - LMR - UCH system, various field data were obtained, analyzed, and graphed to evaluate their quality and availabilities and to obtain a preliminary assessment of physical characteristics of LPR - LMR - UCH system, including freshwater inflows, rainfall, tides, salinity and temperature distributions, wind patterns, etc. Overall, the quality and availabilities of field data in the LPR - LMR - UCH system are found to be marginal with many missing data periods. One important missing piece of data is un-gauged flows, which were first estimated with the HSPF model and the adjusted based on a comparison to results generated by Janicki Environment, Inc. using the SDI method (SWFWMD, 2007).

The dynamically coupled 3D-2DV model was applied to the LPR - LMR - UCH system to simulate hydrodynamics and salinity and temperature transport processes in the three interconnected water bodies. The 3D domain includes the upper Charlotte Harbor, the downstream 1.74km of the Shell Creek, the downstream 15.5km of the LPR, and the downstream 13.8km of the LMR. The 2DV domain includes the LPR from river-km 15.5 to Arcadia, the LMR from river-km 13.8 to river-km 38.4, the Shell Creek from river-km 1.74 to the dam, and the downstream 4.16km of Myakkahatchee Creek. Model simulations were conducted for a 13-month period from June 13, 2003 to July 11, 2004, of which the first 30 days (June 13 – July 11, 2003) were used for the model spin-up run. The model was calibrated against measured water levels, currents, salinities, and temperatures at a total of eight stations in the LPR - LMR - UCH system (current data are only available at one station) during a 3-month period of January 10 – April 9, 2004. It was then verified against field data measured at the same eight stations during a 6-month period before the calibration period and a 3-month period after the calibration period. Gauged freshwater flows were used for upstream boundary conditions, while adjusted un-gauged flow estimates were added to the top cells of the model at their corresponding locations. The downstream boundary conditions on the southern border of the 3D domain were specified with simulation results of another hydrodynamic model (Sheng, et al., 2005).

Although there are many uncertainties in the input data used to drive the LESS model, including measured data, un-gauged flows, boundary conditions provided by the other hydrodynamic model (Sheng et al., 2007), the dynamically coupled model was successfully

calibrated to measured real-time data of water levels, currents, salinities, and temperatures at eight stations during January 10 – April 9, 2004, except for salinity at the North Port station. During the two verification periods before and after the calibration period, the model generally works well in predicting water levels, velocities, and temperatures, but under-predicts salinities in wet months and slightly over-predicts salinities in the driest months.

The dynamically coupled model LESS was used to evaluate estuarine residence times for 16 flow scenarios for the LPR. It was found that the estuarine residence time in the LPR is related to the combined flow of Arcadia, Joshua, and Horse through a power function. Based on an analysis of estimated ERT values for 16 flow scenarios, it was found that the power function takes the form of $ERT = [1747.3 - 375.53 \ln(L)]Q^{-(0.54 + 0.00088L)}$, where L is the percentage of conservative mass remains in the estuary after ERT days and Q is the sum of gauged USGS flows in the Joshua Creek, the Horse Creek, and the Peace River at the Arcadia station. If the ERT is defined as the time when 95% of conservative mass is flushed out of the estuary, then $L = 5$ and $ERT = 1142.91Q^{-0.5444}$.

DRAFT

6. References

- Bicknell, B.R., Imhoff, J.C., Kittle, J.L. Jr., Donigian, A.S. Jr. and Johanson R.C., 1997. Hydrological Simulation Program-FORTRAN, User's Manual for Version 11. EPA/600/SR-97/080. U.S. Environmental Protection Agency, National Exposure Research Laboratory, Research Triangle Park, NC 27711.
- Chen, X. and M.S. Flannery. 1997. Use of a Hydrodynamic Model for Establishing a Minimum Freshwater Flow to the Lower Hillsborough River. In (M. L. Spaulding and A. F. Blumberg, eds.) Estuarine and Coastal Modeling (V), Proceedings of the 5th International Conference, ASCE, pp. 663-678.
- Chen, X. 1999. Three-Dimensional, Hydrostatic and Non-Hydrostatic Modeling of Seiching in a Rectangular Basin. In (M. L. Spaulding and H. L. Butler, eds.) Estuarine and Coastal Modeling (VI), Proceedings of the 6th International Conference, ASCE, pp. 148-161.
- Chen, X., M.S. Flannery, and D.L. Moore. 2000. Salinity Response to the Change of the Upstream Freshwater Flow in the Lower Hillsborough River, Florida. *Estuaries*, 23: 735-742.
- Chen, X. 2003a. An efficient finite difference scheme for simulating hydrodynamics in narrow rivers and estuaries. *International Journal for Numerical Methods in Fluids*. 42: 233-247.
- Chen, X. 2003b. A Free-Surface Correction Method for Simulating Shallow Water Flows. *Journal of Computational Physics*, 189:557-578.
- Chen, X. 2003c, Coupling a 3D model with a 2DV model using a free-surface correction method, In (M. L. Spaulding, ed.) Estuarine and Coastal Modeling (IIX), Proceedings of the 8th International Conference, ASCE, pp. 769 - 783.
- Chen, X. 2004a. Using a piecewise linear bottom to fit the bed variation in a laterally averaged, z-co-ordinate hydrodynamic model. *International Journal for Numerical Methods in Fluids*. 44: 1185-1205.
- Chen, X. 2004b. A Cartesian method for fitting the bathymetry and tracking the dynamic position of the shoreline in a three-dimensional, hydrodynamic model. *Journal of Computational Physics*, 200: 749 - 768.
- Chen, X. 2005. Using a Dynamically Coupled 3D-2DV Model to Simulate Hydrodynamics in the Lower Peace River – Upper Charlotte harbor System in Southwest Florida, In (M.L. Spaulding, ed.) Estuarine and Coastal Modeling (V), Proceedings of the 9th International Conference, ASCE, pp. 72 - 87.
- Chen, X. 2007a. Dynamic coupling of a three-dimensional hydrodynamic model with a laterally averaged, two-dimensional hydrodynamic model. In production, *Journal of Geophysical Research*.
- Chen, X. 2007b. Simulations of Minimum Flow Scenarios for the Lower Myakka River Estuary Using a Dynamically Coupled 3D-2DV Model. Technical Report. Southwest Florida Water Management District, Tampa, Fla.
- Sucsy P.V., F.W. Morris, M.J. Bergman, and L.J. Donnangelo. 1997. A 3-D Model of Florida's Sebastian River Estuary, In (M. L. Spaulding and A. F. Blumberg, eds.) Estuarine and Coastal Modeling (V), Proceedings of the 5th International Conference, ASCE, pp. 59 - 74.
- Johnson, B.H. K.W. Kim, R. Heath, B. Hsieh, and L. Butler. 1991. Validation of a Three-Dimensional Hydrodynamic Model of Chesapeake Bay, *Journal of Hydraulic Engineering*, 117 (1): 2 – 20.

- Mendelsohn, D.L., S. Peene, E. Yassuda, and S. Davie, 1999. A Hydrodynamic Model Calibration Study of the Savannah River Estuary with an Examination of Factors Affecting Salinity Intrusion, In (M. L. Spaulding and L. Butler, eds.) Estuarine and Coastal Modeling (VI), Proceedings of the 6th International Conference, ASCE, pp. 663-685.
- Ross, M.A., A. Said, K. Trout, and J. Zhang, 2005. Hydrologic Modeling of Streamflow from Ungaged Areas in the Upper Charlotte Harbor Basin – Phase 2, Prepared for the Southwest Florida Water Management District. Department of Civil and Environmental Engineering, University of South Florida, Tampa, Florida.
- Sheng, Y.P., T. Kim, and S. Schofield, 2007. Hydrodynamic Modeling of Charlotte Harbor in Support of the Determination of Minimum Flows for the Lower Peace and Myakka Rivers. Prepared for the Southwest Florida Water Management District. Civil & Coastal Engineering Department, University of Florida, Gainesville, Florida.
- SWFWMD, 2001. Peace River Comprehensive Management Plan, Volume I (Draft), Southwest Florida Water Management District Brooksville, Fla.
- SWFWMD, 2007. MFL Report for the Lower Peace River MFL. Southwest Florida Water Management District, Brooksville, Fla.
- Van der Vorst, H.A.. 1992. Bi-CGSTAB: A fast and smoothly converging variant of Bi-CG for solution of non-symmetric linear systems, SIAM J. Sci. Statist. Comput. 13: 631-644.
- UNESCO (1983), Algorithms for computation of fundamental properties of seawater, UNESCO Technical Papers in Marine Science, Number 44, 53 pp., Paris.

Appendix A

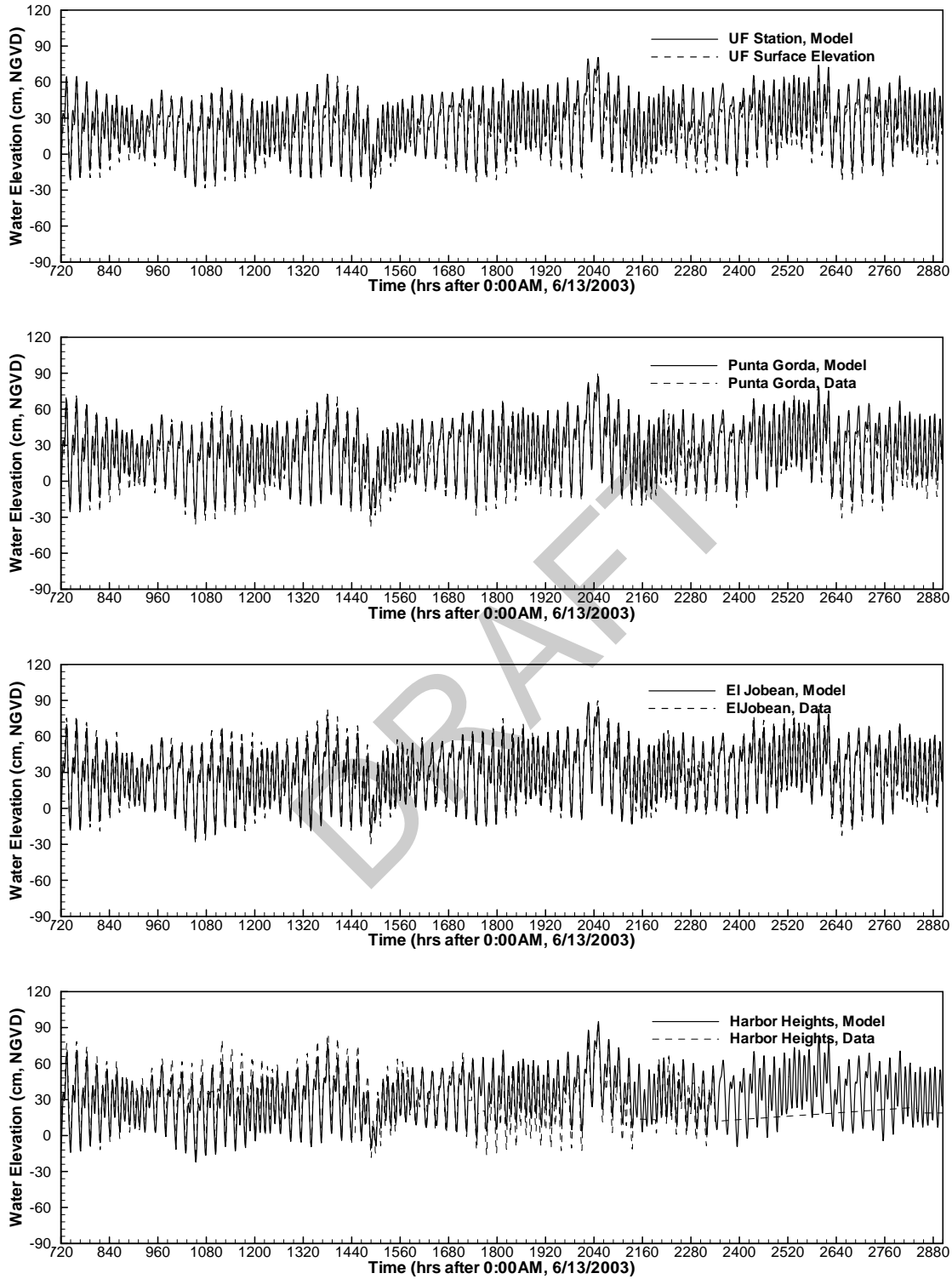


Figure A- 1 Comparisons of simulated and measured water elevations at UF, Punta Gorda, El Jobean, and Harbor Heights during July 12 – October 10, 2003.

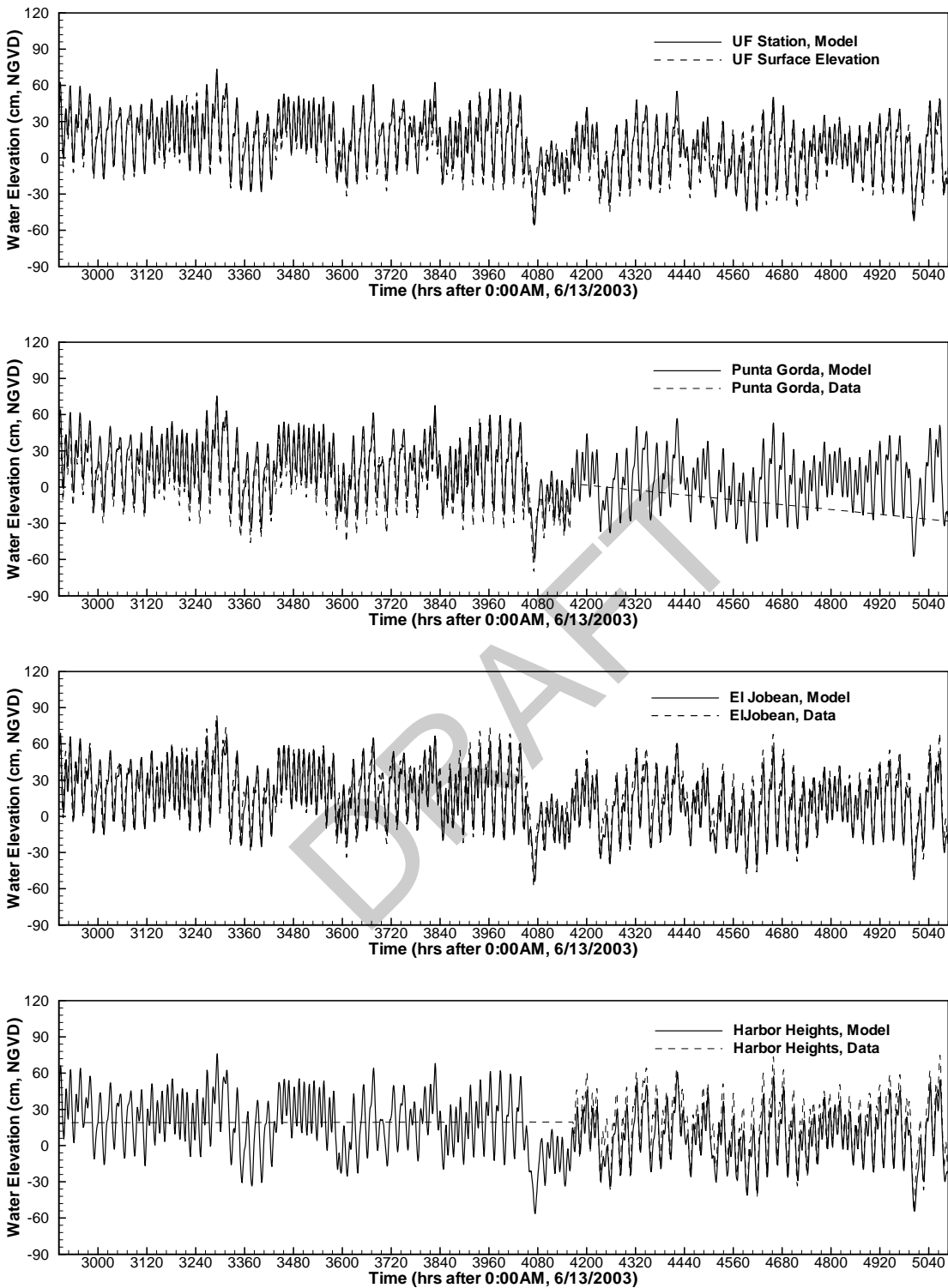


Figure A- 2 Comparisons of simulated and measured water elevations at UF, Punta Gorda, El Jobean, and Harbor Heights during October 11, 2003 – January 9, 2004.

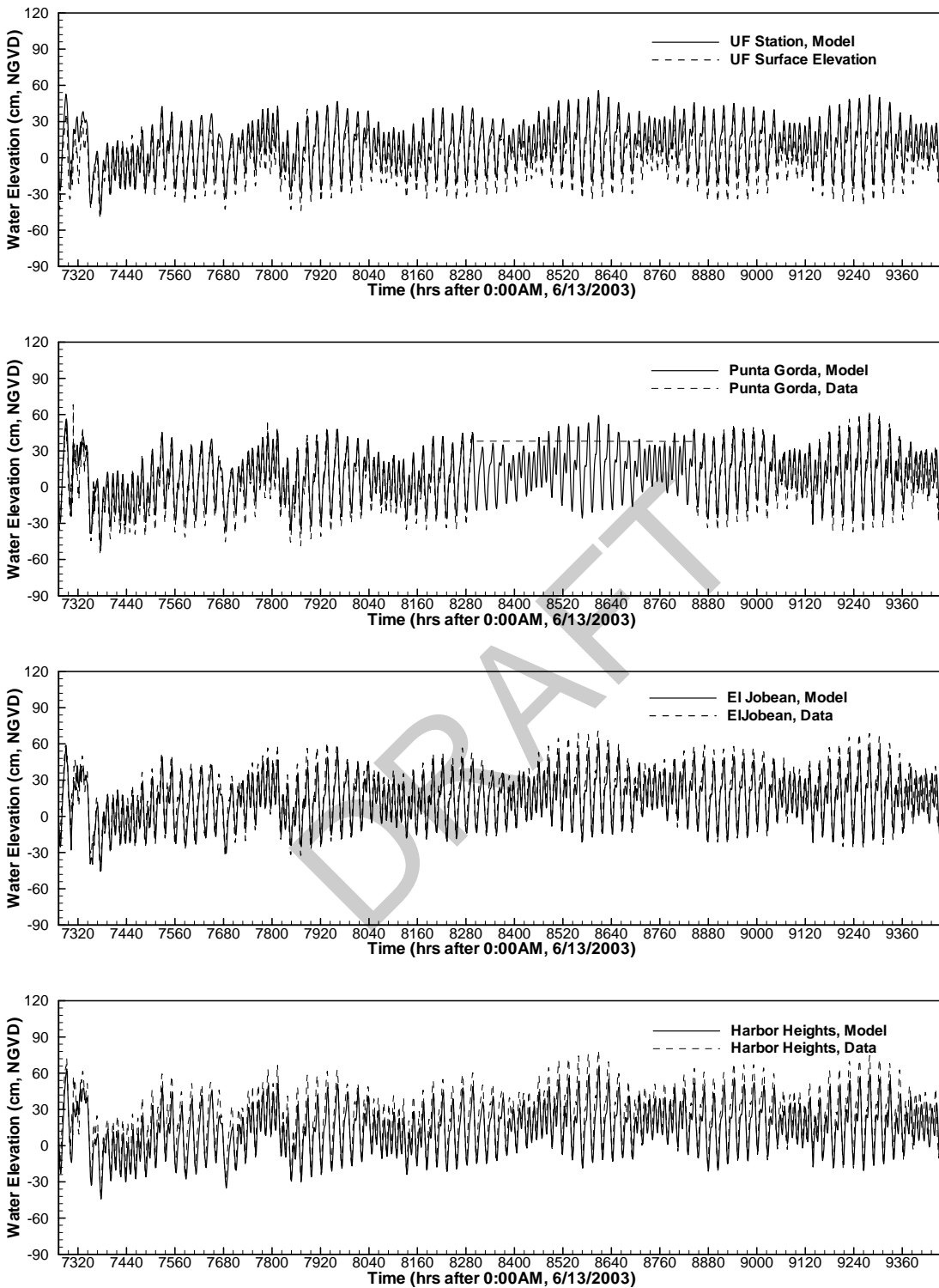


Figure A- 3 Comparisons of simulated and measured water elevations at UF, Punta Gorda, El Jobean, and Harbor Heights during April 10 – July 11, 2004.

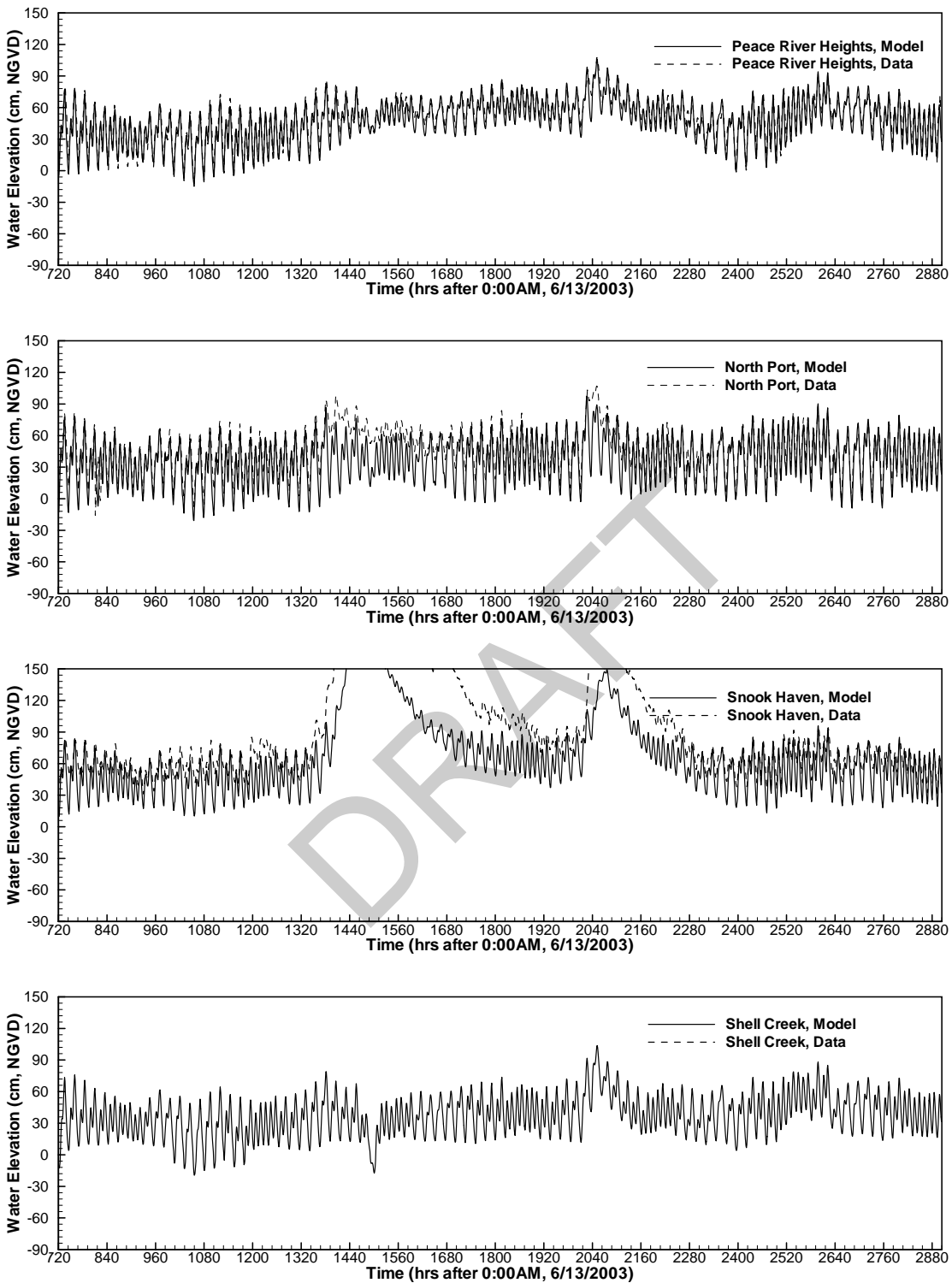


Figure A- 4 Comparisons of simulated and measured water elevations at Peace River Heights, North Port, Snook Haven, and Shell Creek during July 12 – October 10, 2003.

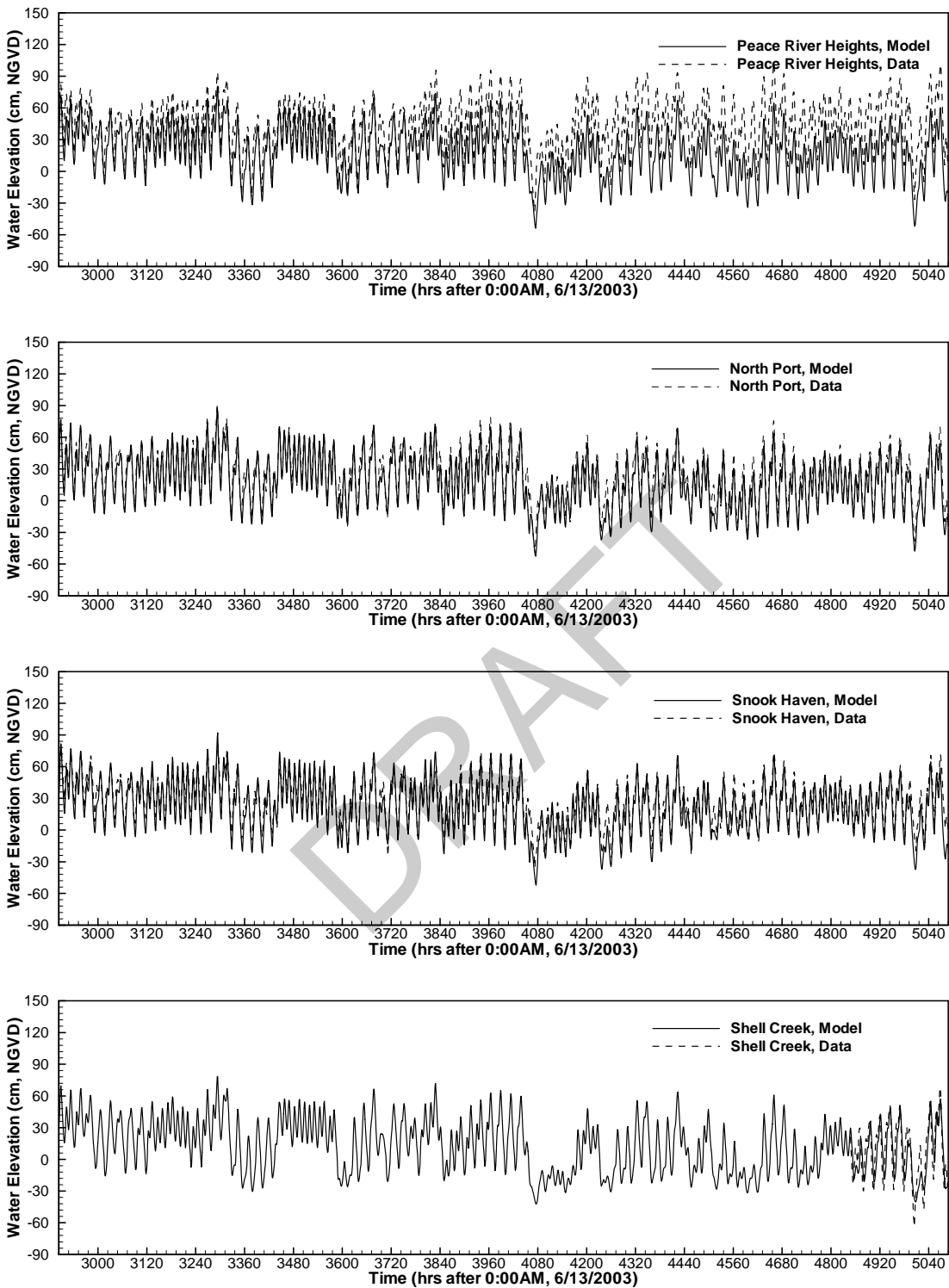


Figure A- 5 Comparisons of simulated and measured water elevations at Peace River Heights, North Port, Snook Haven, and Shell Creek during October 11, 2003 – January 9, 2004.

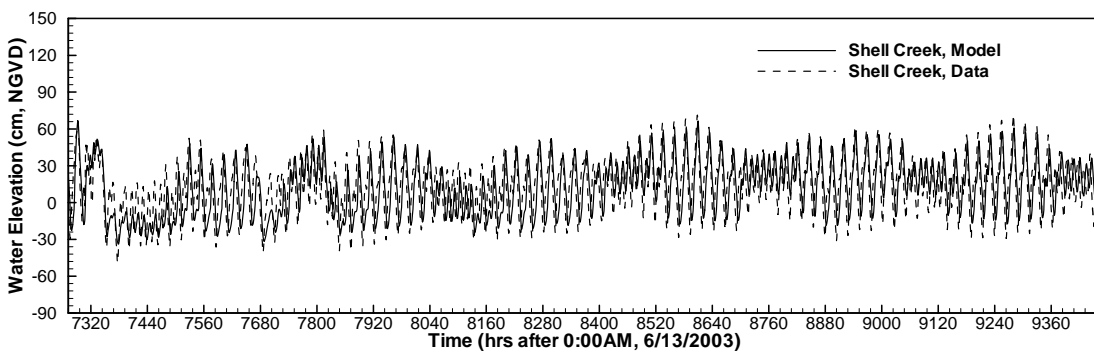
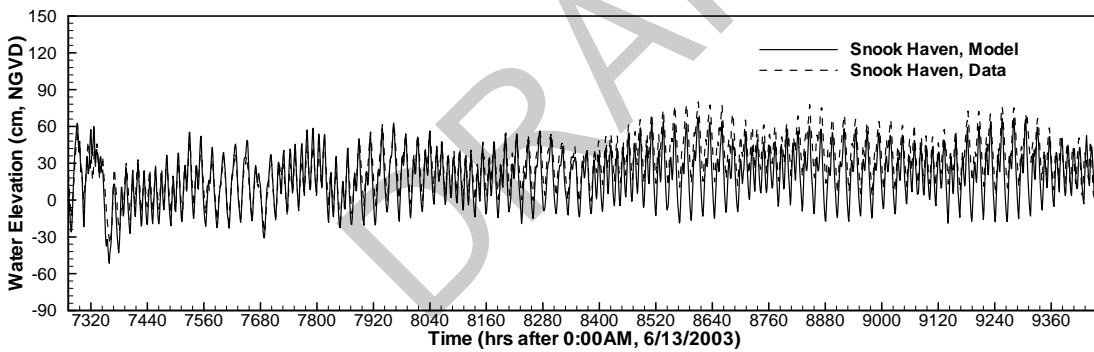
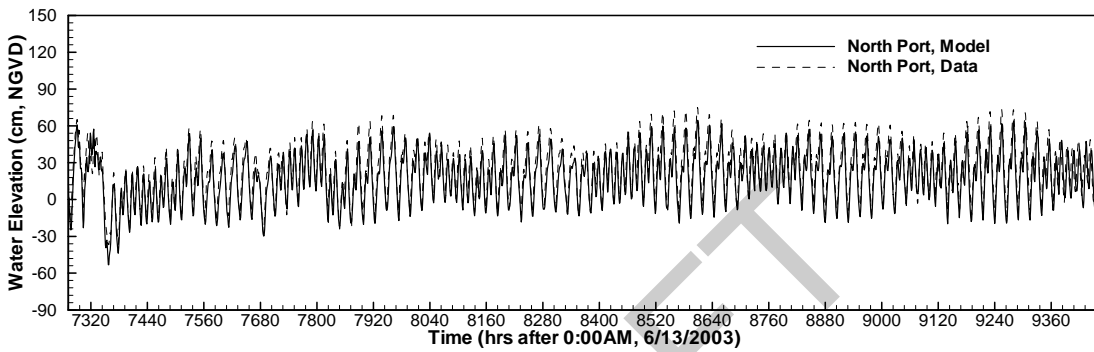
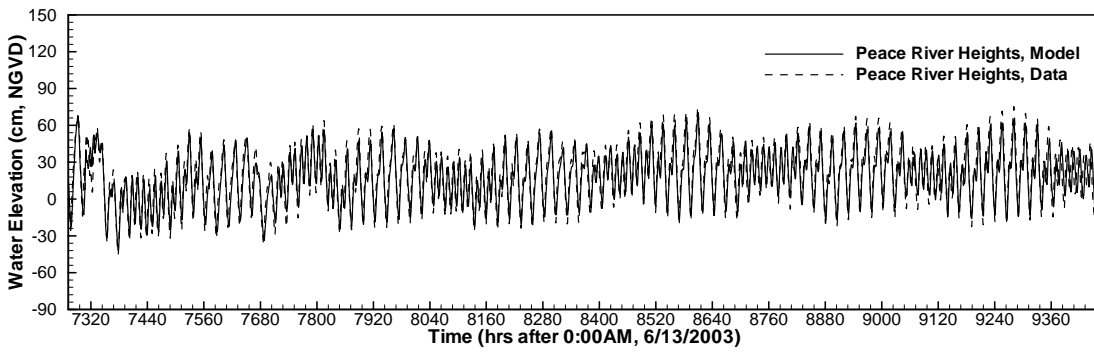


Figure A- 6 Comparisons of simulated and measured water elevations at Peace River Heights, North Port, Snook Haven, and Shell Creek during April 10 – July 11, 2004.

Appendix B

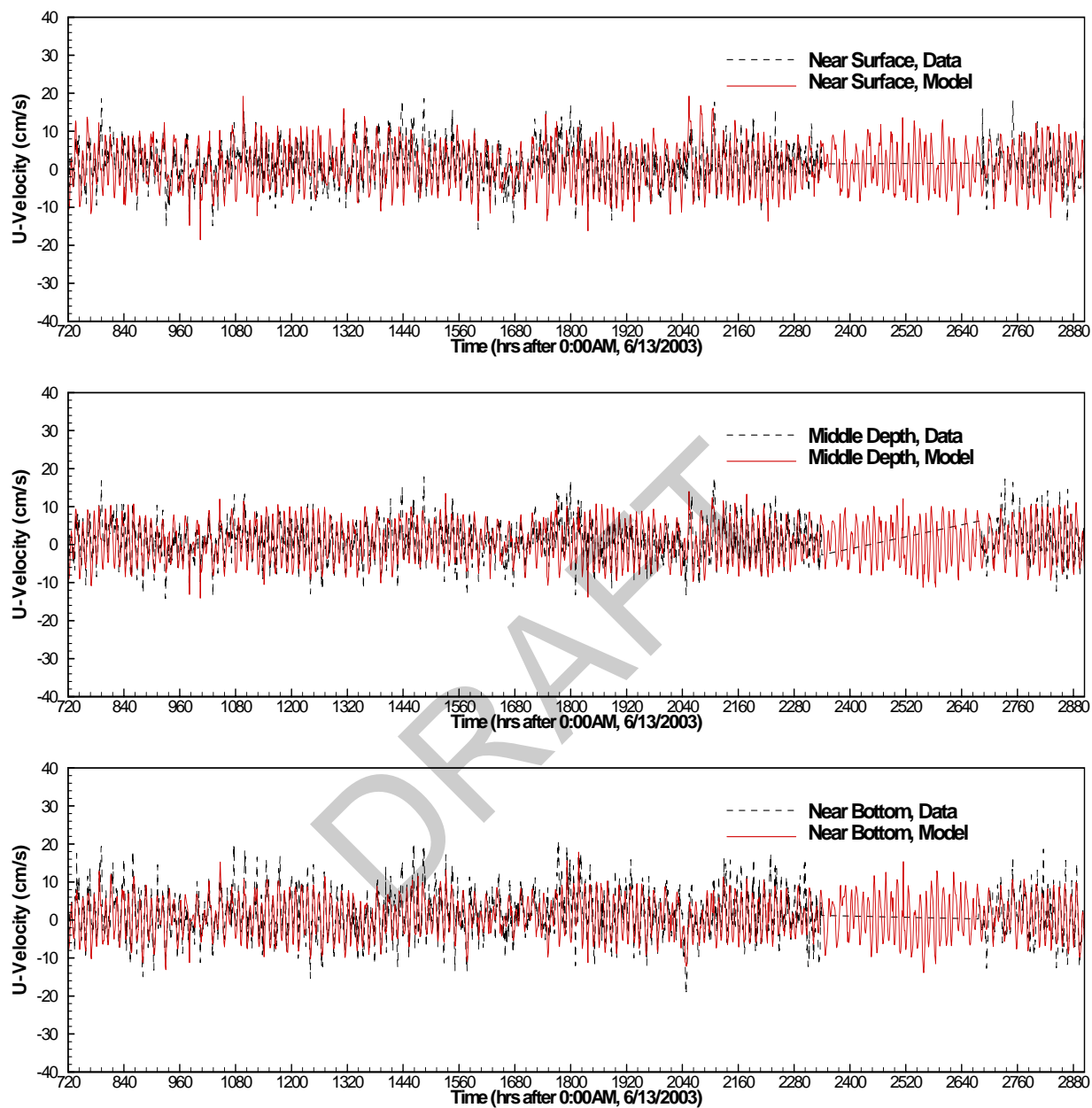


Figure B- 1 Comparisons of simulated and measured u-velocities at three depths at the UF station during July 12 – October 10, 2003.

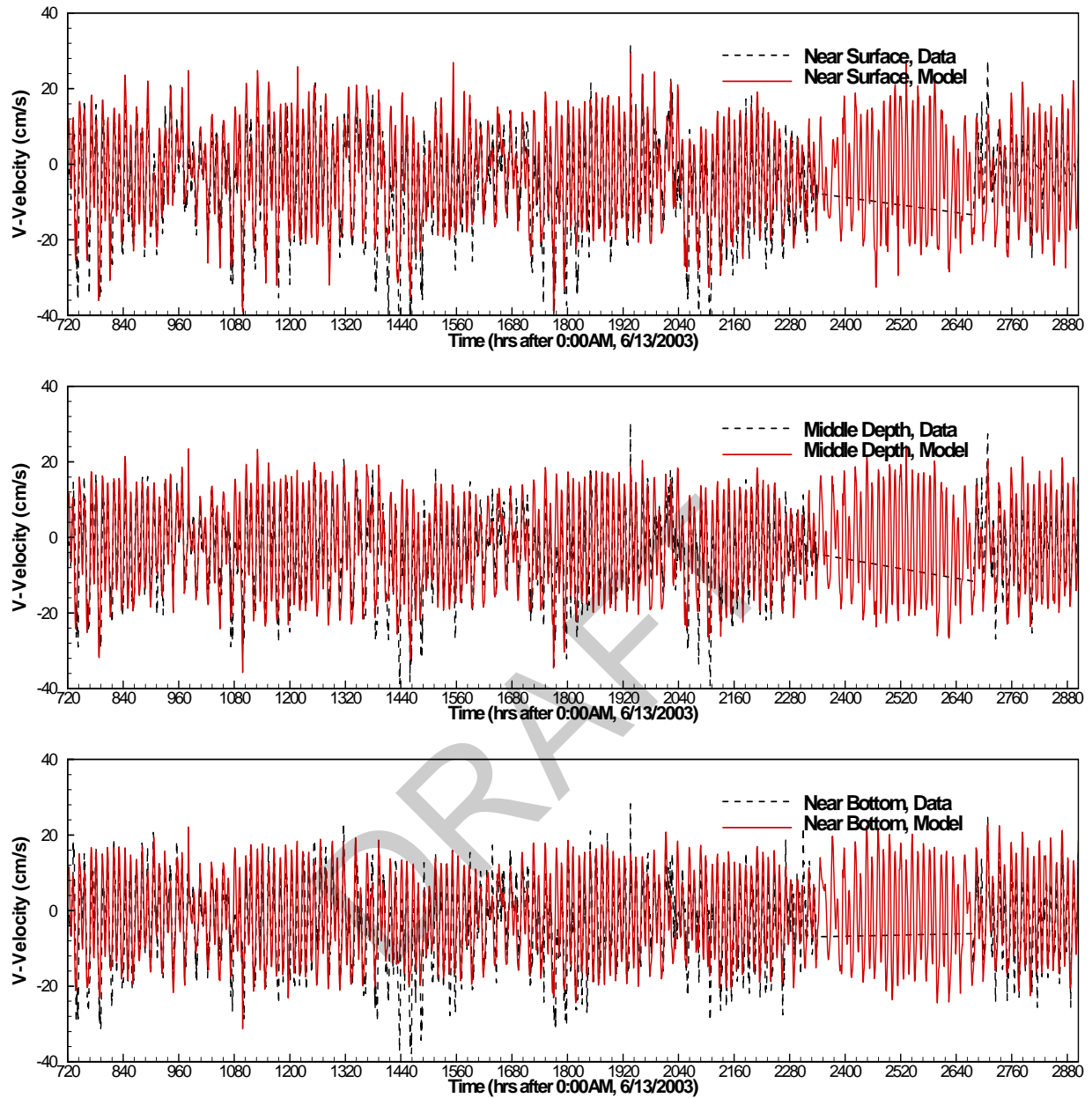


Figure B- 2 Comparisons of simulated and measured v-velocities at three depths at the UF station during July 12 – October 10, 2003.

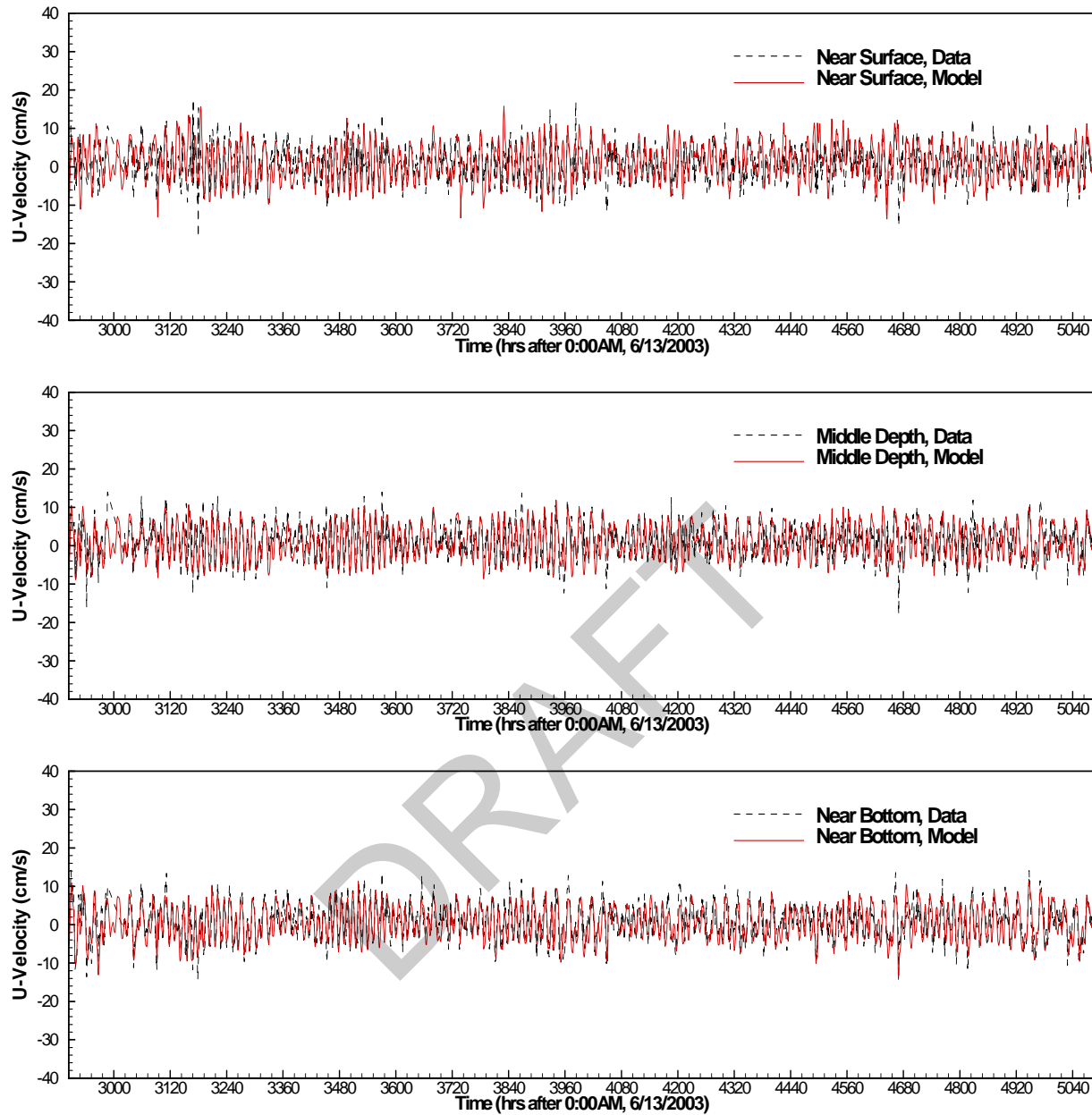


Figure B- 3 Comparisons of simulated and measured u-velocities at three depths at the UF station during October 11, 2003 – January 9, 2004.

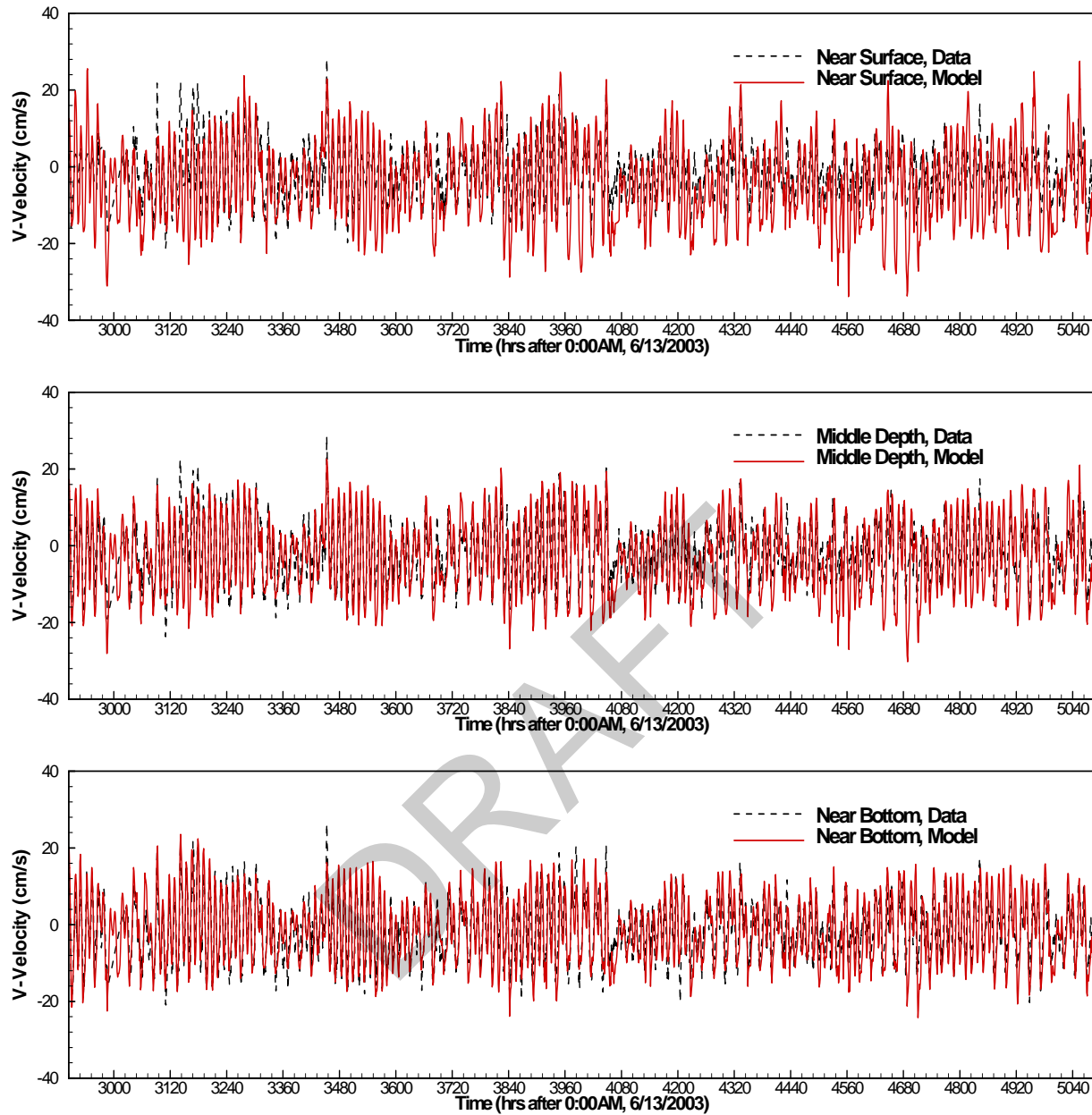


Figure B- 4 Comparisons of simulated and measured v-velocities at three depths at the UF station during October 11, 2003 – January 9, 2004.

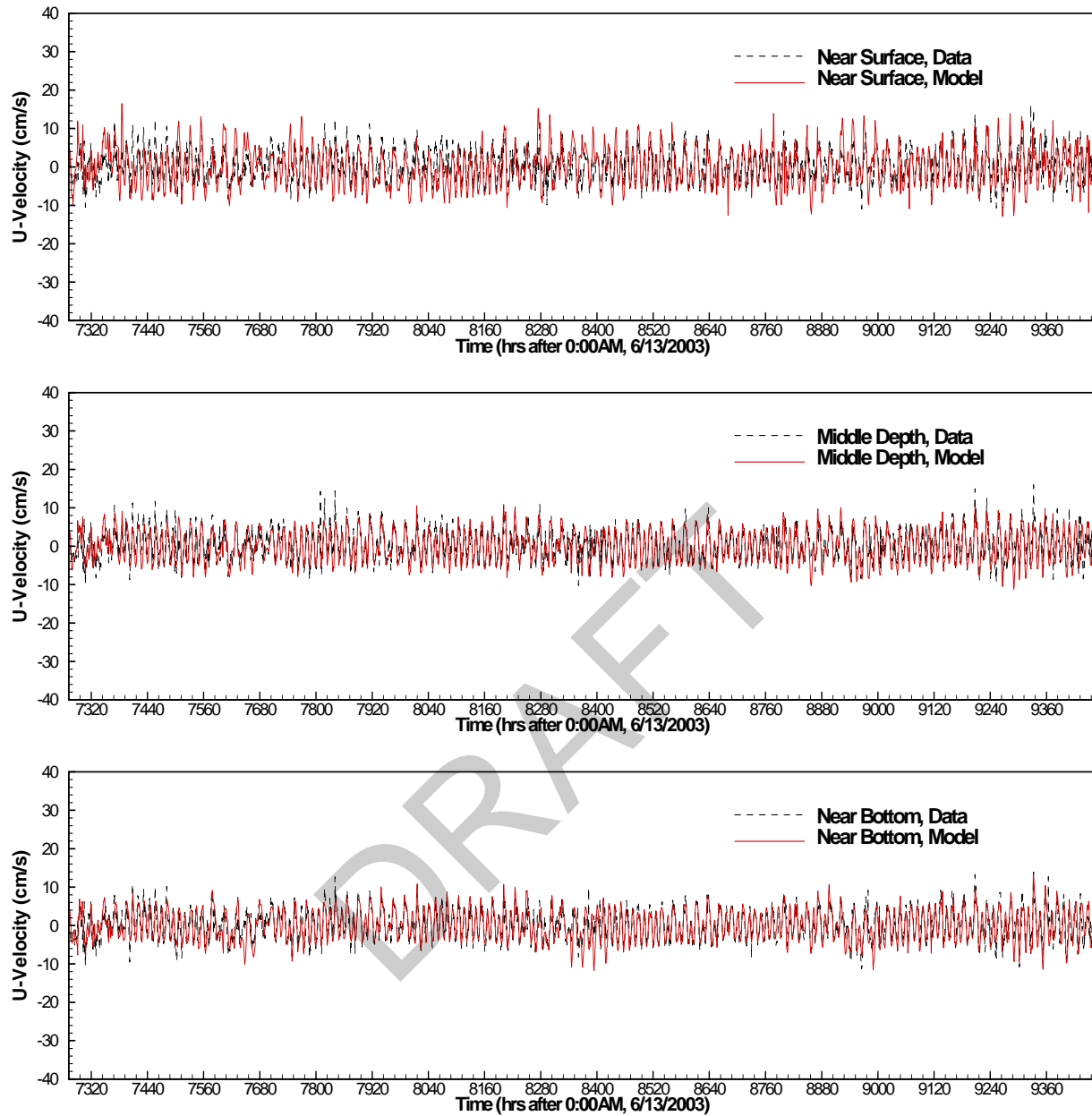


Figure B- 5 Comparisons of simulated and measured u-velocities at three depths at the UF station during April 10 – July 11, 2004.

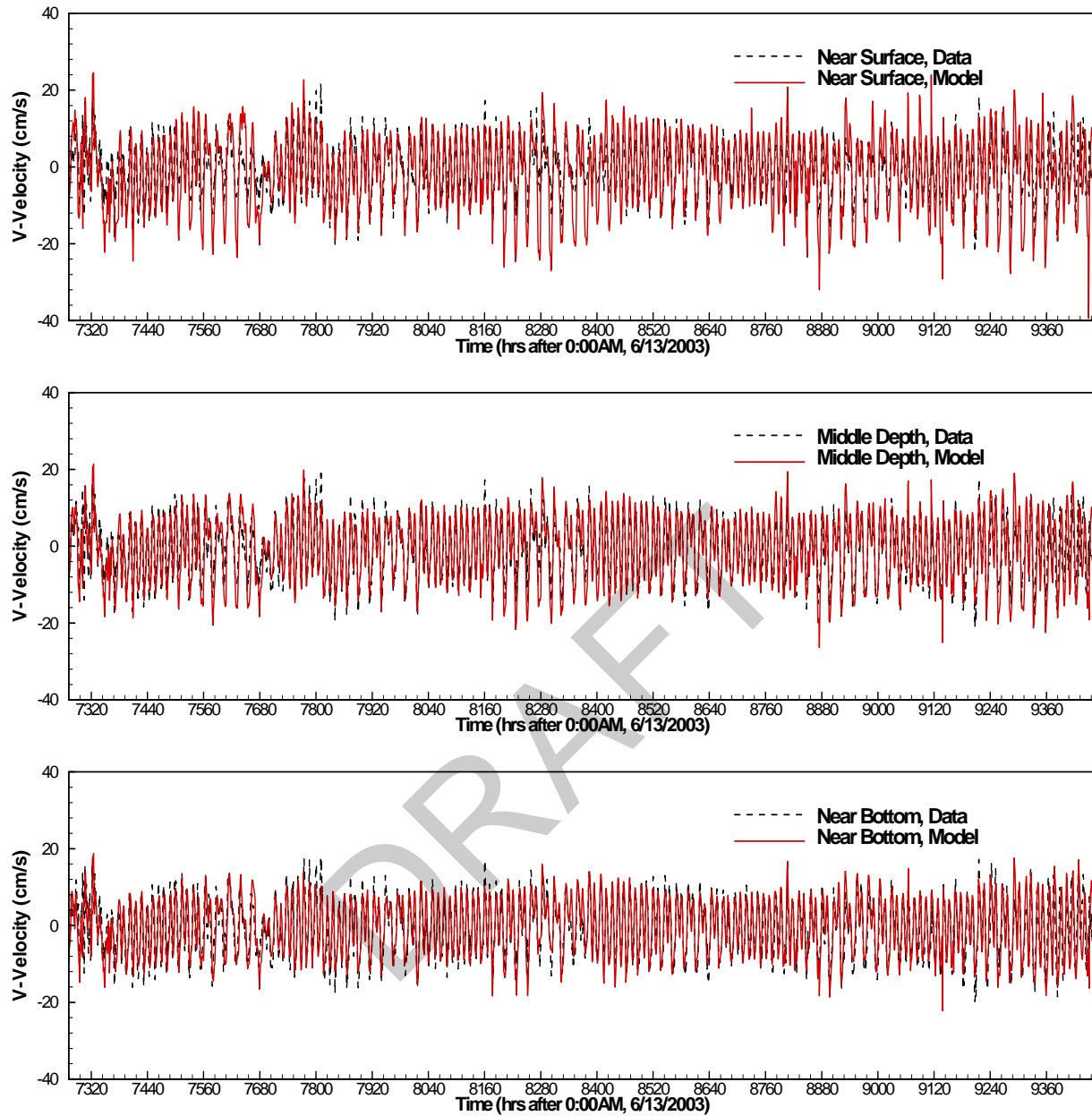


Figure B- 6 Comparisons of simulated and measured v-velocities at three depths at the UF station during April 10 – July 11, 2004.

Appendix C

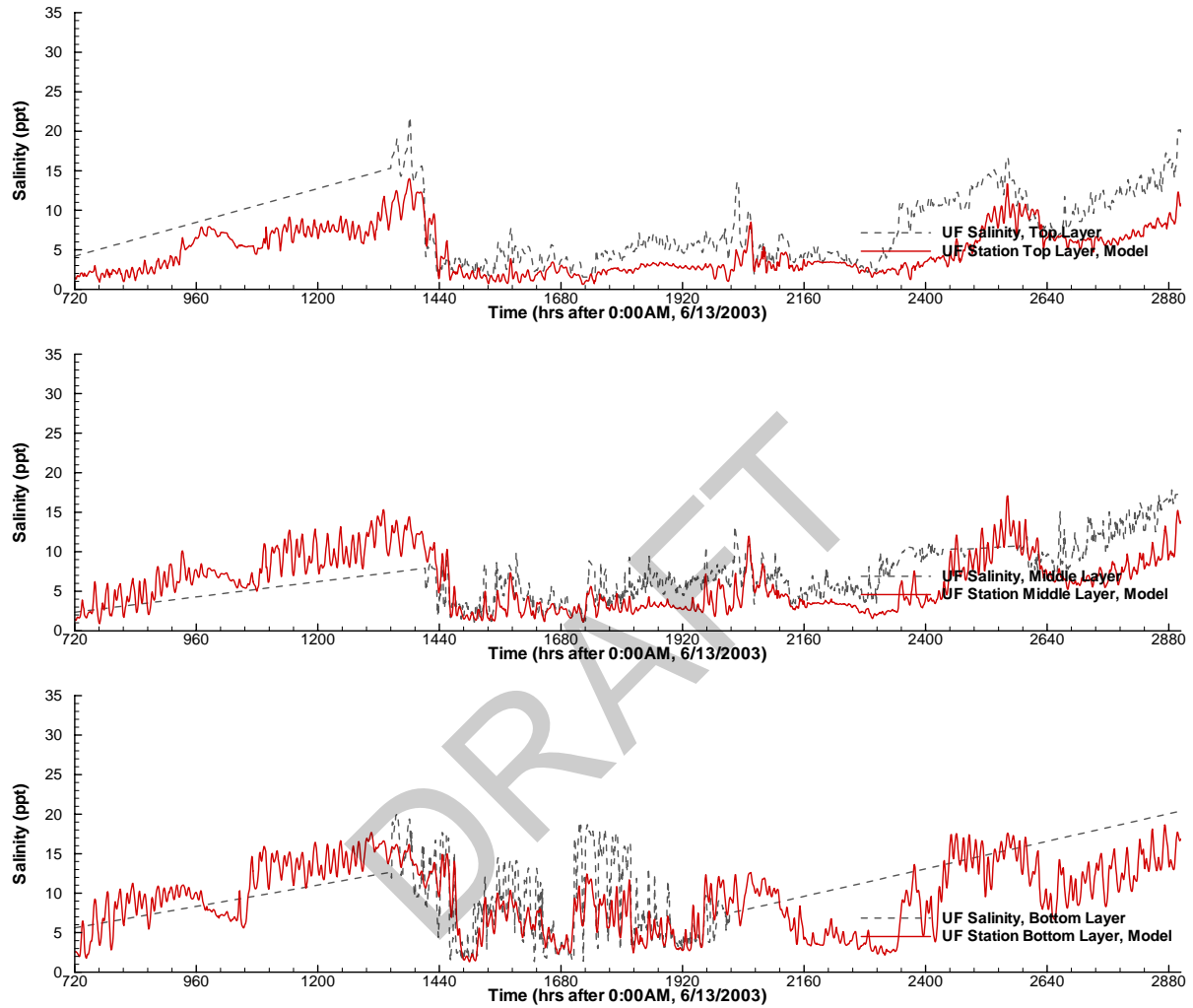


Figure C- 1 Comparisons of simulated and measured salinities at three depths at the UF station during July 12 – October 10, 2003.

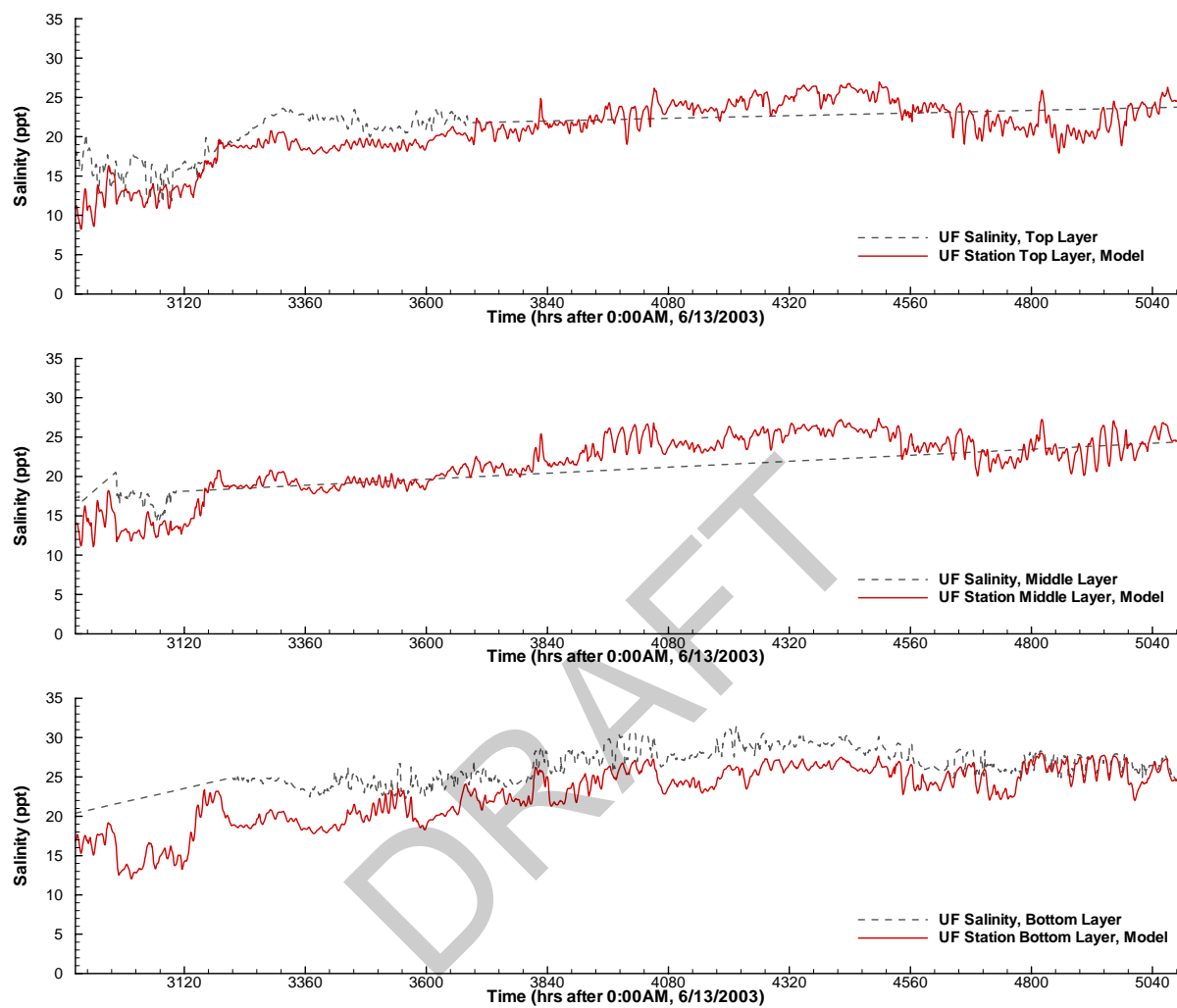


Figure C- 2 Comparisons of simulated and measured salinities at three depths at the UF station during October 11, 2003 – January 9, 2004.

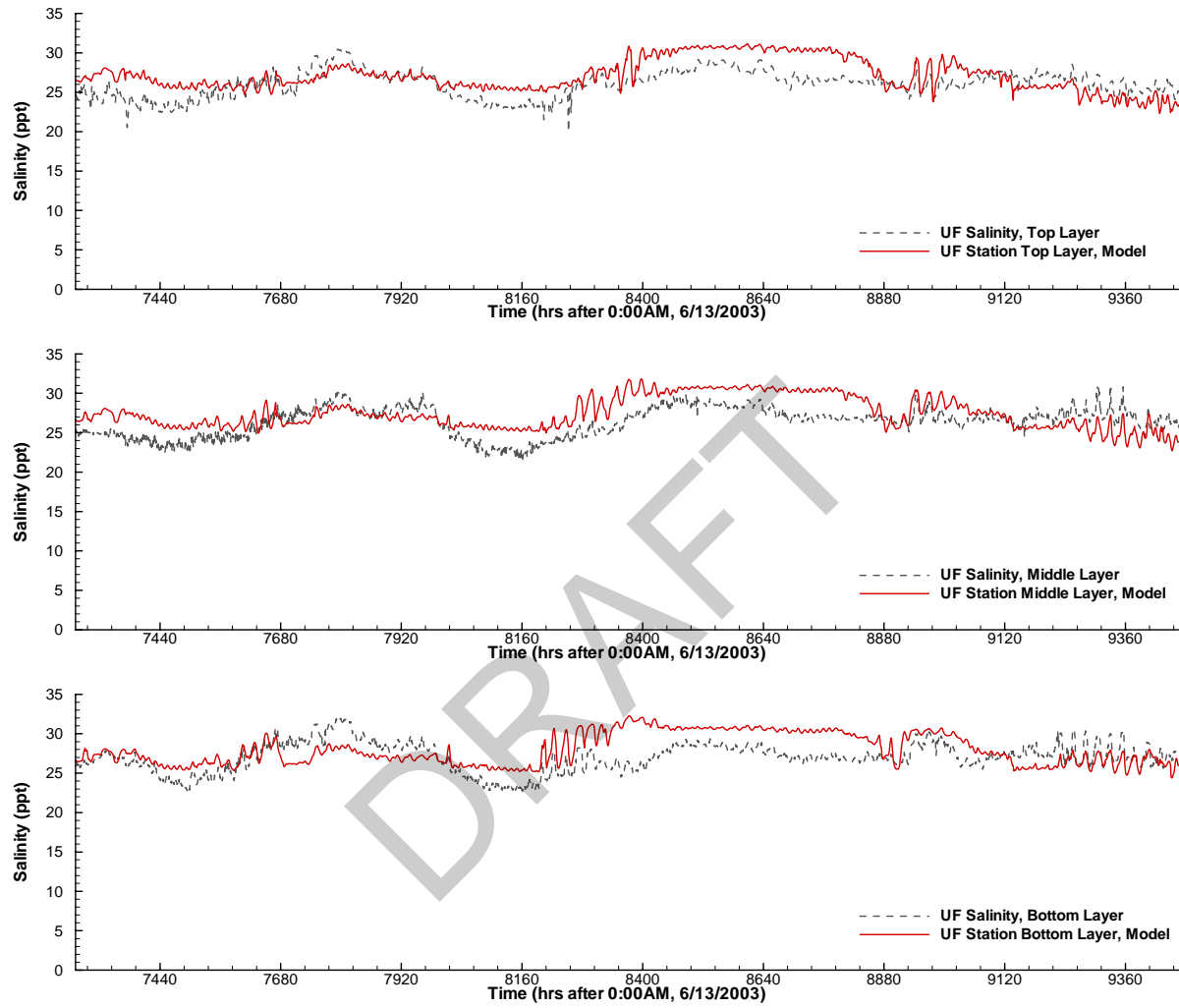


Figure C- 3 Comparisons of simulated and measured salinities at three depths at the UF station during April 10 – July 11, 2004.

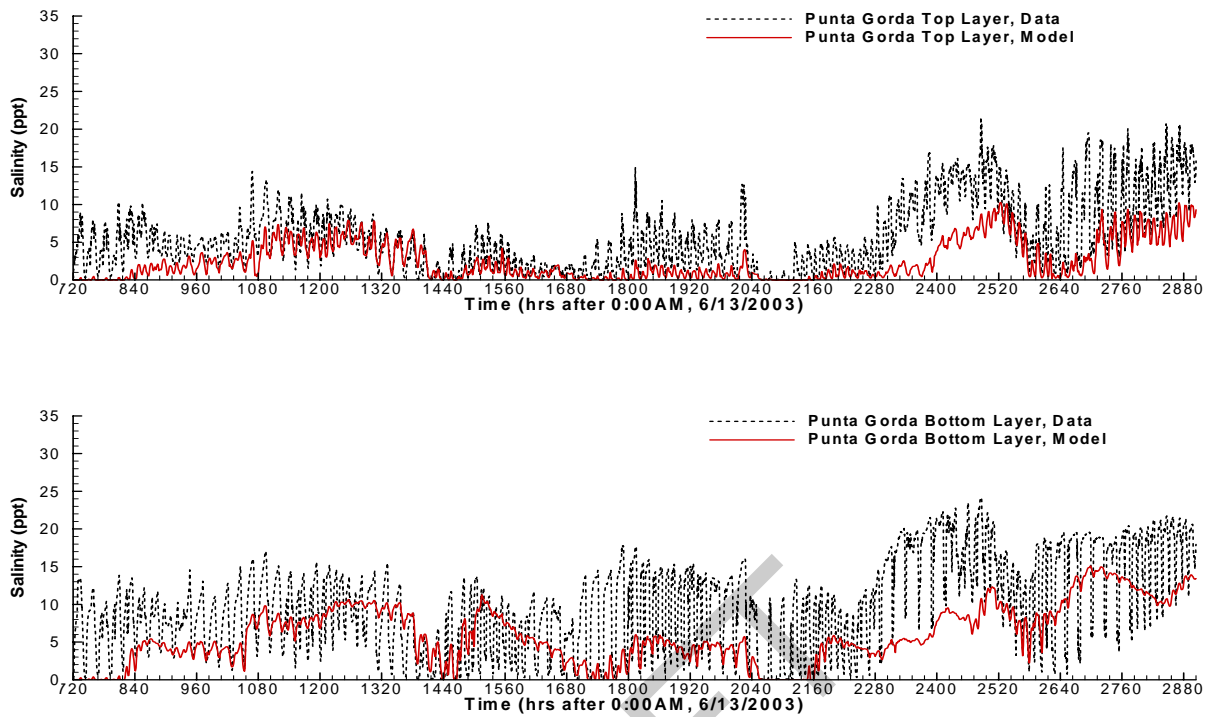


Figure C- 4 Comparisons of simulated and measured salinities at two depths at the Punta Gorda station during July 12 – October 10, 2003.

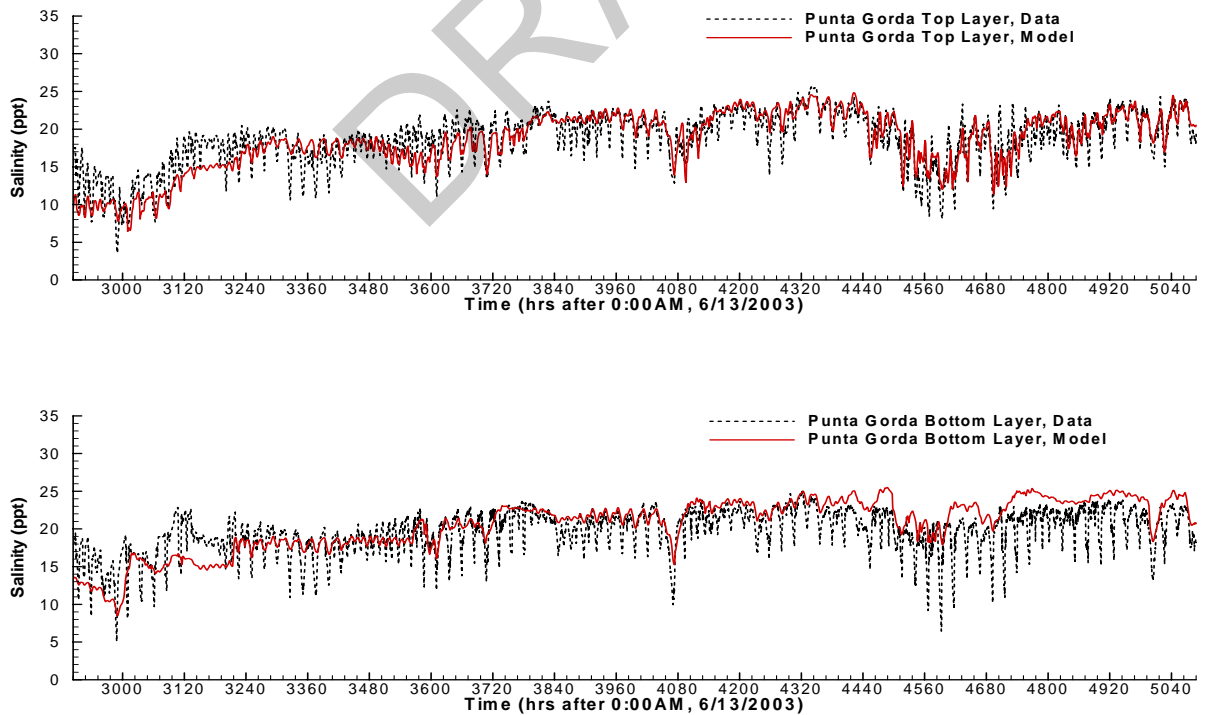


Figure C- 5 Comparisons of simulated and measured salinities at two depths at the Punta Gorda station during October 11, 2003 – January 9, 2004.

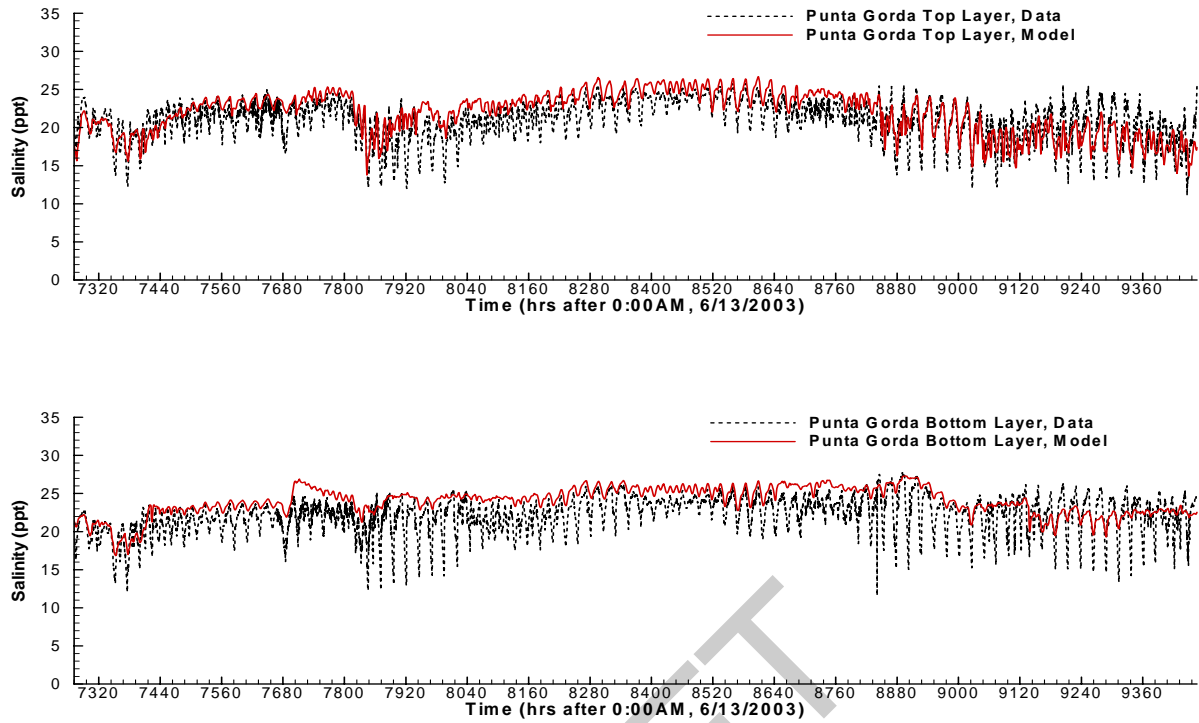


Figure C- 6 Comparisons of simulated and measured v-velocities at two depths at the Punta Gorda station during April 10 – July 11, 2004.

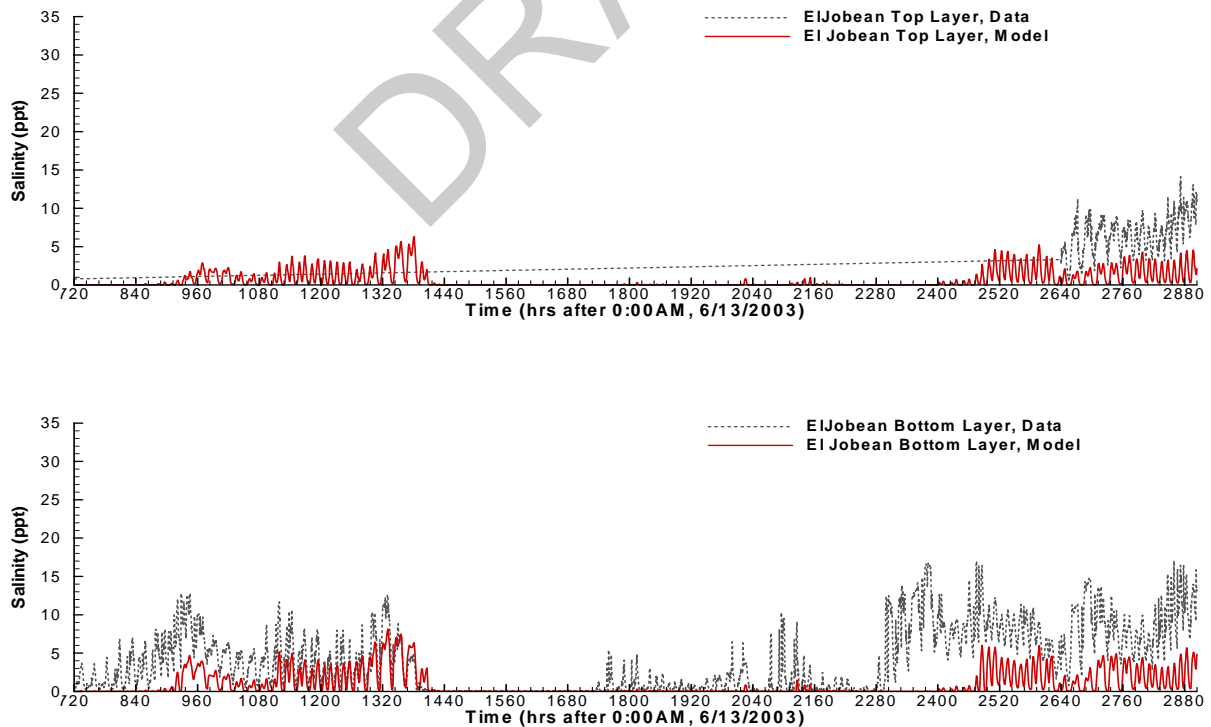


Figure C- 7 Comparisons of simulated and measured salinities at two depths at the El Jobean station during July 12 – October 10, 2003.

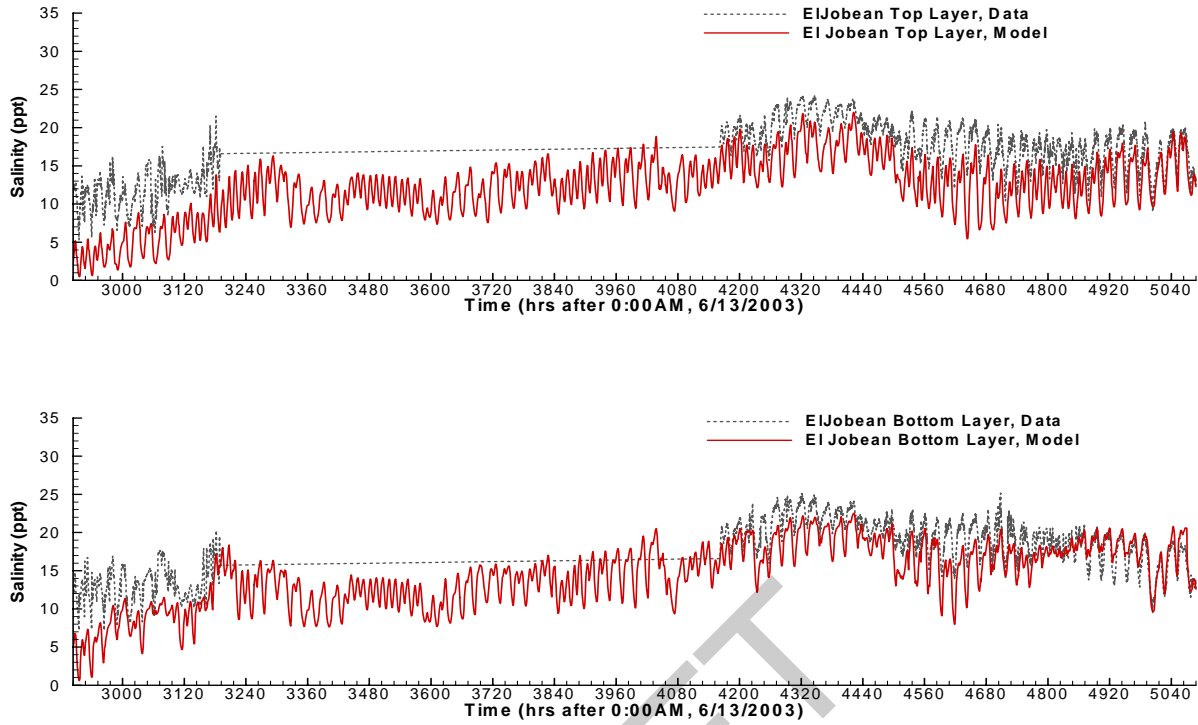


Figure C- 8 Comparisons of simulated and measured salinities at two depths at the El Jobean station during October 11, 2003 – January 9, 2004.

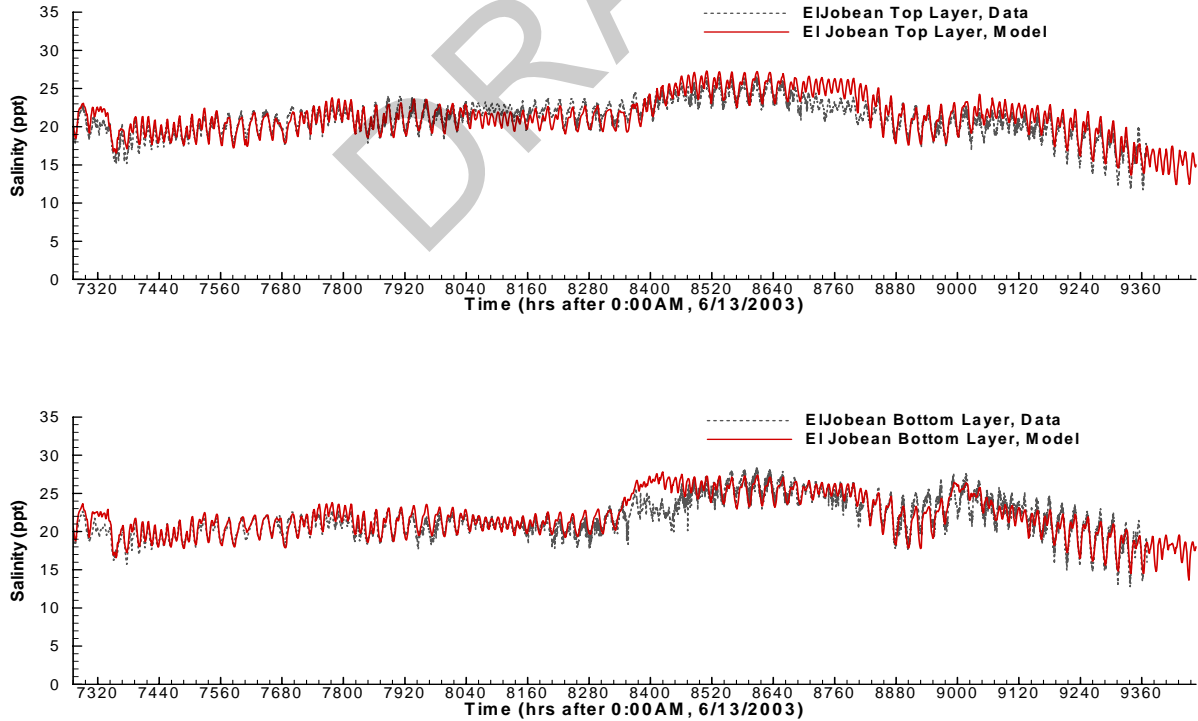


Figure C- 9 Comparisons of simulated and measured salinities at two depths at the El Jobean station during April 10 – July 11, 2004.

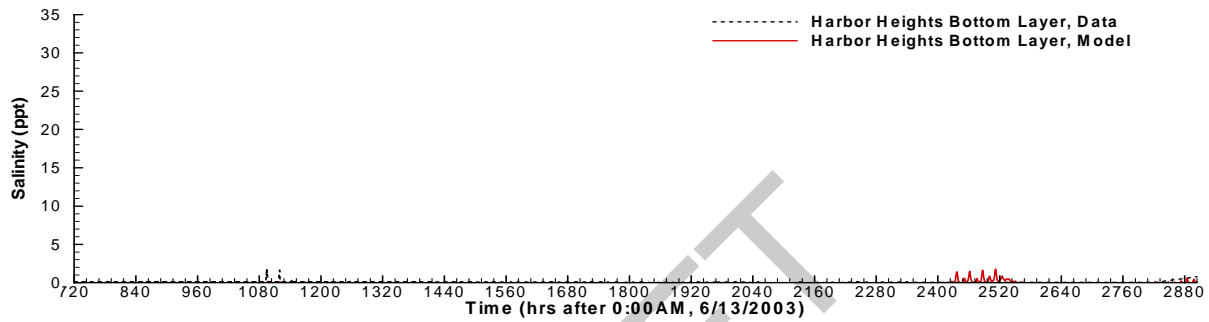
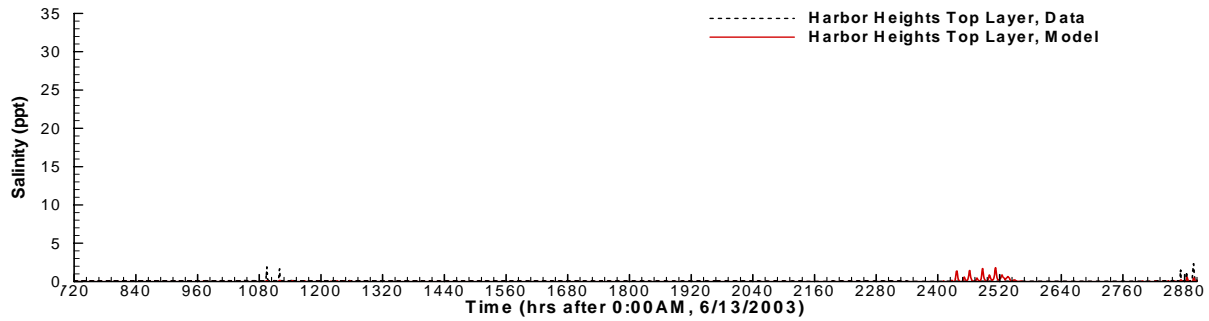


Figure C- 10 Comparisons of simulated and measured salinities at two depths at the Harbor Heights station during July 12 – October 10, 2003.

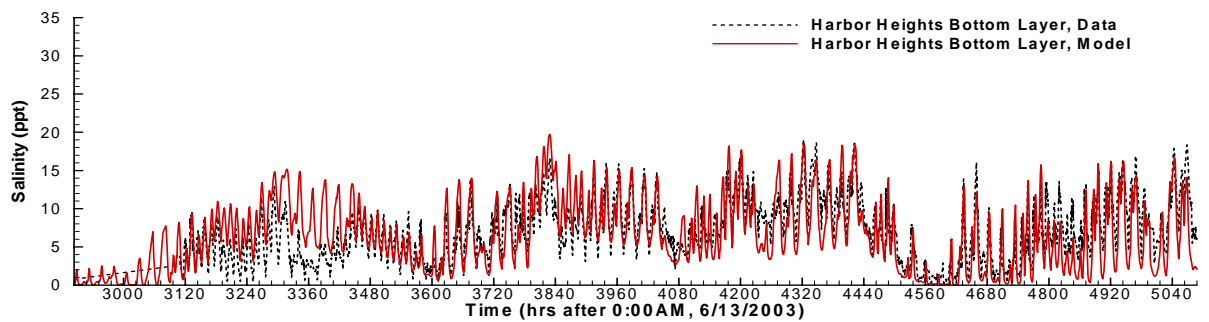
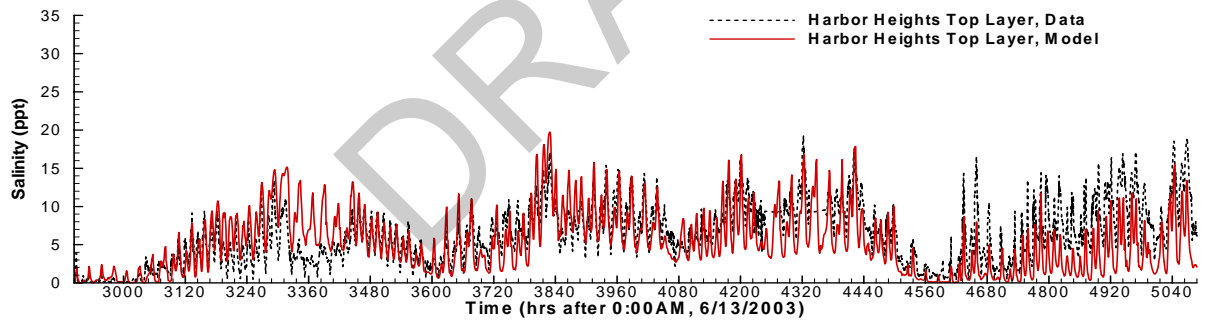


Figure C- 11 Comparisons of simulated and measured salinities at two depths at the Harbor Heights station during October 11, 2003 – January 9, 2004.

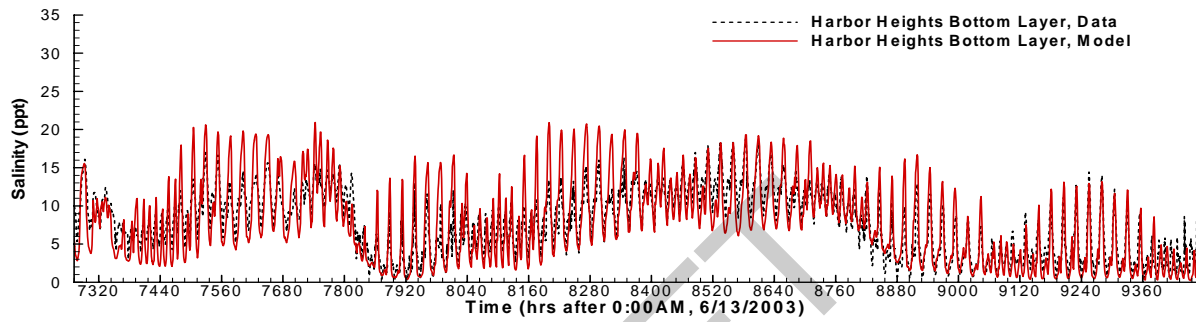
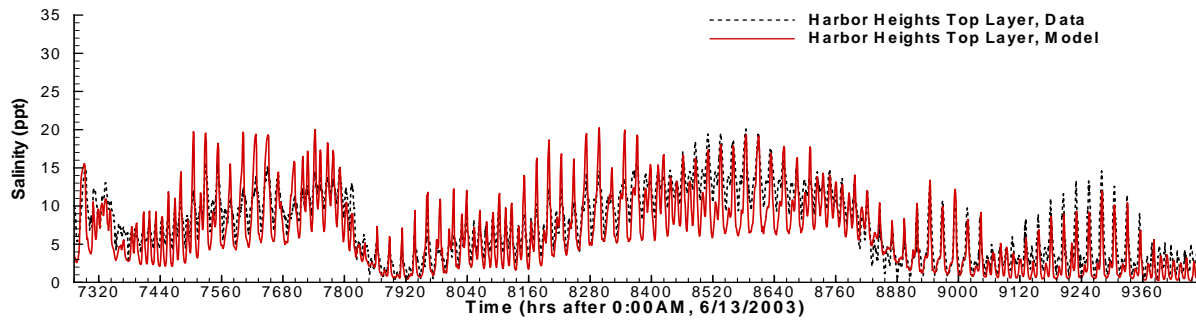


Figure C- 12 Comparisons of simulated and measured salinities at two depths at the Harbor Heights station during April 10 - July 11, 2004.

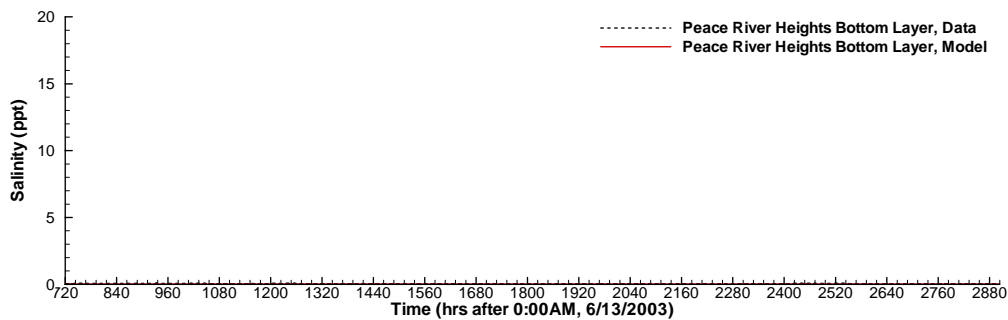


Figure C- 13 Comparisons of simulated and measured salinities at two depths at the Peace River Heights station during July 12 – October 10, 2003.

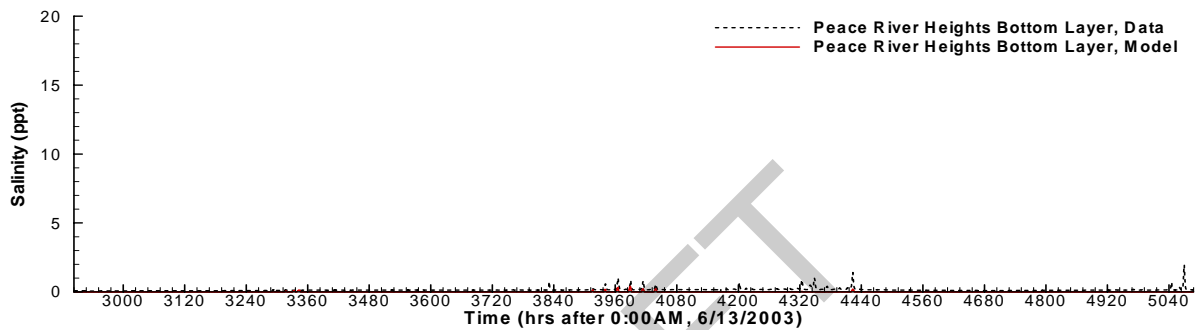
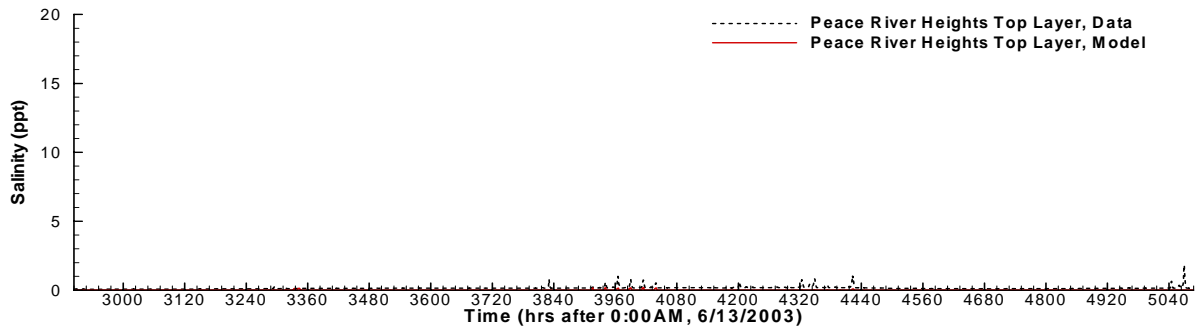


Figure C- 14 Comparisons of simulated and measured salinities at two depths at the Peace River Heights station during October 11, 2003 – January 9, 2004.

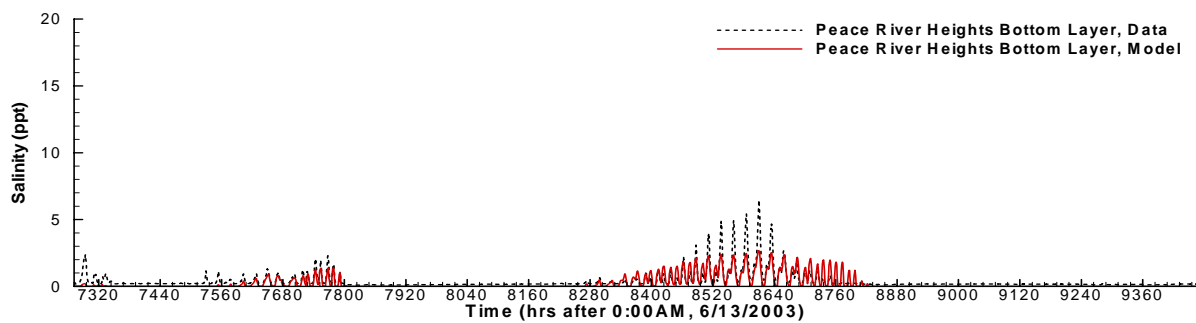
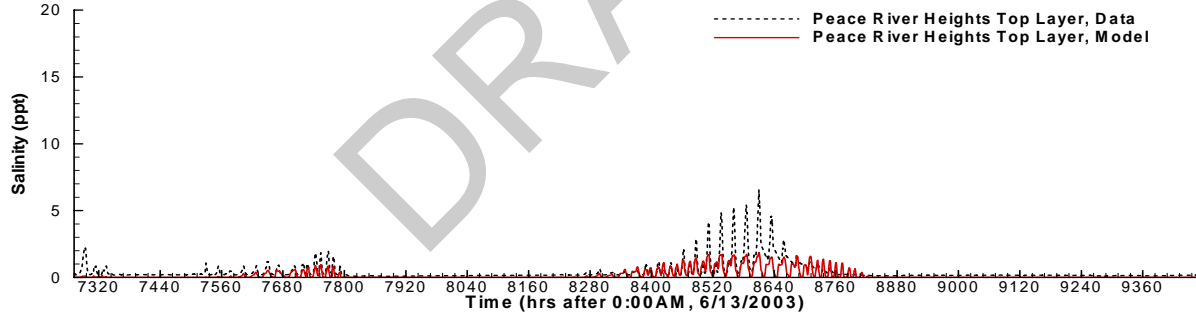


Figure C- 15 Comparisons of simulated and measured salinities at two depths at the Peace River Heights station during April 10 – July 11, 2004.

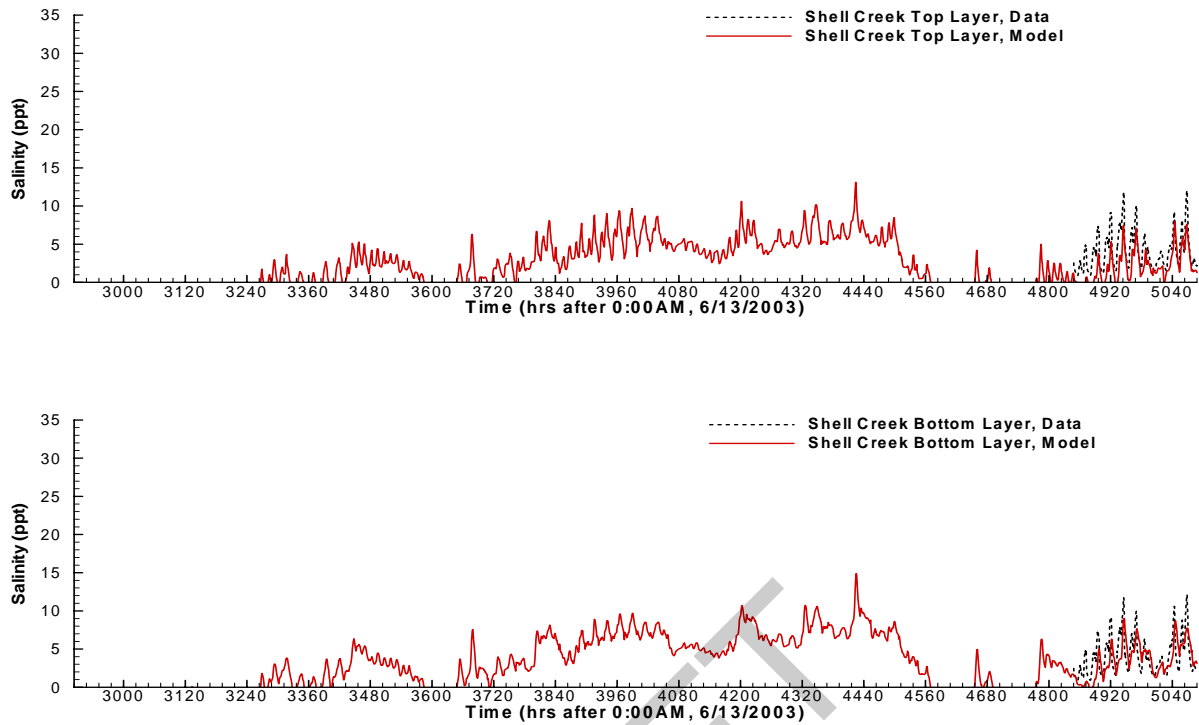


Figure C- 16 Comparisons of simulated and measured salinities at two depths at the Shell Creek station during October 11, 2003 – January 9, 2004.

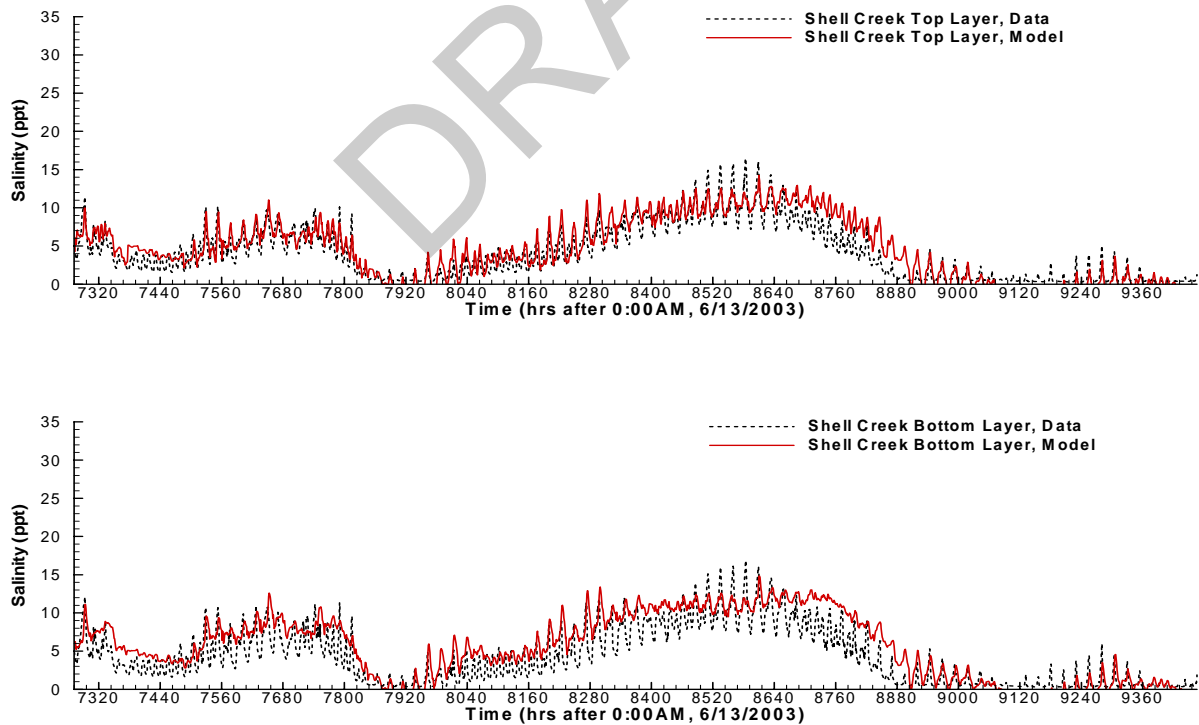


Figure C- 17 Comparisons of simulated and measured salinities at two depths at the Shell Creek station during April 10 - July 11, 2004.

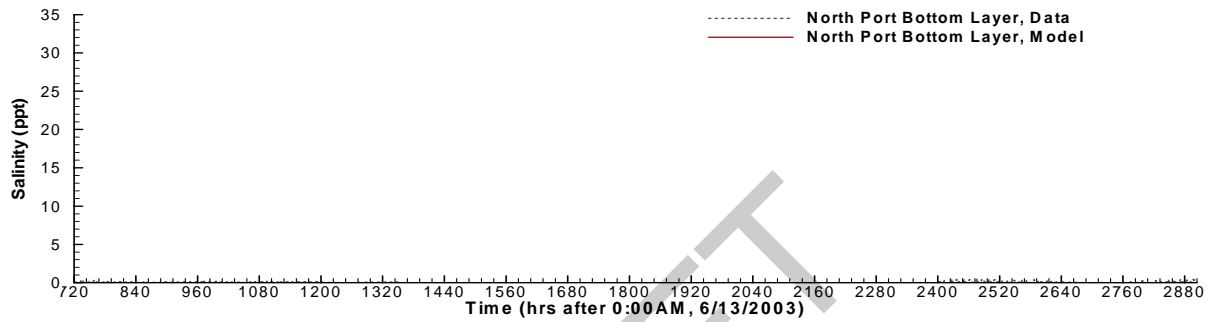
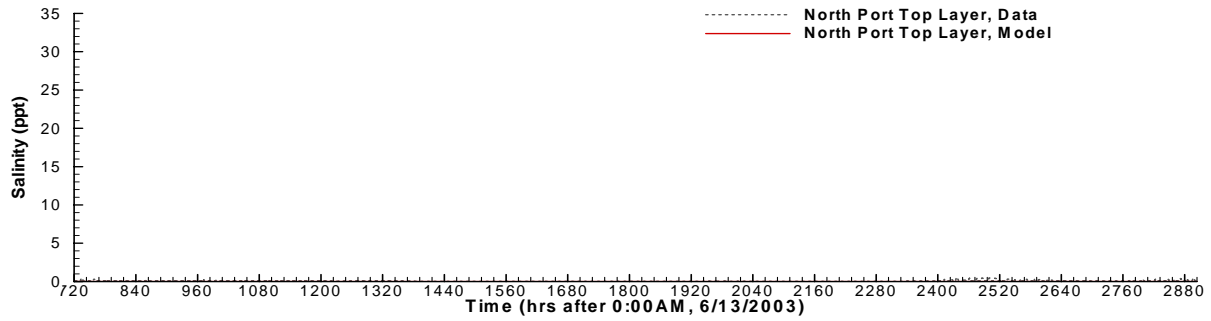


Figure C- 18 Comparisons of simulated and measured salinities at two depths at the North Port station during July 12 – October 10, 2003.

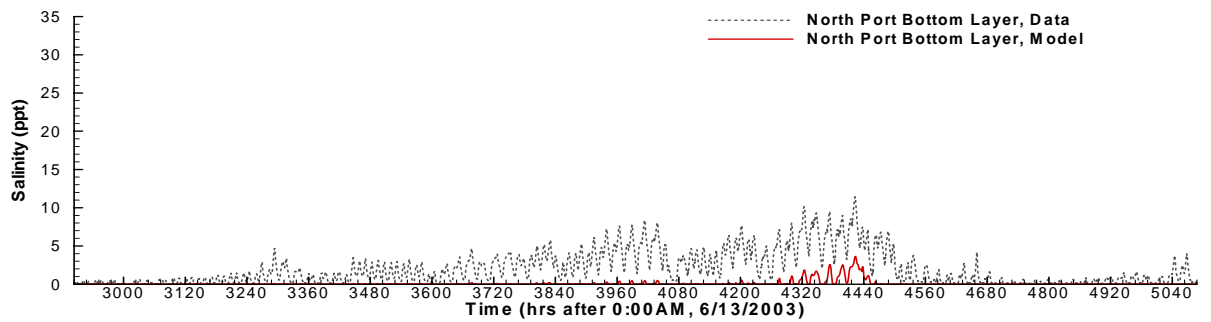
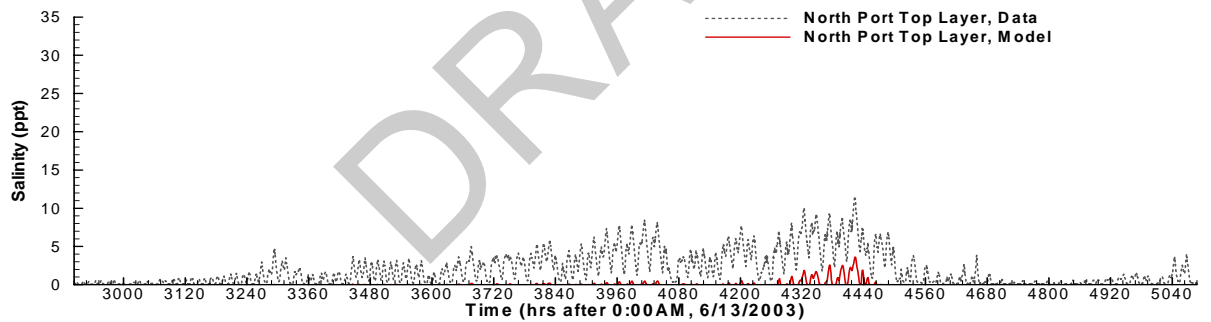


Figure C- 19 Comparisons of simulated and measured salinities at two depths at the North Port station during October 11, 2003 – January 9, 2004.

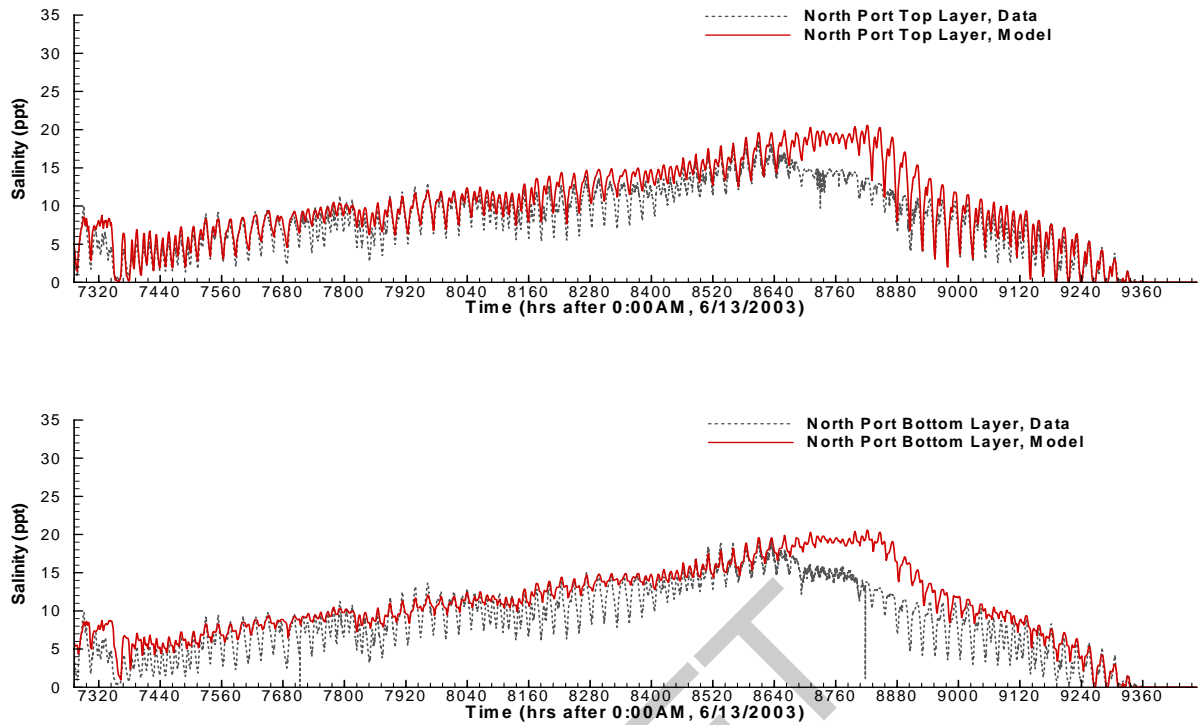


Figure C- 20 Comparisons of simulated and measured salinities at two depths at the North Port station during April 10 – July 11, 2004.

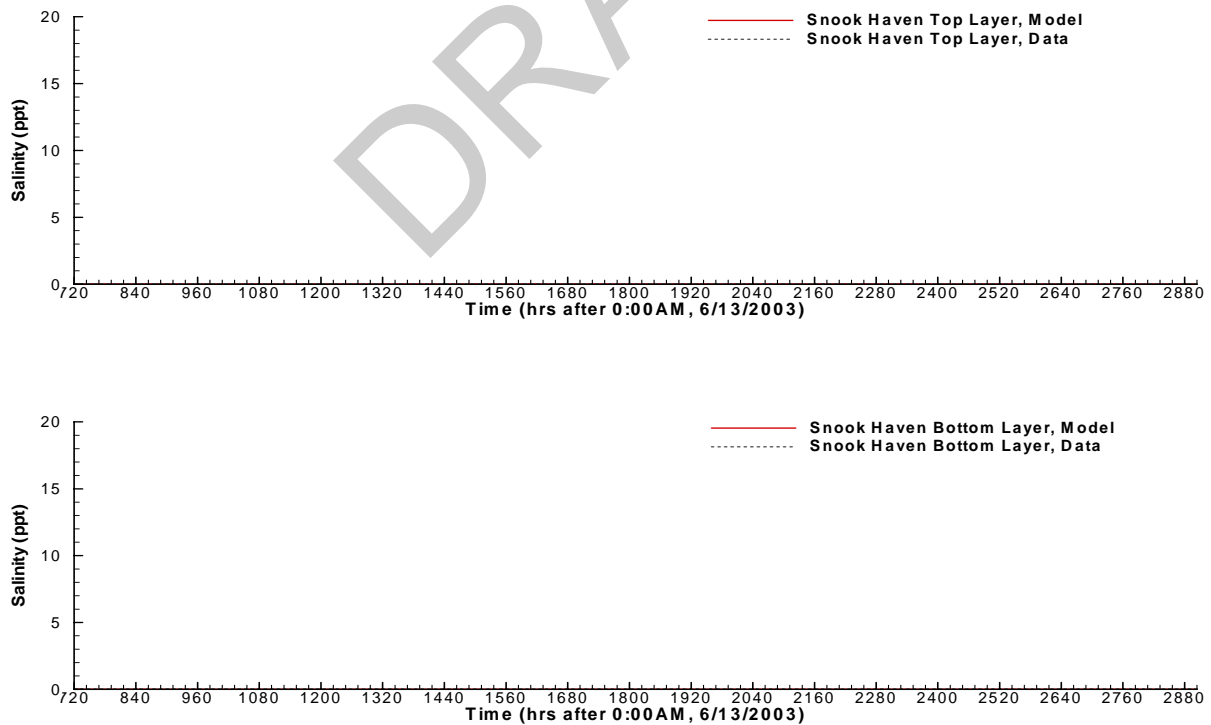


Figure C- 21 Comparisons of simulated and measured salinities at two depths at the Snook Haven station during July 12 – October 10, 2003.

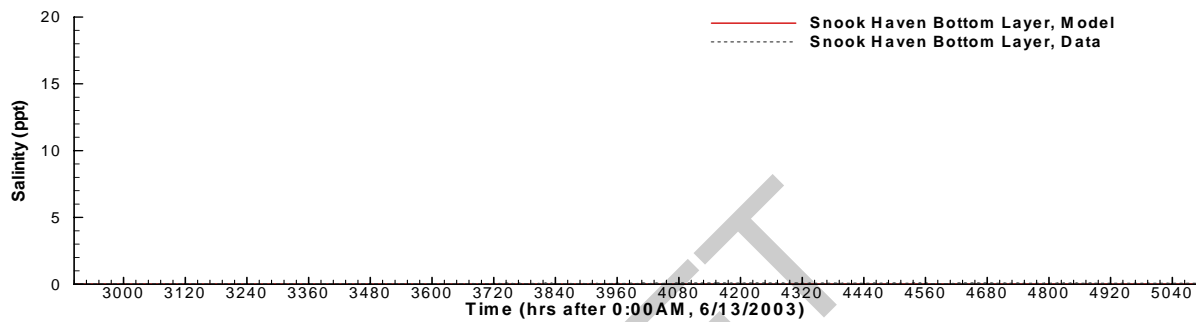
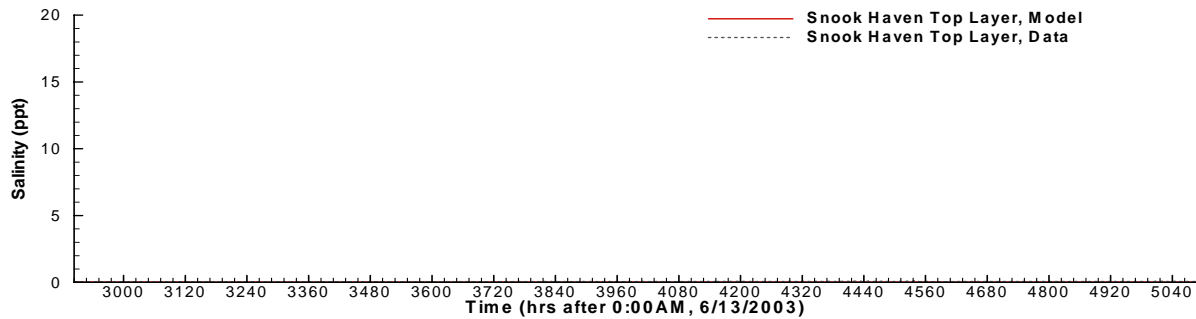


Figure C- 22 Comparisons of simulated and measured salinities at two depths at the Snook Haven station during October 11, 2003 – January 9, 2004.

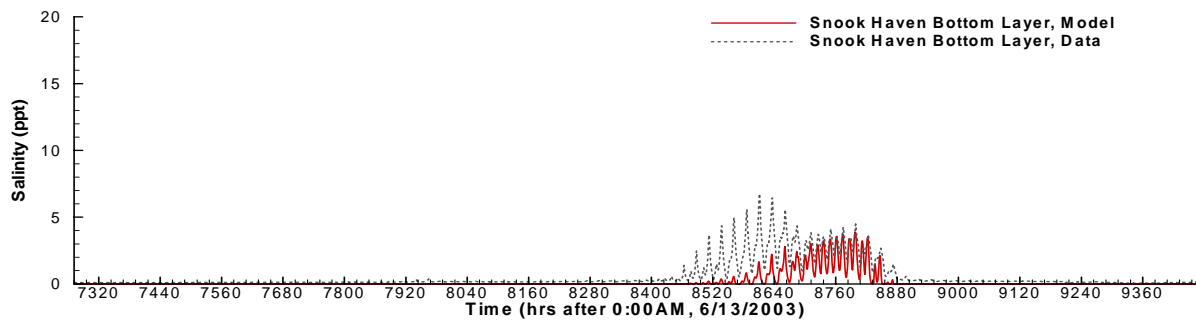
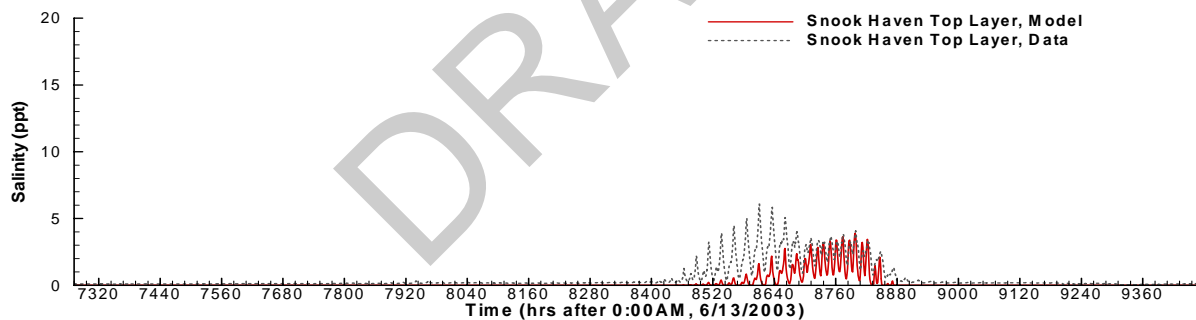


Figure C- 23 Comparisons of simulated and measured salinities at two depths at the Snook Haven station during April 10 – July 11, 2004.

Appendix D

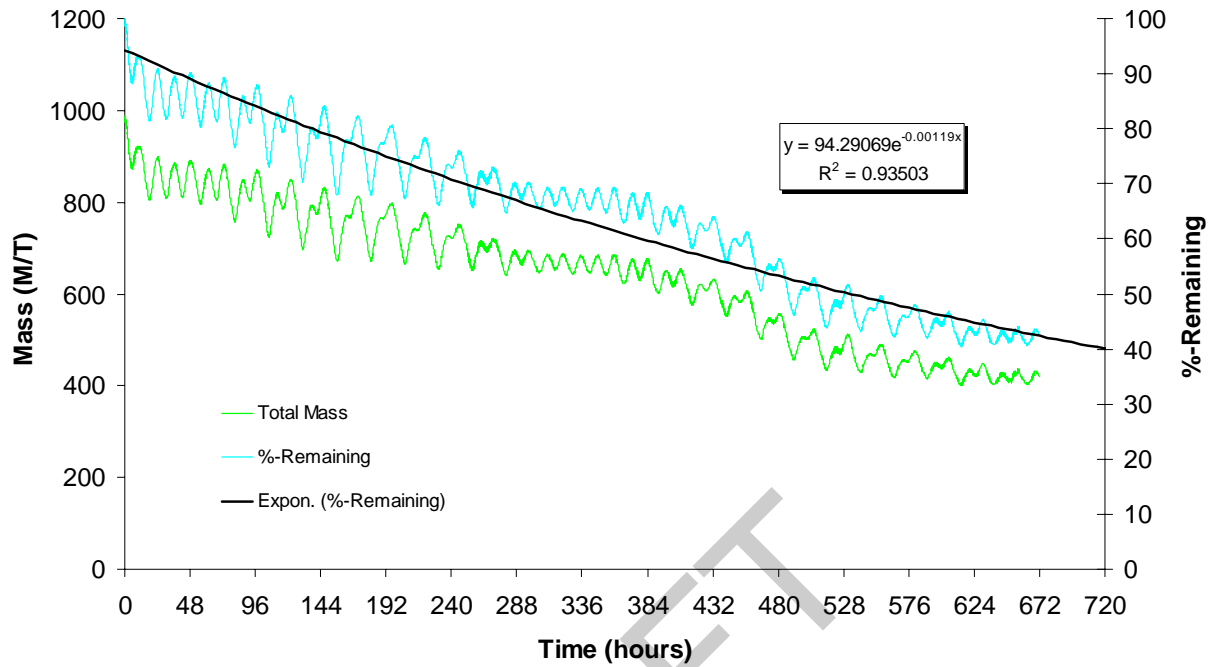


Figure D - 1 Time series of remaining conservative tracer mass in the main stem of the LPR for a combined Arcadia – Joshua - Horse flow rate of 55cfs.

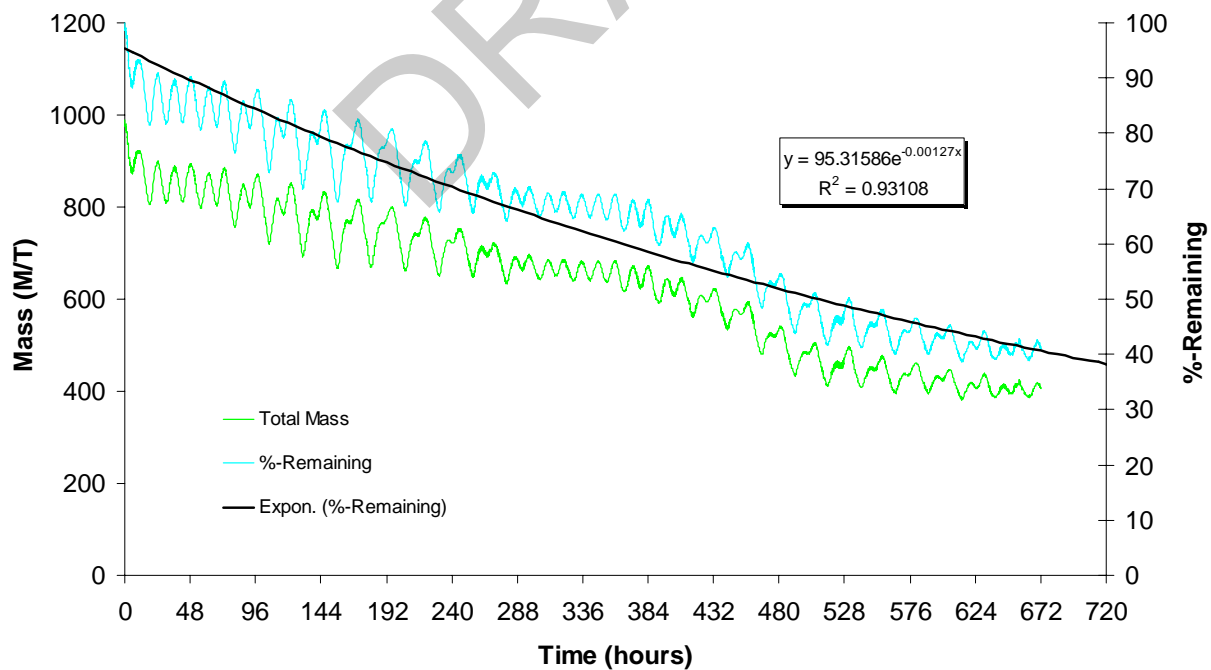


Figure D - 2 Time series of remaining conservative tracer mass in the main stem of the LPR for a combined Arcadia – Joshua - Horse flow rate of 106cfs.

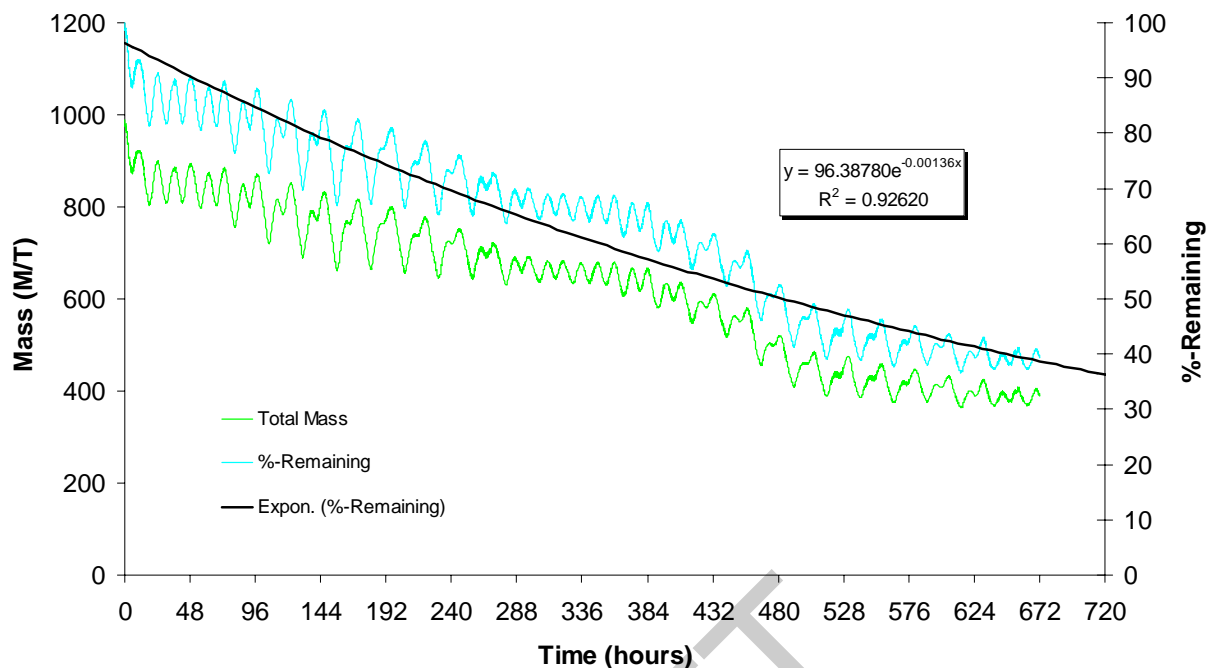


Figure D - 3 Time series of remaining conservative tracer mass in the main stem of the LPR for a combined Arcadia – Joshua - Horse flow rate of 154cfs.

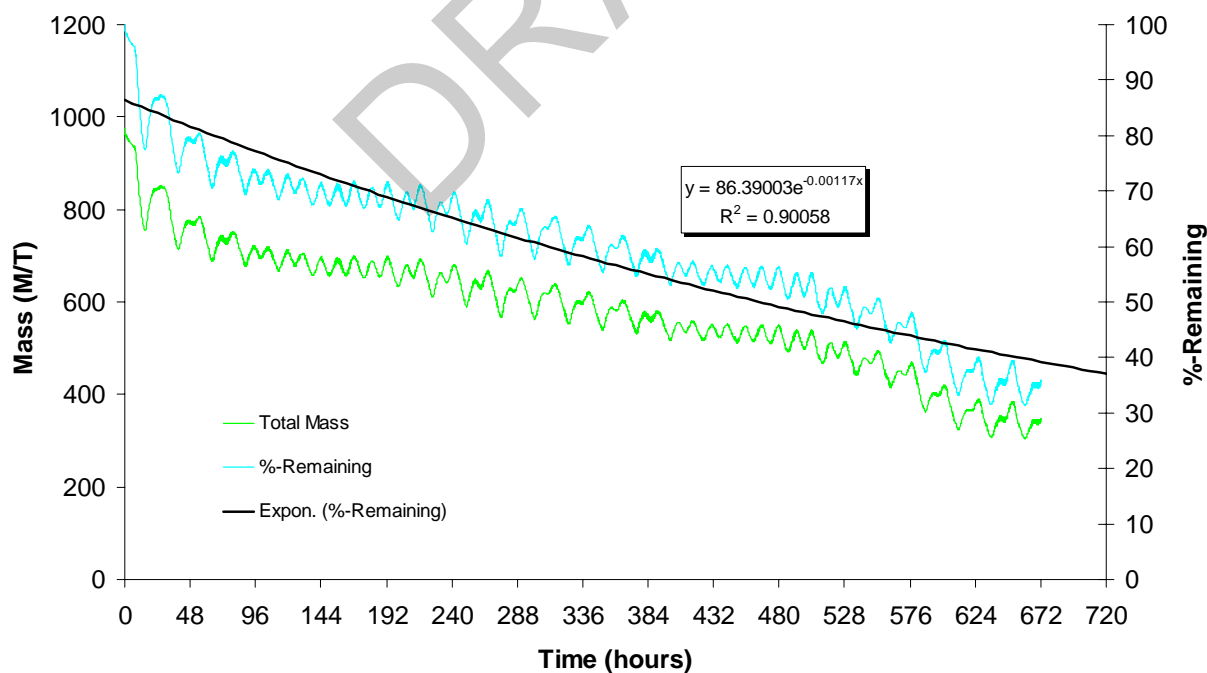


Figure D - 4 Time series of remaining conservative tracer mass in the main stem of the LPR for a combined Arcadia – Joshua - Horse flow rate of 199cfs.

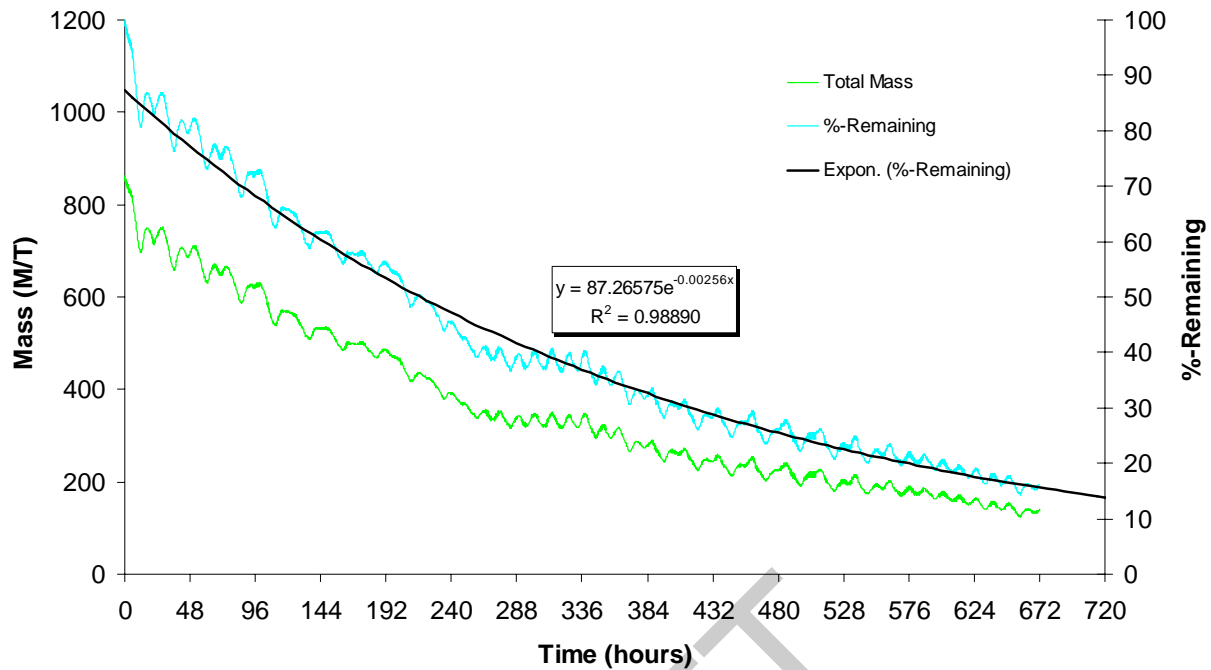


Figure D - 5 Time series of remaining conservative tracer mass in the main stem of the LPR for a combined Arcadia – Joshua - Horse flow rate of 240cfs.

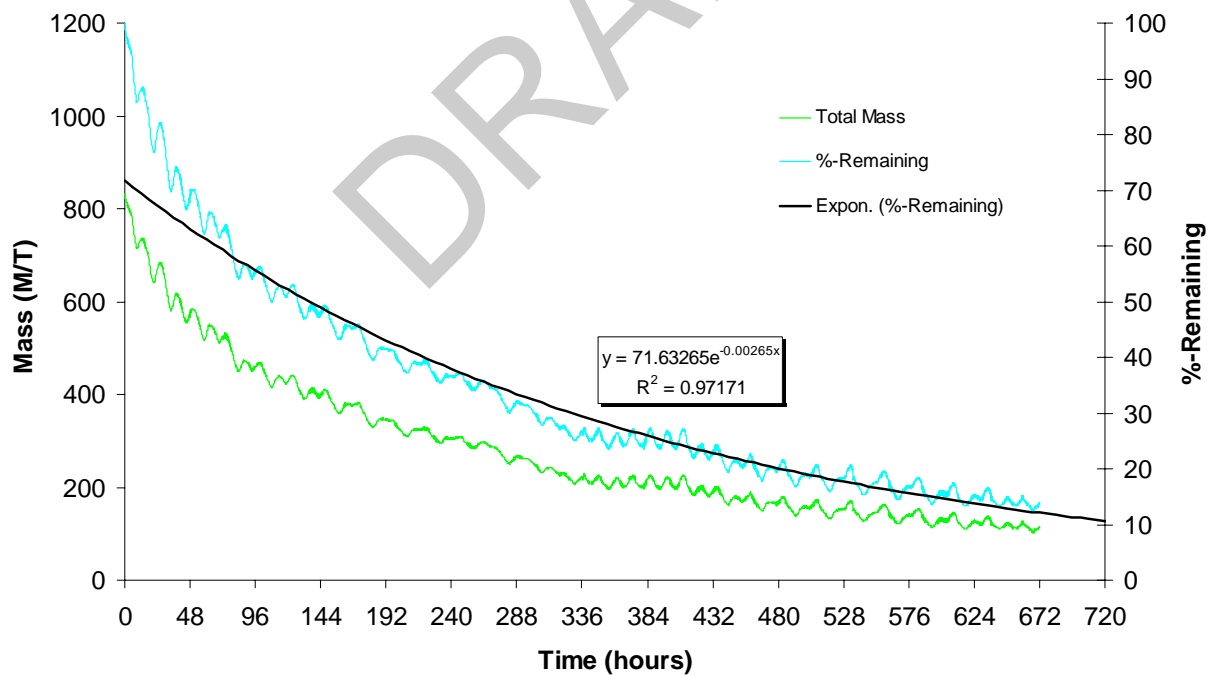


Figure D - 6 Time series of remaining conservative tracer mass in the main stem of the LPR for a combined Arcadia – Joshua - Horse flow rate of 281cfs.

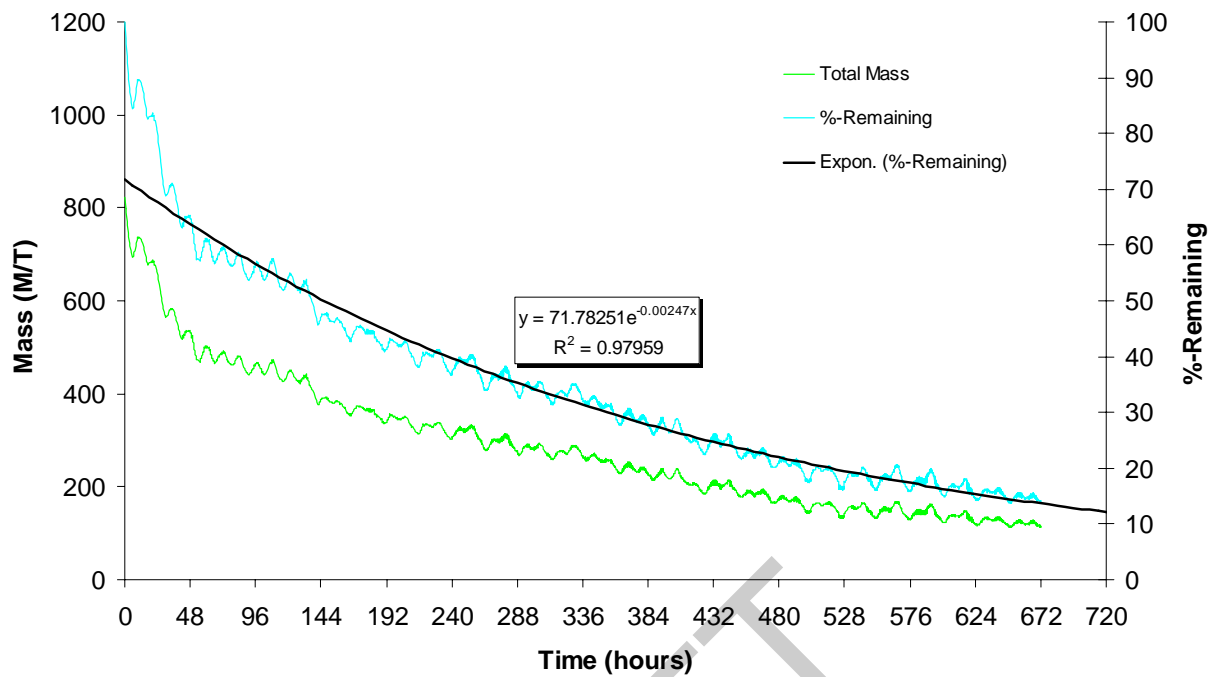


Figure D - 7 Time series of remaining conservative tracer mass in the main stem of the LPR for a combined Arcadia – Joshua - Horse flow rate of 332cfs.

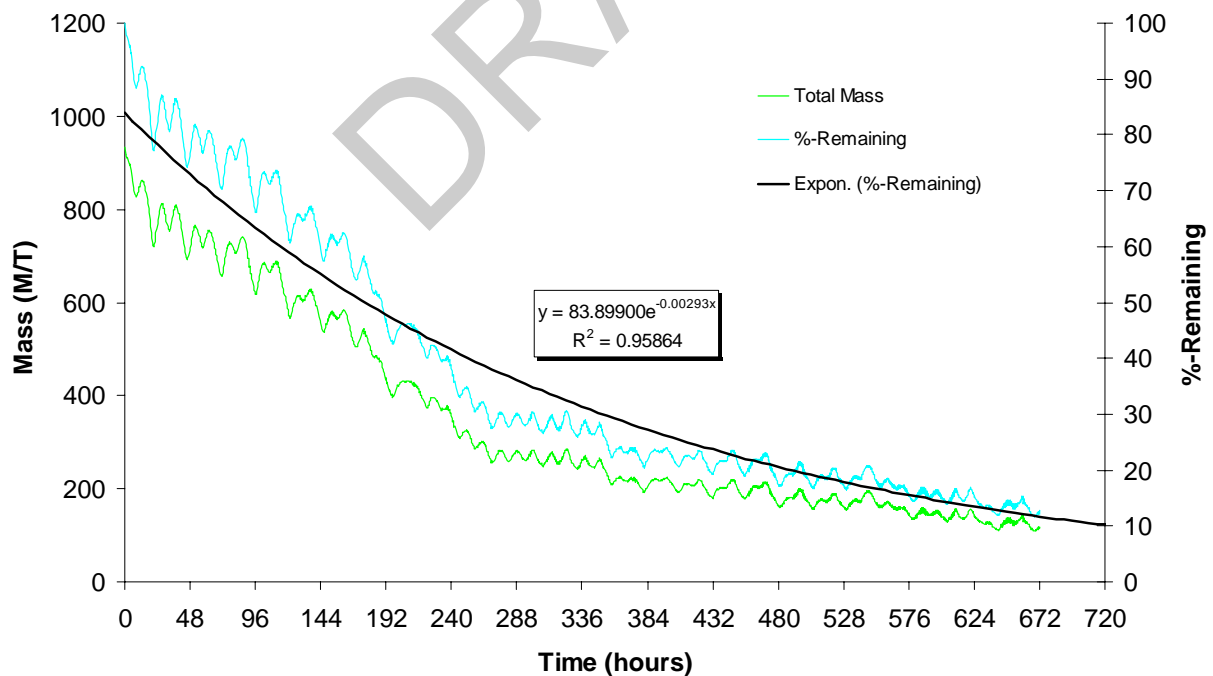


Figure D - 8 Time series of remaining conservative tracer mass in the main stem of the LPR for a combined Arcadia – Joshua - Horse flow rate of 391cfs.

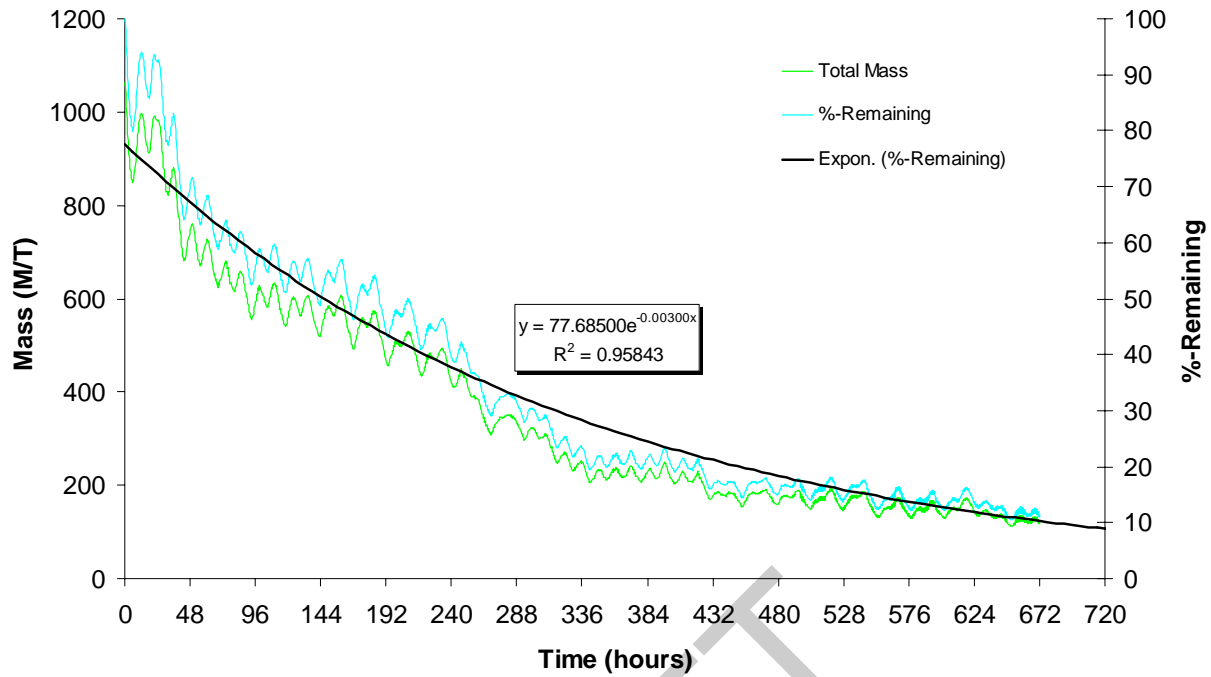


Figure D - 9 Time series of remaining conservative tracer mass in the main stem of the LPR for a combined Arcadia – Joshua - Horse flow rate of 455cfs.

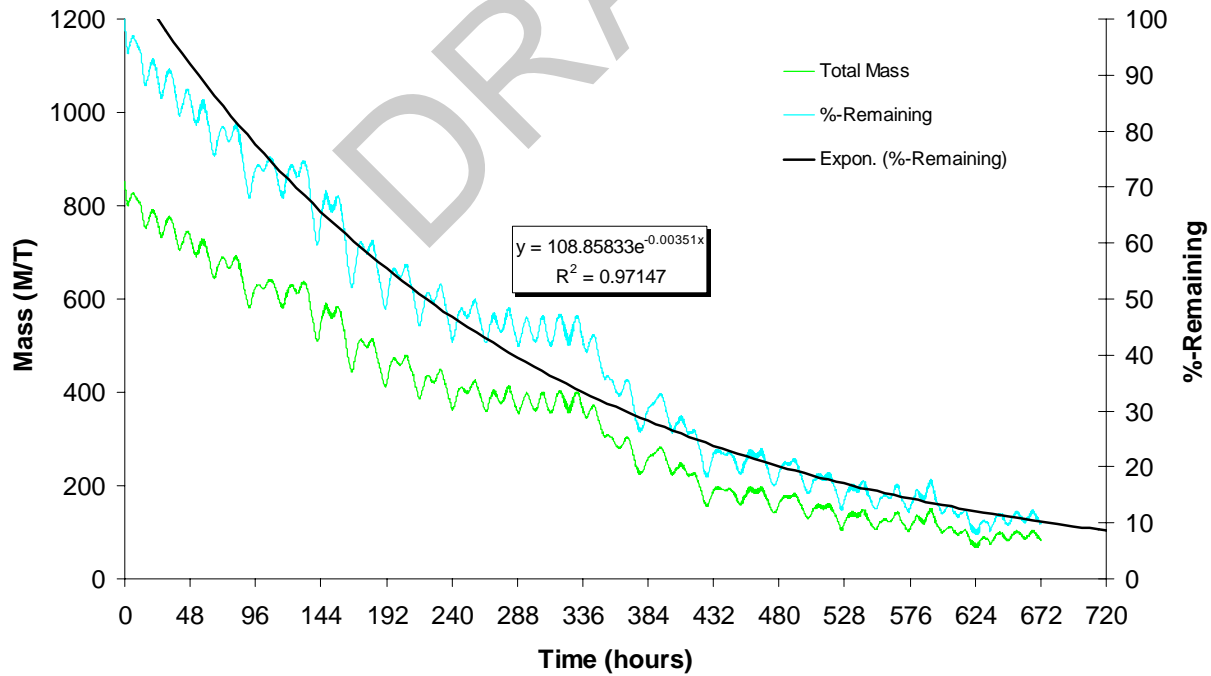


Figure D - 10 Time series of remaining conservative tracer mass in the main stem of the LPR for a combined Arcadia – Joshua - Horse flow rate of 544cfs.

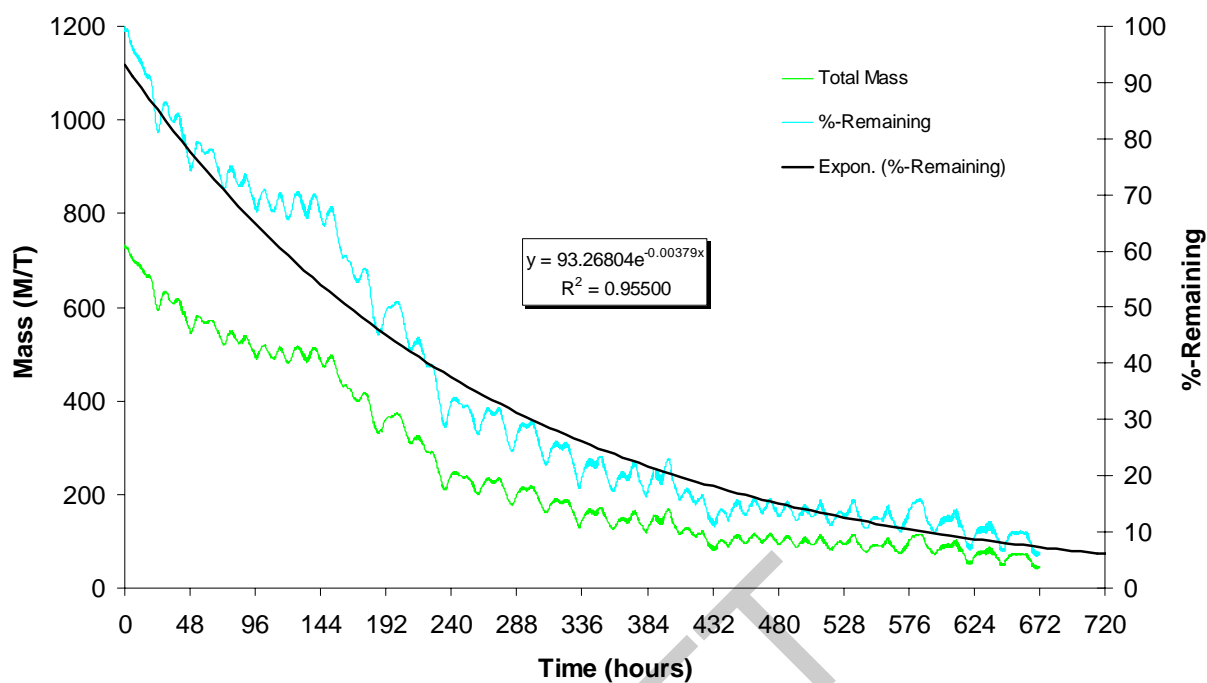


Figure D - 11 Time series of remaining conservative tracer mass in the main stem of the LPR for a combined Arcadia – Joshua - Horse flow rate of 644cfs.

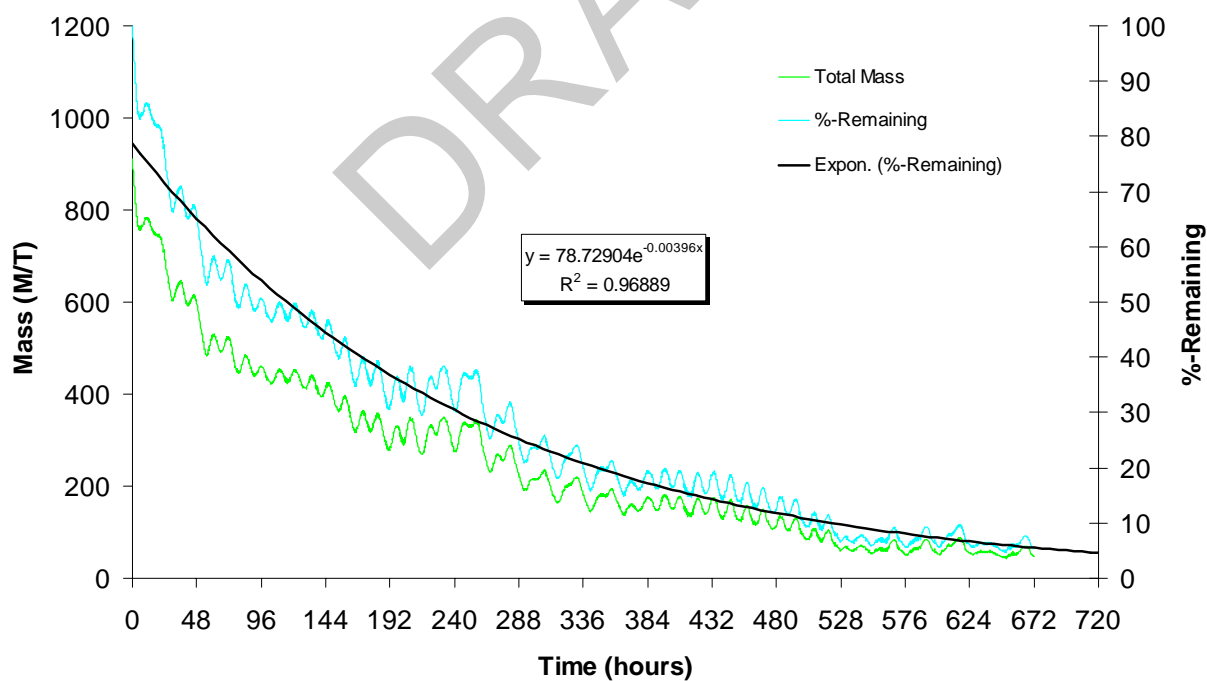


Figure D - 12 Time series of remaining conservative tracer mass in the main stem of the LPR for a combined Arcadia – Joshua - Horse flow rate of 939cfs.

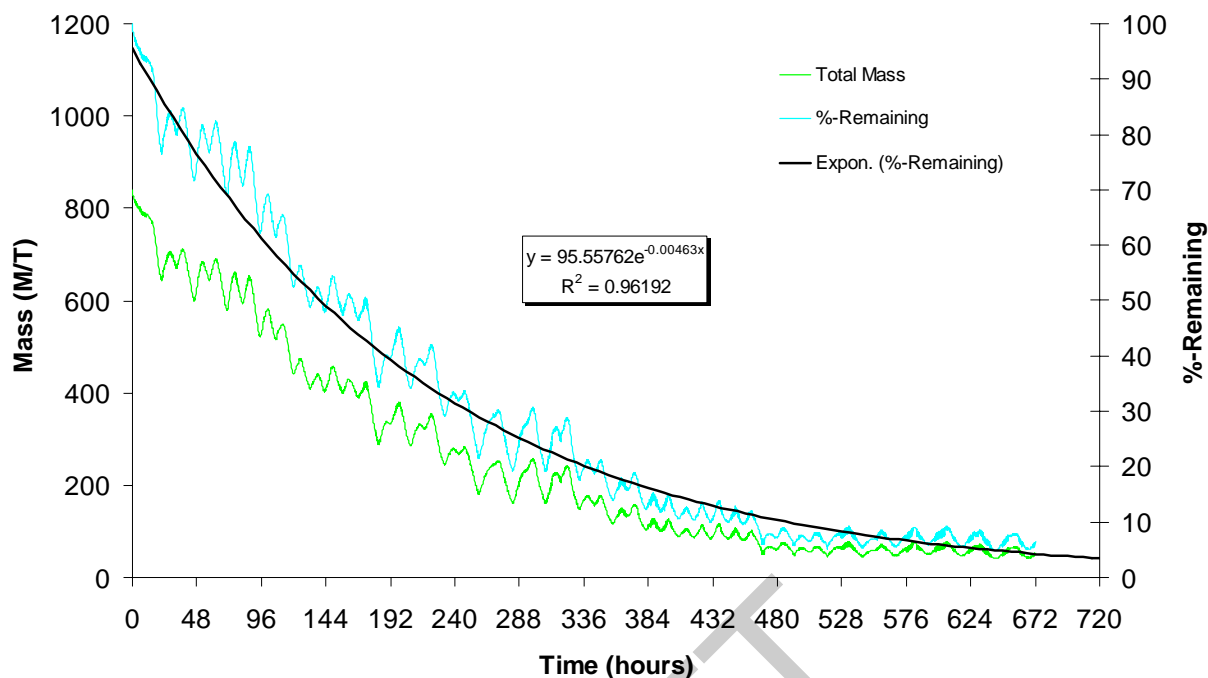


Figure D - 13 Time series of remaining conservative tracer mass in the main stem of the LPR for a combined Arcadia – Joshua - Horse flow rate of 1443cfs.

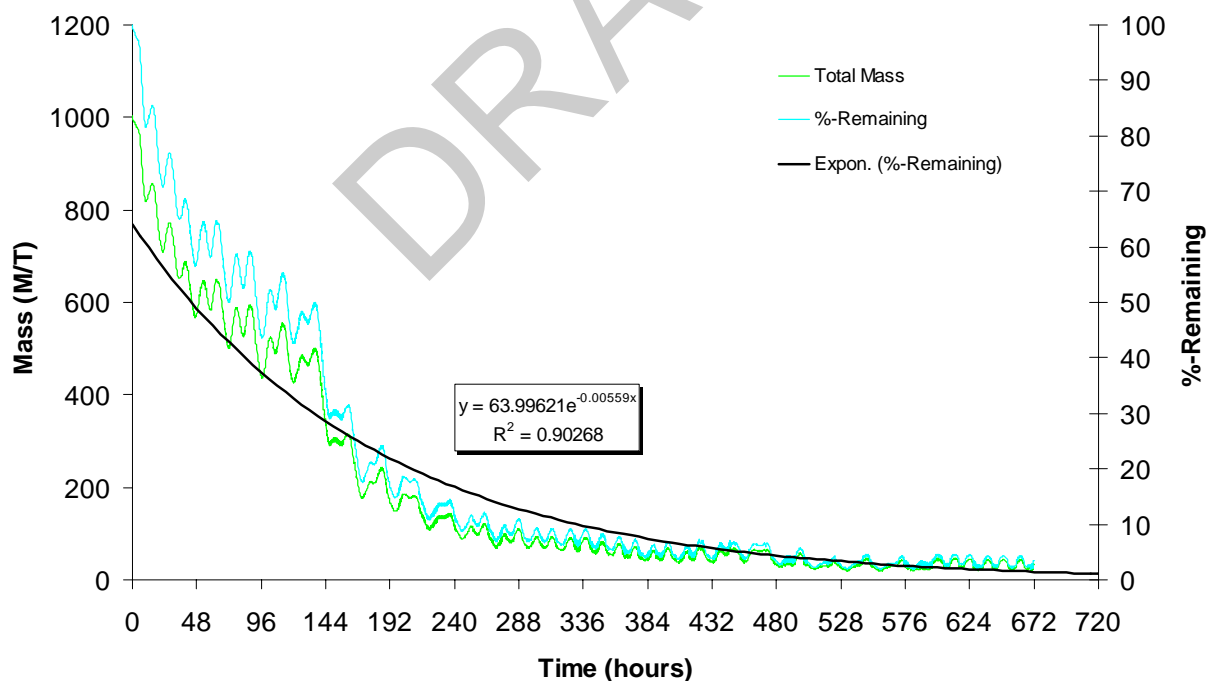


Figure D - 14 Time series of remaining conservative tracer mass in the main stem of the LPR for a combined Arcadia – Joshua - Horse flow rate of 2256cfs.

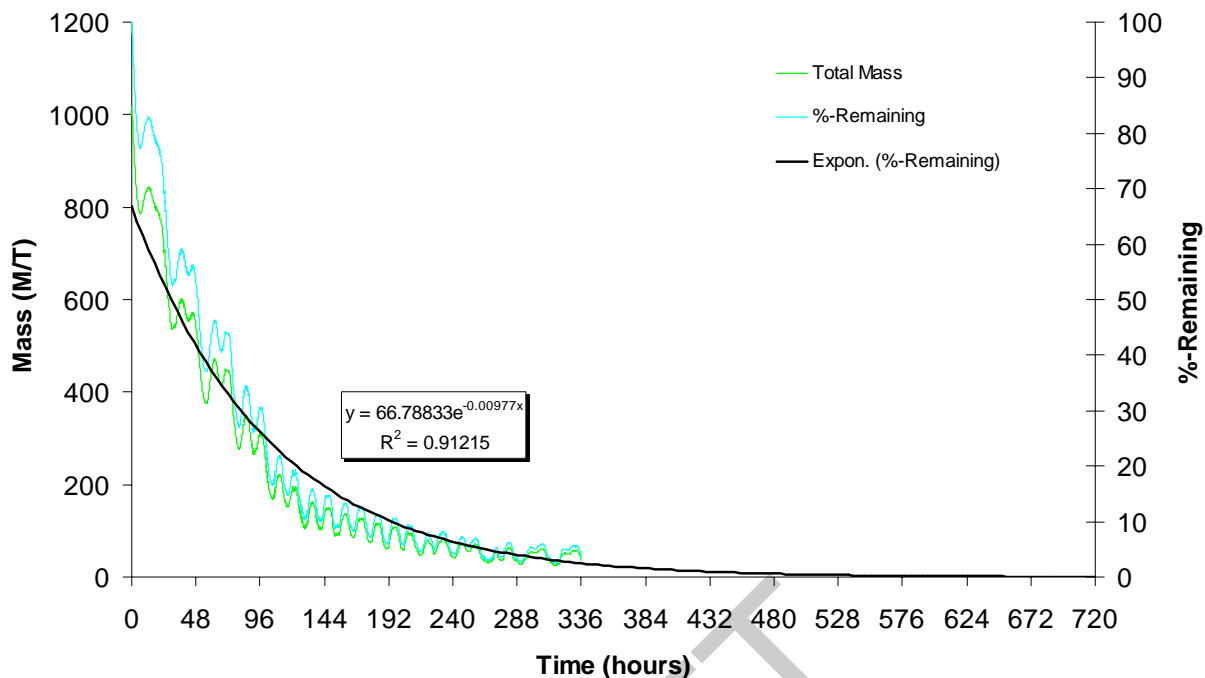


Figure D - 15 Time series of remaining conservative tracer mass in the main stem of the LPR for a combined Arcadia – Joshua - Horse flow rate of 4036cfs.

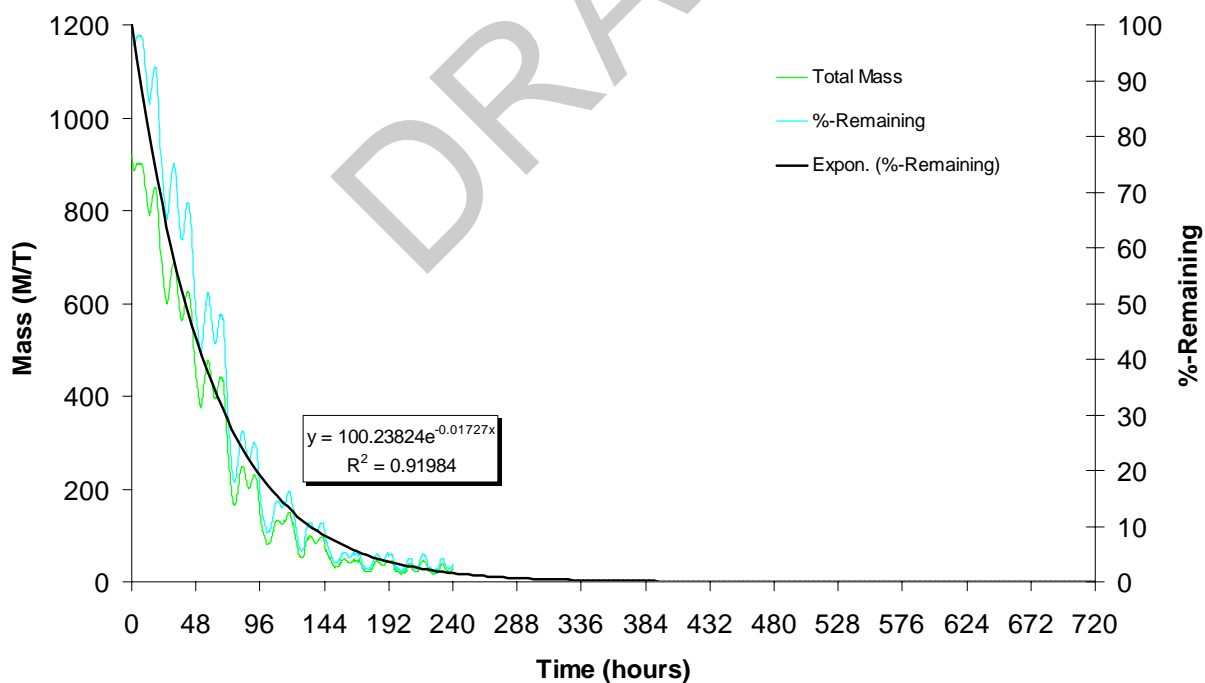


Figure D - 16 Time series of remaining conservative tracer mass in the main stem of the LPR for a combined Arcadia – Joshua - Horse flow rate of 9340cfs.